

Composition, Geochemistry and Conversion of Oil Shales

NATO ASI Series

Advanced Science Institutes Series

A Series presenting the results of activities sponsored by the NATO Science Committee, which aims at the dissemination of advanced scientific and technological knowledge, with a view to strengthening links between scientific communities.

The Series is published by an international board of publishers in conjunction with the NATO Scientific Affairs Division

A Life Sciences	Plenum Publishing Corporation
B Physics	London and New York
C Mathematical and Physical Sciences	Kluwer Academic Publishers
D Behavioural and Social Sciences	Dordrecht, Boston and London
E Applied Sciences	
F Computer and Systems Sciences	Springer-Verlag
G Ecological Sciences	Berlin, Heidelberg, New York, London,
H Cell Biology	Paris and Tokyo
I Global Environmental Change	

PARTNERSHIP SUB-SERIES

1. Disarmament Technologies	Kluwer Academic Publishers
2. Environment	Springer-Verlag
3. High Technology	Kluwer Academic Publishers
4. Science and Technology Policy	Kluwer Academic Publishers
5. Computer Networking	Kluwer Academic Publishers

The Partnership Sub-Series incorporates activities undertaken in collaboration with NATO's Cooperation Partners, the countries of the CIS and Central and Eastern Europe, in Priority Areas of concern to those countries.

NATO-PCO-DATA BASE

The electronic index to the NATO ASI Series provides full bibliographical references (with keywords and/or abstracts) to more than 30000 contributions from international scientists published in all sections of the NATO ASI Series.

Access to the NATO-PCO-DATA BASE is possible in two ways:

- via online FILE 128 (NATO-PCO-DATA BASE) hosted by ESRIN, Via Galileo Galilei, I-00044 Frascati, Italy.
- via CD-ROM "NATO-PCO-DATA BASE" with user-friendly retrieval software in English, French and German (© WTV GmbH and DATAWARE Technologies Inc. 1989).

The CD-ROM can be ordered through any member of the Board of Publishers or through NATO-PCO, Overijse, Belgium.



Series C: Mathematical and Physical Sciences – Vol. 455

Composition, Geochemistry and Conversion of Oil Shales

edited by

Colin Snape

Department of Pure and Applied Chemistry,
University of Strathclyde,
Glasgow, Scotland, U.K.



Springer-Science+Business Media, B.V.

Proceedings of the NATO Advanced Study Institute on
Composition, Geochemistry and Conversion of Oil Shales
Akçay, Turkey
18–31 July 1993

Library of Congress Cataloging-in-Publication Data

ISBN 978-94-010-4140-9 ISBN 978-94-011-0317-6 (eBook)
DOI 10.1007/978-94-011-0317-6

Printed on acid-free paper

All Rights Reserved

© 1995 Springer Science+Business Media Dordrecht

Originally published by Kluwer Academic Publishers in 1995

Softcover reprint of the hardcover 1st edition 1995

No part of the material protected by this copyright notice may be reproduced or utilized in any form or by any means, electronic or mechanical, including photocopying, recording or by any information storage and retrieval system, without written permission from the copyright owner.

Preface

Oil shales are broadly defined as petroleum source rocks containing sufficiently high contents of organic matter (above *ca* 10-15 wt.%) to make utilisation a possibility. Like coal, the world's reserves of oil shales are vast being many times larger than those proven for crude oil. Indeed, some of the largest deposits occur in the USA and Europe where Estonia and Turkey have large reserves. The first recorded interest in oil shale retorting was an English patent in 1694 (Eele, Hancock and Porter, No. 330) which refers to distilling "oyle from some kind of stone". The oil shale retorting industry dates back to the middle of the last century, notably Scotland, Estonia, France and Sweden in Europe. Indeed, my own Department at the University of Strathclyde has a historical link with James "Paraffin" Young, the founder of the Scottish oil shale industry who endowed a chair in Applied Chemistry. The growth of the oil industry saw the demise of the oil shale industry in most countries with the notable exception of Estonia, where kukersite has continued to be used for power generation and retorting. However, oil shale utilisation has attracted renewed attention since the early 1970s as a source of transport fuels and chemical feedstocks due to the the long term uncertainties over crude oil supplies. Indeed, the last 15 years has seen the development of a number of innovative process concepts, such as fluid-bed pyrolysis and hydroretorting which have enabled considerably higher oil yields to be obtained than by the classic retorting procedures.

The yield of shale oil obtained from retorting is governed by the organic matter content and maturity of the shale (crudely classified into Types I, II and III on the basis of atomic H/C and O/C ratios), the retorting regime and interactions between the organic material and the minerals present. To understand these phenomena, detailed structural information is clearly required on the organic matter present. Although microscopy and reflectance measurements enable the visibly distinct organic classes - macerals and the overall thermal maturity to be assessed no information is provided on the chemical structure. The facts that most of the organic matter is insoluble in common organic solvents (kerogen is the generic term used to describe this insoluble matter) and the organic matter occurs in a mineral matrix pose considerable problems for detailed characterisation. Indeed, the problems are more acute than for coals where the mineral concentrations are much lower. Nonetheless, the organic geochemistry and analytical chemistry communities have made considerable strides in the application of gas chromatography, mass spectrometry, nuclear magnetic resonance and a number of other advanced analytical methods to assess the structure and biological origins of kerogens. Therefore, it was considered timely to bring together leading scientists from the analytical/geochemistry and chemical engineering communities involved in fossil fuel research for this NATO ASI.

The aim of the ASI was to provide a comprehensive coverage of oil shale chemistry and conversion technology emphasizing the key role oil shale could have in the future for helping to meet the increasing world's demand for transport fuels and chemical feedstocks. The major themes of the ASI were the (i) composition and geochemistry encompassing microscopy, advanced spectroscopic and pyrolysis techniques, biomarkers and mineral matter and (ii) conversion including static and fluid-bed retorting, hydrolysis, co-processing, gasification, beneficiation, upgrading strategies and environmental considerations. The reviews in first two sections of the book reflect these major themes. In addition to the review lectures, over 25 research contributions were presented as posters at the ASI which contributed greatly to the success of the scientific programme. A number of these have been included the third section of the book.

Special thanks are due to Ekrem Ekinci of Istanbul Technical University for his invaluable assistance in helping me organise the NATO ASI. Further, I wish to acknowledge the contributions from E. Putun, F. Yardim, H. Atakul and D. Ercikan - the local organising committee in Turkey - and that from my wife, Anne who acted as secretary, in helping to make the ASI a success.

Colin E. Snape
9. 10. 94

TABLE OF CONTENTS

Preface	v
---------	---

Part I Reviews: Geochemistry & Characterisation

1.	Organic petrography: principles and techniques. A. Hutton, University of Wollongong, Australia	1
2.	Organic petrography of oil shales. A. Hutton, University of Wollongong, Australia	17
3.	Demineralisation and kerogen maceral separation and chemistry. T.L. Robl and D.N. Taulbee, University of Kentucky, Centre for Applied Energy Research, USA	35
4.	Alkane biomarkers. Geochemical significance and application in oil shale geochemistry. F.J. Gonzalez-Vila, Instituto de Recursos Naturales, Spain	51
5.	Solid state ¹³ C NMR in oil shale research: an introduction with selected applications. F.P. Miknis, Western Research Institute, USA	69
6.	Introduction to mass spectrometric techniques for fossil fuel analysis. G.A. Veloski and C.M. White, Pittsburgh Energy Technology Centre, USA	93
7.	An introduction to open-tubular gas chromatography - analysis of fossil and synthetic fuels. C.M. White, Pittsburgh Energy Technology Centre, USA	107
8.	Speciation of organic sulphur forms in solid fuels and heavy oils. C.E. Snape, K. Ismail, S. Mitchell, University of Strathclyde, UK and K.D. Bartle, University of Leeds, UK	125
9.	Detailed structural characterization of the organic material in Rundle Ramsay Crossing and Green River oil shales. M. Siskin, C.G. Scouten, K.D. Rose, T. Aczel, S.G. Colgrove and R.E. Pabst, Jr., Exxon Research & Eng. Co., USA	143

Part II Reviews: Conversion: Processing, Mechanisms and Products

1.	Economic considerations of the oil shale and related conversion processes. E. Ekinçi, Istanbul Technical University, Turkey	159
2.	Oil shale beneficiation for processing. J.G. Groppo, University of Kentucky, Centre for Applied Energy Research, USA	175

- | | | |
|-----|---|-----|
| 3. | Methods of oil shale analysis.
F.P. Miknis, Western Research Institute, USA | 191 |
| 4. | Relationship between hydrous and ordinary pyrolysis.
A.K. Burnham, Lawrence Livermore National Laboratory, USA | 211 |
| 5. | Fluidized bed retorting of oil shale.
S.D. Carter, U.M. Graham, A.M. Rubel and T.L. Robl,
University of Kentucky, Centre for Applied Energy Research,
USA | 229 |
| 6. | Steam and co-processing of oil shales.
E. Ekinici, Istanbul Technical University, Turkey and Y. Yurum,
Hacettepe University, Turkey | 247 |
| 7. | Chemical kinetics and oil shale process design.
A.K. Burnham, Lawrence Livermore National Laboratory, USA | 263 |
| 8. | Hydropyrolysis: fundamentals, two-stage processing and PDU operation.
M.J. Roberts, Gas Research Institute, USA, C.E. Snape and
S.C. Mitchell, University of Strathclyde, UK | 277 |
| 9. | The bitumen intermediate in isothermal and non-isothermal decomposition
of oil shales.
F.P. Miknis, Western Research Institute, USA | 295 |
| 10. | Aqueous organic chemistry: geochemical aspects.
M. Siskin and A.R. Katritzky, Exxon Res. and Eng. Co., USA | 313 |
| 11. | Asphaltites composition and conversion.
E. Ekinici, Istanbul Technical University, Turkey and Y. Yurum,
Hacettepe University, Turkey | 329 |
| 12. | Oil shale residues as a feedstock for carbon materials.
F.Derbyshire, U. Graham, Y.Q. Fei and M. Jagtoyen,
University of Kentucky, Centre for Applied Energy Research,
USA | 347 |
| 13. | Combustion reactivity of chars.
B.Z. Uysal, Gazi University, Turkey | 365 |

Part III Research contributions

- | | | |
|----|--|-----|
| 1. | A probe for the rapid analysis of Vanadium: An Electron Paramagnetic
Resonance and theoretical perspective.
S.M. Mattar and R. Sammynaiken and I Unger, University of
New Brunswick, Canada | 379 |
|----|--|-----|

2. Characterization of Jurassic black shales from Asturias (Northern Spain): evolution and petroleum potential. 387
I Suárez Ruiz and J.G. Prado, Instituto Nacional del Carbón, Oviedo, Spain
3. *n*-Alkanoic compounds in sulphur-rich macromolecular substances: a detailed investigation of sulphur incorporation and cross-linking. 395
J. Hefter, H.H. Richnow, R. Seifert and W. Michaelis, University of Hamburg, Germany
4. Biodegradation of hydrocarbons by sulphate reducing-bacteria in the Cretaceous Bahloul Formation (Tunisia). 407
M. Pervaz and W. Puttman, Lehrstuhl für Geologie, Geochemie und Lagerstätten des Erdöls und der Kohle, Aachen, Germany
5. Origin, evolution and petroleum potential of a Cambrian source rock: implications of pyrolysate and bitumen composition. 419
S. Bharati, Geolab Nor, Trondheim, Norway and S. Larter, University of Newcastle upon Tyne, UK
6. Carbon isotopic compositions of individual alkanes/alkenes in leaf fossils and sediments from the P-33 site of the Miocene Clarkia deposit. 439
Y. Huang, M.J. Lockheart, J.W. Collister and G. Eglinton, Organic Geochemistry Unit, School of Chemistry, University of Bristol, Bristol, UK
7. Atmospheric pressure temperature programmed reduction (AP-TPR) as a tool to investigate the changes in sulphur functionalities in solid fuels. 449
J. Yperman, D. Franco, J. Mullens, G. Reggers, M. d'Olieslaeger, L.C. Van Poucke, Limburgs Universitair Centrum, Diepenbeek, Belgium and S.P. Marinov, Bulgarian Academy of Sciences, Sofia, Bulgaria
8. Organic geochemical characterization of some carboniferous coal seams of the Zonguldak basin (N.W. Turkey). 461
M.N. Yalçın, TUBITAK, Marmara Research Centre, Turkey
9. X-ray studies of the structure of coals and cokes. 477
P. Wilk and S. Jasieńko, Institute of Chemistry and Technology of Petroleum and Coal, Technical University of Wrocław, Poland
10. The aspects of microscopic studies as exemplified by the macroporous structure of cokes from bituminous coal range. 485
P. Wilk and K. Bratek, Institute of Chemistry and Technology of Petroleum and Coal, Technical University of Wrocław, Poland

11.	Determination of organic sulphur forms in Type I/II kerogens by high pressure temperature programmed reduction.	493
	S.C. Mitchell and K. Ismail , University of Strathclyde, Dept. of Pure & Applied Chemistry, Glasgow, UK, R. Garcia and S.R. Moineo, Instituto Nacional del Carbón, Oviedo, Spain.	
	Index	501

ORGANIC PETROGRAPHY: PRINCIPLES AND TECHNIQUES

Adrian C Hutton
University of Wollongong
Wollongong, NSW, 2522
Australia

1. Introduction

Organic petrography is the study of the organic constituents, known as macerals, in sedimentary rocks, that is, the description and terminology of the properties of the organic matter, whether the rocks be, for example, coal, petroleum source-rocks and oil shales (all of which contain abundant organic matter) or limestone, sandstone and shale (all with minor dispersed organic matter (DOM)).

Traditional petrographic studies utilise transmitted light microscopy for thin-sections and strew mounts (as in palynological and kerogen studies) or incident (also called reflected) white light microscopy for polished blocks. In the last two decades, organic petrography has advanced significantly with the development of fluorescence mode microscopy. Fundamental to fluorescence microscopy is the phenomenon where hydrogen-rich organic matter absorbs wavelengths within the ultraviolet-blue (UV-blue) light range and re-emits longer wavelengths (that is, energy of a lower frequency) that are within the visible light spectrum. This form of fluorescence is known as primary fluorescence or autofluorescence and should be distinguished from secondary fluorescence which relates to fluorescence produced from fluorochromes or chemicals used to "stain" nonfluorescing organic matter, a technique used in biological sciences.

Macerals which have similar properties are placed in groups just as minerals are placed in groups. For minerals, feldspar, amphibole, pyroxene and mica are commonly-known groups. However, whereas there are many groups of minerals, there are only three maceral groups - vitrinite, inertinite and liptinite.

Vitrinite macerals, derived from the cells of plant tissue and precipitated gels, are generally grey, in low rank rocks, becoming light grey to greyish-white in very high rank rocks. In very low rank samples, vitrinite exhibits weak green, orange or red fluorescence grading to weak orange-brown fluorescence at higher rank to no fluorescence in very high rank samples. Several classifications have been developed for the vitrinite group with the most commonly used being the Stopes-Heerlen system, also known as the International Committee for Coal and Organic Petrology (abbreviated to ICCP) system. (The ICCP was known as the International Committee for Coal Petrology until 1990.) This system separates and distinguishes between huminite (low rank 'vitrinite' commonly found in brown coal) and vitrinite ('vitrinite' in higher rank

bituminous coal).

Compared to vitrinite, liptinite is dark grey and has a lower reflectance in incident white light. Most liptinite fluoresces relatively strongly, with much stronger intensities than for vitrinite in the same sample. Fluorescence intensity of liptinite decreases with increasing rank and there is a shift in the wavelength from the blue end to the red end of the spectrum. The fluorescence of liptinite may change after prolonged irradiation. This change may be either a positive or negative shift in both wavelength and intensity. Liptinite is derived from hydrogen-rich precursors such as fats, oils, waxes, spores, cuticle and algal precursors.

Compared to vitrinite, inertinite macerals are light grey to white and have higher reflectance. Inertinite has only very weak fluorescence and generally this can only be observed with special techniques. Inertinite is derived from the cells of plant tissue with initial coalification in a more oxygen-rich environment than for vitrinite.

Organic petrography is particularly useful in the coal industry, the petroleum industry and the oil shale industry. Coal petrography commenced when researchers attempted to determine the origin of coal and to review coal properties that influenced coke manufacture. Of the many concepts used in coal petrography, the two most important are *type* and *rank*. *Type* refers to the nature, that is, variety and abundance of organic matter. Thus type is a function of both the variety of precursor organic matter that was deposited in the pre-peat stage and the nature and degree of alteration that the components of peat underwent during the early stages of diagenesis.

Rank refers to the stage of coalification that the organic matter has reached. Thus rank is determined by the degree to which physico-chemical reactions have coalified or metamorphosed the organic matter in response to time and/or temperature. The reflectance of vitrinite increases almost linearly with rank and thus vitrinite reflectance is a good rank parameter. Reflectance of a maceral is the percentage of light reflected from a polished surface of the maceral and is measured relative to standards of known reflectance and under a narrow set of conditions including specific wavelength of the incident light and temperature.

In coal, macerals rarely occur alone but commonly with other macerals, mineral matter or the same maceral. An assemblage of one or more macerals, where the width of the assemblage is greater than 50 microns, is called a microlithotype.

Whereas coal petrography is quite an old science dating from the early work of Stach, Thiessen and Stopes, oil shale and petroleum source rock petrography are relatively young sciences being not yet three decades old. In the petroleum industry, vitrinite reflectance is used to determine maturity (a term synonymous with rank) which in turn is used to determine the thermal history and other details such as the nature, timing and degree of hydrocarbon generation. Type and abundance of the organic components determines source rock potential. As the organic components are macerals derived from plants, including terrestrial plants and algae, organic petrography is an important technique for studying source rocks.

Oil shale petrography was born of coal petrography and has been nurtured by coal petrographers since its inception. The development of fluorescence microscopy has been of great benefit because many of the liptinite macerals are difficult to distinguish from mineral matter in incident white light, especially in samples of low rank. Petrographic studies of oil shales are basically studies of liptinite macerals (the hydrogen-rich macerals) and an understanding of coal petrography is essential for success and competency in this field.

2. Organic Constituents of Rocks

Over the past twenty years, applications of coal petrography have been extended to include, firstly, the study of oil generation, especially maturation of the organic matter and the thermal history of basins, and more recently, the study of oil shales. Consequently we now see that most organic microscopists are organic petrographers (rather than coal petrographers) who study organic matter in all types of rocks. Most learn the art by studying coals initially because this gives a good background in the principles and techniques.

Petrographers are aware that organic matter is just part of a rock; in coal the organic matter is, by definition, the most abundant part of the rock. In oil shale the organic matter constitutes much less than 50% (by volume) of the bulk rock; in petroleum source rocks, the organic matter constitutes as little as 5% (by weight) of the rock. The message is simple, petrographers need to be aware of the mineral matter as well as the organic matter - the organic constituents are not the only components of the rock examined. One way of looking at the composition of any sedimentary rock is to regard it as comprising one or more of six components, some that are organic and others that are inorganic (detailed definitions of the organic components are given elsewhere):

Vitrinite	-	organic matter derived from woody tissue
Inertinite	-	organic matter derived from woody tissue in an oxidising environment
Primary Liptinite	-	organic matter derived from hydrogen-rich plant tissue
Secondary Liptinite	-	liptinite derived from primary organic components; includes bitumen and oil
Allochthonous Minerals	-	clastic mineral matter, commonly from outside the basin
Autochthonous Minerals	-	authigenic mineral matter precipitated in the basin

3. Techniques Used in Organic Petrography

As with any science, the results obtained and the subsequent importance of any petrographic study is dependent on two factors:

- i. the expertise and equipment used in the preparation of the samples that are to be studied, and
- ii. the expertise and equipment used to make the observations.

Polished blocks can be prepared from outcrop, drill core, sidewall core or cuttings samples and as little as a few grams is all that is required for detailed characterisation of a sample. However, it should be noted that detailed characterisation refers to the interval covered by the sample in the block, however small, and not the seam or deposit.

3.1. SAMPLE PREPARATION

Organic petrography of coal is well documented and the techniques used, including those for sample preparation, have been in use for many years.

Thin sections have been used extensively in the past but tend to be less useful than

polished blocks. The main disadvantages of thin sections are :

- i. aberrant UV-blue radiation is a major hazard;
- ii. larger samples are sometimes required;
- iii. many clay-rich samples do not hold together during preparation and the thin sections produced are commonly of poor quality; and
- iv. cover slips used to protect the thin section reduces fluorescence intensity.

Strew mounts (or kerogen mounts) are important to a palynologist but of limited value for the organic petrographer. Removal of the mineral matter tends to cause the organic matter to form a mat which may impede examination. Demineralisation is first carried out with hydrochloric acid (HCl) to remove carbonates and then hydrofluoric acid (HF) to remove silicates and other mineral groups. Disadvantages of the strew mounts include:

- i. the organic-mineral relationships are commonly destroyed;
- ii. the cover slip reduces fluorescence intensity;
- iii. oxidation of the organic matter may take place and this alters the fluorescence intensity and chemical composition; and
- iv. comminution of the sample may destroy the properties of the palynomorphs.

Polished blocks and reflected light microscopy have the following advantages:

- i. the technique is rapid;
- ii. the technique is easy to learn;
- iii. blocks are easily stored for later use; and
- iv. the amount of sample to prepare a polished block need not be large.

Methods for preparing and polishing samples are given in most text books and it is not proposed to detail these here. No method is prescriptive and many laboratories modify the steps given in text books. For example, a number of laboratories still use manual polishing whereas many others have gone to automated equipment. Some laboratories use alumina powder, others use diamond pastes and others use chromium and magnesium oxides. Likewise the choice of the mounting medium is commonly personal preference. As a general rule, the solid mounting medium should be approximately the same hardness as the sample.

The following points are important.

1. Sample selection is critical; samples may or may not be representative. Whole rock samples (core, outcrop and sidewall core) provide data on mineral-organic textures and boundary features; cuttings samples allow characterisation of larger intervals.
2. Sample preparation is important. Samples should be dry and should not be heated above 50 to 60°C, especially if reflectance data are being taken.
3. All samples should be evacuated before the embedding resin sets as this will make polishing easier; larger grains from preceding polishing steps may be trapped in air bubbles and released during later steps.
4. Samples which contain swelling clays, such as smectite, may have to be polished in an alcohol carrier rather than water.

3.2. ANALYSIS OF SAMPLES

Which microscope should be chosen? The answer is difficult and really depends on the budget and the availability of suppliers. Personal choice may also play a large part in microscope selection. Some researchers prefer digital readout for reflectance measurements, others prefer galvanometers or prefer that data to be input to a computer.

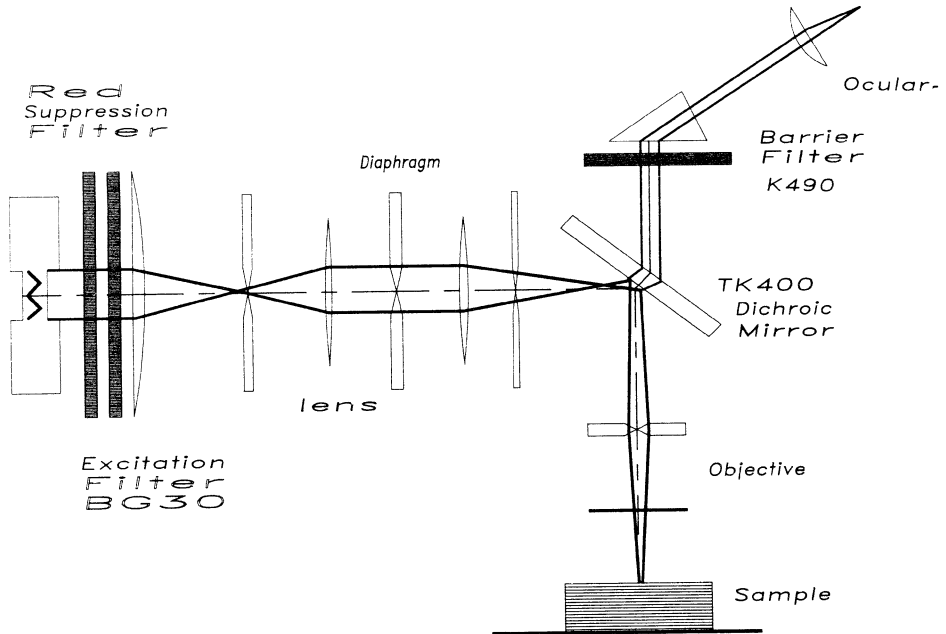


Figure 1. Schematic Light Path for Reflected Light Microscope Using Fluorescence Mode.

Oculars and objectives should be clean. Smears and oil drops can be removed with lens tissue or a clean piece of polystyrene. All samples should be examined in white light as well as fluorescence mode. The fluorescence properties observed in oil immersion are commonly quite different with respect to intensity and even colour, if the same field is observed in air immersion. Likewise changing the filter system changes the fluorescence colours. A commonly used filter system for a Leitz microscope (Fig. 1) comprises a 4 mm BG38 red suppression filter, a 5 mm BG12 excitation filter, a TK400 dichroic mirror and a K490 suppression or barrier filter; fluorescence colours change if one or more of the filters is changed. We commonly forget that colours perceived by the petrographer are rather subjective and quite often few petrographers will give the same colour description when observing the same liptinite. Although standard colour charts have been used, these appear to have had little success in some countries.

It is difficult to describe a 'standard microscope' as manufacturers do not standardise their equipment. Essential components for fluorescence microscope (Fig. 1) are the red suppression or heat filter to reduce the heat energy given off by the lamp, the excitation filter to give a narrow excitation spectrum and the barrier filter to remove harmful primary UV-blue wavelengths that are not absorbed by the sample.

Good photography is an asset to the organic petrographer and the ability to shoot a 'good' photograph improves with experience. Exposure times may be of the order of minutes, especially for fluorescence mode, and fast film speeds are needed - at least ISO

200/24°; ISO 400/27° is better.

Quantitative maceral analyses are usually obtained with standard point count methods using both white light and fluorescence mode counts. Each count should be at least 500 points with the step and traverse intervals calculated to give at least 90% coverage of the block. Percentages should be quoted to realistic figures. In a count of 500, each point represents 0.2% by volume; any figure corrected to 0.1% or less is meaningless. As a general rule the lowest objective magnification should be x32 and preferably x50.

Reflectance measurement should be taken in accordance with a standard. Details of the methods are given in reference books.

4. Organic Petrography of Coal

4.1. BRIEF HISTORY OF COAL PETROGRAPHY

Coal petrography initially employed transmitted light techniques utilising thin sections (TL). Many advances were made using these techniques and amongst those who contributed significantly to the understanding of coal petrography were Thiessen and White who stressed the need for microscopic studies. TL techniques were used extensively in Europe and the USA; benchmark publications came from Reinhardt Thiessen¹ and Mary Stopes², both of whom were palaeobotanists. H and R Potonie were important contributors in Germany.

Reflected light examination of coal was initiated in 1913 and was used in the 1920s and early 1930s by Stach, Thiessen, Stopes, Duparque, (France), Seyler (England) and Hoffman and Jenkner (Germany) who pioneered reflectance measurement and its use as a measure of rank. Two major advances came in 1935. Stach³ published his textbook on coal petrology, which was updated 40 years later and issued as a third edition in 1982⁴, and a meeting of learned coal scientists met at Heerlen (The Netherlands) to resolve some of the many difficulties that had arisen because of the many and varied approaches that had been adopted up to this time. Several ideas on classification had evolved and confusion had arisen over concepts and terminology. At the Heerlen meeting, Mary Stopes proposed her concept of "maceral" to designate the fundamental microscopic constituents of coal. From this meeting was born the Stopes-Heerlen nomenclature system which forms the basis of the present International and the Australian Standards systems of nomenclature.

In the 1950s, the ICCP was formed with the aim of advancing the science of coal petrology through standardisation of methodology and terminology. These attempts have contributed greatly to standardisation but there is still a long way to go. Within the last two decades, automated microscopy and fluorescence microscopy have developed and are now standard techniques in many laboratories. For example whereas subjective estimates of fluorescence colour and intensity were given for liptinite macerals, it is now possible to show a spectrum of wavelengths for fluorescence and quantitative intensities.

Coal petrology is now a multidisciplinary study which includes the petrology of peat, evaluation and causes of rank, detailed studies of coal chemistry and physical properties of coal, technological applications of coal including liquefaction, combustion and carbonisation (coking), petrological studies of coal seam sedimentology and petrological studies of oil shales and petroleum source rocks.

Maceral terminology was first developed for coal and then extended to include petroleum source rocks and oil shales. Coal is an heterogeneous rock that is composed

of organic matter derived from mostly terrestrial plant matter with minor mineral matter of either an authigenic or allochthonous origin.

Today, coal petrography is the study of coal using one or more of the following:

- i. examination of a polished surface in reflected light to identify the vitrinite and inertinite components and in fluorescence mode to determine the type and abundance of liptinite macerals;
- ii. measurement of the vitrinite reflectance to determine rank; the reflectance of other macerals can also be determined although vitrinite reflectance is the accepted rank determiner; and
- iii. estimation of volumetric abundance of macerals; the latter can be either a point count or a visual estimate; many laboratories also measure the wavelength of the fluorescence radiation.

Whilst it is possible to give a number of suggestions, it should be realised that, although the maceral definitions are quite rigidly defined, in practice there is great diversity in the properties of the individual macerals. Experience is the best teacher!

4.2 WHAT IS COAL?

Coal is composed primarily of vegetal matter that was deposited in a number of environments. The vegetal matter forms peat which then changes to coal given suitable conditions. The type and composition of the peat is determined by both contributing plants and the conditions of peat accretion. Both reflect, to a large degree, the position of the water table relative to the swamp surface. It follows that coal will be the end-product of plant type and both physico-chemical and biochemical reactions.

4.3 MACERAL TERMINOLOGY

Maceral terminology and classification is a three-tiered hierarchal system whereby maceral groups are divided into macerals which are further subdivided into sub-macerals. Where very detailed terminology is required, such as in genetic studies, some submacerals are divided into maceral varieties.

It is important to realise from the beginning, that maceral terminology for vitrinite macerals, is not absolute, that is, some vitrinite macerals have more than one name. Maceral terminology is essentially a classification system erected for the description and classification of organic matter in coal. As such, several parameters can be used as the basis for the classification and as a consequence, there are several maceral terminologies in use.

The maceral terminology used in coal petrography has evolved over the years with several of the maceral names suggested by Stopes being adopted at the Heerlen Congress held in 1935. The terminology which has developed under this system has been termed the Stopes-Heerlen system, later adopted, with some revisions, as the International System by the ICCP^{5,6,7}. The Stopes-Heerlen system is widely used by petrographers in Europe, USA and Australia.

One significant historical factor relating to terminology has important consequences; terminology was developed for coals formed in the Northern Hemisphere, especially the Carboniferous bituminous coals and the brown to sub-bituminous coals of Mesozoic and Tertiary age of Europe. As coal petrography spread, it was found that some of the terms did not suit the Permian bituminous coals of the southern hemisphere. Consequently, coal petrographers from a number of countries, especially those living south of the

Equator, began to amend the original descriptions and nomenclature to suit the coals, research needs and applications as required.

4.3.1. Basic Concepts. Phyteral - The term *phyteral* was proposed by Cady⁸ for use where referring to coal fossils or coalified plant fossils. For example, a coalified plant spore is a phyteral; the optically-recognisable coalified spore is referred to as the maceral sporinite; a coalified root is a phyteral that may be composed of several of the vitrinite, inertinite or liptinite macerals. *Phytoclast* is sometimes used synonymously with phyteral; however phytoclast now is used commonly to define an isolated phyteral or part of a phyteral in non coaly rocks.

Maceral - The definition of a maceral as given by the ICCP is: "Coal macerals evolve from the different organs or tissues of the initial coal-forming plant materials during the course of the first stage of carbonification. However, because of variable but severe alteration, it is not always possible to recognise the precursors. Macerals are the microscopically recognisable individual constituents of coal and depending on their quantitative participation and their association, they control the chemical, physical and technological properties of a coal of given rank. In a sense macerals 'may be likened to the minerals of rocks'". A simple definition is - 'a maceral is an elementary microscopic constituent of coal that can be recognised by its morphology and optical properties, that is, by its morphology, reflectance and fluorescence where this occurs'.

The term maceral was introduced by Stopes² to refer to the elementary organic microscopic constituents of coals. Macerals are analogous to the minerals of rocks where the term mineral refers to the elementary microscopic inorganic constituents.

Coal macerals evolve from different organs or tissues of coal-forming plants during the biochemical stage of coalification, and depending on the type, quantity and association of the floral components, these determine the chemical, physical and technological properties of a coal.

All macerals have the suffix '-inite'.

Maceral Group - a *maceral group* comprises several macerals each of which has a set of optically and chemically similar properties. Thus macerals are similar to one another but distinctly different from macerals of another maceral group. Just as minerals which have similar properties, are referred to as groups (for example, feldspars, amphiboles) some of the macerals have similar properties and are grouped into one of three maceral groups - inertinite, liptinite (formerly called exinite) and vitrinite.

The maceral group terms are used in two ways - formally when used as the maceral group name and less formally when used as a general term when specificity of the macerals is not required (for example "vitrinite-rich", "trace liptinite").

4.3.2. Properties of Vitrinite. Vitrinite macerals are commonly the most abundant macerals, generally constituting 40 to 90% of most humic coals; vitrinite is derived from cell walls, cell contents or precipitated gels. Other properties are:

* Density - in the range of 1.2-1.8 g/ml.

* Coking Properties - react during carbonisation to form the bulk of the coke groundmass.

* Chemistry - carbon and hydrogen contents of vitrinite at any given rank below low volatile bituminous coal rank, are intermediate between those of inertinite and liptinite.

* Toughness - after polishing, vitrinite macerals mostly show negative relief.

* Reflectance - in any given coal below the rank of low volatile bituminous coal, vitrinite macerals have a reflectance between that of liptinite and inertinite; in brown coal the reflectance ranges from about 0.2 to 0.5%; in bituminous coal the reflectance ranges from 0.5 to 2%; in anthracite reflectance ranges from 2 to 5%.

* Fluorescence - some vitrinite macerals in coals of low rank show a weak fluorescence.

4.3.3. Vitrinite Terminology. It was stated above that terminology for vitrinite is not absolute, that is, some types of vitrinite have more than one name. The reason one maceral can have two or more names is simply that several classifications or terminologies have developed in much the same way that there are several languages in a country; for example, an object will have a different name in each language. The important point is - a change of name does not change the object. This is the same with vitrinite - a change of name does not change the optical, chemical or physical properties of the vitrinite entity.

A brief look at three terminology systems for vitrinite will illustrate some of the complexities of terminology. Once again it should be remembered that although several systems are used, the organic matter being examined is the same irrespective of the system in use. Each system has a specific name or term that is used for a given maceral and another system has another name (in some cases, the same name may be used in different systems). In summary, no matter what terminology is used, the various macerals are the same and have the same set of optical properties. Confusion arises when the terminology from one system is used with terminology from another system.

A. ICCP (Stopes-Heerlen or International) System

The ICCP (Table 1) is used extensively in most parts of the world, even in the USA and Australia where other systems developed. Because of its widespread use, all petrographers should be familiar with the ICCP system which distinguishes between three classes of petrographic entities - macerals, microlithotypes and lithotypes.

The ICCP system distinguishes between vitrinite macerals in brown coals and vitrinite macerals in bituminous coals (also called hard coals). Vitrinite is the maceral group name for bituminous coal and huminite is the maceral group name for brown coal. It should be noted that several of the maceral terms used for brown coal refer to macerals that are the precursors of other macerals in bituminous coal but which are then given different maceral names. For example, textinite is used for 'structured vitrinite' in brown coal but telinite is the term used for 'structured vitrinite' in bituminous coal. The two macerals differ only in that one is found in low rank coal and the other in high rank coal. Thus the textural or morphological properties are the same but the optical (especially reflectance and fluorescence) and chemical properties are quite different.

Corresponding huminite macerals become vitrinite macerals when coalification has reached the rank of bituminous coal. Correlation between the brown and bituminous coal equivalents is not agreed to by all petrographers and thus some equivalent terms in a given publication are at variance with those given by another author.

One major difficulty with the ICCP System is evident with coals within the rank range between 0.35% and 0.6% vitrinite reflectance. The change in rank is gradational and it is difficult to see any significant change in optical, chemical or physical property of many vitrinite macerals over this range. However, immediately the reflectance or rank changes from 0.49% to 0.5%, a different term must be used even though the properties of the organic matter do not change. (It should be noted that when the ICCP terminology was first detailed, only European coals had been examined and there was evidence of a

Table 1. Maceral Terminology for the Stopes-Heerlen System

Maceral Group	Maceral	Precursor
VITRINITE	telinite	cell walls
	collinite	homogeneous layers
	- telocollinite	homogeneous sphaeroidal or ovoid bodies
	- corpocollinite	gels
	- gelocollinite	homogeneous groundmass
	- desmocollinite	vitrinite fragments
	vitrodetrinite	
LIPTINITE	alginate	large algae
		small algae
	- telalginate	cuticle
	- lamalginate	resins, fats, oils, waxes
	cutinite	spores, pollen
	resinite	suberitized walls of cork tissue
	sporinite	altered algae and humic materials
	suberinite	secondary sweated 'resinite'
	bituminite	intensely fluorescing secondary 'resinite'
	exsudatinitite	fragments of other liptinite
	fluorinitite	
	liptodetrinite	
INERTINITE	fusinite	well-preserved tissue
	semifusinitite	cellular to almost homogeneous, \geq one cell
	sclerotinitite	fungal tissue and fungal spores
	macrinitite	homogeneous bodies
	micrinitite	"granular" inertinitite
	inertodetrinitite	fragments, less than one cell

significant change in chemical and physical properties between 0.4 and 0.6%.

B. Spackman System

Whereas Stopes introduced the term maceral to distinguish the organic components of coal from the inorganic components, Spackman⁹ defined macerals as "... organic substances, or optically homogeneous aggregates of organic substances, possessing distinctive physical and chemical properties, and occurring naturally in the sedimentary, metamorphic, and igneous materials of the earth."

Spackman terminology is based on the concept that each maceral is a substance with a distinctive set of properties which change not only because of type but as a result of rank as well. Consequently, whereas the ICCP terminology implies that the properties of the macerals change with rank (and thus the same maceral of vitrinite, for example, can exist in bituminous coals as well as in anthracites), the Spackman maceral has a narrow range of properties (thus vitrinite, in a bituminous coal, is a different maceral from vitrinite in an anthracite because the two have different sets of properties). Crelling and Dutcher¹⁰ compared the ICCP and Spackman systems as form versus substance. The

practical significance of the Spackman concept is that it:

- i. avoids the proliferation of maceral names based on morphology;
- ii. takes into account the fact that macerals change with rank;
- iii. provides a framework of classification that can express the current knowledge of the various properties of the different macerals; and,
- iv. can be easily adapted for special purposes, such as palaeobotany, by the use of proper adjectives.

C. Australian Standards Association System

The 'Gondwana coals' of Australia, South Africa and India are of Permian age and are highly variable. Many of the ICCP descriptions apply to these coals and a number of "intermediate forms of the organic constituents"¹¹ are not adequately covered by the existing terminology. Consequently a number of the original terms were amended to suite research needs or applications to industry and a proliferation of terminology resulted; standardisation of terminology, as well as results, was difficult.

In 1979, under the sponsorship of the South African Council for Scientific and Industrial Research, a project to produce an illustrated and annotated catalogue of the common microscopic constituents of Permian coals in South Africa was initiated. Falcon and Snyman published the results of this project¹¹.

In response to difficulties with maceral terminology experienced by the Australia coal industry, the Standards Association of Australia set up a subcommittee to prepare a standard for use in Australia. After a number of meetings which attempted to modify the ICCP system, the subcommittee decided to adopt a new system. Under the new system, the liptinite and inertinite groups were essentially unaltered but the vitrinite group was revised. The results are a significant departure from the commonly-accepted ICCP maceral terminology but the advantages of the system are:

- i. it provides a more cohesive description of macerals than the ICCP system;
- ii. it is applicable to coals ranging from low brown coal rank to the low volatile bituminous coals;
- iii. the number of maceral terms is significantly reduced; and,
- iv. the macerals groups are genetic categories.

A summary of the Australian Standards Association system is given in Table 2.

The Australian Standards Association system uses the same maceral groups and macerals as the ICCP system but differs in the maceral subgroup terminology. Telovitrinite comprises phytals or phytoclasts of plant tissue, especially woody plants, which have undergone little or only minor change to the cell wall structure during sedimentation and peatification. Detrovitrinite comprises finely comminuted plant debris. This debris may have been comminuted either during transport or *in situ*. Gelovitrinite is derived from a gel which may have been produced by the living plant, by diagenesis during peatification or metamorphism after burial and is commonly found in fractures and pores and commonly assumes the form of the host (such as a cell infilling); gelovitrinite may be porous or massive.

4.3.4. Properties of Inertinite. Inertinite is derived from plant material that has been strongly altered and degraded in an oxygen-rich environment during the peat stage of coal formation or has been derived from oxidised plant tissue such as charcoal. Inertinite macerals comprise <5% to 60% of most coals; it is claimed, although some dispute this, that inertinite is more abundant in Permian Gondwana coals than in Carboniferous Euro-American coals. Other properties of inertinite are:

Table 2. Australian Standards Association Maceral System

Maceral	Maceral Subgroup	Maceral Group
Textinite*		VITRINITE
Texto-ulminite*		
Eu-ulminite*	Telovitrinite	
Telocollinite		
Attrinite*		
Densinite*	Detrovitrinite	
Desmocollinite		
Corpogelinite		
Porigelinite*	Gelovitrinite	
Eugelinite		
Alginite		LIPTINITE
Bituminite		(Exinite)
Cutinite		
Exsudatinite		
Fluorinite		
Liptodetrinite		
Resinite		
Sporinite		
Suberinite		
Fusinite		INERTINITE
Semifusinite	Telo-inertinite	
Sclerotinite		
Inertodetrinite	Detro-inertinite	
Micrinite		
Macrinite	Gelo-inertinite	

* Density - varies greatly but usually ranges from that of vitrinite to higher values.

* commonly only occur in low rank coals

* Coking Properties - many inertinite macerals are inert in the coking process.

* Chemistry - inertinite macerals have the highest carbon and lowest hydrogen contents of any maceral.

* Toughness - after polishing, inertinite generally shows strong positive relief.

* Reflectance - inertinite macerals have the highest reflectance in coals of rank lower than low volatile bituminous coal.

* Fluorescence - the inertinite macerals generally do not fluoresce.

4.3.5. *Properties of Liptinite.* Liptinite (formerly called exinite) macerals are derived from the waxy, lipid-rich and resinous parts of plants such as spores, cuticles, and resins. The macerals generally constitute about 5-15% of many North American or European

coals but are considerably less in Australian coals.

At a reflectance of 1.3-1.4% or higher, liptinite macerals cannot be distinguished from vitrinite or inertinite macerals. Other properties are:

- * Density - have the lowest density of any maceral group (1.18 to 1.28 g/ml).
- * Coking Properties - liptinite macerals may devolatilise as gases and tars but may also contribute to the coke groundmass.
- * Chemistry - in any given coal the liptinite macerals have the highest hydrogen content and the lowest carbon content.
- * Toughness - after polishing, liptinite macerals generally show positive relief.
- * Reflectance - in any given coal liptinite macerals have the lowest reflectance.
- * Fluorescence - all liptinite macerals, except in coals of very high rank, fluoresce.

5. Microlithotypes

Macerals are not scattered randomly throughout coal but are generally grouped in layers in which one or other maceral group predominates. As early as 1954, Seyler¹² suggested that a number of typical maceral assemblages could be defined. After recognition of these assemblages the concept of microlithotype was introduced.

The following description of microlithotypes is taken from ICCP⁶:

"Three types of microlithotypes, mono-, bi- and trimaceral, can be distinguished on the basis of their compositions and depending on whether they contain macerals of one, two or three maceral groups".

With the various possibilities for composition and band width of associations that could exist, the ICCP was forced to introduce definitions for the microlithotypes with suitable limiting values such as:

- i. the minimum band width of a microlithotype band is 50 microns (0.05 mm),
- ii. the monomaceral and bimaceral microlithotypes contain not more than 5% from maceral groups which are not characteristic of them by definition; the trimaceral microlithotypes contain more than 5% of each maceral group.

A summary of microlithotypes is given in Tables 3 and 4.

6. Mineral Matter

Most coals contain mineral matter. In many coals the mineral matter may constitute 10 to 20% of the coal and can be ubiquitous or restricted to layers where it occurs mostly in one of the microlithotypes. The ICCP and Stach *et al.*^{3,4} introduced terminology for mineral-rich microlithotypes (Table 4).

7. Lithotypes

Lithotypes are the terminology applied to macro-petrographic or hand-specimen entities of coal. They are distinguished and logged on the basis of lustre, fracture pattern, colour, streak, texture and type of stratification. Thus in the words of Stopes, lithotypes are the "visible ingredients in banded bituminous coals". Difficulty is experienced when applying lithotype terminology to coals as several problems with the use of the terminology are related to the fact that the terminology was based on a limited number of coals. Lithotypes are related to types (although relationships are somewhat tenuous)

Table 3. Summary of Microlithotypes (after Stach *et al.*⁴⁾

Microlithotype		Group
<i>Monomaceral</i>		
Collinite	> 95% Collite+	Vitrite
Telinite	> 95% Telite+	
Vitrodetrinite	> 95%	
Sporinite	> 95% Sporite	Liptite
Cutinite	> 95% Cutite+	
Resinite	> 95% Resite+	
Alginite	> 95% Algite	
Liptodetrinite	> 95% -	
Macrinite	> 95% Macroite	Inertite
Semifusinite	> 95% Semifusite	
Fusinite	> 95% Fusite	
Sclerotinite	> 95% Sclerotite+	
Inertodetrinite	> 95% Inertodetrite	
<i>Bimaceral</i>		
V + Sporinite	> 95% Sporoclarite	Clarite
V + Cutinite	> 95% Cuticlocclarite	
V + Resinite	> 95% Resinoclarite+	
V + Alginite	> 95% Algoclarite+	
V + Liptodetrinite	> 95%	
V + Macrinite	> 95%	Vitrinertite
V + Semifusinite	> 95%	
V + Fusinite	> 95%	
V + Sclerotinite	> 95%	
V + Inertodetrinite	> 95%	
I + Sporinite	> 95%	Durite
I + Cutinite	> 95%	
I + Resinite	> 95%	
I + Alginite	> 95%	
I + Inertodetrinite	> 95%	
<i>Trimaceral</i>		
V > I, L	> 95% Duroclarite	Trimacerite
L > V, I	> 95% Vitrinertoliptite	
I > V, L	> 95% Clarodurite	

+ - terms are proposed but are not at present commonly used.

and thus to precursor vegetal matter.

Because of the differences in the hand-specimen properties of brown coals compared to bituminous coals, it has been necessary to devise a lithotype classification for brown coals as well as bituminous coals.

Table 4. Mineral-rich Microlithotypes (after Stach *et al.*⁴)

Microlithotype	Composition	Group
Carbargilite	Coal + 20-60 vol% clay minerals	
Carbankerite	Coal + 20-60 vol% carbonate	Carbominerite
Carbosilicite	Coal + 20-60 vol% quartz	
Carbopolyminerite	Coal + 20-60 vol% mineral matter	

8. Coalification

Coal begins as plant matter deposited in wet peat swamps. On a gross scale the type of plant matter, that is, whether the plants are forest trees, swamp herbs or marsh reeds, will determine the type of coal that is formed. For example, marsh reeds give rise to light brown coals in which the phyterals are small; vitrodetrinite is abundant. Woody forests give rise to dark brown coals with an abundance of large coalified trunks and branches; structured vitrinite, such as telinite derived from woody stems, is abundant. On a smaller scale the type of plant detritus derived from each of the plant communities will determine the composition of the resulting coal. For example, an abundance of resins, fats, waxes and oils will give rise to resinite-rich coals whereas an abundance of pollen and spores will give sporinite-rich coals.

Once the plant matter has been deposited, it is covered with clastic sediment or additional plant matter. Where the plant matter is continually covered with water, little oxygen is available for decay reactions and the coal tends to be vitrinite-rich. If the plant matter is periodically exposed, the plant matter may oxidise giving rise to inertinite-rich coal.

On a larger scale, coals which form in troughs of rapidly subsiding basins will tend to be covered continually with water and the coals will be rich in vitrinite (and the microlithotype vitrite). Australian coals of Permian and Triassic age belong to this category (Smyth¹³ fluvio-deltaic environments of cratonic basins, coals tend to be vitrinite-poor. The composition of coal may change within a seam. This occurs where the water level changes. For example, some Australian Permian coals are vitrinite-rich at the bottom of the seam and inertinite-rich at the top. This is taken to indicate more exposure to an oxidising environment as the later stages of the plant matter was deposited.

After deposition, the plant matter changes into peat which in turn changes through the brown coal stage, bituminous coal stage to anthracite. These changes are known as coalification and the stage that a coal has reached is referred to as the rank as discussed previously. The various changes which occur to the coal during coalification are given in many texts (Stach *et al.*^{3,4}; Bustin *et al.*¹³).

Increased coalification leads to homogenisation of the macerals; this is usually manifested as fewer and smaller cell lumens (cavities), fewer textural differences between macerals and an increase in reflectance - inertinite is white to yellowish white instead of

pale grey-white, vitrinite is pale grey instead of medium grey-grey and liptinite is grey instead of dark grey-black.

9. References

1. R. Thiessen, What is coal? US Bur. Mines Internal Circulation, 1947, **7397**, 1.
2. M.C. Stopes, On the petrology of banded bituminous coals. Fuel, 1935, **14**, 4.
3. E. Stach, M.-Th. Mackowski, M. Teichmuller, G.F. Taylor, G. Chandra and R. Teichmuller, Stach's Textbook of Coal Petrology. 2nd edition, Gebrüder Borntraeger (1975).
4. E. Stach, M.-Th. Mackowski, M. Teichmuller, G.F. Taylor, G. Chandra and R. Teichmuller, Stach's Textbook of Coal Petrology. 2nd edition, Gebrüder Borntraeger (1982).
5. ICCP, Handbook of Coal Petrography. 2nd Edition, Centre National de la Recherche Scientifique (1963).
6. ICCP, Handbook of Coal Petrography. 1st Supplement to 2nd Edition, Centre National de la Recherche Scientifique (1971).
7. ICCP, Handbook of Coal Petrography. 2nd Supplement to 2nd Edition, Centre National de la Recherche Scientifique (1975).
8. G.H. Cady, Modern concepts of the physical constitution of coal. J. Geology, 1942, **50**, 337.
9. W. Spackman, The maceral concept and the study of modern environments as a means of understanding the nature of coal. Trans. New York Acad. Sci., Ser. II, 1958, **20(5)**, 411.
10. J.C. Crelling, and R.R. Dutcher, Principals and Applications of Coal Petrology. Soc. Econ. Paleont. Miner., Short Course, 1980, **8**, Indiana University, Bloomington.
11. R.M.S. Falcon and C.P. Snyman, An Introduction to Coal Petrography: Atlas of Petrographic Constituents in the Bituminous Coals of South Africa. Geological Society South Africa (1986).
12. C.A. Seyler, Unpubl. letter to ICCP (1954).
13. Smyth, The relationship between coal macerals and microlithotypes and depositional environments; in B.G. Jones and A.C. Hutton, (eds), Fluvio-Deltaic Systems Facies Analysis in Exploration. Australian Sedimentologists Specialist Group, 1984. 259.
14. R.M. Bustin, A.R. Cameron, D.A. Grieve, and W.D. Kalkreuth, Coal Petrology. Its Principles, Methods and Applications. Geological Society of Canada, Short Course Notes 3, Victoria (1983).

ORGANIC PETROGRAPHY OF OIL SHALES

Adrian C Hutton
University of Wollongong
Wollongong, NSW, 2522
Australia

1. Introduction

The term oil shale is a misnomer and little agreement has been possible, in the past, as to a definition of oil shale or the nature and origin of the organic matter. Many definitions of oil shale have been published but few address the fundamental feature of oil shales which is the nature and abundance of organic matter. The volume of oil produced during pyrolysis and the chemical composition and subsequent physical properties of the derived oil, are dependent on the nature and abundance of organic matter. It should be noted rocks best termed oil shale, coal, limestone and claystone may all occur in the same sequence. With respect to organic matter, all are end members of transitions, for example, oil shale->limestone and oil shale->claystone. This means that the percentage of organic matter ranges from a minimum (= 0 or at the most <<1%) in claystone and limestone to a maximum in oil shale or coal.

In this paper, an oil shale is defined as a sedimentary rock that contains organic matter that, when retorted, produces sufficient oil to produce more energy than the energy required to produce the oil initially. Where a more rigid definition is required, a cut-off of 5 volume percent (vol%) oil-producing organic matter is accepted as the minimum level. This definition is given because in organic petrography abundance is measured in vol% and we are concerned not with a definition of oil shale but with the components of oil shales and how oil shale petrography can be used in our studies of oil shales.

Organic matter in oil shales can be studied by normal organic petrographic techniques either as macerates devoid of mineral matter or as the whole rock. The latter is considered preferable because the inter-relationships between organic matter and mineral matrix in macerates are lost, as are the inter-relationships between the various organic constituents. Whole-rock petrographic analysis is also preferable because it permits easier identification of the organic constituents, has a minimal effect upon soluble organic matter and can reveal phenomena such as the adsorption of organic matter onto clay minerals. Incident light examination of 'whole-rock' samples has the advantage of allowing simultaneous determination of maturation (diagenesis) parameters such as vitrinite reflectance and liptinite fluorescence. Together with an estimation of organic matter type and quantity, these data are a necessary adjunct to shale oil studies both between and within various deposits.

The dominant organic matter in oil shale is derived from three primary sources - terrestrial plants, lacustrine algae and marine organisms (including algae, acritarchs and dinoflagellates); all are lipid-rich precursors which, in oil shales, are recognised as liptinite macerals. Vitrinite and inertinite macerals are generally minor components. Alginite can be divided, using morphology and fluorescence characteristics, into two types - *telalginite* and *lamalginite*.

A petrographic classification of oil shales, based on the type and abundance of liptinite is advocated in preference to chemical classifications or classifications based on both petrography and chemistry. The primary division of oil shales into terrestrial, lacustrine and marine oil shales, is based on the source of the liptinite whereas secondary sub-divisions are based on the type of liptinite. Secondary oil shale groups recognised are cannel coal, torbanite, lamosite (which can be further subdivided into Rundle-type and Green River-type lamosites), marinite, tasmanite and kukersite. A petrographic classification has the advantages that the components are easily recognised and all groups are related to their origin.

Organic petrography has many uses in oil shale studies including assessment of the various oil shales as potential feedstocks (particularly to assess if an oil shale can be upgraded to produce a higher grade feedstock), oil shale characterisation, spent shale studies and predictions of shale oil yield .

2. Classification of Oil Shales

For most oil shales, animal precursors cannot be sustained and by elimination, this leaves plants as the pre-dominant, if not only, precursors. The organic matter in oil shale is sometimes referred to by two terms - bitumen, the soluble component, and kerogen (or kerobitumen), the insoluble component. Bitumen is a minor component in most oil shales and the use of either the nature or abundance of bitumen in a petrographic classification of oil shales is not warranted.

Kerogen is not a suitable discriminatory term because it has a chemical connotation. The term was first introduced by Cum Brown in 1912 to denote the insoluble organic matter. Cane¹ noted that specificity of the term had been lost and kerogen is now a collective and commonly confusing term for all or any organic matter in oil shale. Kerogen studies generally relate to bulk rock studies and any one or all of the maceral groups may be constituents of the rock.

Where organic petrographic techniques are used to study oil shales, maceral terminology, based on vitrinite, liptinite and inertinite, is the logical language for describing the organic matter.

2.1. MACERAL TERMINOLOGY

Most oil-producing organic matter in oil shale is derived from lipid-rich precursors rather than humic constituents derived from woody plants. Thus vitrinite and inertinite macerals are generally minor components of oil shales and specificity of the individual macerals is not required; the vitrinite and inertinite components can be referred to by the maceral group name. Where these components are abundant, commonly-used terminology, such as defined by the International Committee for Coal and Organic Petrology (ICCP), adequately encompasses these macerals. Likewise, maceral terminology for liptinite derived from terrestrial plants is also adequate.

Much of the liptinite is derived from algae. Such organic matter is referred to as alginite which was defined originally for algal matter in coals. The alginite was thought to have been derived from algae related to, or synonymous with, *Botryococcus*, (such as *Reinschia* and *Pila*) and to a lesser extent *Tasmanites*, *Cladiscothallus* and *Gloeocapsomorpha*. Except in boghead coals, alginite is a minor component of coals and little need for revision of the term was needed until, with the aid of fluorescence microscopy, it was realised that many algae are preserved in rocks other than coals and that many of these are not large, well-structured colonies. The term as defined for coals is not adequate and revision is needed.

The terms alginite A and alginite B were first used for the two types of alginite that can be recognised in oil shales. These terms convey little meaning and subsequently, the terms *telalginite* and *lamalginite* were introduced for the two respectively. 'Tel' is derived from the Latin 'tela' meaning tissue whereas 'lam' is derived from lamellar, the characteristic shape in sections perpendicular to bedding.

Telalginite is derived from large colonial or thick-walled unicellular algae, has strong fluorescence at low rank and exhibits distinctive external botanical structure, and in many cases, internal structure, when viewed in sections perpendicular to bedding.

Lamalginite is derived from small, thin-walled colonial or unicellular planktonic or benthonic algae, generally has weaker fluorescence than telalginite at low rank (especially where both occur in the same sample) and a distinctive lamellar form with little recognisable structure in sections perpendicular to bedding.

Absolute fluorescence intensity has not been included in the definitions. The fluorescence intensity of alginite derived from the same precursor is often quite variable, even in the same sample. If absolute intensity is to be a criterion in the definition, the range of values would either be too large to be meaningful, or alternatively, the range for each group would be too narrow to allow the inclusion of two clearly similar forms of telalginite and a proliferation of groups would result.

Where telalginite and lamalginite occur in the same sample, for example in Australian Tertiary oil shales and marine oil shales of Europe and eastern USA, fluorescence intensity of the telalginite is generally much more intense than that of lamalginite. An exception is in oil shale from the Devonian Huron Member of the Ohio Shale (Kentucky, USA) where telalginite derived from *Foerstia* has very weak intensity, much weaker than the intensity from either telalginite derived from tasmanitids or lamalginite derived from acritarchs and dinoflagellates.

In Australian Tertiary oil shales, lamalginite is derived from three precursors - algae, acritarchs and dinoflagellates. The fluorescence intensity from the acritarchs and dinoflagellates is much stronger than that from algae. Part of this stronger intensity is related to the thickness of the algal walls but part is also thought to be related to the structure of the phytal. If alginite was defined using absolute intensity as a criterion, the alginite from the acritarchs and dinoflagellates would be placed in the telalginite group for some samples and in lamalginite for others. Resolution of the dilemma is relatively simple; the acritarch and dinoflagellates have the typical lamellar morphology and hence lamalginite is the better term.

2.2. PETROGRAPHIC CLASSIFICATION OF OIL SHALES

Classifications facilitate the study of populations if used sensibly because like members of a given population are placed within the same group as they have the same properties or characteristics; unlike members of the population are placed in separate

groups. Most classifications, including rock and petrographic classifications, use an hierarchical scheme involving three operations:

- i. recognising and describing individuals of a population;
- ii. placing like members of the population into formal hierarchical groups; and,
- iii. providing names for the various groups and constituents.

No classification adequately accounts for all members of its population and several classifications can be constructed for the same population. Oil shales are no exception.

Using type of organic matter as the dominant criterion, organic-rich rocks can be divided into three groups - humic coal (including carbonaceous shale), oil shale and bitumen-impregnated rock (including tar sands and petroleum reservoirs). This division allows any of the presently-used coal or bitumen classifications to be incorporated. Tar sands are not included in the oil shale group because the organic matter is bitumen or oil of secondary origin; it has been derived through the alteration of primary organic matter by degradation, metamorphism or maturation of organic matter. Organic matter in tar sands is a petroleum substance not a maceral and, strictly speaking, not kerogen as originally defined.

Because the dominant oil-producing organic matter in oil shales is liptinite, it follows that a natural subdivision should be based on types of liptinite and environments of deposition as the fundamental discriminatory criteria. Such a subdivision was implied by Yen and Chilingarian² when they stated "oil shales were probably deposited in bodies of tranquil, either marine or fresh-water, depositional environments, such as isolated marine basins, lakes or deltaic swamps."

Three primary groups of oil shales (Fig. 1) are:

Terrestrial Oil Shale - oil shale composed of liptinite derived from terrestrial plants.

Lacustrine Oil Shale - oil shale composed of liptinite derived from lacustrine (including brackish, saline or freshwater) algae.

Marine Oil Shale - oil shale composed of liptinite derived from marine algae, acritarchs and dinoflagellates.

Type and abundance of liptinite are the criteria for dividing the primary groups into secondary groups (Fig. 1). Secondary groups of oil shale are referred to as types of oil shale hereafter.

2.3. TYPES OF OIL SHALES

Cannel Coal - a brown to black, homogeneous oil shale composed of liptinite (mostly resinite, sporinite, cutinite, suberinite and/or liptodetrinite) derived from terrestrial

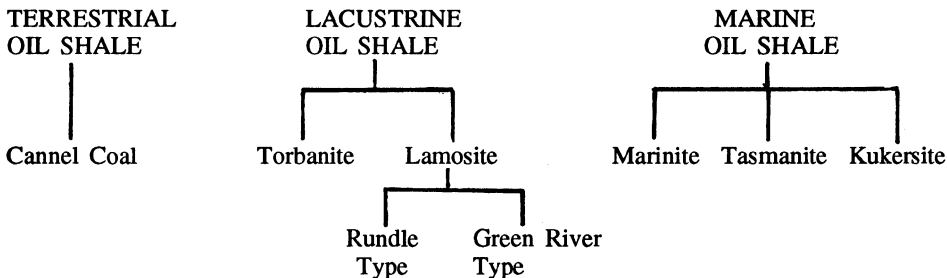


Figure 1. Primary and Secondary Types of Oil Shales.

vascular plants with vitrinite and inertinite. (Note that the term 'cannel coal' is already used in relation to coal. The cannel coals that are oil shales are the same rock as the cannel coals that contain abundant liptinite (and as defined by Stach *et al.*^{3,4}), we are only using the same term in two classifications or different contexts.)

Torbanite - a black to greenish-black oil shale in which the principal liptinite is telalginite derived from *Botryococcus*-related, lacustrine algae; sporinite and liptodetrinite are minor liptinite components; vitrinite and inertinite occur in variable amounts.

Lamosite - a pale brown to dark greyish-brown or olive green oil shale in which the principal liptinite is lamalginite derived from lacustrine algae and other phytoplankton; minor components include vitrinite, inertinite, telalginite and bitumen.

Marinite - a grey to dark-greyish black oil shale in which the principal liptinite is lamalginite derived from marine algae and other phytoplankton, and/or bituminite derived from marine precursors; vitrinite, inertinite, sporinite, telalginite and bitumen are minor components.

Tasmanite - a brown or dark grey to black oil shale in which the principal liptinite is telalginite derived from tasmanitids; lamalginite, vitrinite, inertinite and sporinite are minor components.

Kukersite - a brown oil shale in which the principal liptinite is telalginite derived from *Gloeocapsomorpha prisca*.

A petrographic classification of oil shales is useful as it groups oil shale that have similar organic constituents. Oil shales placed in the same group will behave in a similar manner when retorted and will produce oils that have similar properties.

2.3.1. Lamosite. Lamosite was originally defined as a compact laminated organic-rich rock composed of alginite B (now lamalginite) as the dominant organic entity^{5,6}. Many lamosites are massive rather than "compact laminated" rocks and do not fit the original definition. In addition, lamalginite can be divided into two types:

- discrete lamalginite; thin-walled lamalginite that occurs as discrete entities (generally less than 0.5 mm long) and surrounded by mineral matter in all but very rich oil shale; and
- layered lamalginite; layers composed of numerous sheet-like lamalginite, some or all of which may have been biogenically or physico-chemically degraded.

Oil shales characterised by layered lamalginite, such as Green River lamosite, are generally composed of distinctive lamalginite-rich and mineral-rich laminae whereas laminae are not well developed in lamosite, such as Rundle lamosite, that contains discrete lamalginite. Where specificity is required, the adjectives "Rundle-type" and "Green River-type" are used.

Precursors of discrete lamalginite have been identified to genus level and include the stellate, colonial green alga *Pediastrum*, the acritarch *Cleistosphaeridium* and the dinoflagellate *Septodinium*.

The two types of lamosite should be recognised because:

- i. compared to Rundle-type lamosite, Green River-type lamosite was formed under more saline conditions; and

- ii. organic matter in Green River-type lamosite was probably derived from blue green algae whereas that in Rundle-type lamosite was derived from green algae, acritarchs and dinoflagellates; and,

2.3.2. *Carbonaceous Oil Shale.* Many deposits of Rundle-type lamosite contain laminae with abundant vitrinite and lamalginite and commonly grade into 'normal' lamosite. This subgroup of lamosite is an important oil shale type because the abundant vitrinite significantly alters the properties of the oil shale and the derived shale oil. A new term is not required as the additional organic matter is not liptinite. The adjective 'carbonaceous' as used in relation to coal and carbonaceous shale, overcomes any difficulty in signifying this oil shale. The minimum volume of vitrinite in a carbonaceous oil shale is taken to be 5 vol%.

'Carbonaceous' could also be used in other instances where an oil shale contains >5 vol% vitrinite and/or inertinite, for example carbonaceous torbanite.

2.3.3. *Mixed Oil Shale.* The term mixed oil shale was previously used for marinite in the Julia Creek and other marine deposits³ because it was believed that these oil shales contain a mixed assemblage of organic matter dominated by lamalginite, telalginite, sporinite and vitrinite, that is, liptinite derived from terrestrial and lacustrine precursors. Later studies have shown that bituminite is abundant in many of these oil shales; lamalginite is sparse to abundant and sporinite and vitrinite are generally minor components. Consequently this type of oil shale does not contain a mixed liptinite assemblage. The term as defined originally is quite misleading. 'Mixed oil shale' is only valid where liptinite derived from different precursors are co-dominant.

2.4. MICROLITHOTYPES

In coal petrography, microlithotypes have been defined for maceral associations or maceral-mineral associations that are thicker than 0.05 mm wide. Apart from cannel coals and torbanites, most oil shales contain a very high proportion of mineral matter and the standard terminology for microlithotypes is difficult to apply to oil shales.

Using ICCP and Stach *et al.*^{3,4} systematics, two types of microlithotypes, telalgite and lamalgite, are genetically possible. Both terms have limited use as microlithotypes comprising >95% telalginite and >95% lamalginite rarely occur. Of the two, telalgite is more common, occurring in torbanite and less commonly tasmanite. Lamalginite-rich layers composed of greater than 95% lamalginite are found in the Green River lamosite but the layers, are usually less than 0.05 mm thick.

Torbanite commonly contains subequal telalginite, vitrinite and inertinite. Microlithotypes of this assemblage are called vitrinertoliptite and presumably, if convention is followed, the alginite microlithotype in torbanite called vitrinerto-algite.

Microlithotypes containing greater than 20 to 60% mineral matter are called carbominerite. Many oil shales, such as lamosite and marinite, commonly contain less than 40% organic matter and if nomenclature is strictly followed, these should be called carbominerite with many, because of the high mineral content, regarded as waste. Carbominerite microlithotypes need revision if they are to be useful in oil shale studies.

2.5. OTHER CLASSIFICATIONS

Any classification of rocks should be based primarily on easily recognisable properties

of the key constituents and for oil shales, these constituents are the organic constituents. Many early classifications of oil shales paid little attention to the organic matter. Criteria such as industrial use, mineral matter, physical properties, chemical properties of the organic matter or combinations of two or more of these should not be used in a petrographic classification. Particularly common has been the van Krevelen diagram.

Robert^{7,8} devised a classification of organic matter in source rocks but it is applicable to coal, oil shale and any rock containing organic matter. The classification contains three groups - primary identifiable biological constituents, primary shapeless matter and secondary products produced by the thermal transformation of the first two groups. The 'primary identifiable biological constituents' comprise the ICCP macerals with the exception of alginite. Algal components were listed as "microscopic algae". The 'secondary products' group included bitumen and the ICCP macerals known to be of secondary origin, such as exsudatinite. The 'primary shapeless matter' group contained bituminite, alginite, sapropelic groundmass and humic groundmass.

Although the classification recognises that organic matter in coal and source rocks is derived from a number of precursors, it places algal components into two groups. Recognition of the term "amorphous alginite" is contradictory to the definition as originally defined by the ICCP which based the definition on algae with well-preserved structure. Robert distinguished between "microscopic algae" and "alginite", the latter referring to *Botryococcus* and lamalginite respectively.

Alpern^{9,10} advocated a "universal classification of solid fuels" and argued that the classification "deals with fossil fuels as geological products". It was basically a coal classification, including washed and raw coal, but also included oil shales and source rocks. Oil shales are divided into two groups, one of which is further subdivided into low, medium and high grade whereas the second contains bogheads, sapropelites and cannels. Features of the classification are:

- i. it groups rocks on the basis of type, rank and facies;
- ii. the three categories of rank are lignite, bituminous and anthracite with each further subdivided into hypo-, meso- and meta-; and,
- iii. the three facies divisions are coal, mixtures ("mixte") and shales.

The major problem with this classification is the subdivision of oil shales into grade categories. Any classification based on grade must inherently separate oil shales which have the same organic assemblages. It is possible that two adjacent samples from any deposit, whether it be Green River-type, a torbanite or a marine oil shale, would be placed at either end of the oil shale group despite having the same maceral assemblage and same relative abundances of each organic constituent.

Cook¹¹ published a classification that "develops a systematic treatment of occurrence and chemistry of the organic matter in oil shales". Presumably both organic petrography and chemistry (elemental data) are used as discriminatory criteria. Any classification using discriminatory criteria from different disciplines introduces a large number of categories, which this classification does. This makes use of the classification difficult and at times academic at best.

Classifications, including a petrographic classification of oil shales, have advantages and disadvantages. The tests of any classification are:

1. How well do the populations fit into the groups?
2. Do additional or new data fit into the groups without modification?
3. Can the results of work using other techniques be predicted using the groups of the classification?

For a petrographic classification, chemical properties of the oil shale and derived

oils should be predictable and indeed they are. Rigby *et al.*¹² characterised Australian oil shales using nitrogen isotope abundances and found that tasmanite, torbanite, marinite, cannel coal and lamosite plotted separately as would be predicted from the petrography.

Ekstrom *et al.*¹³ discussed the chemical and retorting properties of selected Australian Tertiary oil shales and found two apparently anomalous results for two samples. When reviewing the shale oils, the authors commented that the phenolic content of the oils from two samples "is characteristic of brown and bituminous coals, and it appears that the kerogen from the carbonaceous shales contains a substantial proportion of material of lignin origin". The oil yields for the two samples were high, 69 and 232 litres per tonne (0 % moisture), the kerogens had low H/C ratios and both gave low oil yields per unit carbon. These properties are predictable given that the samples were taken from stratigraphic units that contain carbonaceous shales and cannel coals which have high liptinite contents. The high oil yields are related to the terrestrial liptinite in the samples and the high carbon contents and low H/C ratios are related to the abundance of vitrinite. In another study, Gannon *et al.*¹⁴ reported on carbon conversion relationships in oil shales from Condor, Daringa and Stuart (Tertiary Australian lamosites). They found that where the oil shales were lamosites, conversion of carbon to oil was 52% or higher (maximum of 62%) whereas samples from carbonaceous shales and cannel coals had carbon conversions of 30 to 40%. For the latter samples they presumed that the kerogen was a mixture of Types I and II. In this case, as for the study by Ekstrom *et al.*¹³, the results are entirely predictable given the types of oil shale used. Where oil shales contain abundant liptinite, more hydrogen is available to produce low molecular weight hydrocarbons whereas with abundant vitrinite and inertinite, less hydrogen per unit organic matter is available and more carbon remains in the char.

3. Petrography and Geochemistry of Oil Shales.

The geochemistry of oil shales and the derived oils have been studied for a much longer period than has the petrography of oil shales. This is logical given the need for characterisation prior to and during the use of retort oils.

Elemental analysis was one of the earliest standard methods of chemical characterisation and the data were, and still are, commonly shown on a van Krevelen diagram. This diagram has been used to show the effects of weathering, comparison of data from different oil shales and maturation paths of the organic matter. The evolutionary paths of the types of kerogen, Types I, II, III (and sometimes IV), are generally shown. Interpretation of several inconsistencies relating to the use of the term kerogen and the interpretation of kerogen plots can be understood using organic petrography.

The major problem with van Krevelen diagrams, as it is with any technique that uses bulk rock properties, lies in the very nature of the kerogen (and thus the nature of the oil shales themselves when the diagram is used for oil shales). Oil shale kerogen is derived from at least two, and commonly many more, chemically different components. Almost without exception oil shales contain liptinite and vitrinite and/or inertinite, the latter being minor components in many oil shales. Notwithstanding this, the relative hydrogen content of vitrinite is much lower than that of liptinite and correspondingly, the oxygen content of vitrinite is higher; the hydrogen content of inertinite is lower

than that of vitrinite. Therefore it is to be expected that the relative abundance of hydrogen and oxygen in any kerogen will be dependent on the proportions of vitrinite, liptinite and inertinite as much as factors such as maturation level and weathering.

It is interesting to note that the van Krevelen diagram was initially used for coal and later for the composition of kerogen derived from demineralised oil shale. Van Krevelen diagrams given for coal and oil shale show three clearly defined zones, corresponding to alginite, liptinite and vitrinite, with a fourth zone sometimes added for inertinite. Clearly, the position of a sample on the van Krevelen plot depends on the relative abundance of each maceral group. Comparing the coal and oil shale kerogen plots, the distribution of Types I, II, III and IV kerogen shows a close relationship between the maceral group distributions and the kerogen type distributions. This is not surprising given that the kerogen or organic matter in both coal and oil shale is composed of macerals. The chemical composition of kerogen should be the same as for chemical composition of the organic matter in the whole rock apart from any loss of organic matter during demineralisation.

3.1. TERTIARY LAMOSITES

An examination of various published van Krevelen diagrams for oil shale kerogen shows that it is difficult to divide the data into clearly defined domains although this is sometimes attempted and is implied by demarcation of Types I, II and III. Considerable overlap of data is evident; this is not a problem if one accepts that oil shales have varying compositions and the position at which an oil shale plots depends on the kerogen composition, that is, the maceral composition. Rapid petrographic examination commonly clarifies apparently anomalous plots.

An excellent example is a kerogen plot for Australian Tertiary lamosite deposits. A lamosite is defined as an oil shale that contains predominantly lamalginite. These oil shales should plot as Type I kerogen, and in the alginite field, on the van Krevelen diagram. Although this is generally the case, exceptions are common. Some samples always plot near the Type II kerogen field and some samples, called 'carbonaceous oil shales' plot as Type III. For the latter, the apparent anomaly is easily explained as the carbonaceous oil shales are resinite-rich cannel coals of brown coal rank. It is therefore only logical that these brown coals with abundant resinite would plot between Types II and III, or if the resinite content is low, they would plot as Type III. As for the oil shales that plot near Type II, these are carbonaceous lamosites.

The apparent anomalous plots for carbonaceous lamosites from the Rundle, Stuart, Nagoorin and Lowmead deposits of Queensland shales, defined previously as a lamosites containing >5 vol% vitrinite and/or inertinite, is one of the major reasons for introducing the term carbonaceous oil shale. Most of these oil shales plot as Type II kerogen and this is clearly misleading as carbonaceous lamosite, although a lamosite by virtue of the abundant liptinite, contains an assemblage of liptinite and vitrinite. Carbonaceous lamosites must plot as Type II kerogen because of the very high vitrinite content. Reference to Type II kerogen in carbonaceous lamosite is uninformative and is of little value.

It can be argued that a van Krevelen diagram shows the average chemical composition of the maceral assemblage rather than the chemistry of a single kerogen type. Subdivision of Tertiary lamosite on the basis of elemental composition is quite arbitrary because of the wide range of chemical compositions; each group is separated by a thin line which represents insignificant changes in chemical compositions.

Torbanites would show similar patterns because as well as containing telalginite which plots as classic Type I kerogen, they also contain abundant vitrinite and/or inertinite. Alginite abundance ranges from 5 vol% to 95+ vol%. Kerogen plots would reflect this composition; plots ranging from Type I (alginite) to Types II and probably Type III are theoretically possible. Examination of data for torbanites in Crisp *et al.*¹⁵ show that as the relative abundance of humic macerals increases, the plot shifts from a position of high hydrogen-low oxygen to one of lower hydrogen-higher oxygen.

3.2. MARINITE

Kerogen derived from marinite mostly plots as Type II or between Types I and II on the van Krevelen diagram. However, petrographic studies show that marinites are composed dominantly of lamalginite and/or bituminite with minor vitrinite, sporinite, inertinite. Marinites thus contain a mixed marine liptinite assemblage and again the kerogen plot is showing this rather than plotting as a single kerogen type.

Some samples of the Devonian Ohio Shale are unusual in that they contain more abundant tasmanitid telalginite than either lamalginite or bituminite. The kerogen for samples which have lamalginite and/or telalginite more abundant than bituminite would obviously plot either as Type I or close to Type I whereas samples in which bituminite is the more abundant maceral would plot nearer to Type II.

Two factors emerge from elemental data and H/C and O/C ratios for marine oil shales. Firstly, the composition of kerogen reflects the maceral assemblage and secondly, it is possible to shed some light on the nature and origin of bituminite. As most marinites which contain abundant bituminite plot as Type II or close to this field, bituminite has higher oxygen and lower hydrogen contents than lamalginite. One explanation for the high oxygen content is bituminite may be derived from alginite, either planktonic or benthonic (although the former appears to be more plausible), which, after deposition, was degraded by mechanical, physico-chemical or biogenic means such as bacteria and blue-green algae. This process could directly alter the relative abundances of oxygen and hydrogen or, indirectly, the remains of the organic matter could be oxidised before compaction thus increasing the oxygen content and reducing the hydrogen content. It also explains the presence of bacterial biomarkers in marine oil shales.

3.3. SHALE OILS

Because liptinite macerals have the highest specific shale oil yields, most of the shale oil comes from liptinite macerals with lesser amounts from vitrinite and gas or very small amounts of oil derived from inertinite. Given that liptinite derived from terrestrial plants is chemically different to that derived from algae, it follows that the oils formed should also have different, if only slightly, chemical properties. Also given the very marked difference in the compositions of vitrinite and inertinite compared to liptinite, there should also be significant differences in the compositions of the oils sourced by the three maceral groups. Thus, if an oil shale is examined petrographically before analysis, it should be possible to predict the nature of the retort oil unless significant cracking occurs during pyrolysis or immediately afterwards.

Crisp *et al.*¹⁵ and Hutton *et al.*¹⁶ presented comparative data for twenty six oil shales and shale oils, mostly from Australian deposits. Two types of oils were analysed - that produced by modified Fischer assay retorting and that produced by 560°C flash

pyrolysis. Analysis of the oils using gas chromatographic techniques showed that in most cases there was a strong correlation between the composition of the two oils.

Five groups of oils were recognised with a strong correlation between the composition of the pairs of oil and the types of oil shales. Clearly the oil compositions were related to the maceral compositions.

Group 1 - flash pyrolysate characterised by alkene/alkane homologues which are most abundant at higher carbon numbers; 1-pristene, phenols and other aromatics are also abundant; oil with very high oxygen contents indicating a terrestrial plant origin; Fischer oil with abundant low carbon alkene/alkane homologues.

Petrography. With the exception of one sample, the oils were produced from cannel coals which contain mostly liptinite derived from terrestrial plants (resinite, sporinite, cutinite and liptodetrinite) with vitrinite and trace inertinite in some of the samples. The exception was an oil from the Tertiary Stuart deposit. The oil contained phenols and aromatic compounds. The apparently atypical composition of the oil is easily explained when the petrography of the samples are reviewed. The parent oil shale was a carbonaceous lamosite composed of interlaminated lamosite and cannel coal, the latter containing abundant vitrinite which gives the apparently atypical molecular signature.

Group 2 - both the pyrolysate and the Fischer oil are typically aliphatic and dominated by homologous alkene/alkane homologues with the Fischer oil showing a monotonous decline in the relative abundance of components having carbon number greater than C_{17} ; the alkenes/alkanes in the flash pyrolysate generally with a slightly bimodal distribution with a low carbon number maximum and a second maximum at, or beyond, C_{17} ; homologous alkene/alkane pairs indicate an algal source; oils contained the lowest sulphur content of any of the oils analysed.

Petrography. The samples were torbanites, dominated by the maceral telalginite which is derived from Botryococcus-related algae.

Group 3 - both oils dominated by alkene/alkane doublets with the pyrolysate oils having a greater proportion of alkenes and a much higher proportion of higher carbon number ($>C_{17}$) homologues; 1-pristene and 2-pristene generally more abundant in the flash pyrolysate than in the Fischer oil; oils typically with low oxygen and sulphur. Petrography. The oil shales were lamosites in which the organic matter was sourced mostly from lamalginite derived from Pediastrum.

Group 4 - oils characterised by complex chromatographic profiles below C_{20} arising from a large aromatic content, including alkyl-substituted thiophenes and benzothiophenes; latter relatively more abundant in the flash pyrolysate, especially beyond C_{17} ; oils had the highest sulphur content of any of the oils analysed and this is thought to confirm a marine origin for the bulk, if not all, the organic matter.

Petrography. The oil shales were marinities which contain mostly bituminite and lamalginite.

Group 5 - both traces dominated by alkene/alkane pairs in the range C_6 to C_{20} with a maximum at C_9 ; tricyclic diterpoids show prominent peaks in the range C_{19} to C_{20} which were more pronounced in the flash pyrolysate suggesting that the Fischer oil may have undergone thermal cracking; pristenes are not detectable and the concentration of aromatic compounds extremely low, reflecting an algal source.

Petrography. The oil shale was a tasmanite in which the dominant liptinite is telalginite derived from tasmanitid algae.

The analytical data for shale oils show that the not only are the chemical properties of the oil shale dependent on the maceral composition but so also are the chemical properties of the shale oils. Saxby and Sato¹⁷ carried out a simple experiment which

demonstrated this for Rundle lamossite. The experiment also showed that chemical properties have limited use for defining boundaries when rocks are composed of two maceral types.

Saxby and Sato compared the properties of oil derived from synthetic mixtures of coal and lamossite with naturally occurring carbonaceous lamossite from Stuart. Using mixtures containing 0, 25, 50, 75 and 100% lamossite, it was found that modified Fischer assays were linearly dependent on the composition of the synthetic mixture and most parameters of oil quality also varied linearly. Oil parameters that did not vary linearly included H/C ratios which, for the mixtures, were slightly lower than predicted.

As the percentage of lamossite in the mixture decreased, the relative abundance of vitrinite macerals increases because of the addition of a component with a much higher vitrinite content. The experimental data clearly showed the variations in properties with increasing vitrinite content and from this it is easy to deduce that there is no single vitrinite content which brings about a significant change in properties of either oil shales or derived oils.

4. Other Uses of Organic Petrography for Oil Shales

Fluorescence microscopy allows the researcher to see the organic matter in an oil shale. This is fundamental to many studies as visual observations of the end products or intermediate products can be highly beneficial during interpretive stages.

4.1. SHALE OIL YIELDS

The modified Fischer assay is the normal method for shale oil yield determination. Estimated errors for this method are not expected to be greater than 5% relative. Organic petrography provides an alternative method for oil yield determinations with approximately the same relative error.

Hutton¹⁸ showed that oil yield (as determined by modified Fischer assay [in litres per tonne at 0% moisture, LTOM]) is linearly related to the percentage of alginite (lamalginite + telalginite) for five Australian Tertiary lamossite deposits. Correlation coefficients ranged between 0.91 and 0.96. For three deposits (Duaranga, Rundle and Stuart) the intercept on the y axis was negative but for the other two deposits (Byfield and Condor) the intercept was positive. The negative intercept was interpreted as indicating that either incomplete pyrolysis had occurred or alternatively, not all the oil was recovered. It has been shown that oil shales with high clay mineral contents give low oil yields and this is the most likely of the two reasons. The positive intercept was thought to be related to an increase in oil volume as a result of cracking of the oil before it was removed from the pyrolysis vessel.

As with many techniques, the petrographic method for oil yield determination requires calibration; the method must be standardised for each deposit. It is unrealistic to expect that each of the six types of oil shales would have the same specific oil yield. For example, Green River lamossite contains abundant bitumen as well as layered lamalginite, Rundle lamossite contains discrete lamalginite and marinite contains bituminite which has a lower specific oil yield than alginite.

Notwithstanding the above, petrographic oil yield determinations provide an easy and rapid method for oil yield determination with approximately the same relative error as the standard modified Fischer assay.

4.2. BENEFICIATION STUDIES

One of the problems hindering development of an oil shale industry in Australia and elsewhere is low grade of the oil shale. Beneficiation to increase the grade of the retort feedstock would greatly improve the economics of an oil project and many studies have been carried out to review beneficiation techniques. Organic petrography is a useful technique for reviewing beneficiation experiments because it allows observation of both the mineral-organic relationships, grain size determination and microscale variations in components.

Hutton¹⁹ studied several beneficiation trials on Australian lamosites, which had shown that upgrading was technically feasible, and compared the results with predictions for torbanite and marinite. It was concluded that upgrading depended on the abundance, type, distribution and size of both the organic and mineral components. Given that lamalginite is less than 0.002 mm thick and generally less than 0.08 mm long, it was concluded that liberation of lamalginite would require a grain size of less than 5 microns to provide significant separation of the mineral matter from the organics. The very small grain size required for separation is a limitation on beneficiation of lamosite.

It was concluded that similar results would be obtained for marinite as for lamosite, especially as bituminite is an amorphous maceral and the lamalginite is also very small. Tasmanitid telalginite would be more readily separated from the mineral matter but it is such a minor component that liberation of this maceral would not greatly enhance beneficiation of marinite. It was concluded that torbanite would be more easily beneficiated because of the larger size of the *Botryococcus* telalginite.

One limitation of petrographic studies of beneficiation products is the difficulty in preparing samples for optical analysis. Where the grain size is less than 2 microns, the mineral and organic components form an incoherent mass which is difficult to resolve optically.

4.3. PARTIAL PYROLYSIS OF OIL SHALES

Just as it is possible to identify the components of oil shales, it is also possible to recognise the constituents of spent (retorted) shales. Spent shale from the partial pyrolysis of Tertiary lamosite has a bitumen impregnated rim to the grains and for one sideritic oil shale, microfractures developed within the rim. The reason for the development of the microfractures is not known; it was noted however, the oil shale evolved 82% of the total recoverable oil whereas the oil shales which did not develop microfractures only evolved 64 % of the total oil¹⁶.

A closely-related study involved petrographic examination of lamosite samples from near a sill which had intruded the Stuart deposit²⁰. The aureole from the sill averages 46 m with a maximum of 64 m. Four zones, with gradational boundaries, are recognised within the aureole. As the sill is approached, there was a dramatic decrease in fluorescence intensity associated with, closer to the sill, a marked shift towards the red end of the spectrum in the fluorescence colours. The lamellar form of the lamalginite was retained within these two zones. In zone 3, the lamalginite is distinctly brown and towards the sill end of this zone, the lamellae become ragged and decomposition is apparent. In the fourth and closest zone, lamalginite is not recognisable but abundant pyrolytic carbon is present.

Near the sill, vitrinite reflectance increases rapidly but in zone 2, the reflectance decreases noticeably; this corresponds with a zone of bitumen which accumulates where porosity is quite high.

4.4. SPENT SHALE STUDIES

Organic petrography of spent shales is a field that invites research as it may provide an insight into mechanisms of pyrolysis. For example, pyrolysed torbanite comprises a network of organic and mineral matter with numerous large ovoid pores where the telalginite was located prior to pyrolysis. There is no recognisable remains of telalginite and this indicates that the alginite has completely devolatilised; there is no fluorescence except for small residual droplets and thin films of presumed high molecular, relatively immobile oil/bitumen fractions which are in and coat pores and fractures.

The very interesting aspect is the composition of the spent shale - homogeneous inert grains, a mozaic and, less commonly, sulphides. Homogeneous inert grains are angular to rounded, have a high reflectance, have diameters ranging from <0.05 mm to 0.5 mm and are enclosed within the mozaic. All grains take a good polish, exhibit a uniform texture or have cell structure and reflectance. Some of the grains have significantly higher relief than the mozaic.

These grains are analogous to the inerts in cokes, produced from bituminous coal, both in appearance and reflectance and as for the inerts in coke, are derived from inertinite, especially inertodetrinite. The homogenous texture of the grains suggests that they remain relatively unchanged during pyrolysis and probably produced only gas, if anything; the reflectance increases marginally.

The mozaic consists of an interlocking mesh of elongate to subequant fine-grained, anisotropic particles of 0.001 to 0.002 mm dimensions which enclose not only the homogeneous inert grains but also patches of isotropic vitrinite-like organic matter that has a lower reflectance than the inert grains but a significantly higher reflectance than the vitrinite in the parent torbanite. The anisotropic mozaic is similar in appearance to the mozaic of coke and as with coke, it is clearly shown using an antireflective or crossed polars. The ratio of anisotropic to isotropic mozaic is quite variable within any field of view; generally the anisotropic mozaic occurs as a rim around the large pores previously occupied by telalginite or as rims around and irregular veins throughout the remaining mozaic.

The mozaic probably develops in either of two ways - condensation of gases derived from the algal components or alteration of vitrinite. The anisotropic character of the mozaic is similar to that of pyrolytic carbon, a relatively common constituent of many organic-rich rocks and products which are thought to form from a gaseous phase. Whilst this mode of formation is an option, especially as it is known that oil shale vapours can form residues during pyrolysis, thus reducing the effective yields, it is not favoured. The texture, composition of the mozaic and association of large pores and mozaic suggests that it is derived from vitrinite, especially desmocollinite that is interstitial to the telalginite in the parent torbanite.

Whereas pyrite is the only sulphide in torbanite, both pyrite and pyrrhotite occur in the pyrolysed torbanite residue. The small pyrite grains that infilled and partly replaced the telalginite in the torbanite are still recognisable in the voids remaining after the devolatilisation of the telalginite but in some cases, have thin rims of pyrrhotite.

4.5. 'FORENSIC' PETROGRAPHY

The main advantage of organic petrography is that the organic components can be recognised and any variations in the morphology or optical properties of any organic constituent is readily noted. Two examples clearly illustrate the usefulness of organic petrography in problem solving.

One Australian company, trialing innovative retorting technology, sent a sample of oil shale overseas for testing. Before shipment, samples were sent for modified Fischer assaying and on arrival at its destination, a second sample was sent for analysis. The latter sample indicated approximately 10% lower grade for the sample. The results were confirmed with duplicate samples. Petrographic examination of a sample of the shipment indicated that many grains possessed a dark, nonfluorescing, partial pyrolysis rim, similar to that identified in the partial pyrolysis study of Hutton *et al.* Further investigation revealed that the samples had been dried in an oven, probably at a much higher temperature than recommended!

The second case study is that of the American Creek deposit, at Mount Kembla, near Wollongong (New South Wales, Australia) which was the site of Australia's first commercial oil shale project. The industry commenced in the 1860s and finished in the early 1870s. This deposit was reported to be a torbanite deposit. However, examination of available data showed that oil yields were much lower than expected for a torbanite. Petrographic examination of a suite of samples showed that far from being a torbanite, the 'oil shale' was a carbonaceous shale that was impregnated with orange fluorescing bitumen. Clearly, the Mount Kembla 'torbanite' was not a torbanite!

5. Petrography of Selected Oil Shales

5.1. AUSTRALIAN TERTIARY LAMOSITES

Australian Tertiary oil lamosites are the Rundle-type lamosite with abundant discrete lamalginites and minor *Botryococcus* telalginites, vitrinite, inertinite and trace sporinite. For most Australian Tertiary deposits, the organic assemblages are such that six 'organic' lithologies are recognisable.

1. Lamosite. Massive or laminated oil shale containing $\geq 5\%$ lamalginites and $< 5\%$ humic macerals. Lamalginites are of three types:

* Type I - lamalginites derived from *Pediastrum*, a stellate colonial alga; fluorescence varies from weak to moderately strong yellow to dull orange but dominantly yellowish-orange to orange; generally < 0.002 mm thick and < 0.08 mm long but rarely 0.1 mm long.

* Type II - minor component constituting $< 5\%$ of the total alginite; derived from acritarchs such as *Cleistosphaeridium* and dinoflagellates such as *Septodinium*; moderately strong yellow or green fluorescence, generally < 0.08 mm long.

* Type III - minor component constituting $< 10\%$ of the alginite; intense green, greenish-yellow or yellow fluorescence, ranging from 0.05 to 0.4 mm long, commonly composed of several interconnected lamellae; origin is unknown but possibly represents fragments of large multicellular sheet-like algal thalli.

2. Carbonaceous Lamosite - massive or laminated lamosite ($> 5\%$ lamalginites) with $> 5\%$ humic macerals; two types: that composed of interlaminated lamosite and coal laminae and that predominantly a lamosite with $> 5\%$ ubiquitous vitrinite and/or

inertinite.

3. Claystone/Shale - fine-grained clastic rock with <5% liptinite; vitrinite-inertinite rare.
4. Carbonate - dolomitic or sideritic rocks with <5% liptinite; rare vitrinite-inertinite.
5. Coal - laminated or massive rock composed of >50% organic matter with predominantly vitrinite-inertinite; where liptinite is >5% (and always derived from terrestrial plants) best termed a cannel coal; alginite mostly absent.
6. Carbonaceous Shale - laminated or massive rock composed of <50% organic matter comprising mostly vitrinite-inertinite and <5% liptinite.

5.2. GREEN RIVER LAMOSITE

Green River lamosite is composed of interlayered pale mineral-rich and brown to dark brown organic-rich laminae ranging in thickness from 0.05 to 10 mm. Higher grade samples contain thicker and more organic-rich layers.

Lamalginitite is the dominant submaceral with layered lamalginitite much more abundant than discrete lamalginitite. Layered lamalginitite has weak to moderately intense yellow, yellowish-green or rarely green to greenish-brown fluorescence. In sections perpendicular to bedding, the layered lamalginitite appears to be composed of numerous lamellae which are continuous over several millimetres suggesting a blue-green algal mat origin. In sections parallel to bedding, the sheets appear to envelop mineral grains. Bitumen is a significant component and occurs as pods and blebs or as an interstitial matrix to mineral grains. It has yellow to yellowish-orange fluorescence and is generally brown or pale brown in reflected light. Minor components include sporinite, vitrinite and inertinite.

6. Summary

The organic matter in oil shales has been studied using many methods including elemental analysis, chemical oxidation, thermogravimetric analysis, infrared spectroscopy, electron microscopy, electron spin resonance, nuclear magnetic resonance and optical microscopy. Of the methods listed above, identification of the organic matter in oil shales is best achieved using a combination of white light and fluorescence mode incident microscopy or organic petrography. With petrographic studies it is possible to characterise and quantify the organic matter, including each type of organic matter, whereas bulk rock chemical methods do not allow separation of the components and thus the properties given are an average of several sets of properties. Organic petrography should be an integral part of any kerogen study. Such integration of techniques is commonly missing in many published chemical accounts of kerogen in oil shales.

The importance of the organic matter in oil shales should not be overlooked as it is the type and abundance of the organic constituents that not only determine the chemical and physical properties of the oil shale, but the oil yield, chemistry and physical properties of the derived shale oil. Data pertaining to probable yield, seam thickness, environment of deposition and both lateral and vertical variation in the type and abundance of organic matter can be obtained using organic petrographic methods.

7. References

1. R.F. Cane, Geological semantics. Nature, 1970, **228**, 1009.
2. T.F. Yen, and G.V. Chilingarian, Introduction to Oil Shales; in T.F. Yen and G.V. Chilingar, (eds) Oil Shale. Elsevier, (1976).
3. E. Stach, M.-Th. Mackowsky, M. Teichmuller, G.H. Taylor, G. Chandra and R. Teichmuller, Stach's Textbook of Coal Petrology, 2nd Ed., Gerbruder Borntraeger, Berlin (1975).
4. E. Stach, M.-Th. Mackowsky, M. Teichmuller, G.H. Taylor, G. Chandra and R. Teichmuller, Stach's Textbook of Coal Petrology, 3rd Ed., Gerbruder Borntraeger, Berlin (1982).
5. A.C. Hutton, A.J. Kantsler, A.C. Cook and D.M. McKirdy, Organic matter in oil shales. J. Aust. Pet. Explor. Assoc., 1980, **20**, 44.
6. A. C. Cook, A.C. Hutton, and N. R. Sherwood, Classification of Oil Shales. Bul. Centr. Rech. Expl. Prod. Elf Aquit., 1981, **5**, 353.
7. P. Robert, Classification des matieres organique et fluorescence application aux roches-meres petrolieres. Bul. Centr. Rech. Explor. Prod. Elf Aquit., 1979, **3**, 223.
8. P. Robert, Classification of organic matter by means of fluorescence; application to hydrocarbon source rocks. Int. J. Coal Geol., 1981, **1**, 101.
9. B. Alpern, Schistes, bitumineux reserves, petrographie, valorisation. Indust. Miner., 1979, August-September, 1.
10. B. Alpern, Les schistes bitumineux: constitution, reserves, valorisations. Bul. Centr. Rech. Expl. Prod. Elf Aquitaine, 1981, **5**, 319-352.
11. A.C. Cook, 1987: Organic petrological studies of oil shale. Abs Prog. Soc. Org. Petrol., **14**.
12. R.D. Rigby, B.D. Batts and J.W. Smith, The characterisation of Australian oil shales by nitrogen isotope abundance. Proc. 2nd Aust. Oil Workshop, Brisbane, Dec. 6-7, 1984, 103.
13. A. Ekstrom, H.J. Hurst, and C.H. Randall, The chemical and retorting properties of selected Australian oil shales. Proc. 1st Aust Oil Shale Workshop, Lucas Heights, May 18-19, 1983, 123.
14. A.J. Gannon, D.A. Henstridge, and A.N. Schoenheimer, Stuart oil shale deposit - relationships of organic carbon with shale oil yield. Proc. 2nd Aust Oil Shale Workshop, Lucas Heights, May 18-19, 1983, 101.
15. P.T. Crisp, J. Ellis, A.C. Hutton, J. Korth, F.A. Martin, and J. D. Saxby, 1987: Australian oil Shales: A Compendium of Geological and Chemical Data. University of Wollongong.
16. A.C. Hutton, J. Korth, P.T. Crisp J. Ellis, Low temperature pyrolysis of three oil shales from Queensland, Australia: a comparative chemical and petrographic study. J. Analyt. Appl. Pyrolysis, 1986, **9**, 323.
17. J.D. Saxby, and S. Sato, Pyrolysis of oil shale/lignite mixtures. Is this a viable option for Australian Tertiary oil shales? Proc. 5th Aust. Oil Shale Workshop, Lucas Heights, Dec. 7-8, 1989, 117.
18. A.C. Hutton, Determination of shale oil yields by petrographic analysis. Fuel, **64**, 1985, 1058.
19. A.C. Hutton, Petrographic approach to beneficiation of Australian oil shales. Fuel, 1987, **66**, 314.
20. D.A. Henstridge, and A.C. Hutton, Pyrolysis of a Tertiary oil shale by a dolerite intrusion, Stuart deposit,, Queensland, Australia. Fuel, 1985, **64**, 546.

DEMINERALIZATION AND KEROGEN MACERAL SEPARATION AND CHEMISTRY

THOMAS L. ROBL AND DARRELL N. TAULBEE
University of Kentucky, Center for Applied Energy Research,
3572 Iron Works Pike, Lexington, KY 40511-8433.

ABSTRACT. Although there are exceptions, the abundance of kerogen is generally small in most oil shales and petroleum source rocks. The presence of the inorganic matrix, which constitutes most of the rock, complicates both the characterization of the kerogen and investigation of pyrolysis chemistry. Kerogen isolation and subsequent separation of its components, or macerals, is important to gaining a fundamental understanding of its chemistry. Techniques to separate kerogen from rocks include both physical and chemical methods. Chemical methods are more effective but may alter the organic matter.

The mineralogy of the rock, for the most part, determines the overall effectiveness of the demineralization reagents. Oil shale contains three broad classes of minerals: carbonates, silicates, and sulfides. The common carbonates are soluble in dilute acids; silicates are soluble in HF. Common sulfides include pyrite and marcasite which are resistant to HCl/HF attack but can be removed with oxidizing or reducing agents. A new procedure for demineralization has been developed which uses HF and HBO_3 to form aqueous BF_3 which is used to remove neo-formed salts. This approach is effective and reduces organic matter alteration.

High speed density gradient centrifugation (DGC) is used to remove pyrite and isolate and concentrate the different kerogen maceral groups. This technique utilizes a dense media of CsCl loaded into a spinning centrifuge to form an in-situ density gradient. Demineralized kerogen particles are then dispersed across the gradient. This method effectively segregates the principal macerals present. Analytical pyrolysis and FT-i.r. analysis on feedstock and separated treated macerals do not indicate any strong alteration of organic matter by this approach.

Our research has focused primarily on Upper Devonian oil shales, including the New Albany Shale from the Illinois basin and the Cleveland Member of the Ohio Shale from the Appalachian basin. These shales are classified as marinities and contain a mixed maceral assemblage. The most abundant maceral present in both shales is bituminite, with both primary forms of alginite, telealginite and lamalginite present in abundance. Vitrinite is an important constituent in both shales. Inertinite is also abundant in the Cleveland but sparse in the New Albany.

The various maceral components fell in all three geochemical type trends. With the alginites plotting in the Type I field, the bituminites in Type II and the inertinites in Type III. Compared to terrestrially deposited macerals of similar rank, the marine materials were found to be considerably enriched in

hydrogen. Comparisons between the New Albany and Cleveland materials found the New Albany macerals to be petrographically and geochemically more degraded than the Cleveland. The New Albany alginites were "red shifted" and had less hydrogen than the alginites of the Cleveland. The New Albany vitrinites were higher in hydrogen than those of the Cleveland suggesting that more of this maceral was derived from the degradation of bituminite precursors.

The relative states of preservation are ascribed to the depositional environment, with the Cleveland deposited under upwelling conditions and the New Albany under stagnant density stratified basin conditions. The Cleveland also had iron limited pyrite, while that of the New Albany had much high concentrations of carbon limited pyrite. More reactive organic matter was consumed in the formation pyrite in the New Albany than the Cleveland resulting in a higher degree of degradation. This and the general enrichment of hydrogen in the shale illustrates the importance of the environment of deposition relative to material source in determining the overall chemistry and oil generating capacity of the kerogen.

1. Introduction

The study of kerogen chemistry and pyrolysis is difficult due to the highly complex heterogeneous nature of oil shales and petroleum source rocks. The inorganic matrix may be composed of a variety of minerals, and the kerogen frequently contains several microscopically identifiable maceral types. Attempts to define fundamental chemical reactions are made complex by interactions among these components.

Complex systems can be better understood by separating them into more fundamental components. Removal of the mineral matrix is the first step in this process. The usual approach is to macerate the mineral by attack with a series of acids, typically HCl followed by HCl in combination with HF. Reducing or oxidizing reagents may be used to remove sulfides. This approach results in the highest purity of organic concentrates but induces chemical alteration of the organic matter.^{1,2,3}

Many kerogens are comprised of a variety of maceral types. Each of these has distinctive chemical and pyrolytic properties that are difficult to differentiate in bulk. Separation and analysis of these macerals can enhance our understanding of the geochemical and pyrolytic properties of the parent oil shale.

2. Chemical Maceration of Mineral Matter

Oil shale contains many different minerals, which can generally be grouped into three classes: carbonates, silicates, sulfides. Phosphates are an important minor component in some shales. Commonly occurring carbonates are calcite, dolomite and siderite. Common silicates include quartz, feldspars and clay minerals. Sulfides include pyrite and marcasite. The mineralogy of the rock determines the effectiveness of the reagents used in demineralizing.

2.1. REMOVAL OF CARBONATES

2.1.1. *HCl Attack.* Although there are several maceration procedures which use HCl, that of the Institut Français du Pétrole (IFP) will be cited here, as it is well documented and widely used.⁴ The first step in this procedure is the removal of carbonates with a strong acid, HCl. Two attacks with 6N HCl solutions are made; the first for 2 hours, followed by a water wash, then a second overnight treatment. This step

is important as calcium or magnesium ions will react with the HF, used later, to form insoluble fluoride salts.

2.1.2. Removal of Carbonates by Resin. Strong acids are not necessary to remove carbonates. They also bring with them an anion, such as Cl, which can result in undesired reactions. One way to avoid the potentially reactive anion is to use cation exchange resin. We conducted a series of experiments at the Center for Applied Energy Research (CAER) to determine if oil shales with a carbonate matrix can be deashed at moderate pH and low ionic strengths using resin. Two oil shales were selected, a sample of the Green River oil shale from the western U.S. and the Rotem oil shale from Israel. The carbonates in the Green River are primarily dolomite ($\text{CaMg}(\text{CO}_3)_2$), and those in the Rotem, calcite (CaCO_3).

The deashing media was FisherRexyn 101(H⁺), a sulfonated polystyrene copolymer cationic exchange resin. The resin was sieved to +40 mesh using a plastic screen (the H⁺ charged resin will attack brass) and the raw shale samples were ground to pass a 100 mesh screen.

The resin was added to the oil shale at a weight ratio of 8:1, resin to shale, in 2000 ml of distilled water. This was reacted at ambient temperature for 3 days. The solution equilibrated after 1 day at a pH of ~3.3 and conductivity of ~250 μS (Figure 1). This conductivity is less than that of the tap water in our laboratory. The resin acts to maintain the low ionic strength of the solution by exchanging protons for dissolved cations, e.g., calcium ions from calcite, as in equation 1:



The carbonate acts to buffer the solution. The net effect is acid dissolution of the carbonates under moderate pH conditions and low ionic strengths.

The resin was then separated from the oil shale by washing the reactants through a 100 mesh plastic screen which retained the resin and passed the deashed shale. A total of 59 wt% of the Rotem shale and 43% of the Green River Shale was eliminated by the resin. Tests conducted on blanks using reagent grade calcite found a low level of cross contamination with this technique, i.e., less than 0.04%.

When compared to samples from the 6N solution HCl attack, similar levels of organic carbon concentration are achieved (Table I). Thus, the carbonates can be effectively removed in very dilute solutions of acid. Although the described approach is too labor intensive and expensive for routine use, it is of value for research and illustrates that strong acid solutions are not required for carbonate removal.

2.1.3. The HF-BF₃ method. The use of strong acids such as HCl is undesirable, as strong acids can hydrolyse the organic matter. Chlorination reactions are also possible, particularly for thermally immature (low ranked) sediments. HCl is not a necessary reagent in the demineralization process, as HF, a much

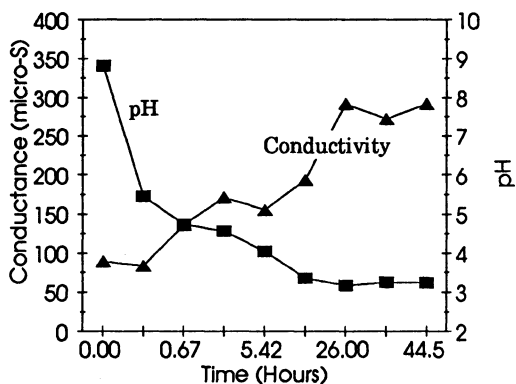


Figure 1. Conductivity and pH of Solution from Resin Demineralization.

Table I. Comparison of Oil Shales Demineralized by Different Methods.

Resin and HCL Deashed Shale			
Rotem	Carbon	Ash	Ash/C
Original 12.0	62.6	5.2	
HCL	27.5	56.1	2.0
Resin	26.8	56.9	2.1
Green River			
	Carbon	Ash	Ash/C
Original 15.1	64.3	4.3	
HCL	24.1	59.0	2.4
Resin	22.4	61.3	2.7
Ash in HF-HCL (IFP) and HF-BF3 Methods			
	HF-HCL	HF-BF3	
Nagoorin	9.82	2.26	
Rotem	10.71	8.88	
Stuart	10.69	8.32	
Toarcian	25.00	22.49	
Irati	33.17	28.70	

weaker acid, can serve to dissolve carbonates. The primary role of HCl is to form water soluble Ca and Mg salts with chloride which are easily removed, thereby suppressing insoluble fluoride salt formation in the silicate dissolution step. An alternate strategy, discussed below, permits the formation of the insoluble fluoride minerals during HF attack, then later utilizes aqueous BF₃ for their removal.⁵

2.2. REMOVAL OF SILICATES

The chemical removal of silicates requires the use of hydrofluoric acid. HF is a weak acid which reacts with silica to form SiF₄, a volatile gas:



Because it is a weak acid (pK=3.45), HF leaves the organic matter largely unaltered.

2.2.1. *HCl in silicate removal.* In addition to reacting with silicates, HF also reacts with other ions, such as Ca and Mg, to form fluoride salts, such as ralsstonite (~Na(Mg₁,Al₅)₆F₁₂(OH)₆·3H₂O) and fluorite (CaF₂), the latter being highly insoluble and difficult to remove once formed.

In the IFP procedure, a 1:1 mixture of 48% HF and 6N HCl is used in the silicate removal step. In aqueous solution, HCl is fully ionized and its presence suppresses the ionization of HF. This retards fluoride ion activity which suppresses fluoride salt formation.

2.2.2. *The HF-BF₃ method.* The overall strategy of the HF-BF₃ method is to remove silica by HF attack and allow fluoride salts to form. The HF is converted to BF₃, a highly water soluble gas, by the addition of excess H₃BO₃:



If H₃BO₃ is not in excess, the following reaction will take place:



This is undesirable as HBF₄ is a strong acid (mixtures of HF and BF₃ are considered superacids).⁶

In an aqueous system at low F/B ratios, BF₃ does not form a strong acid. The aqueous BF₃ is thus free

to react with the neoformed fluoride salts to form soluble fluoride tetrafluoroborate complexes as in eq. 5:



The solubility of these kinds of salts is difficult to determine, but experimental work suggested a solubility of about 0.25 M/L for CaBF₄. It was also found that the sample to reagent concentration for the method must be low, i.e., 20 grams of sample to 800 ml of 24% HF, to provide the lowest ash samples.

The method has been tested on a wide variety of oil shale types including carbonate based shales such as the Rotem (Israel) and Toarcian (Luxembourg) and high silicate shales such as the Stuart and Nagoorin (Australia), and Irati (Brazil). Comparative studies found that the HF-BF₃ method yielded kerogens with lower ash contents (Table I). In addition, significantly lower chlorine contents suggest that this approach results in less alteration of the organic matter. For example, chloride concentrations of 0.22% and 0.15% were measured in the Toarcian and Rotem oil shales using the IFP procedure and less than 0.01% in the same shales macerated with HF-BF₃.⁵

2.3. REMOVAL OF SULFIDES

After the removal of carbonates and silicates, the principal inorganics left are small quantities of resistant minerals, such as rutile and zircon, and sulfides, primarily pyrite and marcasite. The sulfides are difficult to remove without significant chemical alteration of the organic matter¹⁻⁴. Oxidants such as nitric acid cause nitration and oxidation. Reductants such as lithium aluminum hydride (LiAlH₄) reduce C=O and C=N groups. These changes are undesirable and for many purposes unacceptable.

Two promising methods for pyrite removal have been reported. One is based on attack on the pyrite by acidic solutions of cerium (IV)⁷ and the other uses acidic chromous chloride (6).⁸



This latter method appears to achieve significant reductions in pyrite without substantially altering the organic matter, at least as indicated by elemental ratios and FT-i.r. spectra. There does, however, appear to be some chlorination and possibly incorporation of chromium. We have not yet evaluated this method in our own laboratory.

In lieu of chemical dissolution, the approach taken at the CAER is to reduce the sulfide content by centrifugation using dense solutions of CsCl. Chemical attacks on the other minerals disrupts the association between the organic matter and sulfides which facilitates this approach. However, in some shales pyrite is intimately mixed with the organic matter, and clean separations are not easily obtained.

3. Kerogen Maceral Separation by Density Gradient Centrifugation

3.1. INTRODUCTION

The isolation of maceral types in coal has, until recently, been only partially successful. Macerals such as vitrinite, which often occur in bands large enough to permit hand-picking, have been physically and chemically described.⁹ However, isolation of other maceral types, which may be small and/or dispersed, are not amenable to this approach. Isolating macerals from oil shale by hand-picking is even more difficult

due to the larger amount of mineral matter and its intimate association with the organics.

Density gradient centrifugation (DGC) as first described by Dyrkacz and co-workers^{10,11} and later reviewed by Crelling¹² provides an effective approach to the separation of macerals. Our own approach has been similar to those cited with certain modifications, the more significant being the use of larger feed particles and the omission of HCl during demineralization.^{13,14,15,16} The advantages of these changes are suppressed organic alteration, more rapid processing, and more reliable petrographic analyses, particularly for the differentiation of maceral types within a given group. One disadvantage is a higher residual ash due to additional encapsulation of minerals in the larger feed particles. Another disadvantage is an increase in the number of mixed maceral particles and a decrease in maceral purity. We feel that the more reliable petrographic analyses and increased throughput more than offset these disadvantages.

3.2. PROCEDURES FOR THE SEPARATION AND CONCENTRATION OF KEROGEN MACERALS

3.2.1. *Study Samples.* Much of our work on kerogen maceral separation and concentration has been with oil shale from the New Albany Formation and Cleveland Member of the Ohio shale. These are Devonian oil shales from northwestern and northeastern Kentucky, respectively. These shales along with particulars of the maceral concentration techniques have been previously described.^{14,15} We also worked with a high-vol A bituminous coal from the Lower Elkhorn Seam of Pike County (eastern) Kentucky (Table II).¹³

The Cleveland sample was screened to 16x60 mesh whereas the New Albany and coal samples were ground to -100 mesh prior to demineralization. Demineralization was based on commonly used HF digestion procedures with certain modifications^{14,15} including omission of HCl normally used for carbonate dissolution. The chemical removal of iron sulfides was omitted in order to minimize organic alteration.⁴ A separation schematic as applied to the Cleveland oil shale is shown in Figure 2. The New Albany kerogen and coal samples were processed in a similar manner, only for these separations, selected density fractions were recombined and reprocessed by DGC to enhance the maceral concentrate purities.

TABLE II. Selected Properties of the DGC Study Samples. (on an as-Determined basis.)

	New Albany	Cleveland	Coal 3761
% C	14.1	14.0	71.0
% H	1.66	1.78	4.60
% N	0.46	0.44	1.19
% S _t	5.3	1.96	0.99
% moisture	0.8	1.9	0.5
% Ash (HTA)	77.7	76.2	17.1
% Mineral C	0.3	0.1	
Fisher Assay (g/t)	13.7	14.6	
% Liptinites	12.6	35.8	30.6
% Bituminite	78.4	41.0	0.0
% Vitrinites	7.6	10.4	31.9
% Inertinites	1.4	12.8	37.5

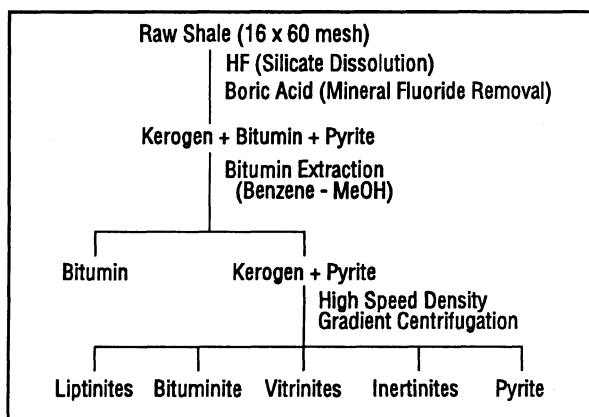


Figure 2. Separation Scheme for the Cleveland Member Kerogen.

3.2.2. *Density Gradient Centrifugation (DGC)*. A DGC method entails pumping aqueous CsCl salt solutions of successively higher density to the outer wall of a spinning centrifuge rotor to form a density gradient in-situ. An aliquot of demineralized sample dispersed in a surfactant solution is loaded to the center of the spinning rotor. The macerals are then forced to disperse across the density gradient at forces ranging up to 25,000xg. Sample loadings ranged from 6-8 g per run. Numerous DGC runs were needed to provide sufficient sample for subsequent analysis.

3.2.3. *Methods of Analysis*. Methods have been discussed in detail elsewhere. Only a summary is presented here.¹³⁻¹⁵

Kerogen petrographic classifications were based on those of Hutton.^{17,18} Alginite (~98%) and sporinite (~2%) were grouped as liptinites. The bituminite maceral, normally classified as a liptinite, was treated separately due to both high abundance and substantial differences in chemistry and pyrolytic behavior. The vitrinite group included vitrinite and degrado-vitrinite. The inertinite group included fusinite, semifusinite, and granular micrinite. Since no density fraction from the New Albany separation contained more than about 1% total inertinites, these counts were added to the vitrinites to which they were most similar in density.

A CDS analytical pyrolysis unit was used to pyrolyze small 1-2 mg samples. This unit utilized a FID detector to monitor hydrocarbon evolution and could be configured to monitor total hydrocarbon yield, relative partitioning of the hydrocarbon components between oil and gas, or interfaced with a capillary GC to determine the relative production of individual oil components.

FT-i.r. transmittance spectra were obtained from 1:100, kerogen or coal:KBr pellets. Spectral subtractions were conducted after the parent and demineralized sample pellets were normalized to a unit carbon basis.

3.3. INVESTIGATION OF CHEMICAL ALTERATION OF THE KEROGEN

Many of our investigations of DGC generated maceral concentrates have focused on the nature of the starting kerogen and its behavior during pyrolysis. Thus, it is important that the maceral concentrates be representative of the parent kerogen. Measuring or estimating the extent of chemical alteration induced by demineralization is not easy. For example, there was no significant change measured in the organic H/C or N/C molar ratios before and after demineralization. However, there is sufficient analytic uncertainty in these determinations to mask small but potentially significant changes. Changes in the organic S/C or O/C are more difficult to measure since the analytical uncertainties for S and O determinations are higher.

Analytical pyrolysis and Ft-i.r. spectroscopy were also used to evaluate chemical alteration of the kerogen during processing. FT-i.r. was used to examine kerogen functional group changes, particularly oxidation, and to ensure that the surfactant employed during DGC was completely removed from the maceral surfaces. Analytical pyrolysis was used to verify that the pyrolysis products were unaffected by the demineralization and to again probe for evidence of surfactant residue.

Unfortunately, evaluating kerogen alteration by either of these techniques is made difficult by the high levels of mineral matter. In the case of FT-i.r., mineral matter in the parent shale reduces the level of absorption by the organic matrix rendering small changes difficult to measure. During pyrolysis, the presence of mineral matter results in secondary reactions, making it difficult to differentiate between

changes induced by mineral matter and those resulting from demineralization. For these reasons, the extent of organic alteration was evaluated with a high liptinite coal which contained considerably less mineral matter than a typical oil shale.

FT-i.r. spectra of the parent and demineralized coal, three maceral group concentrates derived from that coal, and Brij-35 surfactant are shown in Figures 3a and 3b. These spectra are shown expanded between 1800 and 900 cm^{-1} to focus on carbonyl bands, 1760-1690 cm^{-1} ; C-O stretch, 1300- 1000 cm^{-1} ; C-F stretch, 1400-1000 cm^{-1} ; and the strong Brij-35 absorption peak at 1115 cm^{-1} . The parent and demineralized spectra (Fig. 3a) are essentially the same in the carbonyl stretch region indicating no measurable oxidation attributable to the demineralization. These same spectra are also indistinguishable between 1600 and 1200 cm^{-1} . However, they diverge between 1200 and 1000 cm^{-1} due to increased absorption by mineral components, principally illites, in the parent coal. Examination of the three maceral concentrate spectra in Figure 3b reveals no evidence of residual surfactant.

Examination of capillary gas chromatograms from the parent and demineralized coal samples reveal no qualitative differences in their pyrolysis products (Figure 4).

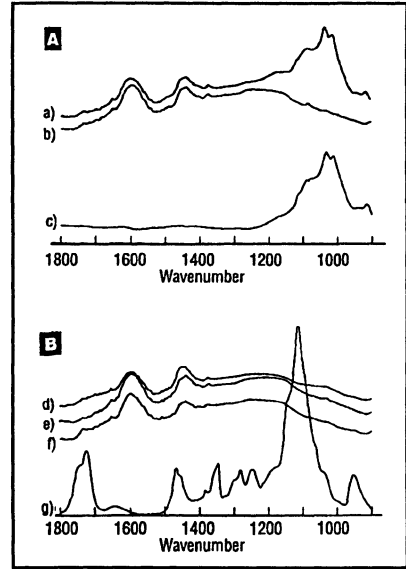


Figure 3. FT-i.r. Spectra of coal 3761 Samples. a) Parent; b) Demineralized; c) Parent minus demineralized; d) Liptinites; e) Vitrinites; f) Inertinites g) Brij-35 Surfactant.

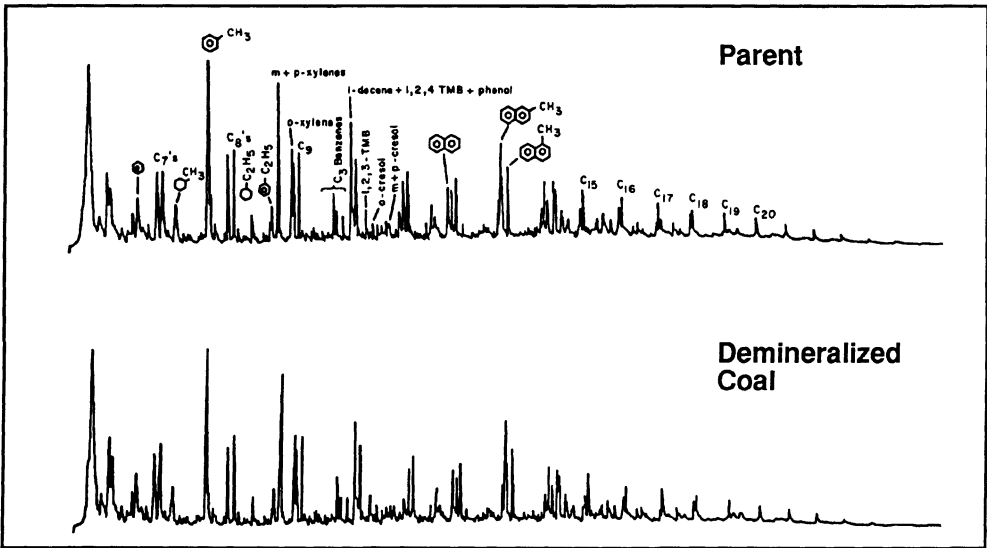


Figure 4. Pyrograms of (A) Parent and (B) Demineralized Coal Samples.

Total HC pyrolysis yield per unit carbon was also essentially the same; 1.16 ± 0.03 for the parent versus 1.19 ± 0.04 for the demineralized sample (relative to an external standard). As a more precise check, the GC area% values for 33 of the major pyrolysis products were summed, normalized to 100%, and grouped according to hydrocarbon class.¹³ No significant differences were discerned between the demineralized and parent samples with the exception of the 1-alkene/n-alkane ratio: 0.89 in the parent versus 0.83 for the demineralized sample. This small difference and the difference in total hydrocarbon yield are most likely a result of the removal of the mineral matrix as the minerals tend to both reduce total pyrolysis production and selectively deplete alkenes relative to alkanes.¹⁹

4. Chemistry and Organic Petrography of the DGC-Separated Kerogen Macerals

4.1. ORGANIC PETROGRAPHY OF THE CLEVELAND AND NEW ALBANY SHALES

The New Albany and Cleveland Member kerogens are composed of varying proportions of terrestrially and marine derived organic matter. The terrestrial components are preserved as vitrinites, inertinites, and trace sporinites. Algal and bacterial decay products were preserved in the form of alginite and bituminite which comprised the bulk of both kerogens. Over 98% of the liptinites (excluding bituminite), consisted of alginite for each kerogen. Both lamalginite and telalginite¹⁸ were present. The telalginite consisted primarily of *Tasminites* which exhibited a wide range of preservation. On average, the Cleveland alginites were better preserved and more brightly fluorescing than those from the New Albany. The New Albany kerogen contained only trace amounts of inertinites. This may have been due to settling out of these denser units prior to reaching the New Albany depositional site which was thought to be farther from the Catskill delta, the source of terrigenous material for both shales.^{20,21}

Bituminite was the most abundant maceral in both shales, accounting for about 41 vol% of the Cleveland and 84% of the New Albany. The term bituminite as used here follows that of Hutton.¹⁸ It is the same material described as “sapropelic kerogen” by Barrows.²² Under Hutton’s classification, bituminite is a liptinite. We have treated it independently due to its high abundance and substantial differences in chemistry and pyrolytic behavior from alginite.

4.2. MACERAL PARTITIONING BY DENSITY GRADIENT CENTRIFUGATION

The maceral distributions for both the New Albany and Cleveland shales are shown in Figure 5 as a function of gradient density. Bituminite recovery maximized at approximately 1.21 g/mL and skewed toward higher densities. This resulted in lower purities for the macerals recovered at higher density in both separations. The cause for this bituminite tailing was identified as contamination of the bituminite with denser materials. Bituminite recovered at a gradient density near 1.21 g/mL was relatively clean of foreign materials; whereas that recovered at a higher density was often associated with either denser macerals or, commonly, with finely disseminated iron sulfides. This observation was confirmed by an increase in the ash/pyrite content of the higher density fractions (Figure 6). X-ray diffraction indicated that residual mineral matter in both kerogens was composed of iron sulfides, pyrite and marcasite, and titanium dioxides, primarily rutile. The concentration of ash and pyrite was about twice as great for the corresponding New Albany density fractions and accounts for a more pronounced tailing of bituminite (Fig. 5a).

Vitrinite enrichment was low for both shales, maximizing around 1.25-1.30 g/mL for the New Albany and 1.28-1.34 g/mL for the Cleveland. The highest vitrinite concentrations from the Cleveland were about

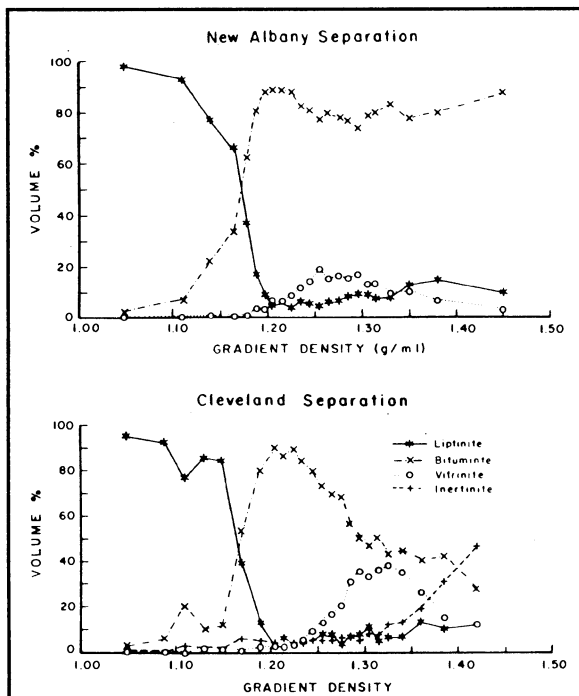


Figure 5. Petrographic Analyses of the Density Fractions Recovered from the New Albany (top) and Cleveland Member (bottom) Kerogens Separations.

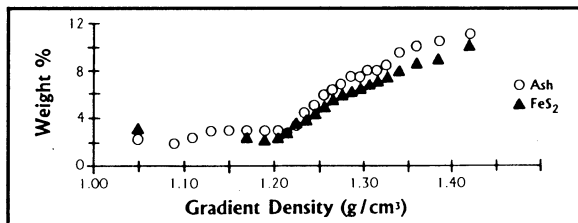


Figure 6. Pyrite and Ash Content of Density Fractions from the Cleveland Member Separation.

twice that from the New Albany. This low enrichment is attributed to the pronounced tailing of bituminites to higher densities resulting in dilution of the vitrinitic fractions as well as lower overall abundance.

4.2.1. *FT-i.r.* FT-i.r. spectra obtained on four selected density fractions from the Cleveland separation are shown in Figure 7. One notable feature of these spectra is the increase in intensity of the 1630 cm^{-1} relative to the 2930 and 2860 cm^{-1} bands. The former is attributed to the carbon-carbon vibrational stretch of aromatic carbons (C=C) while the latter corresponds to the carbon-hydrogen stretch of aliphatic materials (the aliphatic carbon-carbon stretch centered at 1450 cm^{-1} exhibited the same trend). The increase in this ratio is thus an indicator of the greater aromaticity of the higher density fractions.

There is a readily apparent decline in relative intensity of the carbonyl stretch at 1710 cm^{-1} . Not as evident, due to the overall lower absorption of the inertinite concentrate, is a corresponding increase in the intensity of the broadband at $3300\text{--}3500\text{ cm}^{-1}$ assigned to hydroxyl functionalities. This is interpreted as a shift in relative abundance of carbonyl oxygen in the liptinites to hydroxyl oxygen in the higher density macerals. Due to the greater aromaticity of the higher density fractions, hydroxyl oxygen in these denser macerals is more likely present as phenolic oxygen rather than aliphatic alcohols.

4.2.2. *Proximate and Ultimate Analysis.* Organic elemental ratios for the DGC generated density fractions are shown in Figure 8 for both kerogens. Organic H/C and N/C molar ratios for the New Albany density fractions changed rapidly up to a gradient density of about 1.20 g/mL but remained relatively constant at higher densities. The corresponding Cleveland plots exhibited a continuous decrease in the H/C ratio across the gradient. The Cleveland O/C and N/C ratios increased up to about $1.2\text{--}1.3\text{ g/mL}$, corresponding to the maximum frequency of bituminite and vitrinite, and remained relatively constant or declined slightly at higher gradient densities. There was insufficient sample to determine the organic sulfur content of the New Albany fractions but the organic S/C ratios for the Cleveland fractions were essentially

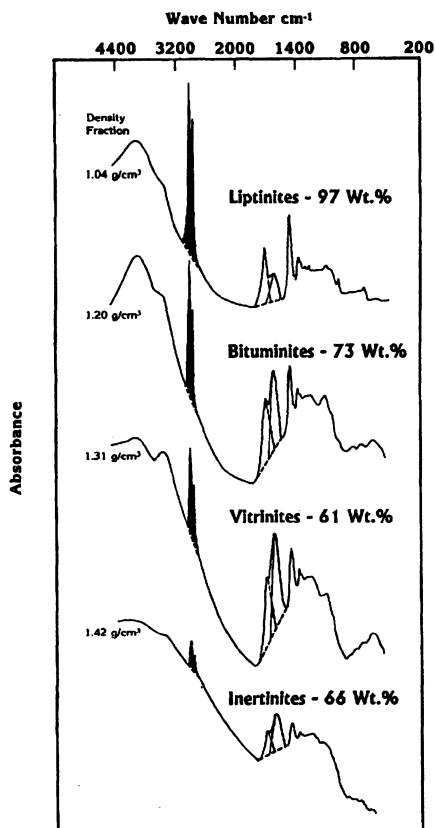


Figure 7. FT-i.r. Spectra of the four Maceral Concentrates from the Cleveland Member Kerogen.

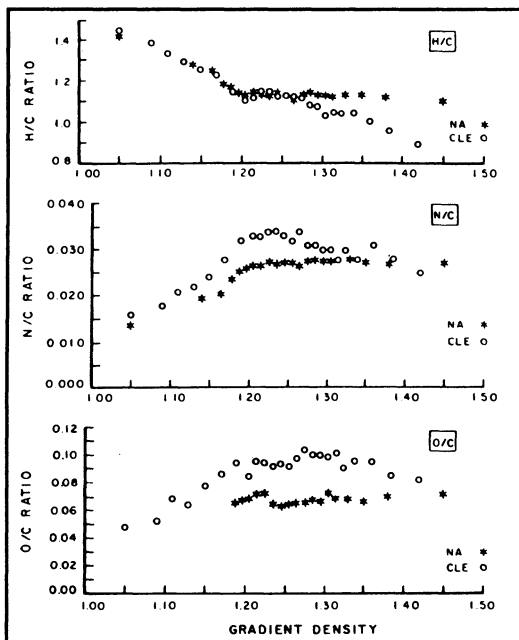


Figure 8. Organic Molar Ratios for the New Albany, *, and Cleveland, O, Density Fractions.

constant across the gradient. The differences in analogous New Albany and Cleveland elemental ratio plots are thought to reflect both improved separation efficiency (less bituminite tailing - Fig. 5a) and a significant contribution from inertinite macerals in the Cleveland kerogen at higher densities.

The New Albany fractions exhibited little change in fixed carbon/total carbon or volatile matter/total carbon ratios beyond about 1.2 g/mL as contrasted to inverse variation of these parameters in the Cleveland density fractions, i.e., increasing %FC, decreasing %VM at higher densities.¹⁴ The mineral matter corrected (dmmf) organic densities for the New Albany fractions showed an increase up to about 1.2 g/mL, maximized at a density near that of maximum vitrinite, and then declined slightly in the higher density fractions. This small decline at higher density corresponded to a decreased vitrinite and increased liptinite content. This, too, was in contrast to the dmmf-Cleveland densities which exhibited a continuous increase across the density gradient, again attributed to the contributions of inertinites in the higher densities Cleveland fractions.¹⁵

The relatively constant values for organic elemental ratios, fixed carbon, volatile matter, and organic density for the higher density fractions in the New Albany separation imply that the alginites and bituminites which partitioned to these higher density fractions were not necessarily chemically different than the equivalent macerals in lighter fractions. Rather, partitioning of these macerals to higher density is thought to merely reflect their frequent association with mineral matter.

4.3. CALCULATION OF PURE MACERAL PROPERTIES

Selected density fractions from the New Albany separation were reprocessed by DGC in an effort to improve maceral type purity prior to calculating individual or 'pure' maceral properties.¹⁴ This resulted in liptinite, bituminite, and vitrinite concentrates of 84.4, 95.7, and 38.5 vol%, respectively (83.4, 95.7, and 39.5 wt%). The concentrates used to calculate pure maceral properties from the Cleveland Member contained 95.5, 90.0, 36.2, and 46.9 vol% (92.7, 89.4, 38.0, 51.8 wt%) liptinite, bituminite, vitrinite, and inertinite, respectively.

Calculating pure maceral properties entailed correcting the empirical density values for each of the maceral concentrates to obtain mineral matter free organic density values.²³ The organic density values coupled with petrographic analyses were then used to calculate pure maceral group densities. These in turn were utilized to convert the volume% petrographic data to a weight% basis thereby permitting the calculation of other pure maceral properties via simultaneous equations.

The results of these calculations, shown in Table III, indicate that the average New Albany liptinite density was significantly higher (1.09 g/mL) than the Cleveland liptinites (1.02 g/mL). Conversely, the average vitrinite density for the New Albany (1.21 g/mL) was lower than for the Cleveland (1.26 g/mL). Pure maceral organic molar ratios exhibited similar trends in both kerogens; that is, the H/C ratios declined with increasing maceral group density, the N/C ratios maximized in the bituminite macerals, and the O/C ratios increased from liptinite to vitrinite. The data in Table III without exception, indicate that the average alginite and vitrinite properties in the New Albany maceral groups are similar to those of bituminite relative to analogous Cleveland maceral groups.

TABLE III. New Albany and Cleveland Member Maceral Properties (Corrected to a 100% Maceral Group and dmmf Basis).

	Liptinites		Bituminites		Vitrinites		Inertinites	
	NA	CLE	NA	CLE	NA	CLE	NA	CLE
Density (g/mL)	1.09	1.02	1.17	1.16	1.21	1.26		1.40
% org C	82.72	81.68	80.19	78.69	78.77	75.67		83.14
% org H	9.19	10.14	7.84	7.40	7.59	6.54		4.53
% org N	1.78	1.43	2.80	3.12	2.63	2.47		2.13
% org S	1.07	1.74	1.68	1.89	1.76	2.22		1.78
% org O	5.24	5.00	7.47	8.91	9.29	13.1		8.42
org H/C	1.32	1.48	1.16	1.12	1.15	1.03		0.65
org N/C	0.019	0.015	0.030	0.034	0.029	0.028		0.022
org S/C	0.0048	0.0081	0.0078	0.0094	0.0084	0.011		
org O/C	0.048	0.046	0.070	0.085	0.089	0.133		0.076
FC/org C	0.25	0.10	0.46	0.46	0.482	0.69		0.90
Pyrolysis Yield								
HC liquids	1.35	1.67	1.10	1.18	0.86	0.65		0.58
HC gases	1.10	0.78	1.29	1.26	1.06	1.20		0.98

Figure 9 shows the calculated pure maceral group molar ratios plotted on an elemental molar ratio diagram. Three major fields are plotted. Type I is derived from the maturation trend of the Green River Shales of the Uinita Basin; Type II is derived from the maturation trend of the Lower Toarcian shales of the Paris Basin; and Type III is characteristic of the Cretaceous shales of the Douala Basin.²⁴ The Cleveland maceral group ratios are plotted as a range of values determined by using the density fractions with the highest concentrations of the respective maceral groups as well as other fractions exhibiting significant maceral enrichment. The New Albany ratios are from the three maceral group concentrates obtained by reprocessing of the initial New Albany fractions as discussed above. Alginites from both kerogens plotted in the Type I field; bituminites as Type II; vitrinites plotted between Types II and III; and the inertinites from the Cleveland as Type III.

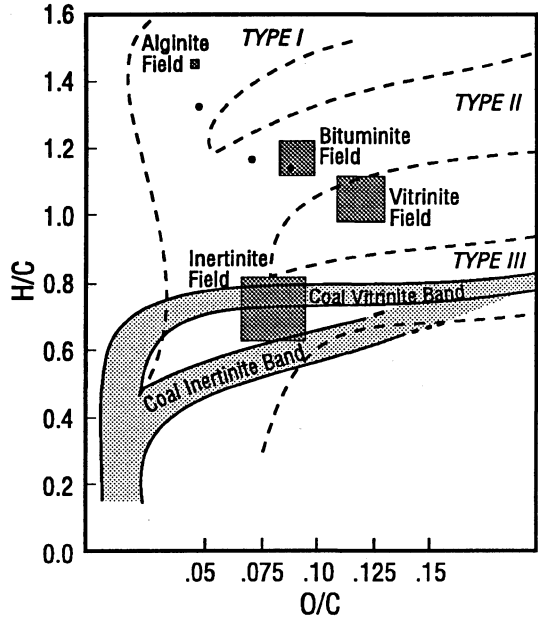


Figure 9. van Krevelen Diagram of Calculated 'pure' Maceral Elemental Ratios

(□ - CLE, ● - NA)

5. The Geochemistry of the Separated Kerogen Macerals

5.1. COMPARISON BETWEEN MARINE AND TERRESTRIAL KEROGEN MACERALS

The marine deposited vitrinites separated from the Devonian kerogens exhibit a higher H/C molar ratio (0.2-0.3) relative to coal vitrinites of the similar rank (Figure 9). Though not as clear due to greater analytic uncertainty, the Cleveland inertinites also appear to be hydrogen enriched relative to coal inertinites.²⁵

This hydrogen enrichment has a bearing on the relative importance of depositional environment and material source. For example, Breger and Brown concluded that Devonian black shales similar to those in this study contained too much terrestrially derived humic material to be considered a good petroleum source rock and should instead be considered a "coaly" material.²⁶ This may be compared to the view of Demaison, who emphasizes the importance of the depositional environment and relates kerogen type primarily to sedimentation rate and the oxygen content of the overlying water column (aerobic vs. anaerobic).^{27,28} The hydrogen enrichment of the vitrinite and inertinite support the importance of the deposition environment in controlling the chemistry of the kerogen.

The specific mechanism for the hydrogen enrichment is uncertain. Humic matter may be adsorbed and incorporated in lipid-rich materials during transport or deposition in the marine environment.²⁹ Alternatively, hydrogen incorporation may take place shortly after deposition during the vitrinite gel phase.³⁰ This latter is supported by evidence that the H/C ratio of coal vitrinites is influenced by the amount of associated liptinites.^{31,32} At any rate, comparison of kerogen and coal maceral chemistries indicates that one must be cautious in drawing conclusions based solely on petrographic analysis.

5.2. COMPARISON BETWEEN THE NEW ALBANY AND CLEVELAND KEROGEN MACERALS

The New Albany and Cleveland kerogens are similar in many respects. Both are comprised of the same maceral types and have similar bulk chemical compositions. However, the New Albany kerogen contains a much higher proportion of bituminite as well as measurable differences in the chemical composition of the other maceral types.

The New Albany alginites exhibited a lower hydrogen content and higher density relative to the Cleveland alginites. Attempts to re-centrifuge the New Albany alginite concentrates indicated that these parameters are inherent and not due to maceral or mineral impurities.¹⁴ On average, the New Albany alginites appeared to be more degraded and exhibited longer wavelength fluorescence (red shifted) than their Cleveland counterparts. Further, there was a continuum in both morphology and wavelength of maximum fluorescence from highly figured, bright-yellow fluorescing alginites to non- or dimly-fluorescing, amorphous bituminites. Visually, the red shift in fluorescence correlated with the extent of morphologic degradation. If the bituminites are derived from degraded alginite precursors as it appears, it is reasonable to expect a continuum in chemical properties which coincide with the extent of precursor degradation. The convergence of chemical parameters between the New Albany alginites and bituminites relative to the same maceral types in the Cleveland can be explained by the fact that, on average, the New Albany alginite precursors appear to have been more extensively degraded.

The New Albany vitrinites were found to contain more hydrogen, were of lower density, and produced more HC product during pyrolysis than did their Cleveland analogues. Similar to the alginite/bituminite continuum, a continuum in morphology and reflectance between vitrinite and bituminite was observed. This, along with the convergence in chemical parameters, suggests that either vitrinite precursors were converted to bituminite precursors during deposition or, more likely, that the New Albany bituminite precursors were more degraded, leading to their petrographic identification as vitrinites. The relatively high hydrogen content of the vitrinites and other chemical and pyrolytic differences between like macerals in the two kerogens also support the significance of the environment of deposition in determining the chemistry of the kerogen.

The differences in chemistry of analogous maceral types in these kerogens may be due to a difference in rank, differences in the precursor or source chemistry, or differences in the environments of deposition. Since both shales show similar vitrinite reflectance ($R_o \sim 0.55$), similar pyrolysis response, and both are Upper Devonian in age, we believe that most of the differences in chemistry can be attributed to the relative extent of decomposition of the maceral precursors during deposition and early diagenesis.

Chemically, the most striking difference between the New Albany and Cleveland is the higher sulfur content and lower carbon to sulfur ratio in the New Albany (3.4 versus 2.7% S, and 1.8 versus 3.9 C/S for the Huron and Cleveland respectively).³³ This difference is a function of the environment of deposition. The Cleveland was deposited under upwelling conditions as indicated by the presence of phosphate nodules as well as the trace element composition.^{34,35} The New Albany, however, was deposited under stagnant basin conditions similar to the present day Black Sea.³⁶ As in the Black Sea sediments, a strong positive correlation and positive intercept is found between organic carbon and total sulfur and organic carbon and degree of pyritisation (DOP) for the New Albany. No correlation is found for the Cleveland.

Pyrite deposition was "carbon limited" in the New Albany and "iron limited" in the Cleveland. That is, the amount of pyrite formed was a function of the availability of reactive organic matter in the New Albany.

In the Cleveland, where upwelling provided large amounts of organic carbon, the amount of pyrite was limited by the availability of iron. Organic matter and pyrite are chemically linked, as the organic matter is the source of the electrons necessary to reduce the sulfate to sulfide and form pyrite. Thus, the higher degree of degradation in the New Albany is a function of the control of pyrite formation in its depositional environment.

6. Acknowledgements

The authors would like to acknowledge the contributions and assistance of Dr. B. Davis, Dr. J. Hower, G. Wild, G. Thomas, L. Barron, K. Sauer, and M. McAlister at the CAER. The work reported here was conducted at the Ky. Center for Applied Energy Research with funding provided by the Commonwealth of Kentucky and the United States Department of Energy.

7. References

1. Saxby, J.D., *Chem. Geol.*, **1970**, *6*, 173-184.
2. Saxby, J.D., *Oil Shale*, 1976, T.F. Yen, G.V. Chilingarian (Eds.), Elsevier Press, Amsterdam, 103-128.
3. Robinson, W.E., *Org. Geoch.*, Ch. 2, 1969, Springer, New York, 181-195.
4. Durand, B. and Nicaise, G., 'Ch. 2: Procedures for kerogen isolation', *Kerogen*, 1980, B. Durand (Ed.), Editions Technip, Paris, 35-53.
5. Robl, T.L. and Davis, B.H., *Org. Geoch.*, **1993**, *20*, 249-255.
6. Ohlah, G.A., Surya Prakash, G.K. and Sommer, J., *Superacids*, 1985, Wiley, New York, 8-15.
7. Audeh, C., U.S. Patent No. 4,640,692, Feb. 3, 1987.
8. Acholla, F.V. and Orr, W.L., *Energy and Fuels*, **1993**, *7*, 406-410.
9. 'Coal Petrography', Edited by E. Stach, 3rd edition, 1982, Gebruder Borntraeger Pub., Berlin.
10. Dyrkacz, G.R., Bloomquist, C.A.A. and Horwitz, E.P., *Sep. Sci. Tech.*, **1981**, *16*, 1571-1588.
11. Dyrkacz, G.R. and Horwitz, E.P., *Fuel*, **1982**, *61*, 3-12.
12. Crelling, J.C., Prepr.: *ACS Div. Fuel Chem.*, **1989**, *34*, #1, Dallas, Tex., 249-255.
13. Taulbee, D.M., Poe, S., Robl, T.L. and Keogh, R.A., *Energy and Fuels*, **1989**, *3*, 662-670.
14. Taulbee, D.N., Seibert, E.D., Barron, L.S. and Robl, T.L., *Energy and Fuels*, **1990**, *4*, 254-263.
15. Taulbee, D.N., Robl, T.L. and Barron, L.S., *Proc.: 1985 Eastern Oil Shale Symp.*, KCERL/85-147, 1986, Univ. of KY-IMMR, Lexington, Ky., 291-300.
16. Taulbee, D.N., Hower, J.C. and Greb, S., *Org. Geoch.*, **1991**, *17*, #4, 557-566.
17. Hutton, A.C., 'Organic Petrology of Oil Shales,' 1982, PhD thesis, Univ. of Wollongong..
18. Hutton, A.C., *Int. J. Coal Geol.*, **1987**, *8*, 203-231.
19. Taulbee, D.N. and Seibert, E.D., *Energy and Fuels*, **1987**, *1*, 514-519.
20. Rich, J.L., *Amer. Soc. of Petr. Geol. Bull.*, **1951**, *35*, 2017-2040.
21. Potter, P.E., Maynard, J.B. and Pryor, W.A., 'Report of Special Geol., Geoch. and Petrol. Studies of Devonian-Mississippian Shales of the Central Appal. Basin,' 1980, H.N. Fisk Lab. of Sedim., Univ. of Cincinnati.
22. Barrows, M.H., Cluff, R.M. and Harvey, R.D., *Proc.: Third Eastern Gas Shales Symp.*; METC/SP-79/6; Morgantown Ener. Tech. Center: Morgantown, WV, **1979**; 85-114.
23. Smith, J.W., 'Report of Investigations,' 1976, LERC/RI-76/6, Laramie Energy Research Center, Laramie, WY, 10 pp.
24. Durand, B. and Monin, J.C., in 'Kerogen: Insoluble Organic Matter from Sedimentary Rocks,' 1980, B. Durand, ed., Paris, Editions Technip, 113-142.
25. Robl, T.L., Taulbee, D.N., Barron, L.S. and Jones, W.C., *Energy and Fuels*, **1987**, *1*, 507-513.
26. Breger, I.A. and Brown, I., *Science*, **1962**, *137*, 221-224.

27. Demaison, G.J., Holck, A.A.J., Jones, R.W. and Moore, G.T., *Prepr., Eleventh World Petr. Cong., 1983, No. PDI(2)*, Wiley, London, 13.
28. Demaison, G.J. and Moore, G.T., *AAPG Bull.*, **1980**, *64*, 1179-1209.
29. Sentfle, J.T., **1983**, personal communication.
30. Durand, B., **1985**, personal communication.
31. Dyrkacz, G.R., Bloomquist, C.A.A. and Ruscic, L., *Energy and Fuels*, **1991**, *5*, 155-163.
32. Masterlerz, K., Wilks, K.R. and Bustin, R.M., *Org. Geoch.*, **1993**, *20*, 555-562.
33. Robl, T.L., Taulbee, D.N. and Barron, L.S., *Prepr.; Div. of Pet. Chem.*, **1989**, *34*, Amer. Chem. Soc., V.1, 81-86.
34. Robl, T. L. and Barron, L.S., *Canadian Soc. Petr. Geol.*, **1988**, *Memoir 14*, V. 2, 377-392.
35. Robl, T.L. Rimmer, S.M., and Barron, L.S, **1992**, *Fuel*, *71*, 276-271.
36. Leventhal, J.S., *Amer. J. of Sci.*, **1987**, *287*, 33-49.

ALKANE BIOMARKERS. GEOCHEMICAL SIGNIFICANCE AND APPLICATION IN OIL SHALE GEOCHEMISTRY

F.J. GONZALEZ-VILA

Instituto de Recursos Naturales y Agrobiologia, C.S.I.C.

P.O. Box 1052

41080-Sevilla

Spain

ABSTRACT. The application of alkane biomarkers for source, palaeoenvironmental reconstruction, maturity and biodegradation of sedimentary organic matter is briefly reviewed. Data on the extractable biomarker composition of a Spanish oil shale, as well as some considerations on future work in biomarker geochemistry are also included.

1. Biomarkers. Concept and Applications

In spite of the progress made in the last decades, understanding the origin and fate of organic compounds in Nature still remains an intriguing and difficult task. However, the concept of using organic compounds as measures of events and processes in the natural world is now widely accepted and applied in a wide range of disciplines.

The organic substances present in recent and ancient sediments are thought to reflect the source inputs and the environmental conditions, including microbial activity, at the time of deposition. A restricted number of these organic substances, the so-called molecular fossils or biological markers (biomarkers for short), are molecules directly inherited from the organisms living at the time of deposition which have been preserved without subsequent alteration, or with only minor changes, so that their basic carbon skeleton remains intact ^(1,2)

The term biomarker stems therefore from the similarity of certain chemical structures in the sedimentary record to precursor molecules which occur in unique biosynthetic products of specific groups of organisms in the natural environment. Compounds whose biological origin is uncertain but whose structural specificity makes them useful as correlation parameters in source diagnosis are also referred to as biomarkers. Small changes in the structures of these biomarkers are due to microbial transformations in the water column and in recent sediments or chemical reactions during diagenesis in ancient sediments. It should be emphasized that, although the inputs contributing to the

sedimentary organic matter are deduced from the presence of specific biomarkers, their absence does not necessarily imply that the biosynthetic precursors and the corresponding biota were not present in the depositional environment.

The biomarker approach, i.e. isolation and recognition of biomarkers from different environments, constitutes a powerful tool in many areas of geochemistry. The use of biomarkers has moved from an academic pursuit (assessment of the nature of the different organic inputs into a sediment, reconstruction of paleo-environments, study of the processes of early diagenesis and thermal maturation, etc) to a highly applied analytical technique in technological fields such as petroleum and gas exploration, based mainly on the determination of source, maturity, migration and biodegradation of hydrocarbons. In all cases, conclusions based on biomarker distribution data are stronger than those based on any single compound or class of compounds.

2. Extraction, Isolation and Analysis of Biomarkers

Biomarker determinations provide a challenge for the analytical chemist. In general, the biomarkers of greatest interest are present in relatively low concentrations in crude oils and rock extracts, which are complex mixtures of organic compounds.

Extraction of biomarkers from sediments and oils is normally accomplished by conventional solid-liquid extraction procedures using different solvents or mixtures of them in Soxhlet apparatus. Over recent years new extraction techniques based on the use of ultrasonic agitation⁽³⁾ and supercritical fluids⁽⁴⁾ have been developed. The supercritical fluid extraction (SFE) seems to have a promising future, since it offers considerable advantages regarding extraction time and elimination of environmental hazards.

After removal of asphaltenes, insoluble in *n*-pentane, the extracts are usually fractionated into saturated, aromatic and polar components by adsorption chromatography on column or on modern solid phase extraction cartridges⁽⁵⁾.

The *n*-alkanes are usually the most abundant compounds in the saturated fractions of crude oils and rock extracts, and sometimes it is necessary to remove them as an analytical step to effectively enhance the concentration of other more specific biomarkers, such as branched and cyclic alkanes. Many concentration techniques have been used quite effectively. Amongst them the clatration with urea and the use of molecular sieves seem to be the most useful to separate *n*-alkanes from their branched/cyclic congeners.

The most common methods for detection and identification of biomarkers in complex mixtures are the computerised Gas Chromatography-Mass Spectrometry (GC-MS) systems, which became readily available and are today indispensable for routine analysis of crude oils and sediment extracts⁽⁶⁾. Relatively different new techniques, such as GC-MS-MS and Supercritical Fluid Chromatography (SFC)-MS have introduced a number of alternative methods for the analysis of stereoisomers and high molecular weight biomarkers.

3. Geochemical Significance of the Various Molecular Classes of Hydrocarbons Found in Sediment Extracts and Petroleum

A comprehensive review of all the areas of biomarker geochemistry which have undergone a number of important reevaluations in the past decade ^(2, 7-10) is beyond the scope of this report. Rather this chapter will essentially comprise an overview of existing data (taken from the above monographs, and only recent references to illustrate trends and developments are included) on those aspects of alkane biomarker distribution which relate to the type of organic matter, the depositional environment, the thermal maturity and indications for biodegradation. Another useful application of biomarkers in oil exploration are the oil-oil and oil-source rocks correlations, as well as the determination of relative migration distances of expelled hydrocarbons. Structures marked throughout the text with Roman numbers are presented in Appendix 1.

3.1. NORMAL ALKANES

n-alkanes are trace constituents of biological lipids. However, these compounds have excellent preservation characteristics and may therefore be regarded as biomarkers. The most common application of *n*-alkanes is to infer the source of the organic material. Input of terrigenous source material is indicated by a strong predominance of high molecular weight odd-numbered alkanes (*n*-C₂₇, *n*-C₂₉ and *n*-C₃₁), which are associated with leaf waxes. Marine algae are known to produce lower molecular weight *n*-alkanes with maximum at *n*-C₁₇, and without any odd or even chain length preference. Freshwater algae synthesize longer chain length *n*-alkanes, with a predominance similar to that in higher land plants. Studies of bacteria have shown them to produce *n*-alkanes in the *n*-C₁₅ to *n*-C₂₈ region with no marked odd/even preference.

The distribution of *n*-alkanes have been used to infer specific depositional environment of source rocks. For example, the occurrence of *n*-alkane distributions with an even-number preference is usually assumed to reflect evaporitic facies or marine carbonate environments ^(10,11). This is probably a function of the highly reducing nature of the depositional environment which causes reduction rather than decarboxylation of the biologically-derived even carbon numbered fatty acids ⁽¹²⁾. The observation of even/odd predominance in well-oxygenated systems has prompted other authors to suggest a possible bacterial autochthonous origin for these alkanes ^(13,14).

Maturity and biodegradation can also influence the distribution of *n*-alkanes. Thus, as maturity increases the odd/even or even/odd predominance decreases. Bacterial degradation of crude oils causes progressive removal of *n*-alkanes beginning from the low molecular weight homologues.

3.2. BRANCHED ALKANES

3.2.1. *Monomethyl branched alkanes*. These compounds occur mainly as the *iso*- (2-methyl) and *anteiso*- (3-methyl) alkanes, and derive from plant waxes (C₂₅-C₃₁ with an

odd chain predominance) or bacteria (C_{13} - C_{19} iso, C_{17} and C_{18} anteiso).

Mid-chain branched alkanes, in particular methyl heptadecanes (C_{18}), with the methyl substituent at C_7 , or C_8 have been proposed as biomarkers of cyanobacteria and hence possibly of hypersaline environments ^(15,16)

3.2.2. Acyclic Isoprenoids. These compounds are known constituents of plants, animal tissues and bacterial cell walls and have been reported in all classes of geological samples. The phytol side chain of chlorophyll-*a* accounts for the widespread occurrence of acyclic isoprenoids in the biosphere. They are chemically formed from various combinations of C_5 isoprene units (I) through three main types of linkages : head-to-tail (the most common, and include compounds such as pristane C_{19} (II), phytane C_{20} (III) and homologues up to C_{45}), tail-to-tail (squalane, perhydro- β -carotane, lycopane, etc), and head-to-head (C_{32} - C_{40} typical of thermophilic and other archaeobacteria).

Isoprenoids, and in particular the ratio of pristane to phytane, have been widely used to obtain information on depositional environments on the premise that both pristane and phytane are derived from phytol. Diagenesis of C_{20} phytol produces by reduction and dehydration in C_{20} phytane in highly reducing conditions, whereas in less anoxic conditions oxidation and decarboxylation prevail yielding C_{19} pristane. However, some important limitations on the use of the pristane/phytane ratio as an indicator for oxygen levels have arisen ^(9,17), and should be taken into consideration before using this parameter.

Since most Recent hypersaline environments are characterised by reducing conditions, the pristane/phytane ratio has also been suggested as an indicator for salinity ⁽¹⁸⁾. Specific acyclic isoprenoids associated with particular environments, such as the regular C_{25} isoprenoid and botryococcane (IV), have been reported by different authors ⁽⁹⁾.

3.3. MONOCYCLIC ALKANES

It is assumed that *n*-alkylcyclohexanes and *n*-alkyl,methylcyclohexanes arise from cyclization of biologically-derived fatty acids ⁽¹⁹⁾. Their distribution in crude oils and sediment extracts follows normally the *n*-alkane distribution with a large odd over even carbon number predominance.

Alkyl cyclohexanes with isoprenoid side chains are probably derived from carotenoids, which are abundant in algae and some higher plants, or are generated from bacterial reworking of previously sedimented acyclic isoprenoids ⁽²⁰⁾. The distribution and catagenesis of cycloalkanes in oils has been recently reviewed ⁽²¹⁾.

3.4. BICYCLIC ALKANES (SESQUITERPENOIDS)

These compounds have been identified in fossil resins, sediments and petroleum ⁽²²⁾. The two main types of bicycloalkanes identified are the drimanes (V) and the eudesmanes (VI). The latter are believed to be derived from eudesmanol, an alcohol found present in higher plants, whereas drimanes are thought to be derived from the degradation of polycyclic alkane precursors in bacteria and appear to be ubiquitous. The large

number of isomers present in the samples also raises the possibility of stereochemical interconversion as a result of diagenesis and maturation.

3.5. TRICYCLIC ALKANES, DITERPENOIDS AND TRICYCLIC TERPANES

The presence of diterpenoid hydrocarbons in fossil fuels and sediments is a very strong indication of a terrigenous input to the oils or source rocks, since these structures are predominant constituents of higher plant resins and supportive tissues, especially in conifers. The skeletal structure types found in fossil fuels consist primarily of derivatives of the abietane (VII), pimarane (VIII) and labdane (IX) series.

Another series of tricyclic alkanes commonly found in marine sediments and crude oils is the homologous series of extended tricyclic terpanes (X) in the range from $C_{19}H_{34}$ to $C_{45}H_{86}$, and possibly higher. They are not reported to be found in terrestrial source rocks or oils derived from terrigenous source material. Different natural precursors, such as the tricyclohexaprenol, formed anaerobically from an ubiquitous cell constituent, hexaprenol, have been proposed for this series ⁽²³⁾.

The tricyclic terpene distribution can be related to the nature of the depositional environment. Thus, oils source from carbonate source rocks usually show a dominant C_{23} homologue ⁽²⁴⁾. On the other hand, several authors have proposed the potential use of tricyclic terpanes as a maturity indicator in the lower maturity levels on the basis of the variation in the relative amount of tricyclic terpanes to hopanes ⁽²⁵⁾, and changes observed in the isomers stereochemistry ⁽²⁶⁾. Tricyclic terpanes are especially useful in correlating nondegraded to biodegraded crude oils since they survive even severe biodegradation processes ⁽²⁴⁾.

3.6. TETRACYCLIC ALKANES

3.6.1. Non-Steroidal Tetracyclic Terpanes. The main types of tetracyclic alkanes found in sediment and crude oils originate from different sources: a) kaurane (XI), beyerane (XII) and phyllocladane (XIII) are produced by diagenesis of tetracyclic alkenes characteristics of conifer resins; b) the series of 4,5-seco triterpanes (XIV) is thought to be formed from plant derived pentacyclic triterpenoids by thermal cracking, and c) the 17,21-secohopanes (XV) and 8,14-secohopanes (XVI) derived from pentacyclic hopanoids by cleavage of the 17(21) and 8(14) bonds respectively, taking place either by microbial activity during early diagenesis or by thermocatalytic degradation of hopanes ⁽²⁷⁾.

Tetracyclic terpanes are usually present in a series from C_{24} to C_{27} . Differences in probable precursors of tetracyclic and tricyclic terpanes makes the ratio of C_{24} tetracyclic terpene over C_{26} tricyclic terpene a source parameter ⁽⁸⁾.

3.6.2. Steroidal Tetracyclanes. Steranes. Steranes commonly found in mature sediments and crude oils are derived via diagenesis from sterols (XVII) which are widely dispersed in plants and microorganisms, with the C_{27} and C_{28} sterols most abundant in marine organisms and the C_{29} sterols in higher plants ⁽²⁸⁾. C_{30} 4-desmethylsterols occur

in marine invertebrates and marine algae ⁽¹¹⁾, and 4-methylsterols are significantly present in dinoflagellates ⁽²⁹⁾.

Generally specific information on the organisms which relies on the position of double bonds and functional groups will be lost, prior to oil generation. However, most of the diagnostic information available from steranes in fossil fuel studies is mainly based on the stereochemical complexity of their basic skeleton, which is often retained and is observed in sediment extracts and oils.

Biomarker maturity determinations are generally based upon changes in steranes and triterpanes ⁽⁷⁾. Sterols generally contain a 5,6 double bond and occur naturally as the 20R epimer with the 14 α (H),17 α (H) configuration. As diagenesis progresses the double bond is hydrogenated and a new epimeric center with a mixture of 5 α (H) and 5 β (H) is formed with a predominance of the 5 α (H) epimer due to its greater thermal stability. As the level of maturity increases the 14 β (H),17 β (H) isomers are formed as a mixture of the 20R and 20S epimers.

Some low molecular weight steranes, such as C₂₁ pregnane and C₂₂ homopregnane (XVIII) have been used as indicators of hypersaline and carbonate environments ^(30,31).

Many parameters involving the complex sterane distribution for source, depositional environment, maturation, migration and biodegradation indicators have been proposed ^(2,8,32). However, some cautions concerning the use of some indicators has been emphasized by different authors ^(33,34). In Table 1 the most widely used parameters are summarized (2)

Diasteranes (XIX) present in oils and source rocks in relatively low abundances are formed by acid-clay-catalyzed rearrangement of regular steranes, and therefore can be used for depositional environment determinations.

3.7. PENTACYCLIC ALKANES

3.7.1. *Hopane-type triterpanes (XX)*. These constitute the group of triterpanes most extensively used in biomarker studies. Their naturally occurring precursors, diploptene and C₃₅ tetrahydrohopane, are widely distributed among bacteria, blue-green algae, some grasses and lichens and several ferns ⁽²⁾.

Diagenesis and maturation of organic material containing the precursors leads to defunctionalization and change of the biological 17 β (H),21 β (H) stereochemistry to the thermodynamically more stable 17 α (H),21 β (H) configuration. At the same time, formation of another series of hopane analogs, known as moretanans (XXI), with the 17 β (H),21 α (H) configuration occurs.

The C₃₁ and higher homologues can occur as either 22S and 22R epimers due to the chiral center at position C₂₂. Increasing maturation leads to mixtures of 22S and 22R (naturally occurring) epimers with an equilibrium ratio of approximately 3:2. The ratio of the C₂₇ 17 α (H)-hopane (Tm), over the C₂₇ 18 α (H) (Ts), more resistant to thermal maturation than Tm, is used as a maturity parameter of oil and source rocks samples.

Most of the samples show the presence of regular hopanes from C₂₇ to C₃₅, with the absence of the C₂₈ homologue. The detection of this compound in a few notable exceptions have been associated with the specific environment of deposition, such as

Table 1.- Summary of biomarkers parameters based on steranes and triterpanes that have been used in petroleum studies, (Philp, 1985).

	Application
* tricyclic terpanes (%)	Source
* change in paraffin concentration plus increase in sterane and triterpane concentration	Migration/Maturation
* $C_{29} + C_{30}$ primary terpanes / $C_{27} + C_{28}$ secondary terpanes	Source/Maturation
* $17\alpha(H)-22,29,30$ -trismorphane (Tm) / $18\alpha(H)-22,29,30$ trismorphane (Ts)	Source/Maturation
* $5\beta(H)$ steranes / $17\alpha(H)$ hopanes	Migration in common sources
* $17\beta(H), 21\beta(H)$ / $17\beta(H), 21\beta(H) + 17\beta(H), 21\alpha(H) + 17\alpha(H), 21\beta(H)$ hopanes	Maturation
* $22R$ / $22R + 22S$ $17\alpha(H), 21\beta(H)$ -homohopanes	Maturation
* $20S$ / $20S + 20R$ $13\beta(H), 17\alpha(H)$ -diacholestane	Maturation
* $24S$ / $24S + 24R$ (20R)-24-methyl- $\alpha\alpha$ -cholestane	Maturation
* $20R$ / $20R + 20S$ -24-ethyl- $\alpha\alpha$ -cholestane	Maturation
* $\alpha\beta\beta$ / $\alpha\beta\beta + \alpha\alpha$ (20R + 20S) 24-ethylcholestane	Maturation
* $\alpha\alpha$ - C_{28} steranes / $\alpha\alpha$ - C_{29} steranes	Source
* $\beta\alpha\alpha$ - C_{27} steranes / $\alpha\alpha$ - C_{29} steranes	Source
* $\beta\alpha\alpha$ (20R) + $\alpha\beta\beta$ (20R) / $\alpha\alpha$ (20R) C_{29} steranes	Migration
* $13\beta(H), 17\alpha(H)$ (20S) / $\alpha\alpha$ (20R) $C_{27} + C_{28} + C_{29}$ steranes	Migration
* $\beta\alpha\alpha$ (20R)- $C_{28} + \alpha\beta\beta$ (20R+20S)- $C_{28} + \beta\beta\beta$ (20R+20S)- C_{29} / $\alpha\alpha$ (20R)- C_{28} steranes	Source
* C_{27} triaromatic steranes / C_{27} triaromatic + C_{28} monoaromatic steranes	Maturation/aromatization
* C_{21} monoaromatic steranes / C_{21} triaromatic + C_{28} monoaromatic steranes	Maturation/bond breaking
* C_{26} triaromatic steranes / C_{20} triaromatic + C_{27} triaromatic steranes	Maturation/bond breaking
* preferential removal of C_{27} -20S diastere over 20R epimer	Biodegradation
* preferential removal of regular steranes over diasteranes	Biodegradation
* $17\alpha(H)$ - C_{30} hopanes / $17\beta(H)$ -($C_{29} + C_{30}$) moretanes	Source rocks by pyrolysis
* $17\alpha(H)/17\beta(H)$ -trismorphanes	Source rocks by pyrolysis

$\alpha\alpha$, $\alpha\beta\beta$, $\beta\alpha\alpha$ refer to the stereochemistry of the H atom at the 5, 14 and 17 positions, respectively, of the regular steranes

mat structures formed by sulphide oxidizing bacteria in upwelling areas (35,36).

In evaporite facies the enhanced reducing character of the environments leads to a greater preservation of the hopane side chain during diagenesis. In hypersaline settings the occurrence of C₃₄ and/or C₃₅ hopanes is characteristic and are found in higher concentrations than the other homohopanes⁽³⁰⁾. A very strong predominance of C₃₁ hopanes has been reported to occur in samples derived from peats and coals. This has been attributed to decarboxylation of C₃₂ hopanoic acids which are abundant in such samples. High concentrations of moretanones have also been noted in them and result from the direct input of moretanol and moretanone into the sediment from land plant sources.

Hopanes having an additional methyl substituent in ring A have been reported by numerous authors to occur in crude oils and sediments, most of them deposited in carbonate and/or hypersaline environments. Summons and Jahnke⁽³⁷⁾ have recently shown that the most commonly reported methylhopanes are 2-methylhopanes. The most significant parameters involving the hopanes are also included in Table 1⁽²⁾.

3.7.2. Non-hopane type triterpanes. Lupanes (XXII), oleananes (XXIII), fernanes (XXIV) and ursanes (XXV) biomarkers characteristic of plant triterpenoids have been frequently found in coals and oils derived from terrigenous source materials. Their precursors are widely distributed in higher plants. C₃₀ bicadinanes (XXVI) found in oils have been shown to be characteristic cracking products of angiosperm fossil resins. The 18 α (H)-oleanane has been observed in a number of deltaic sediments and crude oils related to them^(24,31,38). The biogenic precursors of oleanane are presumed to be oleanene triterpenoids such as β -amyrin, which are associated with highly specialized terrigenous plants.

The origin of gammacerane (XXVII), pentacyclic triterpane, often used as an indicator for salinity, is still unclear. Tetrahymanol, the only pentacyclic triterpenoid found in protozoa and fungus, is the only known potential biological precursor of gammacerane⁽³⁹⁾. As Gammacerane is present in many samples from various environments, its use as a biomarker for salinity is not based on its occurrence, but rather on its relative abundance⁽³¹⁾.

3.8. HEXACYCLIC HOPANOID ALKANES

C₃₁-C₃₅ hexacyclic hopanoid alkanes (XXVIII) have been used as an indicator for anoxic paleoenvironments^(40,41). These authors have suggested that hexacyclic alkanes were derived from bacteriohopanetetrol (C₃₅) precursors through cyclisation of the side chain of extended hopanoids during early diagenesis.

The hexacyclic hopanes are very resistant to bacterial attack and may be very useful for defining palaeoenvironments and biodegradation degree of source rocks and oils.

4. Use of Biomarkers in Oil Shale Geochemistry. Case study of the Puertollano (Spain) Oil Shale

For many years organic-geochemical studies were largely limited to the most economically important organic materials found buried in the Earth, namely coals, oil shales and petroleum. Oil shales have a special geochemical interest both as potential source rocks and as an energy resource in themselves, although most oil shale mining projects are currently non-viable commercially.

Oil shales are a complex group of rocks which were deposited in a wide range of sedimentary environments and have a wide range of largely alginite-dominated maceral assemblages. According to a recent classification of oil shales as regards to their relative abundance of macerals⁽⁴²⁾, they overlap with both coals and petroleum source rocks so that any classification of oil shales has to take these other types into account. In this context the use of biomarker distribution as an alternative to the precise classification of the different types of oil shales might be taken into consideration.

Bitumens are present in some oil shales such as the Green River Formation of the U.S.A. and the Irati Formation of Brazil. The bitumens can impregnate and may partially replace some macerals⁽⁴³⁾. Past work on the biomarkers in oil shale has involved characterization of the biomarkers in bitumen and determination of the manner in which their quantity varied with depth and other characteristics of the shale within a given core. Many outstanding works on the application of biomarkers for source rocks-oil correlations have been carried out on these sedimentary rocks⁽⁴⁴⁾.

To show the utility for oil shale geochemistry of the biomarker approach, we have taken as specific case study the Puertollano deposit, the most important in the Iberian Peninsula, which until now has been only partially characterized from the geochemical viewpoint⁽⁴⁵⁾.

Table 3 shows the composition of the aliphatic extractable hydrocarbon fraction of this deposit. Experimental methods were similar to those recently used for characterization of peat and coal deposits⁽⁴⁶⁾.

The hydrocarbon distribution in the Puertollano Oil Shale is dominated by *n*-alkanes, *n*-alkylcyclohexanes, *n*-alkyl,methylcyclohexanes and mid-chain monomethyl alkanes. The cyclohexanes showed a distribution very similar to that of *n*-alkanes suggesting a common origin. Triterpenoid distributions showed a major contribution of bacterially derived hopanoids. The compounds identified comprised C₂₇-C₃₅ hopanes (no C₂₈), C₂₇-C₃₂ 8,14-secohopanes, C₂₉-C₃₂ ring-D aromatized 8,14-secohopanes, C₃₂-C₃₅ benzohopanes and a C₃₁ hexacyclic saturated hopane. The conifer and angiosperm derived material is expressed in two different groups of diagenetic compounds.

Diterpenoid compounds as abietane, norabietane, simonellite, retene and the sesquiterpenoid cadalene are characteristics of the conifer resins, whereas the terpanes with oleanane and ursane skeleton are characteristics of angiosperms. It is concluded from these results that the Puertollano oil shale has been formed in a lacustrine environment with significant input of higher plant derived organic material.

Some parameters, such as a) the abundance of the C₂₉ and C₃₀ primary terpanes relative to the other members of the series, b) the ratio of C₃₀ 17β(H),21α(H)-moretane

Table 2. Main series of compounds detected in the saturated fraction of the Puertollano Oil Shale extracts.

Series	Range	Main component	o/oo ¹	Structure ²
n-alkanes	C ₁₃ -C ₃₉	C ₂₃	420	
iso-alkanes	C ₁₆ -C ₃₂		20	
anteiso-alkanes	C ₁₆ -C ₃₂		20	
mid-chain methyl alkanes	C ₁₆ -C ₃₂		40	
acyclic isoprenoids	C ₁₅ -C ₂₀	C ₁₉	70	I, II
n-alkyl-cyclohexanes	C ₁₃ -C ₂₈		80	
methyl-n-alkyl-cyclohexanes	C ₁₈ -C ₂₈		80	
bicyclic terpanes	C ₁₄ -C ₁₆	C ₁₆	40	V, VI VII, VIII, IX XI-XVII
diterpanes	C ₁₉ -C ₂₀		35	
tricyclic triterpanes	C ₁₉ -C ₂₈	C ₂₃	40	
tetracyclic terpanes	C ₂₄	C ₂₄	10	
tetracyclic 17, 21 secohopanes	C ₂₄	C ₂₄	10	XV XVI
8,14 secohopanes	C ₂₇ -C ₃₀		5	
id. ring-D aromatized	C ₂₇ -C ₃₁		5	
steranes	C ₂₇ -C ₂₉	C ₂₉	10	XVII-XIX XX
pentacyclic hopanes	C ₂₇ -C ₃₅	C ₃₀	100	
benzohopanes	C ₃₂ -C ₃₅	C ₃₂	10	
hexacyclic hopanes	C ₃₁	C ₃₁	5	XXVIII

(1) relative abundances

(2) Roman numbers refers to the structures shown in Appendix 1

to 17 α (H),21 β (H)-hopane (0.37), c) the predominance of Tm over Ts, and d) the predominance of the biologically occurring $\alpha\alpha$ R isomers over the maturation induced $\beta\beta$ -isomers in the mixture of regular and rearranged steranes are indicative of the low maturity level of this oil shale and the absence of biodegradation.

5. Future Work on Biomarkers

The promising future seen for biomarkers by Eglinton two decades ago ⁽⁴⁷⁾ in basis to the development of a number of applications has been largely realized. Today, now that many of the molecular methods and findings have been adsorbed by the industry (common use of the so-called "biomarker strategy" in exploration studies), the interest in biomarkers has again moved to new applications and extensions of the basic molecular organic geochemical approach. Thus, biomarkers have been applied in the study of recent sediments, to marine sciences, archaeological chemistry, biogeochemical ecology, biomolecular paleontology, molecular stratigraphy, etc.

Important progress in biomarkers geochemistry is expected from future investigations on nonhydrocarbon polar fractions and in particular sulphur biomarkers having well established structural relationships with known precursors ⁽⁴⁸⁾. It has been noted, however, that the "natural sulphurization" during the early stages of diagenesis may lead to selective removal of the specific hydrocarbon biomarker precursor, and therefore to biased palaeoenvironmental reconstruction ^(49,50)

Of especial interest at present is the use of biomarkers in environmental and pollution studies, since these compounds provide information on the chemical and biological degradation of organic molecules in modern environments. Improved abilities to monitor and control waste disposal from modern demands, ranging from the disposal of sewage to improved understanding of landfill waste disposal should be included. Biomarkers have also been useful for fingerprinting the source of oil spills and other organic wastes and tracing the source of this pollution.

A particular goal is to link the patterns of the geological record to the behaviour of the atmosphere, increasing our understanding of the fundamental causes of climate change. An outstanding precedent of these investigations is the use of biomarkers from certain marine algae for paleoclimatic reconstructions based on their ability to synthesize long chain unsaturated ketones (C₃₇-C₃₉) with the degree of unsaturation depending on the ocean water temperature ⁽⁵¹⁾.

The interest in biomarkers depends on the distribution of biochemical precursors in presently living organisms. It should be emphasized, however, that knowledge of the distribution of different precursors in contemporaneous organisms is still insufficient. Progress in this field and consequently in biomarkers geochemistry are dependent on the development and improvement of new technologies and novel analytical schemes to study the complex mixtures of chemicals in geological samples.

Good examples for the new frontiers in biomarker geochemistry are the recent identification of biomarkers of high molecular weights (>C₄₀) by using high-temperature capillar gas chromatography ⁽⁵²⁾, and the development of reliable

instruments for determination of carbon isotopic compositions of individual components of oils and rock extracts⁽⁵³⁾, which seem to be a useful parameter in the correlation of oil to oil or oil to source rock and as indicator to identify the precursor of biomarkers.

5. Acknowledgement

I thanks the Spanish Direccion General de Investigacion Cientifica y Tecnica (Project PB91-0074) for subsidizing this work. Dr.J.C. Del Rio gave invaluable encouragement and advice.

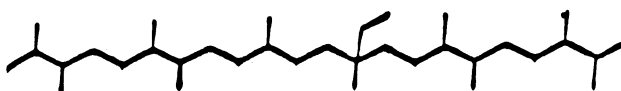
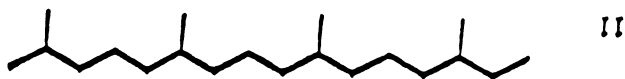
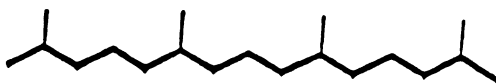
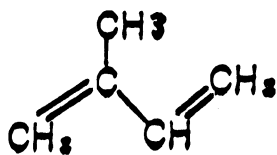
6. References

- 1 . G. EGLINTON and M. CALVIN, *Sci. Am.*, 1967, **216**, 32.
- 2 . R.P. PHILP, *Fossil Fuel Biomarkers. Applications and Spectra*, Elsevier (1985) and references therein.
- 3 . C.G.BLANCO, J.G.PRADO, M.D.GUILLEN and A.G. BORREGO, *Org. Geochem.*, 1992, **18**, 313.
- 4 . J.C. MONIN, D. BARTH, M. PERRUT, M. ESPITALIE and B. DURAND, *Org. Geochem.*, 1988, **13**, 1079.
- 5 . K.H. ALTGELT and T.H. GOUW (eds), *Chromatography in Petroleum Analysis*, Marcel Dekker (1979).
- 6 . C.M. WHITE, *Introduction to mass spectrometric techniques for fossil fuel analysis* in this volume
- 7 . A.S. MACKENZIE, *Advances in Petroleum Geochemistry*, J.Brooks and D.H. Welte (eds), Academic Press (1984).
- 8 . R.B. JOHNS, *Biological Markers in the Sedimentary Record*, Elsevier (1986).
- 9 . R.P. PHILP and C.A. LEWIS, *Ann. Rev. Earth Planet Sci.*, 1987, **15**, 363.
- 10 . J.M. MOLDOWAN, P. ALBRECHT and R.P. PHILP, *Biological Markers in Sediments and Petroleum*, Prentice-Hall Inc.(1992) and references therein.
- 11 . J.M. MOLDOWAN, W.K. SEIFERT and E.J. GALLEGOS, *Am.Assoc.Petrol. Geol. Bull.*, 1985, **69**, 1255.
- 12 . B. TISSOT, R.PELET, J.ROUCACHE and A.COMBA, *Advances in Organic Geochemistry 1975*, R. Campos and J. Gofii (eds), ENADIMSA (1977).
- 13 . J. GRIMALT, J. ALBAIGES, H.T. AL-SAAD and A.A.Z. DOUABUL, *Naturwissenschaften*, 1985, **72**, 35.
- 14 . M.NISHIMURA and E.W. BAKER, *Geochim. Cosmochim. Acta*, 1986, **50**, 299.
- 15 . J. SHIEA, S.C. BRASSELL and D.M. WARD D.M., *Org. Geochem.*, 1990, **15**, 223.
- 16 . N.ROBINSON and G.EGLINTON, *Org. Geochem.*, 1990, **15**, 291.
- 17 . H.L. ten HAVEN, M. BAAS, M. KROOT, J.W. de LEEUW, P.A. SCHENCK and J. EBBING, *Geochim. Cosmochim. Acta*, 1987, **51**, 803.

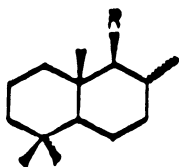
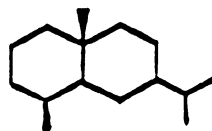
18. J.S.SINNINGHE DAMSTE, H.L. ten HAVEN, J.W. DE LEEUW and P.A. SCHENCK, *Advances in Organic Geochemistry*, D.Leythaeuser and J. Rullkötter (eds), Pergamon Press, (1986).
19. M.G.FOWLER,P.ABOLINS and A.G.DOUGLAS, *Org. Geochem.*,1986, **10**, 815.
20. A. BARBE,J.O.GRIMALT and J. ALBAIGES,*Naturwissenschaften*,1988,**75**, 624.
21. Y.V. KISSIN, *Org. Geochem.*, 1990, **15**, 575.
22. B.R.T. SIMONEIT,In: *Biological Markers in the Sedimentary Record*, R.B.Johns (ed), 43-100, Elsevier (1986).
23. F.R. AQUINO NETO, A. RESTLE, J. CONNAN, P. ALBRECHT and G. OURISSON, *Tetrahedron Lett.*,1982, **23**, 2027.
24. J.E. ZUMBERGE, *Org. Geochem.*,1987, **11**, 479.
25. C.M. EKWEOZOR and O.P. STRAUZS, In: *Advances in Organic Geochemistry* , M.Bjoroy (ed), 746-766, John Wiley (1983).
26. F.R. AQUINO NETO, J.N. CARDOSO, R. RODRIGUES and L.A.F. TRINDALE, *Geochim. Cosmochim. Acta*, 1986, **50**, 2069.
27. J.M. TRENDEL, A. RESTLE, J.CONNAN and P.ALBRECHT, *J.Chem.Soc.Am. Chem. Comm.*, 1982, 304.
28. W. Y. HUANG and W.G.MEINSCHEN, *Geochim. Cosmochim. Acta*, 1979, **43**, 739.
29. R.E. SUMMONS, S.C.BRASSELL, G.EGLINTON, E.EVANS, R.J.HORODISKY, N.ROBINSON and D.M.WARD, *Geochim. Cosmochim. Acta*, 1988, **52**, 2625.
30. H.L. ten HAVEN, J.W. DE LEEUW and P.A. SCHENCK,*Geochim. Cosmochim. Acta*,1985, **49**, 2181.
31. M.R. MELLO, P.C.CAGLIANONE, S.C.BRASSELL and J.R. MAXWELL J.R.,*Mar. Petr. Geol.*,1988, **5**, 205.
32. O. GALLANGO and F. CASSANI F., *Org. Geochem.*, 1992, **18**, 215.
33. H.L. ten HAVEN, J.W. de LEEUW, T.M. PEAKMAN and J.R. MAXWELL, *Geochim. Cosmochim. Acta*,1986, **50**, 853.
34. M.G. STRACHAN, R. ALEXANDER, E.A.SUBROTO and R.I. KAGI, *Org. Geochem.*,1989, **14**, 423.
35. P.J.GRANTHAM and A.G.DOUGLAS,*Geochim. Cosmochim. Acta*,1980,**44**, 1801.
36. B. KATZ and L.W. ELROD, *Geochim. Cosmochim. Acta*,1983, **47**, 389.
37. R.E.SUMMONS and L.L.JAHNKE, *Geochim. Cosmochim. Acta*,1990, **54**, 247.
38. Z. CZOCHANSKA, T.D.GILBERT, R.P.PHILP, C.M.SHEPPARD, R.J.WESTON, T.A. WOOD and A.D.WOOLHOUSE,*Org. Geochem.*,1988, **12**, 123.
39. M.I. VENKATESAN, *Org. Geochem.*,1988, **12**, 13.
40. J. CONNAN and D. DESSORT, *Org. Geochem.*,1987,**11**,103.

41. G.G.L. RINALDI, V.M. LEOPOLD V.M. and C.B. KOONS C.B., In: *Biochemical Biomarkers*, T.F. Yen and M. Moldowan (eds), Harwood Academic (1988).
42. A.C. COOK and N.R. SHERWOOD, *Org. Geochem.*, 1991, 17, 211.
43. M.F. SINGLETON, A.K. BURNHAM, J.H. RICHARDSON and J.E. CLARKSON, In: *Geochemistry and Chemistry of Oil Shales*, F.P. Miknis and J.F. McKay (eds), ACS Symposium Series 230, 433-456, *Am. Chem. Soc.*, (1983).
44. F.P. MICKNIS and J.F. MCKAY, *Geochemistry and Chemistry of Oil Shales*, ACS Symposium Series 230, *Am. Chem. Soc.*, (1983).
45. M.A. KRUGE and I. SUAREZ-RUIZ, *Fuel*, 1991, 70, 1298.
46. J.C. DEL RIO, F.J. GONZALEZ-VILA and F. MARTIN, *Org. Geochem.*, 1992a, 18, 67.
47. B.P. TISSOT and D.H. WELTE, *Petroleum Formation and Occurrence*, Springer Verlag, (1984).
48. J.S. SINNINGHE DAMSTE and J.W. DE LEEUW, *Org. Geochem.*, 1990, 16, 1077.
49. M.E.L. KHONEN, J.S. SINNINGHE DAMSTE and J.W. de LEEUW, *Nature*, 1991, 349, 775.
50. J.S. SINNINGHE DAMSTE and J.W. de LEEUW, *Fuel Processing Tech.*, 1992, 30, 109
51. S.C. BRASSELL, G. EGLINTON, I.T. MARLOWE, U. PFLAUMANN and M. SARNTHEIN, *Nature*, 1986, 320, 129
52. J.C. DEL RIO, J. ALLEN and R.P. PHILP, *Org. Geochem.*, 1992b, 18, 541.
53. K.H. FREEMAN, J.M. HAYES, J.M. TRENDEL and P. ALBRECHT, *Nature*, 1990, 343, 254

APPENDIX 1

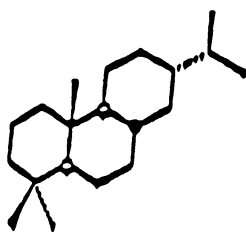


IV

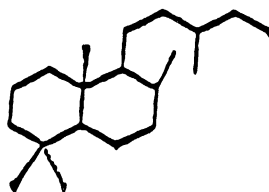
R = CH₃, C₂H₅

V

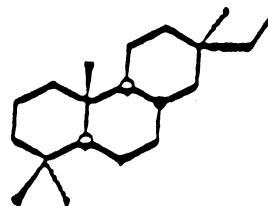
VI



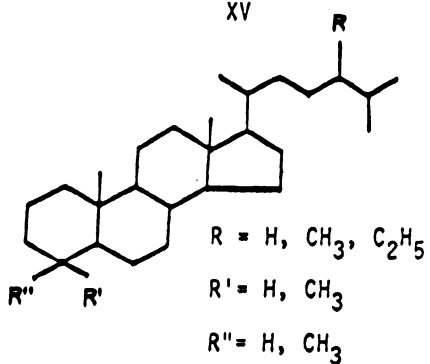
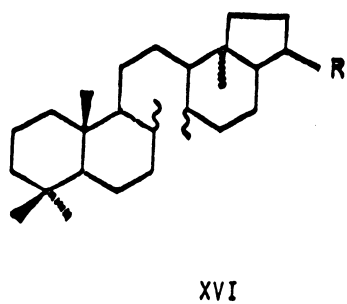
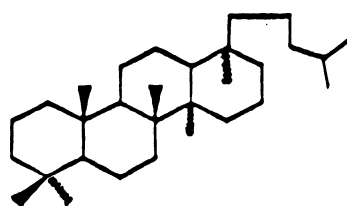
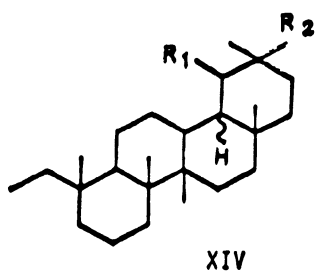
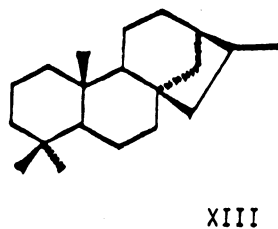
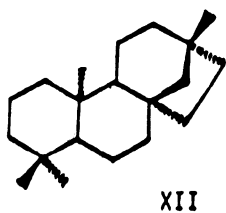
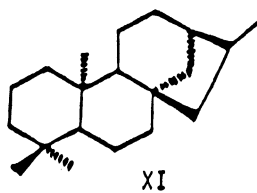
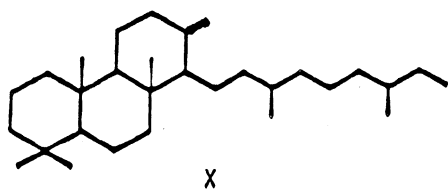
VII



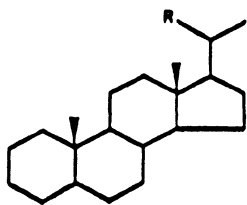
VIII



IX

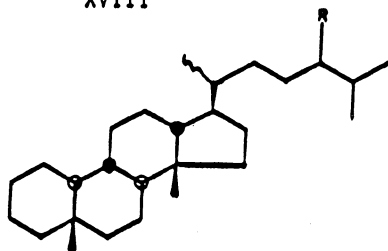


XVII

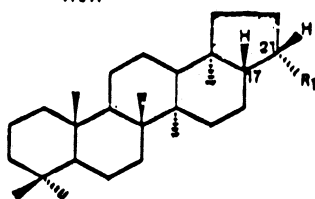


XVIII

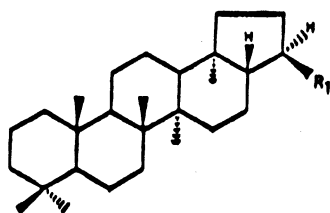
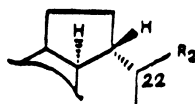
R = H

R = CH₃

XIX

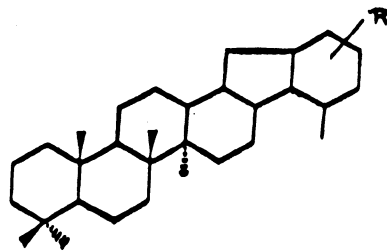
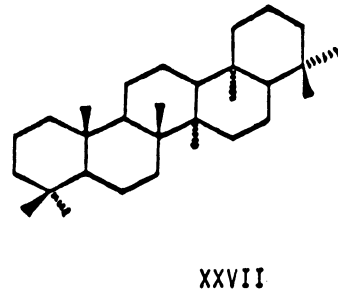
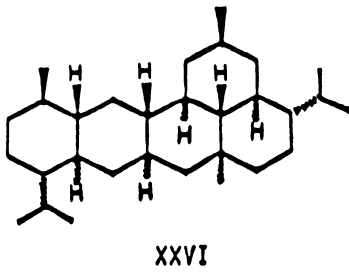
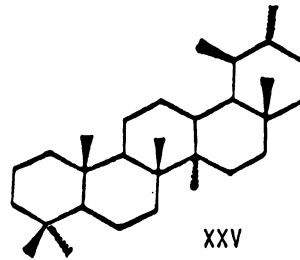
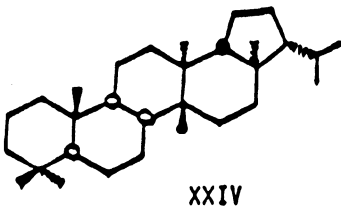
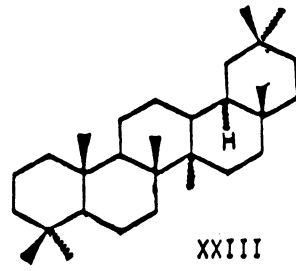
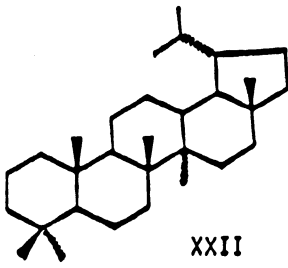


XX



XXI





$R = H, CH_3, C_2H_5, C_3H_7$

SOLID-STATE ^{13}C NMR IN OIL SHALE RESEARCH: AN INTRODUCTION WITH SELECTED APPLICATIONS

FRANCIS P. MIKNIS
Western Research Institute
Box 3395
Laramie, WY 82071
USA

ABSTRACT. An introduction to solid-state ^{13}C NMR techniques and their applications to oil shale research are discussed. Techniques include cross polarization and magic-angle spinning with high-power decoupling, single pulse excitation, dipolar dephasing, and sideband suppression at high magnetic fields. The quantitative reliability of solid-state ^{13}C NMR measurements is discussed also. Results from recent studies on coals show that single pulse methods give more reliable carbon aromaticities than those obtained using cross polarization. This is because a greater percentage of the total carbons are observed in the single pulse experiment than in the cross polarization experiment. Similar comparisons for oil shales have not been made. However, because oil shales generally are more aliphatic than coals, differences in measured carbon aromaticities and percentages of carbons observed may not be as serious a problem for oil shales. Selected applications of solid-state ^{13}C NMR techniques to oil shale resource evaluation, oil shale conversion, and structure are presented.

1. Introduction

Oil shales are fine-grained sedimentary rocks that contain organic matter, which upon heating can be converted to liquid shale oils. The shale oils can then be refined into a slate of products that is similar to that obtained from refining of petroleum crude oil. There are two fractions of organic matter in oil shale: 1) bitumen, which is that fraction that is soluble in organic solvents; and 2) kerogen, which is that portion of the organic matter that is insoluble in common organic solvents. Generally, kerogen constitutes the major portion of the organic matter (~90% or greater), and its insolubility is one reason why an oil shale must be heated to produce liquid products. For an introduction and review of oil shales and kerogen, the reader is referred to books that are available (1-6). Also, Hutton (this monograph) describes methods for classifying oil shale.

Because of kerogen's insolubility, it has been very difficult to obtain information about the chemical structure and composition of kerogen. Compositional data can be acquired after first carrying out laborious and time-consuming preparation of kerogen concentrates. The development of solid-state NMR techniques of cross polarization (CP) and magic-angle spinning (MAS), circa 1976, changed this situation dramatically. With solid-state NMR techniques, information can now be

obtained about the carbon structure of the kerogen in oil shale without the need for preparation of kerogen concentrates. Some of the first CP/MAS ^{13}C NMR spectra that were published were of coals (7,8) and oil shales (9,10), materials that are largely insoluble and for which few good techniques existed at the time to probe the carbon structure of these fossil fuels.

In this chapter, an introduction to solid-state NMR and its applications to the study of oil shales are presented. This chapter does not include a comprehensive review of the literature, nor does it concern itself with the more exotic NMR techniques that might have some application, but are best left in the hands of NMR experts. The objectives are to introduce the concepts of solid-state NMR to the researcher who wishes to acquire an understanding of some of the concepts and terminology that are most often encountered in the literature. While most solid-state NMR studies of fossil fuels have been concerned with coals, in this chapter examples have been taken from oil shale studies, where appropriate, to illustrate these concepts. Omission of relevant literature is an oversight of the author, and is purely unintentional. A number of books (11-13,) symposia proceedings (14-16), and reviews (17-19) have been written. These should be consulted for more comprehensive discussions of solid-state NMR techniques applied to fossil fuels materials.

2. NMR in Solids

In most forms of spectroscopy, sensitivity and resolution are primary concerns. This is particularly true for the observation of ^{13}C NMR spectra in solids such as oil shales. Because the ^{13}C isotope is ~ 1% naturally abundant NMR sensitivity is already low. Coupled with the fact that a "rich" oil shale might contain only 10-15 wt% organic matter, the remaining being mineral matter, it becomes evident that signal averaging must be employed in order to observe an NMR signal. There are also other factors that must be considered for observation of NMR in solids as described in the next sections.

The pursuit of sensitivity and resolution in the solid-state has led to a variety of NMR techniques that are now available to the oil shale researcher. The birth of these techniques is attributable to the development of cross polarization by Pines, Gibby and Waugh (20), coupled with magic-angle spinning (21). The combination of these techniques solved a number of the problems associated with sensitivity and resolution of ^{13}C NMR in solids. Cross polarization overcomes some of the problems associated with sensitivity while magic-angle spinning overcomes some problems of resolution.

There are three major problems that must be overcome in order to acquire NMR spectra that provide useful information about the carbon structure of the organic matter in oil shales. These are: 1) the ^1H - ^{13}C dipole-dipole interaction, 2) the chemical shift anisotropy, and 3) the long-spin lattice relaxation times in solids. Problems 1) and 2) need to be overcome to improve spectral resolution, 3) needs to be overcome to improve sensitivity.

2.1 HIGH POWER DECOUPLING

In solids, the major source of line broadening for ^{13}C is the dipole-dipole interaction between a nearby proton, ^1H , and the ^{13}C nucleus. The interaction is of the form

$$H_{\text{loc}} \propto \mu_{\text{h}} (1 - 3\cos^2\theta) / r^3 \quad (1)$$

where μ is the magnetic moment of the proton, r is the internuclear distance between the proton and the ^{13}C nucleus, and θ is the angle between r and the applied magnetic, H_0 . The ^{13}C nucleus experiences a magnetic field given by the above expression that adds to or subtracts from the main field, H_0 . The strength of the interaction depends on the third power of the separation between the nuclei, so that carbons that have protons attached feel a strong dipolar interaction. The net result of this interaction is a ^{13}C NMR spectrum that is very broad and featureless because of the large number of protons that would be strongly coupled to the carbons in a solid.

The line broadening caused by ^1H - ^{13}C interactions is largely eliminated by irradiating the ^1H nuclei with a strong radio frequency field at their Larmor (resonance) frequency. This induces rapid transitions between the proton energy levels, i.e. spin flips, so that the protons cannot interact strongly with the ^{13}C nucleus. Thus, the ^{13}C nuclei do not feel the strong dipolar interaction because they have been decoupled from the protons. Hence, the term high-power decoupling

2.2 MAGIC-ANGLE SPINNING

While high-power proton (^1H) decoupling removes the dipolar line broadening, the ^{13}C NMR spectra of solids are still much broader than solution spectra of the same material. This residual broadening is due to chemical shift anisotropy (CSA), and without its removal, the spectral lines exhibit anisotropic line shapes that prevent resolution of carbon types that are useful for structural studies.

The chemical shift anisotropy arises from the nonspherical electron density around the ^{13}C nuclei, and is particularly prominent for aromatic and carbonyl ($\text{C}=\text{O}$) carbon types. These carbon types experience different shieldings of the magnetic field depending whether the bond axes are parallel or perpendicular to the external magnetic field. For polycrystalline or amorphous materials all orientations are possible, including these two extremes.

Magic-angle spinning is the one known method that can remove the broadening due to chemical shift anisotropy, while preserving the isotropic chemical shift that is observed in solution. This is accomplished by orienting the sample at an angle of 54.7° with the external magnetic field. In the theoretical description of chemical shift anisotropy, the broadening is proportional to a term, $3\cos^2\theta - 1$. The angle, 54.7° , makes this term zero, hence removing the broadening from chemical shift anisotropy. However, simply orienting the sample at this angle in the magnetic field is not sufficient. The sample must then be rotated about this axes at a rate comparable to the magnitude of the CSA broadening, which for aromatic and

carbonyl carbons can be the entire width of the chemical shift range, i.e. ~ 200 ppm. This has important consequences on the strength of the magnetic field used to observe ^{13}C signals in solids such as oil shales. For example, for a magnetic field strength of 2.3T, equivalent to a ^{13}C NMR frequency of 25 MHz, 200 ppm corresponds to 5,000 Hz. This means that to remove the CSA the sample must be spun about the magic-angle axis at the rate of 5,000 revolutions per second! For a field strength twice this (50 MHz ^{13}C frequency), the spinning rate would have to be twice as great, i.e. 10,000 Hz. Although such rates are achievable, most CP/MAS ^{13}C NMR spectra of oil shales and coals have been acquired using field strengths of 1.4 to 2.3T and spinning rates of ~ 3 to ~ 4 kHz. Increases in sensitivity that might be gained at higher fields are offset by the use of large-volume spinners at the lower fields (22).

The effect of magic-angle spinning on the ^{13}C NMR spectra of oil shales is shown in Figure 1. The improvement in resolution is clearly evident, particularly for shales that have a sizable aromatic component. This is because aromatic carbons have a larger chemical shift anisotropy than the aliphatic carbons. In the absence of spinning, the aromatic carbons yield broad anisotropic line shapes. Note

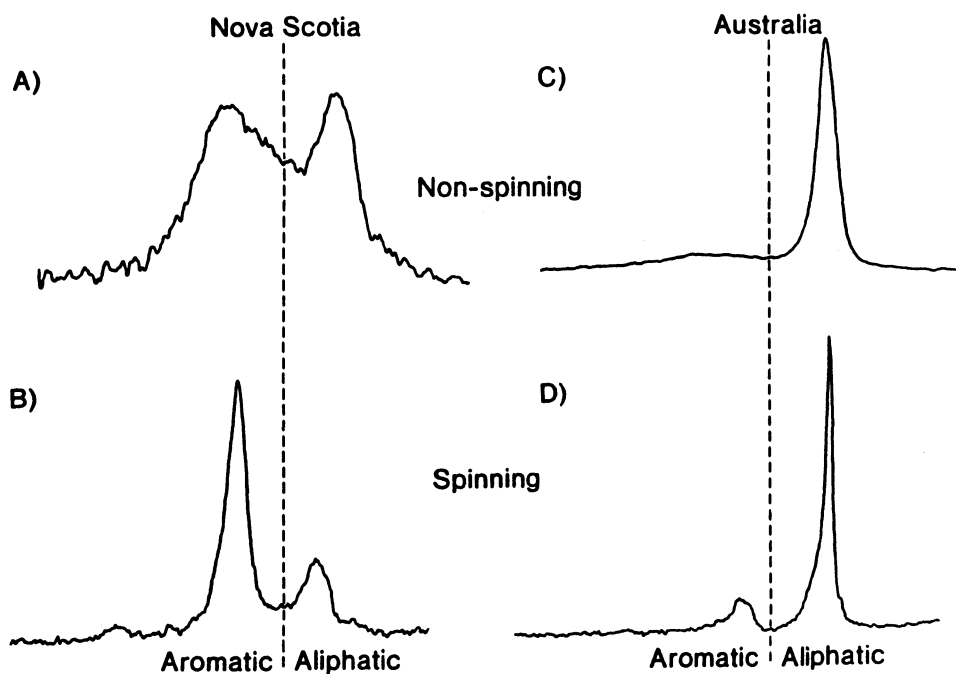


Figure 1. Effect of magic-angle spinning on the ^{13}C NMR spectra of oil shales.

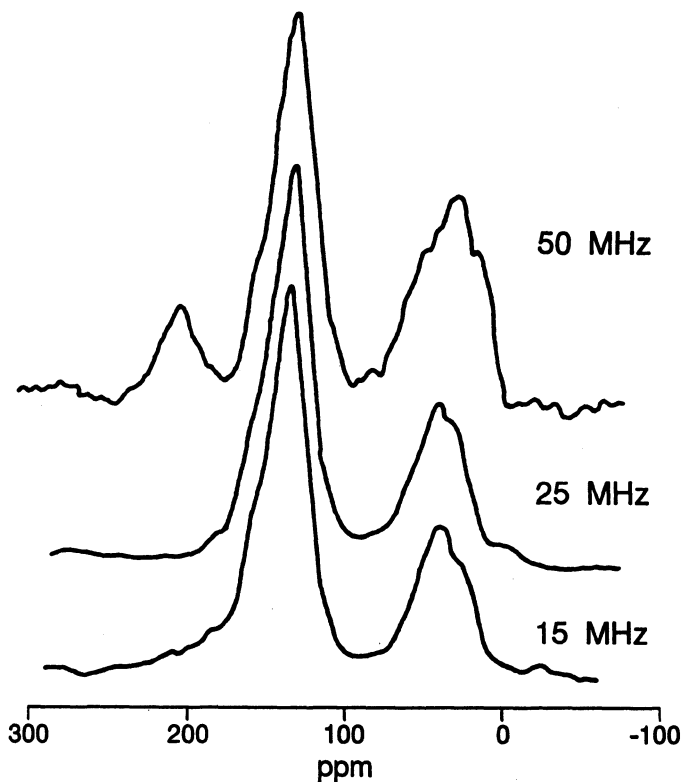


Figure 2. Comparison of NMR spectra of Powhatan coal obtained at 15.1, 24.1 and 50.3 MHz. (Reprinted from ref. 23 by permission of the Amer. Chem. Soc.)

also that for the spinning spectra, the maximum intensity of the aromatic band shifts to the isotropic value which lies between the perpendicular and parallel components of the chemical shift tensor.

If the sample is not rotated fast enough to remove the chemical shift anisotropy, artefacts known as spinning sidebands, are introduced in the spectra that can interfere with the measurements of carbon aromaticities. An example of the effect of sidebands on CP/MAS spectra of a coal for different field strengths is shown in Figure 2(23). All spectra were recorded at a spinning rate of 4.2 kHz. The aromatic carbon sidebands occur at ~ 300 and ~ -30 ppm in the 15 MHz spectrum, and do not interfere with the aliphatic signal intensity. At 25 MHz the high field sideband appears as a shoulder in the aliphatic carbon region near 0 ppm. However, at 50 MHz, the high field sideband is under the aliphatic carbon envelope, and thus gives a non-representative aliphatic carbon resonance. The sidebands are symmetrical about the respective aromatic carbons giving rise to the signal, so that the position of the interfering sideband under the aliphatic envelope can be inferred from the spectrum.

2.2.1. Techniques for sideband removal. A number of ingenious pulsed techniques have been devised to eliminate sidebands from high field spectra so that "normal" CP/MAS spectra are generated(24). These are referred to as PASS(Phase Alternated Sideband Suppression) and TOSS(Total Sideband Suppression) techniques. An example of the use of TOSS to suppress sidebands from the aromatic carbons in Illinois No. 6 coal is shown in Figure 3(25). Two different spinning rates were used to acquire the CP/MAS spectra. The spectra were recorded at 50 MHz so that a 10 kHz spinning speed would be required to obtain spectra free of spinning sidebands. The apparent advantages of using TOSS to suppress sidebands is evident. However, the spectra are misleading because of the issue of the quantitative reliability of these spectra (11,22,26). Advantages and disadvantages of the sideband removal pulse sequences have been discussed by Axelson (11).

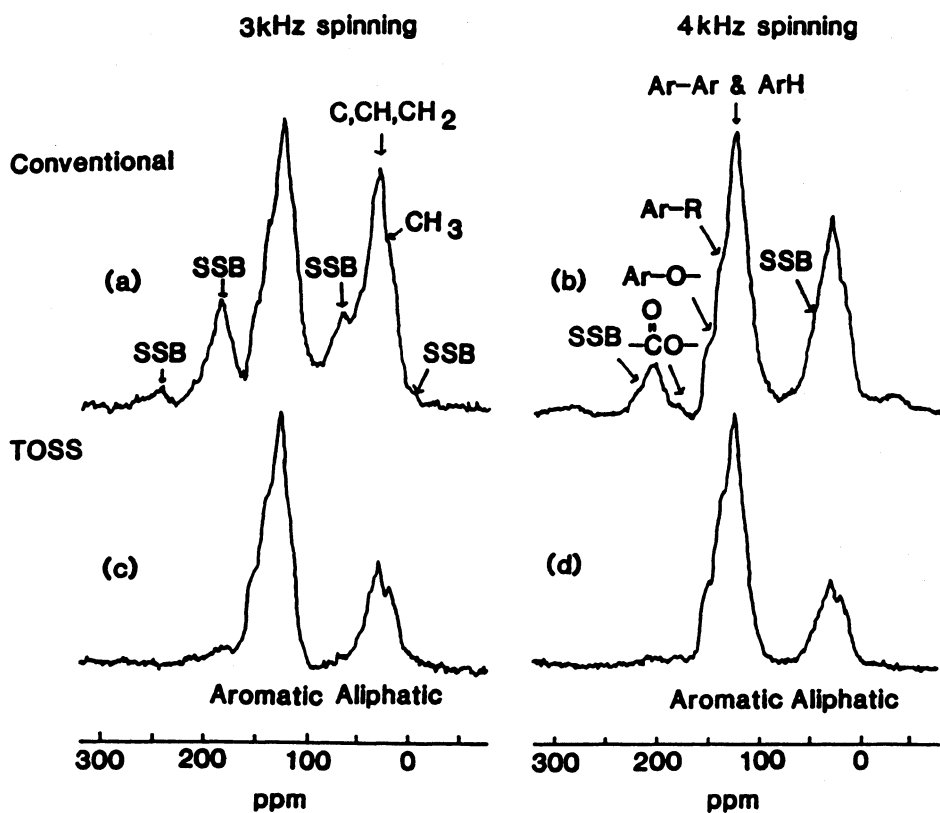


Figure 3. Use of TOSS to suppress sidebands in Illinois No. 6 coal. (Reprinted from ref. 25 by permission of the Amer. Chem. Soc.)

The main reason for acquiring NMR spectra of oil shales and coals at higher magnetic fields is that, in principle, greater resolution and sensitivity should be achievable at the higher fields. In practice, this need not be the case as demonstrated in Figure 2, which shows comparable resolution for 15 and 50 MHz spectra, respectively. Oil shale spectra, especially those of raw shales typically yield only broad aliphatic and aromatic components so that higher fields may not provide any benefits in resolution. There is a gain in sensitivity in going to higher fields (23), but this is partially offset by the fact that smaller sample sizes must be used to achieve the higher spinning rates needed to remove the sidebands. The use of large-volume spinners (22,27,28) at lower fields compensates for the gains in sensitivity at higher fields. The use of large-volume spinners is increasing, mainly because single pulse spectra can be acquired in reasonable times using these spinners. For quantitative work, single pulse methods have been recommended (22,29,30).

2.3 CROSS POLARIZATION

Because ^{13}C has a low natural abundance, NMR measurements on this nucleus require signal averaging. The spin lattice relaxation time, T_1 , determines how rapidly a single pulse ^{13}C NMR experiment can be repeated. The rule of thumb is to repeat the experiment every $3T_1$ to $5T_1$. Suppose the T_1 of a ^{13}C nucleus is 2 min. The single pulse experiment would be repeated every 6 to 10 min. If 1000 signals must be accumulated to obtain a reasonable signal to noise ratio (S/N), the total experiment time would be between 100 and 167 hrs! Fortunately cross polarization overcomes the problems of the long T_1 's and consequent limited sensitivity.

Cross polarization NMR relies on the presence of an abundant spin system (^1H) to enhance the observation of a signal from a dilute spin system (^{13}C). The idea is to transfer polarization (hence signal intensity) from the abundant ^1H spins to the dilute ^{13}C spins. The CP experiment consists of four basic timed sequences of radio frequency (rf) pulses (Figure 4). The left portions of Figure 4 represent the experimental timing sequence and the right portions depict what happens to the nuclei in the sample under the action of the pulses. The four-part procedure consists of (1) polarization of the ^1H spin system, (2) spin-locking in the rotating frame, (3) establishment of ^{13}C - ^1H contact and (4) observation of the ^{13}C free induction decay (FID).

The sample is "prepared" by applying a 90° pulse of intensity $H_{1\text{H}}$ at the ^1H resonance frequency. The action of this pulse rotates the magnetization 90° into the $x'y'$ plane, along y' . Immediately after the 90° pulse, a 90° phase shift is applied to the field, $H_{1\text{H}}$ to bring it colinear with the ^1H magnetization. This causes the protons to precess about $H_{1\text{H}}$ at a frequency, $\omega_{\text{H}} = \gamma_{\text{H}}H_{1\text{H}}$. During the proton spin-lock, a second radio frequency field, $H_{1\text{C}}$ is applied at the ^{13}C resonance frequency. Although there may not be substantial ^{13}C magnetization initially, the ^{13}C nuclei in the sample will precess about $H_{1\text{C}}$ at a frequency, $\omega_{\text{C}} = \gamma_{\text{C}}H_{1\text{C}}$. By adjusting the power levels so that $\omega_{\text{H}} = \omega_{\text{C}}$, then the frequencies of the oscillating components will be the same, i.e. $\omega_{\text{C}} = \omega_{\text{H}}$. By making $\omega_{\text{C}} = \omega_{\text{H}}$, a means is

established to efficiently transfer magnetization from the abundant ^1H spins to the dilute ^{13}C spin system. This transfer is called cross polarization. The Hartman-Hahn condition is maintained for a time, τ_{cp} , the contact time so that a significant buildup in ^{13}C magnetization (dotted line, Figure 4c) is available for detection as a ^{13}C free induction decay (dotted line, Figure 4d). The fourth part of the CP experiment is to terminate the ^{13}C pulse and observe the free induction decay, while maintaining the ^1H field for decoupling (Figure 4d). The entire four-part procedure is repeated many times until a suitable signal-to-noise ratio for ^{13}C is obtained. The resultant FID is then Fourier transformed to give the more common frequency domain spectrum. For solids, the $^1\text{H} - ^{13}\text{C}$ is far more efficient than ^{13}C spin-lattice relaxation so that a CP experiment can be repeated at intervals shorter than $3-5T_1$. For oil shales pulse repetition rates of 1 s and contact times of 1 ms are typical.

3. Dipolar Dephasing

Solid-state ^{13}C NMR spectra of oil shales, obtained by CP/MAS with high-power decoupling are broad because of the multitude of resonances from the different carbon types found in these complex materials. A number of approaches have been taken to improve the resolution of solid-state NMR of fossil fuels. Discussions can be found in the work of Sullivan (23,31), reviews by Miknis (18), Davidson (19) and Wilson et al.(32), and the book by Axelson (11). Such techniques include variable temperature studies, variable frequency studies, mathematical enhancements and deconvolution techniques, and relaxation rate methods. The most popular method of enhancing solid-state NMR spectra is a relaxation rate method called dipolar dephasing (DD)(33), or sometimes referred to as interrupted decoupling (31,34). Wilson et al. (32) have reviewed the exploitation of relaxation in CP NMR of fossil fuels.

Dipolar dephasing is a variation of cross polarization and the timing sequence is shown in Figure 5. The variation is the switching off of the ^1H decoupler for a time, t_1 , after the cross polarization contact time. During t_1 , the signals from different carbon types decay at different rates depending on the strength of the $^1\text{H} - ^{13}\text{C}$ dipolar interactions. the characteristic time for this decay is T_2 , the spin-spin relaxation time. Carbons that are directly attached to hydrogen (primary, secondary, and tertiary carbons) experience strong $^1\text{H} - ^{13}\text{C}$ interactions and decay more rapidly than carbons without attached hydrogen (quaternary carbons). When the decoupler is switched on after a time, t_1 , the resultant signal is due primarily to quaternary carbons. However, methyl groups (CH_3) are not completely suppressed because of their rapid rotation in the solid state and appear in the aliphatic carbon signal. These carbons can be distinguished from the other quaternary aliphatic carbons on the basis of chemical shifts.

In the DD experiment signals are recorded for a series of dephasing times, t_1 , in order to establish the relaxation behavior of the system. Generally, the signal decay is characterized by two components, a rapidly and a slowly relaxing component. Murphy et al. (33) found that the rapid decay is best characterized by

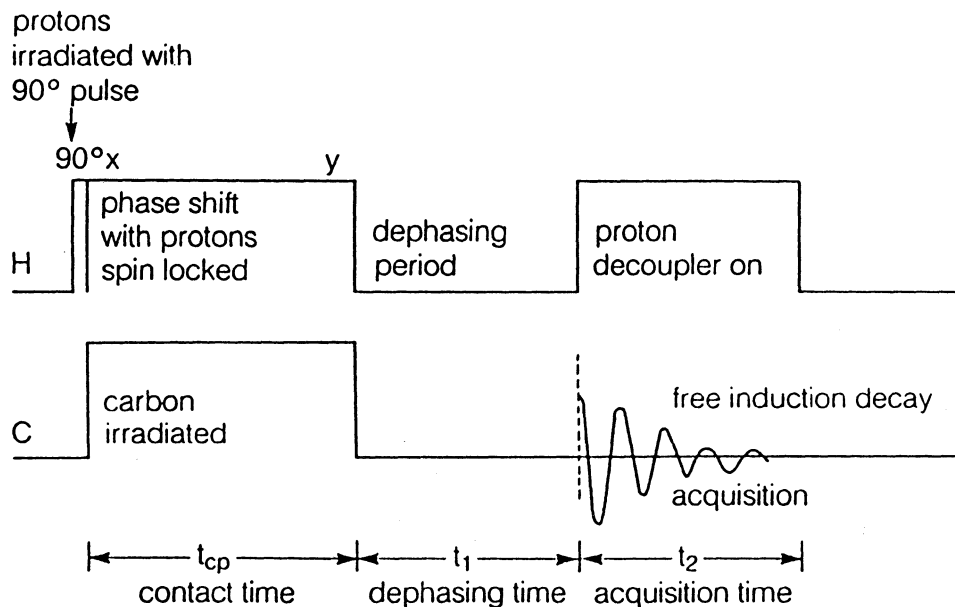


Figure 5. Timing sequence for dipolar dephasing experiment.

a Gaussian or second-order exponential function, and the slow decay is best fit with a Lorentzian or first-order exponential function (Figure 6).

In order to determine the amounts of protonated and nonprotonated carbons, the intensities of the various carbons must be extrapolated to zero dephasing time, $t_1 = 0$. The mathematical expression describing the signal decay is given by,

$$I(t_1) = I_g^0 \exp(-0.5(t_1/T_{2g})^2) + I_l^0 \exp(-t_1/T_{2l}) \quad (2)$$

where the subscripts, g and l refer to Gaussian and Lorentzian components, respectively. At $t_1 = 0$, $I(0) = I_g^0 + I_l^0$, which is the signal intensity for a normal CP spectrum.

For a sufficiently long $t_1 (>40 \mu s)$ the observed signal is due to the Lorentzian component, so that equation (2) reduces to,

$$I(t_1) \sim I_l^0 \exp(-t_1/T_{2l}) \quad (3)$$

By extrapolating this curve to zero time, the contribution of nonprotonated carbons, I_l^0 , to the total signal is obtained. The contribution of protonated carbons is obtained by difference,

$$I_g^0 = I(t_1=0) - I_l^0 \quad (4)$$

Some applications of dipolar dephasing to oil shales are discussed in the next section.

4. Quantitation

4.1 CROSS POLARIZATION

The issue of quantitation in cross polarization has been recognized from the beginning of its application to fossil fuels (11,19,35-42), has been debated (43), and is still a concern in solid-state NMR (22,29,30). The main concerns are whether all carbons are observed equally in the CP experiment, and whether the fraction of carbons observed at true signal intensity are a faithful enough representation so as

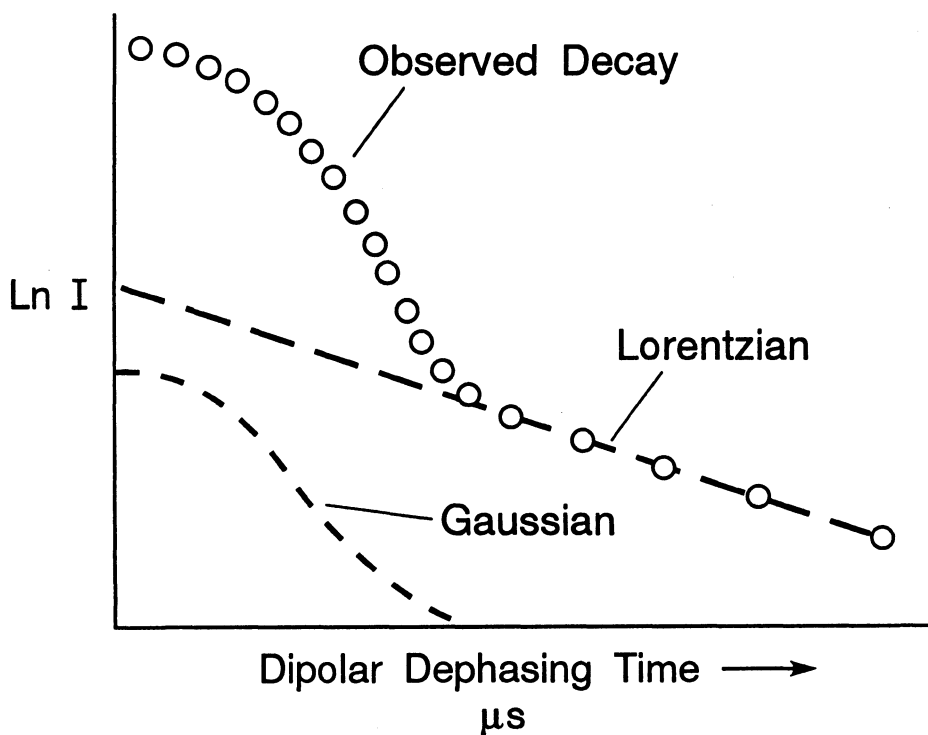


Figure 6. Schematic representation of the Gaussian-Lorentzian two-component decay in a dipolar dephasing experiment. (Reprinted from ref. 11 by permission of the Canadian Government Publishing Centre.)

to be able to ignore the small loss of signal from carbons that are not observed. Other concerns relate to such things as sample heterogeneity, spinning sidebands, unpaired electrons, magic-angle spinning, and the recycle delay. Wind et al. (22) have recently reviewed the problems associated with quantitation of ^{13}C NMR in carbonaceous solids.

The buildup of signal during cross polarization depends on two relaxation processes (Figure 7), the cross polarization transfer time, T_{CH} , and the proton spin-lattice relaxation time in the rotating frame, $T_{1\rho}$. Figure 7 shows that the ^{13}C signal intensity builds exponentially at a rate characteristic of T_{CH} , while at the same time the signal is being truncated by another exponential function, $T_{1\rho}$. The analytic form of the curve in Figure 7 is,

$$M_t = M_0 \exp(-\tau_{\text{CP}} / T_{1\rho}) (1 - \exp(b\tau_{\text{CP}} / T_{\text{CH}})) \quad (5)$$

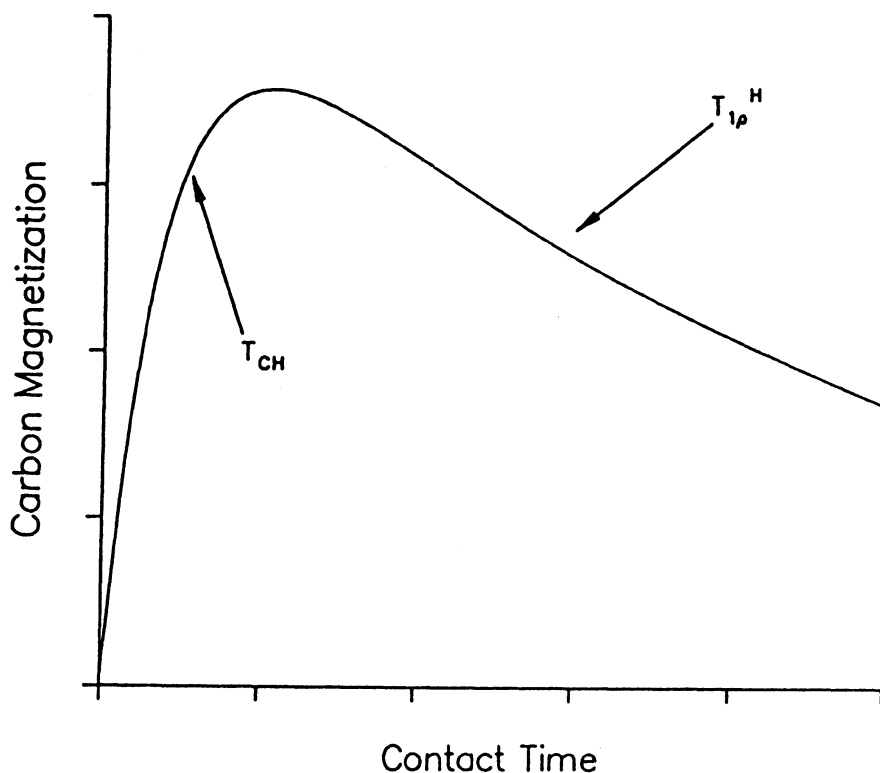


Figure 7. Idealized behavior of the carbon magnetization as a function of the experimental contact time in the cross polarization experiment. (Reprinted from ref. 35 by permission of the Amer. Chem. Soc.)

where $b = 1 - T_{CH}/T_{1\rho}$. The condition $T_{CH} \ll \tau_{CP} \ll T_{1\rho}$ would be the ideal situation. Instrumentally, the contact time, τ_{CP} , should be set at the time that correspond to the maximum in the signal intensity.

Questions of quantitation arise because different carbon types have different T_{CH} and $T_{1\rho}$. Generally, T_{CH} depends on the number of protons attached to the carbons. Thus, aliphatic carbons, aromatic carbons, and carboxylate carbons, for example, should all have different T_{CH} 's. By observing the signal at a single contact time, the true signal intensity of all the carbon types may not be observed, in which case, non representative carbon distributions would be measured. To overcome this problem, CP/MAS spectra should be recorded at different contact times in order to construct curves such as Figure 7, for each carbon type (35). By extrapolating these curves to zero time, the correct signal intensity of each carbon type is obtained, from which the true carbon type distributions can be obtained.

In practice, generating carbon magnetization curves at different contact times can be time consuming. Wilson et al. (44) compared aromaticities for coaly source rocks from the Brent group (North Sea), acquired at a 1 ms contact time, with aromaticities obtained by varying the contact between 10 μ s and 8 ms, and calculating the true intensities by curve-fitting. In seven of eight cases, there was excellent agreement between aromaticities determined by the two methods. They concluded that a contact time of 1 ms could be used with confidence for source rock studies. These conditions are probably acceptable for oil shales, because oil shales are generally aliphatic in nature.

Internal standards can be mixed with oil shale and coals to determine the percentage of carbons observed in CP and single pulse NMR measurements. Hexamethyl benzene has been used successfully (35). An excellent reference material is tetrakis(trimethyl silyl)silane (TKS)(45, 46). Furthermore, treatment with samarium (II) iodide selectively reduces the free radical content which can lead to an increase in the percentage of observable carbon (45,47). For example, treatment of Wyodak subbituminous coal with samarium (II) iodide has been shown to increase the percentage of observable carbons by 27 %, leading to an increase in the carbon aromaticity of ~10 % from 0.66 to 0.73.

4.2 SINGLE PULSE EXCITATION

Single pulse excitation (SPE), also referred to as Bloch decay, can be employed as an independent check on the quantitative reliability of CP/MAS aromaticity measurements. In these experiments, the NMR signal is observed after a 90° pulse using magic-angle spinning and high-power decoupling. The SPE experiments do not enjoy the sensitivity advantage of cross polarization; consequently, they require much longer times to record a spectrum of suitable quality. The signals from SPE experiments arise from different relaxation mechanisms than those in the CP experiment. Therefore, agreement between aromaticities from the two measurements suggest that both measurements are observing the same amounts of carbon, even though the relaxation mechanisms for signal detection are different. In SPE experiments, delay times should be ~5 times the longest T_1 in order to observe all the carbons at full magnetization.

SPE experiments, as checks on the reliability of CP measurements of coals and oil shales, have been employed for some time (32,48,49). However, such measurements were made without the use of spin counting techniques for quantitating the amounts of carbon observed in a CP and SPE experiment. Recent work (29,30,35-37) has demonstrated that generally more carbon is observed in SPE than in CP experiments on coals. The main reason is that paramagnetic centers cause the $T_{1\rho}$ of the protons to relax too quickly for efficient cross polarization to be achieved. Usually, this is more of a problem with aromatic carbons. However, the relationship between aromaticities and observable carbon is not straightforward (Table 1). For example, Bloch decay measurements detect more carbon and generally give higher aromaticities than CP measurements. Yet, the aromaticities observed by CP agree fairly well with SPE values, even though considerably less carbon is observed in the CP experiment. A similar trend was noted by Franz et al. (29), with the greater discrepancies appearing in the aromaticities of low rank coals. Love et al. (30) have also found that SPE measurements combined with dipolar dephasing gave higher values of nonprotonated aromatic carbons than CP with dipolar dephasing.

With regard to oil shales, quantitative comparisons between CP and SPE experiments have not been done. However, because oil shales are generally aliphatic materials, a greater percentage of the total carbon should be observed in oil shales than in coals. Carbon aromaticities of most oil shales should probably lie between the resinite and sporinite values in Table 1. Also, because of the overall lower percentage of aromatic carbons in an oil shale, incomplete observation would not be as big a factor in the measured aromaticity and CP measurements should be reliable.

Table 1. Carbon Aromaticities and Percentage of Carbon Observed in Single Pulse and Cross Polarization Experiments^a

Sample	Aromaticity		% Carbon obsd.	
	CP	SP	CP	SP
resinite	0.16	0.15	105	100
sporinite	0.56	0.57	90	90
vitrinite (Illinois)	0.70	0.73	38	59
fusinite	0.82	0.92	26	43
lignite	0.55	0.58	55	65
Illinois hvC bituminous	0.67	0.67	56	73
Oklahoma mv bituminous	0.81	0.84	40	70

^a Source: modified from Botto et al., Energy & Fuels, 1, 173 (1987).

5. Selected Applications

As mentioned earlier, CP/MAS measurements on coals (7,8) and oil shales (9,10) were among some of the first published applications of the techniques to solids. The main impetus for this was that the CP/MAS techniques provided information about the organic carbon distribution in intractable solids such as coals and oil shales. In addition, the measurements are direct and non destructive, and can be applied to whole rock samples without the prior need to prepare organic concentrates. As with coals, the major parameter obtained by CP/MAS is a measurement of the carbon aromaticity, i.e., the fraction of total carbon that is aromatic. The fraction of aliphatic carbon is obtained also by integration of the appropriate region of the NMR spectrum.

5.1 OIL SHALE RESOURCE EVALUATION

The quality of the organic matter in oil shale largely determines its potential to produce oil upon heating. CP/MAS ^{13}C NMR has proven useful for oil shale resource evaluation because these techniques provide a direct measurement of the carbon distribution (quality) of an oil shale. Examples of CP/MAS ^{13}C NMR spectra of oil shales from different worldwide deposits are shown in Figure 8. These range from highly aliphatic to highly aromatic. Aliphatic carbons are hydrogen rich compared to aromatic carbons. Therefore, oil shales that have a highly aliphatic carbon fraction produce a greater fraction of liquids upon heating than do oil shales that have a highly aromatic carbon (hydrogen deficient) structure.

A number of studies have shown that the aliphatic carbon content of an oil shale correlates with the potential oil yield determined by the Fischer assay(50-55). The aromatic carbon content has also been shown to correlate with the carbon remaining after pyrolysis (53-55,58). A correlation between aliphatic carbon and volatile matter is shown in Figure 9. Coals of rank lignite to bituminous and oil shales of different depositional environments are included in the sample set (53). For the coals, volatile matter is obtained from the proximate analyses. For oil shales, volatile matter is the sum of the oil and the gas determined by Fischer assay. Although the oil shale data are obtained at 500 °C, and the coal volatile matter at 950 °C, the correlation is very good, considering the extreme variation in carbon structure and carbon contents of the samples comprising the sample set. The larger variations are attributed to low rank coals which evolve substantial amounts of CO_2 . These carbons would not be expected to correlate with aliphatic carbons because the source of the CO_2 carbon is probably the carboxylate carbons. It is significant that, despite the continuum of organic matter types from widely different, source materials and depositional environments, a single correlation can be used to evaluate an aspect of the thermal decomposition of fossil fuels.

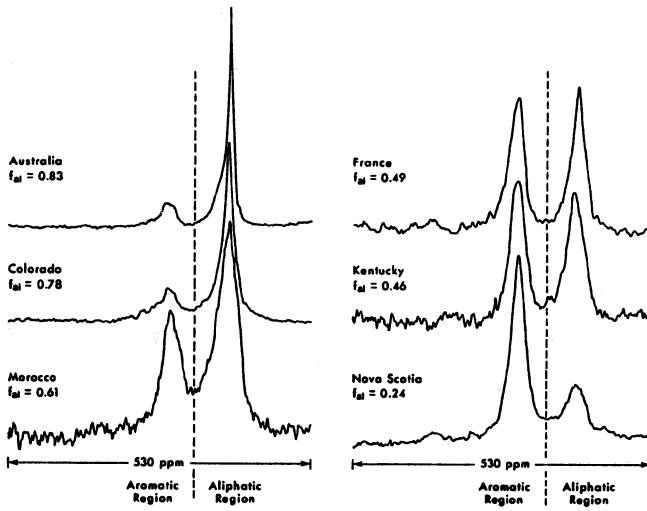


Figure 8. Examples of CP/MAS ^{13}C NMR spectra of oil shales from different worldwide deposits.

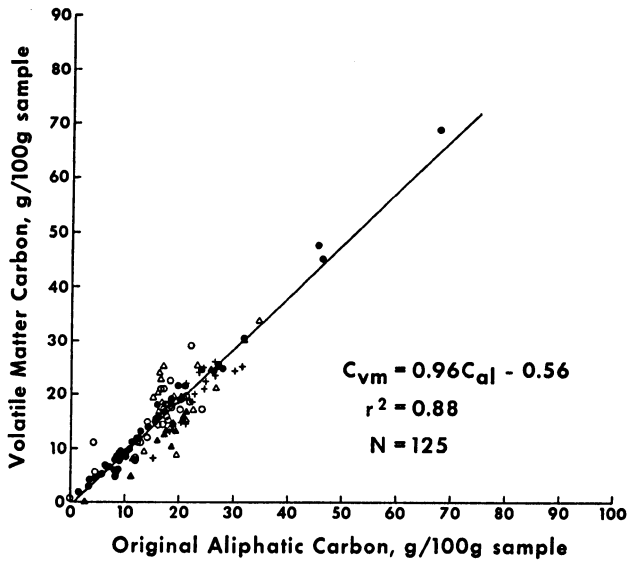


Figure 9. Correlation between aliphatic carbon and volatile matter for coals and oil shales.

5.2 OIL SHALE CONVERSION

The combination of solid- and liquid-state NMR with elemental analyses and mass balance data provides a powerful methodology to gain insight into some of the chemistry that occurs during oil shale conversion. For example, during pyrolysis there is a net increase in the total aromatic carbon in the products (oil plus residue) over that of the starting material. The increase comes from aromatization of the aliphatic carbon moieties and the associated release of light, high hydrogen content aliphatic species. By combining solid- and liquid-state NMR measurements with elemental and mass balance data, the extent of aromatization during pyrolysis can be determined (54,59-61).

Hershkowitz et al. (59) were the first to quantify the increase in the aromatic carbon formed during pyrolysis of Colorado oil shale. Their experiments were conducted at a slow heating rate under high pressure (2600 kPa) N_2 or H_2 , up to $600^\circ C$, followed by a 10 min soak period at this temperature. In a N_2 atmosphere, the total aromatic carbon in the products increased by 83% over that in the raw shale. In H_2 the increase was only 17%. In addition, 87% of the raw shale carbon was recovered in the oil when heated under H_2 , compared to 67% under N_2 . Burnham and Happe (60) also observed an increase in aromatic carbon of about 83% in their pyrolysis studies of Green River oil shale at heating rates of 1 to $720^\circ C/hr$ to $500^\circ C$.

The increase in aromatic carbon during isothermal pyrolysis of a Colorado and a Kentucky oil shale is shown in Figure 10. The increase in aromatic carbon is 29 and 17% for the Colorado and Kentucky oil shale, respectively. An interesting feature of the data in Figure 10 is that the aromatization reaches its maximum value fairly early during thermal decomposition. The Kentucky oil shale, which is an aromatic shale, reaches its limiting value earlier than the Colorado oil shale. Similar results have been observed during coal pyrolysis (61). Thus, aromatization of the aliphatic moieties appears to be a facile chemical reaction. It is not possible from the data to determine whether the aromatization reactions occur directly in the residue or produced oils. However, if the aromatization of aliphatic carbons occurs mostly in the solid oil shale, then these reactions represent an oil loss mechanism. By understanding the kinetics and mechanisms of these reactions, it may be possible to devise methods for preventing their occurrence, thereby enhancing the oil yields.

5.3 STRUCTURE STUDIES

By its nature, a CP/MAS ^{13}C NMR spectrum provides information about the carbon functionalities of an oil shale. However, oil shales contain mostly mineral matter (>~85 %) and usually the spectra consist mostly of a broad aliphatic and a broad aromatic band. For detailed studies of carbon structure, NMR spectra should be acquired on kerogen concentrates which are prepared by removing the mineral matter with HCL/HF treatment. The effects of acid treatment on the NMR spectra of a Colorado and a Kentucky oil shale are shown in Figure 11. Carbonate minerals, if present, are removed by HCL; silicates by HF treatment. Spectra of

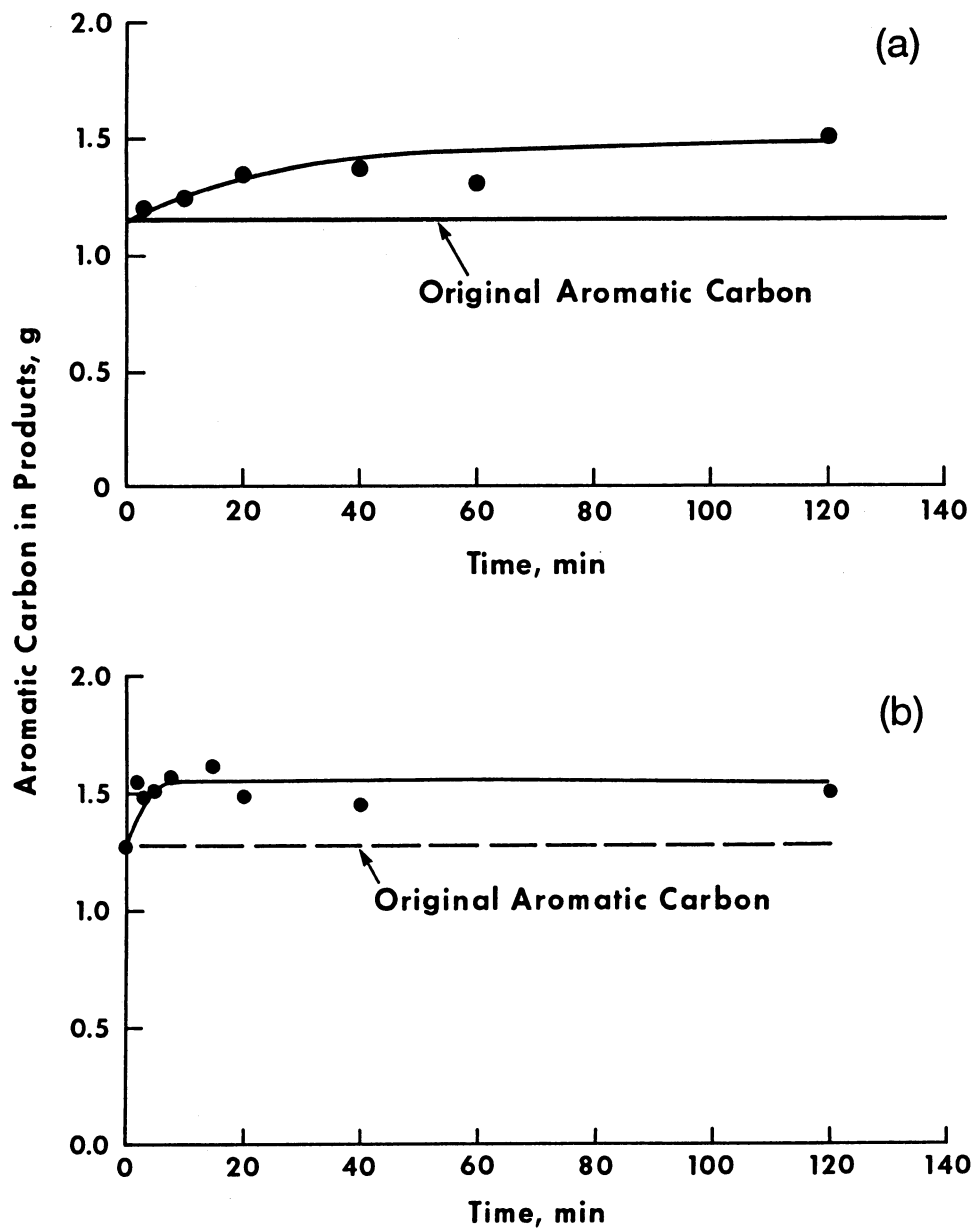


Figure 10. Total aromatic carbon in oil shale conversion products versus temperature at 425°C. a) Colorado oil shale, b) Kentucky oil shale.

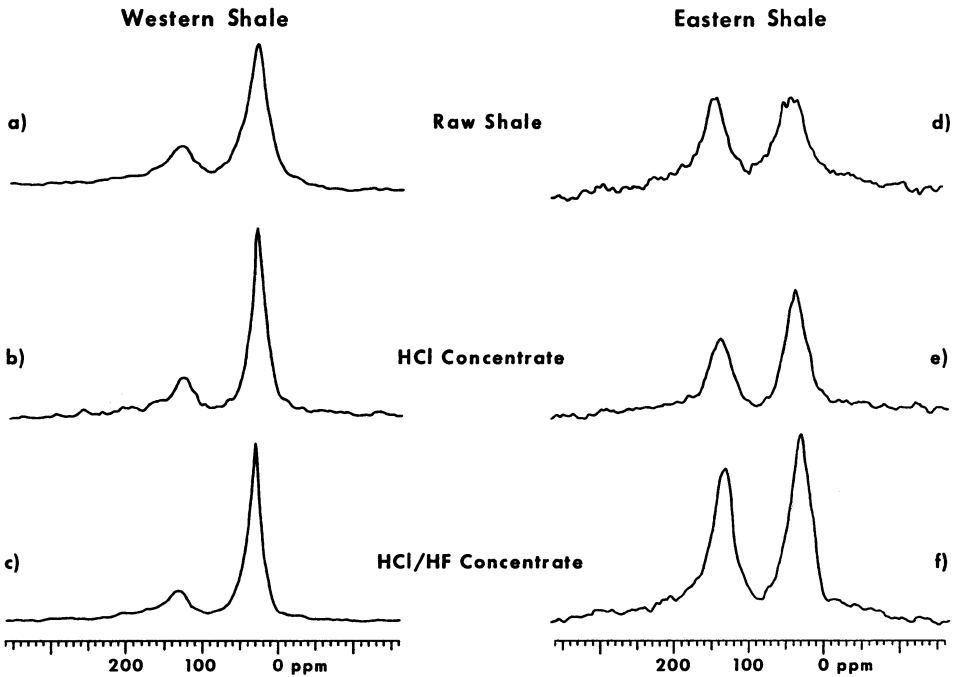


Figure 11. Effects of acid treatment on the CP/MAS ^{13}C NMR spectra of oil shales.

kerogen concentrates are always sharper than those of raw shale. Even simple washing with HCl improves the quality of the spectra of oil shales (28), particularly spent shales (54).

Schmitt and Sheppard (62) used dipolar dephasing techniques to derive structural parameters for a subbituminous coal, and a Colorado, Tennessee and a Kentucky oil shale. Their measurements were obtained on raw shales. Differences in carbon structure among the oil shales were revealed as were some similarities between the eastern shales and the coal (Table 2). The data in Table 2 illustrate the type of carbon center information provided by dipolar dephasing.

Trewhella et al. (63) used curve fitting and dipolar dephasing techniques to determine the amount and types of carbons in a Green River Formation oil shale kerogen. A peak synthesis procedure, based on fourteen representative carbon functionalities was used to derive an average structure for the kerogen. Their analysis showed the kerogen to be composed of long chain aliphatic structures and polycondensed saturated ring structures, which although known from other measurements, were not quantifiable without the use of solid-state NMR.

Solum et al. (64) have used normal CP/MAS, variable contact time and dipolar dephasing to derive a set of 12 parameters related to the carbon skeletal structure of coal. The same procedure is applicable to oil shale. Variable contact time

Table 2. NMR Data and Calculated Results for Coal and Shale Samples^a

	Wyodak Coal	Green River Shale	Chatta- nooga Shale	New Albany Shale
NMR data (Relative areas)				
Total aromatic C	65	16	43	43
Quaternary aromatic C	46	12	32	28
Methyl plus quaternary aliphatic C	12	34	26	17
Carbon centre (mole fractions)				
Methyl	16	13	11	25
Aliphatic CH and CH ₂	21	59	38	34
Quaternary aliphatic	0	11	7.8	0
Aromatic CH	19	4.2	11	14
Quaternary aromatic	45	12	32	27
Methyls per aromatic ring	1.5	4.9	1.6	3.7
Quaternary aromatics per ring	4.2	4.4	4.5	3.9
Minimum aliphatic chain length	2.2	7.0	5.1	2.2
Aliphatic chain length per methyl	2.4	6.3	5.1	2.2

^a Source: Schmitt and Shephard, Fuel, 63, 1241 (1984).

experiments are performed to correct the aliphatic and aromatic signal intensities for relaxation effects.

Using the twelve carbon functionality parameters, a number of structural parameters can be calculated, such as the aromatic cluster size, the attachments per cluster, and the molecular weight of the cluster.

6. Acknowledgment

The author gratefully acknowledges support of this work by the U.S. Department of Energy under Cooperative Agreement DE-FC21-86MC11076.

7. References

1. Yen T.F. and G. V. Chilingarian eds., Oil Shale, Elsevier, New York, 1976.
2. Breger I.A., Organic Geochemistry, Pergamon Press, London, 1963.
3. Durand B., ed, Kerogen, Editions Technip, Paris, 1980.

4. Eglinton G. and M.T.J. Murphy, Organic Geochemistry, Springer-Verlag, New York, 1969.
5. Tissot B.P. and D.H. Welte, Petroleum Formation and Occurrence, Springer-Verlag, New York, 1978.
6. Pelet R. in Petrakis L. and J.P. Fraissard, eds, Magnetic Resonance, Introduction, Advanced Methods, and Applications to Fossil Energy, NATO ASI Series C, 124, D. Reidel Pub. Co., Dordrecht, Netherlands, 1984, pp 219-233.
- 6a Miknis F.P. and J.F. McKay, eds, Geochemistry and Chemistry of Oil Shales, ACS Symp. Series 230, Am. Chem. Soc. Washington, DC, 1983 .
7. VanderHart D.L. and H.L. Retcofsky, Fuel, 55, 202, (1976).
8. Bartuska V.J., G.E. Maciel, J. Schaefer, and E.O. Stejskal, Fuel, 56, 354, (1977).
9. Resing H.A., A.N. Garroway, and R.N. Hazlett, Fuel, 57, 450, (1978).
10. Miknis F.P., and D.A. Netzal, in Magnetic Resonance in Colloid and Interface Science, H.A. Resing and C.G. Wade, eds., ACS Symp. Ser. 34, Am. Chem. Soc., Washington, DC, 1976, Ch. 16.
11. Axelson D.E, Solid State Nuclear Magnetic Resonance of Solid Fossil Fuels, Multiscience Publications Ltd., CANMET and Canadian Government Publishing Centre, 1985.
12. Fyfe C.A., Solid State NMR For Chemists, CFC Press, Guelph, Ontario, Canada, 1983.
13. Wilson M.A., NMR Techniques and Applications in Geochemistry and Soil Chemistry, Pergamon Press, New York, 1987.
14. Petrakis L. and J.P. Fraissard, eds, Magnetic Resonance, Introduction, Advanced Methods, and Applications to Fossil Energy, NATO ASI Series C, 124, D. Reidel Pub. Co., Dordrecht, Netherlands, 1984.
15. Wershaw R.L. and M.A. Mikita, eds., NMR of Humic Substances and Coal, Lewis Publishers, Chelsea, MI, 1987.
16. R.E. Botto and Y. Sanada, eds., Magnetic Resonance of Carbonaceous Solids, Adv. Chem. Ser. 229, Am. Chem. Soc., Washington, DC, 1993.
17. Miknis F.P., Magn. Reson. Rev., 7, 87, (1982)
18. Miknis F.P., in Y. Yurum, ed., New Trends in Coal Science, NATO ASI Series C, V244, Kluwer Academic Publishers, Boston, 1988, pp117- 158.
19. Davidson R.M., Nuclear Magnetic Resonance Studies of Coal, IEA COal Research, London, 1986, Report No. ICTIS/ TR32
20. Pines A., M.G. Gibby, and J.S. Waugh, J. Chem. Phys., 54, 569 (1973)
21. Schaefer J. and E.O. Stejskal, J. Am. Chem. Soc., 98, 569, (1976).
22. Wind R.A., G.E. Maciel, and R.E. Botto, in Magnetic Resonance of Carbonaceous Solids, R.E. Botto and Y. Sanada, eds, Adv. Chem. Ser. 229, Am. Chem. Soc., Washington, DC, 1993, Ch1
23. Sullivan M.J. and G.E. Maciel, Anal. Chem., 54, 1615, (1982).
24. Dixon W.T., J. Magn. Reson., 44, 220, (1981).
25. Adachi Y. and M. Nakamizo, in, Magnetic Resonance of Carbonaceous Solids, Adv. Chem. Series 229, Botto R.E. and Y. Sanada eds., Am. Chem. Soc. Washington, DC, 1993, Ch 13.

26. Sullivan M.J. in Petrakis L. and J.P. Fraissard, eds, Magnetic Resonance, Introduction, Advanced Methods, and Applications to Fossil Energy, NATO ASI Series C, 124, D. Reidel Pub. Co., Dordrecht, Netherlands, 1984. pp 525-533.
27. Zhang and Maciel, J. Magn. Reson., 25, 156, (1989).
28. Miknis F.P., J.Jhou, D.B. MacGowan, and R.C. Surdam, Org. Geochem., 20, 339,(1993).
29. Franz J.A., and J.C. Linehan, in R.E. Botto and Y.Sanada, eds., Magnetic Resonance of Carbonaceous Solids, Adv. Chem. Ser. 229, Am. Chem. Soc., Washington, DC, 1993. Ch20.
30. Love G.D., R.V. Law, and C.E. Snape, Energy and Fuels, 7,639 (1993).
31. Sullivan M.J. and G.E. Maciel, Anal. Chem. 54, 1606, (1982).Yurum Y., ed., New Trends in Coal Science, NATO ASI Series C, V244, Kluwer Academic Publishers, Boston, 1988.
32. Murphy P.D.,T.J. Cassady,and B.C. Gerstein, Fuel, 61, 1233, (1982).
33. Opella S.J., and M.H. Frey, J. Am. Chem. Soc., 101, 5854 (1979)
34. Wilson M.A., Vassallo A.M., and N.J. Russell, Org. Geochem., 5, 35, (1983).
35. Botto R.E., R. Wilson, and R.E. Winans, Energy and Fuels, 1, 173, (1987).
36. Zhang M. and G.E. Maciel, Fuel, 69, 557, (1990).
37. Maciel G.E., C.E. Bronnimann, A. Jurkiewicz, R.A. Wind, and V.H. Pan, Fuel, 70, 925, (1991).
38. Miknis F.P., M.J. Sullivan, V.J.Bartuska, and G.E. Maciel, Org. Geochem., 3, 19, (1981)
39. Dudley R.L. and C. A. Fyfe, Fuel, 61, 651, (1983).
40. Packer K.J., R.K. Harris, A.M. Kenwright, and C.E. Snape, Fuel, 62, 999, (1983).
41. Wilson M.A., P.J. Collin, R.J. Pugmire, and D.M. Grant, Fuel, 61, 959,(1982).
42. Wilson M.A., A.M. Vassallo, P.J. Collin, and H. Rottendorf, Anal. Chem., 56, 433, (1984).
43. Snape C.E., D.E. Axelson, R.E. Botto, J.J. Delpuch, P.Tekely, B.C.Gerstein, M. Pruski, G.E. Maciel, and M.A. Wilson, Fuel, 68, 547,
44. Wilson M.A., A.M. Vassallo, D. Gizachew, and E. Lafargue, Org.Geochem., 17, 107, (1991).
45. Stock L.M., J.V. Muntean, and R.E. Botto, in Yurum Y., ed., New Trends in Coal Science, NATO ASI Series C, V244, Kluwer Academic Publishers, Boston, 1988, pp159-167.
46. Muntean J.V., L.M. Stock, and R.E. Botto, J. Magn. Reson., 76, 540, (1988).
47. Muntean J.V., L.M. Stock, and R.E. Botto, Energy Fuels, 2, 108, (1988).
48. Maciel G.E, V.J. Bartuska, and F.P. Miknis, Fuel, 58, 391, (1979).
49. Miknis F.P., G.E. Maciel, and V.J. Bartuska, Org. Geochem., 1, 169,(1979)47.
50. Maciel G.E, V.J. Bartuska, and F.P. Miknis, Fuel, 57, 505, (1978).
51. Hagaman E.W., F.M. Schell, and D.C. Cronauer, Fuel, 63, 915, (1984).
52. Evans E., B. Batts, and N. Cant, Fuel, 66, 326, (1987).
53. Miknis F.P. and P.J. Conn, Fuel, 65, 248, (1986).
54. Miknis F.P., Fuel, 71, 731, (1993).
55. Sato S., M. Enomoto, and S. Takahashi, Fuel Proc. Technol, 18, 305 (1988).

56. Miknis F.P., D.A. Netzel, J.W. Smith, M.A. Mast, and G.E. Maciel, Geochim. Cosmochim. Acta, 46, 977, (1982).
57. Miknis F.P., N.M. Severenyi, and G.E. Maciel, Fuel, 61, (1982).
58. Qin K., D. Chen, and Z. Li, Org. Geochem. 17, 856 (1991).
59. Hershkowitz F., W.N. Olmstead, R.P. Rhodes, and K.D. Rose, in Geochemistry and Chemistry of Oil Shales, F.P. Miknis and J.F. McKay, eds, ACS Symp. Series 230, Am. Chem. Soc., Washington, DC, 1983, Ch. 15.58.
60. Burhnam A.K., and J.A. Happe, Fuel, 63, 1353, (1984).
61. Miknis F.P., T.F. Turner, L.W. Ennen, and D.A. Netzel, Fuel, 67, 1568, (1988).
62. Schmitt K.D., and E.W. Sheppard, Fuel, 63, 1241 (1984).
63. Trewhella M.J., I.J. F. Poplet, and A. Grint, Fuel, 65, 541, (1986).
64. Solum M.S., R.J. Pugmire, and D.M. Grant, Energy and Fuels, 3, 187, (1989).

Introduction to Mass Spectrometric Techniques for Fossil Fuel Analysis

Garret A. Veloski, Curt M. White*

US DOE
Pittsburgh Energy Technology Center
P.O. Box 10940
Pittsburgh, PA 15236 USA

*Author to whom correspondence should be addressed.

Introduction

Mass spectrometry is a sensitive analytical technique that separates ions according to mass and measures the intensity of the signal derived from ions of each mass. The ions, or ion fragments are generated by bombarding molecules with electrons or other charged particles. A typical mass spectrum is a graphical or tabular report of the measured masses and their corresponding intensities usually normalized to the most intense specie (base peak) in the sample under investigation. Owing to the great sensitivity of most mass spectrometers, as little as a microgram of sample can afford a good spectrum.¹

Much can be learned about a sample through the accurate interpretation of its mass spectrum. The molecular weight of an individual compound or a component in a mixture often can be easily determined. Also, elemental composition and some structural elucidation is possible. In addition, more detailed analyses employing variations in the mass spectrometric technique can provide such physical information as ion kinetics, stability, ion-molecule reactivity, and thermodynamic properties.¹⁻³ The numerous methods of sample introduction, ion generation, and analysis lend themselves to the variety of mass spectrometric techniques that have been developed to accommodate the unique physical properties of certain analytes.

Mass Spectrometer Construction

The general construction of a mass spectrometer consists of a sample introduction system, a source or ionization chamber, ion accelerator, analyzer, detector-amplifier, and recorder (data system) (Fig. 1). The sample introduction system in its simplest form must allow both liquids and volatile solids to enter the mass spectrometer source in the vapor phase. The sample inlet system can also be heated to admit compounds of lower volatility and prevent the sample from recondensing. To maintain the necessary high vacuum in the ion source, some

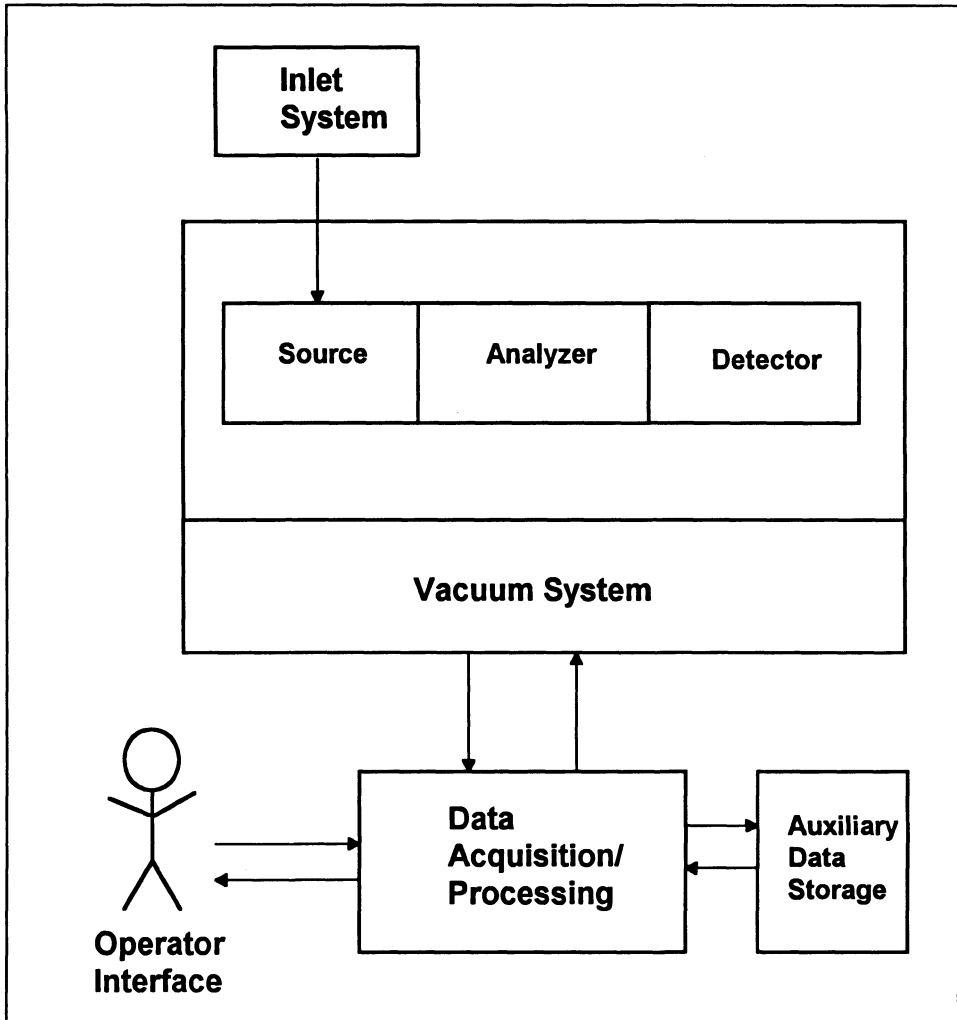


Figure 1.

Mass Spectrometer
block diagram.

sample inlet systems incorporate a differentially pumped vacuum lock mechanism for delivering a sample at atmospheric pressure to source pressure. This often consists of an elaborate system of magnetically actuated valves with precision ground glass seats, glass to metal seals, and other plumbing. Samples having very low volatilities can be introduced by means of a heated probe apparatus. The heated probe contains a small sample well at its tip, which when inserted through a vacuum lock mechanism is in close proximity to the electron beam.

The source is where ionization occurs. The most common form of mass spectrometry, electron impact (EI), employs an incandescent wire or ribbon filament constructed of tungsten or rhenium as a source of electrons to bring about the ionization of neutral sample molecules. A typical magnetic sector mass spectrometer source usually operates at high potentials. These high potentials ($\sim 8\text{kV}$) between adjacent parts and heated surfaces in evacuated spaces require that insulating materials be constructed of high resistivity glass or ceramic. All sample transfer lines and parts associated with the inlet system and in contact with source parts must be constructed with this in mind.

Mass analyzers are most commonly magnetic sector or quadrupole units. The magnetic sector instrument (single focusing) has a fixed wedge-shaped geometry and functions by dispersing the ion beam into its components (Fig. 2). This is accomplished due to the fact that the trajectories of charged particles in a magnetic field and their mass are related by the expression:

$$\frac{m}{e} = \frac{B^2 r^2}{2V}$$

where m/e is the mass-to-charge ratio for a singly charged ion, B is the magnetic field strength, r is the radius of curvature of the magnetic sector, and V is the accelerating voltage. Scanning the magnetic sector instrument involves sweeping the magnetic field. The quadrupole mass analyzer is considerably more complex in theory. In simple terms, mass segregation is afforded by varying the frequency of R.F. voltages applied to the rods in the x and y directions as depicted in Figure 3. Ions entering the analyzer from the source and traveling along the z direction encounter these oscillations resulting in a wobbling motion. There is a specific field oscillation for each m/e that permits the ion to travel the entire length of the analyzer without striking one of the rods. Mass scans are accomplished by sweeping the R.F. voltage. Quadrupole instruments can scan a given mass range much faster than magnetic sector instruments. In both types of instruments, the entire flight path, or space in which the ions traverse, is maintained under high vacuum ($\sim 10^{-5}$ - 10^{-8} torr) to minimize collisions with other molecules.

All types of mass spectrometers require responsive detectors. Typically, the ion current reaching the detector is quite small (as low as 10^{-15}A), and the detector must, therefore, exhibit superior amplification and noise shielding qualities. The most

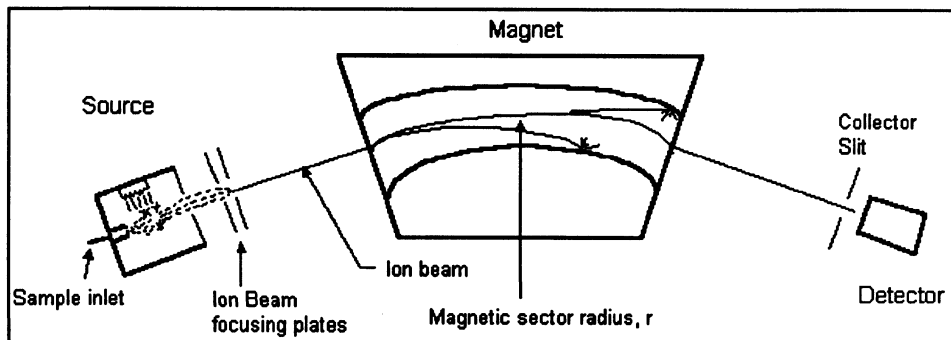


Figure 2.
Magnetic sector mass spectrometer.

common type of detector used for mass spectrometers is an electron multiplier. Electron multipliers contain stages of emissive surfaces (dynodes) that, upon collision with an ion at the first stage, cause a cascading of electrons. The resulting signal gain can be 10^6 or greater.

Electron Ionization (EI)

EI is the most common form of mass spectrometry and will be a focal point for further discussion. In the usual scenario of events, a small stream of neutral sample molecules enters the source via the sample inlet system through a tiny orifice (molecular leak) directed into the path of the electron emission. Ionization occurs when electrons emitted from the filament collide with sample molecules. The mutually repulsive forces between the filament electrons and sample molecules cause an electron to be jettisoned by some portion of the sample molecules, resulting in a net positive charge (Eq. 1).¹⁻⁴



Equation 1.
Formation of a molecular ion.

The specie is referred to as the molecular ion. The molecular ion is frequently the most abundant high mass peak in the spectrum of a chemically pure compound. Not all molecules exhibit prominent molecular ions. Some compounds show none. The presence of M^+ in the mass spectrum is largely dependent on its stability. Since M^+ is a cation-radical, and thus, electron deficient, its stability generally

reflects that of other organic cations and radicals. Compounds having electron-rich substituents and those capable of stabilization through resonance often provide a mass spectrum in which M^+ is the base peak.⁴

The energy of the emitted electron beam is largely dependent on the difference in potential between the filament and the ion block or cage in the source. Normally, 70eV electrons are used to ionize the sample. This is sufficient energy to bring about the ionization of a statistically large population of most if not all molecules. The excess energy imparted to the molecules is the major contributor to unimolecular decompositions which in turn give rise to the familiar fragmentation patterns characterizing most mass spectra. Discussion of the numerous postulated mechanisms and interpretative methods to explain the occurrence of commonly observed ion fragments is beyond the scope of this paper.

Even though the molecular ion may be the most abundant high mass ion in the mass spectrum of a compound, for most organic compounds there are higher mass features of lesser abundance having special importance. These peaks are called isotopic satellites. The intensity of these peaks closely approximates the statistical abundance of the naturally occurring isotopes. All organic compounds contain at least two elements that have more than one naturally occurring isotope (Table 1). Analysis of these isotopic satellite peaks appearing in the mass spectra of compounds showing prominent molecular ions can provide clues in determining the molecular formula. These ion clusters are often all that is necessary to determine the elemental compositions of ions observed in the mass spectra of some compounds. In some of the more advanced EI techniques used in fossil fuel analysis, isotopic satellites of the molecular ion are routinely used to verify the molecular composition of certain components, particularly organosulfur compounds (*vide infra*).

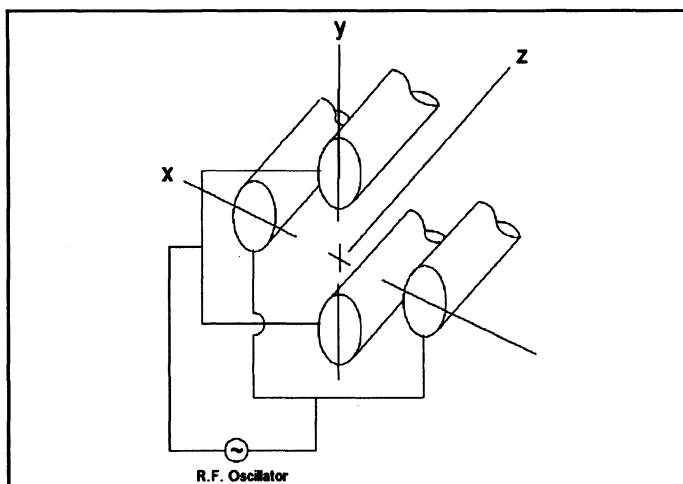


Figure 3.
Quadrupole mass analyzer rod arrangement.

Low-Voltage Electron Impact

Mass spectrometers are traditionally operated at 70eV in the EI mode to optimize the ionization process and to generate characteristic fragmentation spectra that are then compared to libraries of existing spectra for identification purposes. By deliberately reducing the ionization voltage, the energy imparted to the ions and the response or sensitivity of the instrument are considerably lowered. Yet, the low-voltage mass spectrometry (LVMS) technique has several advantages. Low ionizing voltage enhances the detection of the molecular ion (M^{+}) by reducing fragmentation. If a mixture such as a petroleum fraction or coal-derived material is analyzed at 70eV, the resulting mass spectrum in most cases is entirely too complex to derive much useful information. However, if the ionization voltage is lowered to 10-12eV, numerous homologous series of molecular ions from different classes of compounds become obvious. In addition, since the ionization potentials for certain compounds in fossil fuels are lower than others, selective ionization can be accomplished. This method is especially true for fuels rich in aromatic hydrocarbon compounds which typically ionize easier than saturates.

Field Ionization

Field ionization mass spectrometry (FIMS) is considered to be a soft ionization technique, producing spectra that are similar in appearance to LVMS.^{5,6} Ionization occurs when a strong electric field (10^7 - 10^8 V/cm) is applied across two points, one of which contains the sample. After an electron is stripped from the analyte molecules, the resulting low energy ions are analyzed in a manner similar to conventional EI mass spectrometry. FIMS spectra consist primarily of molecular ions. The technique has been extensively applied to fossil fuel analysis, with a particular emphasis on the high molecular weight components. The ionization efficiency of FIMS is lower than LVMS.

Chemical Ionization

The configurations of chemical ionization mass spectrometers (CIMS) are very similar to EI mass spectrometers.^{5,7} The primary difference occurs in the construction of the source. The source ionization chamber for CIMS is designed to operate at locally higher pressures (~ 1 torr). The ionization voltages are typically in the range of 100-400eV. In addition, the inlet system has provisions for metering certain reagent gases into the source. Ionization occurs when the sample molecules react with charged species generated by ionization of the reagent gas (Fig. 4). A proton is abstracted by a sample molecule having a higher proton affinity than the reagent ion resulting in an $(M+H)^+$ ion instead of the molecular ion (M^{+}). The

resulting quasimolecular ion specie $(M+H)^+$, which is located 1 amu higher in the spectrum, is then extracted from the source, accelerated, and analyzed in the usual fashion. Some CIMS instruments have the added capability of analyzing both positive and negative ions. CIMS is also considered a soft ionization technique with some important advantages. In many instances, a compound that will not produce a molecular ion in an EI spectrum will produce a prominent $(M+H)^+$ by CIMS. Selective ionization can also be achieved using CIMS along with the appropriate reagent gas.

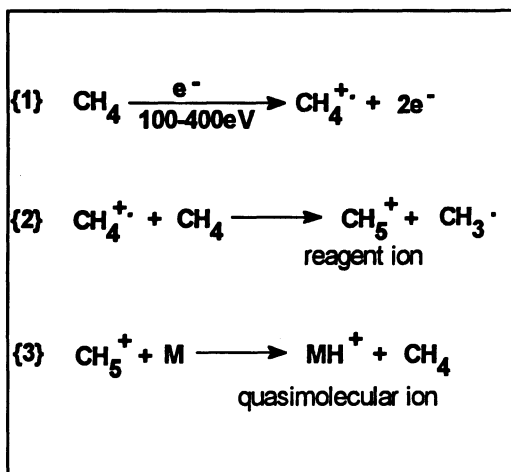


Figure 4.
Methane chemical ionization scheme.

High-Resolution Mass Spectrometry

The high-resolution mass spectrometer (HRMS) combines a magnetic sector mass analyzer with an electrostatic kinetic energy analyzer to achieve high resolving power and precise mass measurements. A very high degree of energy focusing is achieved by the electrostatic analyzer (ESA) which stabilizes and homogenizes the ion beam before entry into the magnetic analyzer. The magnetic analyzer then performs essentially the same function as in low-resolution magnetic sector instruments. The performance of the ESA is independent of the accelerating voltage so that a wide range in mass can be scanned. A common design employs a double sector (180°) configuration (Fig. 5). HRMS instruments are usually scanned from high mass to low mass and much slower than other mass spectrometers.³⁻⁶

The resolving power (R) required to baseline separate a pair of ions (doublet) having the same nominal mass is defined by

$$R = \frac{M}{\Delta m}$$

where M is the nominal mass of both ions in the doublet, and Δm is the absolute difference in mass. Resolutions in excess of 1 part in 100000 are possible with these instruments. However, in practical use HRMS instruments are operated at about 1 part in 25000.^{8,9} Even at these high resolving powers, the highest mass in

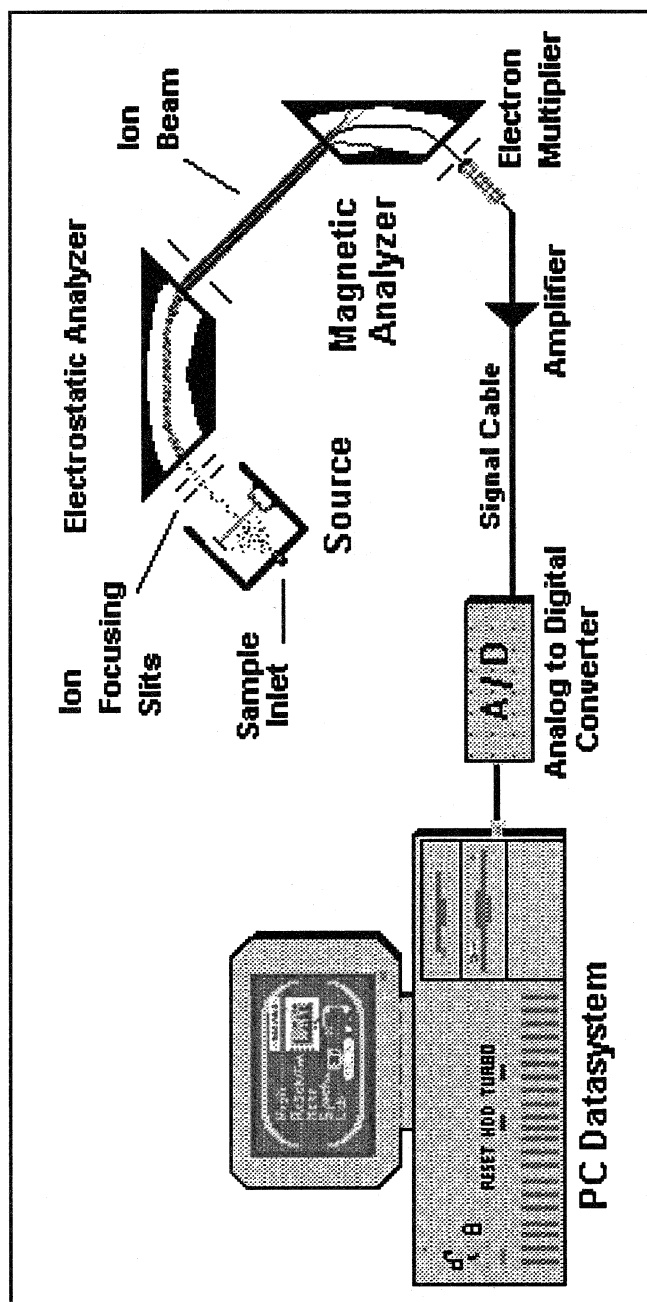


Figure 5.
Nier - Johnson double
focusing mass spectrometer
and data system.

which baseline resolution can be affected is lower than one might expect (Table 2). It is not necessary, however, to baseline resolve a multicomponent peak as long as the center of mass of the components can be accurately approximated. The precise mass measuring accuracy for a HRMS can be better than 1mmu (0.001amu) for ions up to 1000amu under optimum conditions. The major advantages of HRMS are not only the ability to separate close ions commonly occurring at the same nominal mass, but also to determine the elemental compositions of these ions from their precise mass measurements (Table 3). Table 4 provides an example of the output from an atom combinatorial program used to calculate permutations of molecular formulae for a multicomponent peak detected in a Spanish lignite extract by LVHRMS (*vide infra*).

Low-Voltage, High-Resolution Mass Spectrometry

Low-Voltage, High-Resolution Mass Spectrometry (LVHRMS) provides a rapid, efficient method for identifying the numerous classes of volatile and semivolatile organic compounds in matrices as complex as fossil fuels. LVHRMS is well suited for determining how changes in experimental parameters are reflected in the product, or at some other stage in a process, on a molecular level. Low-voltage electron ionization (EI) accomplishes this by reducing fragmentation resulting from unimolecular decomposition reactions (*vide supra*).

LVHRMS is well suited for the analysis of fossil fuels, and in particular, coal-derived materials.⁷⁻¹⁰ This is because the composition of a typical coal-derived material is hydrogen deficient, i.e., most hydrocarbon and heteroatom compounds are mainly aromatic, hydroaromatic, or olefinic. These types of molecules, when subjected to a low voltage (10-12 eV) electron beam, provide intense molecular ions. Precise mass measurements of these molecular ions allows direct calculation of the molecular formulae of all detected ions generated from the sample. Once the relative responses for various classes of compounds typically found in fossil fuels have been reasonably estimated under a given set of operating conditions, the semiquantitative determinations of sample composition are possible. Data arrays consisting of precise mass measurements and their corresponding integrated peak intensities, now having the added dimension of elemental composition, can easily be converted into detailed formula class analyses. The computation of elemental analyses, carbon number distributions, and number average molecular weights can be derived from these data. Based on these properties, successful characterizations of numerous chemical components in coal-derived materials and aromatic fractions of petroleum are all possible. The complexity of fossil fuels, however, imposes special demands, and sets limits even on as powerful a technique as LVHRMS.

Table 1.

Isotopic abundances and precise masses of selected elements.

Element	Symbol	Nominal Mass	Precise Mass	Abundance
Hydrogen	H	1	1.0078	99.99
	D	2	2.014	0.01
Carbon	¹² C	12	12.0000	98.91
	¹³ C	13	13.0034	1.09
Nitrogen	¹⁴ N	14	14.0031	99.6
	¹⁵ N	15	15.0001	0.04
Oxygen	¹⁶ O	16	15.9949	99.76
	¹⁷ O	17	16.9991	0.04
	¹⁸ O	18	17.9992	0.20
Sulfur	³² S	32	31.9721	95.02
	³³ S	33	32.9715	0.76
	³⁴ S	34	33.9679	4.22
Chlorine	³⁵ Cl	35	34.9689	75.77
	³⁷ Cl	37	36.9659	24.32
Bromine	⁷⁹ Br	79	78.9183	50.5
	⁸¹ Br	81	80.9163	49.5
Fluorine	F	19	18.9984	monoisotopic
Iodine	I	127	126.9045	monoisotopic
Phosphorus	P	31	30.9738	monoisotopic

Table 2.

Highest baseline-resolved mass for selected doublets at a resolution of 1 part in 25000.

Doublet	Δ Mass	Highest Resolved Mass (25000 x Δ Mass)
C - H ₁₂	0.0939	2347
C ₂ H ₈ - ³² S	0.0905	2263
CH ₄ - O	0.0364	910
³² S - O ₂	0.0277	692
¹³ CH - N	0.0081	203
C ₃ - ³² SH ₄	0.0034	85

Table 3.

Possible atomic compositions and precise masses for molecular ions at nominal mass 148.

$C_{11}H_{16}$	148.1252	$C_7H_{16}O_3$	148.1099
$C_{10}H_{12}O$	148.0888	$C_7H_{16}OS$	148.0922
$C_9H_8O_2$	148.0524	$C_7H_4N_2O_2$	148.0273
$C_7H_8N_4$	148.0750	$C_6H_{12}O_4$	148.0735
$C_9H_{12}N_2$	148.1001	$C_6H_4N_4O$	148.0386
$C_6H_{12}O_2S$	148.0558	$C_3H_8O_3S$	148.0194
$C_8H_{17}Cl$	148.1019	C_3HF_5O	147.9947
$C_8H_8N_2O$	148.0637	$C_2H_3Cl_3O$	147.9249
$C_8H_4O_3$	148.0160	C_2Cl_3F	147.9049
C_9H_8S	148.0347	$CBrF_3$	147.9135

Table 4

Multiplet detected at nominal mass m/z 268
in Mequinenza lignite pyridine extract.

<u>Measured Mass</u>	<u>Calculated Mass</u>	<u>Molecular Formula</u>	<u>Dev. (milli-amu)</u>	<u>% of Base Peak</u>
268.2146	268.2151	$C_{15}H_{28}N_2O_2$	-0.5	18.01
268.1463	268.1463	$C_{18}H_{20}O_2$	0.0	11.34
	268.1497	$C_{15}H_{24}O_2S$	-3.4	
268.1291	268.1286	$C_{18}H_{20}S$	0.5	20.01
	268.1299	$C_{15}H_{22}O_2^{34}S$	-0.8	
	268.1312	$C_{15}H_{24}S_2$	-2.9	
	268.1252	$C_{21}H_{16}$	3.9	
268.0918	268.0922	$C_{17}H_{16}OS$	-0.4	21.35
	268.0888	$C_{20}H_{12}O$	3.0	
268.0718	268.0724	$C_{17}H_{14}O^{34}S$	-0.6	7.34
	268.0705	$C_{12}H_{16}N_2OS_2$	1.3	
268.0541	268.0524	$C_{19}H_8O_2$	1.7	13.34
	268.0558	$C_{16}H_{12}O_2S$	-1.7	
268.0362	268.0360	$C_{16}H_{10}O_2^{34}S$	0.2	19.35
	268.0347	$C_{19}H_8S$	1.5	
	268.0380	$C_{16}H_{12}S_2$	-1.8	
	268.0394	$C_{13}H_{14}O_2S^{34}S$	-3.2	

References

1. Silverstein, R. M.; Bassler, G. C.; Morrill, T. C. *Spectrometric Identification of Organic Compounds*, Wiley & Sons (1974).
2. Watson, J. T. *Introduction to Mass Spectrometry*, Raven Press (1985).
3. Budzikiewicz, H.; Djerassi, C.; Williams, D. H. *Mass Spectrometry of Organic Compounds*, Holden-Day (1967).
4. McLafferty, F. W. *Interpretation of Mass Spectra*, University Science (1980).
5. Watson, J. T. *Introduction to Mass Spectrometry: Biomedical, Environmental, and Forensic Applications*, Raven Press (1976).
6. Message, G. M. *Practical Aspects of Gas Chromatography/Mass Spectrometry*, Wiley Interscience (1984).
7. Harrison, A. G. *Chemical Ionization Mass Spectrometry*, CRC Press (1992).
8. Batts, B. D.; Batts, J. E. in *Spectroscopic Analysis of Coal Liquids*, pp. 61-128. Elsevier (1989).
9. Schmidt, C. E.; Sprecher, R. F. in *Novel Techniques in Fossil Fuel Mass Spectrometry*, pp. 116-132. ASTM (1989).
10. Schmidt, C. E.; Sprecher, R. F.; Batts, B. D. *Anal. Chem.* **1987**, 59, 2027-2033.

AN INTRODUCTION TO OPEN-TUBULAR GAS CHROMATOGRAPHY-- ANALYSIS OF FOSSIL AND SYNTHETIC FUELS

C. M. WHITE
ANALYTICAL RESEARCH GROUP
PITTSBURGH ENERGY TECHNOLOGY CENTER
P.O. BOX 10940
PITTSBURGH, PA 15236 USA

ABSTRACT

High resolution open-tubular gas chromatography will be introduced, and instrumental aspects will be discussed, along with a substantial amount of practical information concerning its applications. Sample introduction systems, detectors, and column technology will be presented. A block diagram of a gas chromatograph depicting the various components will be shown. Several sample introduction systems will be described including split, splitless, and on-column injection. The concept of retention indices will be introduced, as will the use of gas chromatography for measuring thermophysical properties, such as boiling point and heat of vaporization. Lastly, a molecular topological parameter called molecular connectivity will be presented and it will be shown that it can be used to predict the gas chromatographic retention characteristics of aromatic compounds.

1. Introduction

Chromatography is a word coined by its inventor, M. S. Tswett, and is derived from two Greek words, *chroma* meaning color, and *graphien* meaning to write.¹⁻³ All forms of chromatography have two things in common, *i.e.*, they consist of a mobile or moving phase and a stationary phase. The many forms of chromatography differ from one another based upon the state of the mobile phase and stationary phase. In this chapter, we are concerned with gas chromatography (GC), where the mobile phase is a gas, and the stationary phase is either a liquid or a solid. Specifically, we are concerned with open-tubular (frequently called capillary) gas chromatography where the chromatographic column is an open tube or capillary having an immobile stationary phase coated on the inside surface of the tube. Gas chromatography is an analytical technique used to separate mixtures of substances that are volatile and thermally stable at the operating temperature by moving the vapor phase mixture in a carrier gas over a stationary phase in which the components of the mixture dissolve. Some mixture components are more soluble in the stationary phase than others. The compounds that are least soluble in the stationary phase spend less time dissolved in it and elute (emerge) from the column first. Those constituents that are more soluble in the stationary phase spend more time dissolved in it and take longer to elute from the end of the column. The result is that what entered the column as a mixture elutes from the column as individual compounds.

A block diagram of a gas chromatograph is shown in Figure 1 and consists of (1) a high pressure cylinder of mobile phase commonly called the carrier gas, (2) flow controllers and pressure regulators that reduce the pressure from the cylinder and maintain a smooth delivery of carrier gas to the chromatograph, (3) an injection port where the mixture to be separated and analyzed is introduced to the chromatograph, (4) the chromatographic column that has the stationary phase coated on its inside surface and performs the separation of analytes, (5) the column oven that heats the column at either constant temperature or in a temperature programmed fashion, (6) the detector that detects the compounds when they elute from the column, and (7) the recorder that records the detector signal. The permanent record of the detector signal is called the chromatogram.

A chromatogram consists of a series of peaks arising from a baseline where each peak ideally represents a single compound. The time from sample introduction to the peak maxima is called the retention time and is usually different for each component in the mixture. As described later, the retention times assist in identification of the compounds in the mixture, while ideally, the peak area is directly proportional to the amount of that compound in the mixture. More detailed and complete information concerning various aspects of gas chromatography and open-tubular gas chromatography can be found in texts by Perry,³ Jennings,⁴ McNair,⁵ Hyver,⁶ and Klee⁷.

2. Instrumental And Operational Aspects

2.1 SAMPLE INTRODUCTION (INJECTION)

The sample is injected into the chromatograph using a calibrated syringe. A measured volume of sample is drawn into the syringe and introduced to the gas chromatograph usually by piercing a rubber septum with the needle point, inserting the needle to the base of the syringe barrel, depressing the syringe plunger, and depositing the liquid contents of the syringe into the hot, helium-swept injection port. The syringe is then removed from the septum, allowing the septum to reform a gas tight seal. This is a general description of the mechanics involved in sample injection. Many variations exist depending on the kind of injection hardware mounted in the chromatograph. Some common injection systems used in open-tubular gas chromatography include the following: split injection (vaporizing), splitless injection (vaporizing), and cool on-column (not vaporizing). Other injection techniques are used, but these are the more common ones. Upon injection into a vaporizing injector the liquid sample is converted to a gas *via* flash vaporization of the solvent and/or volatile sample components in the hot injector, and carried out of the injector by the carrier gas (e.g. helium). Klee has written an excellent book on inlet (injection) systems used in gas chromatography.⁷ A much more complete coverage of the topic can be found there and in Hyver's book.⁶

2.1.1 Split Injection. A split injection system is shown in Figure 2.⁶ An open-tubular column contains a very small amount of stationary phase, and thus can dissolve only very small amounts of sample, usually submicroliter amounts. Sample amounts this small are obtained by injecting much larger amounts (0.1 to 1.0 μL) and splitting the carrier gas stream containing the sample so that the major portion of the stream is vented and only a small fraction of the stream reaches the chromatographic column. The split ratio is the ratio of the sum of the flow through the split vent plus the flow through the column to the flow through the column. The injection process is swift, the syringe is removed from the hot injector immediately after depression of the plunger, so that a small slug of sample is delivered to the column in as short a time as possible. Split injection generally results in the narrowest possible peaks. Split injectors vaporize the sample and protect the column from the nonvolatile sample components, which deposit in the injector. The heated injector also causes thermal decomposition of some analytes and discriminates against high boiling sample components as shown in Figure 3, and discussed below. Discrimination is a phenomenon that can occur in vaporizing injectors where the higher boiling sample components are not quantitatively transferred from the syringe to the chromatograph.

2.1.2 Splitless Injection. This injection technique allows much larger sample volumes to be delivered to the chromatographic column (1 to 10 μL). This injection technique is used when the analytes of interest are very dilute. The oven housing the chromatographic column is held about 15°C below the boiling point of the sample solvent so that the solvent condenses and floods the first few coils at the front of the column. During splitless injection, the carrier-gas flow through the split vent is turned off, and the entire contents of the vaporizing injector are swept onto the column. After 20 to 100 seconds the split vent is turned back on and any remaining vapors in the injector are vented. During this entire time the syringe is left in the hot injection port. This would normally result in broad peaks, but because the analytes are refocused at the front of the column by dissolution into the solvent flooding the front of the column, the peaks are narrow. When the column temperature is increased, the solvent vaporizes and elutes from the column followed by narrow analyte peaks. Splitless injectors vaporize the sample, and protect the column from the nonvolatile sample components, which deposit in the injector. The heated injector also causes thermal decomposition of some analytes and discrimination as in the case of split injection.

2.1.3 Cool On-Column Injection. In this injection technique, the liquid sample is deposited directly into the capillary column by inserting the syringe needle tip into the end of the column and depressing the plunger. The front of the column may be either cool or cold. The sample is not exposed to high temperature during introduction as in vaporizing injectors. Several designs of this injector exist. This injection technique has many advantages over other sample introduction methods, such as (1) providing the highest accuracy and reproducibility, (2) eliminating thermal decomposition of analytes

in the hot injector, (3) transferring the syringe contents to the column more quantitatively, (4) eliminating discrimination of high boiling sample components, (5) eliminating the rubber septa used for other injection techniques, thus removing a major source of injector and column contamination. The column oven temperature used in on-column injection can be much higher than that used in splitless injection.

An example of the extent of discrimination against high boiling sample components in a mixture of n-alkanes injected using three different injection techniques is shown in Figure 3.⁸ A mixture of n-alkane standards was prepared so that each was present in nearly identical amounts. Chromatogram A was obtained using split injection where the liquid sample was present in both the syringe needle and the syringe barrel. Upon injection, the syringe plunger was immediately depressed after inserting the needle into the syringe barrel and the syringe removed from the injection port. Chromatogram B was obtained using split injection with the entire sample in the syringe barrel, and the syringe needle was allowed to warm in the heated injection port for several seconds before the plunger was depressed. Chromatogram C was obtained by cool on-column injection. Both types of split injection clearly result in discrimination against higher boiling n-alkanes, while cool on-column injection is relatively discrimination free.

2.2 ANALYTE DETECTION

The most common detector used in open-tubular gas chromatography is the flame ionization detector (FID). The FID responds to almost all organic compounds. The FID responds uniformly to most hydrocarbons on a weight basis. Its response is decreased toward analytes containing oxygen, nitrogen, and other heteroatoms. Element specific detectors, which work well with open-tubular columns include the flame photometric detector (FPD), which is specific for analytes containing either sulfur or phosphorus; the nitrogen-phosphorus detector (NPD); the electron capture detector (ECD), which responds selectively to halogen containing compounds; and the atomic emission detector, which detects the individual elemental composition of each analyte as it elutes. Spectroscopic detectors including the mass spectrometer, the infrared spectrophotometer and others are also used in combination with open-tubular gas chromatography. Operating conditions for commonly used detectors for capillary GC are listed in Table 1.

The FID, shown in Figure 4, will be more fully described because it is the detector most commonly used with open tubular columns. The detector is fed a stream of hydrogen and a stream of air or oxygen that are mixed and combusted at the tip of the FID. The chromatographic column extends to the tip of the FID and as the analytes elute from the column they enter the flame and are combusted. Two electrodes at opposite ends of the flame measure the current in the flame. The apparent electrical conductivity of a gas, such as helium, is directly related and proportional to the number of ions in it. When

no analytes are eluting from the column, only helium is entering the flame and the number of ions in the flame is constant. This is called the background current. As an analyte elutes from the column, it combusts in the flame creating a large number of ions causing current to flow between the electrodes. This produces a signal that is recorded and is called the chromatogram.

The sensitivity of the FID depends upon the hydrogen and air flow rates as well as the use of make-up gas (adding extra helium or nitrogen). This is shown graphically in Figure 5. FID sensitivity is also a function of the ratio of carrier gas (helium) to hydrogen.

The exact position of the capillary column in the FID can have a dramatic effect on the observed chromatogram. Ideally, the end of the capillary column is placed about 1 mm from the end of the FID tip to minimize analyte contact with the metal surface of the FID. As shown in Figure 6, adsorptive analytes that are even slightly polar will adsorb on active surfaces of the FID before they reach the detector.

3. Column Considerations

3.1 COLUMN DIMENSIONS AND MATERIALS OF CONSTRUCTION

Almost all open-tubular columns used today are constructed from fused silica that is coated on the outside with either polyimide or aluminum. Aluminum coated capillaries are used for very high temperature operations (above about 380°C). Less than one dozen stationary phases are in common usage for capillary gas chromatography. Some of them are listed in Table 2 along with their polarity, temperature limits, and some applications. These stationary phases are available on commercial columns in various film thicknesses, column lengths, and diameters. A column coated with a stationary phase from one manufacturer may not display the same retention characteristics as one coated with the same stationary phase available from a different manufacturer. The reasons for this are complex and are due, in part, to batch-to-batch chemical variations in the stationary phase and different column deactivation procedures used by different manufacturers, as shown in Figure 7.⁶

The column internal diameter directly affects the number of theoretical plates (efficiency) of the column. Commercially available columns have internal diameters ranging from 0.1 to 0.75 mm. Generally, the smaller the internal diameter the more theoretical plates per meter the column will have. However, smaller inside diameter columns contain less stationary phase, and can accommodate smaller amounts of individual analytes before overloading occurs and performance is degraded.

3.2 COLUMN TEMPERATURE

Most capillary gas chromatographs in use today are capable of operating in either isothermal or temperature programmed modes. They are equipped with very sophisticated ovens and thermostats that allow column temperatures to be controlled to within 0.1°C or better. They are also capable of extremely accurate and reproducible temperature programming rates. The retention of analytes is directly related to column temperature. The effect of temperature on retention and the effect of temperature programming on the observed chromatogram is shown in Figure 8.⁹ As the isothermal operating temperature is increased, retention time of the analytes decreases. When the sample under analysis consists of a wide boiling range of substances, temperature programming is used to elute the highest boiling analytes in a reasonable operating time. Generally, under temperature programmed operation, the slower the temperature programming rate, the better the observed separation.

4. Treatment Of Retention Data: Qualitative Analysis

4.1 RETENTION INDICES

Two pieces of information are obtained with each peak in the chromatogram, the retention time, and the peak area. Modern gas chromatographs are capable of reproducing the retention times of peaks that elute within the first hour of operation to within a few hundredths of a minute. Retention information is most conveniently expressed as either relative retention or as a retention index. The retention index system proposed by Kovats¹⁰ is strictly for isothermal operation and has been modified by van den Dool and Kratz for linear-temperature-programmed operation.¹¹ In the van den Dool and Kratz method, the retention index of a substance is calculated relative to the retention time of two bracketing standards that are n-alkanes, equation 1.

$$I = 100 \frac{T_{R(\text{substance})} - T_{R_n}}{T_{R_{n+1}} - T_{R_n}} + 100 n \quad (1)$$

In equation 1, I is the retention index of the substance of interest, $T_{R(\text{substance})}$ is the retention time of the substance of interest, T_{R_n} is the retention time of the n-alkane that elutes before the substance of interest, $T_{R_{n+1}}$ is the retention time of the bracketing n-alkane that elutes just after the substance of interest, and n is the number of carbons in the first bracketing n-alkane. Experimentally, a mixture of n-alkanes is added to the sample, injected and chromatographed. The retention indices are calculated by inserting the experimentally determined retention times into equation 1, and solving for I . When using carefully controlled conditions, the calculated retention indices are reproducible within any one lab to about +/- 0.5 index units, and within about 1.5 index units from one lab to another. The retention indices of hundreds of compounds have been measured and are reported in the literature.¹² By comparing the experimentally determined retention indices from the sample with the measured indices in the literature, compounds

in the sample can sometimes be tentatively identified.

The technique of using retention indices to tentatively identify unknown compounds in a synthetic gasoline sample is illustrated in Figure 9 and Table 3.¹³ The retention indices of the unknown compounds are printed next to the previously published retention indices of known compounds. The comparison between the values is excellent, and allows the analyst to tentatively identify the unknown compounds. When this initial identification is combined with spectral information on the same peaks obtained from combined gas chromatography-mass spectrometry and/or combined gas chromatography-infrared spectrophotometry, then identification of the compounds can be positive.

4.2 MOLECULAR CONNECTIVITY

Sometimes the retention index of a compound of interest may not be in the literature, or a pure sample of the compound may not be available for measurement. The retention index of a compound of known structure can be sometimes be estimated using a concept called molecular connectivity, χ , which is a molecular topological index that can be easily calculated for any compound that can be drawn. Molecular connectivity is a description of molecular structure based on a count of skeletal atoms, and weighted by degree of skeletal branching. More detailed information concerning the concept of molecular connectivity can be found in a book by Kier and Hall¹⁴ and a publication by White.¹⁵ The first order valence molecular connectivity, ${}^1\chi_v$, is calculated according to equation 2 .

$${}^1\chi_v = \sum(\delta_i \delta_j)^{-1/2} \quad (2)$$

Each atom is assigned a value (δ), which is the number of bonds to that atom, ignoring bonds to hydrogen. Atoms i and j are bonded. An example calculation of ${}^1\chi_v$ for phenanthrene is given in Figure 10, and examples of how molecular connectivity can be used to estimate thermophysical properties of planar aromatic hydrocarbons are illustrated. The ${}^1\chi_v$ value correlates directly with the molecule's gas chromatographic retention index and its thermophysical properties. Once ${}^1\chi_v$ is computed, the compound's boiling point, T_b , and heat of vaporization, ΔH_v , can be directly calculated using equations 3 and 4.

$$T_b = 76.21 {}^1\chi_v + 225.7 \quad (3)$$

$$\Delta H_v = 6.6464 {}^1\chi_v + 25.147 \quad (4)$$

The planar aromatic hydrocarbon's boiling point can be estimated using equation 5, and

Table 1. Operating Conditions for Detectors Commonly Used in Capillary Gas Chromatography. (Adapted from a table in reference 6.)

Type	Typical Samples	Sensitivity Range	Carrier + Makeup	Flow Rate (ml/min)	
				H ₂	Air
FID	Hydrocarbons	10-100 pg	20-60	30-40	200-500
TCD	General	5-100 ng	15-30	n.a.	n.a.
ECD	Organohalogenates	0.05-1 pg	30-60	n.a.	n.a.
NPD	Organonitrogen and Organophosphorus Compounds	0.1-10 pg	20-40	1-5	70-100
FPD (393 nm)	Sulfur Compounds	10-100 pg	20-40	50-70	60-80
FPD (526 nm)	Phosphorus Compounds	1-10 pg	20-40	120-170	100-150

Table 2. Common Stationary Phase Coatings for Fused-Silica Capillary Columns. (Adapted from a table in reference 6)

Composition	Polarity	Phase with Similar McReynold's Constants	Temperature Limits
1. 100% dimethylpolysiloxane (Gum)	Nonpolar	OV-1 SE-30	-60°C to 400°C
2. 100% dimethylpolysiloxane (Fluid)	Nonpolar	OV-101 SP-2100	0°C to 280°C
3. 5% diphenyl 95% dimethylpolysiloxane	Nonpolar	SE-52 OV-23 SE-54	-60°C to 325°C
4. 14% cyanopropyl phenyl polysiloxane	Intermediate	OV-1701	-20°C to 280°C
5. 50% phenyl 50% methyl polysiloxane	Intermediate	OV-17	60°C to 240°C
6. 50% cyanopropylmethyl 50% phenylmethylpolysiloxane	Intermediate	OV-225	60°C to 240°C
7. 50% trifluoropropyl 50% dimethylpolysiloxane	Intermediate	OV-210	45°C to 240°C
8. polyethylene glycol-TPA modified	Polar	OV-351 SP-1000	60°C to 240°C
9. polyethylene glycol	Polar	Carbowax 20M	60°C to 220°C

TABLE 3. Compounds Identified in the Liquid Condensate and Their Approximate Concentration in the Liquid Condensate. The Liquid Condensate is Approximately 47 Weight % of the Total Product.

Peak #	Compound Name	Method of Identification				Estimated Weight Percent
		GC-MS	FTIR	Measured	Known	
				R.I.	R.I.	
6	Chloroethane	x		423.96	424.09	0.003
9	1-Pentene	x		483.67	483.39	0.004
10	2-Chloropropane	x	x	490.72	491.40	0.012
11	2-Methyl-1-butene	x		493.79	493.58	0.009
13	(E)-2-Pentene	x	x	505.09	504.91	0.027
14	(Z)-2-Pentene	x	x	510.30	510.35	0.014
17	2-Chloro-2-methylpropane	x	x	530.66	530.04	0.146
18	Cyclopentane	x	x	554.24	554.13	0.022
23	2-Chlorobutane	x	x	598.87	598.38	0.030
25	(E)-3-Hexene	x	x	601.03	601.42	0.014
26	(Z)-3-Hexene	x	x	602.28	602.19	0.037
30	Methylcyclopentane	x	x	620.67	620.81	0.296
33	2-Chloro-2-methylbutane	x	x	647.89	647.88	0.911
34	Cyclohexane	x	x	651.09	651.14	0.016
35	2-Methylhexane	x	x	661.02	661.15	0.165
38	Cyclohexene	x	x	667.76	667.80	0.021
39	3-Methylhexane	x	x	670.56	670.60	0.162
54	Methylbenzene	x	x	748.65	749.00	2.452
55	2-Methylheptane	x	x	763.50	763.03	0.078
56	4-Methylheptane	x	x	764.38	764.57	0.044
63	Ethylbenzene	x	x	844.50	844.74	1.473
64	1,3-Dimethylbenzene	x	x	853.85	853.38	8.789
65	1,4-Dimethylbenzene	x	x	854.85	854.75	4.847
67	1,2-Dimethylbenzene	x	x	875.88	875.89	4.041
72	1,3,5-Trimethylbenzene	x	x	954.28	954.69	0.701
74	1,2,4-Trimethylbenzene	x	x	980.80	978.78	45.343
77	1,2,3-Trimethylbenzene	x	x	1004.87	1005.04	0.382
90	1,2,4,5-Tetramethylbenzene	x	x	1102.07	1101.84	5.381
91	1,2,3,5-Tetramethylbenzene	x	x	1104.97	1104.26	0.717
94	1,2,3,4-Tetrahydro naphthalene	x	x	1140.47	1140.85	0.120
95	Naphthalene	x		1160.26	1158.51	0.150

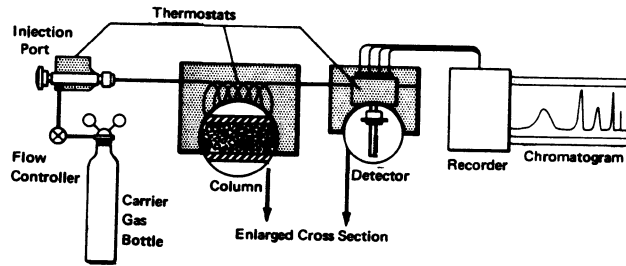


Fig. 1 Block diagram of a gas chromatograph. Reprinted with permission from reference 1.

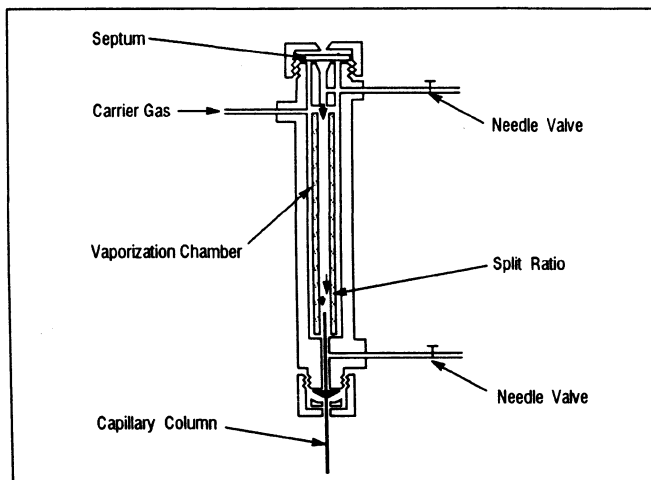


Fig. 2 Drawing of a split injector. Reprinted with permission from reference 6.

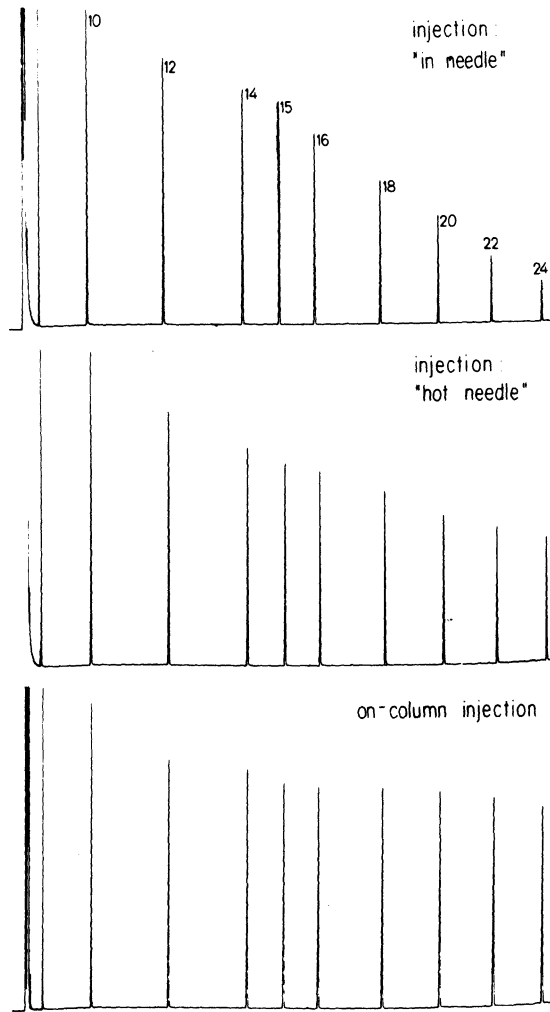


Fig. 3 Discrimination against n-alkanes as a function of injection technique. Reprinted with permission from reference 8.

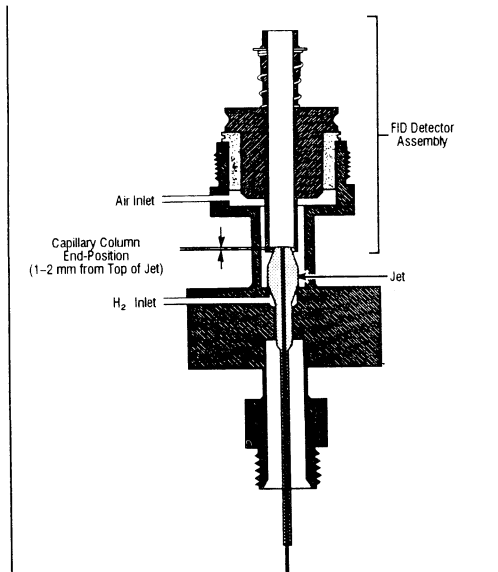


Fig. 4 Schematic diagram of a flame ionization detector. Reprinted with permission from reference 6.

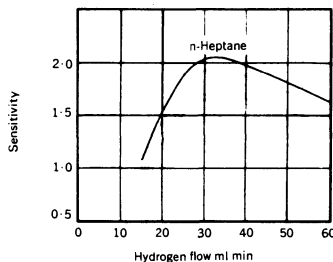


Fig. 5 Sensitivity change of a flame ionization detector toward heptane as a function of H₂ flow rate. Reprinted with permission from reference 5.

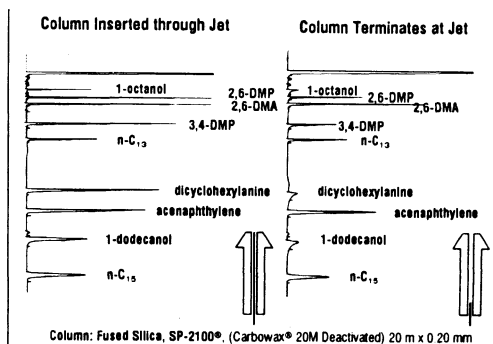


Fig. 6 The relationship between the column terminus in the FID and the quality of the observed chromatogram. Reprinted with permission from reference 6.

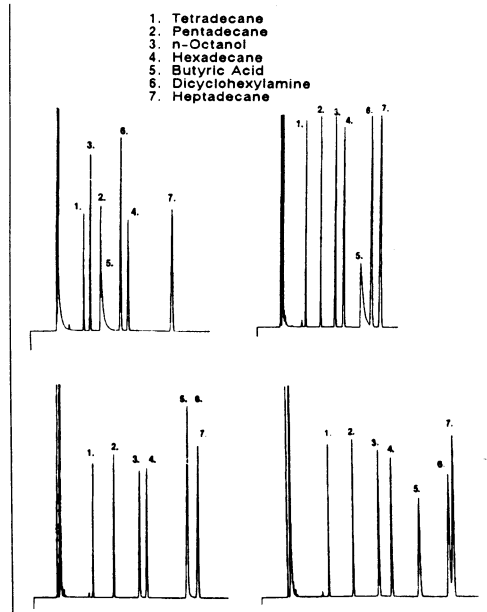


Fig. 7 Chromatograms of a test mixture on four commercially available columns all coated with cross-linked Carbowax 20M. Reprinted with permission from reference 6.

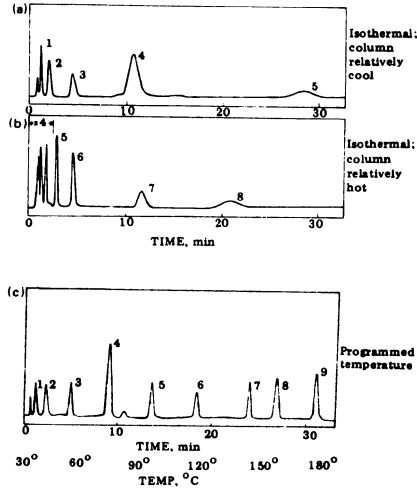


Fig. 8 The effect of different isothermal operating temperatures in the observed chromatograms is displayed in a and b. Chromatogram c shows the effect of temperature programming. Reprinted with permission from reference 9.

CHLOROMETHANE/ZEOLITE LIQUID CONDENSATE

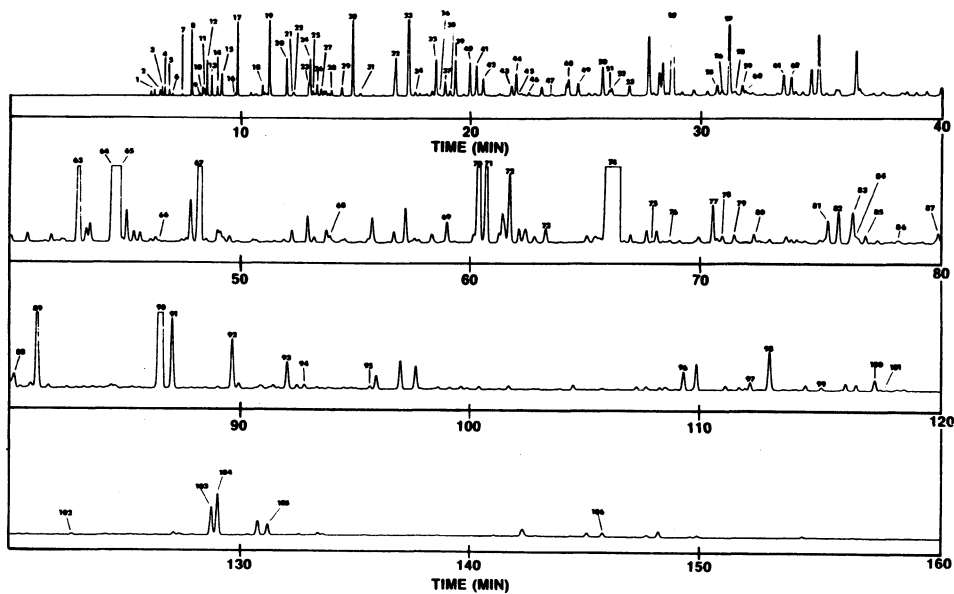
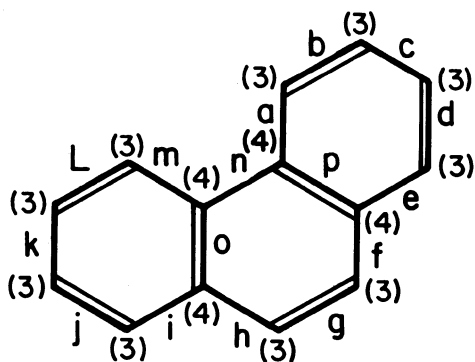


Fig. 9 High resolution gas chromatogram of a synthetic gasoline obtained using a 100m x 0.25mm open-tubular column coated with a 0.5 μ m film of dimethylpolysiloxane. The column was temperature programmed from 30°C to 220°C at 1°C per minute. Some numbered chromatographic peaks are identified in Table 3. Reprinted with permission from reference 13.



$$\begin{aligned}
 {}^1X_V &= \sqrt{\frac{1}{4 \cdot 3}} + \sqrt{\frac{1}{3 \cdot 3}} + \sqrt{\frac{1}{3 \cdot 3}} + \sqrt{\frac{1}{3 \cdot 3}} + \sqrt{\frac{1}{3 \cdot 4}} \\
 &+ \sqrt{\frac{1}{4 \cdot 3}} + \sqrt{\frac{1}{3 \cdot 3}} + \sqrt{\frac{1}{3 \cdot 4}} + \sqrt{\frac{1}{4 \cdot 3}} + \sqrt{\frac{1}{3 \cdot 3}} \\
 &+ \sqrt{\frac{1}{3 \cdot 3}} + \sqrt{\frac{1}{3 \cdot 3}} + \sqrt{\frac{1}{3 \cdot 4}} + \sqrt{\frac{1}{4 \cdot 4}} + \sqrt{\frac{1}{4 \cdot 4}} \\
 &+ \sqrt{\frac{1}{4 \cdot 4}} = 4.815
 \end{aligned}$$

Fig. 10 An example calculation of a first order molecular connectivity for phenanthrene. Reprinted with permission from reference 15.

its retention index can be estimated, with a standard error of estimate of 8.8 index units, using equation 6. Thus, the thermophysical properties of an aromatic compound can be accurately estimated using these techniques.

$$T_b = 1.0672 I + 282.82 \quad (5)$$

$$I = 69.69 \chi_v - 41.93 \quad (6)$$

Information concerning the fundamental physical, chemical, and thermodynamic properties of fossil fuels and individual components present in fossil fuels is needed to properly design and operate fossil fuel processing plants. Since many of these values have not been measured, the estimation techniques illustrated above are particularly useful for engineers designing fossil fuel processing equipment.

5. References

1. V. Heines, Chem. Tech., 1971, 1, 281.
2. M. S. Tswett, J. Chem. Educ., 1967, 44, 238.
3. J. A. Perry, Introduction to Analytical Gas Chromatography, Marcel Dekker (1981).
4. W. Jennings, Gas Chromatography With Glass Capillary Columns, Academic Press (1978).
5. H. M. McNair and E. J. Bonelli, Basic Gas Chromatography, Varian Instrument Division (1969).
6. High Resolution Gas Chromatography, K. J. Hyver, ed., Hewlett Packard (1989).
7. M. S. Klee, GC Inlets-An Introduction, Hewlett Packard (1990).
8. K. Grob, and G. Grob, J. High Resolut. Chromatogr., 1979, 2, 109.
9. H. W. Habgood and W. E. Harris, Anal. Chem., 1960, 32, 450.
10. E. Kovats, Helv. Chim. Acta, 1958, 41, 1915.
11. H. van den Dool and P. D. Kratz, J. Chromatogr., 1963, 11, 463.
12. C. M. White, J. Hackett, R. R. Anderson, S. Kail, P. S. Spock, J. High Resolut. Chromatogr., 1992, 15, 105.
13. C. M. White, L. J. Douglas, J. P. Hackett, R. R. Anderson, Energy & Fuels, 1992, 6, 76.
14. L. B. Kier and L. H. Hall, Molecular Connectivity in Chemistry and Drug Design, Academic Press (1976).
15. C. M. White, J. Chem. Eng. Data, 1986, 31, 198.

SPECIATION OF ORGANIC SULPHUR FORMS IN SOLID FUELS AND HEAVY OILS

C.E. SNAPE, K. ISMAIL and S.C. MITCHELL
*University of Strathclyde
Dept. of Pure & Applied Chemistry
Thomas Graham Building
295 Cathedral Street
Glasgow G1 1XL, UK*

K.D. BARTLE
*University of Leeds
Dept. of Chemistry
Leeds LS2 9JT, UK*

ABSTRACT. The recent advances that has been achieved with X-ray techniques, temperature programmed reduction (TPR) and oxidation (TPO) and selective chemical modification for the speciation of organic sulphur forms present in solid fuels are reviewed. Although each of these approaches has its limitations, a consistent overall picture is beginning to emerge on the nature of organic sulphur groups in solid fuels and heavy oil fractions. As might be anticipated, the more stable sulphur groups are most abundant in the more mature coals and petroleum source rocks. Further, the use of these advanced techniques has enabled the changes to be monitored that occur in the refining of heavy oils and chemical treatments being developed to reduce the sulphur levels of coals.

1. Introduction

Coal and petroleum are derived from sedimentary organic matter of vastly different composition but both contain varying amounts of sulphur. Sulphur was incorporated into oil shales and coals during the early stages of diagenesis via the products obtained from the bacterial reduction of sulphate ions (i.e. S^0 , H_2S , HS_x^-)⁽¹⁻³⁾. In sediments where iron was abundant, pyrite was the predominant form of FeS_2 ⁽¹⁾ produced with the remainder of the sulphur being bound into the organic structure. During maturation of both coal and petroleum source rocks, the distributions of organic sulphur groups are thought to alter markedly with sulphides being converted into thiophenes and the degree of condensation of the thiophenic moieties increasing markedly⁽²⁻⁵⁾. Further, the ease of sulphur removal from oil fractions during petroleum refining processes is known to be heavily dependent on the nature of the organic sulphur groups present⁽⁶⁾. Thus, their speciation is important from the standpoints of being able to fully understand maturation and also to effectively model refinery processes, particularly catalytic cracking and hydrotreatment.

Standard methods are available for the determination of total sulphur contents in all fuels, together with pyritic sulphur in coals (ATSM D2492)^(1,7). Many studies have addressed the molecular characterisation of individual sulphur compounds in (i) light oils and (ii) extracts and pyrolysis products of petroleum source rocks and coals using gas chromatography-mass spectrometry (GC-MS) after appropriate pre-fractionation via liquid

chromatography. The reviews by Sinnighe Damaste and de Leeuw provide a comprehensive coverage of this topic ^(2,3) but, in general, only small proportions of the organic sulphur actually present in coals and petroleum source rocks are actually observed. Indeed, until recently, virtually no information was available on the overall distributions of the thiophenic and non-thiophenic (sulphidic) forms in fossil fuels and the need for suitable techniques has provided a major challenge to the analytical chemist. This review covers the significant advances achieved primarily over the past 5 years using X-ray techniques ⁽⁸⁻¹⁸⁾, temperature programmed reduction (TPR) ⁽¹⁹⁻²⁷⁾ and pyrolysis ⁽²⁸⁻³⁰⁾, temperature programmed oxidation (TPO) ⁽³¹⁻³³⁾ and selective chemical modification ^[34-40]. The latter approach comprises oxidation ⁽³⁴⁾, reduction ⁽³⁵⁻³⁹⁾ and quaternisation reactions ⁽⁴⁰⁾ and invariably involves the use of appropriate techniques, such as nuclear magnetic resonance (NMR) to monitor the resultant changes. Space precludes a comprehensive coverage of all the research on organic sulphur conducted using these techniques but it is hoped that the review illustrates the benefits that can arise from using a variety of analytical approaches to address a complex structural challenge and provides a platform for further reading. For a more detailed account of the application of these techniques to coal, the reader is referred to the recent article by Davidson ⁽⁷⁾.

2. General aspects

As well as pyritic and organic sulphur, sedimentary organic matter (particularly coal) is likely to contain significant amounts of both sulphatic and elemental sulphur. However, there is now overwhelming evidence to indicate that these are both oxidation products from pyrite ⁽⁷⁾. In such weathered samples, it is likely that some of the labile non-thiophenic organic sulphur forms have also been oxidised which gives rise to sulphoxides and sulphones from sulphides and sulphonic acids from di/polysulphides and thiols (Section 3). Hence, it is extremely important to ensure that appropriate handling precautions are taken to avoid oxidation.

The presence of pyrite in sedimentary organic matter poses a problem for most of the techniques described here and its removal prior to analysis is thus desirable. Pyrite can be removed via oxidation with dilute nitric acid as in the standard procedure (ASTM D 2492) for its determination and via reduction using lithium aluminium hydride ^(41,42) (LiAlH_4). However, care is required with both procedures as some of the organic sulphur forms can be affected; nitric acid can oxidise non-thiophenes whilst LiAlH_4 cleaves poly/disulphides to yield thiols. As a result, researchers have preferred to work with samples low in pyrite, for example, the two-high sulphur lignites, Mequienza and Rasa which both contain *ca* 10% organic sulphur but less than 0.5% w/w pyrite. Further, for coals, it has proved relatively easy to compare the results from the different analytical approaches as most researchers have also used the samples across the rank range supplied through the Argonne Premium Coal Sample (APCS) programme. For crude oils and petroleum source rocks, high-sulphur samples have again attracted the most attention, particularly for reductive studies ^[35-37] where a seep oil from Utah (Rozel Point, 14% w/w sulphur) and a Middle East shale (Jurf Ed Darawish, 16% w/w sulphur) have received the most attention.

3. X-ray techniques

3.1 X-RAY PHOTOELECTRON SPECTROSCOPY

Sulphur at or near the surface or particles (electron escape depth is *ca* 3 nm) can be observed via X-ray photoelectron spectroscopy (XPS) using the S 2p peak [8-10,34]. The binding energies of all sulphur compounds fall within a narrow range of less than 10 eV (Table 1) and the differences in binding energy between thiophenes/aromatic sulphides and aliphatic sulphides (sulphur bound to at least 1 sp^3 carbon) are only *ca* 1 eV (Table 1). Further, the S 2p peak comprises a $2p_{3/2}$ and a $2p_{1/2}$ component which have a 2:1 intensity ratio and are separated by 1.2 eV. In addition, there does not appear to be one unique binding energy for thiophenic/aromatic and aliphatic sulphur (Table 1). Not surprisingly, the first investigators to apply XPS to fuels [8,34] both concluded that it was not feasible to resolve thiophenic and different sulphidic environments directly by XPS and both proposed the use of selective oxidation to first convert sulphides into sulphones (Section 5). This gives rise to visually observable differences of 5-6 eV between the resultant sulphones and non-oxidised forms.

Figure 1 shows the XPS spectrum of Rasa coal obtained by Kelemen et al (9) that has been fitted to two signals with binding energies of 164.1 and 163.3 eV corresponding to those of thiophenes and alkyl sulphides, respectively (Table 1). From the peak fitting procedure, they concluded that thiophenic sulphur accounts for 70% of the organic sulphur present in this coal. Diaryl (aromatic) sulphides were not explicitly accounted for with polyphenylene sulphide having a binding energy of 163.7ppm midway between those above for thiophenes and alkyl sulphides. Nonetheless, after air oxidation (5 days at 125°C) to convert the non-thiophenes in to a mixture of sulphoxides, sulphones and sulphonic acids, thiophenic component still accounted for 69% of the sulphur with most of the sulphides (23% out of the original 30% of the sulphur) having been oxidised.

For coals containing significant quantities of pyrite, the peak-fitting procedure becomes more complex with a third component having to be included although the surface concentration of pyrite appears to be less than in the bulk (10). Despite the obvious uncertainties concerning the absolute accuracy of the peak-fitting procedure, the proportion of the thiophenic sulphur component has been found to increase with rank for the Argonne coals (10).(Table 2).

3.2 X-RAY ABSORPTION NEAR EDGE STRUCTURE SPECTROSCOPY

X-ray absorption near edge structure (XANES) spectroscopy has now been used by a number of research groups (10-18) to distinguish between the different organic sulphur forms in coals and heavy oil fractions. However, the requirement of a synchrotron source to provide the intense X-ray beam limits the availability of the technique. Until the very recent report of the sulphur L-edge (17,18), all the studies on fuels have involved observation of the sulphur K-edge where electrons are ejected from the 1s shell (10-16). Table 3 summarises the positions of the first inflection points for a number of sulphur compounds and, as with XPS, there is good resolution between sulphones, sulphoxides and non-oxidised sulphur forms. XANES differs from XPS in that data can be obtained in modes to reflect either the surface or the bulk of a material. Further, Table 3 indicates that the edge energies of thiophenes and diarylsulphides coincide but are resolved from those of aliphatic sulphides (sulphur bound to one or two sp^3 carbons) and disulphides. However,

Table 1 XPS sulphur 2p binding energies for some model compounds

Compound	Binding energy, eV
Dibenzothiophenesulphone	168.2
Polyphenylene ether sulphone	168.2
DL-Methionine sulphoxide	165.8
6-Ethoxy-2-mercaptobenzothiazole (thiazole)	164.2
Dibenzothiophene polymer	164.1
1,2-Benzodiphenylene sulphide	164.0
Sulphur	163.7
Polyphenylene sulphide	163.7
S-Methyl-L- cysteine	163.3
DL-Cysteine	162.7
6-Ethoxy-2-mercaptobenzothiazole (mercapto)	162.1

Taken from Kelemen et al (ref. 9).

Table 2 Comparison of sulphidic (non-thiophenic) sulphur contents derived by different techniques for some coals

	% of organic sulphur				
	Rasa	Mequinenza	Illinois No.6	Wyodak	Upper Freeport
C, % dmmf basis	80.2	68.4	80.7	76.0	88.0
Total sulphur	11.8	9.0	4.8	0.63	2.3
Pyritic sulphur	0.4	0.4	2.8	0.17	0.5
Organic sulphur (%w/w dry basis)	11.4	8.0	2.0	0.43	1.8
High pressure TPR	35	25	25	20	<10
XPS ^(a)	30	66	31	37	19
XANES	26	48	33-37	33-44	5-15
Fluid-bed pyrolysis ^(a)	47	67	-	36	-
TPO ^(a)	12	36	26	43	37

^(a) = refers to aliphatic sulphides with the implication that the total sulphidic content may be significantly higher.

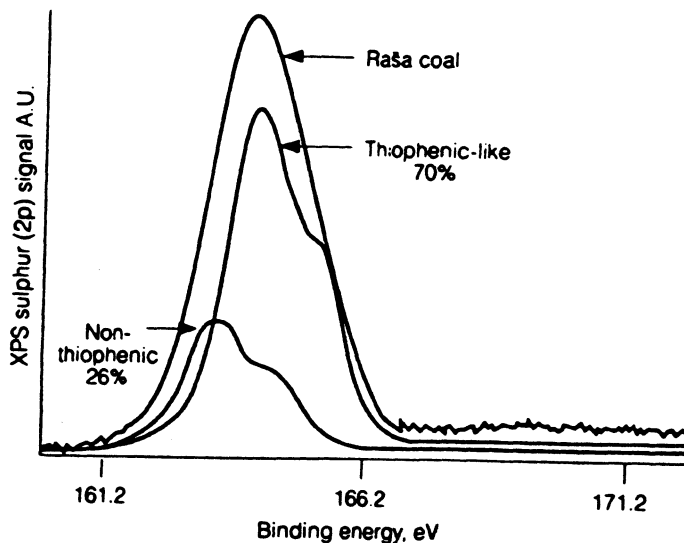


Figure 1

XPS spectrum of Rasa coal showing fit into thiophenic and alkylsulphide components (Kelemen et al, ref. 9). Reproduced by permission of the publishers, Butterworth Heinemann Ltd.

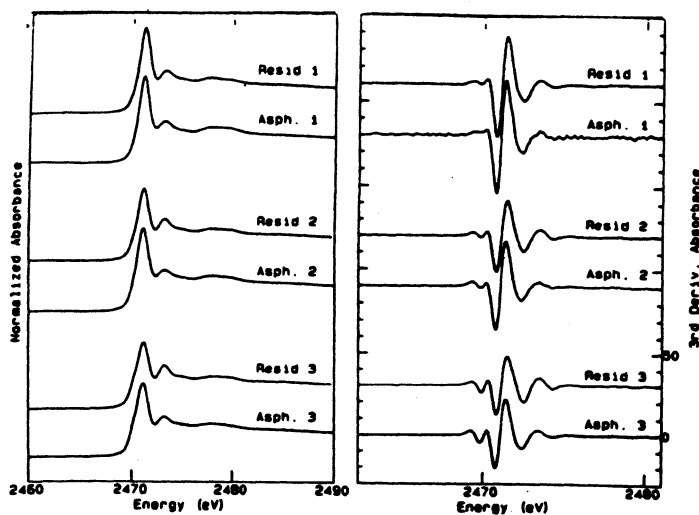


Figure 2

XANES spectra and their third derivatives for heavy petroleum fractions (Gorbaty et al, ref. 11). Reproduced by permission of the publishers, Butterworth Heinemann Ltd.

as with XPS, the energy differences between the different thiophenic and sulphidic environments are small (0.5-1.0 eV, Table 3) meaning that there is virtually no visible resolution observed in the region 2470 eV for fuels which is demonstrated in Figures 2 and 3 for heavy petroleum and coal samples, respectively. Thus, curve fitting procedures once again come into play for quantification. The two approaches that have been used to estimate aromatic and aliphatic-bound sulphur involve (i) taking the third derivatives of the spectra (Figure 2) and using the heights of the features at 2469.8 and 2470.4 eV [10-13] and (ii) least-squares analysis of the near-edge structure into a series of components (Figure 3) for pyrite, the aromatic and aliphatic-bound sulphur, sulphoxide, sulphone and sulphate (15,16). If oxidised sulphur forms are present, calibrations need to be carried out as the observed intensities increase with oxidation state making peaks from sulphones/sulphates look pronounced even when their concentrations are fairly small (Figure 3).

Within the estimated accuracy of both fitting procedures ($ca \pm 10\%$ of the organic sulphur), remarkably close agreement has been achieved for the Argonne coals (Table 2) with the fraction of aromatic-bound sulphur increasing from $ca 60\%$ in sub-bituminous coals to over 85% in low-volatile bituminous coal (7,10,12,15). Although, for the reasons outlined above, the results from XPS and XANES are probably not strictly comparable, good agreement has generally been achieved for heavy petroleum fractions and coals investigated by both techniques (Figure 4) (7,11). However, there is evidence to suggest that XANES might underestimate aromatic-bound sulphur. For example, it appears unrealistic that lignites and sub-bituminous coals (7,11) contain similar proportions of aliphatic sulphur to heavy petroleum fractions despite being significantly more aromatic in character. Further, although the high temperature in-situ measurements conducted by Huffman et al (16) have shown the anticipated decrease in the proportion of aliphatic sulphur with increasing temperature, significant amounts remain above 500°C which is certainly not expected from their thermal behaviour. As with XPS, the use of selective oxidation in which non-thiophenic/aromatic sulphur forms only are converted into sulphoxides and sulphones (S^{II} and S^{IV} species) gives rise to vastly improved the resolution in XANES. Where air oxidation has been used to achieve this, the agreement between XPS and XANES has again been fairly good (13).

Sulphur forms can also be examined by L-edge XANES spectra in which transitions from the 2p orbitals are observed and the first spectrum of a coal was published recently (17). Although distinct peaks are visible because the linewidths are narrower and photon resolution is greater, considerable overlap occurs between thiophenes and the other forms and curve-fitting is still required. In fact, the distribution of 70% thiophenic and 30% arylsulphide which gave the best fit (17) was considerably at variance with that derived from the K-edge spectra (18) and was seen as unrealistic by Calkins, Gorbaty and their coworkers (44). However, this apparent discrepancy probably arises from the fact that not enough standards have yet been analysed under the high-vacuum conditions required for L-edge XANES (18).

4. Thermal techniques

4.1 REDUCTIVE TECHNIQUES

4.1.1 Low pressure TPR TPR is based on the principle that different organic sulphur forms present in solid fuels have different characteristic reduction temperatures at which hydrogen sulphide (H₂S) evolves. Calibration with model compounds has indicated that

Table 3 Sulphur K-edge energies in XANES spectra for some model compounds

Compound	Energy at first inflection point, eV		Formal Ox. state
	Actual value (ref. 11)	Rel. to el. S (refs. 11 and 15)	
Dibutylsulphone	-	- (7.5)	4
Diphenylsulphone	2474.8	4.7	4
Dibenzothiophenesulphone	2474.7	4.6	4
Dibenzylsulphoxide	-	- (3.4)	2
Dimethylsulphoxide	2472.8	2.7	2
Benzothiophene	2470.4	1.3	0
Dibenzothiophene	2470.4	1.3 (1.3)	0
Diphenylsulphide	2470.4	1.3	0
Thiaanthrene	2470.2	1.1	0
Diocylsulphide	2470.1	1.0	0
Benzylphenylsulphide	2469.9	0.8	0
Dibenzylsulphide	2469.8	0.7 (0.7)	0
Cysteine	2469.2	0.1	0
Diphenyldisulphide	2469.2	0.1 (0.1)	0
Sulphur	2469.1	0	0
Pyrite	2468.4	-0.7 (-0.5)	-1

Values taken from Gorbaty et al (ref. 11) and, in brackets, from Huffman et al (ref.15).

Table 4 T_{MAX} for solid calibrants used in high pressure TPR

Calibrant	T _{MAX} , °C
Silica-immobilised dibenzothiophene	470
Silica-immobilised diphenylsulphide	350
Silica-immobilised phenylbenzylsulphide	300
Silica-immobilised thioanisole (S-CH ₃)	250-350
Di/polysulphides in vulcanised coal tar pitch	150-250
Thiol, cysteine	180

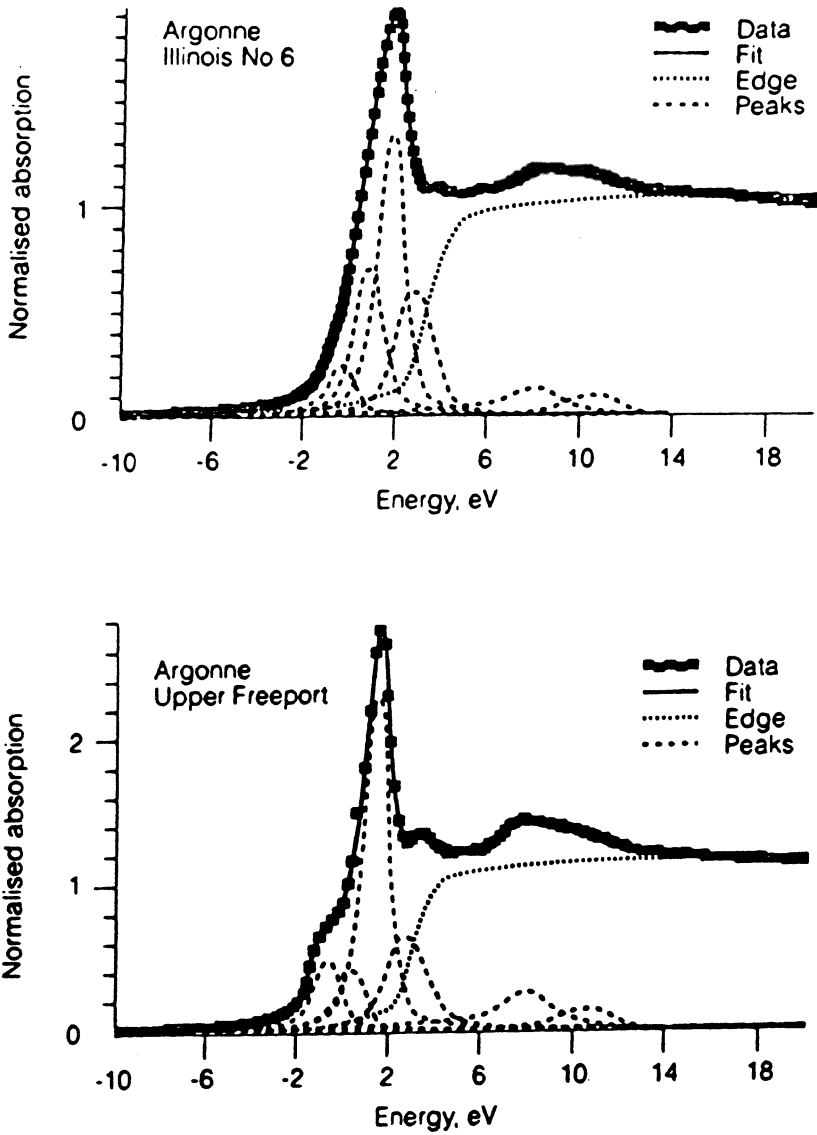


Figure 3

XANES spectra of Illinois No.6 and Upper Freeport coals showing deconvolution into components for pyrite, aliphatic and aromatic-bound sulphur, sulphoxide, sulphone and sulphate. Reprinted from Huffman et al, ref. 15. Copyright [1991] American Chemical Society.

the ease of reduction is in the order of thiols > aliphatic sulphides > aromatic sulphides > thiophenes (19) (Table 4). The method for coals was pioneered by Attar (19,20) and has been used by others (21-23) with few modifications to the original design of the reactor in which coal is refluxed in a mixture of low-boiling solvents and H₂S is swept from the reactor by a stream of carrier gas; a condenser prevents the escape of tar. Attar originally used lead acetate paper to detect H₂S but later workers have used potentiometry (21,22) and flame photometric detection (23). However, only limited success has been achieved thus far primarily because only the labile non-thiophenic forms have actually been observed with sulphur balances being poor. Virtually all the thiophenic sulphur remains in the char due to the use of low hydrogen partial pressures (max. 1 atm.) and inappropriate low boiling reducing agents, such as tetralin. Further, no account has been taken of the reduction of pyrite to pyrrhotite and retrogressive reactions including the conversion of sulphides into thiophenes which are extremely likely due to the long residence time of tar in the reactor. Nevertheless, Attar (19,20) was confident enough to estimate the concentrations of thiolic and aliphatic and aromatic sulphidic sulphur directly from the TPR traces. However, the reported thiol concentrations (ca 20% of the organic sulphur in bituminous coals) are now considered to be unrealistically high (7) whilst those for aromatic sulphides of below 10% are probably too low.

The application of low pressure TPR to study chemical desulphurisation of solid fuels is described in the contribution by Franco and coworkers in this volume.

4.1.2 High pressure TPR The extent of desulphurisation in the pyrolysis of sedimentary organic matter generally increases with hydrogen pressure (44) and typically, in a fixed-bed reactor at a pressure of 150 bar with a dispersed sulphided molybdenum (Mo) catalyst, over 95% of the organic sulphur in both lignites and bituminous coals can be released. Moreover, only about 20% is released as thiophenic compounds in the tars with the remaining 75-80% appearing in the gas phase as H₂S. These findings prompted the authors to overcome the inherent drawbacks of TPR by using a high pressure technique, in which the evolved H₂S is measured with a quadrupole mass spectrometer (24,25). Pyrite contributes significantly to the H₂S profiles and, where present in high concentrations, it has been removed with LiAlH₄.

Figure 5 compares the high pressure TPR traces for Mequinenza lignite and a liptinite concentrate (H rich) separated by density gradient centrifugation [45]. The H₂S evolution profiles comprise a broad shoulder between 200 and 400°C from non-thiophenic sulphur forms followed by the dominant peak above 400°C attributable to thiophenes. These reduction temperatures have been confirmed using novel silica-immobilised sulphur compounds [26] and other appropriate solid calibrants (Table 4). Indeed, the reduction temperature at which H₂S evolution reaches a maximum (T_{MAX}) of 480°C for immobilised dibenzothiophene is close to those of low-rank coals. Given that the T_{MAX} for diphenylsulphide is ca 350°C, it can be concluded that much of the non-thiophenic sulphur in both Mequinenza and Rasa lignites (ca 30% of the total, Rasa gives a similar trace to Mequinenza [26]) occurs as aliphatic sulphides and disulphides with approximately half of the H₂S below 400°C evolving between 200 and 320°C (Figure 5). That below 250°C is attributed to disulphides but the lack of any intensity much below 200°C suggests that thiols are not present in significant concentrations. The resolution is thus considerably superior to that achieved for X-ray techniques, and as might be anticipated from its lower aromaticity, the liptinite contains a greater proportion of non-thiophenic sulphur forms than the whole lignite. Further, T_{MAX} for the thiophenic sulphur in the liptinite occurs at a much

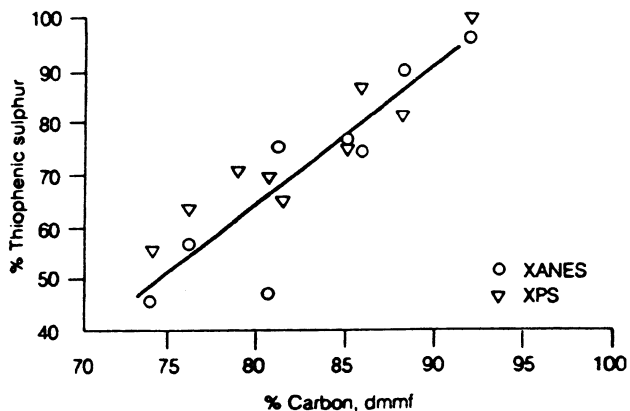


Figure 4 Proportions of thiophenic or, probably more strictly, aromatic-bound sulphur derived from XPS and XANES for the Argonne coals. Reprinted from Gorbaty et al, ref. 10. Copyright [1991] American Chemical Society.

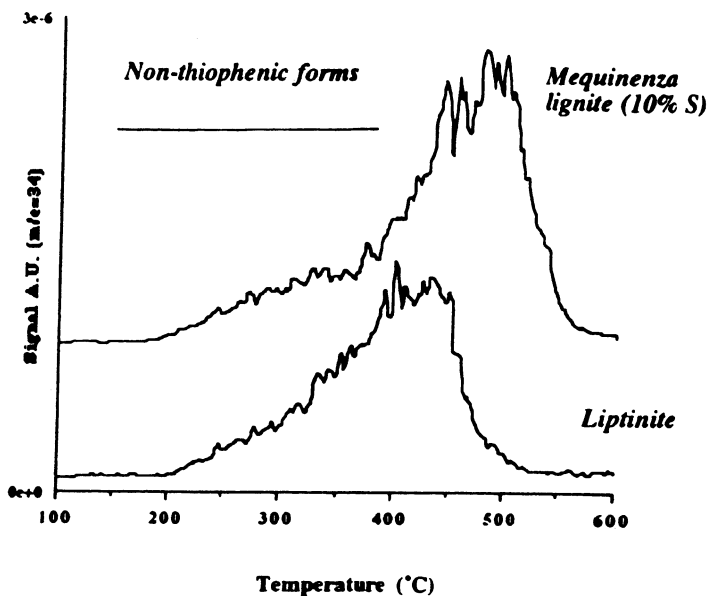


Figure 5 High pressure TPR traces for Mequinenza lignite and its liptinite concentrate (Mitchell et al, ref. 25).

lower temperature strongly suggesting that single ring thiophenes are the dominant form present (Figure 5) compared to probably a mixture of 1-3 ring structures in the whole lignite. These, together with the parallel trends for the distributions of thiophenic compounds in the TPR tars [27] indicate the potential of high pressure TPR to give a good indication of the average ring size of the thiophenic structures present.

The high pressure technique has been applied to Rasa and Mequinenza and indicated that thiophenic forms account for *ca* 70% of the total (24,25) (Table 2). In common with XPS and XANES and other pyrolysis methods, high pressure TPR indicates that thiophenic sulphur increases with rank. However, the proportions of thiophenic sulphur derived from high pressure TPR are consistently higher than by the X-ray techniques with bituminous coals containing no more than 10% of the organic sulphur in non-thiophenic forms (Table 2). The contribution by Mitchell et al in this volume describes the application of high pressure TPR to oil shales.

4.1.3 Flash pyrolysis Calkins and coworkers (28-30) studied the reduction behaviour of a number of sulphur compounds in a fluidised-bed reactor as a function of temperature. The results summarised in Figure 6 indicate that the reduction of aliphatic sulphides, thiols (mercaptans) and disulphides is nearly completed by 800°C whilst aromatic sulphides are stable until higher temperatures are reached and thiophenes are only partially reduced above 900°C. These cut-off points were used for coals to estimate the proportions of aliphatic and aromatic sulphides/thiols. The proportions of aliphatic sulphides derived by this method are generally higher than those from both X-ray and TPR techniques (Table 2) with surprisingly low values for aromatic sulphides (7). These differences might arise from the fact that the desulphurisation behaviour of solids is probably different to that of volatile species in fluidised-beds in that their residence times are much longer implying that some aromatic-bound sulphur may evolve as H₂S below 800°C.

4.2 TEMPERATURE PROGRAMMED OXIDATION

The principal of TPO is the same as that of TPR except the sulphur forms are being oxidised to yield primarily sulphur dioxide (small amounts of COS are also released) at characteristic temperatures, the evolved SO₂ being monitored by Fourier transform infrared spectrometry. The technique has been developed by LaCount and co-workers (31-33) over a number of years and is now referred to as "controlled-atmosphere programmed temperature oxidation" (CAPTO). To limit heating effects, coals are diluted in an excess of tungsten oxide (WO₃) which also acts as a combustion catalyst. Early work was conducted using a mixture of 10% v/v of oxygen in helium (31), but it was found that pyrite produced SO₂ in the temperature range, 250-380°C, the same as that for aliphatic sulphide polymers. This problem was solved using pure oxygen which curtails pyrite oxidation until above 470°C (32,33) which is beyond the oxidation temperature found for aryl sulphides and thiophenes of *ca* 420°C. Typical CAPTO traces for samples of untreated and biotreated Illinois coal are shown in Figure 7 which shows the distinct peaks obtained for aliphatic and aromatic-bound sulphur (290 and 420°C) and pyrite (480 and 580°C). The particular biotreatment used has removed all the pyrite, together with some of the aliphatic and aromatic-bound sulphur (Figure 7).

Table 2 and the information presented by Davidson (7) indicate that, compared to the other techniques described, the estimates of aliphatic sulphide contents from CAPTO occur

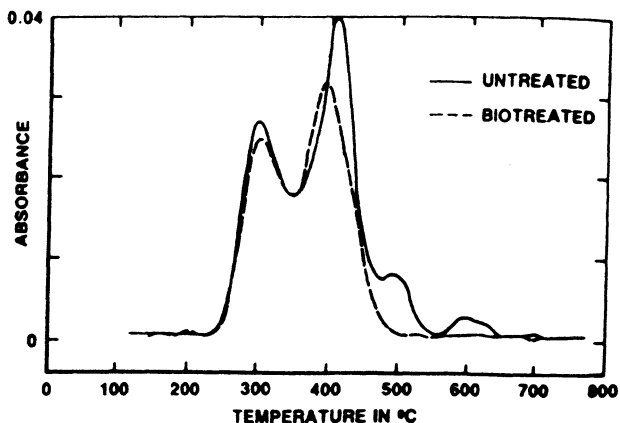


Figure 6 Hydrogen sulphide evolution from reduction of model sulphur compounds in a fluidised-bed reactor. Reprinted from Calkins, ref. 28. Copyright [1991] American Chemical Society.

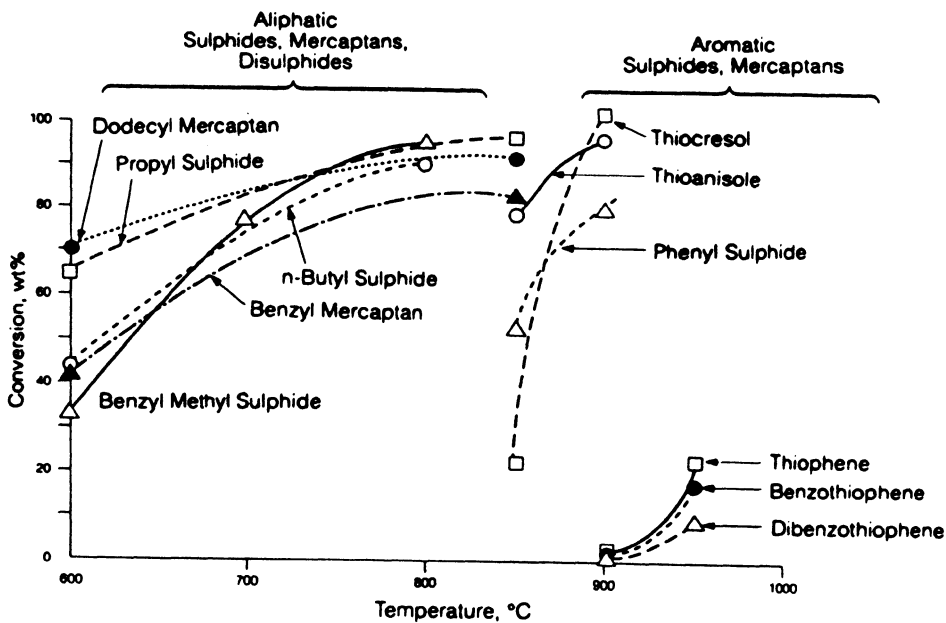


Figure 7 CAPTO sulphur dioxide evolution profiles for samples of untreated and biotreated Illinois No. 6 coal (LaCount et al, ref. 33). Reproduced by permission of the publishers, Butterworth Heinemann Ltd.

across a relatively narrow range (10-35%) and there is no clear rank trend. It seems surprising that a low-volatile bituminous coal, such as Upper Freeport (Table 2), contains similar or greater proportions of aliphatic sulphides than lower rank coals, such as Rasa and Mequinenza lignites. These apparent anomalies might be a consequence of the limited number of standards that have been used to calibrate the technique. As with high pressure TPR, only solid calibrants which will not soften upon heating can be used in the well-swept fixed-bed reactor.

5. Chemical modification

5.1 OXIDATION

The selective oxidation and reduction of particular non-thiophenic sulphur forms prior to analysis offers an attractive approach for speciation. It has already been described how simple air oxidation appears to be fairly effective for non-thiophenic forms (Section 3). Of the many available oxidising agents, *t*-butylhydroperoxide oxidises aliphatic sulphides selectively to sulphoxides⁽³⁴⁾. This approach was used in conjunction with XPS and LiAlH_4 reduction (see following) to show that asphalt contains approximately 50% thiophenic sulphur which appears to be reasonably consistent with direct XPS⁽⁹⁾ and XANES results⁽¹¹⁾, albeit for different samples.

For heavy oils, selective oxidation of the sulphides present to sulphoxides has also been achieved in solution using tetrabutylammonium periodate⁽⁴⁶⁾. Chromatographic separation of the resultant sulphoxides and subsequent reduction with LiAlH_4 to regenerate the sulphides provided concentrates for GC-MS analysis. After separation of the sulphides from the *n*-heptane soluble fractions, the remaining thiophenes were then treated in a similar manner but being selectively oxidised using the stronger reagent, *m*-chlorobenzoic acid. For the suite of samples investigated, the proportions of thiothenes and sulphides varied significantly and the compositions of the sulphur fractions were complex although a good correlation was found between the depth of burial and a maturity index based on the pattern of alkyl substitution for the dibenzothiophenes. Stepwise perchloric acid oxidation has been used to determine pyritic and total organic sulphur contents of coals⁽⁴⁰⁾ and this approach shows promise in attempting to resolve sulphidic and thiophenic sulphur^[48]. However, as for the reduction of insoluble macromolecular organic matter, there is always going to be the uncertainty over accessibility of reagents.

5.2 REDUCTION/HYDRODESULPHURISATION

The points of sulphur incorporation into sedimentary organic matter during diagenesis has been a topic of great interest to organic geochemists (see, for example, refs. 35-37). For high-sulphur oils and source rocks, the hydrocarbons released using relatively specific reducing agents or desulphurisation catalysts indicate the actual moieties involved in sulphur linkages as well as helping to identify the depositional environment. For kerogens (insoluble material in petroleum source rocks), soluble reducing agents are clearly going to be more effective than solid desulphurisation catalysts, such as Raney nickel, which is nonetheless effective for sulphides and simple thiophenes in heavy oil fractions. Indeed, the alkane products obtained using nickelocene/ LiAlH_4 and lithium in ethylamine

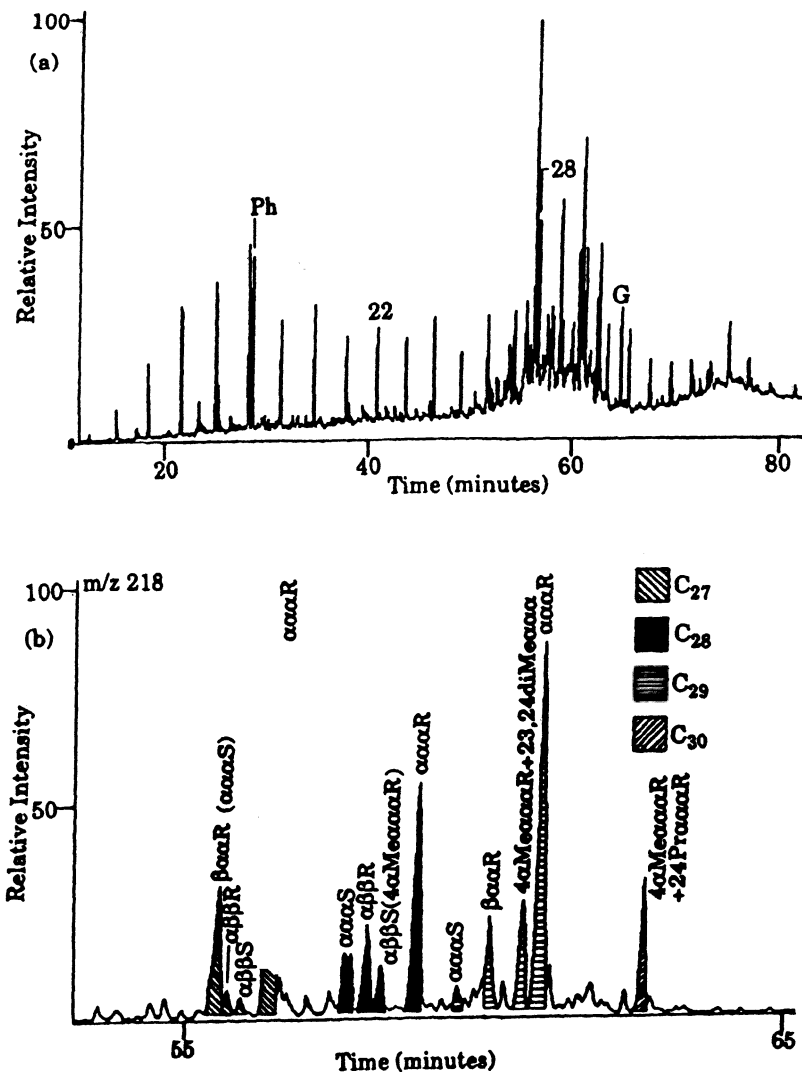


Figure 8

(a) Reconstructed ion chromatogram and (b) partial m/z 218 mass chromatogram (showing the sterane distribution) from GC-MS analysis of the alkane fraction obtained via Li/EtND_2 treatment of JED kerogen. The sterane peaks are marked with stereochemistry at positions 5, 14 and 17 and configuration at position 20. The components in brackets are the minor contributors to peaks for coeluting species. Reprinted from Hofmann et al., ref. 37. Copyright 1991, with kind permission from Elsevier Science Ltd., The Boulevard, Langford Lane, Kidlington OX5 1GG, UK.

(Li/EtNH₂) have been found to be similar to those with Raney Ni for heavy oil fractions (36,37). Moreover, the use of deuterated reducing agents enables the points of attachment of the released alkanes to be assigned with some certainty. As an example of this elegant approach, Figure 8 shows the reconstructed ion chromatogram, together with the partial *m/z* 218 mass chromatogram which is indicative of the sterane distribution for the alkane fraction from Li/EtND₂ treatment of the Jurf EdDarawish (JED) kerogen (37). The deuterium labelled products identified were dominated by the steranes of algal origin with the positions of deuterium incorporation providing confirmatory evidence of sulphide linkages. In contrast, the labelled products from a bituminous kerogen (Serpiano) were dominated by hopanes of bacterial origin which were linked via the side chain (37). The contribution by Hefter and coworkers in this volume is a further example of this approach where deuterated nickel borohydride is used as the reducing agent.

For coals, Lochmann's base, an equimolar mixture of n-butyllithium and potassium *t*-butoxide has been used to reduce sulphides in what, from XANES evidence, appears to be in a fairly selective manner (38); a 30% reduction in organic sulphur was achieved for the Illinois No.6 coal from the Argonne suite. The Lochmann's base treatment was followed by potassium naphthalenide in tetrahydrofuran which converts dibenzothiophene to sulphur-free products (39). This subsequent treatment reduced the organic sulphur content of Illinois No.6 coal by a further 0.55% w/w leaving 0.7% w/w in the final product which suggests that, possibly due to a combination of mass transfer and chemical factors, it is only partially effective for the thiophenic sulphur in coals.

5.3 QUATERNISATION

The low receptivity of ³³S and the fact that it has a quadrupole has made it extremely difficult to observe organic sulphur in fuels directly by NMR. However, for oils and extracts, quaternary iodide salts can readily be formed in solution from the sulphur species present and if ¹³C-enriched iodomethane is used, then ¹³C NMR can be used to estimate the concentrations of non-thiophenic forms present (40). We have applied this approach to the chloroform extract of Mequinenza lignite and Figure 9 shows the ¹³C NMR spectra of the extract before and after quaternisation with ¹³C-enriched iodomethane. The aliphatic region in the quaternised fraction is dominated by methyl peaks from the S⁺-CH₃ groups formed and most of the intensity occurs in the region, 20-30 ppm where peaks from non-thiophenes occur (40). Indeed, from the intensity of this region, it is estimated that non-thiophenes account for over 60% of the total sulphur which is not surprising in light of the low carbon aromaticity of this particular fraction (*ca* 1% w/w) in relation to the whole lignite (0.25 cf. 0.75).

6. Conclusions

Although each of the approaches described here has its limitations, a consistent overall picture is beginning to emerge on the nature of organic sulphur groups in sedimentary organic matter and fuels. As might be anticipated, the more stable thiophenic sulphur forms are most abundant in the more mature coals and petroleum source rocks. Further, the X-ray and pyrolytic techniques described are now at the stage that the changes in organic sulphur distributions which occur during the formation and refining of heavy oils and the chemical desulphurisation treatments for coals can be monitored effectively.

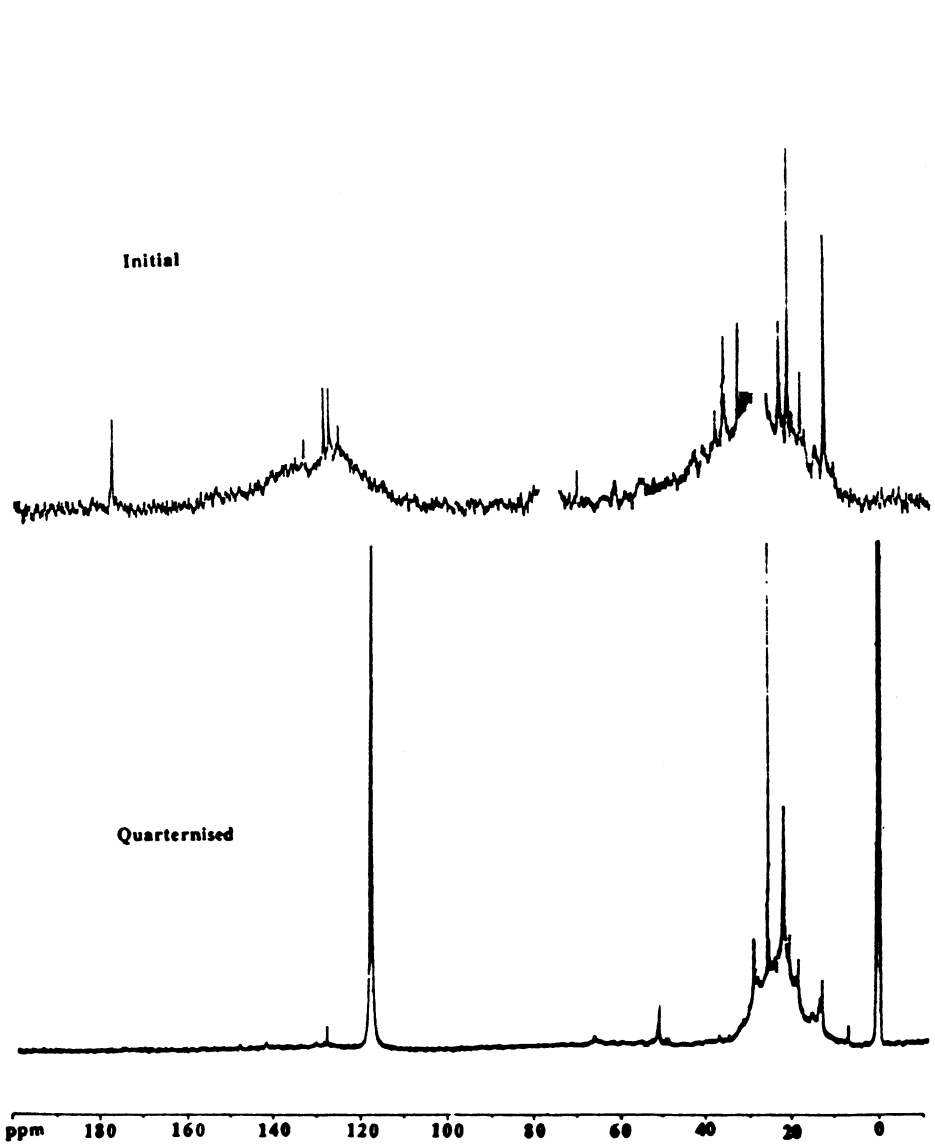


Figure 9 100 MHz ^{13}C NMR spectra of the chloroform extract of Mequinenza lignite before and after quaternisation with ^{13}C -enriched iodomethane.

7. References

1. C-L Chou, 'Geochemistry of sulphur in coal'. In Geochemistry of Sulphur in Fossil Fuels, Am. Chem. Soc. Symp. Ser. No. 429, Eds. W.L. Orr and C.M. White, Am. Chem. Soc., Washington, 1990, p 30.
2. J.S. Sinninghe Damste and J.W. de Leeuw, Fuel Process. Technol., 1992, **30**, 109 and references therein.
3. J.S. Sinninghe Damste and J.W. de Leeuw, Org. Geochem., 1990, **16**, 1077 and references therein.
4. B.P. Tissot and D.H. Welte, 'Petroleum Formation and Occurrence', 2nd Ed., Springer, Heidelberg, 1984.
5. T.I. Eglinton, J.S. Sinninghe Damste, M.E.L. Kohnen, J.W. de Leeuw, S.R. Larter and R.L. Patience. Analysis of maturity-related changes in the organic sulphur composition of kerogens by flash pyrolysis-gas chromatography. In Geochemistry of Sulphur in Fossil Fuels, Am. Chem. Soc. Symp. Ser. No. 429, Eds. W.L. Orr and C.M. White, Am. Chem. Soc., Washington, 1990, p 529.
6. J-F LePage, Applied Heterogeneous Catalysis, IFP Editions Technip, Paris, 1987.
7. R.M. Davidson, Organic sulphur in coal, IEA Coal Research CR/60, August 1993.
8. R.B. Jones, C.B. McCourt and P. Swift, Proc. 1981 Int. Coal Sci. Conf., Verlag Gluckauf, Essen, 1981, p 657.
9. S.R. Kelemen, G.N. George and M.L. Gorbaty, Fuel, 1990, **69**, 939.
10. M.L. Gorbaty, G.N. George and S.R. Kelemen, Direct determination and quantification of sulphur forms in heavy petroleum and coal: sulphur K-edge X-ray absorption and X-ray photoelectron spectroscopic approaches. In Coal Science II, Am. Chem. Soc. Symp. Ser. No. 461, Eds. H.H. Schobert, K.D. Bartle and L.J. Lynch, Am. Chem. Soc., Washington, 1991, Chapter 2, p 127.
11. M.L. Gorbaty, G.N. George and S.R. Kelemen, Fuel, 1990, **69**, 945.
12. G.N. George, M.L. Gorbaty, S.R. Kelemen and M. Sansome, Energy & Fuels, 1991, **5**, 93.
13. M.L. Gorbaty, S.R. Kelemen, G.N. George and P.J. Kwiatek, Fuel, 1992, **71**, 1255.
14. R. Fiedler and D. Bendler, Fuel, 1992, **71**, 751.
15. G.P. Huffman, S.Mitra, F.E. Huggins, N. Shah, S. Vaidya and F. Lu, Energy & Fuels, 1991, **5**, 574.
16. M.M. Taghiei, F.E. Huggins, N. Shah and G.P. Huffman, Energy & Fuels, 1992, **6**, 293.
17. J.R. Brown, M. Kasrai, G.M. Bancroft, K.H. Tan and J.M. Chen, Fuel, 1992, **71**, 649.
18. J.R. Brown, M. Kasrai, G.M. Bancroft, K.H. Tan and J.M. Chen, Fuel, 1993, **72**, 900.
19. A. Attar, Sulphur groups in coal and their determinations. In Analytical Methods for Coal and Coal Products, Vol III, Academic, 1979, Ch.56 and DOE/PC/30145TI Technical Report.
20. A. Attar and F. Dupois, Data on the distribution of organic sulphur functional groups in coals. In Coal Structure, Adv. in Chem. Ser., No. 192, Eds. M.L. Gorbaty and K. Ouchi, Am. Chem. Soc., Washington, 1981, p 239.
21. B.B. Majchrowicz, J. Yperman, G. Reggers, J.M. Gelan, H.J. Martens, J. Mullens and L.C. van Poucke, Fuel Process. Technol., 1987, **15**, 363.

22. B.B. Majchrowicz, J. Yperman, H.J. Martens, J.M. Gelan, S. Wallace, C.J. Jones, M. Baxby, N. Taylor and K.D. Bartle, Fuel Process. Technol., 1990, **24**, 195.
23. B.T. Dunstan and L.V. Walker, Final Report to Australian Nat. Energy Res. Dev. and Dem. Council (1988).
24. C.J. Lafferty, S.C. Mitchell, R. Garcia and C.E. Snape, Fuel, 1993, **72**, 367.
25. S.C. Mitchell, C.E. Snape and R. Garcia, Fuel, 1994, **73**, 1159.
26. S. Mitchell, C.J. Lafferty, R. Garcia, K. Ismail, C.E. Snape, A.C. Buchanan III, P.E. Britt and E. Klavetter, Prepr. Am. Chem. Soc. Div. Fuel Chem., 1992, **37(4)**, 1691 and Proc. 1993 Int. Conf. on Coal Sci., in press.
27. R. Garcia, S.C. Mitchell, C.E. Snape, S. Moinelo and K.D. Bartle, Proc. 1993 Int. Conf. on Coal Sci. Vol. I, p 445.
28. W.H. Calkins, Energy & Fuels, 1987, **1**, 59.
29. R.J. Torres-Ordenez, W.H. Calkins and M.T. Klein, Distribution of organic-sulphur containing structures in high organic sulphur coals. In Geochemistry of Sulphur in Fossil Fuels, Am. Chem. Soc. Symp. Ser. No. 429, Eds. W.L. Orr and C.M. White, Am. Chem. Soc., Washington, 1990, p 287.
30. W.H. Calkins, R.J. Torres-Ordenez, B. Jung, M.L. Gorbaty, G.N. George and S.R. Kelemen, Proc. 1991 Int. Conf. on Coal Sci., Butterworth-Heinman p 985 and Energy & Fuels, 1992, **6**, 411.
31. R.B. LaCount, R.R. Anderson, S. Friedman and S. Blaustein, Fuel, 1987, **66**, 909.
32. R.B. LaCount, D.G. Kern, W.P. King, T.K. Trulli and D.K. Walker, Prepr. Am. Chem. Soc. Div. Fuel Chem., 1992, **37(3)**, 1083.
33. R.B. LaCount, D.G. Kern, W.P. King, R.B. LaCount Jr., D.J. Miltz Jr., A.L. Stewart, T.K. Trulli, D.K. Walker and R.K. Wicker, Fuel, 1993, **72**, 1203.
34. J-M Ruiz, B.M. Carden, L.J. Lena and E-J Vincent, Anal. Chem., 1982, **54**, 688.
35. M.E.L. Kohnen, J.S. Sinninghe Damste, A.C. Kock-van-Dalen and J.W. de Leeuw, Geochim Cosmochim Acta, 1991, **55**, 1375.
36. H.H. Richnow, A. Jenisch and W. Michaelis, Geochim Cosmochim Acta, 1992, and in Adv. in Org. Geochem., Eds. C.B. Eckard et al, Pergamon, Oxford, 1991, p 351.
37. I.C. Hofmann, J. Hutchinson, J.N. Robson, M.I. Chicarelli and J.R. Maxwell, Org. Geochem., 1992, **19**, 371.
38. K. Chatterjee and L.M. Stock, Energy & Fuels, 1991, **5**, 704.
39. K. Chatterjee, R. Wolny and L.M. Stock, Energy & Fuels, 1990, **4**, 402.
40. T. Green, W.G. Lloyd, L.Gan, P. Whately and K. Wu, Prepr. Am. Chem. Soc. Div. Fuel Chem., 1992, **37(2)**, 664
41. D.L. Lawlor, J.I. Fester and W.E. Robinson, Fuel, 1963, **42**, 239.
42. J.W. Smith, N.B. Young and D.L. Lawlor, Anal. Chem., 1964, **36**, 618.
43. W.H. Calkins, M.L. Gorbaty and S.R. Kelemen, Fuel, 1993, **72**, 900.
44. R. Garcia, S.R. Moinelo, C.J. Lafferty and C.E. Snape, Energy & Fuels, 1991, **5**, 582.
45. D.N. Taulbee, S.H. Poe, T.L. Robl and B. Keogh, Energy & Fuels, 1989, **3**, 662.
46. J.D. Payzant, T.W. Mojelsky and O.P. Strausz, Energy & Fuels, 1989, **3**, 449.
47. C.W. McGowan and R. Markuszewski, Fuel, 1988, **67**, 1091.
48. R. Markuszewski, X. Zhou, and C.D. Chriswell, Prepr. Am. Chem. Soc. Div. Fuel Chem., 1992, **37(1)**, 417.

DETAILED STRUCTURAL CHARACTERIZATION OF THE ORGANIC MATERIAL IN RUNDLE RAMSAY CROSSING AND GREEN RIVER OIL SHALES

M. SISKIN, C. G. SCOUTEN, K. D. ROSE, T. ACZEL, S. G. COLGROVE AND R. E. PABST, JR.

Corporate Research Laboratory
Exxon Research and Engineering Co.
Route 22 East, Clinton Township
Annandale, New Jersey 08801 USA

ABSTRACT. The hydrocarbon, oxygen and nitrogen functionalities in Rundle Ramsay Crossing oil shale (RXOS) and Green River oil shale (GROS) have been characterized and quantified using selective/nondestructive chemical derivatizations with isotopically labeled reagents followed by solid state ^{13}C - and ^{29}Si -NMR analysis. In addition, in-depth MS and NMR characterization of the structural features associated with shale oils produced from RXOS and GROS under mild conditions which afford high organic conversions (>85%) have been carried out. The results of these studies have been combined and incorporated into molecular models of the structure of the representative organic material in RXOS and GROS. The models agree well with experimental values for elemental composition, aromaticity, distribution of chain lengths and ring system sizes, hydrocarbon and heteroatom functionalities and the proportion of kerogen and bitumen.

1. History

Oil shale organics are largely present as kerogen, an insoluble and non-volatile material, which is finely disseminated in the rock matrix of the shale, and which must be depolymerized in order to recover shale oil from the rock.¹ This is difficult and expensive. Therefore, there has been intense interest in understanding the molecular structure and chemistry of oil shale kerogens and over the past twenty-five years several research groups have attempted to elucidate the structure of the kerogen of the Green River formation.

Burlingame, et. al.^{2,3} carried out the oxidation of a Green River kerogen concentrate (65.9%) with 3 M chromic acid in sulfuric acid under reflux for 3-48 hours. Most of the organic carbon was converted to carbon dioxide; the remainder, which amounted to only about 9%, was extracted and analyzed by MS and GC. Based upon analysis of these results, the authors proposed a structural model for Green River oil shale organics.

Djuricic, et. al.⁴ carried out the oxidation of a Green River kerogen concentrate in aqueous alkaline potassium permanganate. The corresponding methyl esters were analyzed by GC/MS. Since 70% of the carbon skeleton was converted into carboxylic acids, Djuricic concluded that the "nucleus" probably consisted of long polymethylene bridges connected at tertiary or quaternary branching centers.

Schmidt-Collerus and Prien⁵ used a combination of controlled micropyrolysis and mass spectrometry to investigate the structure of Green River kerogen. They identified (a) normal and branched alkenes, (b) alkyl decalins and tetralins, (c) alkyl-substituted tricyclic terpenoid or phenanthroid type derivatives in the shale oil product. Based upon these results they proposed a generalized kerogen structure with alkyl-substituted decalins or tetralins interlinked by normal or branched alkane bridges (Figure 3). In a kerogen matrix the many sub-units are connected by alkane or ether linkages. There are also trapped sub-units within the matrix. While this model is more detailed than previous models, it is obvious that many of the observed compounds represent secondary pyrolysis reaction products.

Yen and co-workers⁶ recovered over 90% by weight of the original organic carbon content of a Green River kerogen concentrate after mild stepwise alkaline permanganate oxidations. Ten successive fractions were taken and studied by GC, MS, NMR and IR. The carbonate-free oil shale was analyzed by XRD, ESR and ESCA. They concluded that aromatic carbon systems are either absent or present in minute quantities in kerogen and that the bulk of the carbon skeleton is naphthenic and contains 3-4 rings possibly linked by heterocyclic atoms or randomly-substituted short branched hydrocarbon chains.^{7,8} A conceptual model was proposed, largely to accommodate the accumulated physical and chemical evidence.

McGowan and co-workers based their structural model of Green River oil shale kerogen upon characterizations of extracted bitumen, retorted shale oil, and the products obtained by oxidizing the kerogen concentrate with perchloric acid.⁹ The oxidations were carried out by heating the kerogen for 1.5 h in constant-boiling aqueous perchloric acid mixtures. At boiling points up to 150°C (7.99 *N* HClO₄), little oxidation was found; CO₂ yields were less than 2% and essentially all of the kerogen was undissolved. As the boiling point of the perchloric acid was increased from 161°C (8.97 *N* HClO₄) to 180°C (10.18 *N* HClO₄) the CO₂ yield increased from 8.3% to 39.8%, and the amount of undissolved material decreased from 77.4% to 1.9%. At temperatures of 169-180°C, where more than one-half of the kerogen was not insoluble, less than one-half of the starting mass was accounted for in the isolated products. Nevertheless, the products were analyzed. After methylation to convert acids into the corresponding esters, products identified by GC and GC-MS included: methyl esters of C₁₄-C₁₉ fatty acids, phthalate esters, C₁₈-C₂₇ alkanes, and aromatic hydrocarbons (mostly phenanthrene and substituted phenanthrenes). Based upon these results, a model for the structure of the Green River oil shale kerogen was proposed.

Workers at the Institut Francais du Petrole (IFP) have taken a distinctly different approach to kerogen modeling. The studies discussed above were directed toward modeling the structure of kerogen in a particular oil shale. In contrast, Behar and

Vandenbroucke have constructed generalized models representative of Type I kerogen at the beginning of diagenesis, and the end of catagenesis.¹⁰

These models are based upon the results of elemental, IR and ¹³C-NMR analyses, pyrolysis (Rock Eval, artificial maturation) and electron microscopy (fringe analysis) results. Even though the IFP models are generalized and not intended to precisely represent the structure of any particular kerogen, it is useful to point out some key features. First, these models emphasize large, 4⁺-ring aromatics. There is now general agreement that most ring systems are fully aromatized until late in the maturation sequence. Second, based primarily upon electron diffraction results, the IFP models depict aromatic moieties as parallel sheets. Even pure aromatics, especially those of 1-4 rings likely to be important in oil shales, crystallize in a "herringbone" arrangement that maximized edge-to-face interactions. The highly substituted aromatic units in kerogens are even less likely to arrange in parallel sheets. The implications of this kind of ordering to coal structure (Type III kerogen) are important, as recently pointed out by Cody et al.¹¹ The implications for oil shale kerogen structure should be similar, and no less important. Certainly, the X-ray diffraction patterns of amorphous materials, such as kerogens, are properly interpreted in terms of the Debye scattering formalism rather than the diffraction formalism of Bragg. This argument should also apply to electron diffraction. Perhaps reinterpretation using the correct formalism would yield a structure with more physical meaning. Finally, the trends in functional group distributions do not seem unreasonable, but it must be remembered that the details of the IFP models reflect an average over many samples and were not intended to represent any particular kerogen.

Only one attempt to characterize the oxygen functional groups in Green River oil shale kerogen is reported in the literature. Fester and Robinson use acid demineralization (successive treatments with HCl and HF) to prepare a Green River kerogen concentrate containing 14 wt% mineral matter, and wet chemical methods to determine the distribution of oxygen functional groups.¹² Later, Robinson and Dinneen applied this procedure to a series of twelve oil shales from around the world.¹³ While directionally correct, the reported results did not take into account the organic structural changes which may have occurred during the preparation of the kerogen concentrate or during the derivatization reactions, nor did they consider the inabilities of aqueous reaction media to wet and swell the non-porous kerogen concentrates.

2. Introduction

The difficulty of achieving quantitative and selective reactions of insoluble organic solids under mild conditions, and the scarcity of good methods for probing the structures of such materials, have discouraged attempts to characterize the molecular structure of the organic material in solid oil shales. Technical advances in solid state ¹³C- and ²⁹Si-NMR now provide powerful new methods for characterizing hydrocarbon structure and heteroatom functionalities in the solid state^{14,15}. Although questions persist about the quantitative reliability of the cross-polarization NMR technique in coals, compositional effects

responsible for non-quantitative data collection are less common in oil shales and in the bitumen and derivatized samples produced from these materials. Using mild and selective derivatizations with isotopically labeled reagents followed by solid state ^{13}C - and ^{29}Si -NMR analysis has enabled a comprehensive study to chemically characterize the organic functionalities in Rundle Ramsay Crossing oil shale (RXOS) from Queensland, Australia and Green River oil shale (GROS) from the Colony Mine, Parachute Creek, Colorado. Combining this data with in-depth MS and NMR analyses on shale oils produced under mild conditions led to the development of detailed structural models of the organic material.

3. Experimental Results And Discussion

The Ramsay Crossing oil shale used in this work contained 18.69 wt.% organic material finely dispersed in a mineral matrix. Solid state ^{13}C NMR employing CP/MAS indicated an aromaticity of 23% which includes contributions from olefin and carbonyl carbon types. Exhaustive Soxhlet extraction with THF removed 7.6 wt.% of the organics as bitumen. The as-received moisture content was >20%. After drying at 50°C in a nitrogen purged vacuum oven, RXOS has little surface area (16.6 m²/g) or porosity (<0.05 cc/g), hence it is very impermeable to organic solvents and reagents. As a result, organic reactions which do not dissolve the minerals proceed slowly and often do not go to completion. To circumvent this mass transport limitation, acid demineralization of the oil shale, using aqueous HCl/HF at 20°C,¹⁶ to produce the corresponding swellable kerogen concentrate (RXOS-KC) was carried out prior to chemical reactions for derivatization of organic functionalities. The ^{13}C NMR aromaticity and the bitumen content of the kerogen concentrate were unchanged from the raw shale values. However, elemental analysis indicated that the bitumen had a significantly higher hydrogen content, was lower in nitrogen and sulfur than RXOS-KC and had an aromaticity of <1%. Analyses by GC, MS and GC-MS indicated that aliphatic carboxylic acids, esters and amides with long paraffinic chains comprised the major portion of the bitumen. Examination of the empirical formulas for the organics in the raw shale ($\text{C}_{100}\text{H}_{161}\text{N}_{2.3}\text{S}_{0.7}\text{O}_x$) and in the kerogen concentrate ($\text{C}_{100}\text{H}_{161}\text{N}_{1.85}\text{S}_{0.7}\text{O}_{9.2}$) indicate that 0.45 N's/100 C's were lost during the preparation of the kerogen concentrate.

The Green River oil shale used in this work contained 21.4 wt% organic material, 14.7 wt% of which is bitumen. Solid state ^{13}C NMR indicates that 74 wt% of the organic carbon is aliphatic and this value was unchanged after preparation of the kerogen concentrate. GROS also has a low pore volume (~0.005 cc/g) and also required demineralization to overcome mass transport problems during quantitative derivatizations. The empirical formulas for the organic material in GROS and its kerogen concentrate are $\text{C}_{100}\text{H}_{157}\text{N}_{3.1}\text{S}_{0.7}\text{O}_x$ and $\text{C}_{100}\text{H}_{156}\text{N}_{2.2}\text{S}_{0.7}\text{O}_{3.0}$ respectively, indicating that 0.9 N's/100 C's were lost during preparation of the kerogen concentrate.

3.1 HYDROLYZABLE NITROGEN

Nitrogen bases liberated during the acid washings would be retained in the acid solutions as the corresponding ammonium salts. To recover and identify these free bases all of the acid washings were basified with 50% aqueous KOH under a nitrogen sweep. Any volatile free base evolved during basification was swept through HCl solutions where it was trapped as the corresponding hydrochloride. Solvent extraction of the basic solutions and evaporation of the HCl solutions to dryness under reduced pressure recovered dissolved salts (RXOS; %C, 0.39; %H, 7.63; %N, 25.79; %K, 0.21; %Cl, 65.43. GROS; %C, 0.48; %H, 3.85; %N, 13.05; %K, 22.4; %Cl, 62.81). Theoretical for NH_4Cl (%H, 7.54; %N, 26.18; %Cl, 66.28). The very low carbon content ruled out the presence of major amounts of organic amine hydrochlorides. A portion of the salts treated with benzoyl chloride under Schotten-Bauman conditions yielded benzamide as the only nitrogen compound by GC analysis, confirming that ammonia was the only nitrogen base eliminated by the concentration procedure. Powder pattern X-ray analysis further confirmed that ammonium chloride was the major constituent of the salts. In the case of RXOS over 75% of the total ammonia was liberated during the HCl treatments indicating the presence of primary amides which are hydrolyzed by the aqueous acids. The rest of the ammonia liberated during the HF treatment is due to ammonium ions associated with the silicate minerals¹⁷⁻²⁰ and this accounted for about 90% of the ammonia liberated from GROS.

3.2 NON-HYDROLYZABLE NITROGEN: UNHINDERED AND HINDERED BASIC NITROGEN

Quaternization of unhindered basic nitrogen compounds (e.g. pyridines) with iodomethane at 50°C in THF gives the corresponding quaternary ammonium methiodides. Under these conditions hindered nitrogen bases (e.g., 2,6-disubstituted pyridines) do not react, or react slowly. Non-basic nitrogen compounds (e.g., pyrroles) do not react. Thus, methylation with iodomethane (90% ¹³C enriched) was used to quantify unhindered nitrogen bases. The reaction was followed for 28 days by ¹³C NMR. Most of the methyl groups were added to oxygen (as esters) appearing at 51 ppm and to carbon sites at -15 ppm. Nitrogen methyls were added slowly, but after 14 days 0.1 N-methyls/100 C's had been added at -40 ppm and this value did not increase with additional reaction time.

Total Basic Nitrogen - Unhindered Basic Nitrogen = Hindered Basic Nitrogen. A sample of 0.1N KOH washed (to remove any amine hydrochlorides) RXOS-KC was treated with anhydrous HCl in methylene chloride at -70°C for times of 5, 10 and 15 min. The number of chlorine atoms added at each reaction time was obtained by elemental analysis. At the low temperature used, olefin hydrochlorination to give the corresponding alkyl chloride should be much slower than protonation (neutralization) of the basic nitrogen groups. Consequently, the data were extrapolated to zero time to correct for the small interference of the olefin reaction. This gave 1.0 basic N's/100 C's as an estimate of the total basic nitrogens in RXOS-KC. As discussed above, 0.1 unhindered N-bases/100 C's were

identified as the methiodides. Accordingly, the remainder, 0.9 N's/100 C's are ascribed to sterically hindered basic nitrogen functionality. There were 1.1 basic N's/100C's in GROS of which 0.3 were unhindered and 0.8 hindered basic nitrogen functionality.

3.3 NON-HYDROLYZABLE NITROGEN: PYRROLES (AND ALCOHOLS)

Although pyrroles and indoles are not methylated under PT-O methylation conditions (below), even highly hindered pyrroles can be quantitatively methylated under more severe conditions of Phase Transfer Catalyzed - Nitrogen methylation (PTC-N methylation) using methyl tosylate as the methylating reagent, 50% NaOH as the base and tetrabutylammonium bromide (TBAB) as the phase transfer catalyst²¹. PTC-N methylation of RXOS-KC with methyl tosylate (90% ¹³C-enriched in the methyl group) was carried out for 48 h under reflux. ¹³C NMR indicated addition of 3.1 methyls/100 C's; 2.2 O-methyls/100 C's, 0.3 N-methyls/100 C's and 0.6 C-methyls/100 C's. The 2.2 O-methyls/100 C's correspond to the 1.6 esters observed during PT-O methylation at 51 ppm. The additional intensity corresponding to 0.6 O-methyls/100 C's c.a. 56.5 ppm are assigned to derivatives of aliphatic alcohols generally observed in the range of 55-59 ppm. Like pyrroles and indoles, alcohols are much less acidic than carboxylic acids and phenols which are methylated under less severe (weaker base, tetrabutylammonium hydroxide (TBAH)) PT-O methylation conditions. The assignment of the carbon resonance at 57 ppm to derivatives of aliphatic alcohols is also supported by the results of ²⁹Si NMR studies of the silylated derivatives. The 0.3 methyls/100 C's correspond to derivatives of carbazole-like compounds (0.2 N-methyls/100 C's), plus methyl derivatives of pyrroles and indoles (0.1 N-methyls/100 C's) which were formed under more severe PTC-N methylation conditions. When this PTC-N methylated sample was subjected to quaternization conditions (CH₃I, 50°C, in THF, no base) 0.1 N-methyls/100 C's were again added at 40 ppm confirming that N-bases are not derivatized under strongly basic PTC-N methylation conditions. PTC-N methylation of GROS-KC adds 1.7 methyls/100 C's of which 0.5 N-methyls/100 C's are assigned to pyrrolic N-derivatives.

3.4 CARBOXYLIC ACIDS AND PHENOLS

The quaternization reaction described above was carried out in the absence of base. Under the influence of a moderately strong hydroxide base, such as TBAH, acidic O-functionalities, carboxylic acids and phenols, can be quantitatively methylated to give the corresponding methyl esters and methyl ethers. This reaction when carried out in 1:1 THF:CH₃OH at 20°C is very selective for O-methylation. PT-O methylation of RXOS-KC showed by ¹³C NMR to add 2.1 methyls/100 C's. The methyls were distributed as 1.6 esters/100 C's at 51 ppm, 0.3 C-methyls/100 C's and 0.2 N-methyls/100 C's. Results on GROS reveals that 1.0 methyl groups per 100 C's were assigned as methyl esters of aliphatic carboxylic acids at 51 ppm and a small shoulder at 60 ppm indicates only a trace (~0.05/100 C's) of aryl methyl ethers derived from phenols. The difference spectrum indicated essentially no N-, S-, or C-methylation occurred.

3.5 KETONES

Sodium borohydride is a very mild reducing agent which selectively reduces ketones in the presence of esters, carboxylic acids and carboxylate salts. The resulting alcohols can then be converted into the corresponding trimethylsilyl (TMS) derivatives by silylation. A sample of RXOS-KC was treated with 0.5N sodium borohydride in diglyme (2-methoxyethyl ether) for 72 h at 20°C. It was then silylated with MSTFA (N-methyltrimethylsilyltrifluoromethylacetamide) in THF for 1 week at 50°C. Analysis of the resulting silyl derivative by ^{13}C NMR indicated the presence of 3.9 TMS groups/100 C's, corresponding to 2.5 TMS/100 C's derived from acids, alcohols and pyrrolic N-compounds initially present in RXOS, plus an additional 1.4 TMS/100 C's assigned to alcohols derived from the corresponding ketones. Therefore, ketones (1.4 C=O's/100 C's) comprise a major fraction (15%) of the total organic oxygen in the solid RXOS. These carbonyl carbons, as well as those from acids, amides and carboxylates overlap with the aromatic carbons in the ^{13}C NMR and must be subtracted from the aromaticity value. Sodium borohydride reduction followed by silylation of GROS-KC showed the absence of easily reduced ketone and aldehyde functionalities in the GROS organics.

3.6 ESTERS

Lithium aluminum hydride is a powerful reducing agent which rapidly and quantitatively reduces carboxylic acids, esters and ketones to the corresponding alcohols. Consequently, reduction with LiAlH_4 in THF for 16 h at 20°C, followed by silylation with MSTFA and analysis of the silyl derivative was chosen to quantify ester functionalities in RXOS-KC. The disappearance of the strong IR absorption characteristic of -OH and -NH groups and the disappearance of the large resonance at c.a. 20.5 ppm due to the solid state ^{29}Si NMR resonance of TMS derivatives of carboxylic acids were monitored to assure complete reaction. The appearance of a very large resonance at c.a. 13.5 ppm in the ^{29}Si spectrum was observed and is consistent with the presence of TMS derivatives of alcohols. Quantification of TMS groups in the silylated reduction product by ^{13}C NMR indicated the presence of 6.1 TMS/100 C's. Of these 3.9 TMS/100 C's were observed as the TMS derivatives of pyrroles, alcohols and carboxylic acids in the ^{13}C NMR spectrum of the NaBH_4 reduced derivative. The number of pyrroles and alcohols in the two reduced RXOS-KC derivatives should be identical since these groups are not reduced by either NaBH_4 or LiAlH_4 . However, each acid TMS derivative, and each alcohol TMS derivative, contain one silicon atom. Hence, LiAlH_4 reduction of carboxylic acids should have no effect on the total number of TMS groups in the silylated RXOS-KC reduction product. Thus the ^{13}C NMR result indicated the presence of 2.2 TMS/100 C's arising from the LiAlH_4 reduction of esters in RXOS-KC. Since LiAlH_4 reduction produces two

alcohols per ester group, it follows that RXOS-KC contains 1.1 esters/100 C's. The procedure repeated on GROS-KC was also negative as in the sodium borohydride case and shows that all of the carbonyl-containing moieties reduced by LiAlH_4 are carboxylic acids or carboxylate groups.

3.7 OLEFINS

Olefins rapidly react in the dark with bromine in carbon tetrachloride at $\text{C}=\text{C}$ to produce the corresponding dibromides. Interference from phenol bromination was ruled out because only traces of phenols were detected during PT-O methylation. Also, bromination of ketones should be slow in a nonpolar solvent and in the dark. Bromination of one of the double bonds in conjugated dienes or polyenes would result in an undercount of aliphatic unsaturation. Bromination afforded a derivative containing 3.14 Br/100 C's in RXOS-KC and 3.4 Br/100 C's in GROS-KC. Since conversion of an olefin into the corresponding dibromide requires two bromine atoms per olefin, it follows that the RXOS-KC contains 1.5 $\text{C}=\text{C}/100$ C's and the GROS-KC contains 1.7 $\text{C}=\text{C}/100$ C's. Also, these olefinic C's/100 C's must be subtracted from the total aromaticity value seen by ^{13}C NMR.

3.8 THE DISTRIBUTION OF FUNCTIONALITIES

Combining the hydrolyzable nitrogen results with the characterizations on the RXOS-KC and GROS-KC enable a comprehensive description of the distributions of hydrocarbon, and O- and N-heteroatom functionalities in the solid oil shales (Figures 1 and 2). It should be noted that values for the non-derivatizable functionalities, ethers and N-alkylpyrroles, were obtained by difference.

3.9 NON-DERIVATIZABLE FUNCTIONALITIES - ANALYSIS OF LIQUIDS

The selective derivatization chemistries described above led to quantification of 76% of the oxygen (6.95 of the 9.2 O's/100 C's) and 78% of the nitrogen (1.85 N's of 2.3 N's/100 C's) present in RXOS and 86% of the oxygen (2.55 of the 2.95 O's/100 C's) and 80% (2.5 N's of the 3.1 N's/100 C's) present in GROS. The balance of the oxygen and nitrogen, and essentially all of the sulfur (0.7 S's/100 C's in both shales) are present in functional groups which are not easily derivatized. Identification of the bulk of these functionalities was based upon analyses of liquids produced by thermal treatment at 425°C for 1 h, followed by THF Soxhlet extraction of the residue²², which afforded >85% recovery of the total organic matter as liquids and gas. High resolution MS and NMR analyses of the liquid products, and of the fractions separated from these products using HPLC techniques, indicated that these liquids contained appreciable amounts of furans, thiophenes, and pyrroles bearing a substituent group on nitrogen. These results also provided the distribution functions of aromatic condensation, alkyl chain length, and provided information about the average pattern of aromatic substitution.

Key features of the RXOS liquids showed that paraffins (average C23) and olefins (average C20) were essentially all linear, and each comprised about 8% of the HPLC saturates. X-ray analysis of the RXOS-KC (and GROS-KC as well) indicated the importance of paraffin-paraffin interactions (gamma band), and the unimportance of aromatic stacking (no 002 band), in the secondary organic structure. Also the observation of a sharp band corresponding to a spacing of 4.2Å, characteristic of waxy paraffins having long, linear chains, reinforces the importance of the paraffin interactions. Alpha- and beta- olefins in approximately equal amounts comprised the bulk of the olefins, with smaller contributions from gamma- and trisubstituted-olefins. Additional olefins were found as olefinic side chains on aromatics (20% of the liquids), and almost all of these olefins were conjugated with the aromatic nucleus. Condensation of the aromatics in the RXOS liquids averaged 4-6 rings. The average aromatic nucleus bears one methyl group, remnant of the benzylic cleavage of ethylene bridges, and one very long side chain about 30 carbons long. Side chains in RXOS are very linear.

Among the oxygen-containing compounds found in the liquids, there were no carboxylic acids, alkyl ethers or alcohols. Thermal treatment results in decarboxylation of acids to form alkanes, cleavage and dehydration of ethers to form alkanes and olefins and dehydration of alcohols to olefins. Small amounts of esters were present. Long chain methyl ketones (average 20 C's) were prevalent. Most of the observed furans were 2- and 3- ring benzologs. Three ring furans existed as naphthalenofurans.

All of the sulfur in the liquids were present as derivatives of thiophene benzologs. The 3-ring thiophenes (mostly dibenzothiophene S) comprised about half of the total, with contributions from 1-, 2-, and 4-ring derivatives.

Among the nitrogen derivatives found in the liquids were benzologs of pyridine and pyrroles, nitriles and N,O-compounds. Indole derivatives comprised 25% of these N-derivatives - the largest single fraction - followed by pyridines, quinolines and carbazoles. Aliphatic nitriles and smaller amounts of aromatic nitriles (1- and 2-ring) were found. The aliphatic nitriles were essentially linear with very long alkyl chains (average C40). These aliphatic nitriles were probably produced during thermal treatment of RXOS (e.g., by dehydration of primary amides), as no nitrile absorption was detected in FTIR spectra of RXOS. Smaller amounts of di-nitrogen compounds and compounds containing both N- and O- heteroatoms (e.g., 2-pyridone) were also found.

Key features of the GROS liquids show that isoprenoid chains are more abundant in oils produced under mild conditions (425°C vs 500°C). The low level of oxygen in the liquids (0.48 O's/100/C's) indicates ether cleavage followed by dehydration to alkenes and dehydration of naphthenic alcohols followed by dehydrogenation. As such, diaryl ether species and cyclic diaryl ethers represent the only major oxygen types present in the shale oil product. The low oxygen content of the shale also reinforces the absence of extended hydrogen bonding interactions which was verified by lack of increased extractability on O-methylation. Over 70% of the heterocyclic rings and aromatic rings in the oil are one- and two-ring systems. Most of the nitrogen heterocycles in the oil are sterically hindered by a long chain averaging about six carbons adjacent to the nitrogen with two or three methyl groups on the remainder of the molecule. Methyl groups are also abundant on aromatics in

the oil. Both cases are consistent with cleavage of aliphatic bridges and benzylic type bonds. Acid catalyzed hydrogenolysis is very effective in depolymerizing this kerogen. Many of the pyrrolic compounds are N-substituted. Aniline bases represent about 10% of the nitrogen content, but <3% of the oil. Aromatic nitriles, not long chain nitriles are present in low concentration. The 425°C oil contains 0.72 wt% thiophenes, 94% of which are equally distributed at thiophenes and benzothiophenes. A retorted oil contains 2.2 wt% thiophenes, over 90% of which are single ring thiophenes. These results imply that higher temperatures lead to cyclization, e.g. of alkyl sulfides and mercaptans.

4. Results

Representative structural models of organic material in solid Rundle Ramsay Crossing and Green River oil shales have been constructed based upon the functional group analyses in the solid state and detailed characterization of shale oils produced under relatively mild conditions representing >85% of the oil shale organics. The models (Figures 3 and 4) with a formula weight of 30,000 daltons (and an empirical formula of $C_{100}H_{160}N_{2.2}S_{0.68}O_{9.22}$) and 9045 daltons (and an empirical formula of $C_{100}H_{155}N_{3.10}S_{0.62}O_{2.17}$) was required to accommodate the large range of heteroatom functionalities in both shales and the long side chains present in RXOS. It was not possible to accurately represent the range of compound types in the bitumen because of its small amount (8.5% and 12%) and the need to maintain a finite model size. Because carboxylic acids comprise the major part of the RXOS bitumen, all the bitumen in the model was represented as carboxylic acids.

Most of the organic material is insoluble kerogen. From its insolubility and swellability (not discussed here) we infer the presence within the kerogen of a 3-dimensional network structure which must be disrupted prior to dissolution. Accordingly, the models represent one tetrafunctional cross link in an essentially infinite macromolecular network. The linkages comprising the network may be covalent bonds, bonds between heteroatom functionalities (e.g., carboxylates, amines) and minerals, hydrogen bonds, or, (if chains are very long) physical entanglements. We believe that most key linkages are covalent bonds between organic moieties. This is because the bitumen contents of both shales and their KC's are virtually identical after >90% of the minerals were removed which makes it unlikely that organic-mineral interactions are a key to kerogen solubility. Methylation to "cap off" groups (e.g. acids, phenols) which can participate in hydrogen bonding is more significant in RXOS because it increased RXOS-KC extractability from 8.5% to 21% but did not produce complete dissolution of either kerogen. There is no evidence for the very long chains which would be needed to prevent extraction via physical entanglements.

5. Conclusions

Detailed molecular models of the structure of representative organic material in Rundle Ramsay Crossing oil shale and Green River oil shale have been developed. They are based upon characterization results which have (a) non-destructively elucidated the composition, structural features, and significance of hydrocarbon, oxygen and nitrogen functionalities in the solid oil shales and (b) unraveled the structural features associated with the heterocyclic molecules in the shale oils produced under mild conditions which afford high organic conversions. The models agree well with experimental values for elemental composition, distribution of hydrocarbon and heteroatom functionalities (Figures 1 and 2) and the proportion of kerogen and bitumen.

Fig. 1. Comparison of distribution of functionality in Rundle Ramsay Crossing oil shale and model.

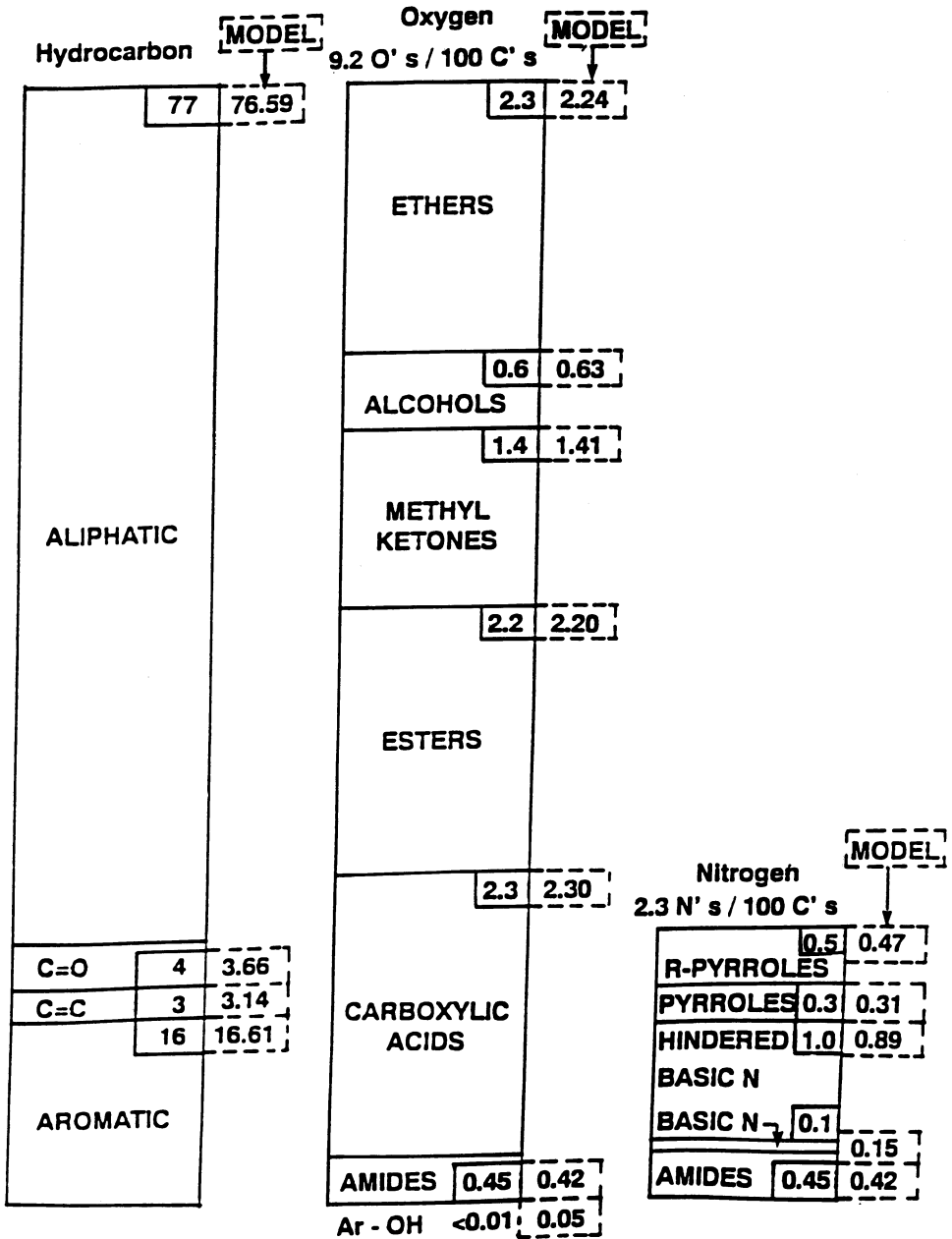


Fig. 2. Comparison of distribution of functionality in Green River oil shale and model.

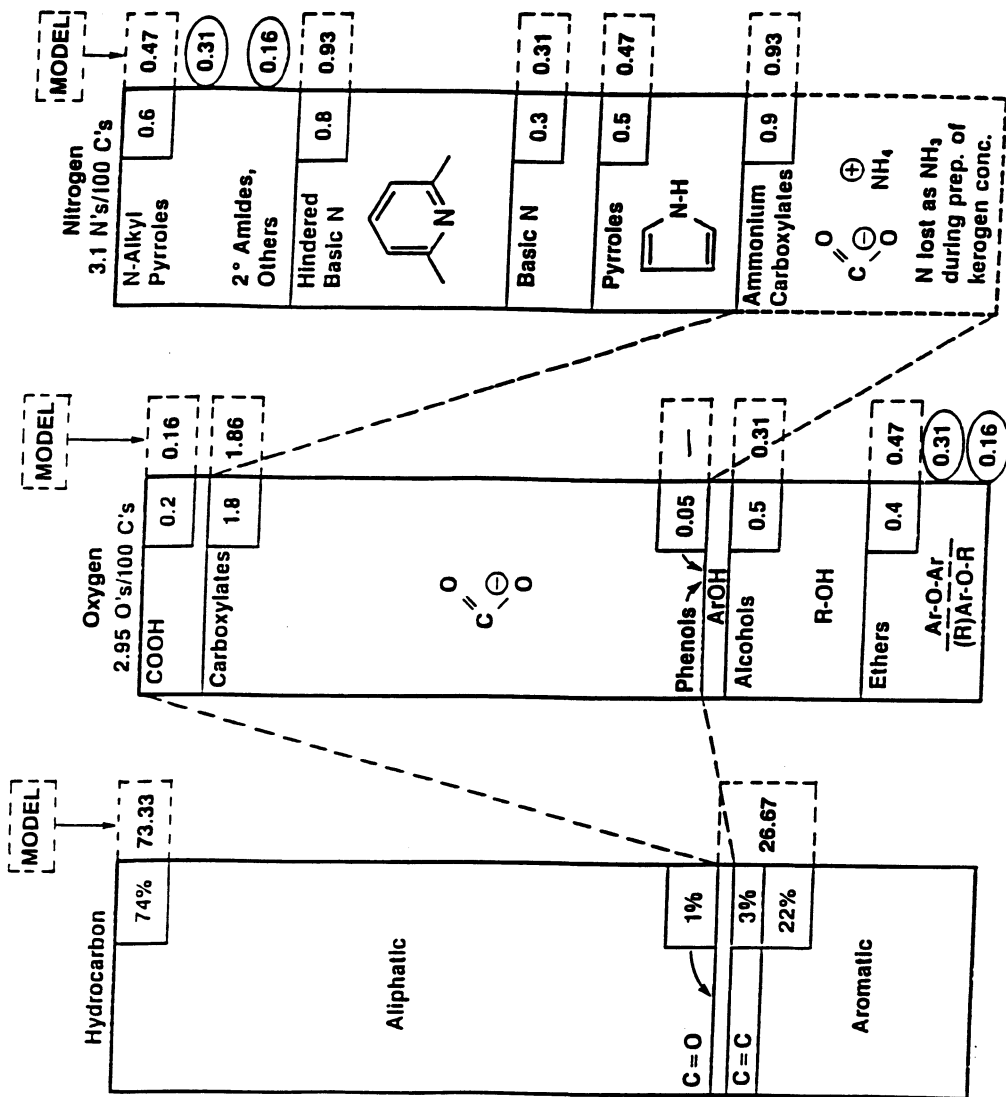


Fig. 3. Section of the model of representative organic material in solid Rundle Ramsay Crossing oil shale.

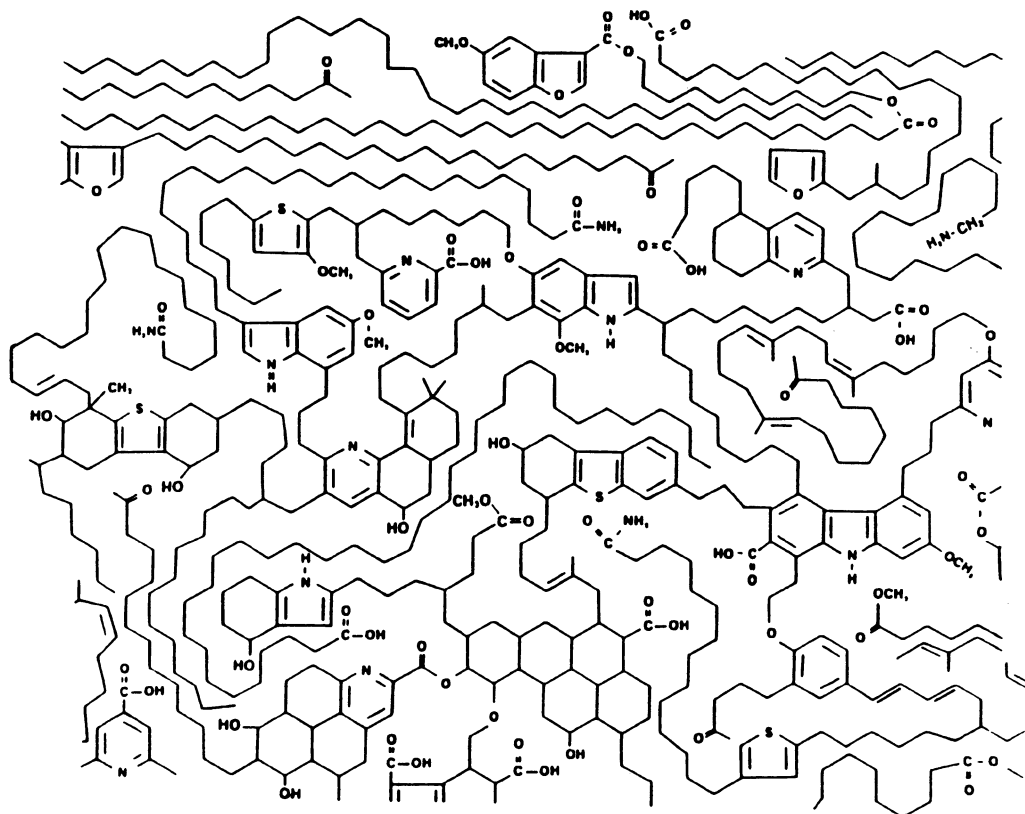
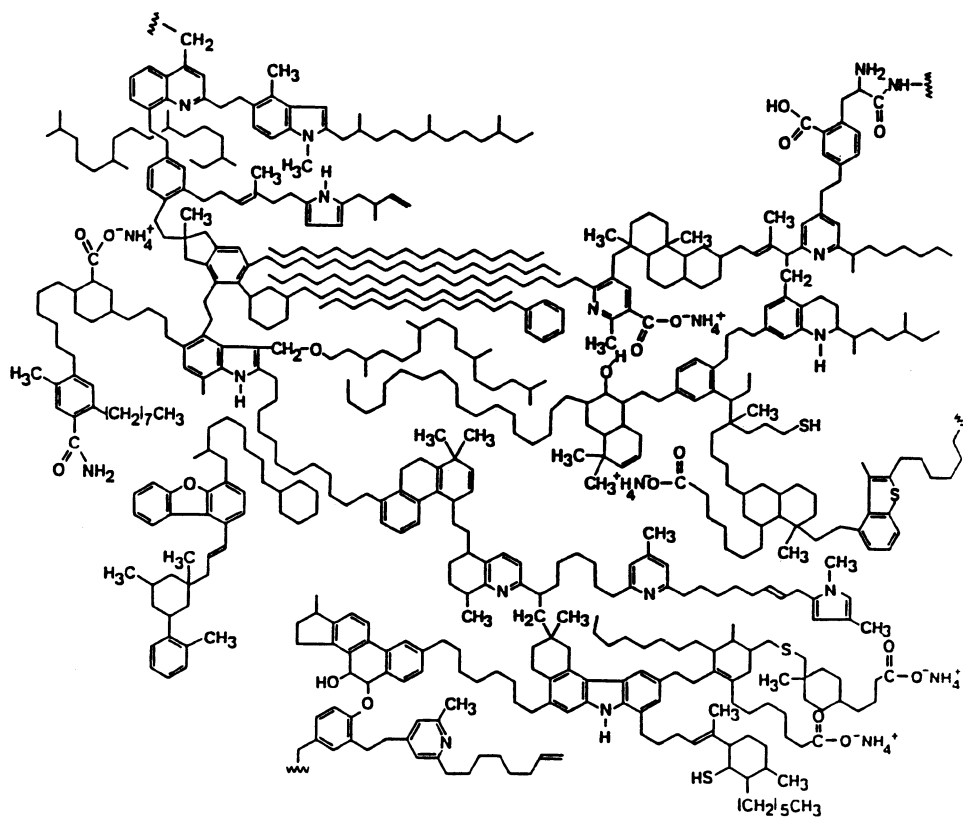


Fig. 4. Model of representative organic material in solid Green River oil shale.



6. References

1. B. P. Tissot and D. H. Welte, *Petroleum Formation and Occurrence*, Springer-Verlag (1978) pp 69-73.
2. A. L. Burlingame and B. R. Simonet, *Nature*, 1969, **222**, 741.
3. A. L. Burlingame, P. A. Huang, H. K. Schnoes and B. R. Simonet, In *Adv. Org. Geochem.*, 4th Int. Conf., P. A. Schenck and I. Haveenar, Eds., Pergamon Press (1968).
4. M. Djuricic, R. C. Murphy, D. Vitorovic and K. Biemann, *Geochim. Cosmochim. Acta*, 1971, **35**, 1201.
5. J. J. Schmidt-Collerus and C. H. Prien, *Prepr. Pap. - Am. Chem. Soc., Div. Fuel Chem.*, 1974, **19**, 100.
6. D. K. Young, S. Shih and T. F. Yen, *Prepr. Pap. - Am. Chem. Soc., Div. Fuel Chem.*, 1974, **19**, 169.
7. T. F. Yen and J. E. Erdman, *Encyclopedia of X-Rays and Gamma Rays*, Reinhold (1963) pp 65-58.
8. T. F. Yen, *Prepr. Pap. - Am. Chem. Soc., Div. Fuel Chem.*, 1974, **19**, 109.
9. (a) C. W. McGowan and H. Diehl, *Fuel Processing Tech.*, 1985, **10**, 169; (b) *ibid.*, 1985, **10**, 181; (c) *ibid.*, 1985, **10**, 195.
10. F. Behar and M. Vandenbroucke, *Rev. Inst. Fr. Petr.*, 1986, **41**, 173.
11. G. D. Cody Jr., J. W. Larsen and M. Siskin, *Energy Fuels*, 1988, **2**, 340.
12. J. I. Fester and W. E. Robinson, In *Coal Science; Advances in Chemistry Series 55*, P. H. Given, Ed., American Chemical Society, Washington, DC (1966) pp 22-31.
13. W. E. Robinson and G. U. Dinneen, *Proc. 7th World Petr. Congress (Mexico City)* 1967, **3**, 669.
14. F. P. Miknis, G. E. Maciel and V. Bartuska, *J. Org. Geochem.*, 1979, **1**, 169.
15. R. Liotta and G. Brons, *J. Amer. Chem. Soc.*, 1981, **103**, 1735.
16. B. G. Silbernagel, L. A. Gebhard, M. Siskin and G. Brons, *Energy Fuels*, 1987, **1**, 501.
17. J. E. Cooper and W. S. Evans, *Science*, 1983, **219**, 492.
18. R. W. Taylor, A. K. Burnham, G. S. Smith, R. H. Sanborn and L. S. Gregory, *Prepr. Pap. - Am. Chem. Soc., Div. Fuel Chem.*, 1985, **30**, 338.
19. J. E. Cooper, *Anal. Chem.*, 1986, **58**, 1571.
20. K. W. Riley, T. D. Moss, H. Orban and R. A. Quezada, *Fuel*, 1987, **66**, 323.
21. N.-C. Wang, K.-E. Teo and H. J. Anderson, *Can. J. Chem.*, 1977, **55**, 4112.
22. J. Bock, P. P. McCall, M. L. Robbins and M. Siskin, *U.S. Patents* 4,458,757 (10 July 1984) and 4,461,696, (24 July 1984).

ECONOMIC CONSIDERATIONS OF THE OIL SHALE AND RELATED CONVERSION PROCESSES

E.EKİNCİ

Department of Chemical Engineering
Istanbul Technical University, Ayazağa Istanbul
Department of Chemical Engineering
TUBITAK Marmara Research Center
Gebze-Kocaeli-Turkey

ABSTRACT

Economical criteria for the evaluation of oil shales depends on the process of utilisation. For combustion the economic grade oil shale is defined as that having a minimum upper calorific value of 750 kcal/kg on dry basis. For pyrolysis, in general, the limiting kerogen content is a function of a lot of parameters but the lower quoted value is 5 % organic content which corresponds to oil yield of 25 l/ton of rock or 6 US gallons per short ton. Shale oil cost components include; mining, crushing, beneficiation and retorting of oil shale, and refining and upgrading of products. The fraction of mining, crushing and beneficiation costs are minor compared to the rest of the items. The grade and type of kerogen directly influences the economics of the process. Oil shale beneficiation, by-product credits from sulphur utilisation and electric power generation are another contributing factor to economics; Efficient combustion adds to revenues and solves solid residues problem. Refining is one of the most important component of cost items of shale oil processing due to high hydrogen consumption. It is generally accepted that proportion of refining cost is about 20-40% of the total cost of production of oil from oil shale.

1.0. Introduction

The economical criteria for the evaluation of oil shales utilisation depend on nature of the process. Organic matter content is the general parameter to evaluate the economical limit but in one report, it was claimed that the sulphur content of low grade fuel was economically more appropriate than the organic content⁽¹⁾. Also, for special low ash and high organic content oil shales, such as Alpha torbanite of Australia and Göynük of Turkey, the adsorbent carbon produced from their pyrolysis residues may be much more valuable than the total syncrude potential⁽²⁾. This comparison is striking when one considers that both Göynük and Alpha torbanite are classified as "very highly economical grade" oil shales according to their Fisher Assay (FA) results.

2.0. Evaluation of Oil Shale Economics

2.1. COMBUSTION

Before technical and processing studies, it is necessary to establish the grade of the oil shale to be utilised. However, this depends on choice of technology. For combustion, the economic grade oil shale is defined as that having a minimum upper calorific value of 750 kcal/kg dry basis (db)⁽³⁾. This limiting calorific value is determined on the basis of heat balance considerations. Of course, this analysis assumes no additional cost load from mining. Further, for surface mined oil shales, this calorific value limit also assumes a minimum thickness of 5 m seams.

No doubt, the choice of combustion technology also affects the limiting calorific value of economic grade oil shales. For example, this limit for fluidised bed combustion of coal washery wastes was investigated in a 2.6 m x 1.6 m bed. La Nauze et.al⁽⁴⁾ calculated the lower operating conditions and heat available for external use for the fluidised bed for different fuels in a nominal plant design with conditions of 2.4 m/s fluidising velocity, 850°C bed temperature, 20% excess air, 85% carbon utilisation and a 5% heat loss to the surroundings. The Turkish oil shales, Göynük and Seyitömer, are included in the La Nauze graph in Figure 1. It is understood from figure that oil shales falling above the solid line evolves heat for recovery. The economics of fuels improve as they are situated away from the solid line. Among the fuels plotted on Figure 1, Göynük oil shale has got the most available extractable heat.

2.2. PYROLYSIS

One of the key economic factors is that oil shale is required to yield energy to process the rock. Taking 500 °C as a typical pyrolysis temperature one would require about 250 cal g⁻¹ for rock heating. If the calorific value of kerogen is typically around 10 000 kcal g⁻¹⁽⁷⁾, then 2.5% by weight of the kerogens total calorific value is required to heat the shale. This value may be taken as a theoretical threshold for oil shale to be considered as an energy input. The limiting kerogen content is a function of many parameters but the lower quoted value is 5 % organic content which corresponds to an oil yield of 25 liter ton⁻¹ (l/ton) of rock or 6 US gallons per short ton (gpt). Ton here is defined as 2000 pounds weight.

To standardise the economical criteria for synthetic oil production capacity from oil shale mineral, modified FA is used. According to FA procedures, 100 g of 2.38 mm particle oil shale are fed to the standardised retort in which a heating rate of 12°C/min up to 500°C and a soaking time of 40 minutes are employed⁽⁸⁾. The classification of oil shales into different economical grades according to FA oil yields is shown in Table 1.

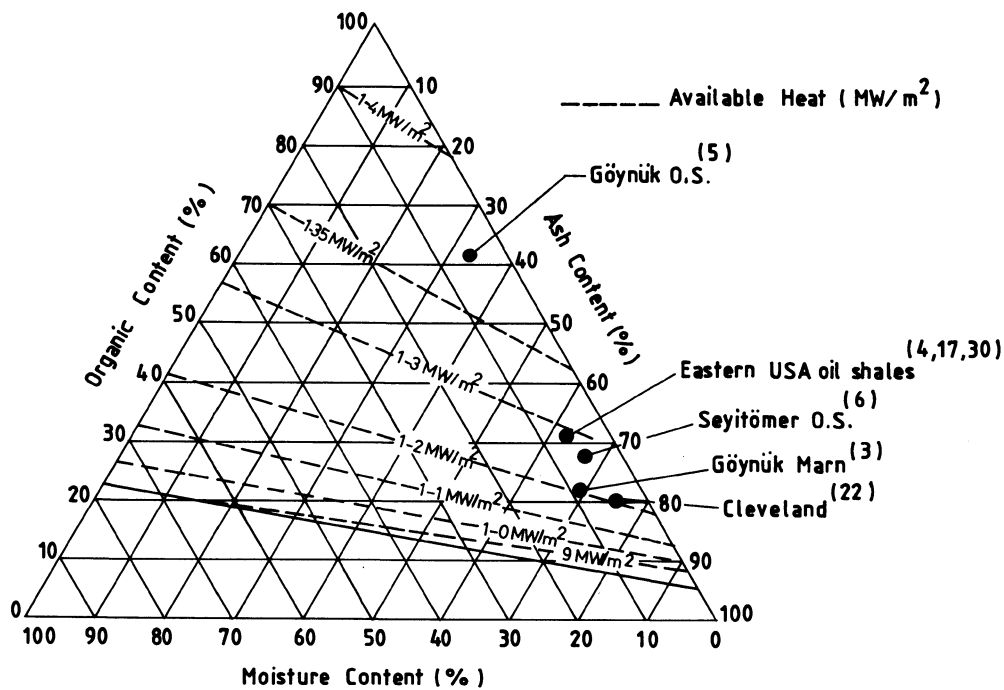


Figure 1. Effect of composition on the combustibility of oil shales (4)

Table 1. Classification of Oil Shales into Economical Classes (9)

	Uneconomical	Medium Economical	Highly Economical	Very Highly Economical
Oil Yield (gal/ton)	10.5	26.7	36.7	61.8
Oil Yield (% weight)	4.0	10.4	13.8	23.6

The distribution of some of the USA oil shale reserves are shown in Table 2. According to FA oil yields the vast majority of them fall into the category of overwhelmingly low economic grade deposits. Combustion seems to be the only suitable process for utilising the 5-10 gpt oil yielding reserves.

Table 2. Distribution of the Main Oil Shale Reserves of the World into Economic Classes⁽¹⁰⁾.

Liquid Fuel Yield	Total Reserves millions tonnes			
	l/ton gpt	21-42 5-10	42-104 10-25	104 - 417 25-100
Green River		636	445	191
Central and Eastern USA		318	159	-
Alaska	wide		32	40
Other Regions		21300	3537	80
Total		22254	4173	311

3.0. Economics of Conversion Processes

The main purpose of producing of shale oil is to meet the shortage in the crude reserves and, therefore, the main factor which governs the economics is the price of crude oil. Johnson⁽¹¹⁾ visualised a stable oil shale derived synthetic fuel option for crude prices at the level of 50 \$/barrel based on 1980 prices.

For calculating the price of shale oil, a number of parameters determine whether shale oil will challenge production of natural crude. The price of raw shale in turn is determined by the type of mining involved. It is well known that direct operating costs per unit excavated by surface mining are lower than for any other mining method. These are dependent upon the characteristics of specific oil shale reserves and include room and pillar mining, caving, sublevel stopping and vertical modified in-situ mining.

The second important price determining factor is sample preparation which may be size reduction and/or pretreatment. The pretreatment may involve beneficiation⁽¹⁾ or drying⁽¹²⁾. The third and the most important factor is the retorting of oil shales. For example, the choice of hydro-retort processing may increase the oil yield up to 2.5 times compared FA at the expense of elevated temperature and pressure. Therefore, the capital investment and processing costs of this route is considerably higher than standard retorting techniques.

For a sound comparison between synthetic crude, from oil shale and natural crude the comparative refinery costs should also be considered.

3.1. SHALE OIL COST COMPONENTS

3.1.1. Mining

Open pit mining involves a number of different operations depending on the reserve and rock characteristics. The costs of these operations were compiled by Banks et. al⁽¹³⁾ in 1977 using the US \$. The cumulative direct operating cost of open pit mining of oil shale is comparable to copper mines which averages between 0.40 and 0.80 \$/ton of rock.

3.1.2. Crushing

Crushing is generally divided into primary and secondary crushing. The first or primary size reduction operation is concerned with the suitability of the oil shale for transportation. The tough and laminated oil shale rock requires considerable crushing work. The most widely used crushers for the primary crushing are gyratory and jaw types.

Table 3. Mining Cost Components (14)

Activity	The Cost (\$/ton)	
	Overburden	Oil Shale
Drilling	0.016	0.019
Blasting	0.076	0.082
Loading	0.077	0.068
Haulage		
Truck	0.13	
Conveyors	0.06	
Primary Crushing	0.071	
Waste Disposal		
Spreader	0.026	
Mining dewatering	0.00042	

Crushing run-of-mine shale to -240 mm size is expected to range from 2-5 cents/ton of oil shale. The capital cost of primary crushers per ton-hr is expected to range between \$ 600 - 1000 in 1978 prices. As operational cost, 0.03-0.15 kwh per ton of throughput and to control the dust, 0.75 % of the weight of oil shale equivalent of water should be considered⁽¹⁴⁾.

Secondary crushing, regulates the size requirement for the processing stage together with sieving. The mostly used types are impact crushers, hammer mills, jaw crushers, toothed rolls and cane crushers. The particle size requirement for a retort running on fine oil shales is -13 mm and that for coarse retorts is 76 to 100 mm top size and 6 to 10 mm bottom size. The cost of crushers depend on the degree of reduction needed which can be specified on case-by-case basis. The power requirement is expected to be between 2-3 kw/h/ton and a similar amount of water as used in primary crushers is needed for dust control⁽¹⁴⁾.

3.1.3. Beneficiation

Shale beneficiation by way of ash reduction reduces the required retort space which lowers the capital investment. On the other hand, operating costs increase due to material handling and beneficiation⁽¹⁾. The calculated production cost dropped 17 % with increasing shale grade from 11.8 to 15.6 gpt for the case of Eastern Oil Shales of US.

The two main ways for increasing the organic content of oil shale are heavy media density separation and size reduction. Beneficiation may also help the retorting process by i) lowering water content as needed in some retorts⁽¹²⁾, ii) giving less spent shale for disposal and iii) the availability of controlled particle sizes.

The cost of heavy media density separation is reported to be comparable to conventional aggregate and gravel separation which are less than \$ 0.50/ton in 1978 prices⁽¹⁴⁾.

Beneficiation by size reduction was applied to Mahoney shale by Bureau of Mines which improved the average oil yield by 2 gpt⁽¹³⁾. On the other hand, coarse cuttings which Gulf has analysed from drilling and boring operations tend to be 3 to 5 gpt richer than the integral core. This is due to undercutting and crushing of more friable lean material, thus translates as a favourable economic operation⁽¹⁹⁾.

The cost of beneficiation by size reduction method is the cost of removed parts. The overall cost of beneficiation is close to zero or less than normal considering the increase in yield of retorting.

4.0. Oil Shale Retorting Economics

The retorting step is the heart of oil shale processing. It is also the most important cost item among the various components. There are also great differences between the types of retorting operation chosen. Surface retorting and in-situ processes have great differences in costs and relative commercial applicabilities. Also, within each of these categories, the procedure of retorting

manifests great differences such as heat transfer mechanism, heat recovery applications, waste disposal and utilisation, gas utilisation, by-product production and synthetic crude stabilization.

Further factors include the grade of oil shale, kerogen extraction, thermal efficiency, make-gas processing requirements, flue gas processing requirements, water processing, retort design and operability, and spent shale processing.

Some of the better known processes that have been either operated commercially or have commercial potential will be evaluated.

4.1. PARAHO RETORTING PROCESS

This process based on limestone calcination practice. The process has the capability of direct combustion or external heating using the recycle gases. The oil yield was reported to range between 85-93 % db on organic rich oil shales (35 gpt) for which the process is best suited. As a part of commercial demonstration a plant of 24 full-size Paraho retorts having a capacity of 100000 bbl/day producing either crude oil or syncrude was basis for economical evaluation. The basis of analysis was 100 % equity, 15 % rate of interest (ROI), no price control entitlements, bonuses and/or other economic constraints. The overall result may be summarized as: cost of 148 million \$/year and crude shale oil price of 11.50 \$/barrel (\$/bbl). For other sets of assumptions investment, operating cost and crude prices are calculated among which the highest values are found to be 1.6 billion \$, 195 \$ million \$/yr and 19.35 \$/bbl, respectively⁽¹⁵⁾.

4.2. SUPERIOR OIL SHALE PROCESS - CIRCULAR GRATE RETORTING PROCESS

This process was adopted from some kiln applications where by the bed of oil shale rotates in the heating zone in which oil is evolved and removed by the circulating gas. The system has fast shut down and start up periods. For a 20 000 ton per stream day (tpcd) using a 24 gpt oil shale and 300 operating days per year a fixed capital investment of 74 million \$ for direct heated and 85 million \$ (1978 prices) for indirect heated retort was quoted⁽¹⁵⁾. Total annual operating cost was calculated to be 14.66 and 12.32 million \$ respectively for the direct and indirect heated cases⁽¹⁵⁾.

4.3. TOSCA II RETORTING PROCESS

In this process, indirect heating by ceramic balls in a separate retort is employed. It has been developed for high grade shales and also applicable to other solid fuels including coal, tar sands and some solid wastes.

Taking a 34.8 gpt shale, 44 400 barrels per stream day of hydrotreated shale oil and liquid petroleum gas, sulphur, ammonia and coke by-products into account, an investment of 1.050 million \$ (1977 prices) and a total operating cost of 92 million \$/year were determined. The selling price of crude oil for 10 and 15 % discounted cash flow (DCF) rate of return was found to be 16.10 and 24.50 \$/bbl respectively. The breakdown of the contribution of the major items on the cost of produced oil is given in Table (4).

Table 4. Colony Project Direct Operating Costs (September 1977 US \$) (19)

	Thousands \$ per Year	\$ per Barrel
Cost Center		
Mining, crushing, and spent shale disposal	35.600	2.27
Plant operating labor	2.300	0.15
Plant maintenance, excluding mining	12.500	0.80
Electrical power costs, excluding mining	15.800	1.00
Catalysts and chemicals	7.800	0.50
Administrative	2.800	0.18
Taxes and insurance	7.600	0.48
Miscellaneous	1.500	0.08
License fee	3.600	0.23
Contingency	2.500	0.16
Total operating costs	92.700	5.85
By-product credits	6.300	0.41
Ammonia	2.900	0.18
Sulfur	2.400	0.15
Coke	11.600	0.74
Total by-product credits	80.400	5.11
Net operating costs		

4.4. SPHER PROCESS (SHELL PELLETT HEAT EXCHANGE RETORTING)

Spher is a fluidised bed retorting process. Two types of inert pellets used in a fluidised and entrained state which was developed in 1980. The process utilises rapid stage heating to enhance kerogen conversion.

The cost analysis for a 51 100 bbl/day plant resulted in a \$ 870 million and another \$ 130 million is spent over the 25-year life of the project to replace mining equipment. The breakdown of the operating costs and costs per barrel of shale oil are given in Table 5.

Table 5. Operating Costs For Spher Retorting Process⁽¹⁶⁾

	Million \$ per Year	\$ per Barrel
Operating costs	44.1	2.63
Mining, crushing, disposal	28.6	1.70
Utilities	7.0	0.42
Catalyst, chemicals, balls	2.6	0.15
Operating labor	24.4	1.45
Maintenance	20.2	1.20
Overhead, taxes, insurance	(4.6)	(0.27)
By product credits	122.3	7.28
Total	248.0	14.77
Capital charge (15 % DCF)	370.3	22.05
TOTAL		

4.5. IGT PRESSURIZED FLUIDISED BED HYDRORETORTING

Institute of Gas Technology (IGT) has carried out a long series of pressurised fluidised bed (PFB) process development work commissioned by the Department of Energy (DOE). The economic analysis of the PFB hydroretorting project is based on 50,000 bpd of raw shale capacity using (1992 prices). The principal components of cost items are taken as: capital, operating, utility, and shale costs. Also credits from sulphur and ammonia recovery and production of power and sulphuric acid are considered⁽¹⁷⁾.

According to the overall economics a total capital investment of 1926.2 million \$, total annual operating cost of 474.7 million \$ and annual by-product credit of 163.8 million \$ was found. These economic figures meant a raw shale oil price of 33.62 \$/bbl. Given the current crude oil prices it is clear that economics of oil shale processing can be appealing with the support of value added products running side by side with synfuel production.

4.6. SOME OTHER RETORTING TECHNIQUES

In-situ retorting is similar to in-situ gasification apart from the target product is oil as opposed to gas. Therefore, there is a higher risk of plugging due to heavy oil condensation. Due to the slow heating for in-situ processes as compared to FA, the oil yields are reduced. Of course, there is the theoretical advantage of reducing the initial investment. There has been a couple of development projects namely Rubble in-Situ Extraction (Rise) costing 93 million \$⁽¹⁸⁾ and the Oxy Modified in-situ process constructed and operated at 57,000 bbl/day capacity by Shell Oil Company⁽¹⁵⁾. Cost comparisons of surface and in-situ retorting and combination of these by Shell Oil Company are summarised in Table 6.

Table 6. Comparisons of Surface, In-situ and Combination for Surface and In-situ Retorting processes (1976 prices)⁽¹⁹⁾

	Surface Retorting	In-Situ Retorting	Combination
Capital investment, million \$			
Initial	775	300	620
Deferred	150	230	220
Total	925	530	840
Operating cost, million \$/year	51	60	69
Annual rate of return, % (oil at \$ 12.50/bbl)	9.5	8.9	11.8
Required oil price for 10 % annual rate of return, \$/bbl	13.10	13.40	10.90
Production			
million bbl	330	290	510
bbl/stream day	52.300	30.500	54.100
Project life, yr	20	30	30

In these comparisons, among other assumptions, the prices of by-product coke and sulfur were taken as 20 and 10 \$/ton, respectively⁽¹⁵⁾.

True in-situ processes are large projects at earlier stages of development. For this reason, they have received less interest due to the unfavorable research climate for oil shales.

In order to explore the benefits of H₂ from the water gas shift reaction, Parkinson and Merson⁽²⁰⁾ conducted semi-continuous laboratory experiments on high performance carbon monoxide (CO)-steam processing of an oil shale. Even though this process resulted in extremely high carbon recovery due to the high pressure retorting section, it was evaluated as an expensive process. Cost comparison studies on Praho (severe hydrotreating), Occidental (severe hydrotreating) and Co-steam process resulted in 18.90, 32.20 and 33.70 \$/bbl respectively, using the 1980 prices.

4.7 FACTORS AFFECTING RETORTING ECONOMICS

The richness and the type of kerogen directly influences the economics of the process. As was pointed out in the earlier sections, the oil shale reserves are classified between uneconomical and very highly economical classes. Oil shale beneficiation is also an important factor since it reduces the capital cost due to reactor volume but increases the operating costs due to material handling costs. The calculated production cost for a low grade Eastern Oil

Shale dropped by 17% with an increase in the oil shale grade from 11.8 to 15.6 gtp. However, for lower grade oil shales, the sulphur content may have a more important effect on the cost. For example, for beneficiated Eastern Oil Shale the calculated production cost dropped by 62% due to an increase in the sulphur content from 2.4 to 7.8 wt% after beneficiation for H₂SO₄ credits. By-product credits from electric power generation is another contributing factor since an efficient combustion adds to revenues and solves solid residues problem which is classified as hazardous waste⁽²¹⁾. Shadle et.al⁽¹⁾, on the other hand, quotes an initial plant capital of 3.84 billion \$ and \$ 25/bbl of produced oil from raw shale feed at a plant capacity of 58000 bbl/d. For the same capacity, the capital investment and operating costs are \$ 2.96 billion and \$ 35/bbl, respectively, for the beneficiated oil shale.

Graham et.al⁽²⁾ reported preliminary results for the production of adsorbent carbons from the high grade Göynük oil shale. For the pyrolysis residue, steam-gasified char and acid treated plus steam-gasified char gave progressively higher specific N₂-BET surface area, as seen in Table 7.

Table 7. Specific Surface Area Measurements of Adsorbent Carbons Produced From Göynük and Alpha Oil Shales

	Specific Surface Area, m ² /g	
	Göynük	Alpha
Pyrolysis Residue	8.7	10
Steam Gasified Residue (4 hrs)	180	170
Acid Treated Steam Gasified Residue	350-400	200-350

Provided that the process characteristics are met, the price of the Göynük adsorbent C is expected to be about 200 \$/ton which is two orders of magnitude higher than the economic potential of synthetic crude. In this process, the gasification stage produces H₂ which may be used to stabilize the synthetic crude oil.

4.8 REFINING - UPGRADING COSTS

Production of oil from oil shale demands relatively milder conditions as compared to coals. However, there are extra difficulties associated with oil shale as compared to coal-based processes. The most severe difficulties are high nitrogen content, viscosity and pour point. Oxygen and sulphur contents are, on the average, the same as natural crudes. Organo-arsenic and vanadium compounds may cause some concern as well⁽²²⁾. The unsaturated, aromatic and nitrogen compounds tend to form gums during storage and

therefore need hydrogenation. At this stage, production of light ends requires more effort and higher cost as compared to natural crude.

Depending on the nature of the shale oil at hand, various upgrading and refining techniques may be employed which also depend on the target products. A general sequence of treatment processes for upgrading may be given as:

- deasphalting-vacuum distillation
- arsenic removal
- hydrotreatment
- dewaxing
- denitrogenation

Sutikno⁽²³⁾ investigated the costs of three different shale oil to transportation fuel refining costs. The processes selected were: hydrotreating-hydrocracking, hydrotreating-fluid catalytic cracking and delayed coking-hydrotreating. The basis for investment costs were 100 000 bbl/day feed (1980 prices), working capital as 15% of the fixed capital, and economic values of by products (ammonia, sulphur, and coke) were not taken into account. The operating costs included utilities, maintenance, taxes and insurance, labour, chemicals, catalyst and royalties. The refining cost includes rate of return on investment. The results of the refining cost of Paraho oil shale are summarised in Table 8.

Table 8. Refining costs of Shale Oil (1980 prices)⁽²³⁾.

Route	Barrel of Product Per Barrel of Feed	\$ Per Product Barrel
Hydrotreating-Hydrocracking	0.96	10.38
Hydrotreating-Fluid Catalytic-Cracking	1.02	9.16
Delayed Coking Hydrotreating	0.83	8.48

Using hydrotreatment process for 100.000 bbl/day for Rocky Mountain shale oil resulted in a 6.50 \$/bbl processing cost. The total investment and operating costs were 600 and 56 million \$ (1978 prices), respectively⁽¹⁹⁾.

A technical and economic assesment of petroleum heavy oil, shale oil and coal liquid refining was carried out by Sikonia et.al⁽²⁴⁾ and their results are summarised in Table 9.

Table 9. Comparison of Heavy Oil, Shale Oil and Coal Liquid⁽²⁵⁾

	Refinery Feed Stock (\$/barrel)	Refining (\$/barrel)	Total (\$/barrel)
Arabian Light	25.15	9.71	34.86
Mexican Maya	20.80	10.20	31.00
Coal Liquid	22.77	10.20	32.97
Shale Oil	19.17	12.81	31.98

5.0. Comparison of Oil Shale With Other Fossil Fuel Alternatives

Green⁽²⁵⁾ made a comparative display of oil shale, tar sand, donor solvent and H-coal options as synfuel alternatives. The tar sands cost data were based on a 100,000 bpd plant at Mildred Lake. The oil shale cost data was based on 50,000 bpd Tosco II retorting with 35 gpt shale. H-Coal technology was assumed to be operating in fuel oil mode in Illinois and Exxon Donor solvent process cost was on 50,000 barrel/day crude equivalent. The error range for the engineering calculations was estimated to go up to $\pm 20\%$.

The range of capital investment, hydrogen consumption and amortised manufacturing costs are shown in Table 10 and the distribution of capital among process steps are given in Table 11.

Table 10. Range of Manufacturing Costs⁽²⁵⁾

Process	Capacity	Hydrogen	Range of Capital	Manufacturing Costs 15 % DCF (\$/barrel)
Tar sands	100000	1050	2020-3030	24-34
Oil Shale	50000	1600	1640-2460	31-43
Exxon Donor Solvent	50000	4500	1430-2140	38-51
H Coal	50000	6200	1760-2635	50-57

Table 11. Percent Distribution of Capital Among Process Steps, Green⁽²⁵⁾

Operation	Tar Sands	Oil Shale	Coal
Reserve Acquisition	3	7	5
Mining	53	14	17
Conversion	16	51	78
Upgrading	28	28	-

Comparison of Arabian light, Mexican Maya, coal liquid and shale oil show that the total \$/bbl price of oil shale is third expensive eventhough it has the highest refining cost per barrel. Hydrogen consumption in shale oil refining is greater than tar sands but smaller than both of the two coal processes listed in Table 10. The distribution of capital investment is allocated mostly to conversion followed by upgrading, mining costs and reserve acquisition for oil shale which shows considerable difference to tar sands and coals.

References

1. L.J Shadle, J.D. Westhoff, A.P. Lui, and J.A. Poku, Assesment of the Economics of Retorting Raw and Beneficiated Eastern Oil Shale, Proc. of 1991 Eastern Oil Shale Symp., 327, 1991.
2. U. Graham, A.M. Rubel, E. Ekinci, and T. Robl, Pyrolysis Processing Characteristics and Product Evaluation of Turkish Göynük Oil Shale, Proc. of 1992 Eastern Oil Shale Symposium, 1992.
3. H. Hufnagel, H.J. Hildebrand, H.H. Schmitz, M. Şener, I. Şengüler, and H. Wehner, Investigation of Oil Shale Deposits in Western Turkey, Part II. Himmetoğlu and Hatıldağ, Technical Cooperation Project No: 84.2127.3, Hannover, 1991.
4. R.D. La Nauze, G.J. Dufty, E.C. Potter, and A.V. Bradshaw, Fluidised Combustion of Coal Washery Wastes, In Fluidization, Ed. Gracei JR and Matsen JW 151-58, 1980 Plenum.
5. E. Pütün, A. Akar, E. Ekinci, and K.D. Bartle, Chemistry and Geochemistry of Turkish Oil Shale Kerogens, Fuel, 67, 1106-1110, 1988.
6. B. Uzluk, Pyrolysis of Seyitömer Oil Shale Under Different Process Conditions, MSc Thesis, ITÜ, 1990 (Tur).
7. B.P. Tissot, and D.H. Welte, Petroleum Formation and Occurance, Chp 9. A Kerogen Rich Sediment With Potential Economic Value, 2nd Ed., Springer Verlag, Berlin, 1984
8. F.P. Miknis, Conversion Characteristics of 10 selected Oil Shales, WRI, Laramie Wyoming, 1989.
9. M. Güneyman, Yields and Chemical Characteristics of Products From Göynük and Seyitömer Oil Shale, ITU, Ph.D. Thesis, 1986.
10. Kirk-Othmer, Encyclopedia of Chemical Technology, Oil Shales, Vol. 16, p 333, 1981.
11. A. Johnson, A Perspective on the Oil Shale in Oil Shale the Environmental Challenges III. Ed. Petersen K.K. Petersen, CSM, 1983
12. T. Yabuishita, Development of Oil Shale Retorting Plant in Japan Part I. Construction of the Pilot Plant. Int. Conf. on Oil Shale and Shale Oil, Beijing, 1988.

13. C.E. Banks, et.al., Technical and Economic Study of an Integrated Single Pass Mining System for Open Pit Mining of Deep Oil Shale Deposits Phase I Report Sun Oil Company, Prepared for U.S. Bureau of Mines, BU Mines OFR 22-1976.
14. M. Perrini, Oil From Shale and Tar Sands, ncd, 1975.
15. Oil Shale Data Book, Prepared by TRW Energy Systems Group for the Naval Oil Shale Reserves Predevelopment Plan, June, 1979.
16. J.E. Gwyn, S.C. Roberts, G.P. Hinds, D.E. Hardsry, and G.L. Johnson, Shell Pellet Heat Exchange Retorting-SPHER, Intensive, Energy Efficiency Process for Retorting Oil Shale, Thirteenth Oil Shale Symposium, Colorado, 1980.
17. M.J. Roberts, M.C. Messinger, D.M. Rue, F.S. Lau, Pressurized Fluidized Bed Hydro-retorting of Eastern Oil Shales, Annual Report, DOE-MC-11089-86, 1992.
18. US Patent 4 017 119
19. P. Nowacki, Oil Shale Technical Data Handbook, ndc, 1981.
20. W.J. Parkinson and J.J. Merson, Cost Analysis of the Carbon Monoxide Steam Process, Report, LA-463-MS, 1982
21. R.M. Coomes, Carcinogenic Aspect of Oil Shale, American Nuclear Society Meeting, Denver Co., 1978.
22. J.D. Erdman, V.G. Ramsey, N.W. Kalenda, and W.E. Hansen, Synthesis and Properties of Porphyrin Vanadium Complexes, J.Am. Chem. Soc., 78, 5844, 1956.
23. T. Sutikno, Cost of Refining Paraho Shale Oil to Transportation Fuels, Energy Progress, 4:2, 94, 1984.
24. J.G. Sikonia, B.R. Shah, and M.A. Ulowitz, A Technical and Economic Assesment of Petroleum Heavy Oil, Shale Oil and Coal Liquid Refining, Coal Technology, 6:5, 169, 1983.
25. C.R. Green, Synsfuels: What's Economical?, Hydrocarbon Processing, June 77, 1988.

OIL SHALE BENEFICIATION FOR PROCESSING

J.G. GROPPPO
University of Kentucky
Centre for Applied Energy Research
3572 Iron Works Pike
Lexington, Kentucky, 40511, U.S.A.

ABSTRACT. Physical beneficiation has frequently been proposed as a method for upgrading oil shale feedstocks in order to improve the economic feasibility of exploiting these resources to produce synthetic fuels. Oil shales typically contain four to six times as much ash-forming minerals as oil-forming kerogen; hence large amounts of inorganic material need to be processed along with the kerogen during retorting which increases the subsequent problems of waste disposal and management. The reduction of inorganic material prior to retorting offers the attractive alternative of reducing the capital and operating costs .

The simplest conceptual method for obtaining higher grade feedstocks is the selective mining of higher grade zones within an ore body. Although this seems feasible, in practice it would be quite difficult, given the large areal extent of the deposits. Beneficiation offers a route to provide consistent, high grade material for retorting.

The beneficiation technologies that can be applied are similar to those employed for concentrating low-grade, finely disseminated metallic ores. The extent to which beneficiation is carried out is a function of the physical and chemical properties of the ore. Oil shale is a special case since the kerogen is finely disseminated in an inorganic mineral matrix and there are essentially no distinct grain boundaries between desirable and undesirable mineral components in the shale.

In order to effectively beneficiate any ore, it is first necessary to liberate the desired mineral components from the gangue minerals in a series of comminution stages. Coarse crushing is carried out in cone, roll or gyratory crushers. Although some liberation of coarse minerals may occur during this stage, there is little, if any liberation of finely disseminated kerogen. Finer grinding is accomplished with rod mills, ball mills, semi-autogeneous (SAG) mills or stirred ball mills until the desired level of liberation is achieved.

Once liberated, various separation processes can be used to isolate the kerogen in a more concentrated form. If a sufficient differences in the specific gravities of mineral (and organic) components exist, gravity-based processing methods such as jigging or dense medium separation can be utilized. For oil shales, the presence of significant amounts of near-gravity material precludes the use of jigs in most cases. Near-gravity material is defined as the weight percent of material that is within ± 0.10 specific gravity units of the desired separation gravity. An attractive alternative to gravity-based separation is froth flotation which exploits the surface chemical differences between mineral components, and, most particularly, wetting behavior.

Flotation is extensively practiced for the recovery of fine mineral ores, and utilizes two types of flotation devices; conventional agitated cells and column cells. Columns have

been shown to be particularly advantageous for very fine particles (<25 μm).

The use of each of these beneficiation processes and their applicability to oil shale will be described. The description will include principles of operation, equipment types, and results that have been obtained on a variety of oil shales. While no single unit operation may be capable of producing the high grade material desired from a given shale, there are specific advantages to each operation which can enable the optimum design of a circuit to maximise upgrading at minimum cost.

1. Comminution

1.1. COMMUNITION FUNDAMENTALS

The purpose of comminution in mineral processing schemes is to reduce particle size, liberate mineral constituents, increase surface area and generate fresh surfaces. Comminution is generally carried out in a series of stages beginning with crushing where the top size of the ore is reduced to achieve a uniform feed for the next stage of size reduction by grinding or pulverising. The distinction between the different stages of comminution is somewhat arbitrary. However crushing typically produces a top size of approximately 1 cm. while grinding reduces the material to approximately 10 μm . Pulverizing reduces material to approximately 1 μm .

The energy consumption for comminution is a major component of the cost of processing and depends upon the hardness of the ore. For a brittle ore, crushing and grinding requires approximately 0.5 to 2 kwhr/ton, while for fine grinding the energy requirements exceed 10 kwhr/ton. For a harder ore, energy requirements are more in the range of 10 to 30 kwhr/ton.

Of the numerous theories that exist to quantify the amount of work required to grind rocks, the most widely used is the Bond Equation or Crack Length Theory. It is applicable to intermediate grinding which covers most commercial grinding operations and is widely used in designing ball and rod mills. The most widely used measure of grindability is the Bond Work Index (W_i) which is tabulated for a variety of ores. The expression for Bond's Equation is given by

$$E = W_i (10/P^{1/2} - 10/F^{1/2}) \quad (1)$$

where E is the energy requirement of the mill (kwhr/t), while F and P are the sizes at which 80% (by weight) of the feed and product, respectively, pass. The experimentally determined value of W_i for oil shale is 15.84.¹ Grinding studies of two specific U.S. oil shales (western Anvil Points and eastern Michigan Antrim formation) found values of W_i to be 23 and 13.6 respectively² which illustrates the variability in the physical properties of oil shales. For comparison, other values of W_i are: quartz, 13.57; granite, 15.05; shale, 15.87; and gneiss, 20.13.¹

For finer grinding, the more applicable theory is Charles' Law which is given by

$$E = A(P^\alpha - F^\alpha) \quad (2)$$

where A and α are constants and P and F are the 50% passing size of the product and

feed respectively.

1.2. COMMINUTION EQUIPMENT TYPES

Primary crushing of run of mine ore is usually conducted at the mine site; underground locations are common. The top size of the feed may be as large as 60 inches and the product size can be 6 to 10 inches. The reduction ratio (R_r) or ratio of feed size to product size in this case would be 60/6 (i.e. 10) or 60/10 (i.e. 6). Normally this stage is carried out with jaw or high capacity gyratory crushers. If secondary crushing is employed, the feed would be the product from the primary crushers with a product top size of 2 to 3 inches or a reduction ratio of approximately 3. Gyratory or cone crushers are typical for secondary crushing. If tertiary crushing is employed, R_r can be in the range 8 and is produced with cone crushers. The product from one or more stages of crushing is fed into a grinding circuit of tumbling mills or stirred media mills.

Tumbling mills utilise the attrition and impact of a medium within a rotating mill which is classified by the type of media used. Rod mills use steel rods, ball mills use steel or ceramic balls, autogeneous mills use the ore itself as medium while semi-autogenous (SAG) mills use both coarse ore and steel balls. Stirred media mills differ in that the medium is stirred by impellers rather than by rotating the mills. In general ore processing, rod mills are used for coarse grinding and the product is fed into ball mills for finer grinding. The use of autogeneous or SAG mills is very ore specific (generally for softer ores) and has the distinct advantage of lower medium consumption. Stirred media mills are used for very fine grinding ($<10 \mu\text{m}$) and because of their high energy consumption are only used industrially for high unit value materials such as calcium carbonate or TiO_2 .

1.3. COMMINUTION APPLICATIONS

A detailed study on coarse crushing of high and low grade Green River oil shales found that the feed grade (20.7 to 24.9 GPT by Fischer assay) had little or no effect on crusher performance.³ Power requirements were essentially the same for the three types of crushers evaluated (gyratory cone, impact and roll crushers) as shown in Table 1. All crusher types had a throughput of near 70% of the rated capacity and the comminution and wear properties were found to be similar to those encountered with a medium hard limestone.

The South Africa Torbanite and Refining Company, Ltd. (circa 1950) used coarse crushing in the beneficiation of a South African torbanite, and primary crushing to 15 cm. (6 in.) was accomplished with single roll crushers.⁴ Secondary crushing to 7.6 to 10 cm. (3 to 4 in.) was provided with a smaller single roll crusher, while tertiary crushing to 2.5 cm. (1 in.) and smaller was done with a double roll crusher. There was no screening between crushing stages and the final product was screened into two products. The +2.5 cm. (1 in.) was charged to Davidson retorts while the -2.5 cm. (1 in.) fines were charged to Salerno retorts. All of the shale was retorted in this particular process.

In the Petrosix process,⁴ primary, secondary and tertiary crushing are accomplished with gyratory and cone crushers with double-deck screens between stages to produce

0.63 and 6.3 cm. (0.25 in. and 1.27 in.) charges for retorts while fines are discarded to the mine with the spent shale from the retort.

There is reasonable consistency in published reports to the effect that the liberation of western U.S. oil shales can be achieved with a grind size of 80% passing 15 to 20 μm or finer. To achieve this grind size with ball or SAG mills, the energy consumption has been reported to be 40 to 50 kwhr/ton.⁵ Optimization tests to minimize power consumption in a stirred ball mill were determined to be a pulp density of 52 percent solids by weight with 85 percent of the mill volume filled with the medium.⁶ With 3 mm. stainless steel beads as the medium, a d_{90} of 21.9 μm was achieved at an energy consumption of 61.35 kwhr/ton. Using 2 mm. stainless steel beads, the same grind was achieved with only 39.42 kwhr/ton. In addition, the mill capacity was increased with the smaller beads. Lower mill speeds reduced the power requirements while higher speeds increased the mill throughput.

The optimization of comminution circuits is dependent on the extent of beneficiation that is required. The obvious conclusion from this discussion is that comminution should be carried out in a series of stages to achieve the desired results, and the minimization of flows through energy-intensive grinding stages will reduce the overall energy requirements.

2. Gravity Concentration

2.1. GRAVITY CONCENTRATION FUNDAMENTALS

Gravity concentration exploits the differences in specific gravity between desirable and undesirable mineral components. It is widely accepted that each type of gravity concentrator has its own characteristic performance curve when treating a given size of material.⁷ These curves effectively measure the efficiency of the equipment, and can be used to predict performance. The most widely used performance curve is the Tromp curve or partition curve as shown in Figure 1. To determine the curve for a particular cleaning operation, one needs to know the recovery of product (weight %) as well as a float-and-sink analysis of both the product and tailings. The cut point (d_{50}) is the gravity at which a particle has an equal probability of reporting to the product or tailings. The sharpness of the separation is the Ecart Probable Moyen or E_{pm} determined by

$$E_{pm} = \frac{(d_{25} - d_{75})}{2} . \quad (3)$$

In general, the lower the E_{pm} , the sharper the separation. An important aspect of gravity separation is the amount of near gravity material or the amount of material within ± 0.10 specific gravity units of the specific gravity of separation. Inefficiencies in gravity-based separation processes result in some material with similar, but not the same, specific gravity being recovered with the product. The more near gravity material that is contained in the feed, the more efficient the process must be to make a sharp separation at the desired specific gravity.

2.2. GRAVITY CONCENTRATION EQUIPMENT TYPES

Relatively simple gravity separation (<15% near gravity material) can be accomplished with a variety of devices including jigs, shaking tables and spirals. Jigs produce a stratification of heavy and light material by pulsating water in a bath, while shaking tables and spirals effectively wash lighter materials away from the heavier ones by moving a slurry across a table with rifts or along a spiral path. While these units are cheap to operate, they find little application in oil shale processing because of the relatively high proportions of near gravity material.

Heavy media devices such as baths and cyclones are more suitable to gravity concentrate oil shale. Rather than using water as a separating medium, a suspension of finely-ground (<37 μm) magnetite is prepared to effectively create a heavy liquid. The higher the magnetite concentration, the higher the suspension gravity. The advantage of these processes is that the specific gravity of separation can be controlled precisely, and magnetite can be recovered by magnetic separators. Heavy media baths are used to separate coarse material (>0.5 mm) while heavy media cyclones are used to separate finer ores. The principle of operation in heavy media cyclones is essentially the same as for any classifying cyclone, except that the specific gravity of the separating fluid can be increased by magnetite addition.

2.3. GRAVITY CONCENTRATION EXAMPLES

A detailed float-and-sink analysis was conducted on Green River oil shale for various size fractions.⁸ An example of the washability curves for the 3/8" X 28 mesh size fraction is shown in Figure 2. A major conclusion of this study was that this shale contained 20 to 40% near gravity material. Because of this, only the most efficient gravity-based beneficiation equipment (heavy medium baths and cyclones) would be suitable for effective separation. At a separation gravity of 2.3, the yield to the float product would be 72 weight percent. The float product quality would be approximately 27 GPT oil, while that of the refuse product would be 8.3 GPT from a feed containing 13.1 GPT. Washability data that is obtained in a float-and sink analysis indicates the theoretical quality of products that can be achieved with gravity-based separation. Performance curves for specific types of equipment can be used to predict the actual separation efficiencies that can be obtained, determined by the E_{pm} . Calculated values of E_{pm} for heavy medium cyclones at different separation gravities for two different feed sizes are shown in Table II. Note that as the specific gravity of separation increases, the E_{pm} also increases for both size fractions. In this study, sharper separations were obtained with coarser material at each separation gravity. For comparison, the E_{pm} values for a Batac jig on several size fractions is shown in Table III. The high values for E_{pm} (0.08 to 0.12) are indicative of inefficient separation or large amounts of near-gravity material contained in the product.

Crushing Green River oil shale to various sizes, grade vs. recovery curves were determined using E_{pm} values for heavy medium cyclone separation and are summarized in Figure 3. A slight improvement in process efficiency was observed as the top size was reduced. At a concentrate grade of 27 GPT, recovery increased from 85 to 86% as the top size was reduced from 1-1/2 inches to 3/8 inch. Using the less efficient Batac jig and

five different grinding schemes (Figure 4), at the same concentrate grade (27 GPT), recoveries of 70 to 79% were achieved.

3. Flotation Concentration

3.1. FLOTATION FUNDAMENTALS

Flotation is a versatile surface-based separation process that exploits differences in surface chemical properties between desirable and undesirable mineral components. The principle surface property of concern in this process is the wetting behavior of the solids. In order for flotation to occur, it is first necessary to form a stable bubble-particle aggregate. The condition for bubble-particle adhesion is expressed by

$$\Delta G = \gamma_{SV} - (\gamma_{LV} + \gamma_{SL}) \quad (4)$$

where γ_{SV} , γ_{LV} and γ_{SL} are the interfacial tensions at the solid/vapor, liquid/vapor and solid/liquid interfaces, respectively. Adhesion occurs if the ΔG is negative.

Young's Equation describes the equilibrium between interfacial energies or:

$$\gamma_{SV} = \gamma_{LV} \cos \theta + \gamma_{SL} \quad (5)$$

where θ is the contact angle between the solid and air interfaces. Combining these equations gives:

$$\Delta G = \gamma_{LV} (\cos \theta - 1). \quad (6)$$

The more negative the value for ΔG , the higher the probability of flotation. Also, the larger the contact angle, the more negative ΔG becomes.

Many kerogen-containing oil shales are naturally hydrophobic and will form a finite contact angle with air bubbles, hence they are amenable to flotation. Hydrophobicity can, in some cases, be increased by the addition of flotation collectors such as fuel oil, which when adsorbed on the particle surface can increase the contact angle.

3.2. FLOTATION EQUIPMENT TYPES

Two distinct types of flotation equipment are commercially available; conventional agitated cells and column cells. Simplified schematic diagrams of both types of cells are shown in Figure 5. These devices differ in their applicability to ores but rely exclusively on the ability to form stable bubble-particle aggregates to separate hydrophobic minerals from hydrophilic gangue.

Conventional agitated cells have been used extensively in the mineral industry for many years. They consist of a large tanks or cells agitated by a mechanical impeller to prevent particles from settling. Air is introduced into the cell and fine air bubbles are produced by the shearing action of the impeller. Surface tension reducing frothers are added in most cases to produce smaller bubbles and to increase their surface area. Hydrophobic

particles attach to the air bubbles and are transported to the top of the cells by buoyancy. At the top of the cells, coalescence of the mineral-laden bubbles occurs and a stable froth is formed. Entrained gangue minerals and water drain from the froth and the hydrophobic minerals are removed by scraping the froth from the top of the cells. These types of cells are commonly used for most mineral separations by flotation.

Column cells were introduced into the mining industry in the early 1960's and by the mid 1980's were used extensively on a variety of ores. They differ from agitated cells in that there is no mechanical impeller to mix particles and bubbles. Rather, particles settle in a column of slurry against a stream of constantly rising air bubbles. The "quiescent" mixing has been shown to be more conducive to fine particle recovery. Another distinct difference is that columns utilise a much deeper froth zone (2 to 4 feet) than agitated cells (4 to 6 inches). The deeper froth zone allows for more effective drainage of entrained gangue from the froth which can be enhanced by counter-current wash water. Bubbles are produced in column cells by a variety of bubble-generating devices, the simplest of which is a sparging rod. Sparging rods are porous rubber or sintered metal tubes at the base of the column cell through which pressurized air is forced to produce fine air bubbles.

3.3. FLOTATION EXAMPLES

Froth flotation of oil shale has been the subject of numerous investigations. Although the results differ significantly, most of these studies have shown that it is first necessary to grind the oil shale to very fine sizes to achieve flotation. A general conclusion is that it is necessary to grind to about 80% passing 15 to 20 μm to achieve liberation.⁵ Most studies have used a flotation feed containing 5 to 15 percent solids by weight and a retention time of 3 to 10 minutes.

Fahlstrom⁵ investigated the flotation of Green River oil shale (16.3% kerogen) and produced a concentrate containing 56% kerogen at 95% recovery. Increasing the concentrate grade to 66% kerogen reduced the recovery to 90%. These results were obtained with high grade material from the Mahogany Zone. Similar material was upgraded from 24 GPT to 50 GPT with 80% recovery by Krishnan et al.² Three additional stages of grinding and flotation produced a final concentrate containing 90 GPT with a recovery of only 47%. At the other extreme, flotation of the Stuart oil shale in Australia was not satisfactory even after grinding to -22 μm .⁹ The most successful example of flotation in the oil shale industry is a kerogen concentrate produced from the Estonian kukersite; this is a commercial process where the flotation product is used as filler for plastics and rubber.¹⁰

Conventional flotation of Devonian shales in the U.S. showed that a shale containing 12 GPT could be concentrated to 36 GPT with a recovery of 78%.¹¹ In the same study, the froth from the first flotation stage (i.e. rougher flotation) was combined with the product obtained from refloating the tailings from the first flotation stage (i.e. scavenger flotation) and refloats four times (i.e. cleaner flotation). This rougher-scavenger-cleaner procedure increased the oil yield of the final concentrate while the grade improved with increasing pH to 9 with no reduction in recovery. Higher concentrate grades were obtained with finer grinding.¹² Without finer grinding, high recovery and grade were not obtained despite the addition of a host of reagents.¹³

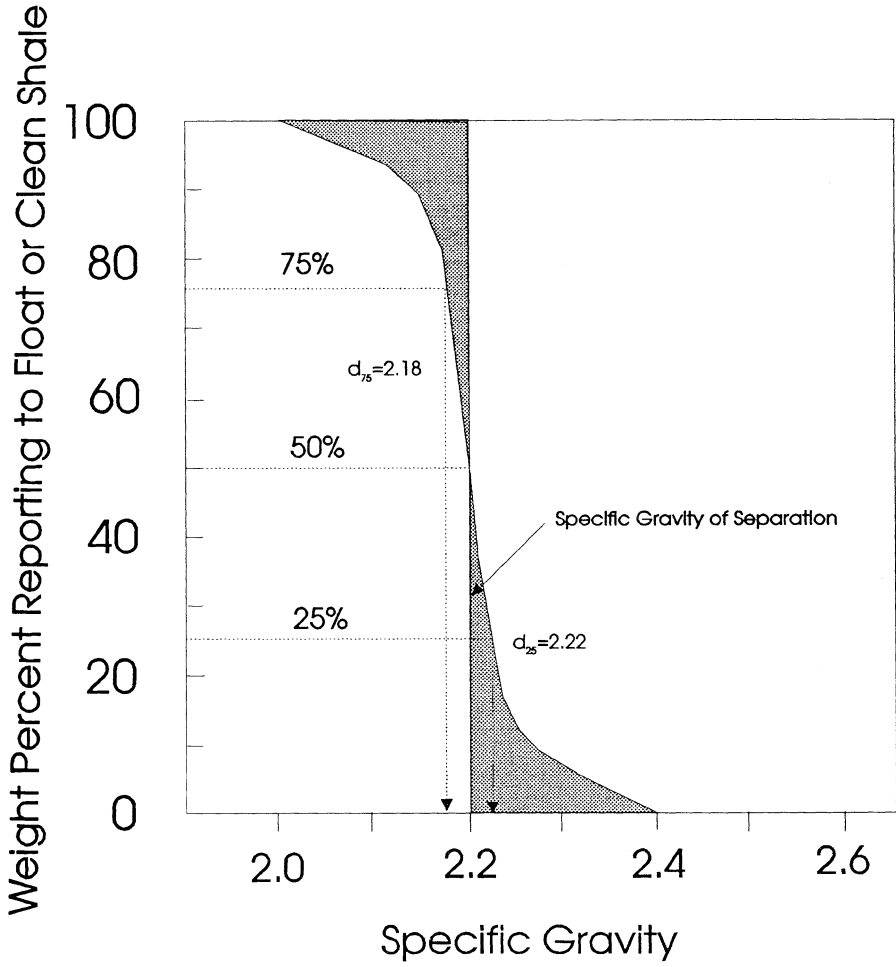


Figure 1. Tromp distribution curve for a proposed density separation process.

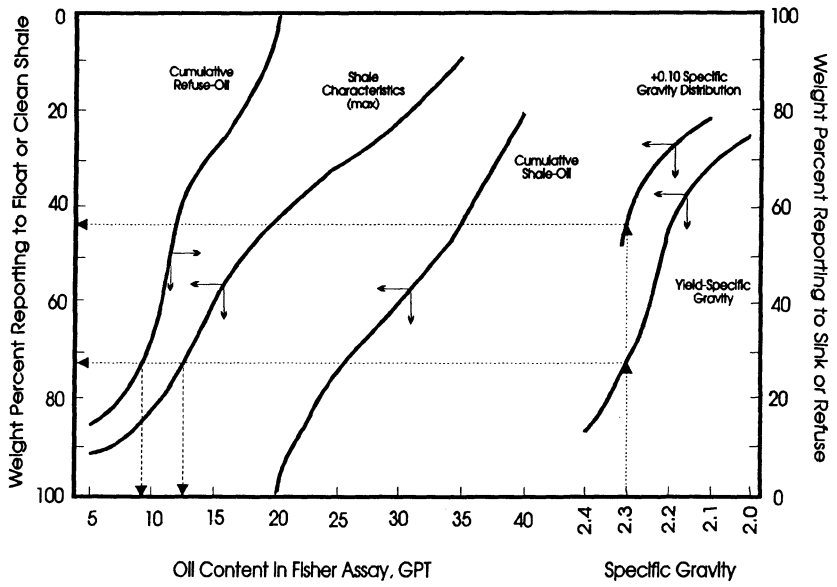


Figure 2. Washability curves for 3/8" X 28 mesh low grade shale showing yields at different specific gravities and the near gravity material.⁶

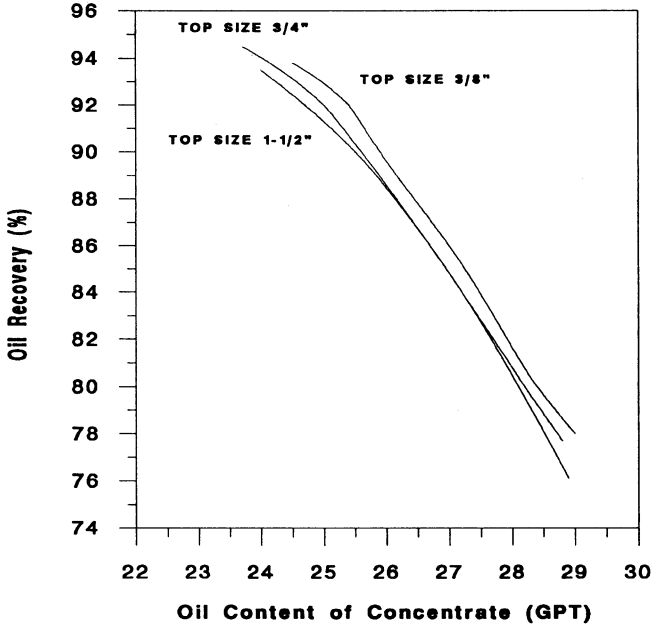


Figure 3. Grade versus recovery curves for low grade shale beneficiated in a heavy medium cyclone.⁸

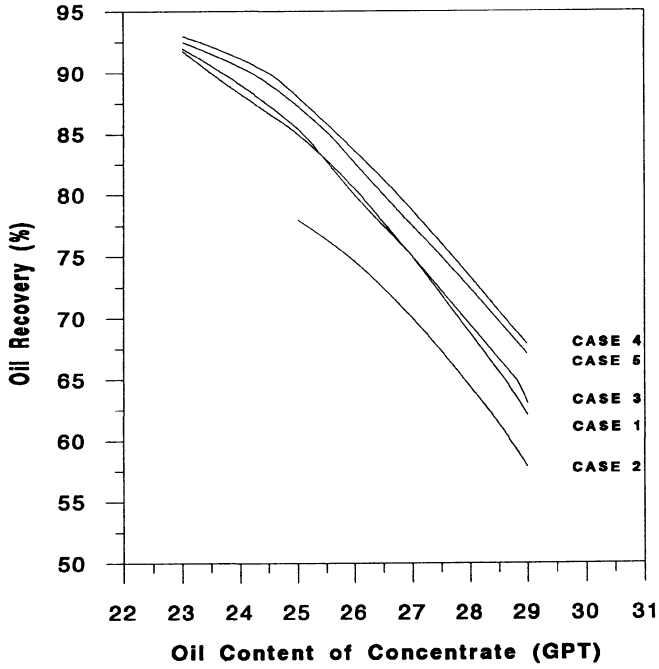


Figure 4. Comparative grade versus recovery curves for five different flow schemes using a Batac jig to beneficiate the oil shale.⁸

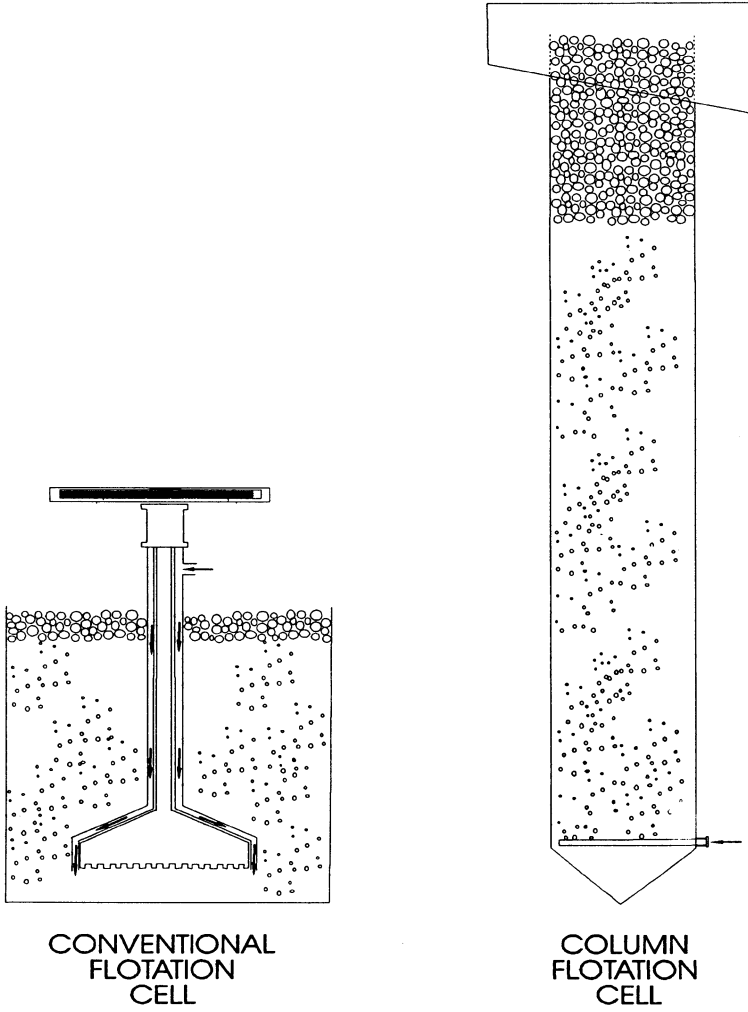


Figure 5. Schematic diagrams of conventional and column flotation cells.

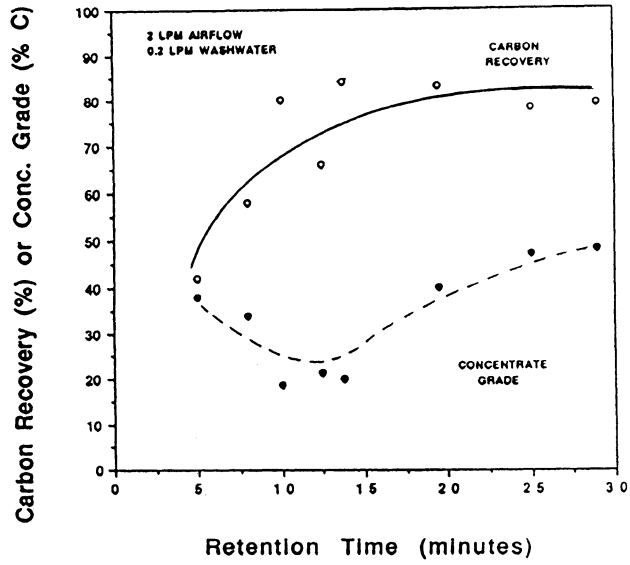


Figure 6. Effect of retention time on carbon recovery and concentrate grade for column flotation of fine-ground eastern U.S. oil shale.¹⁵

Single stage column flotation of eastern U.S. shales has been shown to be as effective as multiple stages of conventional flotation.¹⁴ The minimum retention time required to obtain greater than 80% recovery with high grade concentrate (>40% carbon) from eastern U.S. shales was found to be 20 minutes as shown in Figure 6.¹⁵ Decreasing the retention time lowered concentrate grade and recovery. In this study, the long residence time necessary for effective flotation was attributed to low probabilities of bubble-particle collision and attachment for fine (<10 μm) particles rather than carrying capacity limitations of the froth.

SYNOPSIS

Effective physical beneficiation of oil shale is carried out in a series of stages beginning with comminution. The purpose of comminution is to reduce particle size, liberate mineral constituents, increase surface area and generate fresh surfaces. Energy consumption is a major component of comminution and is dependent on the hardness of the ore, frequently expressed by the Bond Work Index (W_i). A variety of crushing and grinding equipment has been used for comminution of oil shale. The extent to which comminution is carried out is dependent on the type of feed necessary for the concentration method to be used.

Gravity concentration exploits the differences in specific gravity between desirable and undesirable mineral components. Each type of gravity concentrator has its own characteristic performance curve when treating a given size of material, represented by a Tromp curve, from which the sharpness of separation (E_{pm}) can be predicted. The effectiveness of gravity concentration is highly dependent on the type of equipment used and the amount of material within ± 0.10 specific gravity units of the specific gravity of separation. Heavy medium devices are suitable for concentration of oil shale.

Flotation is a surface-based process that exploits differences in surface chemical properties between desirable and undesirable mineral components. Flotation is employed for ores ground to fine sizes that cannot be effectively separated by gravity-based methods. Many kerogen-containing oil shales will form a finite contact angle with air bubbles, hence they are amenable to flotation. Conventional agitated cells and column cells have both been used to effectively concentrate oil shale. In order to produce a high grade concentrate with conventional agitated cells, several stages of flotation may be necessary, while with column cells, similar results may be achieved in a single stage with a longer retention time.

ACKNOWLEDGEMENT

The author gratefully acknowledges the assistance of F.J. Derbyshire, Director of CAER, for his technical and editorial contributions in the preparation of this manuscript.

REFERENCES

1. Anonymous, Mining Engineering, p. 316, 1953.
2. Krishnan, G.N., Farley, E.P. and Murray, R.G., "Beneficiation of U.S. Oil Shales by

- Froth Flotation", Proc. 16th Oil Shale Symposium, Golden, CO, pp. 426-436, 1983.
3. Salotti, C.A. and Datta, R.S., "Size Reduction of Green River Shale", Proc. 16th Oil Shale Symposium, Golden, CO, pp. 394-412, 1983.
 4. Russell, P.L., Oil Shales of the World, Their Origin, Occurrence and Exploitation, Pergamon Press, Oxford, 1990.
 5. Fahlstrom, P.H., "A Physical Concentration Route in Oil Shale Winning", Proc. 12th Oil Shale Symposium, Golden, CO, pp. 252-277, 1979.
 6. Schultz, C.W and Mehta, R.K., "An Integrated Circuit for Beneficiating Eastern Oil Shale", Proc. 1990 Eastern Oil Shale Symposium, Lexington, KY, pp. 367-373, 1990.
 7. Kelly, E.G., Spottiswood, D.J., Spiller, D.E and Robinson, C.N., "Performance of Modern Spirals Cleaning Fine Coal", Preprint No. 84-48, SME-AIME Annual Meeting, Los Angeles, CA, Feb. 26-March 1, 1984.
 8. Datta, R.S. and Salotti, C.A., "Coarse Beneficiation of Green River Oil Shale", Proc. 16th Oil Shale Symposium, Golden, CO., pp. 413-425, 1983.
 9. O'Brien, B.A., "Beneficiation of Stuart Oil Shales", Proc. 2nd Australian Workshop on Oil Shale, Brisbane, pp. 78-82, Dec., 1984.
 10. Urov, K., "Estonian Oil Shales: Composition, Properties, Utilization and Environmental Aspects", Proc. 6th Australian Workshop on Oil Shale, pp. 25-31, Univ. of Queensland, St. Lucia, Brisbane, Dec, 1991.
 11. Lamont, W.E. and Hanna, S.A., "Upgrading of Eastern Oil Shale by Beneficiation", Proc. 1982 Eastern Oil Shale Symposium, p. 175, Lexington, KY, 1982.
 12. Lamont, W.E, Thoedorou, K. and Rex, R.C., "Beneficiation-Hydroretort Processing of U.S. Oil Shales", Proc. 1986 Eastern Oil Shale Symposium, pp. 125-140, Lexington, KY 1986.
 13. Lamont, W.E., Cardoso, J.B., Bates, J.B. and Rigsby, B., "Improvement in Eastern Oil Shale Beneficiation", Proc. 1987 Eastern Oil Shale Symposium, pp. 309-314, Lexington, KY 1987.
 14. Schultz, C.W., Bates, J.B. and Lamont, W.E., "Column Flotation of Eastern Oil Shales", Proc. 1989 Eastern Oil Shale Symposium, pp. 425-430, Lexington, KY, 1989.
 15. Groppo, J.G. and Parekh, B.K., "Column Flotation Studies of Alabama Oil Shale", Preprint No. 93-57, SME-AIME Annual Meeting, Reno, NV, Feb. 15-18, 1993.

METHODS OF OIL SHALE ANALYSIS

FRANCIS P. MIKNIS
Western Research Institute
Box 3395
Laramie, WY 82071
USA

ABSTRACT. The Fischer assay is the traditional method for determining the oil potential of an oil shale. However, the Fischer assay is a specification test and does not provide much information about the quantity or quality of the organic matter in the sediment. A number of other measurements have been suggested to complement or replace the Fischer assay. These include pyrolysis, chromatographic, densimetric, thermophysical, spectroscopic and elemental analysis methods. Of these, the spectroscopic methods, primarily solid-state ^{13}C NMR, are the only ones capable of providing information about kerogen structure. These methods have been used to correlate structural aspects of kerogen with its conversion behavior. As a result, greater insight into the mechanisms of oil generation from oil shales has been obtained. Different methods of oil shale analyses are reviewed in this paper. In addition the use of solid- and liquid-state ^{13}C NMR measurements, combined with the material balance Fischer assay, to study the conversion behavior of oil shales is discussed.

1. Introduction

An oil shale can be defined as a compact rock of sedimentary origin with an ash content of more than 33 percent and containing organic matter that yields oil when destructively distilled, but not appreciably when extracted with ordinary solvents (1). This is an operational definition. There is no geological, or chemical definition of an oil shale. The term is used mostly in an economic sense so that any shallow rock that yields a commercial amount of oil upon pyrolysis may be considered an oil shale. The key words are commercial amount because petroleum source rocks, which often contain only 1% organic matter, can produce commercial amounts of oil over geologic times. On the contrary, oil shales must have a large enough fraction of organic matter to be of economic interest. The organic matter content of an oil shale should be ~2.5 wt%, just to provide the calorific requirements necessary to heat the rock to 500°C in order to produce shale oils by thermal decomposition of the organic matter (2). Below this amount of organic matter, the rock cannot be a source of energy because it takes more energy to heat the rock than can be derived

from the produced shale oil. A lower limit of 5 % organic matter is sometimes used to define a commercial deposit (2). Thus, an oil shale can be a petroleum source rock, if subjected to the proper burial conditions, but a petroleum source rock at shallow depths is not an oil shale because of the requirements of organic matter richness.

Oil shales contain organic matter mostly in the form of kerogen, which is defined as that fraction of the organic matter in a sedimentary rock that is insoluble in common petroleum solvents. The other fraction, called bitumen, is soluble in organic solvents, but represents only a small amount of the organic matter in an oil shale. To evaluate the potential of an oil shale formation as an oil resource, two important factors must be considered: 1) how much organic matter is in the formation, and 2) how much of the organic matter can be converted to oil. The first factor relates to the total quantity of organic matter in the sediment, while the second factor relates to the quality or type of organic matter. The chapters by Hutton (this volume) describe petrographic methods to classify and type oil shales.

Probably the single, most important item of information about an oil shale is its potential to produce oil during heating. The traditional method for evaluating the potential oil yield of an oil shale is the Fischer assay (ASTM method D-3904-80). The Fischer assay (FA) consists of heating a 100 gram sample of -8 mesh (2.38 mm) particle size oil shale to 500° C at 12° C/min and maintaining this temperature for 40 min. During this heating cycle, hydrocarbon vapors are distilled from the rock and condense to form a shale oil. The material is collected, its volume and weight recorded and specific gravity is recorded. From these measurements, the oil potential is reported in gallons of oil per ton of shale. Obviously the greater this number, the greater the commercial viability of the formation.

The Fischer assay is strictly a specification test. It does not provide any information about the quality of the organic matter in the oil shale. Nevertheless, it is the benchmark for evaluation an oil shale deposit, and also for determining the efficiencies of oil shale retorting processes. For issues involving exchange or leasing agreements of public oil shale lands in the western United States, the Fischer assay is the only accepted method to determine the value of the lands in question.

2. Oil Shale Assay Methods

Because the Fischer assay does not provide information about the what chemical properties of oil shales are important for producing liquids, a number of attempts have been made to correlate various chemical and physical property measurements with oil yields determined by the Fischer assay. Even the Fischer assay procedure has been modified for different types of oil shale, or to more closely resemble a certain type of retorting process (4-6).

Table 1. Summary of Methods of Correlating Kerogen Properties with Oil Yields

Method	Measured Property	Reference
Elemental Analysis	organic carbon, total hydrogen	7, 8
Nuclear Magnetic Resonance (NMR)		
Pulsed NMR	total hydrogen	17, 18, 19, 20
Cross Polarization (CP)	aliphatic/aromatic carbon distribution	10
CP with Magic-Angle Spinning	aliphatic/aromatic carbon distribution	11, 12, 13, 14, 15
Electron Spin Resonance (ESR)	unpaired electron concentration	33, 34
Fourier Transform Infrared Spectroscopy	aliphatic hydrogen	
Laser Pyrolysis	acetylene yield	21, 22
Thermal Analysis	weight loss and evolved gases upon heating	23, 24
Densimetric	oil shale density	25, 26, 27, 28
Thermophysical	thermal conductivity, thermal diffusivity, relative dielectric constant	29, 30, 31, 32

A summary of some methods for correlating oil shale properties with Fischer assay oil yields is given in Table 1. In general, these methods attempt to measure a parameter that is associated with the quantity of organic matter in the sediment. As such, most of them are specific to a given oil shale formation so that, for example, a correlation derived for a Green River oil shale is probably not valid for a different oil shale formation, i.e., a new correlation must be established for every new deposit.

2.1. ELEMENTAL ANALYSES

The elemental composition of an oil shale can be correlated with oil yields determined by the Fischer assay (7,8). The best correlation for Green River Formation shales is between organic carbon and Fischer assay oil yields. This is not surprising since organic carbon constitutes the major element in the composition of an oil shale. Cook obtained the equations,

$$\text{oil(wt\%)} = 0.832(\%org) - 0.251 \quad (1)$$

and

$$\text{oil (gal/ton)} = 2.22(\% \text{orgC}) - 0.771 \quad (2)$$

where orgC is the weight percent organic carbon. These correlations were obtained prior to the development of solid-state NMR techniques. However, it is of interest to note that the coefficient, of 0.832 in equation 1 is close to the fraction of aliphatic carbon (0.80) in Green River Formation oil shale determined by ^{13}C NMR measurements (9). The aliphatic carbon for any oil shale has been shown to be a good indicator of oil yield. (10-15).

For Devonian and Mississippian black shales from the eastern United States, organic carbon also correlates with Fischer assay oil yield (Figure 1)(8). However, because of differences in maceral compositions (quality) of the organic matter of the two shale deposits (16), the data are best fit with two separate regressions for the Cleveland and Sunbury deposits.

If the quality of the organic matter does not change significantly in the formation, then correlations based on organic carbon are applicable, and organic carbon is a good indicator of the quantity of organic matter in the sediment. As a rule of thumb, the Fischer assay oil yields in gal/ton for Green River Formation oil shales, are about 2 to 2.5 times the weight percent of organic carbon. For the eastern Devonian oil shales of the United States, the oil yields in gal/ton are about

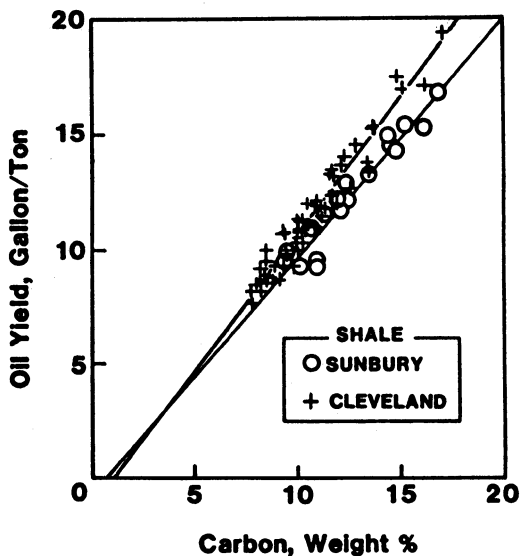


Figure 1. Plot of Fischer assay oil yields and carbon contents for Cleveland and Sunbury oil shales (reprinted from ref 8).

equivalent to the weight percent organic carbon. For the eastern shales in Figure 1, the Sunbury and Cleveland shales produce 1.03 and 1.18 gal of oil per unit wt percent of organic carbon, respectively.

The amount of hydrogen in an oil shale should also be an indicator of the potential oil yield of an oil shale because the amount of available hydrogen is a key factor in producing liquids during pyrolysis. Consequently, a number of correlations have been developed between hydrogen and Fischer assay oil yields (1,17-20). Most of these were based on the use of pulsed NMR methods, which measure signals directly proportional to the amount of hydrogen in the shale. A comparison of a Fischer assay oil yield histogram and a pulsed NMR hydrogen response histogram is shown in Figure 2. The NMR response, which is in arbitrary units, quite faithfully mimics the Fischer assay histogram. Some advantages of pulsed NMR methods are that they are rapid, non-destructive, and can be easily automated. It could be used for rapidly screening an oil shale deposit (Figure 2). Disadvantages are small sample sizes, and interferences due to protons in water and clay minerals. Also, because the pulsed NMR measurement samples a parameter related to organic structure and mineralogy of the oil shale, calibrations must be established for each oil shale deposit.

2.2 LASER PYROLYSIS

Laser pyrolysis chromatography has also been suggested as a method for analyzing oil shales (21,22). The method involves using a laser to rapidly pyrolyze the kerogen in an oil shale, followed by gas chromatographic detection of the pyrolysis products. Because of the extremely high temperatures involved during the pyrolysis, acetylene is the major organic species in the product gas mixture. The amount of acetylene produced correlates with the FA oil yield. With a flame ionization detector, only organic species are detected so that the integrated chromatogram should be proportional to the amount of organic matter. Some disadvantages are that the oil shale must be ground, then pelletized before analysis. Also because the laser is focused onto a small area, it is important that the pellets be uniform in oil shale composition.

2.3 THERMAL CHROMATOGRAPHY

Method for assaying oil shales based on thermal analytical methods have been suggested (23,24). Compared to laser pyrolysis, this method is a low temperature method. In the thermal chromatographic method, an oil shale is heated (~30 °C/min) to a temperature of 600 °C. Hydrocarbon gases that are evolved during heating are monitored with a flame ionization detector. The total amount of evolved gases correlates with FA oil yields. A disadvantage of this procedure is that small sample sizes (mg) must be used; therefore, sample homogeneity and particle sizes could present problems. An advantage is that the evolved gases can be analyzed by GC to obtain information about the organic matter. These methods are similar to the Rock-Eval pyrolysis method for determining kerogen type and

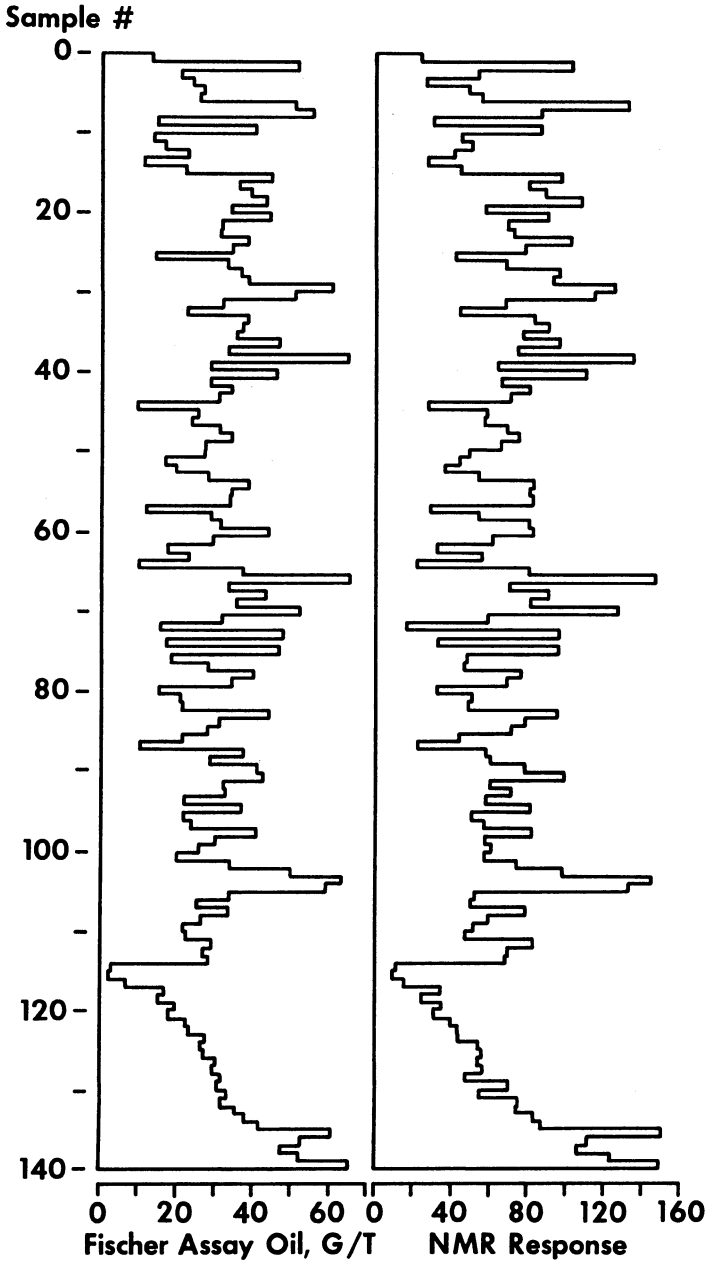


Figure 2. Comparison of histograms of Fischer assay oil yields and pulsed NMR response for a set of 141 Colorado oil shales.

maturity (2). Rock-Eval measurements have been shown to correlate with FA oil yields (1, p 461).

2.4 DENSITY MEASUREMENTS

A simple, but effective, correlation of a physical property measurement with oil yields is the relationship between density and oil yields (25-28). These correlations are based on the simple observation that the richer an oil shale, the lesser its weight for a given volume. Thus, by measuring the density of an oil shale, one is essentially measuring the weight fraction of organic matter in an oil shale. The relationship between density and weight percent organic content has been derived by Smith (25) and has the form,

$$D_T = D_A D_B / [A(D_B - D_A) - D_A] \quad (3)$$

where D_T is the oil shale density; D_A is the average density of the organic fraction; D_B is the density of the inorganic fraction; and A is the weight fraction of the organic matter. Equation 3 is a general expression and should be applicable to any oil shale deposit. However, its use depends on how widely D_A , and D_B vary. For Green River Formation oil shales, D_A is about 1.07, and D_B is about 2.72 g/cm³ (26). An expression relating oil yield (OY) and density for Green River oil shale is

$$OY = 31.6D_T^2 - 206.0D_T + 326.6 \quad (4)$$

In Equations 3 and 4, D_T is the absolute, not the bulk density. Schultz and Bates (27) have also correlated oil shale density with oil yields for oil shales and beneficiated products for oil shales from Alabama, Indiana, Kentucky, Ohio, Michigan, and Tennessee. Their correlations between oil yield, organic carbon and densities is shown in Figure 3. For New Albany oil shales from the eastern U.S., specific gravity has also been shown to correlate with oil yield (28).

The method relating density to organic fraction only works well if the mineral and organic components are fairly uniform throughout the deposit, and the percentage conversion is uniform. Also, the correlation must be developed for each oil shale deposit. These caveats apply to all correlations that measure some chemical or physical property that relates to quantity, and not quality of the organic matter.

2.6 MICROWAVE AND THERMOPHYSICAL CORRELATIONS

Microwave radiation has been suggested as an alternative method for assaying Colorado oil shales (29). The dissipation of microwave energy has been shown to be a strong function of the richness of an oil shale. The loss tangent, which is an index of a materials ability to absorb microwaves and which is also related to the dielectric constant of the material, increases non-linearly as shale richness increases linearly.

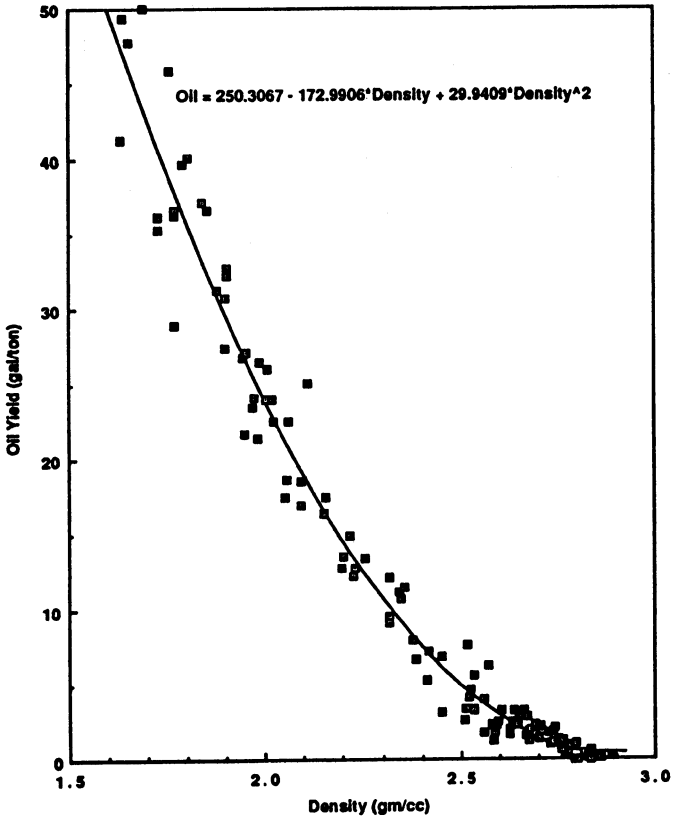


Figure 3. Relationship between density and Fischer assay oil yield for eastern U.S. oil shales (reprinted from ref 27).

Thermal conductivity, thermal diffusivity, dielectric constant, specific heat and sonic velocity measurements have been made as a function of oil shale richness (30-32). However, none of these measurements appear promising as methods for assaying oil shale. In some cases, the measurements are dominated by the mineralogy. Also the correlations are non-linear, as are the microwave correlations, which tends to detract from their usefulness as assay methods.

2.7 ESR MEASUREMENTS

Attempts have been made to correlate electron spin resonance (ESR) measurements with oil yields (33,34). The idea behind these measurements is that the organic free radical concentration might correlate with oil yield. The difficulty with these measurements is that unpaired electrons from the minerals contribute to the ESR signal. Also, stable organic free radicals are associated with aromatic

components, whereas oil yield is more closely associated the hydrogen-rich aliphatic components. Nevertheless, for a set of Colorado oil shales from the same core, the ESR signal gives a fair correlation with oil yields. However, in the case of eastern U.S. oil shale, no correlation between ESR measurements and oil yield was found when samples from different locations were analyzed (34).

3. Solid-State ^{13}C NMR Measurements

All of the assay schemes described in the previous sections have one thing in common. They all measure, or attempt to measure, some parameter associated with the amount (quantity) of organic matter in an oil shale. While these methods might provide reasonably good correlations with oil yields, they are generally only valid for a specific deposit, and only valid if the type of organic matter, or its composition does not vary significantly throughout the deposit. None of the methods provide much insight into what chemical structures are important for producing shale liquids during pyrolysis of oil shales.

The importance of kerogen structure on the conversion behavior of oil shales has been known for a long time (35). However, it has only been during the last decade or so, with the development of solid-state ^{13}C nuclear magnetic resonance (NMR) techniques, that direct information about the carbon structure could be obtained. By combining the NMR measurements of aliphatic carbon ratios of the kerogen, with organic carbon measurements of kerogen, good correlations have been obtained that are independent of depositional environment, geographic location, or geologic age (10-15)(Figure 4). Fourier Transform infrared (FTIR) measurements have also been applied to obtain information about the aliphatic components in oil shales (15,36). However, application of FTIR methods has not been as popular as NMR methods for studying oil shales structure.

3.1 COMBINED NMR AND MATERIAL BALANCE FISCHER ASSAY

The effects of kerogen structure on the conversion behavior of oil shales can be studied by combining solid- and liquid-state NMR measurements with material balance Fischer assays. In a material balance Fischer assay the elemental composition is determined for the raw shale and the gas, oil, and spent shale products. Therefore, the assay data can be normalized to the basis of 100 carbon atoms, and the percentage of carbon converted to carbon in the products can be obtained. The percentage of organic carbon in the raw shale can be used as an indicator of the quantity of organic matter (kerogen) in raw shale. From these combined measurements, greater insight into some of the chemistry of kerogen decomposition can be obtained, which could lead to the development of improved oil shale retorting processes. In this section, the effects of carbon structure on the conversion behavior of several oil shales are described for a set of ten oil shales from different deposits around the world (37). Material balance Fischer data are given in Table 2, and normalized NMR conversion data are given in Table 3.

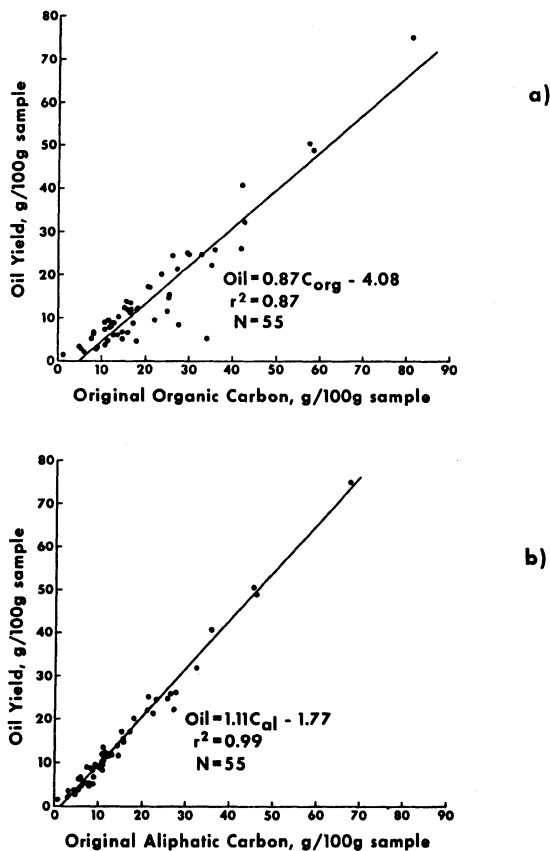


Figure 4. Correlations between total carbon (a) and aliphatic carbon (b) with Fischer assay oil yield.

During pyrolysis, there is an increase in the amount of aromatic carbon in the products (oil plus residue) over that in the original shale (38,39). This increase is produced at the expense of aliphatic carbon moieties, which produce aromatic carbon either by dehydrogenation of hydroaromatic structures or by ring closure of alkyl groups followed by dehydrogenation (40). The combined use of solid- and liquid-state ¹³C NMR, in conjunction with the material balance Fischer assay conversion data, allows some inferences to be made about the extent of aromatization reactions during Fischer assay. The Alaskan shale has the greatest loss of aliphatic carbons, 22, to aromatization reactions (Table 3). The Australia, Kentucky, Morocco, and Turkey shales also show substantial losses of aliphatic carbons to aromatization reactions. When expressed as a percentage of the raw shale aliphatic carbons, a more realistic comparison of the importance of aromatization reactions for the shales is obtained (Table 3). The Kentucky,

Table 2. Material Balance Fischer Assay Results for Oil Shales

Oil Shale	Fischer Assay, wt %			Carbon, wt %			Carbon, Conversion %			
	Oil	Gas	Spent Shale	Raw Shale	Oil	Gas	Residue	Oil	Gas	Residue
Alaska	58.00	8.83	26.66	62.7	84.2	55.7	32.5	78.2	7.9	13.9
Australia-Stuart	11.65	3.03	75.77	20.3	81.6	41.6	12.1	47.7	6.3	46.0
Brazil-Irati	11.14	2.29	83.32	17.5	83.7	36.0	8.6	53.9	4.8	41.3
China-Fushun	8.01	2.29	83.98	13.0	83.9	43.5	6.0	52.7	7.7	39.6
China-Maoming	7.71	2.70	83.11	15.4	85.4	42.7	8.8	43.8	7.7	48.5
Colorado-Anvil Pts.	12.19	1.59	84.94	14.4	83.5	46.1	5.3	66.0	4.8	29.2
Kentucky-Sunbury	5.31	2.76	88.08	16.2	83.4	36.5	11.8	27.9	6.4	65.7
Morocco-Timahdit	4.57	1.88	90.71	8.1	78.7	30.4	4.5	43.8	6.9	49.3
Turkey-Göynük	39.16	9.02	41.87	53.4	81.6	38.6	46.7	58.1	6.3	35.6
Turkey-Seytömer	2.41	1.51	88.67	5.6	85.2	40.3	3.0	38.7	11.4	49.9

Table 3. Summary of NMR Conversion Data for 10 Selected Oil Shales

Oil Shale	Number of Carbons in Raw Shale		Number of Carbons Aromatized	Decrease in Aliphatic Carbons, %	Increase in Aromatic Carbons, %	$C_a^{res}/C_a^{raw 1}$	$C_{al}^{res}/C_{al}^{raw 2}$
	Aliphatic	Aromatic					
Alaska	82	16	22	26.8	137.5	0.813	0.012
Australia-Stuart	67	30	17	25.4	56.7	1.067	0.209
Brazil-Irati	56	43	8	14.3	18.6	0.744	0.161
China-Fushun	57	40	0	0	0	0.700	0.193
China-Maoming	58	39	12	20.7	30.8	0.974	0.172
Colorado-Anvil Pts.	65	34	6	9.2	17.6	0.618	0.123
Kentucky-Sunbury	50	49	21	42.0	42.9	1.143	0.200
Morocco-Timahdit	57	40	18	31.6	45.0	0.975	0.175
Turkey-Göynük	65	32	17	26.2	53.1	0.938	0.092
Turkey-Seyitömer	64	31	18	28.1	58.1	1.161	0.219

¹ Ratio of residue aromatic carbon to raw shale aromatic carbon

² Ratio of residue aliphatic carbon to raw shale aliphatic carbon

Morocco, and Turkey-Seyitömer oil shales show the greatest percentage decrease in aliphatic carbons. These shales also show the lowest carbon conversions to oil and the highest carbon conversions to residue.

The implication of these observations is that coking (aromatization) reactions are more prevalent in, the Kentucky, Morocco, and Turkey-Seyitömer shales. However, it cannot always be established to what extent these reactions occur in the solid or liquid state. For the Alaska shale the net effect of the aromatization reactions is to produce oil because the number of aromatic carbons in the raw shale, 16, is not sufficient to account for the number of aromatic carbons in the oil, 25. For the rest of the shales, the number of aromatic carbons in the shale oil is substantially less than the number of aromatic carbons in the raw shale. Consequently, the origin of the aromatic carbons in the shale oil is not conclusive. In the case of the Kentucky shale, the number of aromatic carbons in the raw shale, 49, is not sufficient to account for the number of aromatic carbons in the residue, 56. Therefore, at least 7 of the raw shale aliphatic carbons formed aromatic carbons in the residue, assuming that coking of the shale oil vapor did not occur during Fischer assay.

A plot of the ratio of the number of aromatic carbons in the residue to the number of aromatic carbons in the raw shale is shown in Figure 5. If this ratio is greater than unity, then the minimum number of aliphatic carbons that aromatized to form residue can be determined. If the ratio is less than unity, the source of the residue aromatic carbons can not be determined. Figure 5 shows that the Australia, Kentucky, and Turkey-Seyitömer oil shales have ratios greater than unity, suggesting that the aromatization reactions to form coke are most prominent in these shales. The Morocco, China-Maoming, and Turkey-Göynük shales have ratios close to unity (>0.93). Except for the Turkey-Göynük shale, all of the shales with ratios greater than or near unity show the lowest carbon conversions to oil during Fischer assay. The data in Figure 5 suggest that the shales can be divided into three groups with regard to coking tendency, based on the ratio of residue aromatic carbon to raw shale aromatic carbon. Thus, the coking tendency is Australia, Kentucky, Turkey-Seyitömer $>$ China-Maoming, Morocco, Turkey-Göynük $>$ Alaska, Brazil, China-Fushun, Colorado.

Some of the original aliphatic carbon ends up as aliphatic carbon in the residue. Although these carbons are not involved in coking reactions, they represent a loss in oil potential. These carbons are most likely short-chain (methyl, ethyl) aliphatic carbons attached to aromatic rings. Figure 6 shows the aliphatic carbon content of the residue, expressed as a percentage of the raw shale aliphatic carbon. The interesting feature of these data is that this percentage is in the range of 10 to 20 % for most of the shales, independent of original kerogen structure and conversion behavior.

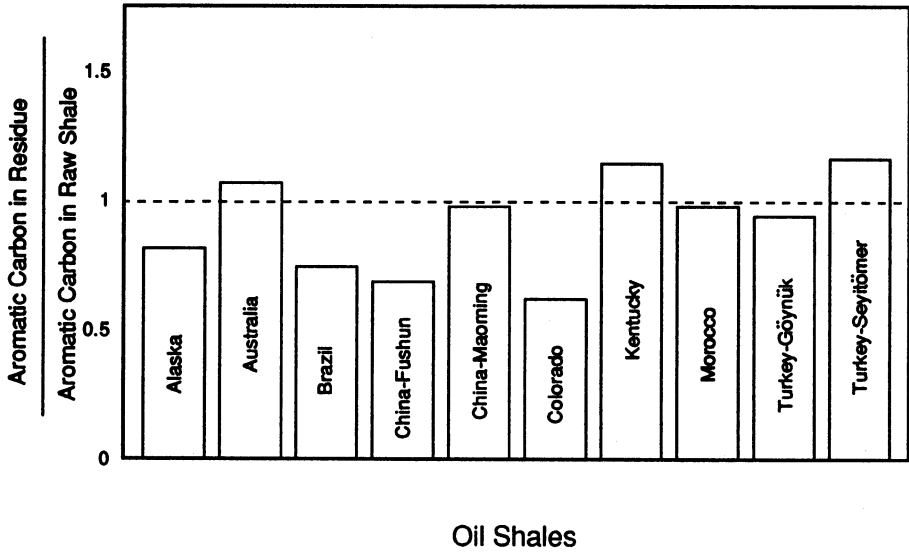


Figure 5. Ratio of aromatic carbon in residue to aromatic carbon in raw shale.

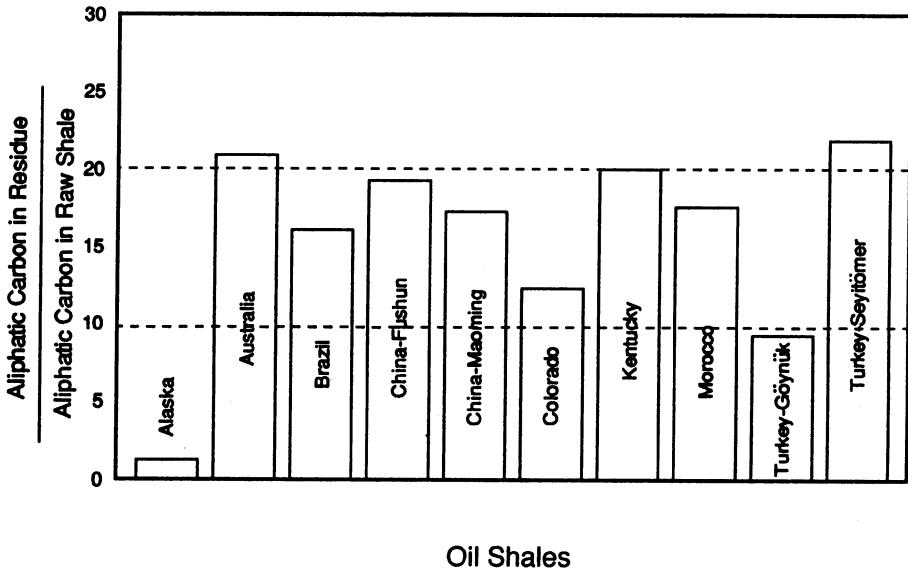


Figure 6. Percentage of raw shale aliphatic carbon in residue.

3.2 SHALE OIL ANALYSES

A limited number of analyses were performed on the shale oils to obtain information about the quality of the shale oils. These data are summarized in Tables 4 and 5. The molecular weights of the shale oils are quite constant, having a mean of 293 ± 28 (95% confidence) daltons, whereas the carbon and hydrogen aromaticities and the specific gravity of the oils are quite variable (Table 4). Thus, a shale oil molecular weight is not a good indicator of compositional differences among the shale oils and is more likely indicative of the temperature at which the oil was produced.

The carbon and hydrogen aromaticities show considerable variation among the shale oils (Table 4). These data do not suggest any relationship between the raw shale carbon aromaticity and shale oil carbon aromaticity. In some cases, the oil aromaticity is greater than that of the raw shale, whereas in other cases, it is less. However, the Kentucky, Morocco, and Turkey-Seyitömer oil shales, which have tentatively been identified as having a high tendency to coke, produce the more aromatic shale oils.

Simulated distillations were obtained on the shale oils to provide nominal data about the distillation properties of the oils (Table 5). The boiling ranges were chosen to correspond to true boiling point distillation fractions. The amount of distillate in each of the fractions does not differ significantly among any of the shale oils, except for possibly the residuum. The bulk of the oil (>50%) distills in two boiling ranges, the atmospheric and vacuum gas oil fractions. The temperature at which 50% of the material has distilled off was determined for the shale oils (Figure 7). The average 50% off temperature for all the shale oils is $369 \pm 16^\circ\text{C}$ ($696^\circ\text{F} \pm 60^\circ\text{F}$) (95% confidence). This temperature is close to the average temperature of the atmospheric gas oil fraction, which is 374°C (705°F).

4. Acknowledgment

The author gratefully acknowledges support of this work by the U.S. Department of Energy under Cooperative Agreement DE-FC21-86 MC11076.

Table 4. Elemental Analyses, Aromaticities, Molecular Weights, and Specific Gravities of Material Balance Fischer Assay Shale Oils

Oil Shale	wt %				Aromaticity		Molecular Weight ¹	Specific Gravity
	C	H	N	S	Carbon	Hydrogen		
Alaska	84.2	11.9	0.3	0.8	0.319	0.073	310	0.9101
Australia-Stuart	81.6	12.3	1.0	0.7	0.297	0.069	280	0.8902
Brazil-Irati	83.7	11.2	0.9	1.2	0.356	0.080	300	0.9151
China-Fushun	83.9	12.2	2.2	0.7	0.222	0.058	300	0.8873
China-Maoming	85.5	12.2	1.2	0.6	0.301	0.064	300	0.9002
Colorado-Anvil Pts.	83.6	12.2	1.9	0.7	0.284	0.049	310	0.9091
Kentucky-Sunbury	83.4	10.0	1.1	2.8	0.495	0.135	280	0.9770
Morocco-Timahdit	78.7	10.0	1.4	7.8	0.422	0.110	270	0.9819
Turkey-Göynük	81.4	11.8	1.3	1.9	0.331	0.081	300	0.9301
Turkey-Seyitömer	85.2	12.4	0.9	0.6	0.346	0.090	280	0.8823

¹ by VPO in toluene

Table 5. Simulated Distillation Fractions of Material Balance Fischer Assay Shale Oils

Fraction	Boiling Range, °F	Oil off, wt %									
		Alaska	Australia Stuart	Brazil Irati	China-Fushun	China-Maoming	China-Anvil Pts	Colorado Sunbury	Kentucky Timahdit	Morocco Göynük	Turkey-Seytomer
Light Straight-run gas	90-190	1.1	0.4	0.3	0.5	0.5	0.4	0.8	0.4	0.0	0.5
Naphtha	190-380	9.9	9.3	11.7	7.8	9.7	9.3	12.6	11.4	6.9	14.6
Kerosene	380-520	12.4	15.5	17.1	12.3	15.6	12.7	15.8	15.9	14.2	21.4
Light gas oil	520-610	10.9	12.9	13.1	12.0	14.0	11.2	12.9	13.7	10.8	15.1
Atmospheric gas oil	610-800	27.9	30.0	28.3	29.2	31.6	28.1	28.9	30.6	27.5	29.0
Vacuum gas oil	800-1,050	28.6	21.6	26.3	25.8	24.2	33.2	21.4	19.9	26.4	18.1
Residuum	1,050 +	9.2	10.3	3.2	12.4	4.4	4.1	7.6	8.1	14.2	1.3

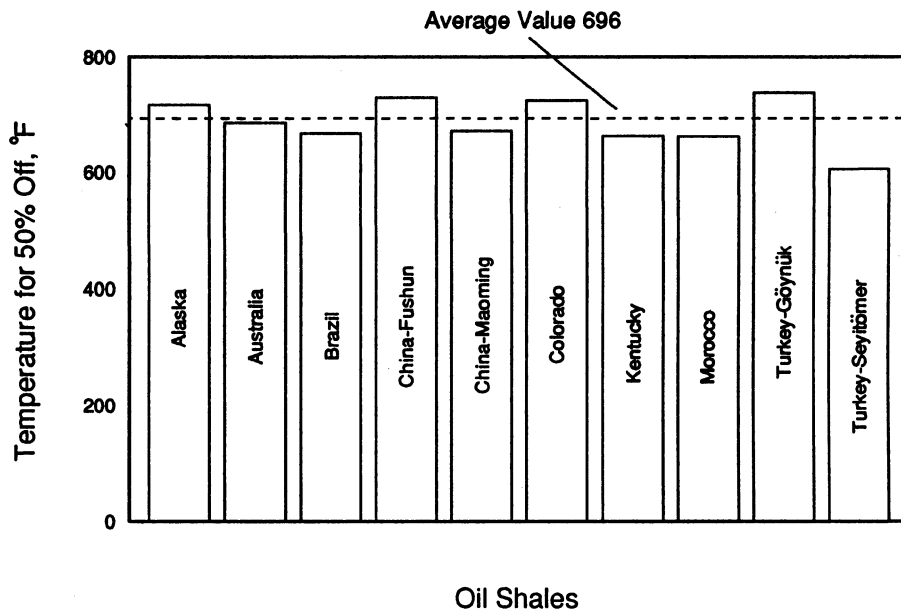


Figure 7. Temperature at which 50 wt % of shale oil distills.

5. References

1. Hunt J.M., Petroleum Geochemistry and Geology, W.H. Freeman Co., San Francisco, 1979.
2. Tissot B.P., and D.H. Welte, Petroleum Formation and Occurrence, Springer-Verlag, New York, 1978
3. Dyni J.R., F. Gay, and T.C. Michalski, Proc. 23rd Oil Shale Symp., Colo. Sch. Mines, J. Gary, ed., Colo. Sch. Mines Press, Golden, CO., 10, (1990).
4. Audeh C.A., Proc. 1990 Eastern Oil Shale Symp., Lexington, KY., J. Stivers, ed., IMMR, Lexington, KY, 263.
5. Dyni J.R., D.E. Anders, and R. Rex, Proc. 1989 Eastern Oil Shale Symp., Lexington, KY., D.J. Lazar, ed., IMMR, Lexington, KY, 270.
6. Watson N.C., Fuel, 63, 1455, (1984).
7. Cook E.W., Fuel, 53, 16, (1974).
8. Robl T.L., A.E. Bland, D.W. Koppenaal, and L.S. Barron, in Geochemistry and Chemistry of Oil Shales, F.P. Miknis and J.F. McKay, eds, ACS Symp. Series 230, Am. Chem. Soc., Washington, DC, 1983, Ch. 9.
9. Miknis F.P., D.A. Netzels, J.W. Smith, M.A. Mast, and G.E. Maciel, Geochim. Cosmochim. Acta, 46, 977, (1982).
10. Maciel G.E., V.J. Bartuska, and F.P. Miknis, Fuel, 57, 505, (1978)
11. Maciel G.E., V.J. Bartuska, and F.P. Miknis, Fuel, 58, 155, (1979)

12. Miknis F.P. in Petrakis L. and J.P. Fraissard, eds, Magnetic Resonance, Introduction, Advanced Methods, and Applications to Fossil Energy, NATO ASI Series C, 124, D. Reidel Pub. Co., Dordrecht, Netherlands, 1984, p 545.
13. Miknis F.P. and P.J. Conn, Fuel, 65, 248, (1986).
14. Hagaman E.W., Schell F.M., and D.C. Cronauer, Fuel, 63, 915, (1984).
15. Evans E., B. Batts, and N. Cant, Fuel, 66, 326, (1987).
16. Robl T.L., S.M. Rimmer, and L.S. Barron, Proc. 1990 Eastern Oil Shale Symp., Lexington, KY., J. Stivers, ed., IMMR, Lexington, KY, 173.
17. Miknis F.P., A.W. Decora, and G.L. Cook, U.S. BuMines Rept. Investig, 7984, 47pp (1974)
18. Miknis F.P., A.W. Decora, and G.L. Cook, in Science and Technology of Oil Shale, T.F. Yen, ed., Ann Arbor Sci. Publ., Ch. 3, (1975).
19. Sydansk R.D., Fuel, 57, 66, (1978).
20. Vitorovic D., D. Vucelic, M.J. Gasic, M. Juranic, and S. Macura, Org. Geochem., 1, 89, (1979).
21. Biscar J.P., J. Chromatogr., 56, 348 (1971).
22. Hanson R.L., N.E. Vandendorgh, and D.G. Brookins, Anal. Chem., 47, 335, (1975)
23. Reed P.R. and P.R. Warren, Quart. Colo. Sch. Mines, 69, 221, (1974)
24. Johnson D.R., Young N. B., and J.W. Smith, Laramie Energy Technology Center Rept. Investig. 77/6, Laramie, WY, 18 pp, (1977).
25. Smith J.W., U.S. BuMines Rept Investig. 7248, 14 pp, (1969).
26. Smith J.W., Laramie Energy Technology Center Rept. Investig. Laramie, WY, 14 pp, (1976).
27. Schultz C.W., and J.B. Bates, Proc. 1989 Eastern Oil Shale Symp., Lexington, KY., D.J. Lazar, ed. IMMR, Lexington, KY, 533.
28. Chong K.P., A.I. Leskinen, and F.P. Miknis, Proc. 1987 Eastern Oil Shale Symp., Lexington, KY., Kent. Energy Cabinet Lab. Publisher, 119, (1987).
29. Judzis A. and B. Williams, Proc. 10th Oil Shale Symp., Golden, CO, 207, (1977).
30. DuBow J, R. Nottenburg, K. Rajeshwar, and Y. Wang, Proc. 11th Oil Shale Symp., Golden, CO, 350, (1978)
31. Rajeshwar K. and J. Du Bow, IGT Symp. on Synthetic Fuels From Oil Shale., Atlanta, GA, Dec. 3-6, 1979, Inst. Gas Technol. Publ., Chicago, 305.
32. Rajeshwar K. and R. Inguva, Fuel, 64, 931, (1985).
33. Sidewell B.L., L.E. McKinney, M.F. Bozeman, P.C. Egbujor, G.R. Eaton, S.S. Eaton, and D.A. Netzel, Geochim. Cosmochim. Acta, 43, 1337, (1979)
34. Choudhury M., K.F. Rheams, and J.W. Harrell, Fuel, 65, 1028 (1986).
35. T.F. Yen and G.V. Chilingarian, Oil Shale, New York, (1976).
36. Solomon P.R., and F.P. Miknis, Fuel, 59, 893, (1980).
37. Miknis F.P., Fuel, 71, 731, (1993).
38. Hershkowitz F., W.N. Olmstead, R.P. Rhodes, and K.D. Rose, in Geochemistry and Chemistry of Oil Shales, F.P. Miknis and J.F. McKay, eds, ACS Symp. Series 230, Am. Chem. Soc., Washington, DC, 1983, Ch. 15.
39. Burhnam A.K., and J.A. Happe, Fuel, 63, 1353, (1984).
40. Vassallo A.M., Wilson M.A., and J.H. Edwards, Fuel, 66, 622, (1987).

RELATIONSHIP BETWEEN HYDROUS AND ORDINARY PYROLYSIS

ALAN K. BURNHAM
Lawrence Livermore National Laboratory
Livermore, CA 94551

ABSTRACT. Pyrolysis results are reviewed briefly with the intent of drawing comparisons between open, high pressure, and hydrous pyrolysis. Empirically, the degree of pyrolysis severity to form volatile products in open pyrolysis is similar to that required to form an expelled oil phase in hydrous pyrolysis. The yields of hydrocarbons from open pyrolysis are close to those from hydrous pyrolysis, but hydrous pyrolysis tends to assist the separation of hydrocarbons from polar materials. Pressure has a small but measurable affect on the generation kinetics.

1. Introduction

The kinetics of oil and gas generation from kerogen have application for modeling both oil shale retorts and natural petroleum formation. Oil generation kinetics have a long history, dating back to the early 20th century.¹ Since that time, many different experimental and data analysis techniques have been developed, with a consequent diversity of results that are difficult to reconcile. One example of an apparent discrepancy is the disagreement between kinetic parameters for oil generation derived from hydrous² and rapid open-system pyrolysis.³

One of the major objectives of LLNL kinetics research over the past decade has been to develop an understanding of how different types of pyrolysis experiments relate to each other.^{4,5} Types of apparatus used include rapid isothermal fluidized-bed pyrolysis, nonisothermal open pyrolysis in flowing helium, nonisothermal open pyrolysis in a self-generated atmosphere, hydrous high-pressure pyrolysis in a closed system, and non-hydrous high-pressure pyrolysis in a closed system. During the same time, we developed more efficient data analysis procedures to compare various models, such as pseudo-nth-order and activation energy distribution kinetics.^{6,7}

The purpose of this paper is to critically evaluate available oil and gas kinetic results from the past ten years in an attempt to more clearly establish the similarities and differences of hydrous and non-hydrous techniques. The paper draws primarily on published data, although some re-analysis is undertaken. Only enough of the literature is used to establish what appear to be general relationships.

2. A Simple Reference Frame for Chemical Kinetics

A first-order reaction is described by the equation

$$dx/dt = k(1-x), \quad (1)$$

where x is the fraction reacted and k is the rate constant at a given temperature. The rate constant is actually temperature dependent, and the dependence is given by the Arrhenius law, $k = A e^{-E/RT}$, where E is the activation energy, A is the frequency factor, R is the gas constant, T is the absolute temperature.

At a fixed temperature, Eq (1) can be easily integrated, giving

$$x = 1 - e^{-kt}. \quad (2)$$

Plotting $\ln(1-x)$ vs t gives a straight line with a slope of k . Determining k at various T , then plotting $\ln(k)$ versus $1/T$ gives a slope of $-E/R$ and an intercept of $\ln(A)$.

Both A and E of a single first order reaction can be determined from a single experiment where T increases linearly with time (constant heating rate). An approximate solution for the resulting exponential integral gives

$$dx/dt = A \exp[-E/RT - ART^2/EH \cdot (1-2RT/E) \cdot \exp(-E/RT)] \quad (3)$$

and

$$x = 1 - \exp[-ART^2/EH \cdot (1-2RT/E) \cdot \exp(-E/RT)] \quad (4)$$

where H is the heating rate. These equations, as well as other integration methods,⁶ can be used in a variety of ways to deduce A and E . If constant heating rate experiments are conducted at more than one heating rate, A and E can be determined from the shift in T_{\max} , the temperature of maximum reaction rate, via

$$\ln(H/RT_{\max}^2) = \ln(A/E) - E/RT_{\max} \quad (5)$$

Unfortunately, the thermal decomposition of most kerogens is not described by a first order reaction, as shown schematically in Figure 1. A concave downward from a first order decay could be attributed to a variety of mechanisms, including a reaction order less than one or a serial reaction aspect of the decomposition. This corresponds to a narrower peak at a constant heating rate. A concave upward deviation from the first-order curve can be attributed to either a reaction order greater than 1 or multiple, overlapping reactions. Further details on these types of models is given in the next section.

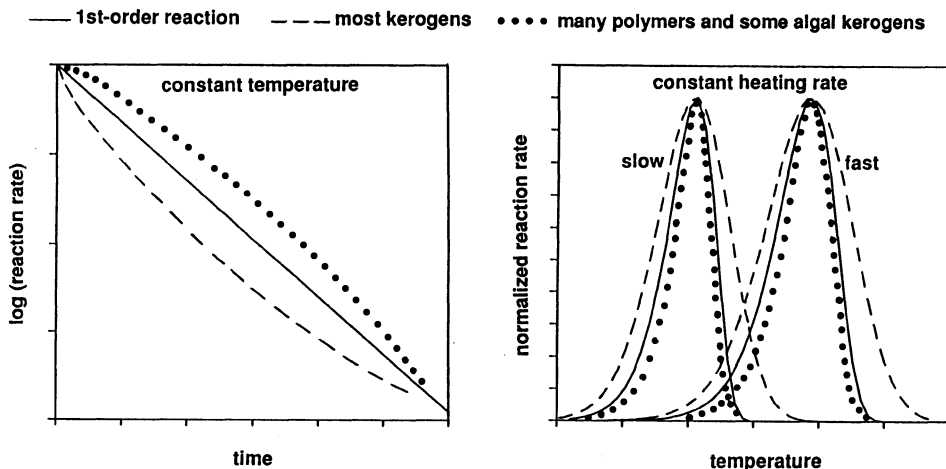
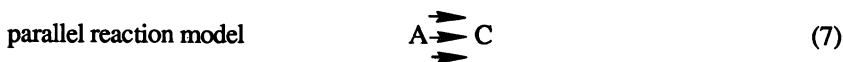


Figure 1. Summary of kerogen pyrolysis characteristics for isothermal and nonisothermal pyrolysis conditions.

3. Atmospheric Pressure Non-Hydrous Pyrolysis

It was noted many years ago that oil generation is normally preceded by generation of a non-volatile bitumen, which subsequently breaks down into oil. This was first explicitly taken into account in a kinetic analysis to my knowledge by McKee and Lyder,¹ and it was clearly present in the classic work on Green River shale of Hubbard and Robinson.⁸ As a second issue, it has been demonstrated for many kerogens that the composition of volatile oil and gas products is not constant throughout the generation process, suggesting that different reactions are occurring. These two observations have led to two commonly applied models:



In these equations, A represents kerogen; B, bitumen; and C, oil and gas. Unfortunately, it is not widely appreciated that they are not mutually exclusive, and neither by itself is truly adequate.

The inadequacy of the serial reaction mechanism for most kerogens can be shown quite simply in theory: a serial reaction by its very nature must have an induction time for the

appearance of product. As a practical matter, all isothermal experiments involving solid decomposition reactions suffer from a finite heating time, which can be confused with a chemical induction time. Braun and Rothman,⁹ in their reanalysis of Hubbard and Robinson's data, attempted to take the heatup time into account by assuming that the initial time could be shifted, but this is probably inadequate. More recent experiments with small samples¹⁰⁻¹⁴ have shown that most kerogens have their maximum rate of hydrocarbon production as soon as the sample reaches temperature. Furthermore, most deviations from first-order generation kinetics are just the opposite of that required for a serial reaction, as summarized in Figure 1, indicating either a reaction order greater than one or multiple generation reactions.

The serial reaction mechanism has additional shortcomings. Braun and Rothman⁹ fitted only the appearance of oil to determine both rate constants (k_1 and k_2) in the serial reaction model. They reached a plausible conclusion that the activation energy for bitumen generation is less than that of oil generation. However, this result leads to an interesting question: does the bitumen generation reaction become rate limiting at high temperatures because of its weak temperature dependence? Subsequent fluidized bed experiments indicated not.^{10,11}

An additional problem with the serial reaction model for Colorado and Kentucky oil shale was found by Miknis et al.¹⁴ The maximum conversion of organic matter to bitumen is related to the ratio of k_1 and k_2 , and the temperature dependence of the maximum bitumen yield gives the relative activation energies of k_1 and k_2 . The maximum bitumen yield increased with temperature for both shales, indicating that the activation energy for bitumen formation must be higher than that for oil generation, just the opposite of what one would expect. Although the issue has not been resolved satisfactorily, it is noteworthy that Ziegel and Gorman¹⁵ found a better fit to Hubbard and Robinson's⁸ bitumen and oil data with an alternate pathway model:

Alternate pathway



(8)

This allows the maximum rate of oil generation to occur at the beginning of pyrolysis while still allowing part of the material to go through a bitumen intermediate.

Nonisothermal experiments overcome two disadvantages of isothermal experiments: the finite heat-up time mentioned earlier and the difficulty in studying the entire extent of reaction over a very wide temperature range. Early nonisothermal experiments in the geochemical community suffered from poor temperature measurements, but over the past few years, careful measurements have yielded close results at several laboratories.¹⁶⁻¹⁹

An extensive database of constant heating rate experiments has established that generation of oil and gas from Green River Mahogany-zone oil shale is described fairly well by a single first-order reaction. However, some Green River and other algal kerogen samples have a narrower reaction profile than calculated for a first-order reaction using the activation energy determined from the shift in T_{max} with heating rate. This is consistent to some extent with a serial reaction, but other polymer decomposition theories may be more appropriate. While the appropriate kinetic model for these kerogens is still in question, a correlation between a

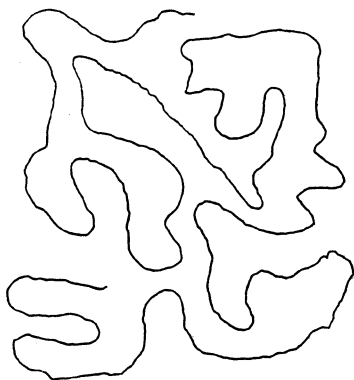
narrow reaction profile and a concave downward deviation from a first-order decay is well established.

Most kerogens, which are typically marine in origin, have a broader reaction profile than is calculated from the activation energy determined from the shift in T_{\max} with heating rate. Numerical studies have shown that the activation energy determined from this shift is still valid for a parallel reaction model having a distribution of activation energies.⁶ Although an nth-order reaction model also works well, the wider profile width would seem to be more properly described by a reactivity distribution because a reactivity distribution is consistent with the heterogeneity of kerogen and with the changing composition of products versus the extent of conversion.

A possible structural interpretation of these kinetic observations is given in Figure 2. Most kerogens may have some weak links (W) that can break and form soluble moieties. However, oil is formed by breaking carbon bonds, and the structure is sufficiently branched that breaking any particular carbon bond will form oil. In contrast, algal kerogens having an induction period must require more than one carbon bond to break to form a fragment small enough to be classified as oil. A single broken bond may lead to a soluble species. Such kinetic behavior is similar to linear polymers.

● Serial reactions

kerogen \rightarrow bitumen \rightarrow oil



● Alternate pathways

kerogen \rightarrow oil
 \searrow bitumen \nearrow

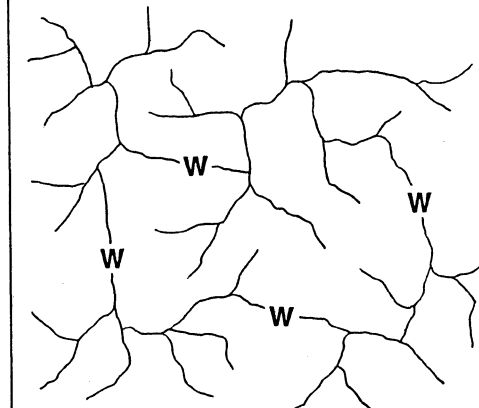


Figure 2. Schematic representation of kerogen structures based on kinetic behavior

4. High Pressure Non-Hydrous Pyrolysis Experiments

High pressure experiments are of interest for a variety of applications, including some oil shale extraction schemes and for natural generation of petroleum. The role of pressure has been controversial, with different workers coming to different conclusions about its importance. Types of high pressure apparatus include sealed, constant volume autoclaves, sealed glass capillaries, pressured gold capsules, and pressurized open systems.

A first step to understand the role of pressure is to realize that not all workers measure equivalent properties, and some experiments are affected by mass transfer phenomena. Burnham and Singleton²⁰ noted that pressure delays the release of oil from a pressurized open reactor, but Burnham and Braun⁴ later showed that most of the effect can be attributed to the influence of pressure on oil vaporization, not its formation.

Schenk and Horsfield²¹ determined very similar kinetics by pyrolysis of whole rocks in an open system and pyrolysis of a the corresponding kerogen in a sealed glass tubes. This is consistent with the result of Freund et al.,²² who found a small but measurable affect of pressure on generation rate, but inconsistent with the results of Price and Wenger,²³ who report that pressure has a profound retarding effect on oil generation. Freund examined several types of reactor configurations to ensure that no artifacts could influence the conclusions, so his results are more convincing. He interpreted his results in terms of an activation volume and obtained values of about 30 cm³/mol, about what one would expect based on polymerization experiments.

5. Hydrous Pyrolysis

Lewan^{24,25} has promoted the hydrous pyrolysis technique as one that is more representative of natural maturation. In hydrous pyrolysis, as strictly defined, there is enough liquid water to cover the sample, and an expelled hydrocarbon phase is found at the top of the water at the end of the experiment. The expelled hydrocarbon phase is said to be much more like natural petroleum than either the whole hydrous pyrolysis extract or pyrolysates obtained from non-hydrous pyrolysis.

My experience indicates that the differences between hydrous and non-hydrous pyrolysis, though real, have been overstated. The original paper by Lewan et al.²⁴ compares the composition of expelled pyrolysates to Fischer assay oil composition and notes that they are significantly different. However, it has been well established that the composition of oil from Fischer-Assay-like experiments depends on both the heating rate and pressure.²⁰ With no added water, the pyrolysate produced at 1°C/h and 27 bar has little alkene content and substantially reduced polar content, making it much more like the expelled phase and natural petroleum. The 1°C/h heating rate causes the oil to be formed at roughly the same temperature as in hydrous pyrolysis for 72 h.

A more detailed comparison between hydrous pyrolysis fractions and modified Fischer assay pyrolysates from a Posidonia shale is given in Tables 1 and 2.²⁶ The hydrous pyrolysates were generated by Marzi²⁷ and obtained from the KFA. The open system pyrolysate produced in a self-purging reactor at 2°C/h²⁸ is fairly close to the expelled oil in aromatic content and elemental composition. The absolute yields of individual compounds and hydrocarbon groups is also quite similar. The difference in chain length and total normal

Table 1. NMR analysis of hydrous pyrolysates generated at two temperatures and evolved oils generated at two heating rates. The maximum yield of extracted bitumen occurs at 310°C and the maximum yield of expelled oil occurs at 329°C.

property	native bitumen		72h/310°C		262h/329°C		self-purging reactor	
	bitumen	oil	bitumen	oil	bitumen	oil	2°C/h	2°C/min
proton NMR^a								
aromatic	5.5	11.2	13.8	11.2	21.7	11.1	8.1	8.6
olefinic	0.0	0.0	0.0	0.0	0.0	0.0	0.6	1.2
aliphatic	94.5	88.8	86.2	88.8	78.3	88.9	91.3	90.1
benzyllic	13.9	21.4	21.4	17.3	30.4	17.6	21.9	25.1
methylene	55.1	48.8	45.8	48.8	35.6	50.7	47.6	44.0
methyl	25.6	22.7	19.1	22.7	12.3	20.6	22.0	20.2
carbon NMR^b								
aromatic	24	43	43	30	58	36	35	39
br+cycl	65	45	45	53	33	44	35	31
normal	11	12	12	17	9	20	30	30
C1	1.6	2.0	2.0	2.3	1.4	3.3	6.4	5.0
C2	2.1	1.9	1.9	2.5	1.6	2.9	5.7	5.4
C3	0.7	1.5	1.5	2.6	1.0	2.0	4.5	4.5
Cn	6.9	6.7	6.7	9.7	5.0	11.9	11.3	14.5
chain length								
method A ^c	15.5	13.5	13.5	13.9	13.5	14.6	10.8	11.8
method B ^d	14.5	12.3	12.3	14.8	13.1	12.3	9.4	11.7
method C ^e	25.5	14.7	14.7	13.6	16.1	17.6	12.0	12.4
a% of total H								
b% of total C								
$c_L = 6(C1+C2+C3+Cn)/(C1+C2+C3)$								
$d_L = 2(C1+C2+C3+Cn)/C1$								
$e_L = 2Cn/C3+6$								

alkane yield may be due to the near absence of C₆-C₉ in the hydrous pyrolysate, possibly due to handling. The overall similarity suggests that much of the earlier difference between hydrous and open system pyrolysis products is due to temperature, not pressure or water.

Table 2. Gas chromatographic analysis of expelled and evolved oils. The expelled oil represents conditions for maximum oil yield from hydrous pyrolysis.

Property	Expelled oil 262h/329°C	Evolved oils	
		2°C/h	2°C/min
oil concentration, %:			
pristane	0.19	0.17	0.09
pris-1-ene	—	0.02	0.04
phytane	0.08	0.09	0.06
n-C ₁₇ ane	0.36	0.39	0.23
1-C ₁₇ ene	(.03) ^a	0.10	0.13
n-C ₁₈ ane	0.30	0.29	0.18
1-C ₁₈ ene	(.02) ^a	0.05	0.07
C ₇ -C ₃₁ anes	5.0	7.3	4.5
C ₇ -C ₃₁ enes	(.4) ^a	1.5	1.9
alkene + alkane ratios:			
pr/ph	2.3	2.2	1.9
pr/n-C ₁₇	0.57	0.34	0.25
ph/n-C ₁₈	0.30	0.27	0.26
alkene + alkane yields, mg/g TOC:			
pristane	0.64	0.76	0.60
phytane	0.28	0.35	0.31
n-C ₁₇	1.2	1.9	1.6
n-C ₁₈	1.0	1.3	1.2
C ₇ -C ₃₁	17	34	31
total normal ^b	68	116	146

^aconsidered to be interfering compounds because proton NMR detected essentially no alkenes

^bfrom ¹³C NMR

Another difference between hydrous and open pyrolysis is the yields from the two types of experiments. Table 3 compares the bitumen and expelled oil yields for a variety of samples to the hydrogen index of the same or similar material. The expelled oil yields are always significantly lower than the hydrogen index. Additional information on gas yields indicates that most of the difference is related to differences in liquid yields. Given that slower open system experiments produce an oil more similar to the expelled oil due to the coking of polar material in the oil, it appears that another part of the difference between hydrous and open pyrolysis is that much of the polar fraction in hydrous pyrolysis remains absorbed on the rock, while it is volatilized in the open system experiments.

Table 3. Maximum yields of extracted bitumen and expelled oil (mg product/g TOC) along with TOC and Rock-Eval HI

Source rock	TOC	HI	max bit	max oil	source of data
Green River	10.6	877	319	575	Peters (1986)
Monterey	4.5	501	204	319	"
Monterey	11.6	615	249	285	"
Woodford	12.1	588	388	264	Lewan (1985, 1989)
Phosphoria	20.9	644	911	313	"
Phosphoria	22.8			380	Winters et al. (1981)
Kimmeridge	11.2			362	"
Kimmeridge	25.2			334	"
La Luna	4.2	650	607	440	Vallejos (1990)
Posidonia	12.1	660	347	331	Marzi (1989)

Even though the differences may have been overstated, there do seem to be some real effects due to water. Lewan²⁹ has reported otherwise identical experiments with no added water and enough water to form a liquid phase covering the sample. He finds that in the early stages, hydrous and ordinary pyrolysis produce about the same amount of pyrolysate. At higher temperature, hydrous pyrolysis produces more oil plus bitumen, but most of the difference is in bitumen extracted from the rock in the hydrous case. Apparently, water inhibits the coking reactions that cause major yield loss in ordinary sealed vessel pyrolysis. The hydrous pyrolysis oil-plus-bitumen yields are fairly similar to the yield in open pyrolysis, indicating that the inhibiting effect of water on coking is comparable to that of escape by volatilization. Lewan also found that water caused a substantially greater generation of CO₂, suggesting that it is acting as both an oxidizer and source of hydrogen in its reaction with kerogen. Further details on how water might be acting as a chemical reaction are given by Siskin in this volume.

Given the differences in product yields and composition, it is not obvious how the rate parameters of hydrous and non-hydrous experiments should compare. Kinetics in the literature for hydrous pyrolysis experiments have generally been based on a first-order

assumption using expelled oil yields as a function of temperature at a single time. Unlike the fairly narrow range of activation energies found from accurate open pyrolysis experiments, typically 50 to 56 kcal/mol, reported activation energies for hydrous pyrolysis range from the mid-30 kcal/mol range to the low-60 kcal/mol range.

After numerous comparisons of hydrous and open system kinetics, evidence appears strong that the wide range of activation energies from hydrous pyrolysis is due to a misapplication of first-order kinetics. Burnham²⁸ showed that first-order hydrous pyrolysis kinetics predict fairly well the formation of volatile oil in open-system pyrolysis where the heating rate is such (1 to 2°C/h) that the temperature of oil formation is similar to that in hydrous pyrolysis. However, most of these first-order kinetic parameters predict that oil is formed at a much higher temperature than is observed for higher heating rates. In contrast, kinetic parameters derived from open pyrolysis using activation energy distribution models accurately predict the timing of expelled oil in hydrous pyrolysis as well as the formation of volatile oil in open pyrolysis over a wide temperature range. A comparison is shown for four samples in Figure 3.

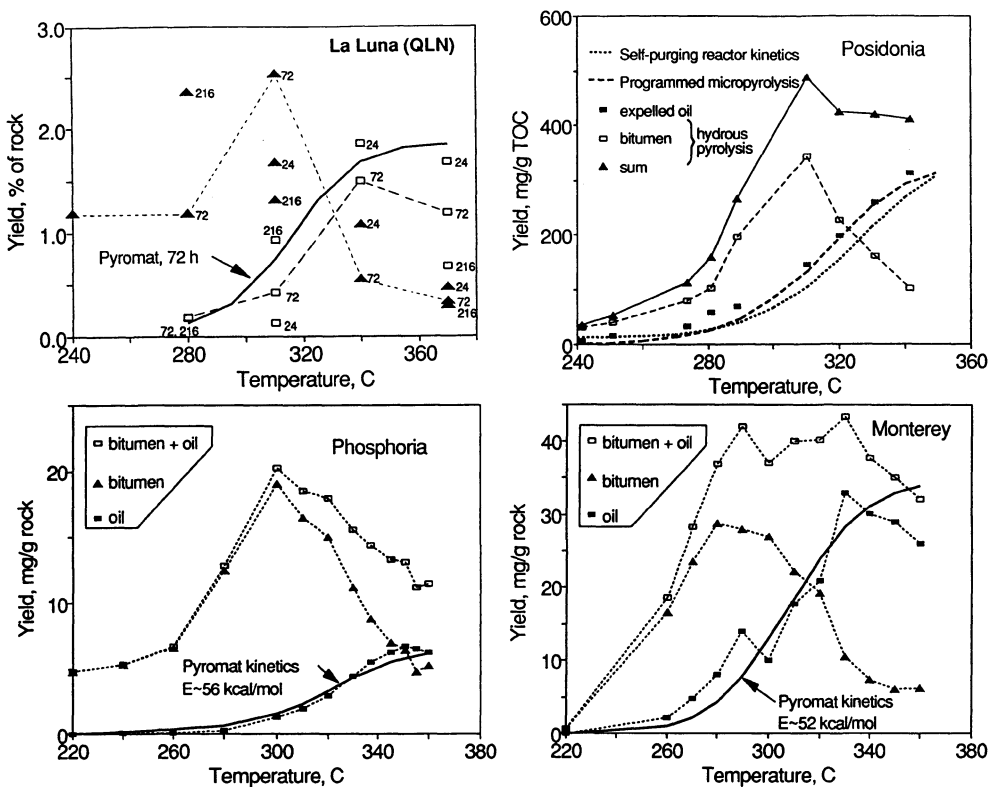


Figure 3. Comparison of hydrous pyrolysis yields with open system kinetics. The open system yields have been scaled to the maximum expelled oil yield. The numbers by the La Luna data points indicate the time of pyrolysis in hours.

The Monterey shale deserves special attention because it has the largest discrepancy between reported activation energies for hydrous and open pyrolysis. Tabular hydrous pyrolysis yield data supplied by Ken Peters³⁰ was analyzed using the assumption that the appearance of both bitumen and expelled oil can be described by a first-order reaction. The results are shown in Figure 4. Even though the noise in the oil generation data is substantial and there is uncertainty in the maximum yield of both oil and bitumen, it is clear that the first-order activation energy for oil generation is less than that of bitumen, counter to what one would expect. The oil generation activation energy is similar to that reported by Lewan for hydrous pyrolysis of a different Monterey sample.

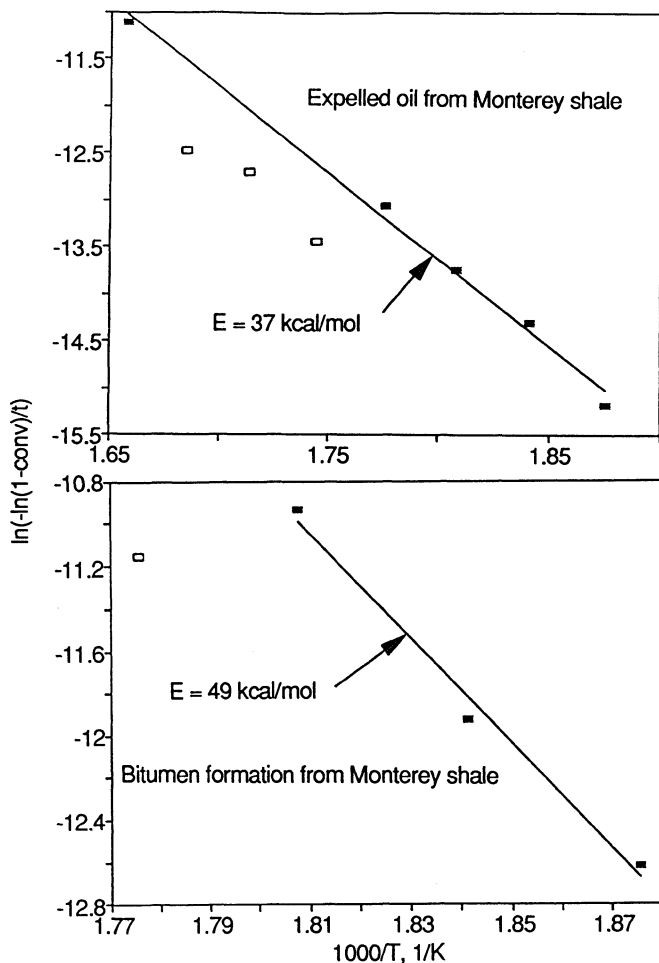


Figure 4. Arrhenius plots for bitumen and expelled oil formation from Monterey shale, using data from Baskin and Peters.³⁰

The problem with these kinetic parameters is readily apparent if viewed at both laboratory and geologic heating rates, as shown in Figure 5. If the reactions are assumed to be independent and extrapolated to a geological heating rate, one finds that oil generation is predicted to occur below 100°C, despite geologic observations to the contrary¹⁹ If one requires the oil to form from bitumen, one is forced to justify and use a serial reaction model, not a first-order model, to analyze the expelled oil data. One also needs to explain away the contradiction of the lack of an induction time in the isothermal open system experiments¹³

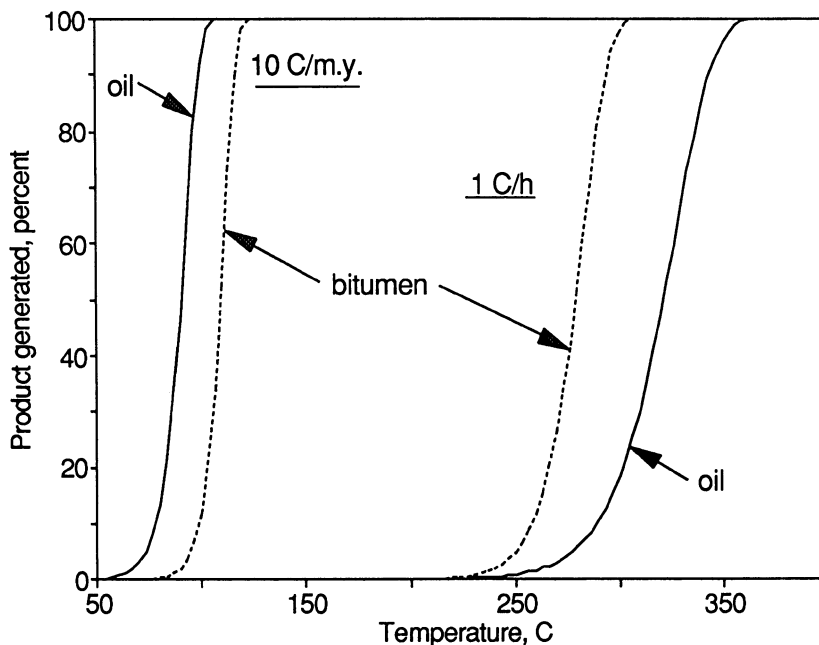


Figure 5. Extrapolation of Monterey kinetics to geological heating rates.

Open-system kinetic parameters for a similar Monterey sample were measured with a Pyromat instrument. In agreement with others,^{3,19} we obtained a principal activation energy in the low 50 kcal/mol range. Oil generation was calculated at hydrous pyrolysis conditions with these kinetics, and the calculated temperature range agreed well with the temperature range over which oil is expelled during hydrous pyrolysis (Figure 3). This is the sixth such favorable comparison made (following Green River, Woodford, Phosporia, Posidonia, and La Luna samples), indicating that it is not a fluke. Furthermore, Schenk and Horsfield²¹ recently reached a similar conclusion when comparing open and sealed-tube pyrolysis. While the mechanistic interpretation is still unclear, there now seems to be little doubt that the low activation energies reported by Lewan²⁵ and Hunt et al.² are artifacts of an improper kinetic analysis.

Is it possible to analyze hydrous pyrolysis data with activation energy distribution models? There are two problems. First, either multiple heating times at various temperatures or two series of constant heating rate experiments quenched at various temperatures are required for experiments in which expelled oil is measured separately. No such data sets with adequate accuracy exist. Second, the expected deviation from first-order behavior is such that oil generation should persist longer than extrapolated from initial production rate, but oil destruction reactions that occur in the closed system probably mask this persistence. It is questionable whether it is possible to adequately test the expelled-oil first-order kinetic hypothesis. On the other hand, Burnham²⁶ demonstrated that disappearance of S2 potential (both before and after extraction) in the residues of hydrous pyrolysis requires an activation energy distribution. The latter are shown in Figure 6.

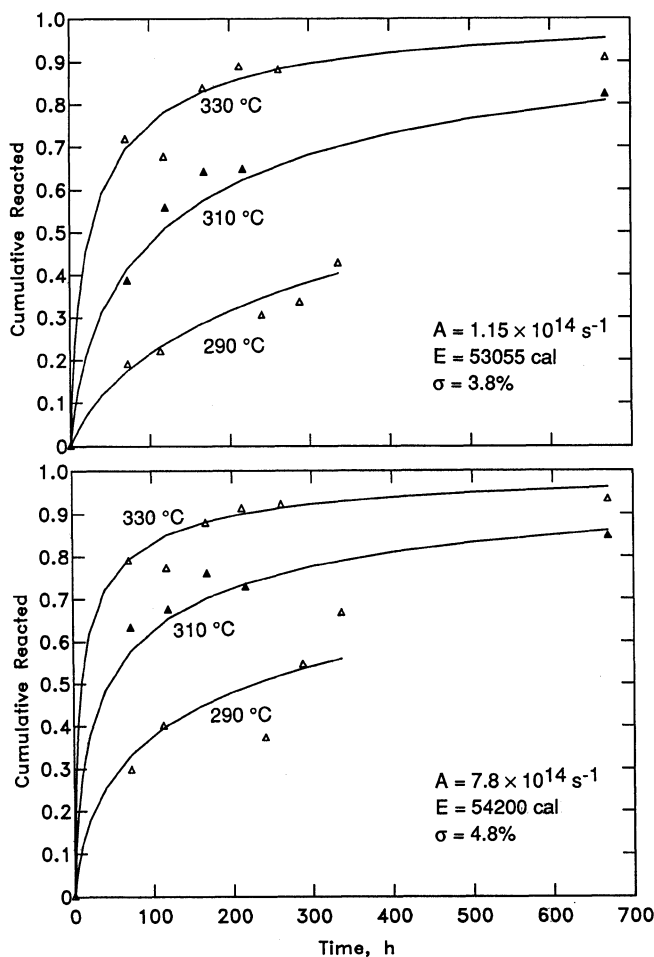


Figure 6. Kinetic analysis of remaining Rock-Eval potential, before and after extraction, with a Gaussian activation energy model.

It cannot be merely another coincidence that the kinetics of S2 disappearance before extraction are virtually identical to those determined from formation of volatile hydrocarbons in open pyrolysis. It is also encouraging that the S2 kinetics extrapolate fairly well to a geological heating rate (Figure 7). In addition, Castelli et al.³¹ generated enough data for total pyrolysate yield to demonstrate that an activation energy distribution is required and derived a mean activation energy of about 55 kcal/mol.

6. Limitations of Parallel Reaction Models

While the need for some type of distributed reactivity model for most kerogens is clear, it is less clear that a simple parallel reaction model is adequate. Early support for a parallel reaction model over a single reaction model came from the observation that the T_{\max} of the remaining material increased as a function of maturity as was observed for geological maturation of type II and type III kerogens. However, on closer inspection, the parallel reaction does not match the precise natural maturation trend. One of the properties of a parallel reaction model is that the T_{\max} of the remaining material does not change until a significant fraction of the potential is generated. In contrast, geologic maturation causes a 10-15°C increase in T_{\max} before significant generation occurs. Burnham and Dahl³² found for the North Viking Graben that T_{\max} increases steadily with depth, but significant oil generation does not occur until T_{\max} has increased from about 420°C to between 430 and 435°C. Further discrepancies between natural maturation and parallel reaction model calculations have been found for the Bakken shale³³ and San Juan basin coals.³⁴

One can understand the source of the problem when one considers that kerogen undergoes considerable changes during maturation, particularly the elimination of oxygen, prior to generating significant hydrocarbons. Why this would cause the hydrocarbon T_{\max} to increase is not certain, but it has been proposed³⁵ that elimination of oxygen substituents from an aromatic ring increases the energy required to break the bond between a hydrocarbon substituent and the same aromatic ring. This would cause T_{\max} to increase during early maturation as the oxygen is eliminated.

The importance of oxygen in the hydrocarbon generation mechanism has other implications. Our earlier comparisons between hydrous and open-system pyrolysis for the La Luna formation indicated that carbon dioxide is generated more easily during hydrous pyrolysis than predicted by open-system pyrolysis kinetics.³⁶ As a result, more oxygen is still present in the kerogen during the hydrocarbon generation phase when very immature samples undergo open-system pyrolysis than when the samples reach the hydrocarbon generation phase in nature. In addition, the oxygen appears to form refractory cross-links during open pyrolysis.³⁴

Because of the unforeseen ways in which these reactions might affect the apparent activation energy, we have tentatively concluded that open-system kinetics from highly immature source rock samples are not reliable predictors of natural maturation. We found in the past³⁷ that very immature coal samples appeared to have higher mean activation energies than those in the incipient oil generation phase. While a subsequent study of the San Juan basin coals³⁴ saw less of a trend, very high (<60 kcal/mol) mean activation energies have been observed for high-oxygen Monterey and Norwegian samples. The evidence is not as strong as desired, but it suggests that reliable predictions of geologic maturation require

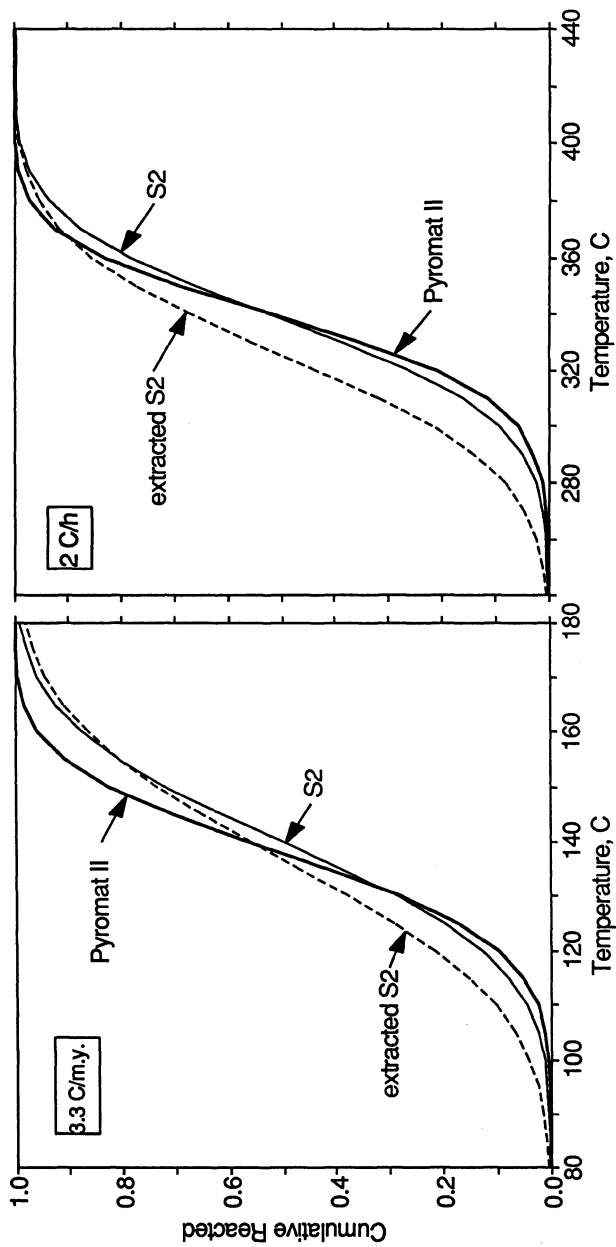


Figure 7. Open system kinetics compared with those derived from the S2 of hydrous pyrolysis residues.²⁶

samples in which most of the oxygen has been eliminated naturally. Unfortunately, that makes it impossible to measure the kinetics of early hydrocarbon generation coincident with oxygen elimination.

Because hydrous and high-pressure pyrolysis experiments follow the natural van Krevelan trend more closely, partial maturation of an immature sample under these conditions prior to open-system pyrolysis may produce satisfactory kinetics. Also, it will probably be necessary to introduce some type of serial character into the reaction network in order to properly model both the oxygen elimination and hydrocarbon generation aspects of kerogen maturation.

Acknowledgements. This work was conducted under the auspices of the U.S. Department of Energy by the Lawrence Livermore National Laboratory under contract W-7405-Eng-48.

7. References

1. McKee, R. H. and Lyder, E. E., (1921) *J. Ind. Eng. Chem.* **13**, 613-618.
2. Hunt, J. M., Lewan, M. D. and Hennet, J.-C. (1991) *AAPG Bulletin* **75**, 795-807.
3. Tissot, B. P., Pelet, R. and Ungerer, P. (1987) *AAPG Bulletin* **71**, 1445-1466.
4. Burnham, A. K. and Braun, R. L. (1985) *In Situ* **9**, 1-23.
5. Burnham, A. K. and Braun, R. L. (1990) *Org. Geochem.* **16**, 27-39.
6. Braun, R. L. and A. K. Burnham (1987) *Energy & Fuels* **1**, 153-161.
7. Burnham, A. K., Braun, R. L., Gregg, H. R., and Samoun, A. M. (1987) *Energy & Fuels* **1**, 452-458.
8. Hubbard, A. B. and Robinson, W. E. (1950) U.S. Bur. Mines, Rept. Inv. 4744.
9. Braun, R. L. and Rothman, A. J. (1975) *Fuel* **54**, 129-131.
10. Wallman, P. H., Tamm, P. W. and Spars, B. G. (1981) in *Oil Shale, Tar Sands, and Related Materials*, ACS Symp. Ser. 163, H. C. Stauffer, Ed., American Chemical Society, Washington, pp. 93-113.
11. Burnham, A. K., Braun, R. L., Taylor, R. W. and Coburn, T. T. (1989) *Preprints ACS Div. Petrol. Chem.* **34**(1), 36-42.
12. Bar, H., Ikan, R. and Aizenshtat, Z. (1988) *J. Anal. Appl. Pyr.* **14**, 73-79.
13. Klomp, U. C. and Wright, P. A. (1990) *Org. Geochem.* **16**, 49-60.
14. Miknis, F. P., Turner, T. F., Berdan, G. L. and P. J. Conn (1987) *Energy & Fuels* **1**, 477.
15. Ziegel, E. R. and Gorman, J. W. (1980) *Technometrics* **22**, 139.
16. Schaefer, R. G., Schenk, H. J., Hardelauf, H. and Harms, R. (1990) *Org. Geochem.* **16** 115-120.
17. Braun, R. L., Burnham, A. K., Reynolds J. G. and Clarkson, J. E. (1991) *Energy & Fuels* **5**, 192-204.
18. Sundararaman, P., Merz, P. H. and Mann, R. G. (1992) *Energy & Fuels* **6**, 793-803.
19. Jarvie, D. M. (1991) *Chem. Geol.* **93**, 79-99.
20. Burnham, A. K. and Singleton, M. F. (1983) in *Geochemistry and Chemistry of Oil Shales*, ACS Symp. Ser. 230, F. P. Miknis and J. F. McKay, eds., American Chemical Society, Washington, pp. 335-351.
21. Schenk, H. J. and Horsfield, B. (1993) *Geochim. Cosmochim. Acta* **57**, 623-630.

22. Freund, H., Clouse, J. A. and Otten, G. A. (1992) *Preprints, ACS Div. Fuel Chem.* 37(4), 1628-1635.
23. Price, L. C. and Wenger, L. M. (1992) *Org. Geochem.* 19, 141-159.
24. Lewan, M. D., Winters, J. C. and McDonald, J. H. (1979) *Science* 203, 897-899.
25. Lewan, M. D. (1985) *Phil. Trans. R. Soc. Lond. A* 315, 123-134.
26. Burnham, A. K. *Pyrolysis Kinetics and Composition for Posidonia Shale* (1990) LLNL Report UCRL-ID-105871.
27. Marzi, R. (1989) *Kinetik und quantitative analyse der isomerisierung und aromatisierung von fossilen steroidkohlenwasserstoffen im experiment und in natürlichen probensequenzen*. PhD thesis, Kernforschungsanlage Jülich GmbH, Nr. 2264, Jülich, Germany.
28. Burnham, A. K. (1991) *Energy & Fuels* 5, 205-214.
29. Lewan, M. D. (1992) *Preprints, ACS Div. Fuel Chem.* 37(4), 1643-1649.
30. Baskin, D. K. and Peters, K. A. (1992) *AAPG Bulletin* 76, 1-13.
31. Castelli, Chiamonte, M. A., Beltrame, P. L., Carniti, P., Del Bianco, A. and Stroppa, F. (1990) *Org. Geochem.* 16, 75-82.
32. Burnham, A. K. and Dahl, B. (1993) to be presented at the 16th International Organic Geochemistry Meeting, Stavanger, Norway.
33. Sweeney, J. J., Gosnold, W. D., Braun, R. L. and Burnham, A. K. (1992) *A Chemical Kinetic Model of Hydrocarbon Generation From the Bakken Formation, Williston Basin, North Dakota*, LLNL Report UCRL-ID-112038.
34. Reynolds, J. G. and Burnham, A. K. (1993) *Energy & Fuels*, in press.
35. Solomon, P. (1992) personal communication.
36. Burnham, A. K., Braun, R. L., Sweeney, J. J., Reynolds, J. G., Vallejos, C. and Talukdar, S. (1992) *Kinetic Modeling of Petroleum Formation in the Maracaibo Basin: Final Report, Annex XII*, Report DOE/BC/92001051, Avail. NTIS, Springfield, VA.
37. Burnham, A. K., Oh, M. S., Crawford, R. W. and Samoun, A. M. (1989) *Energy & Fuels* 3, 42-55.

FLUIDIZED BED RETORTING OF OIL SHALE

S.D. CARTER, U.M. GRAHAM, A.M. RUBEL, and T.L. ROBL
Center for Applied Energy Research
University of Kentucky
3572 Iron Works Pike
Lexington, KY 40511
USA

ABSTRACT. Atmospheric pressure fluidized bed technology offers many processing advantages for retorting oil shale. The one advantage which has been most studied and emphasized is that oil yield, as compared to Fischer assay, is increased. While the nature of the shale greatly influences the degree of oil yield enhancement that is realized, there is little doubt that fluidized bed technology increases the yield of oil, at least marginally, for all oil shales. Concomitant with an increase in oil yield and decrease in gas yield by the fluidized bed technique is that the oil, compared to Fischer assay oil, has higher aromaticity, density, heteroatom content, viscosity, and Conradson carbon content. With improved heavy oil upgrading catalysts and promising non-fuel, added-value applications for the heavy fraction, however, the generation of more, but heavier, oil can be a distinct advantage for a fluidized bed process. While increased oil yield is the most renowned benefit of fluidized bed retorting, there are several other aspects of this technology which should be considered just as highly such as: precise temperature control, utilization of fine particles, rapid pyrolysis kinetics, and processing flexibility without mechanical complexity and moving parts. The Center for Applied Energy Research (CAER) is developing a multi-stage fluid-bed process called KENTORT II which incorporates pyrolysis, gasification, and combustion zones. The main features of the process are that the heat of the process is provided by the combustion of char from pyrolysis and this heat is transferred to the pyrolysis zone with recirculating shale without diluting the overhead pyrolysis products with combustion flue gases. The KENTORT II process will be used as the primary example of a fluidized bed retorting process because it includes all of the major gas/solid reactions which are relevant for thermal processing of oil shale at atmospheric pressure. While the KENTORT II process has been initially developed to process the Devonian shales of the eastern U.S., the CAER has also investigated the fluidized bed characteristics of Brazilian (Irati), Moroccan (Timahdit and Tarfaya), and Turkish (Goynuk) oil shales. These results will be compared to fluidized bed pyrolysis results from other laboratories including those for the Green River shales of the western U.S. and the oil shales from various Australian deposits.

1. Overview

The efficiency of atmospheric-pressure fluid-bed retorting of oil shale has been touted for several years. Fluidized bed retorting is generally considered as "second-generation" technology compared to the packed-bed retorts which were used at the start of the oil shale industry. While no commercial fluidized bed ventures ever came to fruition in the United States, there were two planned projects in the late 1970's to early 1980's which had potential for success. The Shell Pellet Heat Exchanger Retort (SPHER)¹ and the Staged Turbulent Bed

Retort (STB)² both included a fluidized bed pyrolysis section, but neither project was initiated because of the poor economics for synthetic liquid production which developed at that time and which we still face. The oil shale retorting industry has simply not developed enough for second-generation technologies to take root. At this time there are only a few commercial-scale retorts operating in the world,^{3,4} so it should not be inferred that fluidized bed technology has been dismissed in favor of more efficient processes.

One of the advantages that fluidized bed technology offers is higher oil yield compared to Fischer assay. Oil yields of up to 110% of Fischer assay have been reported for the Green River oil shale of the western U.S. by fluidized bed pyrolysis,⁵ whereas oil yields of approximately 150% of Fischer assay have been reported for the Devonian shales of the eastern U.S.^{6,7,8,9,10} The amount of oil yield enhancement depends primarily on the nature of the kerogen within the shale. The oil yield from an aromatic kerogen as in the Devonian of the eastern U.S. will be more enhanced by fluidized bed pyrolysis than the aliphatic kerogen of the western U.S. shales. The mineral matrices of oil shales have been shown to promote secondary reactions differently, so the inorganic portion of the shale can also affect the oil yield which is achieved during fluidized bed pyrolysis.^{11,12,13,14,15}

Concomitant with an increase in oil yield and decrease in gas yield by the fluidized bed technique is that the oil, compared to Fischer assay oil, has higher aromaticity, density, heteroatom content, viscosity, and Conradson carbon content. These oil properties are consistent with the assertion that oil yield enhancement is accomplished through the reduction of secondary reactions. The largest and most aromatic primary pyrolysis products will undergo cracking and coking reactions most easily. It is these species that are not converted to char and gas during fluidized bed pyrolysis and are responsible for the enhanced oil yield and heavier oil.¹⁶ It should be noted, however, that with improved heavy oil upgrading catalysts and promising non-fuel, added-value applications for the heavy fraction, the generation of more, but heavier, oil can be a distinct advantage for a fluidized bed process. It will be seen that oil properties are a strong function of fluidized bed conditions. Bed temperature is the most influential parameter when utilizing externally heated laboratory retorts,¹⁰ but the utilization of solid heat carriers in integrated demonstration units also significantly affects oil quality.¹⁷ It is possible to adjust oil quality within the regime of fluidized bed conditions so that the oil quality is (within limits) best suited to the prevailing market forces.

While increased oil yield is the most renowned benefit of fluidized bed retorting, there are several other aspects of this technology which should be considered just as highly. As evidence of this, consider that the two commercial fluidized bed oil shale processes which were planned in the U.S. were designed for the western U.S. oil shale reserves, so it was more than the modest 10% increase in oil yield that made fluidized bed processing attractive. One advantage of fluidized bed technology is that temperature control within a fluidized bed of

solids is precise. A properly operated fluidized bed is isothermal which differs in comparison to packed, moving beds which can have poor temperature control resulting in under- or over-heated shale. Another important advantage is that fluidized bed technology can process fines from the crushing of raw shale so that no shale needs to be returned for disposal without processing. Additionally, the rapid heating of the shale in a fluidized bed shortens the required residence time of the shale for complete pyrolysis to occur which means that throughput is rapid and vessel size is reduced. Finally, the fluid-like behavior of the shale permits processing flexibility without mechanical complexity and moving parts. The retort can be staged, much like a distillation column, to preheat or cool the shale or to incorporate additional processes like gasification or combustion to take advantage of the specific properties of a particular shale. This sort of multi-stage fluid-bed technology is nearly identical to that used in the now-mature fluid catalytic cracking (FCC) industry, so there is much relevant commercial experience from which to draw even though fluidized bed retorting of oil shale has not yet been applied commercially.

The Center for Applied Energy Research (CAER) is developing a multi-stage fluid-bed process called KENTORT II which incorporates pyrolysis, gasification, and combustion zones. The main features of the process are that the heat of the process is provided by the combustion of char from pyrolysis and this heat is transferred to the pyrolysis zone with recirculating shale without diluting the overhead pyrolysis products with combustion flue gases. The process was shown to be viable in a 2.3-kg/hr bench-scale version of the process,^{18,19} and with this success, a 23-kg/hr process demonstration unit has been recently designed and constructed. The KENTORT II process will be used as the primary example of a fluidized bed retorting process because it includes all of the major gas/solid reactions which are relevant for thermal processing of oil shale at atmospheric pressure.

Many of the shales of the world cannot be processed by the full KENTORT II configuration because either the minerals will not permit high-temperature processing or there is not sufficient char following pyrolysis to support both gasification and combustion. In these cases, however, one or more of the zones of the KENTORT II process can be removed, but with the same overall advantages of the fully configured system. With the exception of some rich oil shales which may agglomerate during fluidized bed pyrolysis, the KENTORT II technology is not a resource-specific technology because the configuration can be adjusted for the characteristics of the shale. This is not to say, however, that it is impossible to process agglomerating oil shales in fluidized beds, but that more research is needed to find engineering solutions to this problem. While the KENTORT II process has been initially developed to process the Devonian shales of the eastern U.S., the CAER has also investigated the fluidized bed characteristics of Brazilian (Irati), Moroccan (Timahdit and Tarfaya), and Turkish (Goynuk) oil shales. These results will be compared to fluidized bed pyrolysis results from other

laboratories including those for the Green River shales of the western U.S. and the oil shales from various Australian deposits.

2. Fluidized Bed Pyrolysis

Fluidized bed pyrolysis studies can be put into two categories. The first classification deals with laboratory-scale reactors which heat the fluidized bed with a combination of heat transferred through the reactor wall and with preheated fluidizing gas. These types of experiments generate the highest oil yields because the beds are small and the bed material is the spent shale itself which generally promotes less coking and cracking than non-carbonized heat-carrying solids. The second type of fluidized bed pyrolysis experiment is more representative of a commercial-scale design and includes heating the retort by a solid heat carrier. Laboratory-scale studies are presented in the following section and pyrolysis studies in conjunction with a solid heat-carrier are described in Section 3.

2.1 EXPERIMENTAL

The results which will be described for eastern U.S. shale in the following sections were obtained in a 7.6-cm diameter fluidized bed reactor which was heated by an electrical resistance furnace. The detailed operating procedures for this apparatus are described by Carter and Taulbee,¹⁰ but a brief discussion is provided here for the reader's convenience. The fluidized bed system (see Figure 1) was capable of fluidization with nitrogen, steam, or recycled pyrolysis gas. Raw shale was fed continuously at a rate of up to 2.3 kg/hr above the fluidized bed. The bed height was controlled by an adjustable standpipe which withdrew pyrolyzed shale by gravity from the retort. Gases and vapors from pyrolysis were sent without cooling through a cyclone to recover entrained fine particles. The vapor stream was then cooled in an air-cooled heat exchanger which resulted in the formation of an oil aerosol which was then trapped downstream by an electrostatic precipitator at 120-150°C. The rest of the system consisted of further cooling and filtering the vapor stream to recover oil and water. A sampling loop on a refinery gas chromatograph took on-line samples for analysis at 30 minute intervals. Two different Devonian shales, both from Kentucky, were used in the fluidized bed studies. The New Albany shale contained more organic material and sulfur than the Cleveland shale that was studied (see Table 1).

2.2. EFFECTS OF PROCESSING CONDITIONS ON EASTERN U.S. OIL SHALE

2.2.1. *Temperature.* Bed temperature is the most influential parameter on oil and gas yields and compositions for fluidized bed pyrolysis of eastern U.S. shale. Oil

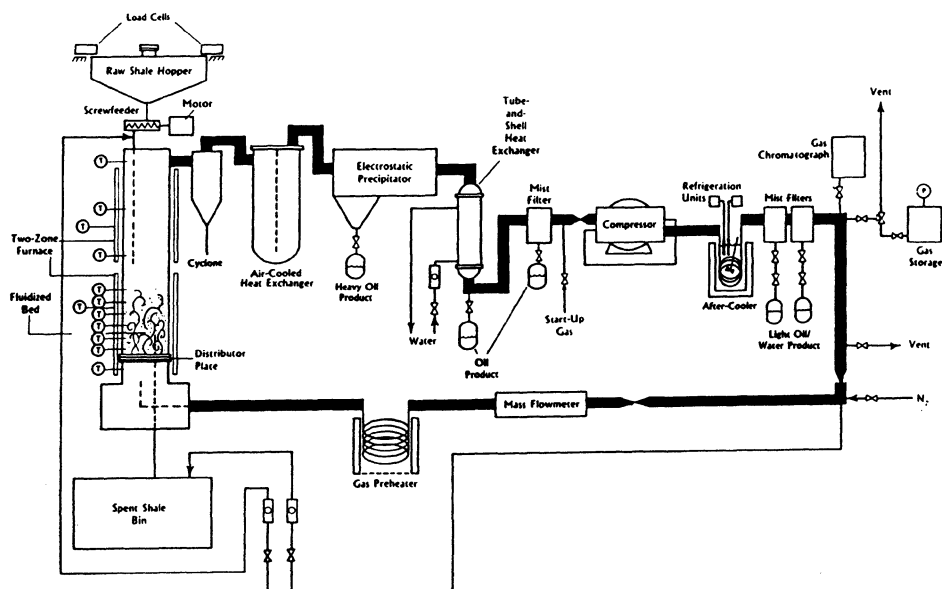


Figure 1. Flow diagram of 7.6-cm diameter fluidized bed retort and oil collection system. The system shown is for recycle-gas operation, but similar configurations were used for steam and nitrogen fluidization.

Table 1. Average Analyses of the Eastern U.S. Devonian Oil Shales Used for the Fluidized Bed Pyrolysis Studies.

Shale Type: Location Mined:	Cleveland Montgomery County, KY	New Albany Bullitt County, KY
Fischer assay, l/Mg gal/ton	51.6 12.4	59.5 14.3
Ultimate Analysis (as-received)		
Carbon, wt%	10.3	13.3
Hydrogen, wt%	1.3	1.6
Nitrogen, wt%	0.4	0.6
Sulfur, wt%	2.7	5.6
Ash, wt%	83.6	78.4

yield has been found to maximize at approximately 530°C which corresponds to a 28% increase above Fischer assay on a unit carbon basis (Figure 2). The gas yields increase linearly with increasing temperature from 2.5% to 7% of the carbon in the raw shale. Hydrocarbon gases (C_1 - C_4) make up 90% of the carbon-bearing gases with CO and CO_2 constituting the balance. Vapor phase oil (C_5 +) was measured chromatographically and considered in the oil yield. At 530°C the gas yield for fluidized bed pyrolysis is nearly equivalent to the Fischer assay yield on a unit-carbon basis, but the composition of the gas is quite different. The hydrocarbon gases from fluidized bed pyrolysis are nearly evenly distributed in terms of carbon number between 1 and 4 on a weight basis. Fischer-assay gas, on the other hand, has proportionally more lighter species (CH_4 , C_2H_4 , and C_2H_6) which indicates that more cracking has taken place.

The oil produced by fluidized bed pyrolysis increases in aromaticity with increasing temperature (see Figure 3). This increase in aromaticity is generally attributed to increased secondary reactions which include cyclization, dehydrogenation, and cleavage of aliphatic chains into gaseous components. The aromaticity of fluid-bed oil, as determined by the H/C ratio and NMR analyses, is much higher than Fischer assay oil (see Table 2). Since coking reactions are minimized by the rapid removal of pyrolysis vapors from the fluidized bed, aromatic oil vapors which are prone to char formation survive and are collected as oil. Accordingly, it has been found that fluid-bed oil is higher boiling, denser,

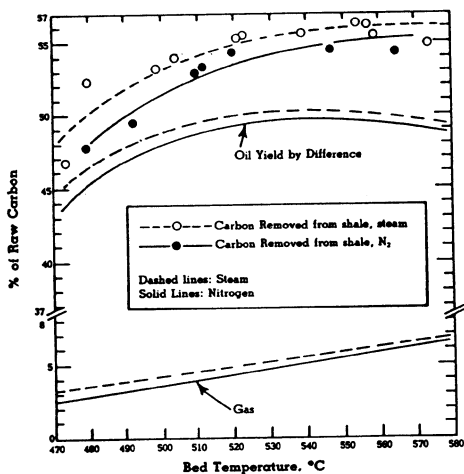


Figure 2. Oil and gas yields from fluidized bed pyrolysis of Cleveland oil shale in a 7.6-cm diameter retort using nitrogen and steam for fluidization. (Ref. 10)

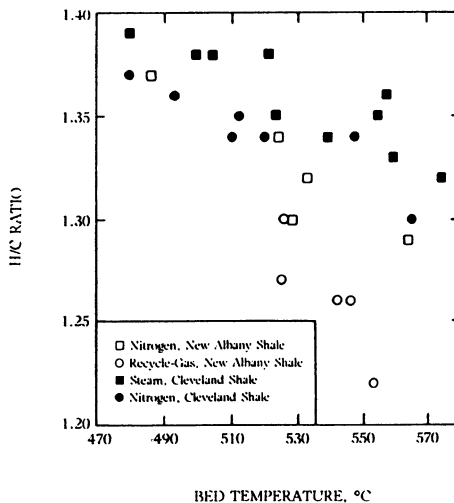


Figure 3. Hydrogen/carbon molar ratios of oil collected from fluidized bed pyrolysis of eastern U.S. shale.

Table 2. Characteristics of Oils from Fischer Assay and Fluidized Bed Retorting of Eastern U.S. Oil Shale. Data Taken from Ref. 10.

Ultimate Analysis (DAF)	Fischer Assay	Fluidized Bed Steam, 539°C
C, wt%	85.0	85.4
H, wt%	10.9	9.5
N, wt%	1.1	1.5
S, wt%	1.8	1.7
H/C	1.53	1.34
Density (60/60)	0.921	1.016
Viscosity, cP 25°C	NA	870
¹ H and ¹³ C NMR		
% Aromatic H	13.2	16.9
% Aromatic C	31.9	42.0

more viscous, and more heteroatomic than Fischer-assay oil (see Table 2). How this trade-off between oil quality and oil yield is resolved depends mainly on the intended slate of products for the oil shale process. Promising, non-fuel products from oil shale liquids such as asphalt and carbon fibers depend on the heavy fraction of oil which fluid-bed retorting produces in large proportions. So, from this point of view, a heavier, more aromatic oil product is more desirable than an oil which is more suited for transportation fuels.

2.2.2. Fluidizing Medium. At atmospheric pressure there are three fluidizing media which are practical for industrial application: combustion flue gases, steam, and recycled pyrolysis gas. The experimental fluid-bed program was designed to examine all of these possibilities. While hydrogen gas is certainly industrially viable, hydrogen provides no benefits at low pressure, so it has not been studied at the CAER. Nitrogen was considered as an appropriate substitute for combustion flue gas since nitrogen is the majority component of flue gas. Steam was of particular interest because of various claims that it is reactive during pyrolysis and that oil yield or quality may be enhanced compared to inert-gas pyrolysis.^{20,21,22,23,24,25,26,27} The effects of steam during fluid-bed or other types of rapid pyrolysis are not conclusive in the literature, however.^{28,29,30}

The finding at the CAER was that steam increased the conversion of carbon to volatile products by 2% and that half of that increase could be attributed to enhanced oil production (see Figure 2). Steam did not measurably alter the

characteristics of the shale oil, so it was concluded that steam played no reactive role during the pyrolysis of the kerogen. It was found that steam facilitated the production of H_2S from the iron sulfides and that 90% sulfur removal could be attained when the shale was reacted with steam for approximately 30 minutes.¹⁰ One of the most significant roles that steam plays during pyrolysis is that it aids the condensation of the lighter oils. It is, therefore, important to possess thorough carbon balances when comparing results between fixed-gas and steam retorting. It is possible that some of the high oil yields that have been attributed to steam in the literature have been due to more efficient oil collection compared to the parallel fixed-gas experiments.

The utilization of recycle gas for fluidization resulted in lower oil yields and higher gas yields compared to nitrogen fluidization. The loss of oil production was not balanced by the additional gas generation, so there was a net increase in char production. The H/C ratios of the oils from recycle-gas retorting are much lower compared to the parallel experiments using nitrogen for fluidization (see Figure 3). Capillary GC tracings of the recycle-gas oils indicated a lack of the normally predominant, high-boiling, n-alkane/1-alkene pairs. These compounds are not recycled to the reactor which suggests that recycle-gas is reactive and results in the destruction of saturated hydrocarbons.

2.2.3. Shale Residence Time. The residence time distribution for particles in a well-operated fluidized bed closely approximates the relationship for a perfectly mixed reactor which is given by:

$$F = 1 - e^{-\frac{t}{\tau}} \quad (1)$$

where F indicates the fraction of the particles in the exit stream which are older than t , and τ is the mean holding time of the vessel. Therefore, studying the kinetics of pyrolysis (i.e. the effects of shale residence time) in a continuously-fed fluidized bed is difficult. To overcome this characteristic of fluidized beds, a technique has been used by several workers in which a small pulse of oil shale is injected into a batch of fluidized solids and the total hydrocarbon vapors are measured quantitatively by a flame ionization detector (FID).^{5,8,31} The CAER adopted this technique to investigate the pyrolysis kinetics of New Albany oil shale.³² The evolution of hydrocarbons from the shale for all these studies was characterized by an initial rapid rate period followed by a much slower rate regime (see Figure 4). Two first-order reactions in parallel have been found to fit the data well. The CAER study also included a heat transfer time constant, θ , to more closely model the behavior when the shale particles are first introduced to the bed, transforming the pyrolysis kinetics model into the following:

$$C_k(t) = f_1 e^{-k_1 t} + f_2 e^{-k_2 t} \quad (2)$$

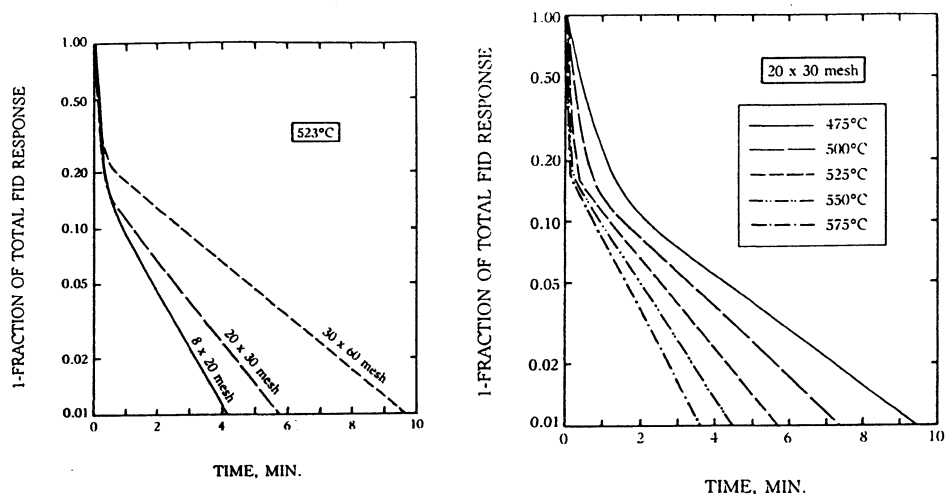


Figure 4. Least-squares solution to the first-order, parallel reaction model for New Albany shale. a) various particle sizes at 523°C. b) 20x30 mesh shale as a function of temperature.

$$k_i = A_i e^{-\frac{E_i}{RT_p}} \quad (3)$$

$$T_p = (T_{init} - T_{bed}) e^{-\frac{t}{\theta}} + T_{bed} \quad (4)$$

For simplicity, the particle temperature for the slower rate constant, k_2 , was assumed to be constant and equivalent to the bed temperature. The results of fitting this model to the data using a non-linear least squares routine are shown in

Table 3. Mean Kinetic Parameters for the First-Order Parallel Reaction Model for Fluidized Bed Pyrolysis of New Albany Oil Shale.

Mesh Size	f_1	A_1 , min ⁻¹	E_1 , kJ/mol	f_2	A_2 , min ⁻¹	E_2 , kJ/mol	θ , min
8x20	0.812	1.39E9	125.6	0.188	1.32E5	80.3	0.033
20x30	0.815	1.97E10	141.8	0.185	9.23E2	49.7	0.022
30x60	0.751	2.71E9	129.2	0.249	7.97E-1	5.8	0.015

mean variance=0.000971

Table 3. The rapid rate constant, k_1 , was responsible for approximately 80% of the total evolved hydrocarbons, and at temperatures above 500°C this portion of the pyrolysis curve was completed within one minute. The initial kinetics depended little on particle size, and the results for the rapid reaction regime corresponded well with values in the literature.³² The effect that particle size had on the kinetics during the rapid-rate stage was to vary the heat-up time of the particles themselves. The fitted heat transfer time constant in the model, θ , was found to increase according to particle size and was within a factor of two of what would be expected from heat transfer considerations alone.

A slow-rate period accounting for approximately 20% of the products was observed under all conditions of this study, and this still remains as a subject for conjecture. The smallest particle sizes display a slower rate than the largest (see Figure 4b), but as Wallman et al.⁵ showed for western U.S. shale, this is attributable to increased oil production from the smallest particles. In Wallman's study, however, the apparent activation energy for the slow-rate period, E_2 , was independent of the size of the shale particles. In the case of the CAER study with eastern U.S. shale, E_2 is dependent on particle size, and the trend is in the wrong direction to be explained by diffusion limitations. One suggestion has been that the smallest particles produce the largest and most unstable molecules which exit the pyrolyzer as vapor and which subsequently become trapped in the constant-temperature (350°C) transfer line to the FID and then slowly evolve gases. Another suggestion by Coburn and co-workers is that dust in the line to the detection device can delay the measurement of the release of hydrocarbons.^{33,34} Whatever the cause, it is most likely that the long tail associated with the kinetics studies is at least partially indicative of the experimental apparatus.

2.3 FLUIDIZED BED PYROLYSIS OF WORLD-WIDE OIL SHALES

A large amount of fluidized bed pyrolysis work has also been conducted at the CAER using a 3.8-cm diameter laboratory-scale fluidized bed reactor. Most of these studies have focused on eastern U.S. shale,⁶ and the results have compared well with those from the 7.6-cm diameter retort at the CAER.³⁵ In addition to studies with eastern U.S. shale, however, recent investigations with Moroccan and Turkish oil shales have also been completed.^{36,37} The oil yields from these and other fluidized bed pyrolysis studies for important oil shales of the world are summarized in Table 4. In general, the greater the aromaticity of the kerogen, the greater the oil yield enhancement that is possible by fluidized bed pyrolysis. It appears that highly paraffinic oil shales produce a maximum of 110% of Fischer assay oil from fluidized bed pyrolysis. Accurate H/C ratios of the Moroccan kerogens were not available, but they appear to be in the range of 1.1 to 1.3. It is important to note that the minerals can play a large role in the oil yields that are realized. In the case of the Turkish Goyruk oil shale, a carbonless shale was mixed with the Goyruk shale to retard its agglomerating behavior during pyrolysis.

Table 4. Comparison of Fluidized Bed Pyrolysis Results for Various Oil Shales of the World.

Shale	Kerogen H/C Ratio	% of Fischer Assay Oil Yield	Ref.
Eastern U.S. Cleveland	1.1	155	6
Moroccan Tarafaya R4	NA	146	36
Moroccan Timahdit M	NA	157	36
Australian Nagoorin	1.3	134	29
Australian Condor	1.4	128	29
Turkish Goynuk A	1.5	111	37
Western U.S. Green River	1.5	110	5
Australian Rundle	1.5	110	29

The diluent shale provided additional surface area for coke formation and certainly lowered the oil yield. The Goynuk shale is so rich in organic matter, however, that the added rocks actually provided a more equitable basis of comparison to the other oil shales.

3. Commercial Fluid-Bed Retorting Process Concept (KENTORT II)

3.1 OVERVIEW

To this point, only the characteristics of fluidized bed pyrolysis have been discussed. In a commercial retorting process, pyrolysis is just one step in a large system, and it is just as important that the rest of process be efficient also. While fluidized bed pyrolysis of eastern U.S. shale significantly increases carbon conversion to liquid and gaseous products, approximately 40% of the carbon remains in the spent shale. This material is ideal for immediate combustion since it has already been heated in excess of the 500°C and is of no value once removed from the process. Additionally, it is a good heat carrier because of its small size, relatively low rate of decrepitation, and high volumetric heat capacity. Accordingly, pyrolyzed shale combustion and its use as a heat carrier have been included as integral features of the KENTORT II process.

Several processes have been proposed that utilize char combustion with hot solids recirculation for generating and transferring heat in the retort.³⁸ However, direct combustion of the char does not represent the best approach for processing eastern U.S. oil shale. Since only a portion of the carbon in the char from pyrolysis is required by the combustor to meet process heat requirements, total carbon utilization would require the removal of heat from the reactor. This excess

heat could be used in the plant or power could be exported. The economics of cogeneration are highly site-specific, and this is generally not considered advantageous for an oil shale process. In addition, rapid pyrolysis concentrates sulfur in the spent shale compared to carbon, so direct combustion of the char would generate substantial SO_2 emissions. Environmental considerations make it imperative that these emissions be minimized.

The knowledge that steam would react with the shale to remove inorganic sulfur and the need to efficiently utilize the pyrolysis char provided the impetus to include a mild gasification stage between pyrolysis and combustion in the KENTORT II process concept. The removal of sulfur from the solid residue prior to combustion creates a relatively concentrated stream of H_2S which is easier to scrub than a dilute stream of SO_2 from a combustor. The H_2S serves as feedstock for elemental sulfur production. Moreover, the generation of syngas eliminates the need to export power. The synthesis gas has potential applications ranging from in-plant use to feedstock for liquid fuel synthesis to crude oil upgrading. The nearly complete removal of sulfur from the shale by oxidation of the iron sulfides through gasification and combustion greatly reduces the potential for acid drainage upon disposal of the shale.³⁹

3.2 EXPERIMENTAL

3.2.1. *Apparatus.* An integrated 7.6-cm diameter, 2.3-kg/hr prototype of the KENTORT II process was first used to investigate the viability of the concept (see Figure 5). The pyrolysis and gasification zones are stacked vertically and share steam as their common fluidizing medium. Raw shale is metered onto the pyrolysis bed and following pyrolysis, the solid residue is transferred through a gravity-fed standpipe to the gasification zone. The gasifier serves as the central distribution center for the retort. Hot, gasified solids are pneumatically transferred from the gasifier to the pyrolyzer to heat the incoming raw shale, and gasified solids are also pneumatically transferred to the fluidized bed combustor to raise the temperature of the solids before they are returned by gravity back to the gasifier. The system was completely enclosed in an electrically-powered furnace to preheat the system and to compensate for heat loss. More details of the apparatus and operating procedures are given elsewhere.^{18,19}

3.2.2. *Shale Samples and Test Matrix.* A Cleveland oil shale from Kentucky and an Irati oil shale from Brazil have been tested in the KENTORT II prototype (see Table 5). The similarity of the inorganic portion of the Irati shale to Devonian shales of the eastern U.S. permitted testing of the Irati shale in the full KENTORT II configuration. The Irati shale ($\text{H/C}=1.24$) has a more aliphatic kerogen compared to Devonian shale ($\text{H/C}=1.11$) and represents the major difference between the shales. For all prototype runs, the pyrolyzer temperature was held at 530°C and the combustor was operated at $850\text{-}900^\circ\text{C}$. The gasifier

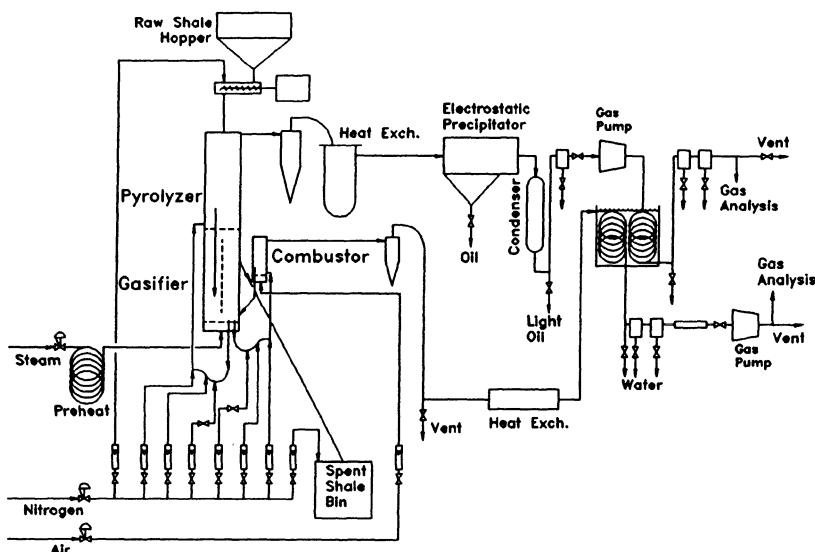


Figure 5. Schematic diagram of the integrated 2.3-kg/hr KENTORT II prototype system including the oil collection system.

temperature (740-850°C) was the primary operating variable and resulted in the solid-recycle ratio between the gasifier and pyrolyzer to range from 1.3 to 2.7.

3.3 PROTOTYPE RESULTS

3.3.1. Oil Yield. Since the temperature of the pyrolysis zone was held constant throughout the test series, the rate and temperature of hot gasifier solids being injected into pyrolyzer were the only parameters that could affect the oil yield. When the raw shale feedrate is held constant, the solid-recycle rate and the gasifier temperature are inversely related, so it is sufficient to characterize the conditions by only one of these

Table 5. Analyses of Cleveland and Irati Oil Shale Samples Processed in the 2.3-kg/hr KENTORT II Prototype.

	Cleveland	Irati
Ultimate Analysis		
C, wt%	16.1	16.5
H, wt%	1.7	1.8
N, wt%	0.6	0.5
S, wt%	1.8	4.0
Ash, wt%	74.7	76.9
Moist., wt%	2.2	2.2
Modified Fischer Assay		
Oil Yield, wt%	7.0	9.7
Oil Yield, l/ton	74	108
Water, wt%	4.2	3.0
Gas, wt%	2.6*	2.2
Loss, wt%	--	1.0
* Gas+loss.		

parameters. For convenience, the gasification temperature was chosen.

Oil yield from the Cleveland oil shale displayed little dependence on gasifier temperature (see Figure 6). This result is at odds with a previous study using the same Cleveland oil shale which did not include the combustor during operation of the prototype.¹⁸ With combusted solids present in the system, there appears to be a certain balance between the effects of temperature and recycle-solid rate on oil yield. When the prototype was operated without recycle-solids to provide baseline data, the average oil yield for the Cleveland shale was 129% of Fischer assay. The average oil yield obtained in the solid-recycle mode of operation for eastern U.S. shale was 111% of Fischer assay.

Therefore, regardless of the combination of recycle-solid rate and temperature, a net decrease in oil yield of approximately 14% was observed.

Owing to its more aliphatic character, the Irati shale produced higher absolute oil yields compared to the Cleveland shale which corresponds to 112% of Fischer assay. No non-solid recycle runs were performed with the Irati shale, but it is believed that the maximum fluidized bed oil yield should be approximately 115% of Fischer assay based on the study by Lisboa et al.³ The more aliphatic Irati shale is less sensitive to conditions that can cause secondary reactions, so the oil yield reduction caused by recycle solids is relatively small.

3.3.2. Carbon Distribution. Under half of the carbon from the Cleveland shale was distributed among oil and hydrocarbon gas products (see Table 6), so the majority of the carbon was available for gasification and combustion. The temperature of the combustor was controlled by diluting the combustion air with nitrogen. This was done because the recycle ratio between the combustor and gasifier (approximately 5:1) was too low to maintain the combustion temperature at less than 900°C. This procedure limited the amount of carbon that could be combusted, and explains the large amount of carbon remaining in the spent Cleveland shale. A larger combustor-gasifier recycle ratio will remedy this situation. The amount of residual carbon in the spent Irati shale was lower than for the Cleveland shale because there is less residual carbon available following the pyrolysis of Irati shale. Similar levels of gasification were achieved for the two shales, but approximately twice as much carbon was burned in the combustor for the Cleveland shale compared to the Irati shale.

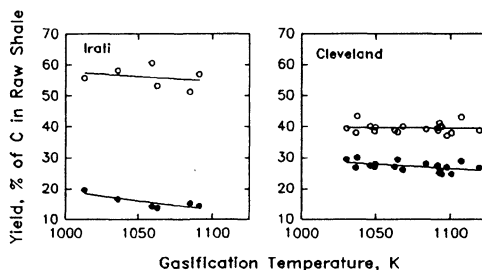


Figure 6. Oil (○) and char (●) yields for the Irati and Cleveland oil shales tested in the KENTORT II prototype reactor. (from Ref. 19)

3.3.3. *Sulfur Distribution.* The majority of the sulfur for both shales was in the form of H_2S gas (see Table 6). Even greater H_2S production can be expected at mean shale residence times over 20 minutes. It may be especially important to extend the gasification holding time for the Irati shale in order to convert its large amount of inorganic sulfur to H_2S . Much more sulfur partitioned to the oil for the Cleveland shale compared to the Irati, indicating that the Cleveland has a much higher organic sulfur content while having much less inorganic sulfur.

3.4 SUMMARY AND FUTURE WORK

The operation of the 2.3-kg/hr KENTORT II prototype was stable and reliable. Design conditions were achieved in all instances with the exception of insufficient solid recycle between the gasification and combustion zones. Therefore, true autothermal conditions were not attained, but sufficient carbon remained in the spent shale to heat balance the system if the solid recycle loop had been larger. A significant conclusion of this work was that the viability of the KENTORT II concept was demonstrated. Not only did the system work well physically, but enhanced oil yields were attained and the sulfur distribution was skewed toward H_2S production as expected. The results from the prototype were encouraging enough to scale the process up to a 23-kg/hr process demonstration unit (PDU). The PDU will further address the effects of scale-up on oil yield, and it will also permit autothermal operation to be achieved. A full-scale cold-flow model of the PDU was used to verify its fluid and particle dynamics.⁴⁰ At the time of this writing, the PDU is nearly ready to be operated for the first time. Following verification of the process using an eastern U.S. shale, adaptation of the KENTORT II process to other shales around the world will be investigated.

Table 6. Typical carbon and sulfur distributions for the Irati and Cleveland shales at a gasification temperature of 818°C in the KENTORT II prototype.

	Cleveland	Irati
Carbon, wt%		
Spent Shale	27.3	14.4
Oil	39.6	56.9
HC gases(C_1 - C_4)	4.8	6.1
CO_x -gasifier	9.3	8.0
CO_x -combustor	12.2	6.0
Water	1.6	2.3
Sulfur, wt%		
Spent Shale	19.9	24.6
Oil	8.4	2.6
H_2S	57.9*	42.7
SO_2	5.6	13.0
Water	8.2	0.2
* by difference		

4. References

1. Gwyn, J.E., Roberts, S.C., Hinds, Jr., G.P., Hardesty, D.E., and Johnson, G.L., *Thirteen Oil Shale Symposium Proceedings*, 1980, Colorado School of Mines, Golden, CO.
2. Tamm, P.W., Bertelsen, C.A., Handel, G.M., Spars, B.G., and Wallman, P.H., *Energy Progress*, 1982, 2 (1), 37.
3. Lisboa, A.C., Novicki, R.E., and Piper, E., *1989 Eastern Oil Shale Symposium Proceedings*, University of Kentucky, Lexington, Ky.
4. Urov, K., *6th Australian Workshop on Oil Shale*, 1991, Univ. of Queensland, St. Lucia, Brisbane, pp. 25-31.
5. Wallman, P.H., Tamm, P.W., and Spars, B.G., *Oil Shale, Tar Sands, and Related Materials*, American Chemical Society Symposium Series, 1981, 163, pp. 93-113.
6. Rubel, A.M., Margolis, M.J., Haley, J.K., and Davis, B.H., *1983 Eastern Oil Shale Symposium Proceedings*, 1983, IMMR83/089, University of Kentucky, Lexington, KY.
7. Margolis, M.J., *1981 Eastern Oil Shale Symposium Proceedings*, 1981, IMMR82/066, University of Kentucky, Lexington, KY.
8. Richardson, J.H., Huss, E.B., Ott, L.L., Clarkson, J.E., Bishop, M.O., Gregory, L.J., and Morris, C.J., Lawrence Livermore National Laboratory Report No. UCID-19548, 1982.
9. Ahmed, M.M., Parker, D.W., and Archer, D.H., *1982 Eastern Oil Shale Symposium Proceedings*, 1982, University of Kentucky, Lexington, KY.
10. Carter, S.D. and Taulbee, D.N., *Fuel Processing Technology*, 1985, 11, 251.
11. Coburn, T.T., *1988 Eastern Oil Shale Symposium Proceedings*, 1989, IMMR89/201, University of Kentucky, Lexington, KY, p. 325.
12. Dung, N.V., Wall, G.C. and Kastl, G., *Fuel*, 1987, 66, 372.
13. Wall, G.C. and Udaja, P., *Fuel*, 1988, 67, 1340.
14. Udaja, P., Duffy, G.J., and Chensee, M.D., *Fuel*, 1990, 69, 1150.
15. Rubel, A.M., Rimmer, S.M., Keogh, R., Robl, T.L., Carter, S.D., and Derbyshire, F.J., *Fuel*, 1992, 71, 1427.
16. Burnham, A.K. and Happe, J.A., *Fuel*, 1984, 63, 1353.
17. Taulbee, D.N. and Carter, S.D., *Fuel*, 1991, 70, 1245.
18. Carter, S.D., Robl, T.L., Rubel, A.M., and Taulbee, D.N., *Fuel*, 1990, 69, 1124.
19. Carter, S.D., Robl, T.L., Taulbee, D.N., and Rubel, A.M., *Fuel*, 1991, 70, 1347.
20. Gavin, M.J. and Desmond, J.S., *U.S. Bur. Mines*, 1928, No. 315.
21. Wells, W.E. and Ruark, J.R., *U.S. Bur. Mines Rep. Invest.*, 1952, No. 4874.
22. Lewan, M.D., Winters, J.C., and McDonald, J.H., *Science*, 1979, 203, 897.
23. Tyler, A.L., Bullen, E.A., and Jacobs, H.R., *14th Oil Shale Symposium Proceedings*, 1981, Colorado School of Mines, Golden, CO.
24. Cummins, J.J. and Robinson, W.E., *Amer. Chem. Soc., Div. Fuel Chem., Prepr.*, 1976, 21 (6), 94.

25. Campbell, J.H. and Taylor, R.W., Lawrence Livermore National Laboratory, 1978, UCID-17770.
26. Allred, V.D., *Symposium Papers: Synthetic Fuels from Oil Shale*, 1979, Institute of Gas Technology, Chicago, IL.
27. Rubel, A.M. and Coburn T.T., *1981 Eastern Oil Shale Symposium Proceedings*, 1981, IMMR82/066, University of Kentucky, Lexington, KY.
28. Sohns, H.W., Jukkola, E.E. and Murphy, W.I.R., *U.S. Bur. Mines*, 1959, Rep. Invest. No. 5522.
29. Wall, G.C., *17th Oil Shale Symposium Proceedings*, 1984, Colorado School of Mines, Golden, CO.
30. Steedman, W.G., Appelbaum, H.R. and Shirley, F.W., *Symposium Papers: Synthetic Fuel from Oil Shale*, 1983, Inst. of Gas Technology, Chicago, IL.
31. Forgac, J.M., AIChE 1984 Spring National Meeting, 1984, Paper 57b, Anaheim, CA.
32. Carter, S.D., *1986 Eastern Oil Shale Symposium Proceedings*, 1986, University of Kentucky, Lexington, KY.
33. Coburn, T.T., Taylor, R.W., and Morris, C., *1988 Eastern Oil Shale Symposium Proceedings*, 1988, IMMR88/101, University of Kentucky, Lexington, KY.
34. Coburn, T.T. and Morris, C.J., *1990 Eastern Oil Shale Symposium Proceedings*, 1990, IMMR90/201, University of Kentucky, Lexington, KY.
35. Rubel, A.M. and Carter, S.D., *Prepr. Am. Chem. Soc., Div. Fuel Chem.*, 1984, 29, 3, 202-208.
36. Graham, U.M., Bekri, O., and Robl, T.L., *Am. Chem. Soc. Prepr., Div. Fuel Chem.*, 1992, 37 (2), 778.
37. Graham, U.M., Rubel, A.M., Ekinici, E., and Robl, T.L., *1992 Eastern Oil Shale Symposium Proceedings*, 1992, IMMR93-01, University of Kentucky, Lexington, KY.
38. Lewis, A.E., Braun, R.L., and Diaz, J.C., *Seventeen Oil Shale Symposium Proceedings*, 1984, Colorado School of Mines, Golden, CO.
39. Robl, T.L., Cisler, K., Thomas, G., and Koppenaal, D.W., *1985 Eastern Oil Shale Symposium Proceedings*, 1985, KCERL/85-147, University of Kentucky, Lexington, KY.
40. Vego, A., Stehn, J.L., Carter, S.D., and Neathery, J.K., *1991 Eastern Oil Shale Symposium Proceedings*, 1991, IMMR91-07, University of Kentucky, Lexington, KY.

STEAM AND COPROCESSING OF OIL SHALES

E.EKİNCİ^{1,2}, Y. YÜRÜM³

¹ ITU, Department of Chemical Engineering, Ayazağa-İstanbul, and

² TUBITAK-MRC, Department of Chemical Engineering, Gebze-Kocaeli, Turkey

³ Hacettepe University, Department of Chemistry, Beytepe-Ankara, Turkey

ABSTRACT

Steam pyrolysis is receiving particular interest due to the oil yield increase, ease of removal of the product, and steam's role as reagent in shale oil processing. The experiments on fixed bed steam and nitrogen sweep show that greater oil yields than Fisher Assay (FA) ranging upto 25 % were observed. The effect of steam on oil yield in fixed beds was found to be greater than nitrogen which diminished as higher sweep velocities are used. The highest fluidised bed yield for oil shales was reported as 155-160 % in excess of FA.

There are obvious advantages in considering co-utilisation of oil shales and lignites since they often co-exist in the same sedimentary sequence. Copyrolysis experiments with Turkish oil shales and lignites and asphaltites resulted in increase of oil yield as well as alteration in product distribution.

1.0. Introduction

Steam pyrolysis is receiving particular interest in oil shale processing due to the oil yield increase, ease of removal of the products, its compatibility with the environment and its already accepted role as a means for shale oil processing for production of special chemicals like ethylene, propylene, benzene, toluene, and xylene⁽¹⁾. Positive effect of steam in pyrolysis atmosphere was reported by earlier studies of Bureau of Mines⁽²⁾. The first report was as early as 1920's during the study of Colarado oil shale in "Pumperston" retort and another in the study of "Royster" retort⁽³⁾.

Steam was used in pyrolysis of oil shales in variety of ways. Numerous studies have utilised steam in fluidised state, for example Carter and Taulbee⁽⁴⁾, Dung⁽⁵⁾, Richardson et.al⁽⁶⁾; in fixed bed Cambell and Taylor⁽⁷⁾, Minkova et.al⁽⁸⁾, Çitiroğlu⁽⁹⁾; as supercritical solvent Yanik et.al⁽¹⁰⁾ and; in fixed and fluidised bed mode when oil shale was copyrolysed with lignite Çitiroğlu et. al.⁽¹¹⁾ In literature, the effect of atmospheric steam, steam under pressure, steam together with CO Cummins and Robinson⁽¹²⁾, Parkinson and Merson⁽¹³⁾ and super heated steam in-situ conditions Udell⁽¹⁴⁾ on pyrolysis were some of the topics that were studied.

Coprocessing was first realised and extensively studied in coal liquefaction with heavy oil slurrying media, such as heavy crudes, residual oils etc.⁽¹⁵⁾ This has given rise to improvements in oil yield, reduction of sulphur and nitrogen contents in the liquid product and other process advantages. Similarly, coprocessing of oil shales with asphaltites and lignites have also investigated for possible synergism and processing improvements Erdem-Şenatalar et.al⁽¹⁵⁾, Çıtıroğlu et.al.⁽¹¹⁾.

In the first part of this manuscript the effect of steam on the pyrolysis of oil and other shales is reviewed upon variations obtained with. The different contact systems, nitrogen sweep, process parameters and product yield and quality are described. In the second part, coprocessing of oil shale with lignite is then discussed.

2.0. Utilisation of Steam in Pyrolysis of Oil Shales

2.1. FIXED BED APPLICATIONS

Under static conditions used in oil shale retorting such as Gray-King, Fisher assay, and Heinze, two factors limit the oil yield considerably. These are the retrogressive char-forming reactions and cracking of volatiles at the hot surfaces during evolution. The former is aided by the catalytic activity of the inorganic matrix. In order to overcome the mass transfer limitations that force the desirable potential condensable liquids to gas and char, steam and inert gases are used to sweep volatiles out of the fixed-beds.

Nearly in all comparative fixed bed studies between steam and inert gas (nitrogen) under slow heating conditions and atmospheric pressure, it has been observed that steam sweep is more beneficial to oil yields than is inert gas sweep. Results for two Turkish oil shales (Göynük and Seyitömer) pyrolysed under steam and nitrogen sweep at different sweep velocities are summarised in Table 1.

Table 1. Yields from pyrolysis experiments on Göynük oil shale at 550 °C (wt% daf shale)⁽¹⁶⁾

	Göynük Char Oil		Seyitömer Char Oil	
Heinze retort				
static	55	33	static	64 28
steam, 0.7 cm/s	46	40	steam, 4.3 cm/s	51 38
steam, 1.3 cm/s	40	44	steam, 7.7 cm/s	46 42
steam, 3.3 cm/s	25	55	steam, 12.3 cm/s	42 45
nitrogen, 3.3 cm/s	47	39		
Fixed Bed				
static	48	38	static	56 33
nitrogen 22 cm/s	23	61	nitrogen 22 cm/s	48 42

From the results presented in Table 1. The mass transfer limitation are clearly evident. The difference in magnitude of oil yields between the steam and nitrogen sweep processes diminishes at higher gas velocities. For the higher ash content Seyitömer lignite much greater steam velocity is required for similar conversion as compared to Göynük oil shale. Similar to Ekinci et.al⁽¹⁶⁾, Cambell and Taylor⁽⁷⁾ reported earlier that for Colorado oil shale oil yields up to 109 % of Fischer Assay (FA) were obtained for steam whereas argon sweep at similar velocities resulted in yields up to only 100 % FA. Rubel and Coburn⁽¹⁷⁾ reported that fixed bed steam sweep retorting provided oil yields up to 125 % of FA and nitrogen sweep under similar conditions provided oil yields up to 112 % of FA. These authors also reported that the maximum steam flow rate possible was limited by the system as 0.7 L min^{-1} and optimum steam flow was yet to be achieved. Minkova et. al⁽⁸⁾ carried out steam pyrolysis of a lignite, a high volatile bituminous coal and oil shale. Fixed-bed steam pyrolysis resulted in oil yields 20-50 % higher than that obtained in FA.

2.2 EFFECT of STEAM on the PRODUCT YIELD

The favourable effect of steam on the pyrolysis of oil shales has been attributed to a variety of reasons. There are both points of agreement and contradiction amongst the different researchers. There is a general agreement that steam affects both the quantity and quality of the oil. Ekinci et.al⁽¹³⁾, report that for increasing sweep velocity of steam and N_2 , the yields of alkanes and aromatics are increased whereas that of polars decreased and that this is more pronounced for steam as compared to nitrogen. From these results, it might be inferred that alkanes may be involved in retrogressive char-forming reactions via dehydrogenation to alkenes and subsequently cyclisation. Thus, either steam promotes bond cleavage reactions and creates a greater demand for transferable hydrogen, or merely provides a more protective environment, limiting the extent of cyclization and aromatization of alkanes by passivating the acidic clay minerals. Minkova et.al⁽¹⁸⁾ measured lower CO and higher CO_2 concentrations in the gas for the steam pyrolysis indicating a probable reaction between CO and steam in the presence of Fe catalyst. The characteristics of the oils obtained from Heinze retort were different for static, steam and nitrogen sweep conditions^(9,16). Comparison of the steam and static pyrolysis products of Göynük and Seyitömer oil shales showed that they contained similar amounts of n-hexane solubles but the concentrations of alkanes and polars were distinctly different Figure 1. As the velocity of steam increased the proportion of paraffins increased while the proportion of the polars decreased. $^1\text{H-NMR}$ studies of oils showed greater aromaticity for steam pyrolysis as compared to static pyrolysis. The changes for nitrogen sweep oils were in similar trend as steam but not so intense.^(9,19)

Minkova et.al.^(8,18), in addition to the explanation given above, proposed that steam had a physical influence on the heat transfer favouring the desorption of low molecular weight products from solid phase surfaces where by subsequent

cracking or coking is avoided. This may be paralel with Allred's⁽²⁰⁾ results who reported an earlier starting temperature for oil evolution for steam as compared to nitrogen. However, there have been claims that the improvement in the lower molecular weight compounds for steam pyrolysis was also affected by the efficiency of liquid collection⁽⁴⁾. Minkova et. al.⁽¹⁸⁾ also claimed the probability of donor-acceptor interaction and desorption of hydrophobically retained low molecular weight products from the cavities of cross-linked macromolecules.

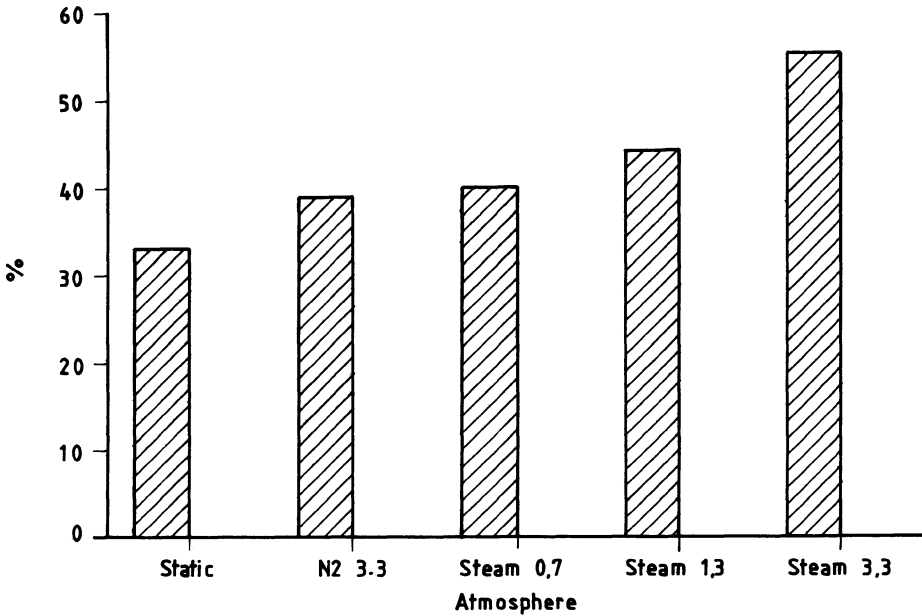


Figure 1. Comparison of Tar Yields for Pyrolysis of Göynük Oil Shale in Heinze Retort With Static, Self-Generated, Nitrogen and Steam Atmospheres

Furthermore in a different study⁽²¹⁾, the same group of workers observed the formation of semicoke with a strongly developed porous structure and high adsorption capacity. The increase in porosity is measured in terms of specific surface area for fixed bed and steam sweep chars of Göynük oil shale as $8.7 \text{ m}^2\text{g}^{-1}$ and $170 \text{ m}^2\text{g}^{-1}$ respectively⁽²²⁾. For the same oil shale, fixed bed residue and steam pyrolysed (1 hr) residue had $8 \text{ m}^2\text{g}^{-1}$ and $300\text{--}400 \text{ m}^2\text{g}^{-1}$ N_2 -BET surface areas⁽²³⁾. The increase in surface area is claimed to ease the evolution of supplementary volatile products from the inner volumes. Steam is claimed to penetrate into the pores, accelerate the diffusion of enclosed low molecular weight components and destroy some bonds in the macromolecular structure⁽¹⁸⁾. Therefore, this may be one explanation that steam prevents the char-forming reactions even at low velocities. Comparative pyrolysis studies of a coal in fixed-beds in inert and steam atmospheres also indicated that steam behaved different than inert atmosphere and is claimed to be a better extractor of volatile matter⁽²⁴⁾.

2.3 FLUIDISED BED APPLICATIONS

Fluidised-beds have a considerable number of advantages for oil shale processing applications. Some of these features are highlighted in a delightful disposition by Levenspiel⁽²⁵⁾ and include high thermal efficiency, high through-put, simpler and smaller equipment, ease of transportation for continuous mode operations and high heat transfer rates. These characteristics open new options for a number of process combinations. The oil shale retorting development work at University of Kentucky Center for Applied Energy (CAER) is a good example for these systems of fluidised beds in which pyrolysis, gasification and combustion of Eastern oil shales are accomplished to maximise of efficiency and minimisation of environmental pollution⁽²⁶⁾. The fact that fluidised-beds improve the oil yield considerably over fixed beds makes it possible to include many oil shale reserves into an economical class which otherwise would be classed as uneconomical.

In experiments carried out in nitrogen sweep fixed-bed and nitrogen fluidised-bed, a 9.3 % increase in oil yields was obtained in favour of the latter Ekinci et. al.⁽²⁷⁾. This clearly demonstrates that the type of contact may significantly affect the oil yield. There have been relatively few studies on the fluidised-bed steam pyrolysis of oil shales. Dung⁽²⁵⁾ reports yield data for FA and fluidised-bed pyrolysis with nitrogen and steam sweep for eight Australian oil shales. Compared with the FA, fluidised-bed nitrogen and steam pyrolysis gave 7 and 15 % more oil respectively. Carter and Taulbee^(4,29) observed oil yields for fluidised bed exceeding FA yields by 20-30 %. Fluidised-bed steam retorting is observed to give higher carbon conversion for gas, oil and shale as compared to nitrogen. The highest fluidised-bed yield for oil shales was reported as 155-160 % of FA⁽²⁹⁾. The same authors report a 29 % increase over FA carbon conversion to oil for an integrated gasifying, pyrolysis and combustion system namely the Kentort II reactor^(30, 31). The effect of fluidised-bed temperature on oil and gas yield from steam and nitrogen fluidisation were studied for Kentucky oil shales and the trend for nitrogen fluidisation was

similar to steam but the oil yield obtained for steam fluidisation was approximately 1 or 2 % greater depending method of evaluation. Continuous fluidised-bed studies on Rundle Oil Shale gave yields close to FA at 480 °C but increased to 145 % FA at 540 °C⁽³²⁾. A number of researchers observed a decrease in oil yield at higher temperatures, therefore an optimum oil production temperature was quoted. Carter and Taulbee⁽⁴⁾ reported this temperature as 520 °C. Which is 20 °C lower than that from Dung⁽⁵⁾ and Litster and Newell's⁽³¹⁾ results. This difference was attributed by Dung⁽⁵⁾ to the possible low residence times (3-6 minutes) employed by Carter and Taulbee⁽⁵⁾. However, Carter and Taulbee's results also give 540 °C as optimum temperature for both N₂ and steam if oil yield was determined by the difference method [organic C-(char + gas)]. Of course in order to make meaningful comparisons between such results the differences in reactor geometry, gas velocity, particle size, and other process paramaters should be considered.

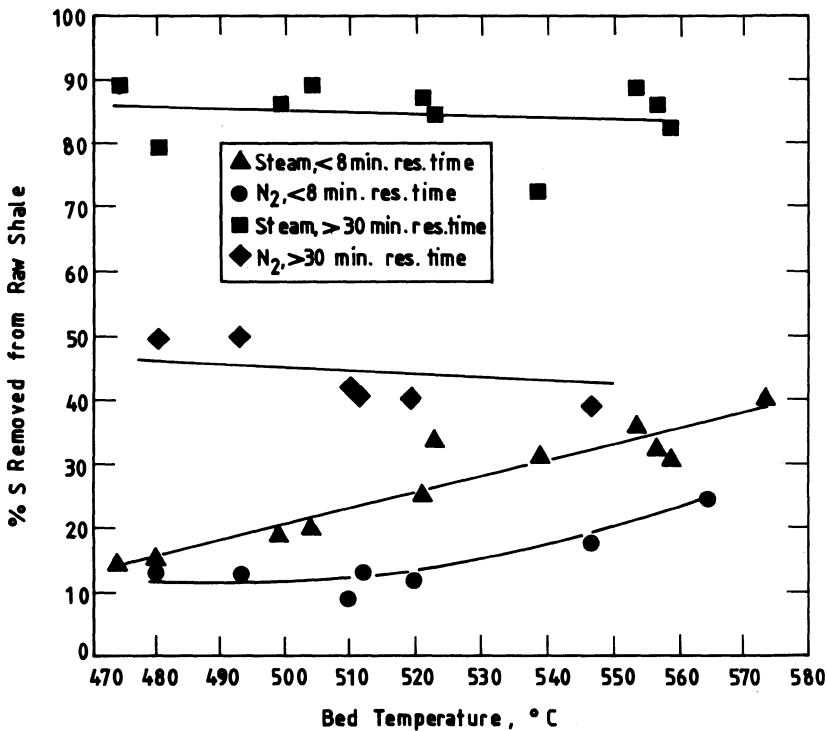


Figure 2. Effect of Bed Temperature on Carbon Removal

For the case of pyrolysis of Condor and Stuart shales in a fluidised bed, oil yields close to modified FA was obtained but when ash to shale ratio was increased to 2 up to 28 % oil loss was obtained⁽²⁸⁾. There are some studies which report the effect

of ash/shale ratio on the oil yield⁽³³⁾. Experiments with pure minerals such as illite and montmorillonite are found to be destructive with respect to oil Espetiale et.al.⁽³⁴⁾

Most of the reasons forwarded for the favourable oil yield for sweeping fixed bed retorts are relevant to fluidised beds. In the case of fluidised beds, generally higher space velocities, 3-4 times in excess of minimum fluidisation velocity are used which are expected to work against the mass transfer limitations and cracking reactions relevant at fixed and low sweeping velocity cases. Also, the increase in the efficiency of condensation of lower molecular weight compounds is emphasized strongly by many researchers^(4,8,18,29).

2.4. COMPOSITION OF OILS OBTAINED FROM STEAM PYROLYSIS

The oils obtained from fluidised beds were determined to be different in character as compared to FA. The former were realised to be more dense, less volatile, more aromatic and higher in nitrogen content⁽²⁹⁾. Therefore, increase in oil yield has to pay a price of some magnitude in terms of being more difficult to refine.

There are significant differences on the yield and composition of products obtained from steam and nitrogen pyrolysis. The gas composition for FA and fluidised bed retorting were substantially different but the gas distribution and yield for steam and nitrogen fluidised beds were similar. This was interpreted as steam not playing an extra role in hydrocarbon gas kinetics under the given experimental conditions⁽⁴⁾. This point was substantiated by the measurement of 1-alkene/ n-alkane ratios for C₂ to C₅ products for varying temperatures for steam and nitrogen fluidisation. The difference in the obtained yields for fluidised bed steam and nitrogen was attributed to the improvement in oil collection efficiency which was believed to be much greater than its role as a reactive pyrolysis medium by increasing the fraction of kerogen converted to C₅⁺ products. Indeed the increase in the lighter fractions of the collected oil was reported as well by other researchers for steam^(4,9,19).

Compared to the FA and similar to fixed bed sweep experiments, the contents of acyclic and cycloalkanes and polar compounds increased in the fluidized bed oil. Steam oil was found to have slightly higher H/C ratios and lower nitrogen content than did the nitrogen oil. The order of difference was attributed also to the efficiency of light ends recovery. Otherwise the oils from steam and nitrogen atmospheres were found to be essentially identical⁽⁴⁾.

Steam oil results in more alkenes as for case of fixed bed sweep experiments with increasing steam velocity. Çıtıröğlü⁽⁹⁾ detected increased yield of terminal alkenes. N-alkene/n-alkane ratio increased to 0.44 from 3.3 cm/sec steam sweep compared to static retorting. The increase in the alkenes (internal and external) was believed to be due to cyclisation reactions catalysed by mineral matter that are curtailed by steam. Indeed experiments with n-hexadecane has shown that cyclisation reaction occur during pyrolysis.

Some investigations indicated that process conditions such as temperature, steam flow rate, and heating rate affect characteristics of the oil product. As fluidised bed temperature was raised, the H/C ratio of oil was reduced, but it was still reported to be slightly higher than for nitrogen fluidisation⁽⁴⁾. Increasing the temperature also increased the aromaticity of the oil^(4,29). Increase in the steam flow rate decreased the H/C molar ratio from 1.48 to 1.43 for Cleveland and 1.51 to 1.41 to Sunbury oil shales. Furthermore, steam velocity is reported to increase the aromaticity of the oil⁽³⁵⁾.

2.5 SULPHUR BEHAVIOUR UNDER STEAM

Sulphur, together with nitrogen and organometallic compounds, constitute an important quality aspect of pyrolytic synthetic fuel processes. Therefore, their distribution among char, gas and liquid products is of paramount importance. Carter and Taulbee⁽⁴⁾ followed the sulphur removal from the shale in steam and nitrogen fluidised beds at the same temperature, and the magnitude of removal was greater for steam fluidisation. It has been reported that while pyrolysis was essentially complete at a mean residence time of 3 minutes, sulphur evolution was found to be a much slower process. Supportive findings were reported by Attar⁽³⁶⁾ who concluded that the rate-limiting step for desulphurisation is the decomposition of FeS₂. The great difference between nitrogen and steam sulfur removal of 45 and 85 % at long reaction times Figure 3. are partly explained in terms of steam reacting with FeS to produce iron oxides with possible reduction to iron⁽³⁷⁾.

It should also be noted that for steam fluidisation, sulphur removal was activated faster compared to other media; 90 % S removal could be activated at residence times greater than 30 minutes and temperatures less than 600 °C⁽³⁸⁾.

3.0. Coprocessing of Oil Shales With Lignites

Coprocessing is generally used in conjunction with liquefaction of coal with petroleum derived oil or another heavy oil slurring media, such as heavy crudes, residual oils and similar material that have potential to increase through put and reduce hydrogen demand other benefits include utilisation of a waste component, possible synergistic increases in conversion is not and linking the process to current refining technology.

Apart from coal and petroleum derived heavy oils, two solid fuels such as an oil shale and lignite and an oil shale and an asphaltite pairs could be coprolysed with the aim of maximising of resources^(39,40). Often the oil shale deposits co-exist in the same sedimentary sequence. For example both Göynük and Seyitömer oil shale reserves overlie the lignite deposits. For this reason there are obvious advantages in considering co-utilisation of these two fuels. Oil shales and lignites may be blended as an input to combustion and/or pyrolysis systems.

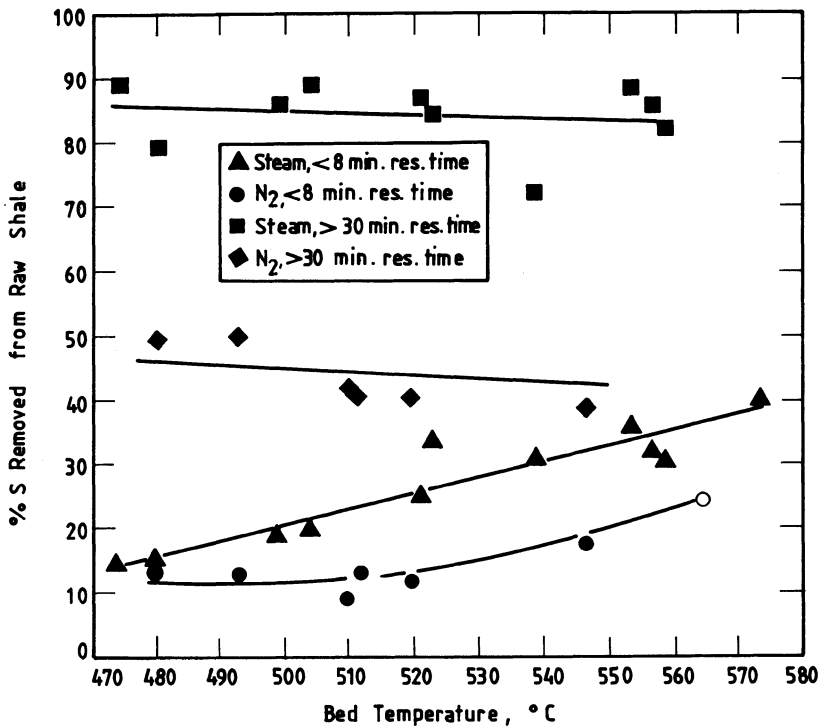


Figure 3. Effect of fluidization gas, bed temperature, and oil shale residence time on sulfur removal⁽⁴⁾

3.1. EFFECT OF COPROCESSING ON OIL YIELD

Saxby and Sato⁽⁴⁰⁾ coprolysed Rundle/Stuart oil shale and lignite as naturally occurring deposits using a range of mixtures. Mixtures containing 25, 50 and 75 % lignite were prepared and dried prior to pyrolysis using a modified Fisher assay apparatus. A linear relationship between oil yield and the proportion of oil shale in mixture was obtained. There were distinctive changes in the characteristics of produced oils from coprocessing compared to non-interacting components.

Çitiroğlu et. al.⁽⁴¹⁾ coprocessed mixtures of Göynük and Seyitömer oil shales (GOS) and (SOS) and Seyitömer and Yatağan lignite (SL) and (GL) using a modified Heinze retort at 550 °C under static and nitrogen sweep conditions. The mixtures contained 25, 50, 75 % lignite. Contrary to Saxby and Sato⁽⁴⁸⁾ higher than predicted oil yields (2-5 % daf) have been found. The coprocessing results for GOSYL and SOS/SL are shown in Figure 4.

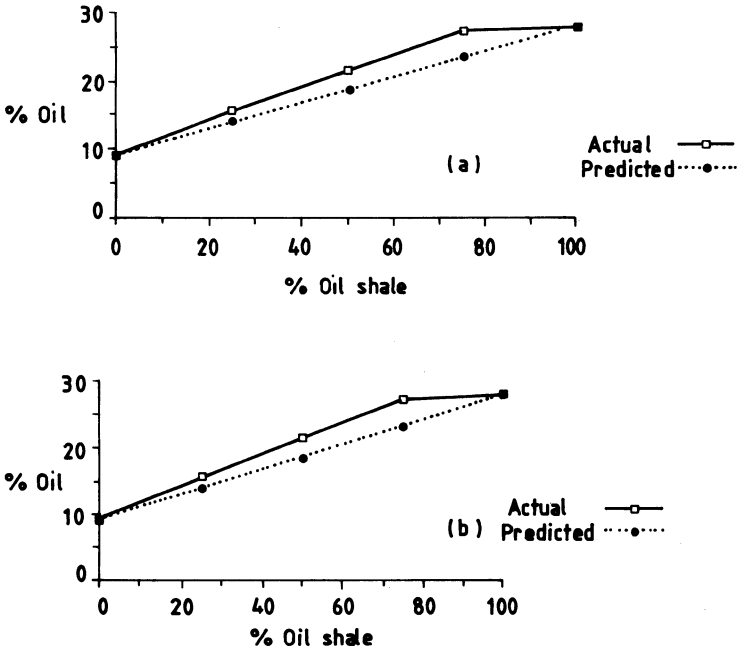


Figure 4. Oil Yields From Göynük Oil Shale/Yata'an Lignite (a) and Seyitömer Oil Shale/Lignite (b) Mixtures

The highest increase in oil yield (synergism) was observed for the highest oil shale to lignite ratio investigated. This was interpreted as the oil shale partly preventing retrogressive char forming reactions in the lignite. The reason for the maximum synergism is further explained in terms of poor compatibility between the shale and lignite. The highly aliphatic shale oils produced during the initial stages of pyrolysis in the form of pyrobitumen are expected to be relatively poor solvents for phenolic lignite materials.

Coprocessing of Turkish Avgamasya asphaltite and three lignites were investigated by Şenatalar et. al.⁽³⁹⁾ in a modified Heinze retort. For all three combinations oil yields increased above the theoretically calculated values from the individual components. The maximum synergistic increase was obtained for 25 % asphaltite and 75 % lignite. Asphaltites originating from petroleum origin may have much greater compatibility with lignites remembering that pioneering and mainstream coprocessing experiments are carried out between heavy oils and coals^(42,43). It has been concluded from asphaltite/lignite coprocessing results that the synergism had a direct relationship with the gas evaluation and ash content of the fuel, indicating the possible role of retrogressive char forming reactions.

3.2. TARS OBTAINED FROM OIL SHALE/LIGNITE COPROCESSING

Saxby and Sato⁽⁴⁰⁾ reported substantial changes in the structure of coprocessed oil shale/lignite oils compared those obtained from the individual components. H/C values of oils from mixture pyrolysis (FA) are slightly lower than the calculated values from pure oil shale and lignite. Aromaticity of the oil resulting from FA of mixture is observed to have higher aromaticities compared to the calculated values from pure component pyrolysis. The H/C and aromaticity changes are shown in Figure 5. Increasing the lignite content of the mixture resulted in lower molecular weight products qualified as a more desirable feedstock for gasoline production.

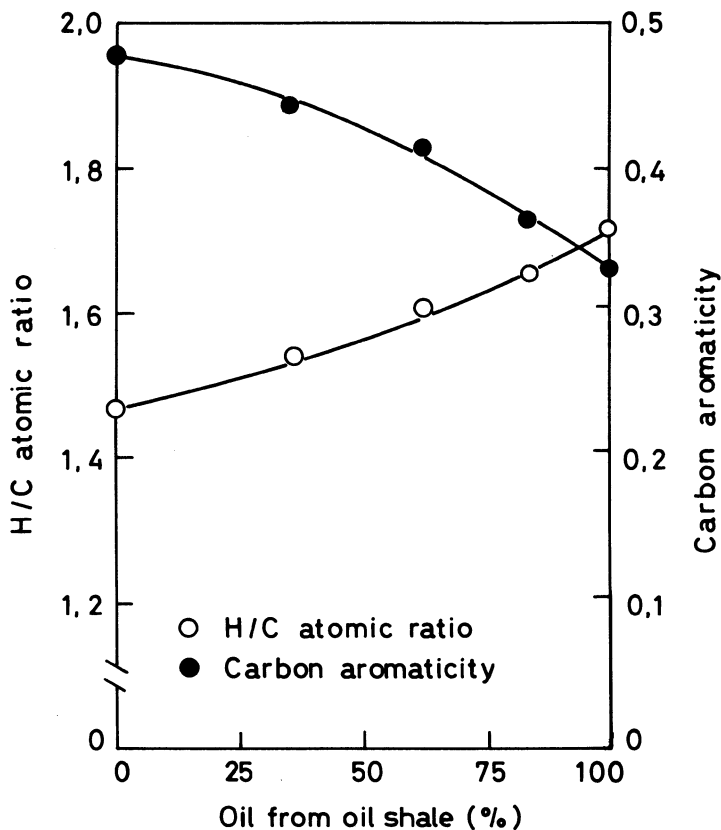


Figure 5. The H/C and Aromaticity Changes for Coprocessing

The mechanisms that may play an important role in the structural changes in the composition of tars obtained from coprocessing are proposed to be: carbon dioxide from liginites assisting the rapid release of oil vapours; hydrogen from pyrolysis of oil shale particles being available for hydrogenation of tar molecules from lignite; and aliphatic free radicals "capping" reactive sites on lignite-derived small aromatic fragments⁽⁴⁰⁾.

Çitiroğlu, et.al.⁽⁴¹⁾ sought information on the interactions between oil shale and lignite during copyrolysis by observing the changes in solubility classes namely aliphatics, aromatics and polars. The results showed that for the synergistic cases the concentration of alkanes and aromatics increased and the concentration of polars decreased. This was interpreted as interaction between the oil shales and lignites go some way to limit retrogressive char forming reactions. Further substantiation may be seen from three different evidences. The first of these is similar changes were observed for nitrogen and steam sweep compared to static pyrolysis. This may indicate similarities between the copyrolysis and sweep pyrolysis mechanisms. Also a direct correlation found between the highest synergistic case and lowest ash content of the related mixture⁽³⁹⁾. For the distinct synergistic mixture of 1:2 mixture of YL and GOS use of nitrogen as a sweep gas gave rise to significantly higher conversion and with maximum sweep gas velocity of 6.0 cm s^{-1} , conversions of oil shale and lignite are slightly higher than their volatile matter contents. This suggested that synergism would appear to be evident under static conditions or with low sweep gas velocity where there are severe mass transfer limitations on the release of volatiles.

REFERENCES

1. Griswold, C.F., Yesavage, V.F., and Dickson, P.F, Steam Pyrolysis of Tosco Shale Oil For Production of Chemical Intermediates, 172nd National Meeting, ACS Div. Fuel. Chem., Vol. 21, No 6, 207.
2. Gavin, M.J., and Desmond, J.S., U.S. Bur. Mines, No 315, 1928.
3. Wells, W.E., and Ruark, J.R., U.S. Bur. Mines, Rep. Invest. No 4874 1952.
4. Carter, S.D. and Taulbee, D.N., Fluidised Bed Steam Retorting of Kentucky Oil Shale, Fuel Processing Technology, 11, 251-272, 1985.
5. Dung, N.V., Yields and Chemical Characteristics of Product From Fluidised Bed Steam Retorting of Condor and Stuart Oil Shales: Effect of Pyrolysis Temperature, Fuel, 69, 368-76, 1990.
6. Richardson, J.H., Nuss, E.B., Ott L., Clarkson, J.E., Bishop, M.O., Gregory, L.J., and Morris, C.J., Fluidised Bed Pyrolysis of Oil Shale, Oil Yield, Composition and Kinetics UCID-19548, Lawrence Livermore Nat. Lab., 1982.
7. Campbell, J.H., and Taylor, J.R., Lawrence Livermore Laboratory, UCID-17770, April 10, 1978.
8. Minkova, V., Angelova, G., Ljutzkanov, L., Goranova, M., and Razvigorova, Effect of Water Vapour on the Pyrolysis of Solid Fuels, 1987 ICCS Ed. Moulijn et. al Elsevier, 1987.
9. Çıtıröğlü, M., Pyrolysis Studies on Turkish Oil Shales and Lignites, MPhil Thesis, University of Strathclyde, 1989.
10. Yanık, J., Sağlam, M., Yüksel, M., Olukçu, N., Bartle, K.D., and Frere B., Investigation of Products of Extraction with Water and Pyrolysis of Göynük oil Shales, Annual Chemistry and Chemical Engineering Symposium, İstanbul 1992 (Tur).
11. Çıtıröğlü, H., Önen, A., Çıtıröğlü, M., and Ekinci, E., Effect of Different Processes on Liquid Product Distribution, Erdöl und Kohle Erdgas Petrochemie, 46:4, 1993.
12. Cummins, J.J, and Robinson WE, ACS Div. Fuel, Chem. Prepr. 21(16): 94, 1976.
13. Parkinson, W.J., and Merson, T.J., Cost Analysis of Carbon Monoxide Steam Process , Report, LA-9463-MS, 15pp, 1982.

14. Udell, K.S., and Jacobs, H.R, ASME Publications, 79-HT-3, 1979.
15. Erdem-Şenatalar, A., Arabacıoğlu, B., and Ekinci E., Copyrolysis of Turkish Lignites and Asphaltites, Proc of. 1992 Eastern Oil Shale Symposium, Lexington 1992.
16. Ekinci, E., Çıtıroğlu, M., Pütün, E., Love, G.D., Lafferty, C., and Snape, C.E., Effect of Lignite Addition and Steam on Pyrolysis of Turkish Oil Shales, Fuel, 71, 1511-14, 1992.
17. Rubel, A.M., and Coburn, T.T., Influence of Retorting Parameters on Oil Yield From Sunburry and Ohio Oil Shales from Northern Kentucky, 1981 Eastern Oil Shale Symposium Proceedings, 1981, Lexington.
18. Minkova, V., Razvigorava, M., Gergova, K., Goranova, M., Ljutzkanov, L., and Angelova, G., Effect of Water Vapour on the Pyrolysis of Solid Fuels 2. Effects of Water Vapour During Pyrolysis of Solid Fuels on Formation of Porous Structure Semicoke, Vol 71, 263, Fuel 1992.
19. Okutan, H., Uzluk, B., Çıtıroğlu, M., and Ekinci E., Pyrolysis of Seyitömer Oil Shale and Lignite Under Different Processing Conditions, Jour. Analy. Pyr., 1993 (submitted).
20. Allred, V.D., Symp. Papers: Synth. Fuels from OS, IGI Atlanta, GA., Dec. 1979
21. Minkova, V., Rajvigorova, M., Goranova, M., Ljutzkanov, L., and Angelova, G., Effect of Water Vapour During the Pyrolysis of Solid Fuels on the Yield and Composition of the Liquid Products, Fuel, Vol. 70, 713, 1991.
22. Çıtıroğlu, M., Pyrolysis Processes and Characterisation Studies on Three Solid Fuels, PhD Thesis, ITU, 1993.
23. Graham, U.M., Rubel, A.M., Robl, T., and Ekinci E., Pyrolysis Processing Characteristics and Product Evaluation of the Turkish Göynük Oil Shale, 1992 Eastern Oil Shale Symposium, Lexington, 1992.
24. Sharma, D.K., Sulimma, A., and Van Heek, K.H., Comparative Studies of Pyrolysis of to Coal in Inert Gas Steam and Hydrogen Under Pressure, Erdol und Kohle-Erdgas Petrochemische, Bd 39, Heft 4, Under, 173, 1986.
25. Levenspiel, O., Chemical Engineering's Grand Adventure, Chemical Engineering Science, Vol. 43, No:7, 1427-1435, 1988.
26. Carter, S.D., Rubel, A.M., Robl, T., and Taulbee, D.N Development of the Kentort II Process for Eastern Oil Shale, DE90, 009680, May 1990.

27. Ekinci, E., Yardım, M.F., Graham, U.M., and Robl, T., An Integrated Pollution Prevention Process for the Utilisation of Göynük Oil Shale, NATO CCMS Workshop on Pollution Prevention Techniques and Technologies, Graz, 1993.
28. Dung N.V., Pyrolysis Behaviour of Australian Oil Shales in a Fluidized Bed Reactor and Material Balance in a Modified Fischer Assay Retort, *Fuel*, 1570, 1989.
29. Carter, S.D., and Taulbee, D.N, Fluidised Bed Retorting of Eastern Oil Shale: An Evaluation of Steam As a Fluidizing Medium, 1984 Eastern Oil Shale Symposium, 267, 1984.
30. Carter, S.C, Robl, T., Rubel, A.M, and Taulbee, D.N, Processing of Eastern US Oil Shale in a Multistage FB, *Fuel*, 1124, 1990.
31. Carter, S.D., and Taulbee DN., Operation of the 5 lb/hr Kentort II Reactor in the Solid Recirculation Mode, *Proceedings of Eastern Oil Shale Symposium*, 1989.
32. Litster, J.D, Newell, R.D, and Bell, P.R, Pyrolysis of Rundle Oil Shale in a Continous Fluidised Bed Retord, *Fuel*, 67, 1327, 1988.
33. Dung, N.V., Wall, G.C., and Kastl, G., Continous Fluidised Bed Retorting of Condor and Stuart Oil Shale in a 150 mm Diameter Reactor, *Fuel* 66, 372-376, 1987.
34. Espitalie, J., Madec, M., and Tissot, B., *Am. Assoc. Petrol. Geol. Bultein*, 64, 59, 1980.
35. Taulbee, D., Coburn, T., Rubel, A.M., Thomas, G., and Yates, L., Analysis of Products from Bench Scale Retorting of Kentucky Oil Shale, 1982 Eastern Oil Shale Symposium Proceedings, 1982, Lexington.
36. Attar, A., Chemistry, Thermodynamics and Kinetics of Reactions of Sulphur in Coal Gas Reactions, *Fuel*, Vol. 57, pp. 201-212, 1978.
37. Burham, A.K., and Ward, R.L., *Oil Shale, Tar Sands and Related Materials*, ACS Symp. Ser. 163: 79, 1981.
38. Rubel, A.M., Morgolis, M.J., Haley, J.K., and Davis, B.H., 1983 Eastern Oil Shale Symposium Proc. 399-405, Lexington Kentucky, 1983.
39. Erdem-Şenatarlar, A. Arabacıoğlu, B., and Ekinci, E., Copyrolysis of Turkish Lignites and Avgamasya Asphaltite, *Proc. of Eastern Oil Shale Symposium*, Lexington, 1992.

40. Saxby, J.D., and Sato, S., Liquid Products from Pyrolysis of Synthetic and Natural Blends of Australian Low Rank Oil Shales and Lignites, *Fuel*, 69 (9), 1109-1112, 1990.
41. Çitiroğlu, M., Okutan, H., Uzluk, B., Erdem-Şenatalar, A., and Snape, C.E., Coprolysis of Turkish Lignites With Oil Shales and Asphaltites, *Proc. ICCS*, 548-551, Newcastle, 1991.
42. Rahimi, P.M., Dawson, W.H., and Kelly, J.F., The Significance of Hydrogen Donor Ability and Characteristics of Heavy Oils/Bitumens in Coprocessing, *ACS Div. Fuel Chem. Div.*, 39, 1988.
43. Fouda, S.A., and Kelley, J.F., Coprocessing of an Eastern Canadian Bituminous Coal and Petroleum Residue, *Proc. of ICSC*, 899-903, Tokyo, 1989.

CHEMICAL KINETICS AND OIL SHALE PROCESS DESIGN

Alan K. Burnham
Lawrence Livermore National Laboratory
Livermore, CA 94551

ABSTRACT. Oil shale processes are reviewed with the goal of showing how chemical kinetics influences the design and operation of different processes for different types of oil shale. Reaction kinetics are presented for organic pyrolysis, carbon combustion, carbonate decomposition, and sulfur and nitrogen reactions.

1. Introduction

The processing of oil shale involves numerous chemical reactions, not only those leading directly to oil and gas generation but also those required for process heat. In addition to desired products, the chemical reactions also generate by-products that can lead to environmentally undesirable emissions. An understanding of all these chemical reactions and their rates can help design processes that minimize the total processing cost, including the cost associated with meeting environmental regulations. The chemical kinetics can be incorporated, where appropriate, into mathematical models that simulate the interaction of various chemical and physical processes.¹⁻³

2. Types of Oil Shale Processes

A first step in understanding the role of chemical reactions in process design is to outline the various kinds of processes that are used to generate shale oil. All oil shale processes require heat to generate oil. Therefore, the first step in designing a process is to decide how to generate the heat and how to transfer it to the raw shale. Many approaches have been tried,⁴ and various authors have attempted to classify these approaches.^{5,6}

Fundamentally, most processes can be separated into four types based on the medium used to heat the shale, i.e., those that use hot gas to heat the shale, those that use hot solids, those that use hot liquids, and those that use electromagnetic radiation. The hot-solids retorts can be further subdivided into two types according to whether the heat carrier is reactive (e.g., burned shale, as in the case of the 4-ton per day retort at LLNL) or inert (e.g., ceramic balls as for the Tosco II process). The hot-gas retorts can be further subdivided into two types: direct (internal combustion) and indirect (external combustion). Both the hot gas and hot liquids might also be subdivided into reactive and unreactive heat carrier types. An example of a reactive hot gas would be high-pressure hydrogen,⁷ although combining high-pressure hydrogen with a solid heat carrier would greatly reduce gas pumping costs. Hot

liquids retorting⁸ might use a recycled hydrogen donor solvent to extract a bitumen.⁹ The electromagnetic types consist of radio-frequency (rf) and solar methods. Radio-frequency energy can penetrate the oil shale and deposit over lengths of meters.¹⁰ Solar methods could be classified in different ways depending how the solar energy is transferred to the shale. Hot-gas and rf methods can be used in situ.

A combustion retort and a hot-recycled-solids retort are shown in Figure 1 along with most of their important chemical reactions. The combustion retort is considered a hot-gas retort because the primary mechanism of heat transfer in the direction of the propagation of the flame front is via the gas phase. The combustion wave can either propagate down a

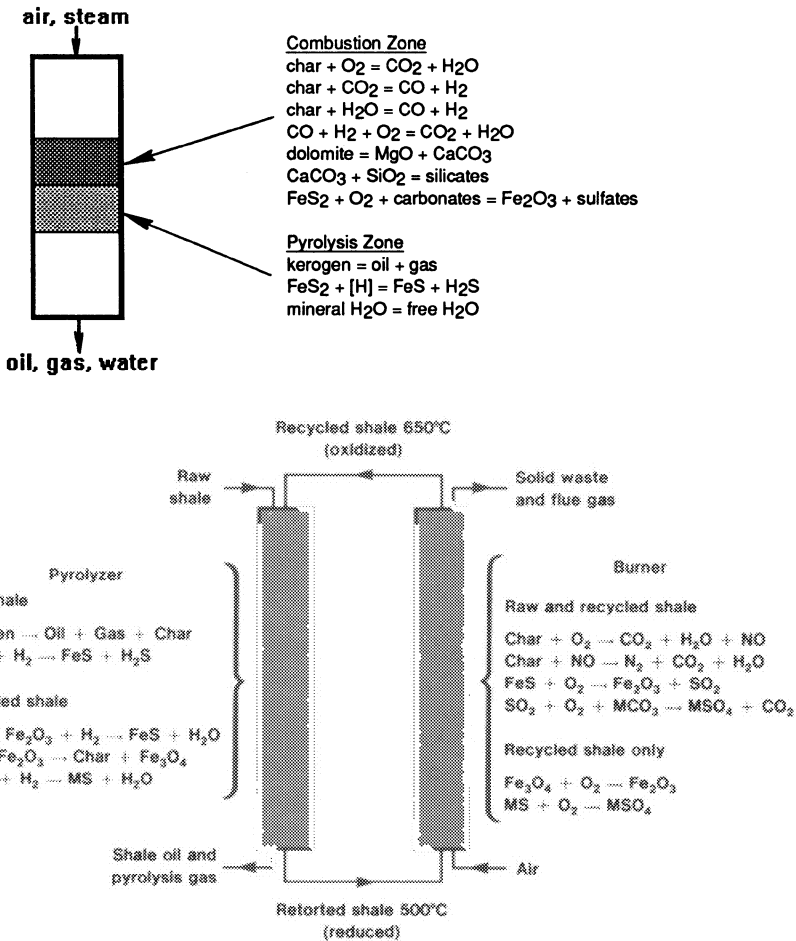


Figure 1. Combustion and hot-recycled-solids retorts with important chemical reactions. In the hot-recycled-solids reactions, M represents magnesium and calcium.

stationary bed or be maintained in a fixed position as the shale passes through the reactor vessel. In some cases, the combustion zone is stabilized by injection of part of the off-gas in the middle of the retort. A disadvantage of the combustion retort is that the off-gas is diluted by N_2 and CO_2 . The hot-recycled-solids (HRS) retort uses iron oxide in the recycled burned shale to scrub most of the sulfur out of the pyrolysis gas, thereby producing a high-quality fuel gas in addition to the shale oil. For carbonate-containing shales, the dilute phase combustion and short residence times allow the residual carbon fuel to be burned with minimum carbonate decomposition, even though the carbonates still effectively scrub the SO_2 produced from iron sulfide oxidation.

An important design aspect is heat transfer. Within this topic, there are two issues: the heat capacity of the heat carrier, and the time it takes to transfer the heat from the carrier uniformly through the raw shale.

For either hot-solids or indirect hot-gas retorts, roughly the same mass of heat carrier must contact the raw shale. The exact ratio depends on the entering temperatures of the raw shale and heat carrier and whether the flow is co-current (same exit temperature) or counter-current (outgoing heat carrier reaches the temperature of incoming shale for more complete heat exchange). Hot-gas retorts are easier to conceive as counter-current, but a counter-current hot-solids retort could be designed based on differences in particle sizes flowing in opposite directions in a fluidized bed.⁶ For hot-gas retorts, since the density of gas is about 1000 times less than shale, a large volume of gas must be pumped through the shale to heat it. This requires a design that balances shale particle size and gas flow rates to make sure that fluidization occurs only where desired.

The time required to transfer the heat from the carrier to the shale depends crucially on particle size, because of both the surface-to-volume ratio and the time needed to conduct the heat to the interior of the particle. The heatup time scales roughly as diameter squared for large particles (>1 cm). Approximate heatup times are 2.5 min for 1 cm, 4 h for 10 cm, and 17 days for 1 m. Breaking rock into small pieces costs money, so one does not want to create any smaller particles than required. However, reactor volumes and process costs increase with processing time, so one needs to reduce the shale to particles sufficiently small for effective processing. In reality, it is impossible to reduce particle size uniformly, so an optimized industry could conceivably involve several processes using different sized shale. Radio-frequency methods avoid traditional heat transfer issues. Instead, the heat is deposited according to the electric field density, enabling one to deposit energy more uniformly in large particles.¹⁰ However, the greater cost of rf energy relative to thermal energy is a disadvantage.

3. Chemical Reaction Rates in Oil Shale Processing

3.1. HYDROCARBON GENERATION AND CRACKING

The most important reaction in oil shale processing is that leading to shale oil. It is possible to develop global rate constants for this reaction that predict the timing of oil generation at virtually all time scales, including rapid fluid-bed retorting, slow in-situ retorting, and even natural petroleum formation. These rate constants can help determine processing times and, consequently, reactor volumes, since reactor volume depends on throughput times the processing time. Rate constants have also been developed for secondary reactions that affect

both oil quality and quantity. The pyrolysis reactions generate gas as well as oil. The composition of the gas depends on the processing time and the way the shale is heated.

An examination of the extensive literature leads to an incredible diversity of kinetic models (reaction networks and rate expressions) for conversion of kerogen to oil and gas. To establish some sense of order, it is useful to establish two guidelines: (1) any activation energy less than 170 kJ/mol (40 kcal/mol) is probably not a valid measure of intrinsic chemical kinetics, and (2) bitumen generation is faster than oil generation by about 25°C at all temperatures, requiring that the mean activation energies cannot be more than a few kcal/mol different. A partial justification of these conclusions is given in a separate paper in this volume.¹¹

As a reference, consider the time scale for hydrocarbon generation from a type I oil shale (Green River Formation) and a generic type II oil shale using kinetics that are reasonable at both laboratory and geological heating rates (type I: $A=5 \times 10^{13} \text{ s}^{-1}$ and 7, 90, and 3% of the potential at 49, 53, and 54 kcal/mol, respectively; type II: $A=3 \times 10^{13} \text{ s}^{-1}$ and 5, 15, 45, 20, 10, and 5% of the potential at 49-54 kcal/mol, respectively). Type I oil shales (50-80% conversion of kerogen to oil) are usually lacustrine and type II oil shales (30-50% conversion to oil) are usually marine. The generation curves for several heating rates of potential interest are shown in Figure 2. The time to complete retorting for the four heating rates are 8 years, 8 days, 50 min, and 2 min. When compared to the heatup times mentioned in the preceding section, it is evident that rapid oil-shale processing (retorting in a few minutes) is limited to particles no greater than a centimeter or so. Slow above-ground processing (retorting within an hour or so) might use particle sizes several times larger. Modified in-situ processing would most likely retort particles between 10 cm and 1 m,

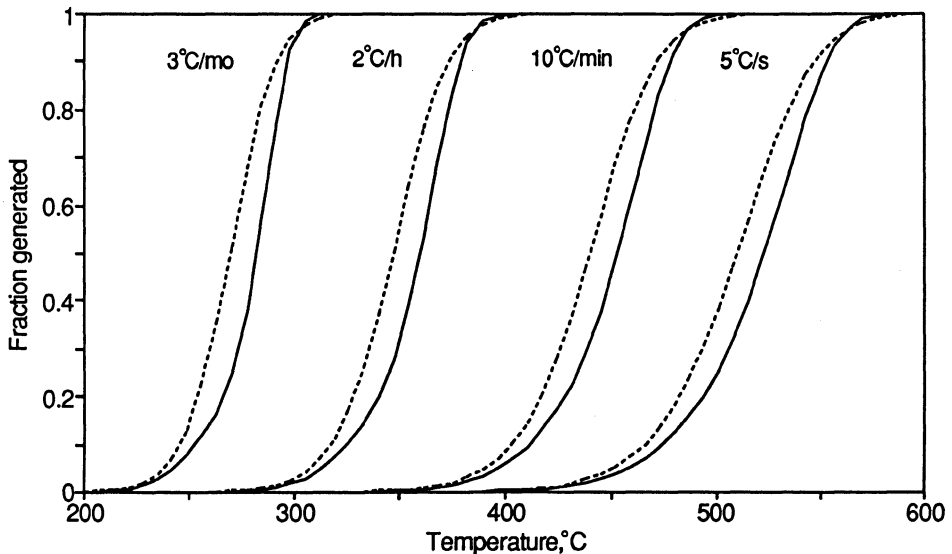


Figure 2. Hydrocarbon generation curves for type II (dashed) and type I (solid) oil shales for shale heated at constant rates ranging from 3°C/mo to 5°C/s.

thereby requiring even longer processing times. These in-situ retorts involve the propagation of a combustion wave down a rubble column, giving effective heating rates at a fixed point ranging from about 1°C/min to about 1°C/h. The slowest heating rate represents the lower limit of human-processing interest and could conceivably represent the processing of very large volumes of oil shale by rf heating.

A more general understanding of the kinetics of oil generation comes primarily from organic geochemistry, both from source rock kinetic analyses and standard Rock-Eval analyses.^{12,13} Type II shales generate most of their oil faster than type I oil shales (e.g., lower Rock-Eval T_{max}), although type II shales contain a broader reactivity distribution that requires about the same time to complete retorting. However, type II kerogen kinetics depend more strongly on natural maturation: the overall reactivity slows by about a factor of two (increase in Rock-Eval T_{max} from 420 to 435°C) as kerogen eliminates its oxygen during diagenesis prior to substantial generation. Type I kerogens ordinarily start with less oxygen in the kerogen, and the kinetics are nearly independent of natural maturation until most of the oil has been generated naturally. The kinetics of both can be accelerated by the incorporation of sulfur during early diagenesis.¹⁴ Oil shales with well-preserved algal bodies, whether of marine or lacustrine origin, have similar kinetics and tend to have an induction time for oil generation.^{15,16}

One special issue for oil generation kinetics from fluidized beds is that most early measurements of this type suffered from a large apparent tail to the generation curve. At first, it was thought that the tail was due to the generation of additional heavy oil.¹⁷ However, more recent work¹⁸ has demonstrated that most of the tail is an artifact of oil adsorption on dust in the apparatus, as shown in Figure 3. When removed, the shape of the pyrolysis curve agrees with that predicted by non-isothermal kinetics.¹⁹ When the oil adsorption artifact is removed, type II oil shales tend to have a longer tail than type I oil shales, which is consistent with the need for an activation energy distribution to describe nonisothermal kinetics.

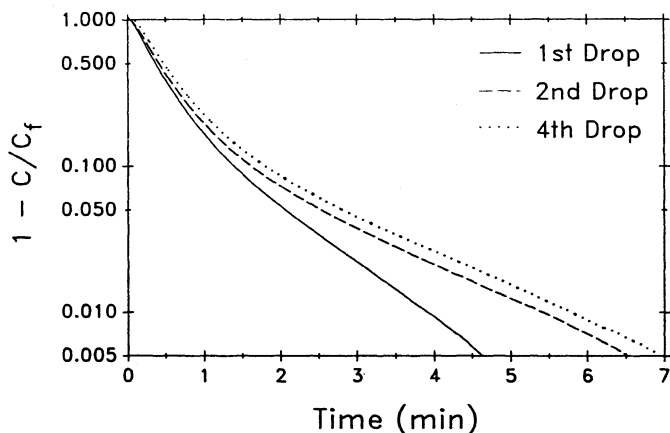


Figure 3. Logarithm of the fraction of remaining potential as a function of time for a type II oil shale (New Albany, 54 L/Mg). The longer tail on the successive drops is due to oil hold-up on a dust filter in the apparatus that accumulates more dust with each drop.

There has been considerable confusion about the relative generation kinetics of oil and gas. Early nonisothermal experiments²⁰ suggested that gas generation from Green River kerogen peaked at a higher temperature, implying slower kinetics, than oil. However, later nonisothermal and isothermal experiments have shown that most of the hydrocarbon gas from type I oil shales has the same kinetics as oil, although some of the methane is generated by a slower process.²¹ For type II oil shales, most of the hydrocarbon gas still has the same kinetics as oil, but a much larger fraction of the methane is generated by the slower process. Hydrogen generation from Green River oil shale peaks and continues to a higher temperature than hydrocarbons during nonisothermal pyrolysis. Hydrogen also shows an induction period for isothermal pyrolysis,²² indicating that it is formed primarily from a product of kerogen decomposition. Therefore, more complete retorting should give a higher hydrogen content in the product gas.

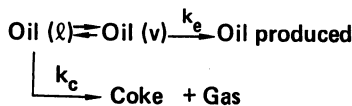
Oil yield depends on heating rate because of secondary reactions, as shown in the general scheme in Figure 4.²³ Oil yield decreases with heating rate due to liquid-phase coking reactions. The coking tendency is related to the aromatic content of the oil so has a larger effect for type II shales than type I shales. The beneficial aspect of coking is that it tends to increase oil quality by increasing the H/C ratio and decreasing nitrogen content. Pressure seems to enhance coking, at least initially, by increasing the liquid-phase residence time.²⁴

Oil cracking decreases oil yield by converting aliphatic material to mostly gas. Most published oil-cracking kinetics suffer from an artificially low apparent activation energy, probably because of the distribution of reactions occurring. The role of pressure on oil cracking is complicated.²⁵ At high temperatures, pressure increases chain transfer reactions that increase the destruction of a particular molecule, but the overall conversion to gas is partially mitigated by enhanced recombination and alkylation reactions. At temperatures below about 350°C, recombination reactions dominate, so pressure actually decreases the overall cracking rate. Oil cracking and coking are accelerated by the presence of a clean mineral surface and can be modeled by an adsorption isotherm approach.²⁶

- Oil production



- Oil coking



- Oil cracking

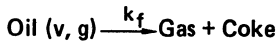


Figure 4. Kinetic scheme for oil generation and destruction. Coking occurs in the liquid phase producing mostly coke; cracking occurs in the gas phase producing mostly gas.

High-pressure hydrogen increases oil yield by providing the driving force to prevent recombination reactions by reactive fragments, and the increased yield is primarily aromatic oil.^{27,28} The yield enhancement is especially important for type II oil shales because they tend to be more hydrogen deficient.⁷

It has been proposed that steam has a beneficial effect on the organic reactions of oil shale retorting.²⁹ At present, it seems certain that steam decreases the pour point of the oil³⁰ and gives a slight yield enhancement,^{31,32} possibly due to the inhibition of surface-catalyzed coking reactions.³³ However, a purported increase in oil generation rate²⁹ seems to be an artifact of the experimental apparatus because it is not observed in other experiments.³⁴

A separate paper by myself in this volume addresses the mechanism of oil generation and that kerogen in most oil shale breaks down initially into soluble material and then into volatile oil and gas, though not by an ideal serial reaction. Some have proposed that kerogen be extracted by thermal dissolution, thereby recovering a higher fraction of the organic matter.³⁵ It is often postulated that, once the organic matter is in a form that can access catalysts, a more efficient pathway to products might be achievable than via the traditional thermal cracking. The relevant kinetic issue is the time-temperature severity required to extract the kerogen. Miknis³⁶ found that nearly all the kerogen from Green River shale could be recovered as oil and bitumen in 20 minutes at 425°C. Actual kinetic parameters for bitumen generation are much less well determined than for oil generation; most published activation energies are too low for the reasons discussed earlier. The low apparent activation energies predict that kerogen is not stable on a geologic time scale, although we know that the natural generation of bitumen occurs at about 100°C. The correct activation energies appear to be about 210 kJ/mol (50 kcal/mol).

3.2 THE ROLE OF SULFUR IN PYROLYSIS

Sulfur in the kerogen is important for two reasons: (1) it affects the overall generation rate of oil and gas, and (2) it leads to sulfur species in both the oil and gas that must be removed. Although the factors affecting the relative generation kinetics of various kerogens are not clearly understood, the evidence that organic sulfur accelerates the process is strong.¹⁴ High-sulfur kerogens, such as in the Monterey shale, produce oil as much as 50°C in Rock-Eval pyrolysis lower than well-preserved, low-sulfur algal kerogens, such as the Green River oil shale. Less well understood is the effect on the activation energy. Ordinary pyrolysis gives activation energies about 220 kJ/mol.^{12,37} Other work³⁸ tends to overestimate the effect of sulfur on the activation energy due to the assumption of a single first-order reaction.

Sulfur in the oil and gas can affect upgrading and utilization costs. The sulfur content of the oil depends primarily on the sulfur content of the kerogen.³⁹ Incorporation of inorganic sulfur into the oil seems to be minor. Sulfur content of the gas depends on both kerogen and pyritic sulfur. The reactions leading to sulfur-containing gases occur slightly faster than the overall kerogen decomposition rate.⁴⁰ Pyrite reacts with both water and organics during pyrolysis to produce additional sulfur-containing gases. The rate of this reaction depends on both the reactivity of the pyrite (primarily particle size)⁴¹ and the gas-solid contact.⁴⁰ About 95% of the gaseous sulfur is in the form of H₂S, with most of the remainder in methanethiol, ethanethiol, and carbonyl sulfide.⁴² There seems to be little difference in the relative amounts of H₂S and mercaptans formed from organic and inorganic sulfur, although

inorganic sulfur does not form thiophenic compounds.⁴³ Some shales contain a separate (Mg,Fe)CO₃ phase, which decomposes readily at or below 500°C, providing a source of iron to capture H₂S as FeS. The iron-rich surface layer of ankeritic-dolomite can also capture some sulfur. In hot-recycled solids retorts, iron oxide formed from combustion of iron sulfides is an effective capture agent. However, the fate of the captured sulfur in the combustor depends on the presence or absence of carbonates, as discussed in the next section.

3.3 HEAT SOURCE AND SINK REACTIONS

Although the enthalpy of the conversion of kerogen to oil and gas is fairly small, oil-shale processing requires a substantial heat source because the sensible heat recovered from the products is usually far less than required to heat the raw shale to pyrolysis temperatures. Oil-shale retorting leaves a carbonaceous residue, and efficient oil-shale processes will burn this residue to provide process heat (about 380 kJ/kg shale per wt% residual C). Oxidation of sulfide minerals can lead to a substantial exothermic contribution (107-320 kJ/kg per wt% sulfur, depending on the pyrite/pyrrhotite ratio and the degree of sulfate formation). Decomposition of carbonate minerals can be a substantial heat sink (18-28 kJ/kg per wt% CO₂, depending on the degree of silication). Gasification of char by the mineral CO₂ is also endothermic, but oxidation of the resulting CO in the gas stream is exothermic. The sulfide, carbonate, and gasification reactions are affected by steam. Carbonate minerals also play a key role in reducing sulfur dioxide in the flue gas.

The reactivity of the pyrolysis residue (char) to oxygen and other gases depends on its generation history, with rapid pyrolysis leading to more a more reactive char.^{44,45} The reason for the heating rate dependence is not known. The limited information on surface area suggests that the surface areas are not substantially different. The residues from Green River shale at all heating rates are far more reactive than typical coals, probably because of the higher hydrogen content. There are two practical implications of this high reactivity: (1) the oxidation reactions are diffusion-limited except for small particles at relatively low temperatures,⁴⁶ and (2) the residence time in the combustion zone does not have to be very long for hot recycled shale retorts using fine particles. For the small particles associated with the HRS process, most of the fuel value of the char can be extracted in less than one minute residence time at 530°C, and substantially less at a more typical combustor temperature of 700°C.³ In contrast, diffusion limitations cause combustion times of 1-2 days at comparable temperature for the 15-cm particle sizes typical of modified in-situ retorts.⁴⁷

The carbonate decomposition reactions, for those shales that have carbonate, depend on gas atmosphere, as shown in Figure 5.^{48,49} Decomposition of dolomite is only weakly and indirectly affected by CO₂; the primary difference is in whether CaO or CaCO₃ is formed. Calcite decomposition is frequently inhibited because of its low equilibrium vapor pressure. In a flue gas containing 15% CO₂, the calcite cannot decompose to CaO unless T is greater than about 800°C, although it does react directly at lower temperatures with quartz and other silicates. Most of the iron contained in carbonates in Green River shale is ordinarily contained in the dolomite, often in an iron-rich surface layer³⁴ that decomposes slightly faster than the bulk.

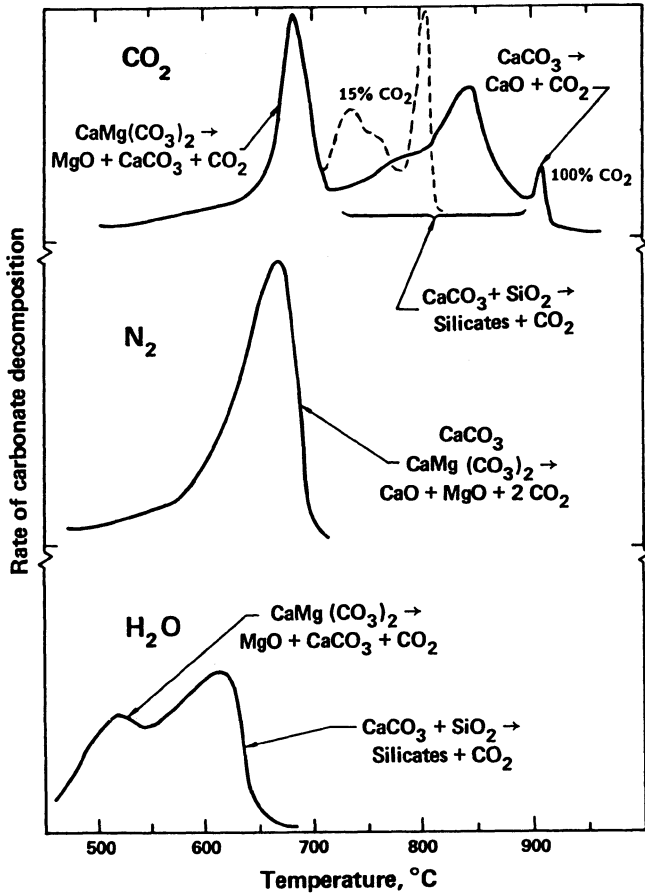


Figure 5. Thermal decomposition profiles of carbonate minerals in Green River shale heat at $2^{\circ}\text{C}/\text{min}$ in various gas atmospheres.

The sulfur captured during pyrolysis either by iron carbonates or recycled iron oxides, when returned to the combustor in a HRS process, provides additional heat to the process. The kinetics of capture are favorable for both Green River and New Albany shale, but the net heat gain is slightly different for the two cases because about 30% more energy can be obtained forming sulfates from carbonates than by forming SO_2 in the absence of carbonates.⁴⁰

The overall energy released during combustion depends on spent shale composition and the final products. Char and pyrite are the major energy sources, and carbonate, if present, is the major heat sink when the temperature is high enough to decompose it. The fraction of kerogen carbon remaining in the shale correlates with both the H/C ratio of the kerogen and pyrolysis conditions. Most marine shales, such as the Eastern U.S. Devonian shales, leave a much higher fraction of their carbon as char.

The amount of heat required for the process depends largely on the exit temperature of the products. About 700 kJ/kg of heat is required for products of Green River shale exiting at 500°C.^{50,51} The heat requirement increases from 600 to 800 kJ/kg over the range of 20 to 200 L/Mg, and the distribution of sensible heat between volatile and solid products and the contribution of heats of reaction vary. The spent shale organic carbon is roughly equal to 0.028 times the oil yield in L/Mg, so the retorting process would be energy self-sufficient at 65 L/Mg for no pyrite oxidation or carbonate decomposition. A higher grade would be needed to sustain the process if the shale in an HRS process leaves the recycle loop at the peak combustion temperature, as discussed in the next paragraph. Type II shales have a much higher coke/oil ratio, so they would be energy self-sufficient at lower oil grades than type I shales.

The excess energy in the char of shale grades that would be exploited first might be used to generate electricity. Such a scheme markedly increases the economics of processing Green River Formation oil shale,⁵² where the flue gas is self-scrubbed by the carbonate minerals. For Eastern U.S. Devonian oil shales, there is more carbon available, but this advantage is counter-balanced by the lack of carbonates to scrub SO₂. The Kentort II process⁵³ (and Carter in this volume) adds a gasification reactor section to maximize the recovery of the fuel value as a reduced gas, thereby allowing removal of the sulfur as H₂S rather than as a more difficult, dilute SO₂ in the flue gas. The economic value of the H₂S is then recovered as elemental sulfur rather than electricity. The gasification also removes a potential source of acid drainage from the disposed spent shale.

Counter-current combustion retorts (e.g., Paraho direct) have the advantage that the inlet air can cool the shale to about 200°C, thereby potentially reducing the heat required by about 200 kJ/kg, equivalent to the fuel value of 0.5 wt% C. In practice, however, counter-current retorts require large enough particles that carbon accessibility is severely limited by diffusion, thereby cancelling any beneficial effect of heat exchange. Furthermore, the increased time and temperature required to access the carbon causes more carbonate decomposition for dolomite-containing oil shales, thereby cancelling most of the energy gain.

3.4 COMBUSTION EMISSIONS

Environmental considerations will undoubtedly limit SO₂ and NO_x emissions: no more than 0.001 kg SO₂/kg oil and 2.5 10⁻⁷ kg NO_x/kJ of combustion energy in Colorado. Fortunately, there are favorable reactions in some oil shales that minimize emissions.

The high Ca/S ratio in Green River shale makes sulfur capture very thorough at high temperatures; the important question for kinetics is whether the SO₂ can be captured at the relatively low combustion temperatures desired to minimize carbonate decomposition. The capture reactions are quite effective for temperatures greater than 530°C. Release of <0.1% of the sulfur is easily achieved, which corresponds to <10⁻⁴ kg SO₂/kg oil for a shale containing 1 wt% S and yielding 15 wt% oil. Ca-Mg sulfates are formed below 650°C, apparently by a direct reaction of the SO₂ with the dolomite, and Ca sulfate is formed at higher temperatures.⁴⁰ However, shales with above average sulfur content would need higher temperatures because of the inhibition of a surface sulfate layer on the capturing carbonate at low temperature.⁵⁴

The combustion reactions also lead to NO_x through oxidation of fuel nitrogen and mineral nitrogen. The relative amounts of each depend on the shale. The resulting NO_x levels are strongly affected by secondary reactions with the carbonaceous residue, inorganic components, and co-generated ammonia. Early work found that (1) retorted shale was an effective reductant of NO_x ,⁵⁵ (2) most of the NO_x was formed after most of the carbon was burned,⁵⁶ and (3) the mineral nitrogen source, buddingtonite, burned slower than the char.⁵⁶ This led to the hypothesis that the char limited the survival of NO_x until the char was gone, then oxidation of mineral nitrogen could result in NO_x . The kinetic model shown in Figure 6 reproduced the experimental results. More recently it has been found that oxidized shale under the correct conditions can serve as a de- NO_x catalyst,⁵⁷ and work is in progress to use that property to minimize NO_x emissions from Green River oil shale.

Reactions:

char \rightarrow CO_2 by k_1

Inorganic N \rightarrow NO by k_2

NO \rightarrow N_2 by k_3

$$\text{NO}_x(t) = \frac{k_2 N_o \exp(-k_2 t)}{1 + k_3 \tau C_o \exp(-k_1 t)}$$

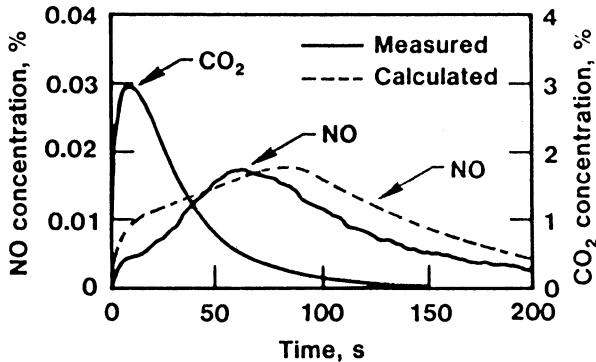


Figure 6. CO_2 and NO release from Green River Formation oil shale during combustion at 540°C in a bed of sand fluidized with 10% O_2 . The model assumes that NO is formed from inorganic nitrogen and destroyed by reaction with char, where τ is a contact time.

3.5 CONCLUDING REMARKS

There are many ways to design an oil shale retort, and advances in the understanding of oil shale chemistry has aided the conceptual development of new oil shale processes. Hot-recycled-solids processes can achieve high yield while processing the shale completely in less than 5 minutes with minimal environmental impact. Prospects are excellent for producing a nonhazardous spent shale while minimizing air emissions. Furthermore, the overall thermal efficiency (energy in shale oil and net electricity produced per energy content of raw shale plus input from mining, transportation and capital equipment) of an HRS plant co-generating of electricity²⁶ exceeds earlier processes.⁶ Including estimates for the energy value of fuel, explosives, and capital goods according to the estimates of Gwyn et al., thermal efficiencies are estimated at 75-80% for oil yields of 90-100% of Fischer assay from 125 L/Mg (0.8 bbl/tonne) oil shale. Ironically, it was questioned in a congressional debate during the writing of this article that it may not be possible to recover shale oil with a net energy gain. A subsequent vote may have ended U.S. oil shale research for the foreseeable future, leading it to yet another nadir.

Acknowledgements. This work was performed under the auspices of the U.S. Department of Energy by the Lawrence Livermore National Laboratory under contract W-7405-Eng-48.

References

1. Lewis, A. E., and Braun, R. L. (1981) *J. Energy* **5**, 355-361.
2. Braun, R. L., Diaz, J. C., and Lewis, A. E. (1984) *Soc. Petrol. Eng. J.* **23**, 75.
3. Cena, R. J., and Thorsness, C. B. (1992) *25th Oil Shale Symp. Proc.*, J. H. Gary, ed., Colo. School of Mines Press, Golden, CO, pp. 187-214.
4. Baughman, G. L. (1978) *Synthetic Fuels Handbook*, 2nd Ed., Cameron Engineers, Denver, CO.
5. Lewis, A. E., Braun, R. L., and Diaz, J. C. (1984) *17th Oil Shale Symp. Proc.*, J. H. Gary, ed., Colo. School of Mines Press, Golden, CO, pp. 1-16.
6. Gwyn, J. E., Roberts, S. C., Hinds, G. P. Jr, Hardesty, D. E., and Johnson, G. L., *13th Oil Shale Symp. Proc.*, J. H. Gary, ed., Colo. School of Mines Press, Golden, CO, pp. 35-45.
7. Roberts, M. J., Rue, D. M., and Lau, F. S. (1991) *1990 Eastern Oil Shale Proc.*, J. Stivers, ed., Institute for Mining and Minerals Research, Lexington, KY, pp. 323-341.
8. Cha, C. Y., Guffey, F. D., and Fahy, L. J. (1989) *1988 Eastern Oil Shale Proc.*, D. J. Lazar, ed., Institute for Mining and Minerals Research, Lexington, KY, pp. 301-311.
9. Baldwin, R. M., Lane, G. S., and Chen, K. W. (1985) *18th Oil Shale Symp. Proc.*, J. H. Gary, ed., Colo. School of Mines Press, Golden, CO, pp. 176-181.
10. Bridges, J. E., and Sresty, G. C. (1991) *24th Oil Shale Symp. Proc.*, *Quart. Colo. School of Mines* **83**, 35-43.
11. Burnham, A. K. (1993) this volume
12. Tissot, B. P., Pelet, R., and Ungerer, P. (1987) *AAPG Bulletin* **71**, 1445-1466.
13. Braun, R. L., Burnham, A. K., and Reynolds, J. G., and Clarkson, J. E. (1991) *Energy & Fuels* **5**, 192-204.

14. Tegelaar, E. W. (1993) unpublished results.
15. Bar, H., Ikan, R., and Aizenshtat, Z. (1988) *J. Anal. Appl. Pyr.* **14**, 73-79.
16. Klomp, U. C. and Wright, P. A. (1990) *Org. Geochem.* **16**, 49-60.
17. Wallman, P. H., Tamm, P. W. and Spars, B. G. (1981) in *Oil Shale, Tar Sands, and Related Materials*, ACS Symp. Ser. 163, H. C. Stauffer, ed., American Chemical Society, Washington, pp. 93-113.
18. Coburn, T. T., Taylor, R. W., and Morris, C. J. (1989a) *1988 Eastern Oil Shale Proc.*, J. Stivers, ed., Institute for Mining and Minerals Research, Lexington, KY, pp. 325-332.
19. Burnham, A. K., Braun, R. L., Taylor, R. W. and Coburn, T. T. (1989) *Preprints ACS Div. Petrol. Chem.* **34**(1), 36-42.
20. Huss, E. B., and Burnham, A. K. (1982) *Fuel* **61**, 1188-1196.
21. Reynolds, J. G., Crawford, R. W., and Burnham, A. K. (1991) *Energy & Fuels* **5**, 507-523.
22. Richardson, J. H., Huss, E. B., Ott, L. L., Clarkson, J. E., Bishop, M. E., Taylor, J. R., and Morris, C. J. (1982) Lawrence Livermore National Laboratory Report UCID-19548.
23. Campbell, J. H., Koskinas, G. H., Stout, N. D., and Coburn, T. T. (1978) *In Situ* **2**, 1-47.
24. Burnham, A. K., and Singleton, M. F. (1983) in *Geochemistry and Chemistry of Oil Shales*, ACS Symp. Ser. 230, F. P. Miknis and J. F. McKay, eds., American Chemical Society, Washington, pp. 335-351.
25. Mallinson, R. G., Braun, R. L., Westbrook, C. K., and Burnham, A. K. (1992) *I&EC Res.* **31**, 37-45.
26. Wallman, P. H., Fields, D. B., Morris, C. J., Singleton, M. F., Thorsness, C. B., and Watkins, B. E., (1991) Lawrence Livermore National Laboratory Report UCRL-JC-108770, presented at the *6th Australian Workshop on Oil Shale*.
27. Burnham, A. K., and Happe, J. H. (1984) *Fuel* **63**, 1352-1356.
28. McMahon, M. A., and de Paz, E. F. (1989) *22nd Oil Shale Symp. Proc.*, J. H. Gary, ed., Colo. School of Mines Press, Golden, CO, pp. 127-137.
29. Allred, V. D. (1979) *12th Oil Shale Symp. Proc.*, J. H. Gary, ed., Colo. School of Mines Press, Golden, CO, p. 241.
30. Burnham, A. K. (1981) unpublished results.
31. Carter, S. D. and Taulbee, D. N. (1986) *Fuel Proc. Technol.* 251-72.
32. Dung, N. V. (1990) *Fuel* **69**, 497-501.
33. Coburn, T. T., and Morris, C. J. (1991) *1990 Eastern Oil Shale Proc.*, J. Stivers, ed., Institute for Mining and Minerals Research, Lexington, KY, pp. 289-297.
34. Coburn, T. T., Taylor, R. W., and Morris, C. J. (1989b) *22nd Oil Shale Symp. Proc.*, J. H. Gary, ed., Colo. School of Mines Press, Golden, CO, pp. 118-126.
35. Patzer J. F., Moon, W. G., Jones, G. L., and King, A. B. (1986) *Chem Eng. Sci.* **41**, 1005-1011.
36. Miknis, F. P., Turner, T. F., Berdan, G. L., and Conn, P. J. (1987) *Energy & Fuels* **1**, 477-483.
37. Jarvie, D. M. (1991) *Chem. Geol.* **93**, 79-99.
38. Hunt, J. M., Lewan, M.D., and Hennet, J.-C. (1991) *AAPG Bulletin* **75**, 795-807.
39. Burnham, A. K. (1991) *Energy & Fuels* **5**, 205-214.

40. Burnham, A. K., and Taylor, R. W. (1982) *15th Oil Shale Symp. Proc.*, J. H. Gary, ed., Colo. School of Mines Press, Golden, CO, pp. 299-319.
41. Hoare, I. C. (1987) *Proc. 4th Australian Workshop on Oil Shale*, pp. 113-120.
42. Wong, C. M., Crawford, R. W., and Burnham, A. K. (1984a) *Anal. Chem.* **56**, 390-395.
43. Wong, C. M., Crawford, R. W., and Burnham, A. K. (1984b) *Prepr. ACS Fuel Div.*, **29**(3), 317-321.
44. Fujumoto, R. D., Braun, R. L., Taylor, R. W., and Morris, C. J. (1987) *Energy & Fuels* **1**, 320-323.
45. Thorsness, C. B., Watkins, B. E., Aldis, D. F., and Morris, C. J. (1992) *25th Oil Shale Symp. Proc.*, J. H. Gary, ed., Colo. School of Mines Press, Golden, CO, pp. 55-70.
46. Aldis, D. F., Singleton, M. F., Watkins, B. E., Thorsness, C. B., and Cena, R. J. (1992) *25th Oil Shale Symp. Proc.*, J. H. Gary, ed., Colo. School of Mines Press, Golden, CO, pp. 71-93.
47. Mallon, R. G., and Braun, R. L. (1976) *Quart. Colo. School of Mines* **71**(4), 309-333.
48. Campbell, J. H. (1978) *The Kinetics of Decomposition of Colorado Oil Shale. II. Carbonate Minerals*, Lawrence Livermore National Laboratory Report UCRL-52089-2.
49. Burnham, A. K., Stubblefield, C. T., and Campbell, J. H. (1980) *Fuel* **59**, 871-877.
50. Camp, D. W. (1987) *20th Oil Shale Symp. Proc.*, J. H. Gary, ed., Colo. School of Mines Press, Golden, CO, pp. 187-214.
51. Burnham, A. K. (1989) *Energy* **14**, 667-674.
52. Wallman, P. H. (1992) *Energy* **17**, 313-319.
53. Carter, S. D. and Taulbee, D. N. (1990) *1989 Eastern Oil Shale Proc.*, D. J. Lazar, ed., Institute for Mining and Minerals Research, Lexington, KY, pp. 511-518.
54. Taylor, R. W., Morris, C. J., and Coburn, T. (1989) *1988 Eastern Oil Shale Proc.*, D. J. Lazar, ed., Institute for Mining and Minerals Research, Lexington, KY, pp. 147-161.
55. Taylor, R. W., and Morris, C. J. (1984) *Prep. ACS Div. Petr. Chem.* **29**(1), 277-283.
56. Taylor, R. W., Morris, C. J., and Burnham, A. K. (1985) *18th Oil Shale Symp. Proc.*, J. H. Gary, ed., Colo. School of Mines Press, Golden, CO, pp. 278-290.
57. Reynolds, J. G., Taylor, R. W., and Morris, C. J. (1992) *Prepr. ACS Fuel Chem. Div.* **37**(4), 1840-1846.

HYDROPYROLYSIS: FUNDAMENTALS, TWO-STAGE PROCESSING AND PDU OPERATION

M.J. ROBERTS
Institute of Gas Technology
3424 South State Street
Chicago
Illinois 60616
USA

C.E. SNAPE and S.C. MITCHELL
University of Strathclyde
Dept. of Pure & Applied Chemistry
Glasgow G1 1XL
United Kingdom

ABSTRACT Fundamental aspects of hydrolysis in terms of how both reaction conditions and reactor geometry affect product yields and compositions are reviewed, followed by a description of the pressurised fluidised-bed hydroretorting (PFH) process developed at the Institute of Gas Technology (IGT) as an example of an oil shale hydroretorting process that has been successfully operated on a PDU scale. The use of low temperatures and long solids residence times in well-swept fixed- and fluidised-bed reactors are essential to achieve high selectivity to liquid products in hydrolysis. For oil shales, hydrogen pressures of *ca* 5-10 MPa are generally sufficient to approach the maximum economical oil yield compared to those of over 30 MPa for coals, unless suitable dispersed catalysts are used. Hydrolysis oils generally more aromatic with lower heteroatom contents with increasing hydrogen pressure. The PFH process developed at IGT has been scaled-up from a 100 g batch unit to a 100 kg hr⁻¹ semi-continuous PDU. To assess the potential oil yields from PFH, a hydroretorting assay unit was used extensively. Compared to Western U.S. (Eocene, Type I kerogen) oil shales, which give high oil yields in conventional retorting processes, Eastern Devonian shales (Type II kerogens) have considerably lower atomic H/C ratios which severely restricts the attainable oil yields. In hydroretorting at 538°C and 6.9 MPa, the oil yields from Eastern U.S. shales were substantially improved and usually doubled using the PFH process.

1. Introduction

Hydrolysis, or hydroretorting, refers to pyrolysis conducted using relatively high hydrogen pressures and is potentially an attractive route for the production of liquid fuels from both oil shales and coals. Historically, hydrolysis has received considerably more attention in relation to coal liquefaction and gasification⁽¹⁻³⁾ probably due to their volatile matter contents being considerably lower than those of most oil shales which gives rise to a much greater potential for improving liquid yields. Nevertheless, hydroretorting is still an attractive option for the production of liquid fuels from oil shales, particularly for those classified as type II kerogens where the liquid yields are significantly higher than in standard assays^(4,5). For coal liquefaction, hydrolysis provides a process configuration that avoids the use of recycle solvent which constitutes up to two-thirds of

the reactor stream for conventional liquefaction processes. Although technology for feeding ground solids into high pressure reactors is well-established, coal pyrolysis processes are usually associated with relatively low conversions to liquid products⁽¹⁻³⁾. Further, hydrogen consumptions are high due to large quantities of methane invariably being produced via char hydrogasification and cracking of the primary volatiles at temperatures above 600°C, normally required to achieve substantial liquid yields. Selectivity to liquid products can be improved by operating at relatively low temperatures (*ca* 500°C) where methane yields are below 3% daf coal/shale but long solids residence times are required to maximise liquid yields.

Fundamental aspects of hydrolysis in terms of how both reaction conditions and reactor geometry affect oil yields, selectivity and composition are reviewed here with the development of the pressurised fluidised-bed hydroretorting (PFH) process at the Institute of Gas Technology (IGT), an example of an oil shale hydroretort that has been successfully operated on a PDU scale.

2. Fundamental aspects

2.1 REACTOR TYPES

To investigate the effects of hydrogen pressure on conversions for solid fuels, fixed-bed^(1,3, 6-8), wire-mesh (captive sample)^(1,3 9-11) and entrained-flow reactors^(2, 12) have been studied extensively, together with the small-scale fluidised-beds described in Section 4. The characteristics of these different reactors are summarised in Table 1. In all cases, the use of small particles (*ca* < 200 μ) is desirable to overcome mass transfer restriction to volatiles release.

Table 1 Comparison of reactors used for small-scale experiments

	Fixed-bed	Fluidised-bed	Wire-mesh	Entrained-flow
Sample size, g	> 1	> 1	0.01	> 1
Heating rate, °C s ⁻¹	0.01-10	> 1000	> 1000	> 1000
Pressure range, MPa	0.1-30	0.1-7	0.1-10	0.1-10
Solids residence time, s	> 100	> 100	1-30	1-10
Effective sweep gas through particles	Yes	Yes	No	No
Temp. for max. yields, °C	500-650	500-650	> 800	> 800

The scope of this review precludes an in-depth analysis of each type of reactor (see references 1,3 and 11 for comprehensive descriptions) but in terms of maximising the selectivity to liquid products, the use of low temperatures and long solids residence times (fluidised and fixed-beds) are essential. For entrained flow reactors^(2, 11) with equally short vapour and solids residence times, high temperatures (*ca* > 800°C) are required to achieve conversions comparable to the volatile matter of solid fuels. The consequence of using high hydrogen pressures is that the volatiles are hydrocracked to yield predominantly methane and light aromatics (benzene, toluene, xylene). Thus, their main application has been for hydrogasification and are not considered further here.

Heated-grid or wire-mesh reactors provide extremely high heating rates and minimise secondary cracking reactions due to the small sample bed and minimal heating of the surrounding sample volume.^(1,3,9-11) However, high temperatures are required to attain high conversions because, even if the carrier gas can be swept through the sample grid, the gas velocities remain low compared to those used in fixed and fluidised-beds. As a consequence, overall conversions have been found to actually decrease with increasing hydrogen pressure (although methane and light aromatic yields have been found to increase due to some hydrocracking taking place within the actual sample). This is because the increased resistance to mass transfer is not overcome by the beneficial effects of hydrogen transfer in promoting bond cleavage reactions which lead to higher conversions. Further, as with entrained-flow reactors, the high temperatures used gives rise to high methane and light aromatic yields, with poor overall selectivity to liquid products (% liquids/% hydrocarbon gas).

For the reasons outlined above, fixed-bed reactors have received the most attention for fundamental work where the objective has been to maximise liquid yields and selectivity. Although heating rates are generally limited by their high thermal mass, the use of large sample sizes means that mass balances and product analysis are relatively straight forward. Further, the use of slow heating rates means that intrinsic kinetics can be probed when the volatiles are analysed on-line, for example, via mass spectrometry⁽⁸⁾.

2.2 FIXED-BED REACTORS

2.2.1 Temperature, pressure and heating-rate effects. The combination of relatively small sample beds and high sweep gas velocities in fixed-bed reactors should, in principle, be sufficient to overcome mass transfer limitations to volatiles release. Once this has been achieved, liquids yields increase linearly with hydrogen pressure to over 30 MPa for bituminous coals as shown in Figure 1. However, if the gas velocity through the devolatilising particles falls below the critical value necessary to prevent mass transfer effects, decreased oil yields can be observed with increasing pressure (Figure 1, constant volumetric flowrate, i.e. gas velocity decreases linearly with increasing pressure). For oil shales classified as both Type I and II kerogens, significant increases in conversion are achieved as the pressure is raised from atmospheric to 5 MPa (Table 2). The increases are most pronounced for the Type II kerogen but, notably for both samples, these are relatively small above *ca* 50 bar. Table 2 indicates that at 520°C the selectivity to liquid products is

Table 2 Effect of pressure on hydropyrolysis yields from Goynuk (Type I) and Kentucky (Type II) oil shales at 520°C.

	Pressure (Mpa)	Char	% daf basis	
			Oil	C ₁ -C ₄ gases
Goynuk	0.1 ^a	29	60	3.3
	5	13	77	4.3
	15	8	81	5.8
Cleveland	1	53	41	2.0
	50	27	68	2.6
	150	22	69	3.4

^a = nitrogen

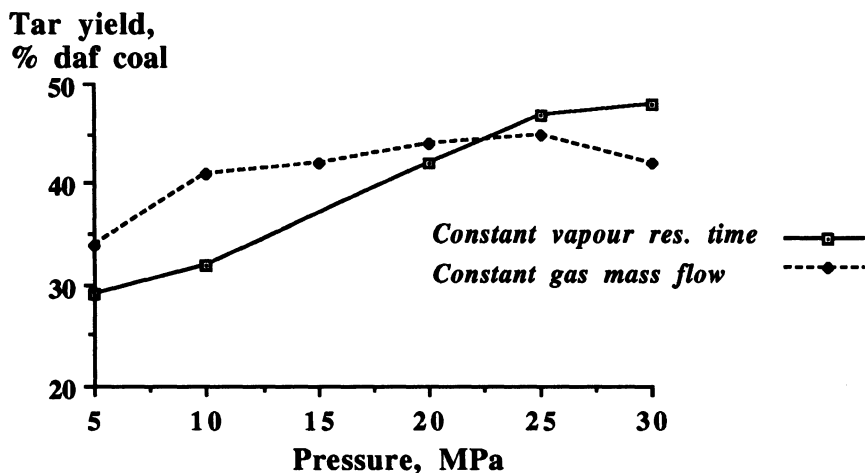


Figure 1 Effect of hydrogen pressure on tar yield for a bituminous coal.

extremely high for oil shales where the oil yield passes through a broad maximum. For coals, the highest oil yields are obtained at somewhat higher temperatures but the selectivity to liquid products is lower due to high methane yields.

At high hydrogen pressures, slow heating has been found to give rise to both increased conversions and tar yields, the effect being particularly noticeable for low-rank coals (Figure 2). This effect contrasts with the situation for inert gases where faster rates tend

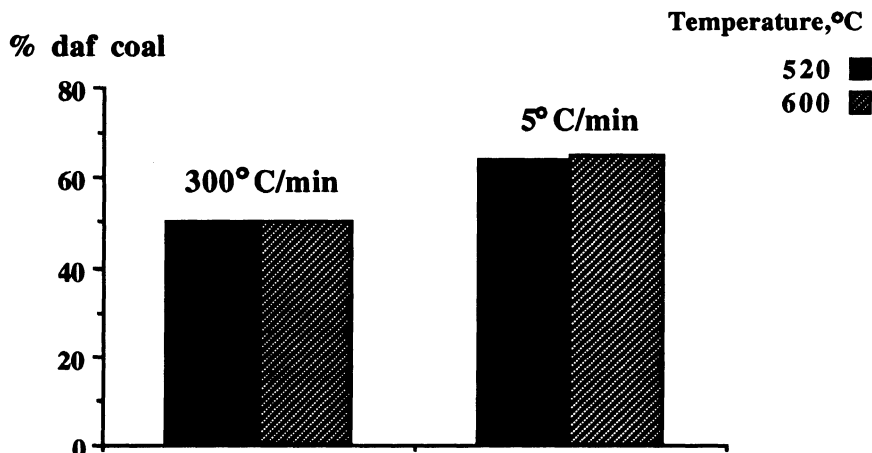


Figure 2 Comparison of tar yields obtained from Wyodak sub-bituminous coal with relatively fast and slow heating rates in fixed-bed hydrolysis at 15 MPa pressure.

to favour higher yields of liquid products in most reactor types (1,3,9). In hydropyrolysis, the slower the sample passes through the critical temperature window around 400°C, the more favourable it should be for forming liquid products. This is due to bond cleavage reactions being promoted prior to any retrogressive chemistry, which at higher temperatures leads to char formation.

2.2.2 Oil composition. Increases in hydrogen pressure invariably give rise to more aromatic oils (lower atomic H/C ratios) with lower heteroatom contents and molecular mass distributions (7,13,14) but the differences tend to be less pronounced for oil shales than for coals (4) as a consequence of the generally lower devolatilisation temperatures. For coals, little variation in bulk composition is observed as a function of rank due to the relative high severity of hydropyrolysis. Further, catalysts (see following) have little effect on the molecular mass profiles for oils (13,14), demonstrating that the composition of the tars in terms of solubility fractions and molecular mass is primarily determined by reactor geometry.

Although the bulk compositions of hydropyrolysis tars are relatively uniform, a number of rank trends have been identified in the yields and distributions of the alkanes (14,15). For example, the ratios of β,α to α,β hopanes are highest for low rank coals, while relatively large amounts of the immature β,β hopanes are released via hydropyrolysis despite the relatively high thermal severity.

2.2.3 Dispersed catalysts. It is now recognised that tar yields in coal hydropyrolysis can be increased considerably by using catalysts such as Lewis acids (16,17) and metal sulphides, particularly molybdenum (Mo) (18,19) but high loadings of active metal are generally required as in hydroliquefaction (20-22). However, the high conversions achieved for oil shales using hydrogen pressures of no more than 5-10 MPa provides little incentive to use dispersed catalysts simply for increasing conversions, although further increases in oil yield have been reported (4). Nevertheless, catalytic effects are important in providing insight into the competing reaction pathways and to illustrate their effects for different forms of Mo and Fe, the results from a recent study at the Univ. of Strathclyde on

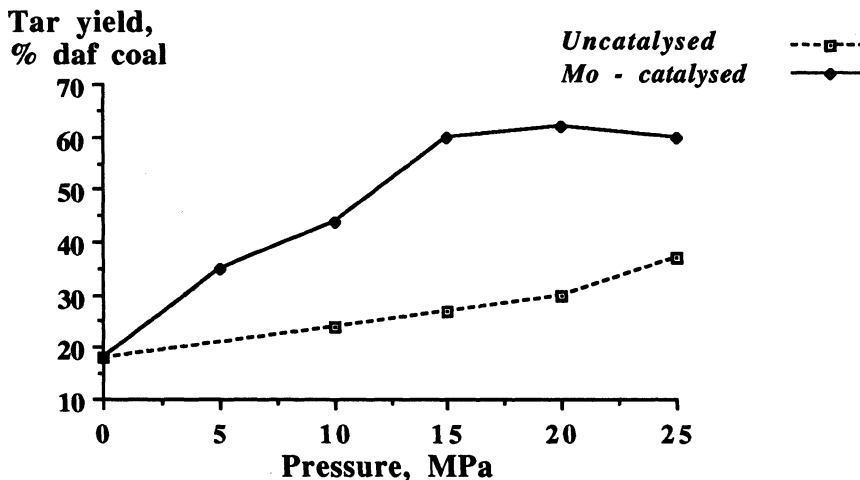


Figure 3 Effect of sulphided Mo catalyst on tar yield for a bituminous coal.

bituminous coals^(14,23) are described here.

Figure 3 demonstrates that sulphided Mo can raise oil yields from *ca* 30 to 60% (daf basis) with the maximum oil yield being attained at 15 MPa pressure. Gas yields do not increase significantly provided that relatively low temperatures (<550°C) are used^(15,16). The yields of tar, char and hydrocarbon gases obtained from a UK bituminous coal with a number of Mo-containing precursors (nominal loading of 1% daf Mo) are listed in Table 3. The maximum conversion of close to 80% daf coal is maintained until the Mo concentration drops below 0.2% for the two sulphur-containing Mo precursors used⁽²³⁾. The conversion achieved with the C₈-dithiophosphate is only slightly lower than that with the other two sulphur-containing precursors. Table 3 also indicates that the naphthenate and the chloride are considerably less effective than the S-containing precursors for an equivalent Mo loading of 1% active metal.

Table 3 Effect of molybdenum and iron precursors on hydropyrolysis yields for a UK bituminous coal (Linby)

Catalyst	Conc. of metal (%)	% daf Coal		
		Char	Tar	C ₁ -C ₄ gases
None	-	55	33	7
Mo Naphthenate	1.0	27	55	9
(NH ₄) ₆ Mo ₇ O ₂₄ ·4H ₂ O	0.2	27	54	N.D.
"	1.0	25	58	10
(NH ₄) ₂ MoO ₂ S ₂	1.0	21	62	10
Mo(C ₂ H ₅) ₂ S ₂ CN	1.0	20	65	6
C ₈ -Mo DTP	1.0	23	59	8
MoCl ₅	1.0	28	56	9
FeS ₂	0.3	49	42	4
FeSO ₄ ·7H ₂ O	1.0	47	40	8
Red Mud	50	62	33	N.D.

N.D. = not determined

1. The Mo precursors used were a naphthenate (octanate), ammonium heptamolybdate and dioxydithiomolybdate, a dithiocarbamate - Mo(C₂H₅)₂S₂CN, a C₈ - dithiophosphate (DTP) and molybdenum chloride. Except the naphthenate and dithiophosphate which are soluble in n-hexane, aqueous/methanol solutions were used for impregnation.

2. For Fe, ferrous sulphate, colloidal iron sulphide (prepared by adding sodium sulphide to ferrous sulphate) and red mud were used as precursors with nominal Fe loadings of 1.0 for the first two precursors and 10 % daf coal for the red mud.

The relatively low conversion obtained with the naphthenate appears surprising in view of their well-documented activity in both batchwise hydrogenation⁽¹⁸⁾ and, more recently, in co-processing of coals and petroleum resids⁽²²⁾ often with low Mo loadings (*ca* 0.1%). This has led to the hypothesis that the lower conversions obtained with the naphthenate and other non-sulphur containing precursors are due to their inability to form the active phase (sulphided Mo) at low enough temperatures in hydropyrolysis (<400°C) to promote hydrogenation and heteroatom removal at the much higher heating rates used compared to direct liquefaction. Thermogravimetric analysis has shown that both the dioxydithiomolybdate and the dithiocarbamate decompose to species corresponding closely

to MoS_2 at approximately 400°C . For the dioxodithiomolybdate, a species corresponding to MoOS_2 is formed at 250°C which is probably also catalytically active. Therefore, the choice of Mo precursor is much more critical in coal hydrolysis than in batchwise hydrogenation and direct liquefaction where there is significantly more time for the non-sulphur containing Mo precursors to acquire sulphur from the coal. Further, sulphided Mo and, indeed, all hydroprocessing catalysts are considerably more effective at temperatures close to 400°C which are used in direct liquefaction than at the higher temperatures required to maximise tar yields in hydrolysis where dehydrogenation reactions are more thermodynamically favoured.

To introduce the active metal by ion-exchange as opposed to impregnation, a bituminous coal was coated with a hydrous titanium oxide (HTO) film ⁽²³⁾ and the results are listed in Table 4. For purposes of comparison, the results from control experiments with (i) the initial coals, (ii) the coals coated with HTO films but not ion-exchanged with Mo and (iii) sulphided Mo (1% loading of Mo) prepared by impregnation with $(\text{NH}_4)\text{MoO}_2\text{S}_2$ are included. Table 4 indicates that a Mo loading of 0.3% Mo on the HTO-coated coal gives a higher conversion than the sulphided Mo (1% loading) prepared by impregnation. Further, 0.03% Mo-HTO gives a conversion intermediate between those

Table 4 Hydrolysis yields from a Mo-HTO coated coal (Illinois No.2)

Catalyst	Char	% daf Coal	
		Tar	C ₁ -C ₄ gases
None	45	38	7
1% Mo as MoS_2	16	68	9
0.3% Mo-HTO	15	69	9
0.03% Mo-HTO	28	59	8
0.003% Mo-HTO	35	51	6
HTO Film	47	37	5
HTO Film acidified to pH = 4	35	52	7

Hydrous titanium oxide (HTO) coatings were prepared by contacting the coal with titanium tetraisopropoxide and a methanolic solution of sodium hydroxide ⁽²³⁾, the coatings corresponding to a nominal loading of approximately 2% daf coal. Mo was introduced by anion-exchange to give a similar range of loadings, the pH of the ammonium molybdate solution used being varied between *ca* 2 and 6.

obtained for 0.3 and 0.003% HTO but lower than that with the sulphided Mo. The same conversion is achieved with 0.003% Mo-HTO as the acidified substrate (10% more than for the initial coal) demonstrating that the latter, rather than the low Mo concentration, is responsible for the catalytic effect; a neutral HTO coating gives no increase in conversion. These results demonstrate that much lower concentrations of Mo (approximately ten-fold) are effective when ion-exchange rather than impregnation is used to disperse the Mo onto coals.

Iron catalysts have a significant cost advantage over Mo, particularly if industrial wastes such as red mud can be utilised. However, Table 3 indicates that the iron-based catalysts tested on the UK bituminous coal only increased tar yields by *ca* 5% daf coal compared to 25% for sulphided Mo. Indeed, the difference in activity between Fe and Mo-based catalysts is much more pronounced for hydrolysis than in direct liquefaction ⁽²⁰⁾.

As for the non-sulphur containing Mo compounds (Table 3), the ineffectiveness of Fe in hydrolysis is undoubtedly attributable to the fact that the active phase, pyrrhotite, is not formed in sufficient quantities below 400°C under the relatively rapid heating regime used here. These results further illustrate the more stringent requirements required for dispersed catalysts in hydrolysis in relation to those used in direct coal liquefaction.

2.2.4 Hydrogen replacement. The major additional cost for hydrolysis over low pressure pyrolysis processes is hydrogen generation. Recently, the effects of partially substituting other gases, such as steam ⁽²⁴⁾ and methane ⁽²⁵⁾ for hydrogen have been investigated. Although increases in conversion were obtained with increasing steam pressure, these were relatively small in relation to those achieved with hydrogen and, consequently, the level of conversion is dictated primarily by the hydrogen partial pressure. Nonetheless, the use of red mud as a catalyst was found to be effective for steam/hydrogen mixtures ⁽²⁴⁾.

Cypres and coworkers have used a mixture of 55% hydrogen, 30% methane and 15% nitrogen by volume to simulate the use of coke oven gas in hydrolysis ⁽²⁵⁾. At temperatures up to 720°C, the oil yield obtained with the mixture was intermediate between that obtained with hydrogen and methane, indicating again that conversion is dictated by hydrogen partial pressure. However, although the oil yield decreased in going to higher temperatures, the yields obtained with the coke oven gas mixture were similar to those obtained with pure hydrogen due to the disproportionation of methane into primarily tar, solid carbon, hydrogen and ethane.

2.3 TWO-STAGE REACTORS

2.3.1 Vapour phase hydrotreating. One major advantage of hydrolysis that has not been fully exploited for oil shales is the ability to pass the primary oil vapours over a suitable hydrotreating catalyst in a two-stage reactor to produce low boiling distillates directly. For bituminous coals ⁽²⁶⁾, two-stage hydrolysis at pressures up to 15 MPa with both traditional γ -alumina supported Ni/Mo catalysts and the novel Ni/Mo exchanged HTOs have given distillates with low heteroatom contents (*ca* 50 ppm nitrogen) containing over 50% material which boils below 300°C. However, the composition can vary considerably as a function of vapour residence time, pressure and temperature ⁽²⁶⁾. Additionally, the performance of the catalyst obviously deteriorates with time on stream. Nonetheless, even after a substantial level of carbon deposition, the level of upgrading achieved in terms of heteroatom removal (50% reduction in nitrogen), hydrocracking to yield naphtha (10-15 cf 25% for fresh catalyst) is still significant ⁽²⁶⁾. In practice, the effect of catalyst deactivation can be overcome to some extent by increasing the vapour residence time.

2.3.2 Mineral interactions. Two-stage operation is useful from a fundamental standpoint in that the secondary vapour phase reactions between oil and the mineral matter in shales can be investigated ⁽²⁷⁾. Table 5 compares the oil and gas yields from hydrolysis at 50 bar pressure when the primary oil vapours (from a Cleveland shale) are passed through a bed of combusted shale. Compared to nitrogen, the use of high hydrogen pressure virtually eliminates the deposition of carbon onto combusted shale ⁽²⁷⁾ (Table 5). The hydrocarbon gas yields increase after the second stage due to the disproportionation of the primary oil into lighter liquids, coke and gas over the combusted shale.

Table 5 Comparison of product yields for single and two-stage hydrolysis at 5 MPa hydrogen pressure for a Cleveland shale

<u>% daf shale</u>	<u>Single</u>	<u>Two-stage</u>
Oil	61	51
Methane	1.1	1.5
C2-C4 hydrocarbons	1.8	2.9
C deposited	-	<1

3. Pressurised fluidised-bed hydrotorting

3.1 PROCESS DEVELOPMENT AND PDU PRODUCT YIELDS

Over the past decade, a number of retorting approaches have been tested for the hydrogen deficient Eastern U.S. oil shales (28). The results of these tests show that the highest oil yields are obtained by retorting these shales in the presence of hydrogen at elevated pressures. Most of the research conducted at IGT during 1987 focussed on the development of the process for moving-bed hydrotorting (HYTORT). It was concluded that oil yield decreases and gas yield increases with increasing particle size and that hydrotorting of beneficiated shale significantly improves the overall economics of producing oil, together with the use of small particles.

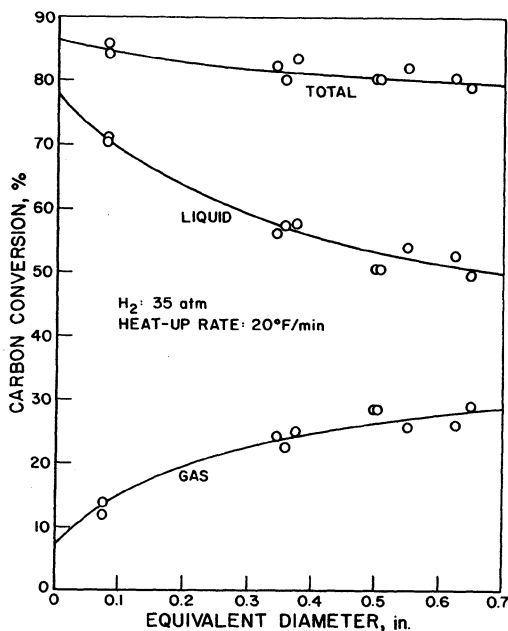


Figure 4 Variation of oil and gas yields with particle size.

Efforts to improve the economics of hydroretorting have led to the development of a second-generation process, the pressurised fluidised-bed hydroretorting (PFH) process at IGT. Research conducted in a laboratory-scale thermobalance confirmed that oil and gas yields obtained during hydroretorting of U.S. Eastern shales depend on the particle size, Figure 1 showing that, the smaller sized particles yield more oil and less gas (29). Improved selectivity to oil reduces hydrogen consumption which, in turn, increases overall process efficiency.

The overall process concept for PFH of oil shale includes the major components for crushing and beneficiation, the hydroretort, hydrogen generation and combustion of the spent shale. The difference between PFH I and II (a more advanced technology) is in the method of hydrogen generation (30,31). In PFH I, the hydrogen is generated by the conventional steam retorting of methane while, in PFH II, it is made by cracking the product gas (primarily methane) to carbon and hydrogen. The carbon is then combusted to generate heat to drive the methane cracking (endothermic) reaction. PFH II technology can potentially eliminate the conventional hydrogen plant and its steam requirement for reforming. PFH II technology may also produce a simplified plant and improve the overall process economics. Block flow diagrams of the major integrated components for the two processes are shown in Figures 5 and 6, respectively. Since the hydroretort is common to both processes, the remaining discussion of PFH results will not differentiate between PFH I and II.

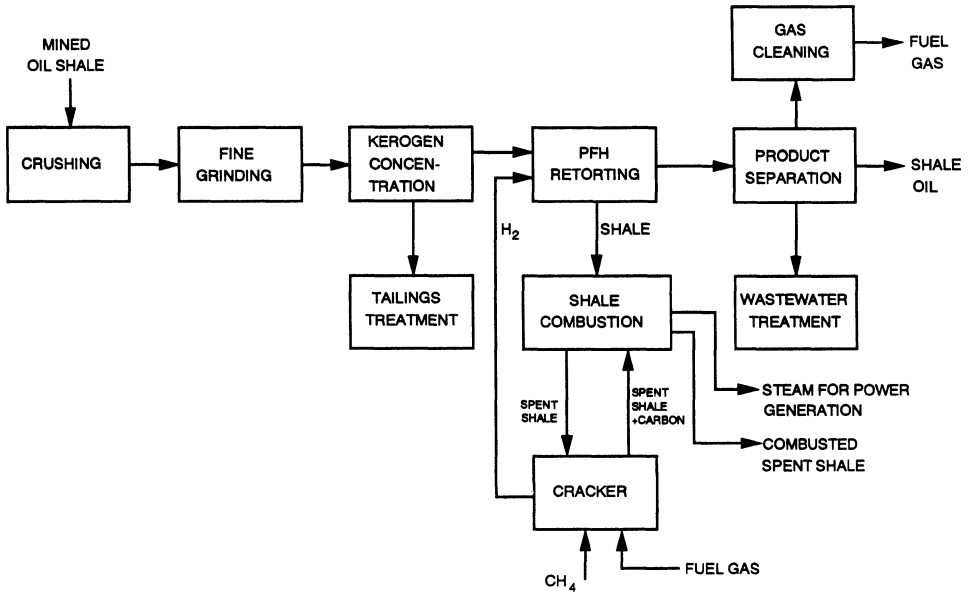


Figure 5 Major components of PFH I process concept.

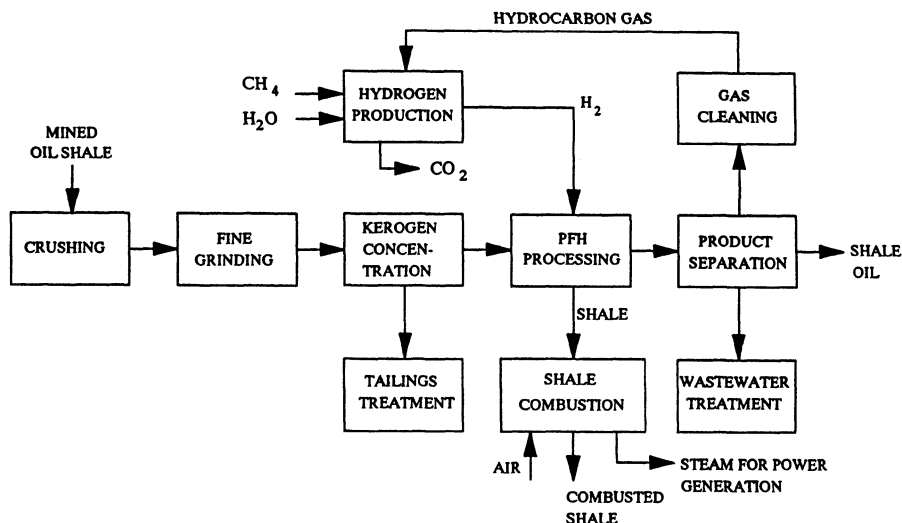


Figure 6 Major components of PFH 2 process concept.

IGT has recently concluded a major program to develop the PFH process and establish a data base for several U.S. Eastern oil shales (32-34). The program also included the development of support technologies including beneficiation, product separation, combustion and waste disposal to improve the economics and environmental acceptability of the PFH process.

The effect of temperature and hydrogen pressure for PFH processing of Indiana New Albany oil shale in the range of 450 to 700°C and 28 to 69 bar on carbon conversion to oil and gas and on the normalised oil yield are shown in Figures 7 and 8, respectively. The highest pressure produces the most oil and, with increasing temperature above 500°C, the oil yield decreases at the expense of more gas. Oil yields are expressed in dm^3 per metric tonne per %w/w organic carbon and can be compared directly with Fischer assay (FA) yields expressed on the same basis. A comparison of PFH and FA yields for six Eastern U.S. shales is presented in Figure 9. All PFH tests were conducted at 6.9 MPa in the laboratory-scale reactor.

The PFH process has been scaled up from a 100 g batch unit to a 100 kg h^{-1} semi-continuous PDU. The latter was designed to operate at any combination of temperature and pressure up to 100°C and 7 MPa. The major components include the feed hopper, reactor, residue receiver, product gas filters, gas-fired preheater, coolers and condensers and recycle compressors. The solids elutriated from the bed are collected by an external cyclone to permit measurement of quantity and particle size. The cyclone piping can also be configured to return fines to the reactor. A summary of operating conditions and the results of the tests with Alabama shale, designated PDU-4 and 5 are presented in Table 6. Carbon conversion to oil for PDU-4 is 42.1 % which corresponds to 149% of the FA yield. When the pressure was raised to 6.89 MPa in PDU-5, the carbon conversion to oil increased to 58.1% of the feed corresponding to 201% of the FA oil yield. Carbon conversions to gas in PDU-4 and 5 were 20.1 and 14.6%, respectively. The raw Indiana New Albany shale gave the somewhat lower than expected oil yield of 170% the FA value.

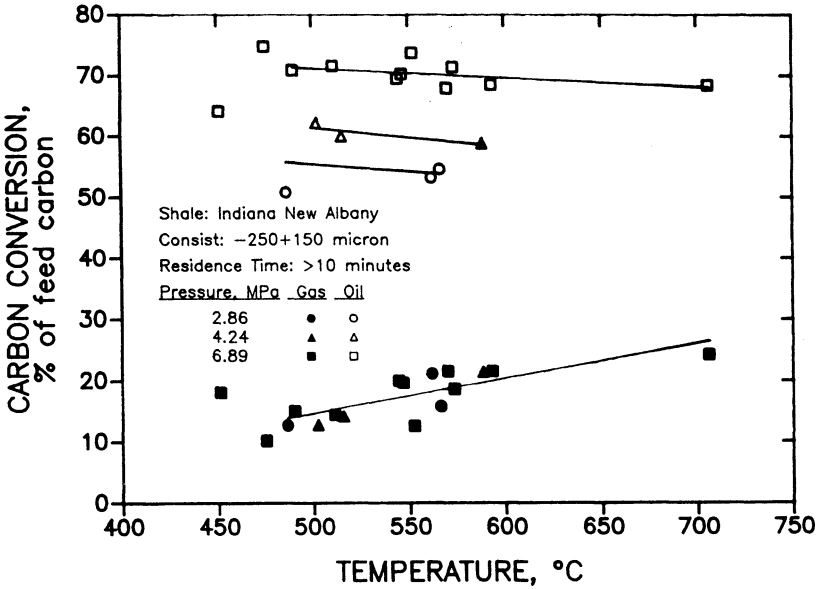


Figure 7 Effect of temperature and hydrogen pressure on carbon conversion to gas and oil for Indiana shale.

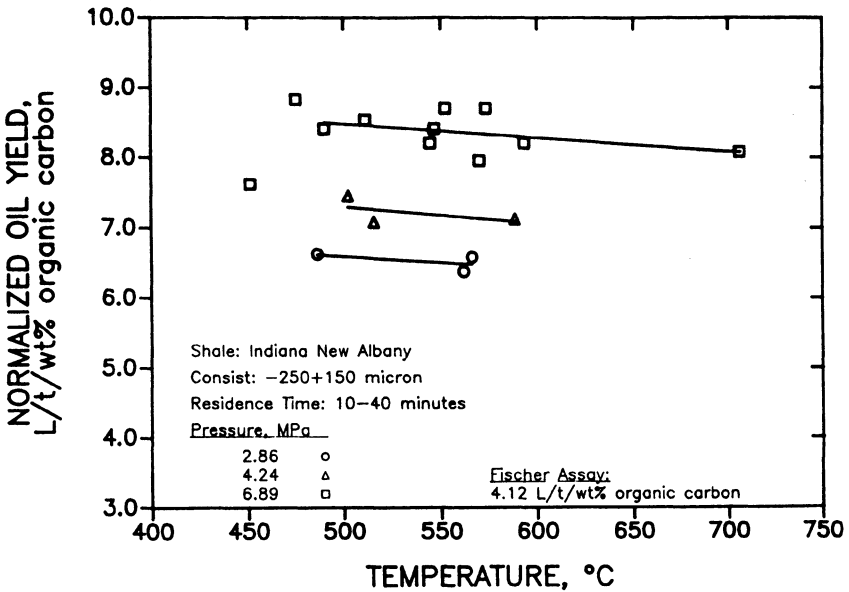


Figure 8 Effect of temperature and hydrogen pressure on carbon conversion on normalised oil yield for Indiana shale.

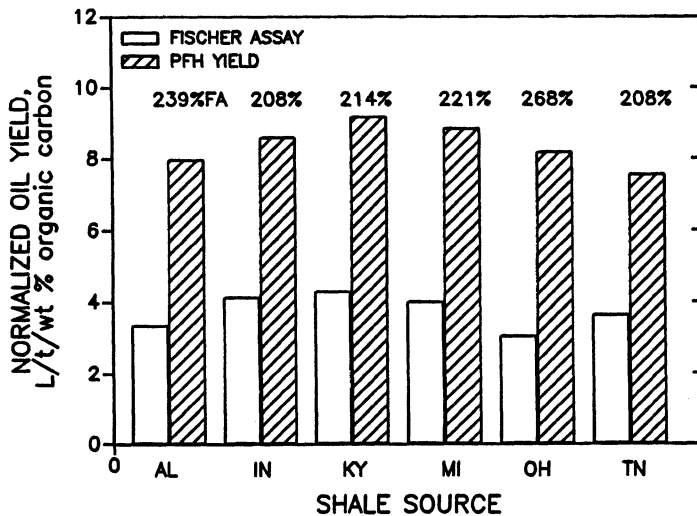


Figure 9 Comparison of Fischer Assay and PFH retorting yields for six Eastern U.S. oil shales.

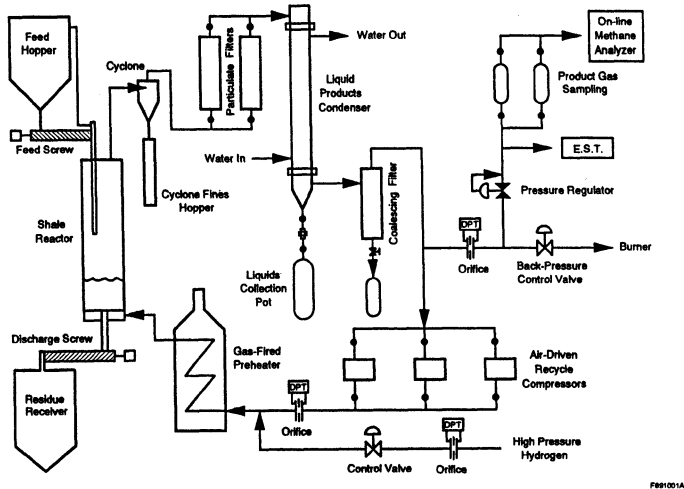


Figure 10 Schematic diagram of PDU-scale PFH test unit.

Table 6 PDU operating conditions and results

	PDU-4 Alabama	PDU-5 Alabama	PDU-9 Indiana	PDU-10 Indiana benf.
<i>Operating conditions</i>				
Average reactor T, °C	519	523	513	519
Shale residence time, min.	26	24	26	19
Pressure, MPa	4.14	6.89	6.89	6.89
Shale particle size, μ	150–180	150–850	150–180	150–850
Shale feedrate, kg h ⁻¹	15.0	14.9	34.3	25.1
Gas flowrate, m ³ h ⁻¹	393	574	561	501
Gas velocities, m ³ s ⁻¹				
superficial	0.38	0.34	0.34	0.30
complete fluidisation	0.36	0.32	0.32	0.26
Shale feedtime, h	3.2	3.6	3.1	3.3
Steady-state period, h	2.0	2.0	1.8	1.5
<i>Product carbon (wt. % feed C)</i>				
Residue shale	37.4	26.9	25.3	19.2
Product gas	20.1	14.6	15.6	18.9
Oil	42.1	58.3	58.9	61.6
Water (as sol. hydrocarbon)	0.4	0.2	0.2	0.2
Total	100.0	100.0	100.0	100.0
<i>Oil</i>				
Yield (dm ³ tonne ⁻¹)	78.7	106	91.4	211
Yield (% of FA)	149	201	170	195
Density (°API)	7.8	5.2	10.6	12.5
Density (kg m ⁻³)	1016	1035	996	983

benf. = beneficiated

However, processing the beneficiated shale gave 195% the FA yield (211 dm³ tonne⁻¹), compared to the laboratory hydroretorting assay (see following) of 208% of FA.

3.2 HYDRORETORTING ASSAYS

The modified FA technique developed by the U.S. Bureau of Mines for evaluating oil yields evolved from tests originally designed to measure the potential liquid yield obtained in coal pyrolysis. During the early decades of this century, procedures and operating conditions for the FA were gradually modified to bring the results into line with oil yields obtained by typical retorting processes of the day. The resulting test is now an ASTM standard (designation D-3904-90). While modern thermal retorting processes - when applied to Western U.S. shales - may produce oil yields which differ slightly from those of the FA test, their yields are sufficiently close for the FA results to be accepted as a standard for assessing the potential of oil shale resources. With the development of hydroretorting processes, it became necessary to devise an assay technique capable of measuring the substantially greater oil yields obtained. Thus, an oil shale is assessed in IGT's hydroretorting assay unit (HAU) prior to PFH processing⁽³⁵⁾.

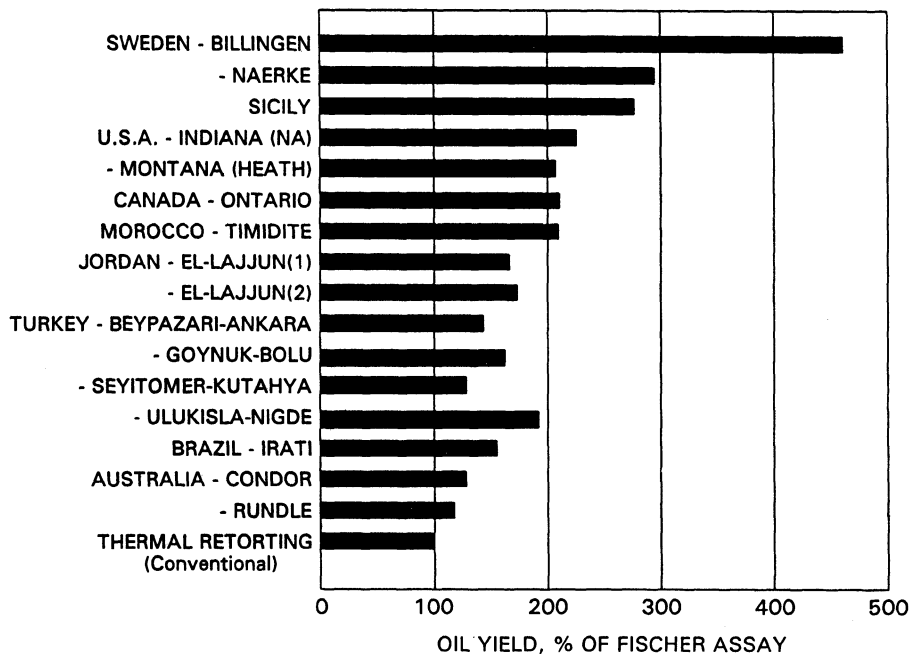


Figure 11 Hydroretorting assay results for World oil shale samples

Table 2. Selected Fischer Assay (FA) and Hydroretorting Assay Unit (HAU) oil yields

Sample	FA (dm ³ tonne ⁻¹)	HUA (dm ³ tonne ⁻¹)	HUA/FA %
Australia - Condor	68.4	88.4	129
- Rundle	102	120	118
Brazil - Irati	77.6	121	156
Canada - Ontario	41.7	88.0	211
Jordan - El-Lajjan (1)	84.6	141	167
- El-Lajjan (2)	137	238	174
Morocco - Timidite	45.0	94.6	210
Sicily	18.3	50.9	277
Sweden - Billingen	15.8	73.0	461
- Naerke	45.4	134	295
Turkey - Beypazari - Ankara	102	147	144
- Goynuk - Bolu	24.6	40.0	163
Seyitomer - Kutahya	277	333	129
Ulukisla - Nigde	41.7	80.0	192
United States - Indiana NA	51.9	133	226
- Montana Heath	67.5	140	207

World oil shales vary significantly in their ability to produce oil. The Western U.S. oil shales (Eocene, Type I kerogen) give high yields when retorted by conventional processes due to their high atomic H/C ratios. However, many of the other world oil shales are comparable to the Eastern U.S. Devonian shales (Type II kerogens) with a hydrogen deficiency which restricts the amount of organic matter in the shale that can be converted to hydrocarbon products in conventional retorting processes. As has been shown earlier, oil yields can be improved substantially by hydrotretorting in the PFH process.

HAU results have been obtained for shales from Australia, Brazil, Canada, Jordan, Morocco, Turkey and elsewhere using the standard operating conditions of 538°C and 6.9 MPa. Oil yields from these shales (Figure 11) show improvements up to 300% over the FA yields, and for one particular shale (Billingen, Sweden), the improvement is over 400%. The actual oil yields are presented in Table 2 which indicates that yields of 125 dm³ per tonne can be obtained from oil shale resources which would be considered too lean for commercial exploitation by conventional thermal retorting processes. Beneficiation may present an opportunity to further exploit these lean oil shale resources.

4. Acknowledgements

Financial support is acknowledged from (i) the European Community [Contract No. EN3V-0048-UK(H)] and (ii) the US Dept. of Energy through Sandia National Laboratories for research at the University of Strathclyde and from the US Dept. of Energy through Morgantown Energy Technology Centre for the PFH process at IGT.

5. References

1. G.R. Gavalas, *Coal Pyrolysis*, Elsevier (1985).
2. S.K. Chakrabarty and M.P. du Plessis, *Modern Coal Pyrolysis; Information Series 95*, Alberta Research Council, Canada (1985) and references therein.
3. S. Furfari, IEA Report No. ICTIS/TR20 (1983) and references therein.
4. E. Ekinci, A.E. Putun, M. Citioglu, C.J. Lafferty and C.E. Snape, Proc. 1991 Int. Conf. on Coal Science (Newcastle), 520 and M. Citioglu, Ph.D thesis, Istanbul Technical University (1993).
5. M.J. Roberts, D. Rue and F. Lau, Fuel, 1992, **71**, 1433.
6. G. Fynes, W.R. Ladner and J.O.H. Newman, Fuel, 1980, **59**, 397.
7. C. Bolton, C. Riemer, C.E. Snape, R.J. O'Brien and R. Kandiyoti, Fuel, 1987, **66**, 1413.
8. H. Juntgen, Fuel, 1984, **63**, 731 and references therein.
9. E.M. Suuberg, W.A. Peters and J.B. Howard, Ind. Eng. Chem. Process Des. Dev., 1978, **17**, 37.
10. P. Arendt and K.-H. van Heek, Fuel, 1981, **60**, 779.
11. J.B. Howard in Chemistry of Coal Utilisation 2nd. Supp. Vol., (Ed. M.A. Elliott), J. Wiley, 1981, p 655.
12. P.T. Fallon, B. Bhatt and M. Steinberg, Fuel Process. Technol., 1980, **3**, 155.
13. C.E. Snape, W.R. Ladner and K.D. Bartle, Fuel, 1985, **64**, 1394.
14. C.E. Snape, C.J. Lafferty, S. Mitchell, F. Donald and C. McArthur, G. Eglinton, N. Robinson and R. Collier, Final report on EC Contract No. EN3V - 0048 - UK (H), October 1991.

15. N. Robinson, G. Eglinton, C.J. Lafferty and C.E. Snape, Fuel, 1991, **70**, 249.
16. R.E. Wood and W.H. Wiser, Ind. Eng. Chem. Proc. Des. Dev., 1976, **15(1)**, 144.
17. J.R. Kershaw, G. Barass and D. Grady, Fuel Process Technol., 1980, **3**, 115.
18. C. Bolton, C. Riemer, C.E. Snape, F.J. Derbyshire and M.T. Terrer, Fuel, 1988, **67**, 901.
19. C.E. Snape, C. Bolton, R.G. Dosch and H.P. Stephens, Energy & Fuels, 1989, **3**, 421 and Am. Chem. Soc. Div. Fuel Chem., 1988, **33(3)**, 251.
20. D. Garg and E.N. Givens, Prepr. Am. Chem. Soc. Div. Fuel Chem., 1983, **28(5)**, 200.
21. J.A. Ruether, J.A. Mima, R.M. Kornosky and B.C. Ha, Energy & Fuels, 1987, **1(2)**, 198.
22. C.W. Curtis and J.L. Pelligrino, Energy & Fuels, 1989, **3(2)**, 160.
23. C.E. Snape, C.J. Lafferty, H.P. Stephens, R.G. Dosch and E. Klavetter, Fuel, 1991, **70**, 393.
24. D.K. Sharma, A. Sulimma and K.H. van Heek, Fuel, 1986, **65**, 1571.
25. C. Braekman-Danheux, R. Cypres, A. Fontana, P. Laurent and M. Van Hoegaerden, Fuel, 1992, **71**, 251.
26. C. Bolton, C.E. Snape and H.P. Stephens, Fuel, 1989, **68**, 161 and references therein.
27. S.D. Carter, M. Citiroglu, J. Gallacher, C.E. Snape, S.C. Mitchell and C.J. Lafferty, Proc. 1992 Eastern US Oil Shale Symp., Univ. of Kentucky and Fuel, 1994, **73**, 1455.
28. D.V. Punwani, Presented at 12th Energy Technology Conference & Exposition, Washington, D.C., 24-26 March, 1985.
- 29.. S.A. Weil *et al*, Presented at Synthetic Fuels from Oil Shale II, Nashville, Tennessee, 26-29 October 1981.
- 30.. M.J. Roberts *et al*, Proc. 1989 Eastern US Oil Shale Symp., pp 487-498, Univ. of Kentucky.
31. F.S. Lau and D.V. Punwani, Presented at US DoE Oil Shale Contractors meeting, 19-21 July 1988.
32. M.J. Roberts *et al*, Final Report on US DoE Contracts DE-AC21-87MC11089 (4 volumes) and Reports on US DoE Contract DOE/MC/11089-47 to 50 (March 1992).
33. M.J. Roberts *et al*, Final Report on US DoE Contract DOE/MC/11089-68 (June 1991-May 1992).
34. M.J. Roberts *et al*, Final Report on US DoE Contract DOE/MC/11089-79 (June 1992-January 1993).
35. P.A. Lynch *et al*, Prepr. Am. Chem. Soc., Div. Pet. Chem., 1984, **29(1)**, 71.

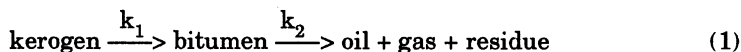
THE BITUMEN INTERMEDIATE IN ISOTHERMAL AND NONISOTHERMAL DECOMPOSITION OF OIL SHALES

FRANCIS P. MIKNIS and THOMAS F. TURNER
Western Research Institute
Box 3395
Laramie, WY 82071
USA

ABSTRACT. A common feature of oil shale decomposition models is the bitumen intermediate, which is defined to be a soluble, nonvolatile primary product of kerogen decomposition. Despite the large number of studies that have been conducted on oil shale thermal decomposition, there is a scarcity of data on the bitumen intermediate. The problem with the bitumen intermediate is that, while it is often used in oil shale decomposition, it is seldom measured experimentally. The lack of experimental data can lead to deficiencies in understanding the mechanism and kinetics of oil generation. In this chapter some comments on the role of the bitumen intermediate during oil shale decomposition are examined, with emphasis on its temperature dependence under isothermal and nonisothermal conditions. Data are presented to illustrate that significantly greater conversions of kerogen to soluble products can be accomplished by paying attention to the kinetic behavior of the bitumen intermediate, particularly for oil shales that have a large aliphatic carbon component.

1. Introduction

Oil shale thermal decomposition is generally considered to be a first-order rate process that proceeds through different intermediate stages before the final products are produced. Various decomposition schemes have been proposed to model the process. One of the most frequently used decomposition models is shown in equation 1,



where k_1 and k_2 are the rate constants for the kerogen and bitumen decomposition. Kerogen is defined as that portion of the organic matter in oil shale that is insoluble in common organic solvents. It is figuratively a "blackbox" from which products evolve upon application of heat. The bitumen is defined as the benzene-soluble organic material formed during the heating period that is nonvolatile and

remains in the shale sample. Residue is defined as the benzene-insoluble portion of the kerogen remaining in the spent shale.

Burnham (1) points out that the above model is inadequate for most kerogens. The main reason is that the serial model in equation 1 must have an induction time for oil generation, which means that the slope of the oil generation curve must be zero at zero time. For most kerogens this is not the case. An easy solution is to write a more general expression for kerogen decomposition, i.e.,



and



This model allows for any reaction product to be produced from either the kerogen or the bitumen. The relative amounts of each decomposition product would be determined from stoichiometric coefficients. Thus, a non zero stoichiometric coefficient for oil in equation 2 addresses the problem of allowing the maximum oil generation to occur at the beginning of pyrolysis and still having bitumen as an intermediate in the decomposition.

Although bitumen has been considered an important intermediate in kerogen decomposition (2-9) its chemical and physical properties have not been thoroughly investigated. Historically, models such as equation 1 were proposed for oil shales containing type 1 kerogen, which is highly aliphatic and which exhibits high conversions to oil during pyrolysis. These kerogens, which include Colorado and Baltic oil shales, Australian torbanites, and sapropelic coals, show similar first-order rate constants for kerogen decomposition (4). Eastern Devonian and Mississippian shales have a more aromatic kerogen structure than do the Tertiary oil shales from the Green River Formation (10). Little attention has been paid to whether the bitumen is a significant reaction intermediate in the pyrolysis of these more aromatic shales.

There is a paucity of published data on the time dependence of the chemical and physical properties of oil shale pyrolysis products. In particular, there is very little information on the bitumen intermediate. For a long time, the data of Hubbard and Robinson (11) were the most comprehensive on the thermal decomposition of Colorado oil shale. However, even in that study, chemical and physical properties of the reaction products were not measured. Instead, overall decomposition data were reported, which subsequently have been used by others (2-4) to develop global models of kerogen decomposition. For eastern U.S. oil shales some properties of the bitumen have been investigated (12-14). For other shales from different worldwide deposits, comprehensive decomposition data have not been reported, and the significance of the bitumen intermediate has not been addressed for these shales.

In this chapter, the role of the bitumen intermediate during oil shale decomposition is discussed with emphasis on the temperature dependence of the bitumen under isothermal and nonisothermal conditions. Possible relationships between bitumen formation and kerogen structure are also discussed that can lead to improvements in oil shale conversion. In addition, some compositional differences between the bitumen produced from eastern and western U.S. oil shales are presented.

2. Experimental

2.1 OIL SHALE SAMPLES

The Fischer assay data for the oil shales are listed in Table 1. Organic carbon conversion data are given in Table 2. The shales were crushed to pass a 20-mesh (841μ) screen and the 20/45 mesh ($841\mu/354\mu$) fraction was separated for decomposition studies. An initial 1500-gram fraction of each shale was thoroughly mixed and was then split eight ways in two stages to yield 64 samples each weighing about 22 grams. Twenty-gram samples were weighed from these for kinetic measurements.

Table 1. Fischer Assay Data for Oil Shales

	Kentucky Shale	Colorado Shale		Wyoming
	New Albany	Anvil Points	Exxon Colony	Tipton
Oil, gal/ton	14.4	52.2	27.5	22.0
Oil, wt %	5.7	19.3	10.2	8.8
Gas, wt %	3.2	4.9	4.6	2.0
Spent Shale, wt %	89.5	74.4	83.5	86.0
Water, wt %	1.6	1.4	1.7	3.2

Table 2. Fischer Assay Organic Carbon Conversion for Oil Shales

	Kentucky Shale	Colorado Shale		Wyoming
	New Albany	Anvil Points	Exxon Colony	Tipton
Oil	35.1	71.5	61.7	62.3
Gas	9.1	12.7	13.8	8.0
Spent Shale	55.8	15.8	23.7	29.7

2.2 PYROLYSIS REACTOR SYSTEM

Isothermal measurements were carried out in a heated sand-bath reaction system that has been described in detail elsewhere(14-16)). Briefly, 20-gram samples are heated to reaction temperature by immersing a tubular reactor containing the shale sample into a pre-equilibrated fluidized sand bath. The reaction is quenched by removing the reactor from the sand bath and spraying liquid CO₂ onto its surface. A helium sweep gas flow rate of 30 cc/min is used to remove the products from the reaction zone. The liquid product is collected in a dry ice-cooled trap and gaseous products are analyzed by gas chromatography, either by collecting the total gaseous product in an evacuated vessel or by analyzing the product gas on-line. The amount of bitumen was determined by extracting the residue shale from each experiment with benzene for 24 hr in a Soxhlet apparatus, followed by rotary film evaporation to obtain the bitumen for analysis.

Material balances were calculated by measuring the weight change of the shale sample, the weight of liquid collected, the volume of water collected, and the weight of each component in the gas. The gas evolution curves were integrated, taking into account analytical system delays and backmixing, to give the total amount of gas evolved in each timed experiment. Material balances were typically 100 ± 1%. Typical heat-up and cool-down curves for isothermal are shown in Figure 1 for 30-min isothermal runs at 400 and 425°C.

3. Results and Discussion

3.1 BITUMEN FORMATION UNDER ISOTHERMAL CONDITIONS

As already mentioned, an objective of this work was to investigate the transient nature of bitumen during thermal decomposition of oil shales. The temperature dependence of the bitumen is shown in Figure 2. The data are plotted on a carbon basis to facilitate comparison. The data show that, in the temperature range of 375°C to 425°C, the maximum amount of extractable bitumen from the Kentucky

New Albany shale is about 14% of the original kerogen (425°C data). However, the Colorado and Wyoming oil shales show greater amounts of extractable bitumen, reaching maximum values between 40 and 60% at 425°C. The lower maximum value at 440°C for the Exxon-Colony is probably due to experimental constraints that prevent rapid heating and quenching of the shale in a time sufficiently short to observe the maximum value at this temperature. The differences in carbon structure and conversion to oil between the shales suggest that bitumen formation may be a function of the original kerogen structure, i.e., the more aliphatic the oil shale, the more bitumen that is formed during pyrolysis.

A reasonable explanation for the low bitumen yields of the New Albany shale is that direct kerogen conversion to residue, oil and gas competes with bitumen formation. Because the overall carbon conversion of the New Albany shale is about 35 and 56% to oil and residue, respectively, during Fischer assay (Table 2), direct residue formation appears to be a major pathway for kerogen decomposition in this shale. It is also possible that for the New Albany shale, given the high aromatic carbon content (10), a certain portion of the original kerogen resembles a residue product. Unfortunately, there is no way to discriminate between a residue that is formed and a residue-like material that is already part of the original kerogen.

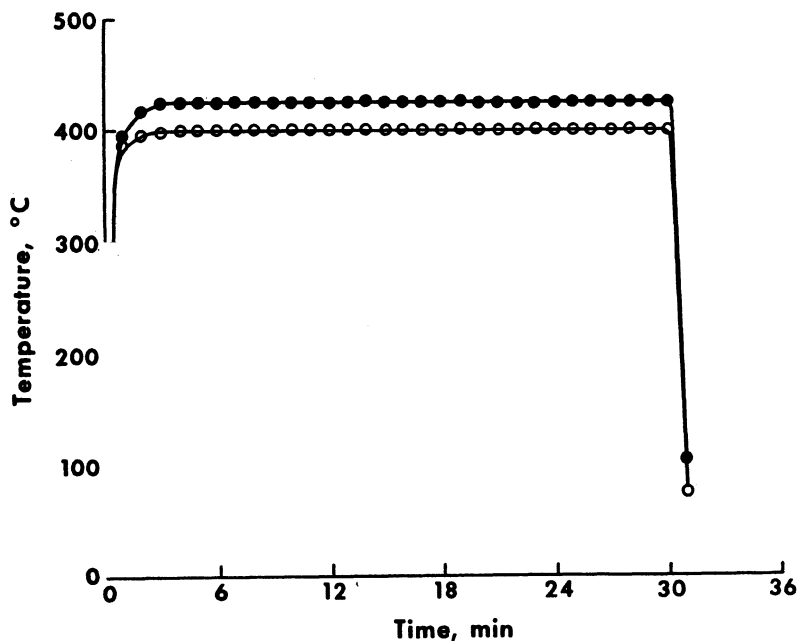


Figure 1. Heat-up and cool-down curves for 30-min isothermal runs at 400 and 425°C.

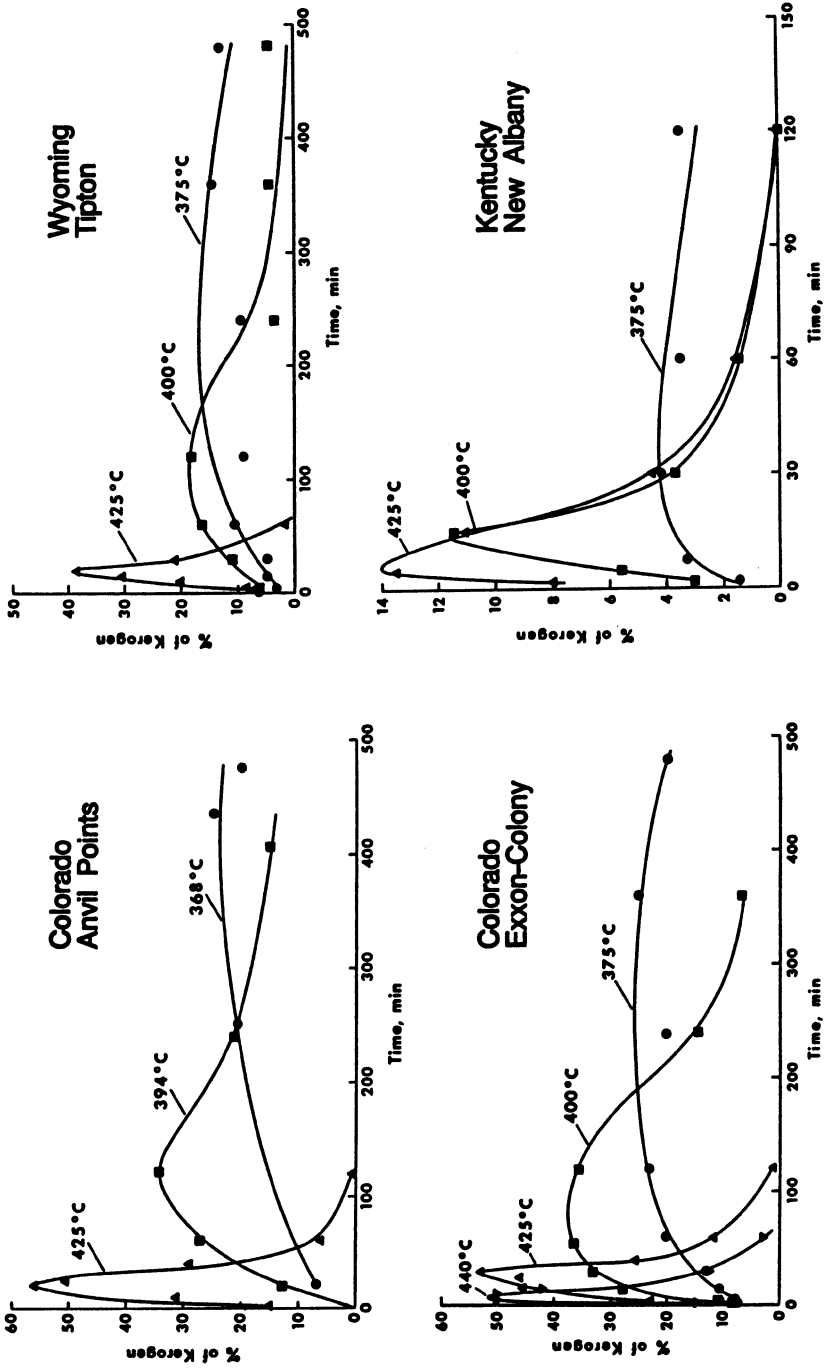


Figure 2. Time and temperature dependence of bitumen for Colorado, Wyoming, and Kentucky oil shales.

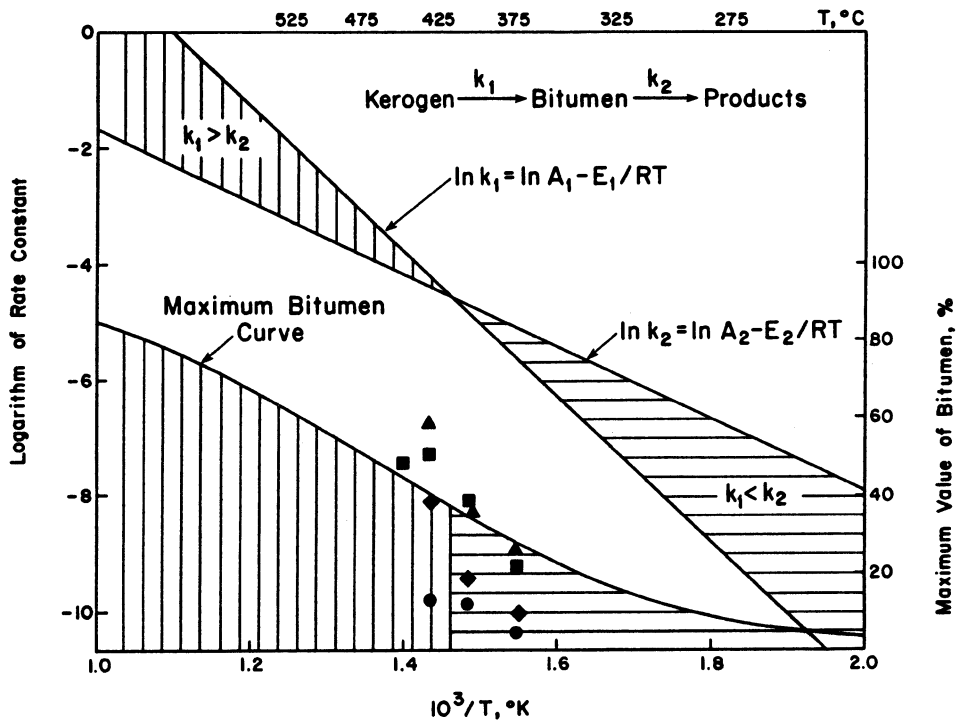


Figure 3. Temperature dependence of kerogen and bitumen decomposition rate constants and maximum bitumen concentration (▲ Colorado Anvil points, ■ Colorado Exxon-Colony, ◆ Wyoming Tipton, ● Kentucky New Albany).

There is one aspect of the data in Figure 2 that is important for understanding kerogen decomposition, but which has been largely ignored (3,5,8,9) in the development of oil shale decomposition kinetics. That is, experimentally the maximum amount of extractable bitumen increases with temperature. The implications of this trend on oil shale decomposition kinetics are best explained with the aid of Figure 3, and equation 1. For the model given by equation 1, the bitumen concentration is

$$B/K^0 = f_1 k_1 / (k_2 - k_1) [\exp(-k_1 t) - \exp(-k_2 t)] \quad (4)$$

where K^0 is the amount of original kerogen, f_1 is the fraction of kerogen converted to bitumen, and k_1, k_2 are the first-order rate constants for kerogen and bitumen decomposition. The time for the bitumen to reach its maximum value at a given temperature can be obtained by setting the time derivative of equation 4 equal to zero, and solving for the time. This yields

$$t_{\max} = (k_2 - k_1)^{-1} \ln(k_2/k_1) \quad (5)$$

By substituting equation 5 into equation 4, the maximum value of the bitumen can be obtained from

$$\%B_{\max} = 100f_1(k_1/k_2)^{k_2/(k_2-k_1)} \quad (6)$$

The temperature dependence of each rate constant can be described by the Arrhenius equation:

$$k = A \exp(-E/RT) \quad (7)$$

where A is the frequency factor, R is the ideal gas constant, E is the activation energy, and T is the temperature. By taking the logarithm of both sides of equation 7, the temperature dependence of the logarithm of the rate constant can be expressed in the form of a straight line with intercept, $\ln A$, and slope, $-E/R$, as shown in Figure 3. The lines in Figure 3 are calculated from a model in which $E_1 > E_2$, and $A_1 > A_2$. For purposes of discussion, only the ordering of E_1 , E_2 , and A_1, A_2 is important; experimentally determined values are not necessary. Because the slopes and intercepts are not the same, the lines for the rate constants, k_1 and k_2 , cross at some temperature. The point at which the crossover occurs is when $k_1 = k_2$, and the maximum amount of extractable bitumen is 37% at this point for the given model. Less than this amount is extractable in the region where $k_1 < k_2$, and greater than this amount is extractable in the region where $k_1 > k_2$ (equation 6).

The curve for the maximum extractable bitumen as a function of temperature is also shown in Figure 3. This curve is calculated from equation 6 where k_1 and k_2 are first calculated at a given temperature from equation 7. The fraction of kerogen converted to bitumen is assumed to be unity for purposes of illustration. Experimental data for the maximum bitumen from Colorado, Wyoming and Kentucky oil shales are also shown on Figure 3.

The key point to be made about the maximum bitumen curve is that it increases with temperature if the activation energies of the kerogen and bitumen decomposition are ordered as shown in Figure 3, that is $E_1 > E_2$. It is difficult to reconcile the temperature dependence of the bitumen with an activation energy of kerogen decomposition that is less than the activation energy of bitumen decomposition. One way to reconcile this is for the fraction of kerogen converted to bitumen (f_1 in equation 4) to be temperature dependent, increasing with increasing temperature. However, this behavior has not been demonstrated in any work published to date and does not appear to have been considered in models of oil shale thermal decomposition. If the fraction of kerogen converted to bitumen, f_1 , is less than unity, the maximum bitumen curve still increases with temperature, but scales accordingly to lower values of maximum concentration.

A number of studies have reported activation energies for kerogen and bitumen decomposition that were based on analysis of TGA weight loss curves (6,9), liquid product yields (3), yields of total hydrocarbons (7), or combined yields of oil and bitumen (8). In all cases, experimental data were not obtained for the bitumen, although bitumen was included as an intermediate in the analysis of the kerogen decomposition kinetics. Only one of these studies (7) reported an activation energy of kerogen decomposition that was greater than that of the bitumen decomposition.

An interesting aspect of the 425 °C liquid product data that can be important for oil shale processing is illustrated in Figure 4. These data show maxima in the oil plus bitumen curves for the Colorado oil shales. By quenching the reaction at the time of the maximum (~30 min), 85 to 95 % of the carbon in the kerogen is recoverable as soluble products. For longer times, lesser amounts of soluble products are recoverable due to coking of the bitumen. Ultimately, the liquid yields will be that of the oil only since the bitumen will have decomposed to form oil, gas, and residue products.

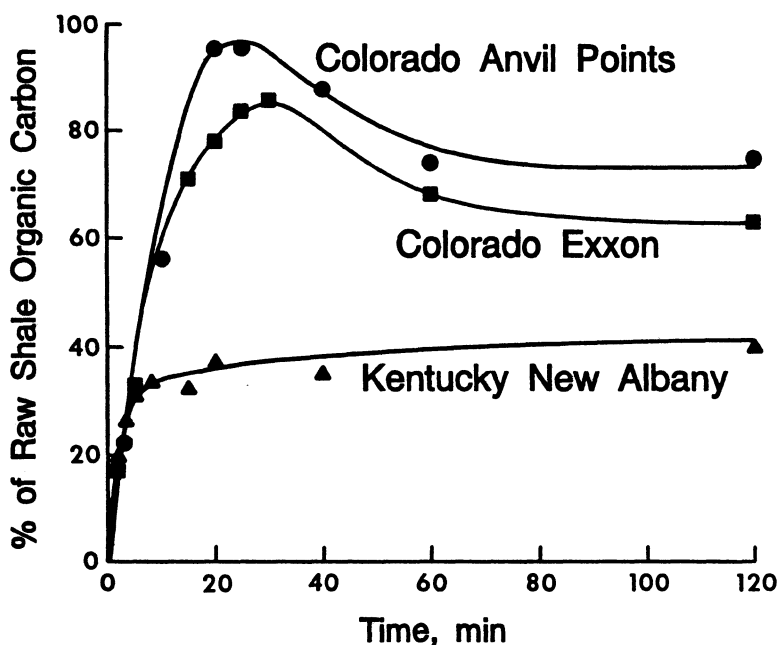


Figure 4. Sum of oil and bitumen produced from Colorado and Kentucky oil shales at 425 °C.

The maximum in the oil plus bitumen curve from the Colorado oil shales results from the large fraction of extractable bitumen generated at 425°C (Figure 2). An insufficient amount of bitumen is extractable during pyrolysis to produce a maximum in the oil plus bitumen curve from the New Albany shale. As a result, no improvement in conversion to soluble products can be obtained by quenching the reaction after a specified time as has been shown for the Colorado shales.

Yields greater than Fischer assay have been obtained from eastern shales by hydrolysis (17,18), donor solvents (19), and rapid heating (20,21). In view of the lack of a substantial intermediate concentration for these shales, it appears that the increased oil yields are brought about by effectively blocking the direct residue formation step or by redistribution of products to produce less gas and more oil. However, more detailed studies are needed to understand the reasons for increased oil yields under different pyrolysis conditions for shales in which the bitumen is not an important intermediate in the decomposition.

3.2 QUALITATIVE BEHAVIOR OF THE BITUMEN UNDER NONISOTHERMAL HEATING

For nonisothermal heating, the temperature dependence of the bitumen can also be used to infer the ordering of activation energies. This is most easily understood with the aid of Figure 5, which shows the theoretical behavior of bitumen and kerogen for the model described by equations 2 and 3 for heating rates of 2 and 10 K/min assuming a stoichiometric coefficient of unity ($f_1 = 1$) for the formation of bitumen from the kerogen. Figure 5a illustrates the case, $E_1 > E_2$ and Figure 5b illustrates the case, $E_1 < E_2$. The values of E_1 , E_2 , A_1 , and A_2 are chosen only for the purposes of illustration.

Figure 5 shows that the temperature at the maximum in the bitumen curve shifts to higher temperature as the heating rate increases. For $E_1 > E_2$, the maximum amount of bitumen also increases with heating rate; whereas for $E_1 < E_2$, the maximum amount of bitumen decreases with increasing heating rate. Furthermore, the maximum in the bitumen will always lie outside of the kerogen decomposition curve when $E_1 > E_2$. If $E_1 < E_2$, the maximum of the bitumen curve will always lie inside the kerogen curve. The predicted properties of the temperature dependence of the bitumen can be used to infer the ordering of activation energies for nonisothermal behavior.

Experimentally, the behavior of the bitumen and kerogen under nonisothermal heating is shown in Figure 6 for the Wyoming oil shale. The maximum in the bitumen lies outside the kerogen curve, and the maximum shifts to higher temperature as the heating rate increases. Also, the maximum amount of bitumen increases with heating rate. These experimental observations support the notion that the activation energy of kerogen decomposition (E_1) is greater than the activation energy of bitumen decomposition (E_2).

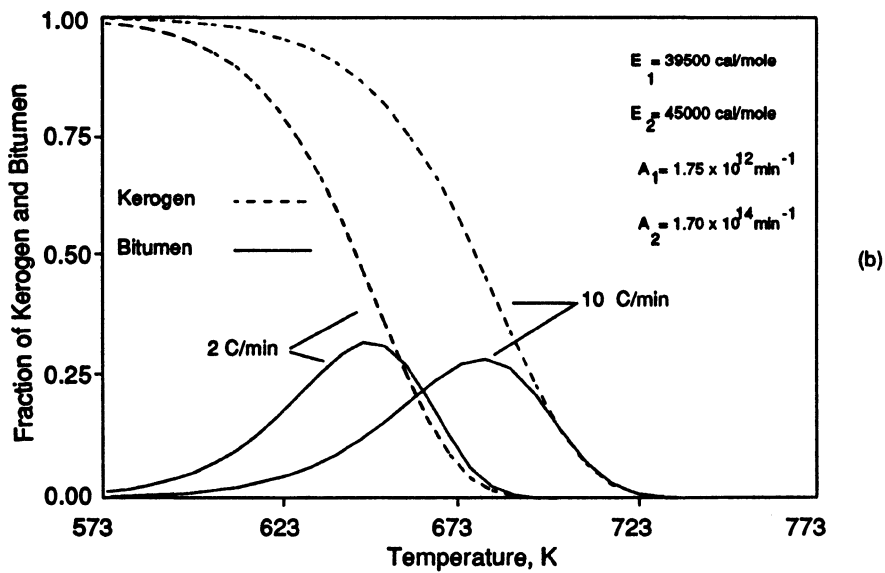
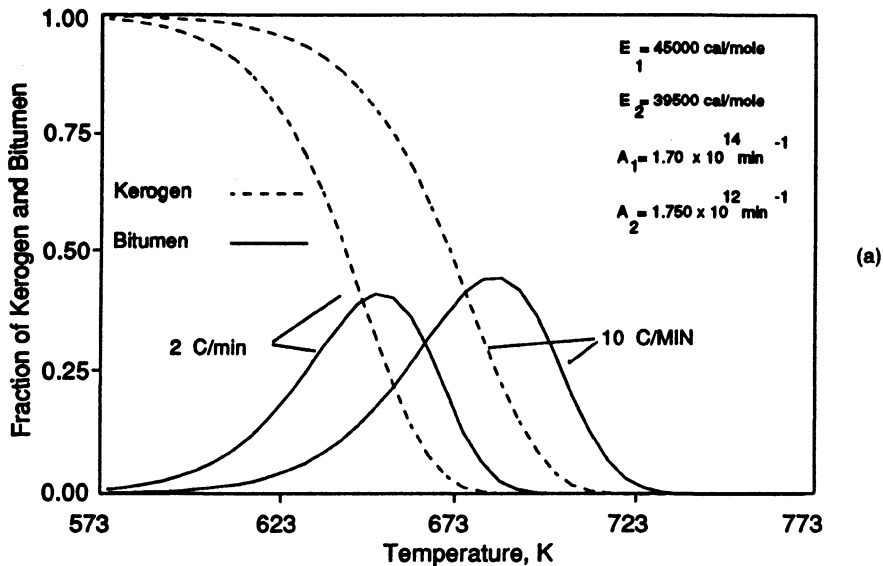


Figure 5. Theoretical curves for kerogen and bitumen evolution under nonisothermal conditions, (a) $E_1 > E_2$, (b) $E_1 < E_2$.

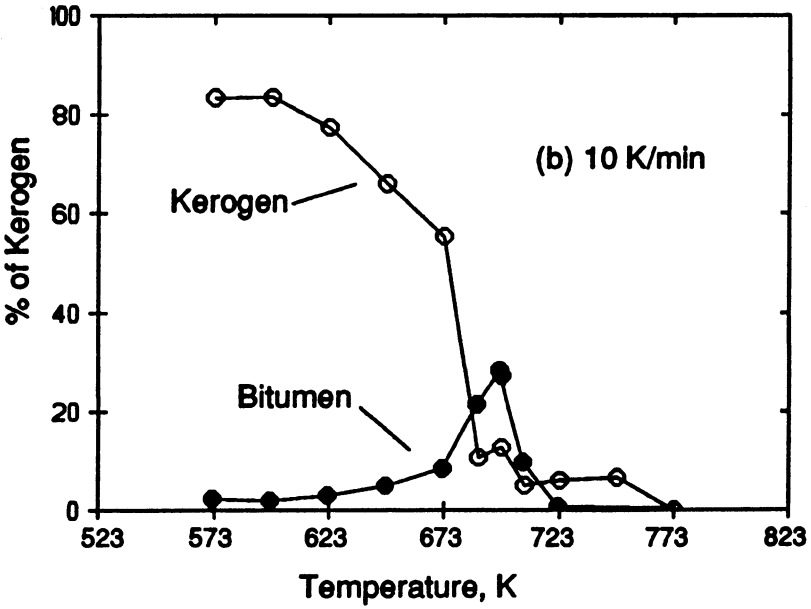
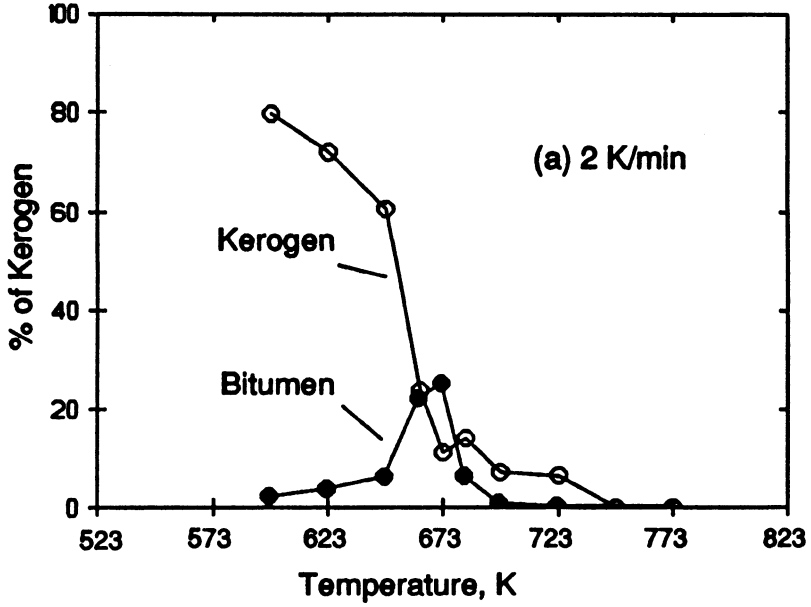


Figure 6. Temperature dependence of kerogen and bitumen in Wyoming oil shale heated at (a) 2 K/min and (b) 10 K/min.

Another nonisothermal study that incorporates data for the bitumen is that of Li et al. (22). They studied the nonisothermal decomposition of Fushun oil shale at a heating rate of 2 K/min in the range of 653 to 793 K and obtained activation energies of 30 and 48 kcal/mole for E_1 and E_2 , respectively. Because only one heating rate was used, the ordering of activation energies could not be established from their work. Based on the above discussion, at least two heating rates must be employed in quenched nonisothermal experiments to determine the ordering of activation energies. Clearly, additional measurements of the bitumen under nonisothermal heating and different heating rates are needed for all types of oil shales.

3.3 OTHER PROPERTIES OF THE OIL AND BITUMEN

Hydrogen-to-carbon ratios and molecular weights were determined for the oils and bitumens produced from isothermal decomposition of the Colorado Exxon-Colony and Kentucky New Albany oil shales (Figures 7 and 8). Similar results have been obtained for other Colorado and Kentucky oil shales (14).

For the shale oils, the H/C ratios and molecular weights were remarkably constant at all times and temperatures for each type of shale oil. Average values from all the time/temperature data are given in Table 3. The differences in average properties of the two shale oils reflect the differences in the original kerogen structure, i.e., the more aromatic nature of the Kentucky oil shale kerogen compared with the Colorado oil shale kerogen.

Table 3. Average properties of Colorado and Kentucky Shale Oils

	H/C	Carbon Aromaticity	mol wt
Colorado	1.71 ± 0.03	0.02 ± 0.02	358 ± 40
Kentucky	1.50 ± 0.06	0.41 ± 0.04	257 ± 16

Chemical property measurements of the bitumen were limited by the small amounts of bitumen extracted from the 20-g samples of shale. This was especially true for the Kentucky oil shale in which little bitumen was extracted throughout the decomposition and for the Colorado oil shale at longer reaction times where little bitumen remained. In general, the composition and properties of the bitumen change during the course of the reaction. This is most evident from the molecular weight data in Figures 8a and b. These data indicate that the bitumen molecular weight passes through a maximum during the decomposition. This effect had been noted previously by Mityurev (23) in his analysis of the thermal decomposition of Baltic shales. Because of this, Mityurev concluded that a kinetic intermediate whose composition changes with time is untenable in a reaction sequence. Instead,

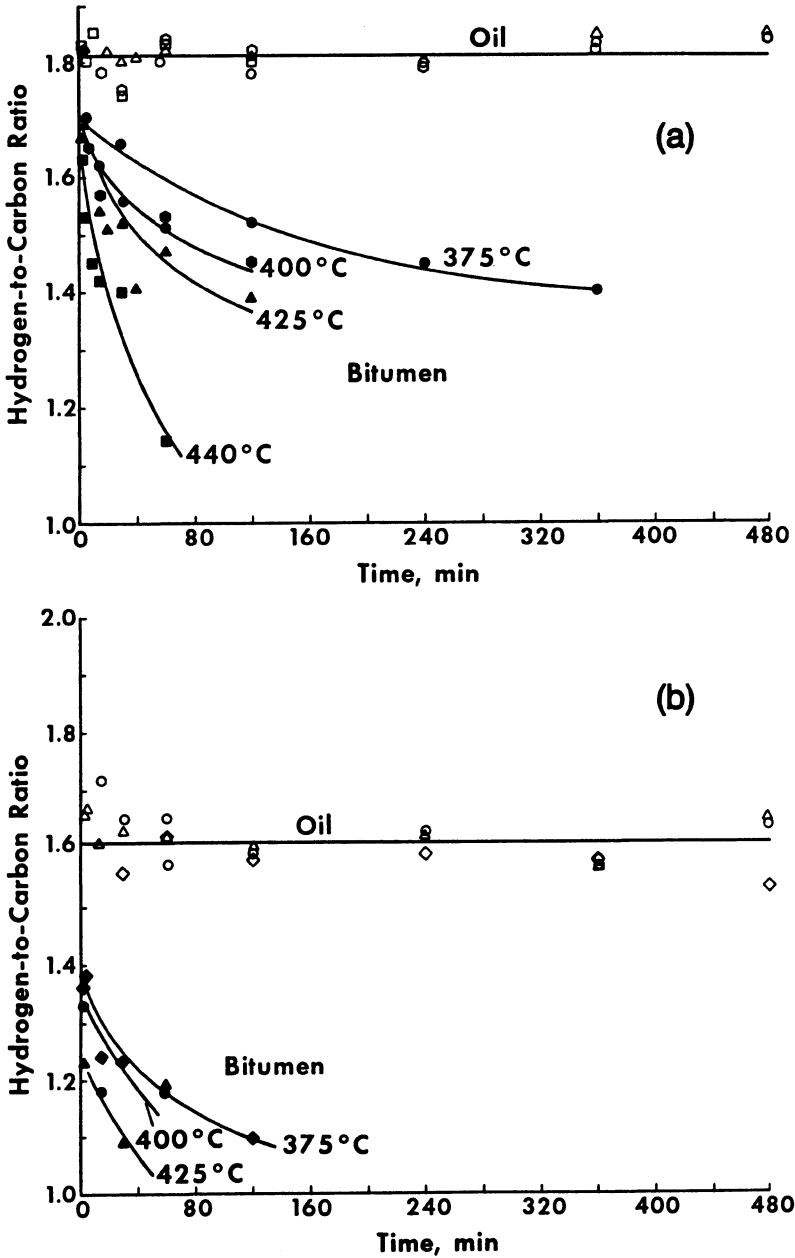


Figure 7. Hydrogen-to-carbon ratios of oil and bitumen vs. time and temperature for (a) Colorado (Exxon-Colony) and (b) Kentucky (New Albany) oil shale.

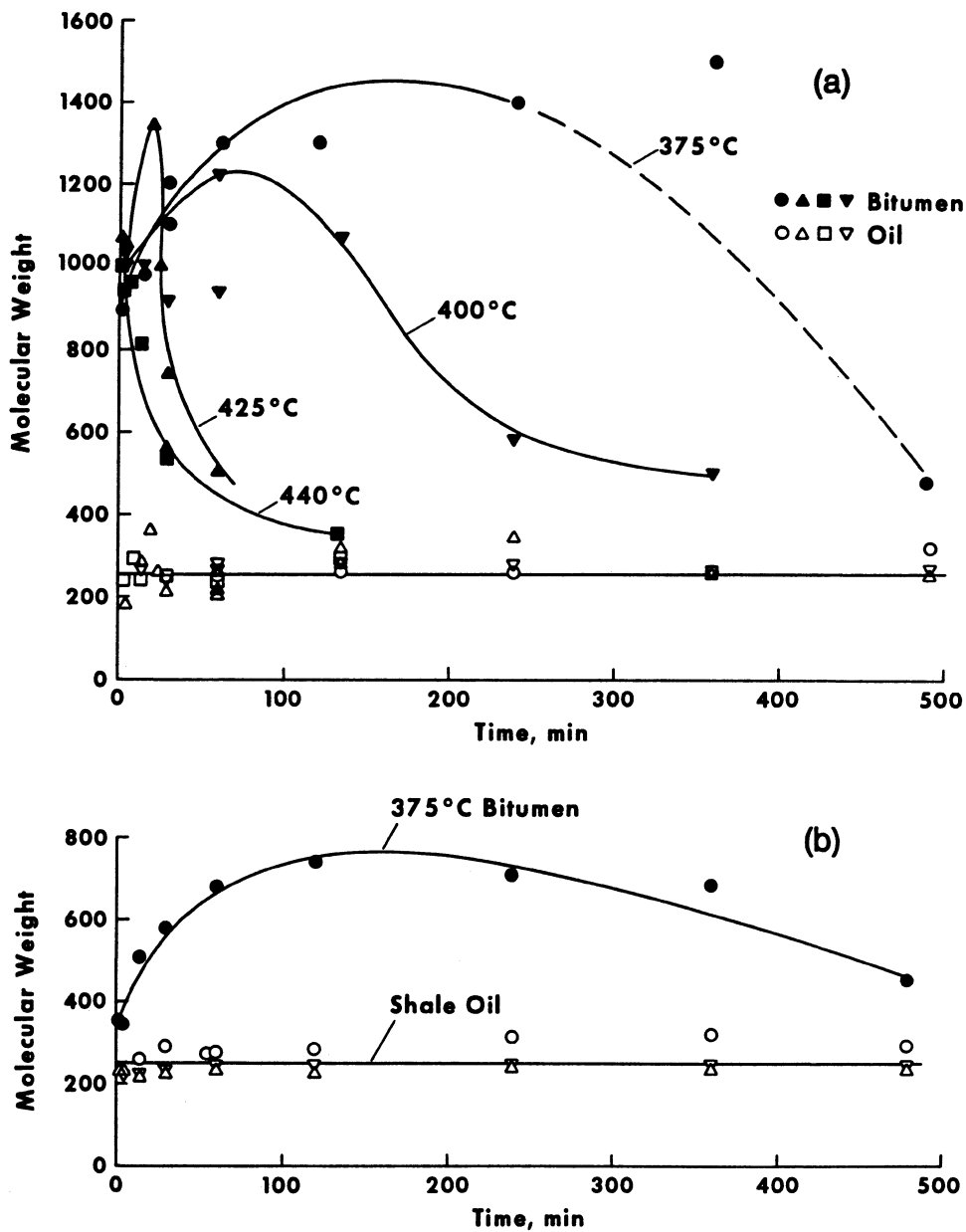


Figure 8. Molecular weights of oil and bitumen vs. time and temperature for (a) Colorado (Exxon-Colony) and (b) Kentucky (New Albany) oil shale.

Mityurev considers bitumen to be a mixture of tar and unconverted kerogen. The changing composition of the bitumen is attributed to the variation in the amount of unconverted kerogen in the tar at any given time. Allred's postulate of an autocatalytic reaction between the bitumen and kerogen is also a consequence of the changing composition of the bitumen (2).

More recently, Suuberg et al.(24) have shown that the molecular weights of the bitumens differ significantly from the oils produced during rapid pyrolysis of Colorado oil shale. They suggest that oil production is partly vaporization controlled and that current models are inadequate for predicting oil release under conditions of rapid heating. The reason for this is that the details of the reactions for formation and destruction of the bitumen are not yet satisfactorily understood and may be related to the nature of the cross-links in kerogen (25). This is a neoteric concept in oil shale studies although in coal research, the nature of the cross-links has been shown to play a significant role in the amount of tars and extractable materials formed during pyrolysis (25). The differences in the product distribution (including the bitumen) between the Colorado and Kentucky oil shales may be governed by the nature of the cross-links in the parent kerogen. For example, the low oil yields from the Kentucky shale may be the result of a more highly cross-linked kerogen which upon heating produces more char than oil.

4. Acknowledgment

The author gratefully acknowledges support of this work by the U.S. Department of Energy under Cooperative Agreement DE-FC21-86 MC11076.

5. References

1. Burnham A.K., Relationship between hydrous and ordinary pyrolysis, this monograph.
2. Allred, V.D. Chem. Eng. Prog. **1966**, *62*, 55-60.
3. Braun, R.L., and A.J. Rothman. Fuel **1975**, *54*, 129-131.
4. Johnson, W.F., D.V. Welston, H.H. Keller, and E.J. Couch. Quart. Colo. Sch. Mines **1975**, *70*, 237-272.
5. Drescher, E.A., C.A. Bassil, and E.J. Rolinski. In Alternative Energy Sources v. Part D: Biomass/Hydrocarbons/Hydrogen; Veziroglu, T.N., Ed; Elsevier Sci. Pub. B.V.: Amsterdam, **1983**, pp. 307-324.
6. Rajeshwar, K. Thermochemica Acta **1981**, *45*, 254-263.
7. Wallman, P.H., P.W. Tamm, and B.G. Spars. ACS Symposium Series 163, American Chemical Society: Washington, DC, 1981, 93-113.
8. Wen, C.S., and T.P. Kobylinski, Fuel **1983**, *62* 1269-1273.
9. Shen, M.S., L.S. Fan, and K.H. Castleton. ACS Div. Petrol. Chem. Preprints **1984**, *29*(1), 127-134.

10. Miknis, F.P., D.A. Netzel, J.W. Smith, M.A. Mast, and G.E. Maciel. Geochim. et Cosmochim. Acta **1982**, 46, 977-984.
11. Hubbard, A.B., and W.E. Robinson. USBM Rept. Investig. 4744, **1950**.
12. Miknis, F.P., P.J. Conn, T.F. Turner, and G.L. Berdan. Western Research Institute, Laramie, WY. August **1985**, [Rep] DOE/FE/60177-2213.
13. Miknis, F.P., T.F. Turner, and L.W. Ennen, 1987 Eastern Oil Shale Symposium Proceedings, Lexington, KY, p. 323-328.
14. Miknis, F.P., T.F. Turner, G.L. Berdan, and P.J. Conn., Energy and Fuels, **1987**, 1, 477.
15. Conn, P.J., H.J. Rollison, and F.P. Miknis. Western Research Institute, Laramie, WY, Oct. **1984** [Rep] DOE/FE/60177-1791.
16. Miknis, F.P., P.J. Conn, and T.F. Turner. Western Research Institute, Laramie, WY, May **1985**, [Rep] DOE/FE/60177-2288.
17. Feldkirchner, H.L., and J.C. Janka. Proc. IGT Symp. on Synthetic Fuels from Oil Shale, Atlanta, GA, Institute of Gas Technology Dec. **1979**, 489-524.
18. Kahn, D.R., A.Y. Falk, and M.P. Varey. Proc. 1983 Eastern Oil Shale Symp., Lexington, KY, Nov. **1983**, 225-233.
19. Cronauer, D.C., J. Solash, D.A. Danner, and L.G. Galya. Proc. 1983 Eastern Oil Shale Symp., Lexington, KY, Nov. **1983**, 17-23.
20. Carter, S., D. Taulbee, and D. Collins. Proc. 1983 Eastern Oil Shale Symp., Lexington, KY, Nov. **1983**, 113-122.
21. Richardson, J.H., E.B. Huss, J.R. Taylor, M.O. Bishop, and L.L. Ott. Lawrence Livermore National Laboratory, Livermore, CA, December **1981**, [Rep] UCRL-86587.
22. Li, S., J. Qian, K. Qiu, and Y. Zhu, Ranliao Huaxue Xuebao, 15(2), 118-123 (1987).
23. Mityurev A.K., in Chemistry and Technology of Combustible Shale and Their Research Products, G. Geller, ed. , Israel Programs for Scientific Translation, Jerusalem, 205-221 (1962).
24. Suuberg E., J. Sherman, and W.D. Lilly, Fuel, **66**, 1176-1184 (1987).
25. Suuberg E., P.E. Unger, and J.W. Larsen, Energy and Fuels, **1**, 305 (1987).

AQUEOUS ORGANIC CHEMISTRY: GEOCHEMICAL ASPECTS*

MICHAEL SISKIN¹ AND ALAN R. KATRITZKY²

¹Corporate Research Laboratory
Exxon Research and Engineering Co.
Route 22 East, Clinton Township
Annandale, New Jersey 08801 USA

²Department of Chemistry
University of Florida
Gainesville, FL 32611

ABSTRACT. Study of the reactivity of organic molecules in hot water is developing from studies aimed at understanding how organic matter (kerogen) forms in natural environments and then breaks down into energy source materials. In natural systems where kerogens are depolymerized, hot water is ubiquitous and usually contains salt and minerals. Reactions such as ionic condensation, cleavage, and hydrolysis are facilitated by changes in the chemical and physical properties of water as temperature increases. These changes make the solvent properties of water at high temperature similar to those of polar organic solvents at room temperature. Therefore, reactions with organic compounds are facilitated. An understanding of aqueous organic chemistry may lead to potential applications in areas as diverse as petroleum exploration, coal liquefaction, synthesis of chemicals and plastics recycling.

1. Introduction

This presentation describes an emerging area of chemistry: the transformations of organic compounds in hot water at elevated pressure. Although conventional wisdom holds that most organic compounds do not react with water under normal conditions, our overview demonstrates that water frequently participates as catalyst or reactant as well as solvent. Specifically, the behavior of compounds with functional groups and linkages corresponding to those found in shale kerogens and coals, and their precursors, implies that water has important effects on the conversion of plant and animal material into organic fuels under geologic conditions of time, heat, and pressure. These results are of broad interest to geologists, chemists, and anyone who is concerned with the environment.

Common organic molecules that were previously considered to be unreactive in liquid water undergo many chemical reactions when the temperature is increased to 250° to 350°C; these reactions were previously expected only in the presence of strong acid or base. For example, ethers and esters, which are unreactive to heat alone, undergo facile

* Excerpted largely from Science 1991, **254**, 231 with permission.

cleavage and hydrolysis, respectively, in water at 250° to 350°C (1). Similarly, polyethylene terephthalate polymers (found in plastic soft drink bottles) can be hydrolyzed quantitatively back to their starting materials in hot water in less than an hour (2). Other polyesters and also polyamides (like nylon) are equally susceptible to hydrolysis. A major analogy in nature of polymers to such reversion reactions is catagenesis: the process by which solid petroleum kerogens, which are cross-linked macromolecular structures, are converted in source rocks into liquid petroleum. Natural catagenesis takes place at temperatures below 200°C over millions of years in aqueous environments at pressures of about 61 MPa. Because of the relatively low temperatures, it has been hypothesized that some of the chemistry by which petroleum is formed is catalyzed by clay minerals in the sediments (3). Two additional factors can affect and catalyze kerogen and thus are important to petroleum formation. One is that simple aqueous chemistry generates water-soluble products that are acidic or basic, or have redox properties. The other is the effect of salts present in sea water or aqueous environments (4,5).

Should one expect organic chemical reactions to take place in hot water? Dramatic changes in the physical and chemical properties of water suggest the possibility: as temperature increases, water becomes more compatible to reaction with organics. For example, as temperature rises from 25°C to 300°C, the density of water decreases from 0.997 to 0.713 g/cm³ (6), its dielectric constant decreases from 78.85 to 19.66 (7), and its solubility parameter decreases from 23.4 to 14.5 (cal/cm³)^{1/2} (8). The ionic product (dissociation constant) of water increases by three orders of magnitude, from 10^{13.99} to 10^{11.30} (9), even though the dielectric constant falls with rising temperature. These changes in physical properties make the solvent properties of water at 300°C roughly equivalent to those of acetone at 25°C. Therefore, ionic reactions of organics should be favored by increased solubility in water. The increase in the dissociation constant will increase the rate of both acid- and base-catalyzed reactions in water far beyond the natural acceleration due to increased temperature.

The reactivity of organics in water in the temperature range of 200° to 350°C (10) has been systematically studied with the use of reactants that include aliphatic and aromatic species containing oxygen, sulfur, and nitrogen functional groups. Many of these are representative of structures found in kerogenous resources such as coals and oil shales. In many cases, salt (brine) and minerals were added to the model organic compound-water systems to simulate the chemistry of diverse natural environments. These reactions are carried out in closed reactors, such as an autoclave, in which a liquid water phase is maintained (5). Pressures range from ~4 MPa at 250°C to ~17 MPa at 350°C. From these studies, new understandings of aqueous organic chemistry have emerged, and several key concepts governing these reactions have been recognized, including: (1) Water can act as a highly effective acidic or basic catalyst, and indeed, as a powerful acid-base bicatalyst. Such catalyzed reactions are often further accelerated by acidic and basic minerals like clays and carbonates. (2) Ionic chemistry predominates as high-temperature water opens reaction pathways that are alternative to and preferred over thermal (free radical) routes. This ionic chemistry is often facilitated in brine. (3) Reactions can be autocatalyzed by water-soluble reaction products.

On the basis of these fundamental concepts, we present in this article an overview of the reactivity of a broad range of organic molecules in hot water, including in the presence of minerals and brine. These advances have increased our confidence in our ability both to understand organic geochemical processes and to promote new desired reactions under environmentally clean and safe conditions.

2. Geochemical Background

Plant substances are transformed in the relatively quiescent waters of swamps to peat. The subsequent burial of the peat in an aqueous anoxic environment causes further chemical and physical changes, and the peat is converted into lignite during the first stage of coalification. From a chemical point of view, coalification can be grossly viewed as a progression of molecular changes, some microbiological, that converts lignocellulosic plant material to coal, over millions of years and with increasing severity of geological conditions (especially temperature and pressure). Coalification is largely a deoxygenation-aromatization process; as the rank (degree of metamorphosis) of the coal progressively increases during heating, the organic oxygen content decreases and aromaticity increases by a series of condensations that include dehydration, dehydrogenation, alkylation, and elimination reactions. The concept is further illustrated by comparison (Fig. 1) (11) of two parameters of rank in the principal reactive component of coal (vitrain): percent oxygen and percent carbon. During formation of bituminous coal, which lies about halfway along the metamorphic pathway between peat and high-ranked anthracite coal, the initial organic material becomes largely an insoluble, cross-linked macromolecular network. Parts of two-dimensional structural models believed to be representative of a low-rank lignite (12) and a medium-rank bituminous coal (13) (Type III kerogens) are illustrated in Fig. 2. To be solubilized or converted into liquid products, these structures must be chemically or thermally broken down, or depolymerized. Most current technologies convert solid coal to synthetic fuel liquids by thermal free-radical depolymerization.

The organic material in oil shale is derived largely from algal material deposited in the mineral sediments of a lacustrine or marine environment. This process, called diagenesis, consists of condensation and aromatization pathways similar to those for coals and forms insoluble cross-linked macromolecular structures (Types I and II kerogens). These kerogens typically have a higher aliphatic carbon content than coals. It is generally believed that shale kerogens, which in an aqueous environment were exposed to increasing temperature and pressure, are the immediate precursors for most of the naturally occurring gaseous (natural gas) and liquid (petroleum) hydrocarbons. Because the temperature remains below 200°C during oil generation, many researchers have postulated that catalysis would have been required to sufficiently lower the activation energies of the decomposition reactions. The most obvious natural catalysts are the clay minerals of the matrix in which the kerogen is dispersed. Grim (3) suggested that the clay minerals in

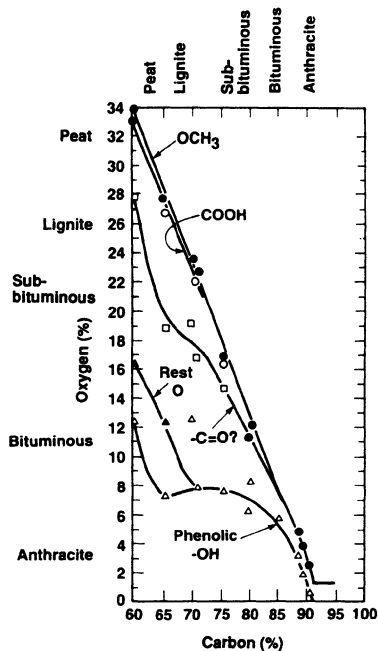


Fig. 1. Oxygen functional groups in coals vary according to rank. [Adapted from van Krevelen (11) with permission]

shale and sediments concentrate organic substituents by absorption and then act as acid catalysts in converting kerogens into petroleum.

Typical coals and kerogens (14) in oil shales consist of two- to three-ring aromatic clusters connected largely by cross-links, or bridges (Fig. 2), of carbon as diaryl methanes and ethanes, oxygen as diaryl and alkylaryl ethers and some esters, and sulfur as diaryl and alkylaryl sulfides. Hydroxyaromatics are abundant in coals, whereas carboxylic acids, ammonium carboxylates, primary amides, and smaller amounts of esters predominate in oil shales as pendant groups on aliphatic chains. In both coals and oil shales, most of the sulfur and nitrogen is present in heterocyclic rings.

The models in Fig. 2 also suggest that carbon and oxygen cross-links need to be broken if solid coals and oil shale kerogens are to be converted into liquids usable as synthetic fuels. Thermal conversion at 400°C easily cleaves diaryl ethane bridges, but diaryl methanes are less susceptible and biphenyl type linkages are thermally unreactive. Methylene-bridged cross-links are not reactive in hot water at 350°C except in the presence of strong acids. In contrast, ether and ester cross-links are only slowly cleaved thermally at 350°C, but in water they can be readily broken by hydrolysis at much lower temperatures (250° to 300°C). Moreover, some of the water-soluble products generated (for example, acids and bases formed by hydrolysis of pendant ester, amide, and nitrile groups and by decarboxylation of acids and carboxylate salts) can be expected to autocatalyze these and other reactions in both commercial processes and in nature.

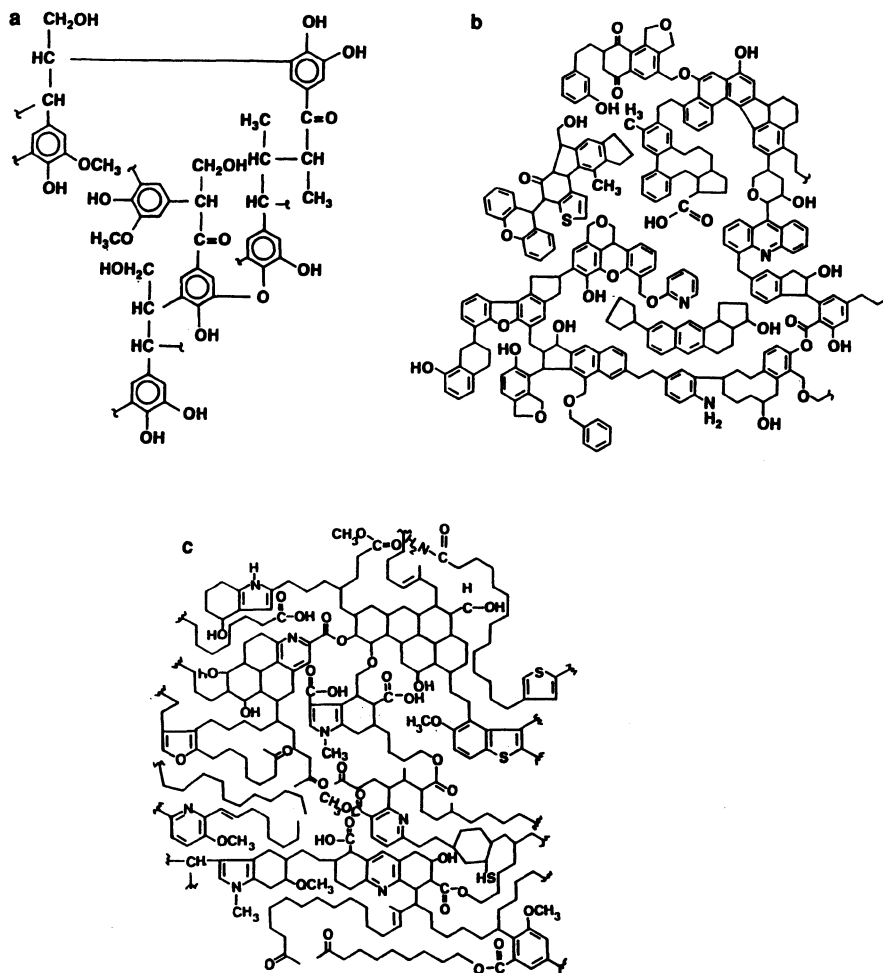
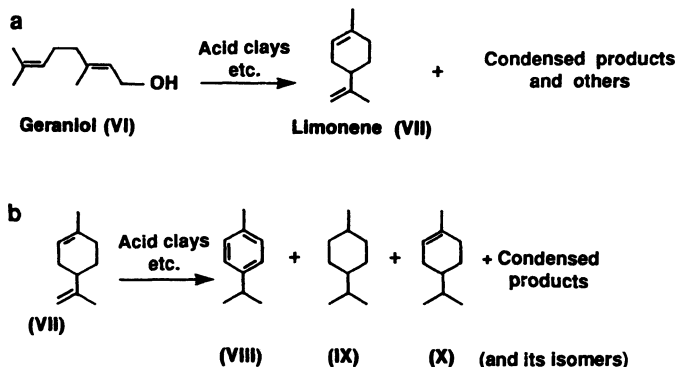


Fig. 2. Portions of structural models of the representative organic material in resources: (a) lignite coal [from (12) reprinted with permission from Pergamon Press PLC]; (b) bituminous coal [from (13), reprinted with permission from Butterworth-Heinemann Ltd. and the author]; (c) oil shale kerogen (14).

During diagenesis, condensation reactions predominate in the conversion of the initial plant and algal materials into the macromolecular network structures characteristic of kerogen. During catagenesis (the macromolecular depolymerization that generates petroleum) cross-link cleavage and hydrolysis reactions become dominant. Generally, in many model compound studies, the aliphatic derivatives typify the structures found in oil shale kerogens and the aromatic structures those found in coals.

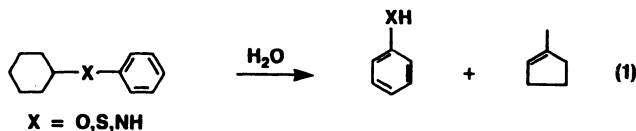
sequence demonstrates that such structures in kerogens could be converted by surface-active materials in sediments to low-molecular-weight aromatic compounds of the type found in petroleum (Scheme 2). A subsequent study by Goldstein (19) showed that geraniol (VI), a biologically synthesized unsaturated alcohol, undergoes a similar stepwise catalytic conversion in the presence of water, clays, and other sediments at $<100^{\circ}\text{C}$ initially to form polymeric materials. These polymeric materials were converted into the thermodynamically stable phenyl, naphthyl, and higher condensed aromatic products. This model system study nicely demonstrates that clay, limestone, and other sediments catalyze a wide variety of reactions in closed, water-containing systems of varying pH (3.9 to 9.7).



Scheme 2. Reactions of geraniol (a) and limonene (b) in the presence of clay. [Adapted from (17) with permission from Pergamon Press PLC]

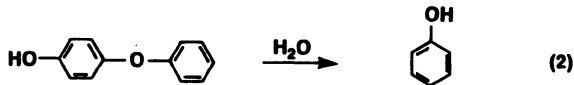
3.2 BOND CLEAVAGE REACTIONS

Studies of cyclohexyl phenyl compounds with oxygen, sulfur, and nitrogen links showed that they were relatively unreactive thermally, but readily cleaved in water at 250°C to form methylcyclopentene together with phenol, thiophenol, or aniline, respectively (Eq. 1)

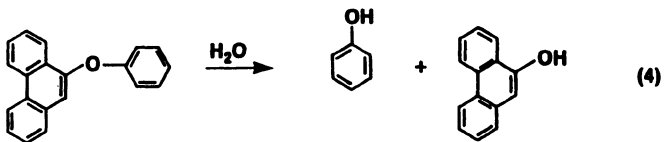
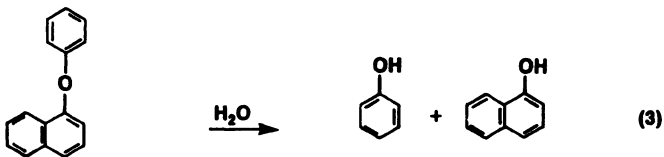


(20). These ionic reactions are enhanced in brine (10% NaCl) and in the presence of an acidic clay but depressed by basic calcium carbonate. This evidence supports the notion that an acid-catalyzed carbocation mechanism operates in water at high temperature for this system. Cycloalkyl-X-aryl ($\text{X} = \text{O}, \text{S}, \text{N}$) structures are representative of the major cross-links in a sample of a Kimmeridge shale, which is a source rock for petroleum found in the North Sea (21). Other aryl ethers, especially diaryl ethers, are more representative of the structures found in coals. Although an acyclic diaryl ether (diphenyl ether) and a

cyclic diaryl ether (dibenzofuran) were unreactive under both aqueous and thermal conditions, an activated diaryl ether (4-phenoxyphenol) was preferentially cleaved in water to form large amounts of phenolic products (Eq. 2) (1).



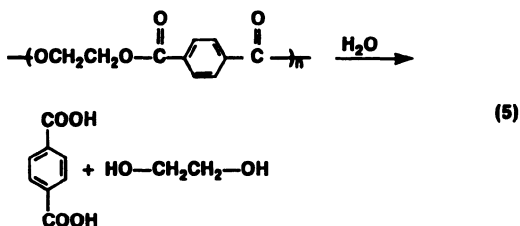
Similarly, benzyl aryl ethers were much more susceptible to cleavage under aqueous than thermal conditions at 250°C. Significantly, the unactivated diaryl ethers 1-phenoxyphenanthrene and 9-phenoxyphenanthrene are cleaved in water at 315°C in 2 hours to phenol and 1-naphthol or 9-phenanthrol, respectively (Eqs. 3 and 4) (22).



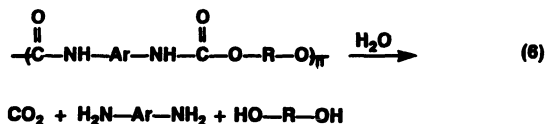
Ester groups, which are bound into the network of resource structures and serve as cross-links, although thermally unreactive, are easily cleaved in water at 250-350°C (4).

3.3 HYDROLYSIS REACTIONS

Synthetic polymers can be considered analogous in structure to and contain many of the functional groups found in the macromolecular structure of resource materials. Hydrolysis reactions have been used to effect desired chemical changes in synthetic polymers in a manner similar to natural geochemical reactions (as discussed later). Mandoke (2) described a simple approach for the neutral hydrolytic decomposition of condensation polymers like polyethylene terephthalate (soda bottles), nylon 6 and 66, other synthetic fibers, and polycarbonates in water at 200° to 300°C (Eq. 5).



Similarly, polyurethane foams can be hydrolyzed to reusable diamines and glycols (Eq. 6) (23).



In other studies (16) modeling kerogen reactivity, decyl decanoate was readily hydrolyzed in water at 250°C, in an ionic reaction catalyzed by brine and calcium montmorillonite. Norton (24) describes a hydrolytic process for making aromatic carboxylic acids from nitriles at 200° to 300°C. In this approach, no catalyst is added directly, but the aqueous solution from earlier hydrolyses is used in order to take advantage of autocatalysis by ammonia formed during the hydrolysis of the amide intermediate. Analogous autocatalytic approaches have been used to form glycols by hydrolysis of the corresponding acetic acid diesters (25) in order to produce formic acid from methyl formate (26) and glycerin by hydrolysis of glycerol triacetate with water at 180° to 245°C (27). Evstratova, et al. (28) hydrated 2,6-dicyanopyridine stepwise to the diamide in boiling water in a reaction that is acid- and base-catalyzed.

Benzonitriles, pyridinecarbonitriles, benzamides, and pyridinecarboxamides are almost unaffected by thermolysis but are rapidly hydrolyzed in water at 250°C to the corresponding ammonium carboxylates (the nitriles via the amides). The ammonia formed autocatalyzes these hydrolyses and the subsequent decarboxylations (29).

3.4 AUTOCATALYSIS

In the formation and depolymerization of resource materials, autocatalysis appears to be a major mechanistic pathway. During the diagenesis of kerogens, oxygen functionalities such as carboxylic acids, aldehydes, and alcohols are lost directly by cleavage and indirectly by condensation reactions that form methylene bridged, ether, and ester cross-links. The cleavage reactions release water soluble products such as carbon dioxide, formic acid, and formaldehyde (Scheme 1). In the water-filled pore systems of oil-bearing rocks, the acids and formaldehyde can autocatalyze diagenesis and subsequent catagenesis chemistry. In addition to acid catalysis by carbon dioxide and formic acid, the formaldehyde and formic acid act as hydride ion transfer agents and thereby reduce oxygen functionalities to alkyl groups and polycyclic aromatics to their partially hydrogenated hydroaromatic derivatives. When the three oxygenated pyridine derivatives are allowed to react in added formic acid or in formaldehyde generated in the forward reactions (Scheme 1), the course of the reaction changes such that methylated reduction product (II) is favored over pyridine (V) (5).

The effect on reaction rates of benzyl alcohol emphasizes the significance of autocatalysis. Benzyl alcohol undergoes 30% conversion to toluene, benzaldehyde, and dibenzyl ether in water after 1 day at 250°C. Under these conditions, benzyl acetate is

rapidly hydrolyzed to benzyl alcohol and one equivalent of acetic acid; in the presence of acetic acid, conversion of the benzyl alcohol is three times as fast, and not only are more toluene, benzaldehyde, and dibenzyl ether produced, but also a series of alkylated products (benzylated benzyl alcohols and benzylated toluenes) not observed with the pure benzyl alcohol (30). Many aqueous reactions are facilitated by increasing the ionic strength of the medium and catalyzed by acidic and basic minerals in the geological formation, as well as by generation of organic acids (from aqueous hydrolysis of, e.g., esters) and bases such as ammonia (by hydrolysis of nitriles and amides). Other more practical examples of autocatalysis were discussed above.

3.5 RELATED REACTIONS

Henderson (31) showed that montmorillonite, in water at 375°C, catalyzes the conversion (90%) of octacosane ($C_{18}H_{38}$) into an insoluble black carbonaceous material and small amounts of alkenes and aromatics. Without water, only 1% of the octacosane was converted to other alkanes and aromatics.

Jurg and Eisma (32) reacted samples of behenic acid ($n-C_{21}H_{43}COOH$) with montmorillonite in sealed tubes in the presence and absence of water at 200°C for 89 and 760 hours. They found that hydrocarbon formation was significant only in the presence of the clay catalyst. The ratios of iso- to normal-butane (1:40) and iso- to normal-pentane (1:40) were raised significantly in the presence of water (1:1) in both cases; the data indicate that the water induced carbocation chemistry. The increase in the proportion of saturated hydrocarbons with time at the expense of unsaturated hydrocarbons suggests that alkylation or hydrogenation reactions were occurring. Among the higher molecular weight hydrocarbons (C_{14} to C_{34}), there was a strong predominance (55 to 60%) of $C_{21}H_{44}$, the direct decarboxylation product of behenic acid. On the other hand, the aromatic carboxylic acid, 1-naphthoic acid, was decarboxylated slowly in water at 250°C, but reacted quantitatively in <2 hours at 343°C. Under anhydrous conditions there was no reaction at 250°C; reaction at 343°C was slow (1).

Johns (33) studied the kinetics of the decarboxylation of behenic acid using a series of clays under anhydrous conditions. Arrhenius plots of the data show large decreases in activation energy (from 58.4 to 24.7 kcal/mol) for decarboxylation in the clay-catalyzed reactions compared to the reaction without clay catalysis. The time required for 90% decarboxylation at 60°C ranged from 2.9×10^{20} years for the thermal conversion to only 0.03 year when nontronite, an iron-containing clay, was present. Johns pointed out that the catalytic activity measured in these laboratory studies surpasses that of the natural shale kerogen systems, a finding consistent with the sharp decrease in clay acidity with increasing water content (19).

The dimerization at the alkene bond in mono-unsaturated fatty acids was carried out at 200° to 260°C in the presence of 2 to 5% of an acid-activated clay and 1-5% water in a pressure vessel or under reflux (34,35). The yield of dimerization products was about 60% for oleic acid.

Clark and co-workers studied the reactions of thiophene and tetrahydrothiophene in

water at 240°C: these compounds were converted slowly in water (36), but more rapidly in acidic media (37) and in the presence of metal cations (38,39). A small quantity of H₂S was produced, as well as CO₂ and low-molecular-weight hydrocarbons as gaseous products, and a complex array of liquid sulfur-containing products. Tetrahydrothiophene was more reactive than thiophene and showed some reactivity at high pH. More recently, Clark and co-workers (40) studied the reactions of benzothiophene with water and in the presence of metal cations and identified several higher molecular weight products.

4. Hydrous versus Anhydrous Pyrolysis of Kerogen

The studies of organic compounds discussed above have led to a better understanding of aqueous organic chemistry. In addition, several other studies have considered the reaction of resource materials (kerogens) in hot water as an alternative to anhydrous pyrolysis at higher temperature. Simulation of petroleum formation requires the presence of hydrous conditions because water is ubiquitous in sediments.

Winters et al. (41) demonstrated that the characteristic low olefin (high saturates) content of natural petroleum oils could be produced by hydrous pyrolysis of Woodford (Devonian), Phosphoria (Permian), and Kimmeridge (Jurassic) source rock shales at 330°C. Thus, hydrous pyrolysis in a closed system appeared to be a more realistic reaction system than anhydrous pyrolysis in an open system which, by contrast, generated large amounts of olefins.

This work is complemented by that of Tannenbaum and Kaplan (42) who carried out a comparative study in which low molecular weight hydrocarbons were generated from Green River oil shale kerogen by both hydrous and anhydrous pyrolysis. At 300°C, production of initial C₂ to C₆ olefins was comparable in both systems, but under aqueous conditions, their concentrations then started to decrease with time (also observed by Jurg and Eisma (32)). This high reactivity of the olefins may explain why olefins were not previously observed under hydrous conditions.

Hydrous pyrolysis (43) of a Messel shale, extracted with benzene-methanol, at 330°C for 3 days in the presence of D₂O gave saturated hydrocarbon products multiply substituted (1-14) by deuterium. Heating the saturated hydrocarbon docosane (C₂₂H₄₆) with a sample of solvent-extracted shale in an excess of D₂O showed only minor deuteration of the reisolated docosane (80%). This result suggests that simple hydrogen exchange on saturated molecules can be ruled out as a major pathway. However, under similar conditions in the aqueous system, the olefin 1-octadecene was completely reduced to octadecane (60%) with simultaneous significant deuterium incorporation. Hoering applied similar treatment to a kerogen-2-methylheptadecanoic acid mixture and found that the acid decarboxylated to 2-methylheptadecane in 10% yield, whereas facile deuterium exchange took place at hydrogen atoms adjacent to oxygenated functional groups. In other studies, Hoering and Abelson (44) showed that deuterated hydrocarbons are generated from kerogen heated in D₂O at 100°C and then dried and pyrolyzed in an inert atmosphere.

They proposed that olefins, or olefin intermediates generated during pyrolysis, exchanged with the D_2O . Alexander et al. (45) found that there was considerable exchange of isotopic hydrogen between naphthalenes and the acidic clay surfaces at 23°C or in aqueous slurries at 70°C.

In later studies, Huizinga et al. (46) found that the presence of clay minerals influenced the production of aliphatic hydrocarbons during laboratory thermal maturation studies of immature Type I and II kerogens at 200 to 300°C in a manner critically dependent on the water concentration. During dry pyrolysis, where only pyrolyzate water is present, normal alkanes of 12 or more carbon atoms and acyclic isoprenoids are almost completely destroyed by montmorillonite but undergo only minor alteration in the presence of illite. The presence of both clay minerals caused significant reduction in alkene formation and preferential retention of large amounts of the polar constituents of the bitumen (soluble, petroleum-like portion) but not alkanes or acyclic isoprenoids. Therefore, in the presence of these clay minerals, especially when dry, the constituents of bitumen fractionate according to their polarity. By this process, alkanes and acyclic isoprenoids are concentrated in the bitumen or petroleum fraction that is not strongly adsorbed on the clay matrices. The extent of these concentration effects is greatly diminished during hydrous pyrolysis. Under hydrous conditions (a mineral:water ratio of 2:1), the acidity, and therefore the effect of the clay minerals, is substantially reduced.

Eglinton et al. (47) carried out the hydrous pyrolysis of a Kimmeridge kerogen (Type II) at 280° or 330°C for 72 hours in the presence of clay or carbonate minerals. They found that more organic-soluble pyrolyzate was formed when calcium carbonate was the inorganic phase, which suggests that base-catalyzed cleavage of cross-links can be significant.

Kawamura (48) also reported that water present during the 200° to 400°C pyrolysis of Green River kerogen either enhanced the release of long-chain carboxylic acids (C_{10} - C_{32}) or reduced the rate of their thermal destruction. These results suggest that decarboxylation is not an important mechanism for generating aliphatic hydrocarbons during hydrous pyrolysis, a theory that agrees with some (16), but not all (32,33,43) of the studies on reactions of alkyl carboxylic acids in water. However, Kawamura logically suggested that carboxylic acids may be decarboxylated once they are released into bitumen, especially in a clay-rich mineral matrix.

More recently, Eglinton (49) showed that significant quantities of carboxylic acids are generated from bitumen-free (solvent extracted) kerogen concentrates, especially Type II kerogens, and that the presence of minerals significantly influences the amount of acids produced. The major acid product in all cases was acetic acid, suggesting that ester hydrolysis is a key route.

Graff and Brandes (50) found that a steam pretreatment of an Illinois bituminous coal (Type III kerogen) between 320° and 360°C dramatically improved the yield of liquids upon subsequent conversion or solvent extraction. The steam-modified coal contained twice the hydroxyl groups of the raw coal. This result leads to the conclusion that steam reacts with the ether linkages in coal; this reaction forms hydroxyl groups and thereby substantially reduces an important covalent cross-link in the coal structure (51). These

conclusions are consistent with model compound studies on ether reactivity in hot water (1,20,21).

5. Implications for Technology

Chemical reactions carried out in hot water have the potential to provide a cleaner, safer environment than reactions in hydrocarbon solvent media. In addition, water acting as a catalyst or reagent could minimize, or possibly eliminate, the need for catalyst synthesis, recycle, regeneration, and disposal. Application to the recycle of condensation polymers such as plastics, synthetic fibers, and polycarbonates is attractive (2,23). Another potential application is the use of hot water treatment to upgrade low-value by-products of operating processes. A demonstrated example occurs in the hydration of propylene with sulfuric acid to form isopropyl alcohol and diisopropyl ether as a by-product. Hydrous cleavage of this ether at 315°C for 30 minutes readily forms essentially equimolar amounts of the desired product, isopropyl alcohol, and recyclable propylene (52). Di-sec-butyl ether, a by-product in the hydration of butylene to sec-butyl alcohol in the methyl ethyl ketone process similarly can be converted to the alcohol in hot water (52).

Kerogens are generated in an aqueous environment largely by condensation reactions followed by depolymerization. Aqueous pretreatment of coals at moderate temperatures could increase the amount of extractable liquids or enhance subsequent liquefaction conversion (50). Other potential applications for hot water in by-product upgrading, waste-stream cleanup, recycling of off-spec materials, and so forth, are numerous and await innovative ideas.

6. Conclusions

In this presentation, we have emphasized the geochemistry of the reactivity of organic molecules in hot water. Outside of biological processes, where aqueous chemistry predominates and is catalyzed by enzymes, kerogen formation and its subsequent depolymerization into petroleum is the major arena in nature where aqueous chemistry is observed. In this chemistry, water participates as catalyst, reactant, and solvent. Although the geochemical aspects serve as a foundation for understanding the aqueous chemistry, the implications for a wide variety of other organic chemical transformations and technological applications are potentially large and just beginning to emerge.

The ability of water to carry out condensation, cleavage, and hydrolysis reactions and to effect selective ionic chemistry (not accessible thermally) is largely due to changes in its chemical and physical properties of, which become more compatible with the reactions of organics as the temperature is increased. Therefore, the solvent properties of water at 250° to 350°C approach those of polar organic solvents at room temperature. Water can

act as an acidic or basic catalyst, and its reactivity can often be reinforced by autocatalysis from water-soluble reaction products. Additional positive aspects of the use of aqueous chemistry are its simplicity, low cost, and favorable environmental impact.

7. References and Notes

1. M. Siskin, G. Brons, S. N. Vaughn, A. R. Katritzky and M. Balasubramanian, Energy Fuels, 1990, **4**, 488.
2. J. W. Mandoki, U.S. Patent 4,605,762 (12 August 1986).
3. R. E. Grim, Am. Assoc. Pet. Geol. Bull., 1974, **31**, 1491.
4. M. Siskin, G. Brons, A. R. Katritzky and M. Balasubramanian, Energy Fuels, 1990, **4**, 475.
5. A. R. Katritzky, A. R. Lapucha, R. Murugan, F. J. Luxem, M. Siskin and G. Brons, *ibid.* (1990), **4**, 493.
6. CRC Handbook of Chemistry and Physics (61st Edition, 1981) p. E57.
7. G. C. Akerloff and H. I. Oshry, J. Am. Chem. Soc., 1950, **72**, 2844.
8. Calculated from specific internal energy of vaporization in J. H. Keenan and F. G. Keyes, P. G. Hill and J. G. Moore, Steam Tables, Wiley-Interscience (1969).
9. W. L. Marshall and E. U. Franck, J. Phys. Chem. Ref. Data, 1981, **10**, 295.
10. Series of 18 initial publications, Energy Fuels, 1990, **4**, 475-584.
11. D. W. van Krevélen, Coal: Typology-Chemistry-Physics-Constitution, Elsevier (1961) pp. 171-173.
12. P. G. Hatcher, Org. Geochem, 1990, **16**, 959.
13. J. H. Shinn, Fuel, 1984, **63**, 1187.
14. C. G. Scouten, M. Siskin, K. D. Rose, T. Aczel, S. G. Colgrove and R. E. Pabst Jr., Preprints Am. Chem. Soc. Div. Petrol. Chem., 1989, **34**, 43.
15. J. A. Ballantine, J. H. Purnell and J. M. Thomas, Eur. Pat. A-1 EP31252 (1 July 1981); J. M. Adams et al., Angew. Chem. (Int. Ed. Engl.) 1978, **17**, 282.
16. M. Siskin, G. Brons, A. R. Katritzky and M. Balasubramanian, Energy Fuels, 1990, **4**, 475.
17. H. Mueller and D. Voges, U.S. Patent 4,539,415 (3 September 1985).
18. M. Frenkel and L. Heller-Kalai, Org. Geochem., 1977, **1**, 3.
19. T. P. Goldstein, Am. Assoc. Pet. Geol. Bull., 1983, **67**, 152.
20. M. Siskin, G. Brons, A. R. Katritzky and R. Murugan, Energy Fuels, 1990, **4**, 482.
21. M. Siskin and C. G. Scouten, unpublished results.
22. M. Siskin, A. R. Katritzky and M. Balasubramanian, Energy Fuels, 1991, **5**, 770.
23. J. F. Kinstle, L. D. Forshey, R. Valle and R. R. Campbell, PrePrints. Am. Chem. Soc. Div. Polym. Chem., 1983, **24**, 446; G. A. Campbell and W. C. Meluch, Environ. Sci. Technol., 1976, **10**, 182.
24. R. V. Norton, U.S. Patent 3,873,610 (25 March 1975).
25. Y. Tanabe, J. Toriya and I. Kasahare, Ger. Offen. DE2645030 (14 April 1977).

26. J. D. Leonard, U.S. Patent 4,299,891 (10 November 1981).
27. W. Vogt and H. Glaser, Ger. Offen. DE2062376 (29 June 1972). (See also, GB1,320,280).
28. M. I. Evstratova et al., Khim.-Farm. Zh. 1985, **19**, 196.
29. A. R. Katritzky, A. R. Lapucha and M. Siskin, Energy Fuels, 1990, **4**, 555.
30. A. R. Katritzky, M. Balasubramanian and M. Siskin, Energy Fuels, 1990, **4**, 499.
31. W. Henderson, G. Eglinton, P. Simmonds and J. F. Lovelock, Nature, 1968, **219**, 1012.
32. J. W. Jurg and E. Eisma, Science, 1964, **144**, 1451.
33. W. D. Johns, Dev. Sedimentol., 1982, **35**, 655.
34. F. O. Barrett, U.S. Patent 2,793,219 (21 May 1957).
35. O. Schmint and K. Huttner, U.S. Patent 1,988,021 (15 January 1935).
36. P. D. Clark, J. B. Hyne and J. D. Tyrer, Fuel, 1983, **62**, 959.
37. P. D. Clark, J. B. Hyne and J. D. Tyrer, Fuel, 1984, **63**, 125.
38. P. D. Clark and J. B. Hyne, Fuel, 1984, **63**, 1649.
39. P. D. Clark, N. I. Dowling, J. B. Hyne and K. L. Lesage, Fuel, 1987, **66**, 1353.
40. P. D. Clark, K. L. Lesage, G. T. Tsang and J. B. Hyne, Energy Fuels, 1988, **2**, 578.
41. J. C. Winters, J. A. Williams and M. D. Lewan, Advances in Organic Geochemistry, Wiley (1981) pp. 524-33.
42. E. Tannenbaum and I. R. Kaplan, Nature, 1985, **317**, 708.
43. T. C. Hoering, Org. Geochem., 1984, **5**, 267.
44. T. C. Hoering and P. H. Abelson, Carnegie Inst. Wash. Yearbook, 1963, **62**, 229; T. C. Hoering, ibid. 1968, **67**, 199.
45. R. Alexander, R. I. Kagi and A. V. Larcher, Geochim. Cosmochim. Acta, 1982, **46**, 219.
46. B. J. Huizinga, E. Tannenbaum and I. R. Kaplan, Geochim. Cosmochim. Acta, 1987, **51**, 1083.
47. T. I. Eglinton, S. J. Rowland, C. D. Curtis and A. G. Douglas, Org. Geochem., 1986, **10**, 1041.
48. K. Kawamura, E. Tannenbaum, B. J. Huizinga and I. R. Kaplan, Org. Geochem., 1986, **10**, 1059.
49. T. I. Eglinton, C. D. Curtis and S. J. Rowland, Mineral Mag., 1987, **51**, 495.
50. R. A. Graff and S. D. Brandes, Energy Fuels, 1987, **1**, 84.
51. S. D. Brandes, R. A. Graff, M. L. Gorbaty and M. Siskin, Energy Fuels, 1989, **3**, 494.
52. M. Siskin, G. Brons, S. N. Vaughn and R. Y. Saleh, U.S. Patent 5,043,486 (27 August 1991).
53. We thank our colleagues at Exxon Research and Engineering Company and the University of Florida, whose names are mentioned in the references, for their contributions to the aqueous chemistry studies and Joyce C. Barrett for editorial assistance.

Asphaltites: Composition and Conversion

Y. YURUM¹ and E. EKINCI^{2,3}

¹Hacettepe University, Department of Chemistry, Beytepe-Ankara, Turkey

²TUBITAK-MRC, Department of Chemical Engineering, Gebze-Kocaeli, Turkey

³ITU, Department of Chemical Engineering, Ayazağa-Istanbul, Turkey

1.0. Introduction

Turkey has insignificant reserves of crude oil and natural gas. Consequently, the amount of foreign currency spent on importation of petroleum and electricity is equivalent to the total exportation from the country. The increasing trend in crude oil prices, is an important threat to the industrialisation of Turkey. There are two possible ways in which Turkey can approach the problem of providing crude oil for the industry and decrease the balance of payments problems: Firstly, in the acceleration of exploration for oil, and secondly in the development of synfuels technology from solid fuels that are present in Turkey. Due to the shortage of appropriate technologies and investment easy liquefiable sources should be given preference. Compared to the world standards Turkey is not rich in solid fuel resources, but it contains considerable amounts of lignites, oil shales and asphaltites. The former two have a plant origin, and require complex and expensive technologies, while the latter is formed by migration of petroleum followed by biodegradation and other maturation processes during burial, and liquefies at moderate conditions using simpler technologies.

In this manuscript it has been aimed to review the related work on the occurrence and conversion of Southeastern Anatolian Asphaltites.

1.1. BACKGROUND

The asphaltite reserves have been considered as "coal" and were originally burnt as coal for domestic, industrial and transportation purposes as fuel⁽¹⁾. It was used in steamers on Tigris river. At present there is still some domestic utilisation of asphaltite which is one of the main causes for Diyarbakir rated as the 13th and 2nd dirtiest city in Turkey, during the winter of 1992, in SO₂ and smoke emissions respectively. The winter average emissions measured were 194mg/m³ and 187mg/m³ for SO₂ and smoke respectively.

Tasman⁽³⁾ reported that asphaltites are formed by the leakage of petroleum into coal formations Aydoğan⁽¹²⁾ was first to report that its origin is all petroleum.

Generally asphaltic materials are formed by the migration of petroleum into cracks during tectonic movements. During and after the migration petroleum loses its light weight components and becomes subject to a series of complex chemical

and physical changes. Depending on the extent of these changes, the new formation may end up to be natural asphalts, asphaltites and asphaltic pyrobitumen in the given order⁽⁴⁾.

The ash content of the asphaltite formation in Turkey differ from the general asphaltic substances in other parts of the world which tend to have low ash content of about 1 %. This has caused great differences in the chemical structure due to the catalytic activities promoted by the inorganic matrix in the case of the former.

2.0. Formation, Reserves and Characteristics of Turkish Asphaltites

Şirnak asphaltites are found in the Germav formation of Cretaceous-Paleocene age in the form of almost vertical dykes: the Germav formation consists of alternating sand stone, shale and limestone and has been intercut with asphaltite. The age of deposition of the asphaltites is Miocene or younger. The main rock is carbonate of the Cudi formation and in probably Junassic-Cretaceous age Lebküchner and Orhun⁽⁵⁾, Williams⁽⁶⁾, Tasman⁽³⁾ Erdem-Şenatalar et al.⁽⁷⁾.

The Avgamasya bitumen, Soxhlet extracted with chloroform, was characterised⁽⁸⁾ and classified as an aromatic asphaltic oil⁽⁹⁾. The oil formation was originated from open water marine sediments laid down in an anoxic environment. Asphaltic minerals are generally believed to be formed by migration of petroleum followed by alteration during burial. Light fractions are lost and variety of biodegradation, oxidation, evaporation, water washing and other chemical reactions occur with concomitant increase in the molecular weight and decrease in H/C ratio. The changing mineral, as a result of metamorphosis, has higher melting point and lower CS₂ solubility as compared to the original input. The stratigraphic/tectonic history of asphaltites^(1,3,8) suggest an origin from inspissated petroleum. There is a striking similarity between the average structures of asphaltites and Athabasca bitumen^(8,9,10).

The different veins of asphaltic material reported in Table 1 have different physical and chemical characteristics depending on the location of asphaltic material, geological formation and degree of metamorphosis⁽¹¹⁾. During the full process of migration, semi asphaltic and asphaltic petroleum transform to natural asphalt after losing its light fractions. Then, through the process of metamorphosis asphaltite and asphaltic pyrobituminous structures are followed. Therefore, natural asphalt is a product of petroleum asphaltite which had its light components evaporated while asphaltites and asphaltic pyrobitumens are products resulted from chemical reactions in the presence of catalytic activity of mineral matter⁽⁴⁾. Turkish asphaltites are mostly classified between asphaltites and asphaltic pyrobitumens in terms of the degree of metamorphosis⁽¹¹⁾ and Lebküchner and Orhun⁽⁵⁾ from considerations of the surrounding geological features, suggested that southeastern Anatolian asphaltites arises from an aromatic intermediate oil by alteration during migration.

Average values for the analysis of the asphaltite reserves are reported to be: (1-5.33) % water, (33-47) % ash, (4.3-6.4) % sulphur, (24-40) % volatile matter, (47-59) % fixed carbon, (3.4-5.6) % hydrogen and (4.9-30) % solubility in CS₂ (12). The spread of analytical data on the parameters indicate that the asphaltites similar to Turkish coals show a ready changing characteristics⁽¹³⁾.

A comparative study of the Avgamasya asphaltite and neighbouring Raman-Dinçer crude that is within migration distance is made by Erdem-Şenatalar et. al⁽⁷⁾. The neighbouring Raman-Dinçer crude oil is situated in an anticlinal structure which ends with a fault at the northern end. The reservoir rock is Beloka formation of Campanian age. It is overlaid by the lower clayed Sinan Maastrichtian formation. The Beloka formation is represented by limestone, dolomite and dolomitic limestone. Porosity has been formed after burial of the formation. Petroleum produced from this area originates from calciferous rock of the Jurassic-Cretaceous Cudi group. The West Raman crude of south eastern Turkey has been classified as aromatic intermediate by Huc et.al.⁽¹⁴⁾. Raman Dinçer crude study by Erdem-Şenatalar et.al.⁽⁷⁾ classified the oil as an extreme aromatic intermediate type.

Table 1. Some of the Important Reserves of Asphaltites of Turkey⁽⁸⁾.

Name	Reserve (1000 Tones)	Higher Calorific Value (kcal/kg)	Mineral Matter Content (%)
Avgamasya	14300	4000-5000	37.4
Milli	6500	3000-4000	50.2
Anılmış	5510	5000	-
Seridalhi	4000	5000	58.4
Nivekar	1700	4250	45.9
Ispindoruk	1215	4000	42.1
Segürük	1000	4000	38
Harbolite	18000	5000-7000	42

Comparison of the Avgamasya asphaltite oils produced by various extractive methods are compared with the Raman Dinçer crude on similar fractionation and characterisation methods. One of the distinct differences observed between the oil and the asphaltite is on the n-alkanes distribution. The asphaltite is severely depleted in C₁₀-C₃₁ n-alkanes and is dominated by the unresolved branched/cyclic compounds on which are superimposed the peaks of the isoprenoid and terpenoid compounds which are all more resistant to bacterial attack.

The water washing and biological attack is believed to remove the low molecular weight compounds from oils as well. However the comparative study on Avgamasya asphaltite and Raman-Dinçer crude indicated that the effects are not as significant⁽⁷⁾.

Avgamasya and Raman-Dinçer crude is found to show distinctive similarities in molecular weight distribution, aromaticity and alkyl chain length calculated by structural analysis⁽⁷⁾.

The ¹H and ¹³C-NMR spectra of the two hydrocarbonaceous minerals are virtually identical confirming the conclusion reached by that biodegradation does not affect alkyl side chain of large aromatics.

3. Utilisation and Structural Studies on Turkish Asphaltites

The asphaltite reserves found in Southeastern Turkey in the province of Siirt (Şırnak) and Mardin (Silopi) were burnt as coal originally in 21 provinces but its usage as coal has been restricted. There have been various researches conducted to find out the best usage for these asphaltites. These may be classified as pyrolysis, solvent extraction at atmospheric and higher pressures, supercritical gas and fluid extraction, hydrogen donor solvent extraction, mineral matter extraction, fluidised bed combustion and the use of asphaltite as ammonia feedstock. A brief summary of these studies is presented below.

3.1. PYROLYSIS

Due to the simplicity of this method and low capital and operational costs it has been applied earlier than other methods. The first reported work on Turkish asphaltite is by Tasman⁽³⁾ on Harbolite. In this study Harbolite was subjected to Fischer distillation and the following results were obtained: Liquid product 13 %, water decomposition 3.5 %, coke and free coal 25.3 %, inorganic matrix 44.6 % and gaseous products 13.6 %. Orhun⁽¹¹⁾ pyrolysed Avgamasya asphaltite in Fischer retort up to 530°C. In this study he investigated the samples obtained from different depths of burial.

The results indicated that the liquid product yield for pyrolysis got smaller as the depth of burial was increased.

The most detailed pyrolysis study was carried out on Avgamasya asphaltite by MTA researchers (Maden Tetkik Arama Enstitüsü, Mining Research and Development Institute) to produce synthetic gaseous, liquid and solid fuels as main products, hydrogen sulfide and ammonia as by-products⁽¹⁶⁾. The optimum yield is obtained for three different temperature ramps of 800, 900 and 900°C from room temperature with pyrolysis times of 300, 300 and 375 minutes respectively. The optimum product distributions are reported to be: 64.6 % pyrolysis coke, 19.1

% gaseous fuel, 11.8 % synthetic crude oil, 2.9 % liquor, 0.5 % hydrogen sulphide and 0.13 % ammonia. The net heating value of the pyrolysis coke is 3900 kcal/kg but it is unsuitable for metallurgical purposes. The synthetic crude oil has an API gravity (at 60/60°F) of 26.6, sulphur content of 3.8 %, carbon-hydrogen ratio of approximately 8 and a net heating value of 9400 kcal/kg. The liquid product therefore has very similar properties to natural crude oil even without hydrogenation. The gaseous product contains 37.8 % hydrogen by volume and has a higher calorific value of 4800 kcal/Nm³. In the report it is emphasized that recovery of rare metals may be an important economical incentive. Also, from this laboratory scale study a flow diagram for an integrated process has been proposed.

Table 2. Pyrolysis Results for Avgamasya Asphaltite Samples From Different Depths⁽¹¹⁾.

Depth of the samples taken	m	21.7-37.5	76.8-95.4	131.6-147.7	160-170
Water (Moisture Structural)	%	0.67	0.80	0.53	0.54
Gaseous Product	%	8.02	6.19	6.47	7.41
Liquid Product	%	12.0	11.2	9.8	8.0
Distillation Residue	%	79.35	81.8	83.2	84.0

Two asphaltites namely Harbolite and Avgamasya were pyrolysed at 525 and 840°C and the liquid and gaseous products were characterised by Ekinci et.al. The main purpose of the study was to make structural comparisons with the solvent extraction products obtained from the same asphaltites^(17,18). Preparative pyrolysis was carried out in a bench-scale Gray-King apparatus as used for coal. Samples of both asphaltites were heated from room temperature up to 525 or 840°C over 75 and 150 minutes respectively. The final temperature was maintained for 30 minutes.

The water free liquid products were separated into pentane solubles, asphaltenes (pentane insoluble, benzene soluble) and benzene insoluble material. Oil and asphaltene fractions were further separated into paraffinic, neutral aromatic and polar fractions by column chromatography as described by^(15,13). Chromatographic, spectroscopic and other related methods are used to characterise the liquid product fractions and the product gas.

From the experiments greater yields of liquid products are obtained from the less metamorphosised Harbolite asphaltite. Pyrolysis tended to produce a greater proportion of paraffinic products, asphaltenes, and large polar aromatic fractions. The results of this study may be summarised as follows:

Table 3. Pyrolysis Results of Harbolite and Avgamasya Asphaltite

	HARBOLITE		AVGAMASYA	
	525	840	525	840
Temperature, T(°C)	525	840	525	840
Pyrolysis Loss (% wt/wt)	27.5	41.6	16.9	19.3
Oil Yield (% wt/wt)	19.0	24.4	10.8	11.1
Volume Evolved (gas/cm ³ g ⁻¹ asp)	67	208	70	118

Önen et al.⁽²⁵⁾ carried out comparative pyrolysis of two Turkish asphaltites (Silopi, Şırnak) and two oil shales (Göynük and Seyitömer). The pyrolysis was carried out using a Heinze retort under a heating rate of 5 °C/min and was maintained half an hour at the peak temperature of 540 °C. As a result of this study, it has been stated that shale oil was more aliphatic in character than the asphaltite oil. The oils from asphaltites have shorter alkyl chain lengths. The average length of alkyl side chains of asphaltites were reduced on pyrolysis but similar effects were not observed for oil shales.

3.2 SOLVENT-EXTRACTION OF TURKISH ASPHALTITES

Avgamasya and Harbolite asphaltites were subjected to solvent extraction using different solvents, with and without acid extraction and at atmospheric and higher pressures. The best solvents for the extraction of Minacar asphaltites at different temperatures and pressures were linseed oil followed by cresols, anthracene oil and pyridine⁽²¹⁾. Tolay⁽²²⁾ also observed best yields for linseed oil but found this solvent to be degradative. Among benzene methanol, pyridine, aniline and tetraline Bartle et al.⁽⁸⁾ obtained best yields for chloroform extraction for Avgamasya and Harbolite.

3.2.1. Acid Extraction of the Inorganic Matrix of the Asphaltites

As shown in Table 1 all of the reported Turkish asphaltites have high mineral matter content. One possible way of producing synfuels from these solid minerals is the elimination of the mineral matter⁽²³⁾. Bartle et al.⁽⁸⁾ extracted the carbonates and sulphates using zinc dust and hydrochloric acid. This pretreated and original asphaltite were solvent extracted to observe the effects of acid pretreatments.

In addition to the pretreatments reported by Bartle et al.⁽⁸⁾, Tolay⁽²²⁾ extracted Silicates using 15 % HF. At the end of the three acid pretreatments, the highest inorganic matter removal efficiency was obtained to be 88.4 %.

3.2.2. Solvent Extraction at Atmospheric Pressure

Saraçoğulları⁽²⁴⁾ carried out soxhlet extraction studies on what he called "Şırnak" asphaltites which categorically include (Avgamasya, Milli. Seridalhi, Nivekar and Segürük veins). Asphaltite/solvent ratio of 1/10 of benzene, chloroform and carbontetrachloride were used. On the average 10-12 % crude oil is obtained from the original asphaltite. The particle size of -9 and -32 mesh did not change the extraction efficiency considerably. The resultant crude was reported to be viscous. His results are compiled in Table 4.

Table 4. Soxhlet Extraction of Şırnak Asphaltite

Solvent	Time (hr)	Particle Size (mesh)	Yield of Crude Oil (%)
Benzene	8	-9	10.25
Benzene	12	-9	11.33
Chloroform	12	-9	11.50
Chloroform	8	-32	13.00
Chloroform	24	-32	12.60
CCl ₄	8	-9	7.0
CCl ₄	8	-32	9.67

Table 5. Solvent Extraction of Avgamasya and Harbolite Asphaltites⁽⁸⁾.

Solvent	Treatment	Extraction Time (hr)	Yield %	
			Avgamasya	Harbolite
3/1 benzene-methanol	-	24	4.8	6.5
3/1 benzene-methanol	-	Exhaustion	4.8	18.0
3/1 benzene-methanol	HCl, HCl-Zn	Exhaustion	5.9	17.0
Aniline	-	24	5.3	5.6
Tetralin	-	24	6.0	11.5
Chloroform	-	24	6.1	12.5
Chloroform	HCl, HCl-Zn	Exhaustion	8.8	24.8

Prior to pyrolysis work mentioned earlier⁽¹⁸⁾, Bartle et. al.⁽⁶⁾ have done solvent extraction of Avgamasya and Harbolite both with and without acid pretreatments. The aim of this study was to provide a base for comparison with the yield and product quality of pyrolysis. The results for both asphaltites, with and without pretreatments, are shown Table 5 for the 5 different solvents that are used.

The pretreated chloroform extracts are analysed by use of size exclusion chromatography and spectroscopy, particularly ¹H and ¹³C nmr.

More recently Tolay⁽²²⁾ carried out Soxhlet extraction on the pretreated and original Avgamasya using toluene, CS₂ and chloroform as solvents. The results of his experiments are compiled in Table 6.

Table 6. Soxhlet Extraction of Avgamasya Asphaltite

Solvent	Sample	Ash (%)	Extraction Time, (hr)	T, (°C)	Yield, (%)
Toluene	Original	37.6	76	110	9.16
Toluene	Acid Extracted	5.0	76	110	10.02
CS ₂	Original	37.6	76	46	13.04
CS ₂	Acid Extracted	5.0	76	46	15.22
Chloroform	Original	37.55	76	61	10.58
Chloroform	Acid Extracted	5.0	76	61	12.28

3.2.3. Mild Pressure Solvent Extraction

Similar to the line of Saraçoğulları, Evgin⁽²⁵⁾ carried out benzene, methanol/benzene, toluene, chloroform and carbon tetrachloride extraction of Avgamasya asphaltite and obtained yields varying between 8-13 %. Chloroform resulted in highest yield among the solvents used. Tolay⁽²²⁾ extended his study of solvent extraction at pressures higher than atmospheric of original and acid pretreated Avgamasya. On the original asphaltite autoclave extractions were done at pressures 1, 5, 10, 15, 20 and 30 atmospheres. The highest yield was observed at 10 atmosphere as 16 % for toluene which was 59 % increase as compared to the atmospheric yield Table 7.

Table 7. Autoclave Extraction of Avgamasya Asphaltite

Solvent	Acid Extraction	Pressure, att	Crude Oil Yield, %
Toluene	Treated	1	10.02
Toluene	Treated	5	14.45
Toluene	Treated	10	15.96
Toluene	Untreated	10	13.30
Toluene	Treated	15	15.13
Toluene	Treated	20	14.90
Toluene	Untreated	20	11.86
Toluene	Treated	30	14.31
Toluene	Untreated	30	11.4
Chloroform	Treated	1	12.28
Chloroform	Treated	10	14.92
Chloroform	Treated	20	10.32
Chloroform	Treated	30	9.51

Similarly, Saraçoğulları obtained an optimum (22.7 %) yield at 200 °C and 7.8 atmosphere for Şırnak. These mild pressure extraction results indicate a possible start to an effective asphaltite utilisation complex process.

3.2.4. Supercritical Gas and Liquid Extraction and Hydrogen Donor Solvent Extraction

In a detailed study Erdem-Şenatalar⁽²⁶⁾ has done extensive studies on supercritical gas and liquid extraction and hydrogen donor solvent extraction. The experiments involved temperatures between 325-345 °C and pressures upto 150 atmosphere and variation of yields and composition of the extracts are investigated. The parameters taken for the supercritical gas extraction included temperature, gas density and acid treatment. The solvent used was toluene. Hydrogen-donor extraction was performed using tetraline and the parameters investigated included: temperature, time, particle size, solvent/asphaltite ratio and extraction atmosphere (N₂/air ratio).

During the comparative experiments temperature was found to have the strongest effect on the yield for all extraction methods. The rate of increase in the yield with

temperature slowed down above 425 °C. Hydrogen donor extraction conversion and yield were found to be higher than all other extraction methods.

The explanation given for the higher yields for H₂-donor extraction was the capping by hydrogen of radical centers formed by pyrolytic bond breaking which becomes more important at higher molecular weight components which are less stable and will otherwise polymerise into insoluble char.

Erdem-Şenatalar's⁽²⁶⁾ investigation of the H₂-donor solvent extracts showed that with increase in temperature there is a tendency for greater percentage of lower molecular weight fractions. The pyrolysis effects on the average structural parameters of the neutral oil and asphaltene fractions of the extracts such as their aromaticity, average molecular weight, degree of alkyl and naphtenic substitution and average chain length become evident above 400 °C and especially above 425 °C. These temperatures are considerably higher than the corresponding oil shale pyrolysis reactions. This is explained for asphaltites by nature of the organic input in the asphaltites which predominantly are asphaltenes and preasphaltenes of which cracking becomes important above 400 °C and 425 °C respectively. The oil formation is attributed to be from asphaltite and preasphaltenes 400 °C-425 °C, oil formation was mainly by the cracking of asphaltenes. The increase in both oil and gas yield were due mainly to the cracking of the alkyl chains⁽²⁶⁾.

The investigation of super critical gas extraction products differed from other extraction methods by its selectivity towards relatively lighter and less condensed oils with shorter and fewer alkyl substitutions. Supercritical liquid-extraction is found to increase the Soxhlet yield by solubility of higher molecular weight asphaltenes with long alkyl chains and relatively condensed average aromatic skeleton but the lighter oil extracted by the supercritical gas from the pores of organic structure, are not present for soxhlet extraction⁽²⁶⁾.

3.2.5. Feedstock for Ammonia Synthesis

Turkey has a shortage of ammonia in 1993⁽¹⁷⁾. Considering the future plans for increasing the agricultural products of the country by four fold by the south-eastern irrigation project (GAP). The deficit will be getting greater, therefore, sources for ammonia production may be necessary. Having generally high hydrogen/carbon ratios asphaltites may be used for this purpose, especially the residues, after a synfuel process. As reported by MTA⁽¹⁶⁾ the coke obtained after the pyrolysis does not meet metallurgical purposes. This carbon residue or residue from solvent extraction may be used in ammonia synthesis⁽²⁸⁾

3.2.6. Fluidised Bed Combustion

From the relatively high calorific valued pyrolysis residue⁽¹⁶⁾ solvent extraction residues, it is not possible to obtain metallurgical coke for this reason combustion of the residue may be an efficient utilisation and environmental control

technology. Because, even if another process follow pyrolysis or solvent extraction, i.e. ammonia synthesis, it is still necessary to burn the residue for environmental reasons. Since the residue contains unspent carbon and the calorific value is in the order of Turkish lignites, therefore it may be considered as a fuel. The high sulphur content of the residue makes fluidised bed combustion essential. On the fluidised bed combustion of Avgamasya asphaltite various studies have been carried out. Avgamasya asphaltite with sulphur and nitrogen content of 7.05 % and 1.1 % was burnt in a fluidised bed 10 cm in diameter⁽²⁹⁾. As burnt the fuel had much higher SO₂ emissions than EPA, or Air Quality Assurance Act of Turkey⁽³⁰⁾.

Ekinci et.al.⁽³¹⁾ investigated the SO₂ and NO_x capturing capacity of the inorganic matrix of Avgamasya asphaltite by burning the fuel as received and after the elimination of the calcium and magnesium by acid washing. It is observed that the inorganic matrix has an inherent SO₂ and NO_x capturing capacity due to the Ca content which a Ca/S mole ratio of approximately one. The indigenous Ca was found to be better SO₂ absorber than limestone especially at high excess oxygen conditions. The electron microscope studies showed that this was due to the resultant pore structure of asphaltite which is much larger than limestone.

In their comparative study of the ash content limit of combustion of Avgamasya and Harbolite asphaltites in a fluidised bed, Ekinci et.al.⁽³²⁾ noted that it is possible to burn synthetically prepared Avgamasya and Harbolite asphaltites with ash contents of 86 and 85 % at 800°C. These ash contents corresponded to calorific values of 2.83 MJ/kg and 3.74 MJ/kg which indicated that asphaltite residues with very low calorific values may be burnt in fluidised bed for refuse reclamation and steam generation purposes.

3.2.7. Rare Metals Recovery

During the pyrolysis experiments MTA researchers⁽¹⁶⁾ noted that loss of rare metals such as Ni, Mo, V, Ti and radioactive minerals such as U₃O₈ was not significant.

Akçetin⁽³³⁾ in his metal recovery study of Harbolite, Milli and Avgamasya asphaltites found presence of valueable metals however the economically viable ones are reported to be U, V, Mo and Ni. The metals contents in asphaltite ashes are shown in Table 8 as determined.

From Table 8 it is obvious that leaching of nickel, molybdenum, vanadium and U₃O₈ may be an essential part of an integrated asphaltite technology (28).

Table 8. Economically Viable Metal Potential of Turkish Asphaltites (kg/tonnes)

Asphaltite	U ₃ O ₈	V	Mo	Ni
Harbolite	0.24	3.45	3.33	2.76
Milli	0.21	2.94	3.20	2.27
Avgamasya	0.29	4.76	4.15	2.89

4.0 Integrated Asphaltite Utilisation Technological Alternatives

Considering the most important 3 reserves of asphaltites Harbol, Avgamasya and Milli MTA reserchers⁽²⁸⁾ have chosen Avgamasya asphaltite as a representative mineral since its chemical and physical characteristics and the stage of metamorphosis is nearly the average of the other two extreme asphaltites. Therefore, the average characteristics and quality of Southeastern asphaltites may be compared with those of Avgamasya.

Following on from this evaluation MTA⁽¹⁸⁾ has proposed the following synfuel and other utilisation technologies for Avgamasya asphaltite.

I. Direct combustion in a power plant in order to produce electricity: 1.000.000 Tonnes/year of asphaltite would provide enough fuel for a 2x150 MW power plant. From the 85 % captured ash (358 000 t), 5390 tonnes of concentrated nickel sulphate, molybdenum sulphate, vanadium sulphate and U₃O₈ would be obtained.

II. As a second alternative asphaltite is proposed to be utilised as a source for ammonia synthesis. Again on the basis of 1.000.000 tonnes/year 308.000 tonnes of ammonia may be produced. The remaining ash may be leached using sulphuric acid and 5706 tonnes of concentrated nickel sulphate, molybdenum sulphate, vanadium sulphate and U₃O₈ would be obtained.

Considering the lignite deposits of approximately 6 billion tonnes⁽¹³⁾ and recent technologies such as underground coal gasification applicable for ammonia synthesis, it would be wise to consider lignite deposits for ammonia plant projects as well⁽²⁴⁾.

III. Pyrolysis of asphaltite to produce synthetic crude oil, gas fuel and pyrolysis coke The latter may be utilised as power plant fuel. As in the first two alternatives rare metal recovery is considered. Beloff⁽²¹⁾ also notes that Minacar asphaltite is an excellent raw material for gas production.

It has been calculated that if 1.040.000 tonnes/year of asphaltite is fed to the synfuels plant 118.000 tonnes/year of synthetic crude oil having API gravity of 26.6 will be obtained. Also 252.000.000 Nm³/year of 4800 kcal/Nm³ of gas and

646.100 tonnes of pyrolysis coke having a calorific value of 3.900 kcal/kg and 5000 tonnes of H₂S may be produced. With 600.000 tonnes/year of pyrolysis coke 1x150 MW fluidised bed power plant may be operated. 5.333 tonnes/year of concentrated nickel sulphate, molybdenum sulphate, vanadium sulphate and U₃O₈ may be obtained.

IV. As in the third alternative it is proposed that the pyrolysis coke will be used in an ammonia plant. If this process is chosen 1.145.300 tonnes/year asphaltite would yield 118.000 tonnes/year of API gravity 26.6 crude oil, 252.000.000 Nm³/year gas with calorific value 4800 kcal/Nm³. From the remaining 415.800 tonnes/year pyrolysis coke 180.000 tonnes/year ammonia and from the ash 6.215 tonnes/year sulphates and U₃O₈ would be obtained.

V. Apart from alternatives stated by⁽²⁸⁾ solvent extraction at atmospheric and higher pressures should be considered.

As stated in alternative 4, on the basis of product yield pyrolysis is more advantageous over solvent extraction of original asphaltite. However, pretreatment of Avgamasya asphaltite increased 13.04 % to 15.22 % for carbonsulfide. These reported increases are obtained at high economical costs. Using Tolay's⁽¹⁴⁾ data it is clear that in order to process one metric ton of Avgamasya asphaltite 27.500 liters of 15 % HCl, 7.500 liters of 15 % HF and 100 kg of Zn powder would be necessary. As results of these enormous inputs only 17 kilogrammes of extra crude oil is obtained which makes it uncompetitive.

Table 9 : Analyses of lignite bituminous coal and oil shale

	BITUMINOUS		
	LIGNITE	COAL	OIL SHALE
Proximate Analyses (wt/%)			
Volatile matter (daf)	60.0	38.7	71.0
Ash (dry)	19.8	9.7	78.8
Moisture	6.3	1.7	3.0
Sulphur (total.dry)	4.7	1.1	2.3
Ultimate analysis (wt %)			
Hydrogen	6.8	5.8	8.5
Carbon	64.1	82.5	74.9
Nitrogen	0.7	2.6	1.7
Sulphur. S _{org}	1.5	0.9	1.0
Oxygen (by difference)	26.9	8.2	13.9

Table10: Yield of the Products of Pyrolysis

	LIGNITE		BITUMEN COAL		OIL SHALE	
	Fischer	Steam Pyrolysis	Fischer	Steam Pyrolysis	Fischer	Steam Pyrolysis
Products (%)						
Semicoke	53.2	47.8	76.0	72.0	88.0	80.4
Liquid Product	11.0	15.4	11.5	17.5	6.3	10.9
Gas-water-losses	35.8	36.8	12.5	9.8	5.7	8.7
Distribution of organic matter						
Semicoke	48.5	40.4	70.1	66.6	32.0	24.8
Liquid products	15.4	21.4	12.7	19.4	35.0	60.9
Gas-water-losses	36.1	38.2	17.2	14.0	33.0	14.3
Total Yield of volatiles(%)	51.5	59.6	29.9	33.4	68.0	75.2

References

1. Lebküchner, R.F., Occurrences of the Asphaltic Substances in Southeastern Turkey and Their Genesis., Maden Tetkik Arama Enst. Bull., No. 72, 74-96, 1969. (Tur)
2. Enviromental Statistics, Air Pollution, State Statistics Institute, News Bulletin, Ankara (Tur), 3.2.1993
3. Tasman,C., Harbolite, a Carbonaceous Hydrocarbon. Bull. Am. Assoc. Pet. Geol., 30:1051-1053, 1946
4. H. Abraham, Asphalts and Allied Substances, 6.Ed. Van Nostrand Co, Inc. 1960.
5. Lebküchner R.F., Orhun, F., and Wolf M., Bull. Amer. Assoc. Petrol. Geol. 56, 1939, (1972)
6. Williams, P.V.F., In Brooks, J. (Ed.) Organic Maturation Studies on Fossil Fuel Exploration, p255, Academic Press, NY, 1981
7. Erdem-Şenatalar, A., Ekinci, E., Bartle, K.D., and Frere, B., Hydrocarbon Minerals From South Eastern Turkey, Erdöl und Kohle, Erdgas-Petrochemie vereinigt mit Brennstoff-Chemie, Bd 44 Heft 7/8 Jul./August, 1991
8. Bartle, K.D., Ekinci, E., Frere, B., Mulligan, M., Saraç, S. and Snape, C., The Nature and Origin of Harbolite and a Related Asphaltite From Southeastern Turkey, Chemical Geology, 34-151-164, 1981.
9. Tissot, B.P. and Welte, D.H., Petroleum Formation and Occurrence Springer, Berlin, Part IV, Ch. 2, 1978.
10. Speight, J.G. and Moschopedis, S.E., Some Observations on the Molecular Nature of Petroleum Asphaltenes, Am. Chem. Soc., Div. Pet. Chem., 24:910-923, 1979.
11. Orhun, F., Characteristic Properties of Asphaltic Substances in Southeastern Turkey, Their Degree of Metamorphosis and Their Classification Problems., Maden Tetkik Arama Enst. Bull., No: 72, 97-109, 1969 (Tur)
12. Nakoman, E., Southeastern Anatolian Asphaltic Formations, Madencilik Bull. MMO Publications, p.41, Nov.1977. (Tur)
13. Maden Tetkik Arama Enst., Coal Inventory , Ankara, 1977. (Tur)

14. Huc, A.Y., Behar, F., and Roussel, J.C., Proc. Int. Symp. on Charct. of Heavy Oils and Petroleum Residues, Lyon France, p 99 (1984)
15. Snape, C.E., Ladner, W.R., and Bartle, K.D., in Schultz, H.D. Structural Characterization of Coal Extracts by NMR, Ch.4, Wiley, NY (1983).
16. Maden Tetkik Arama Enst., Investigation of the Possibility of Producing Synthetic Gas, Liquid and Solid Fuels From Southeastern Anatolian Asphaltites by Pyrolysis., Internal Report, 1977.
17. Ekinci, E., Pakdel, H., Jones, D.W., Bartle, K.D., Olcay, A., and Özel, F., The Organic Geo- chemistry of Harbolite and Avgamasya Asphaltites, *Chimica Acta Turcica*, Vol. 9, No 3, 465-473, 1981
18. Ekinci, E., Saraç, S., and Bartle, K.D., Characterisation of Pyrolysis Products of Harbolite and Avgamasya Asphaltites: Comparison with Solvent Extracts, *Fuel*, 61, 346, 1982
19. Bartle, K.D., Ladner, W.R., Martin, T.G., Snape, C.E., and Williams, D.F., Structural Analysis of Supercritical Gas Extracts of Coals., *Fuel*, 51: 156-159, 1979.
20. Önen, A., Saraç, S., Önen, A., and Ekinci, E., Estimation of Structural Parameters from Asphaltites and Oil Shale Pyrolysis Products by ^1H and ^{13}C NMR Spectroscopy, *Fuel Processing Technology*, 32, 151-58, 1982
21. Beloff, E.J., Minacar Asphaltite: an Asphaltite From Argentina, *Fuel*, 51: 156-159, 1972
22. Tolay, M., Elimination of Mineral Matter by Solvent Extracion of Şirnak-Avgamasya Asphaltite, MSc Thesis, İTÜ, 1982. (Tur)
23. Yen, T.F., Science and Technology of Oil Shale, Ann Arbor Pub. Michigan, 226, 1976.
24. Saraçoğulları, M., Solvent Extraction of Şirnak Asphaltite, Internal Report, MTA, 1976 (Tur).
25. Evgin, K.U., Investigation of Temperature and Pressure Effects on Solvent Extraction, MSc Thesis, İTU, 1981.
26. Erdem-Şenatalar, A., Investigation of Liquefaction Potential and Extract Structure of Avgamasya Asphaltite, PhD Thesis, İTU, 1984.
27. VI. Development Plan, State Planning Organisation, 1989, Ankara (Tur)

28. Maden Tetkik Arama Enst., Evaluation of the Utilisation Possibilities of Southeastern Anatolian Asphaltites Deposits, Internal Report, 1976. (Tur)
29. Ekinci, E., Combustion of Avgamasya Asphaltite in a Fluidised Bed, Doz. Thesis, İTÜ, 1981 (Tur)
30. Air Pollution Quality Assurance Legislation, Official Gazette, 19269, 1986, Ankara (Tur)
31. Ekinci, E., Pogson, B., and Fells, I., Sulphur Dioxide Capture by the Anorganic Matrix of a Low Grade Fuel in a Fluidised Bed Combustor, Journ. of Inst. of Energy 57, 368-72, 1984.
32. Ekinci, E., Türkay, __, Kadio^olu, E., and Fells, I., Ash Content Limit of Solid Fuels Combustion in a Fluidised Bed, Turkish-German Energy Symposium, İzmir, 1981.
33. Akçetin, D., Analytical Investigation of Some Usage of Asphaltites by N.A.A. as a Part of Turkish Energy Resources, Doz. Thesis, İTÜ, 1979. (Tur)
34. Yardım, M.F., Investigation of Pyrolysis Products of Avgamasya Asphaltite and Structural Analysis, MSc Thesis, İTÜ, 1984.

OIL SHALE AS A FEEDSTOCK FOR CARBON MATERIALS

Frank Derbyshire, Uschi Graham, You Qing Fei, Tom Robl, Marit Jagtoyen
University of Kentucky Center for Applied Energy Research,
3572 Iron Works Pike, Lexington, KY 40511-8433, USA

Introduction

Other chapters have considered oil shale in terms of its composition, characterization, and processing to produce, primarily, liquids. This chapter is concerned with the use of oil shale and oil shale products as starting materials for the production of high added-value materials. The focus is on the synthesis of carbon materials, although it should be recognized that a range of other materials can also be produced: oil shale can be used in cement and brick manufacture; shale liquids can be used as a source of nitrogen heterocycles for the chemical industry, and as asphalt additives and binders (1,2).

Later in this chapter, specific examples will be given from recent research that has demonstrated the formation of adsorbent or activated carbons, carbon fibers, and activated carbon fibers from oil shale. First it is useful to review the processes involved in the conversion of carbon-containing precursors to carbon products.

Carbon Formation

In hydrocarbon processing and the reactions of other carbon-containing compounds, carbon is almost invariably formed as a by-product. Carbon is formed by routes involving the loss of hydrogen and addition. In many cases, carbon formation is undesirable and can lead to the blockage of tubes and valves; deposits on the walls of vessels and tubes can reduce heat transfer; and deposition on catalysts can cause loss of activity. In oil shale processing, the secondary cracking of pyrolysis liquids can reduce the product yield, with the attendant formation of carbon deposits.

In other cases, carbons are produced either as a major co-product (e.g. in the pyrolysis of different starting materials for the production of liquids and gases) or the process is intended primarily for the manufacture of carbons. Depending on the type of carbon, the product may be manufactured in large volume (examples: metallurgical coke, petroleum cokes, activated carbons) or as a low-volume specialist material (carbon fibres, carbon-carbon composites, graphites).

It should be recognised that the words "carbon", "graphite", "coke" and "char" are used interchangeably, and inexactly, to refer to a very wide range of materials with very different properties. Carbon in its elemental form shows the same sort of versatility as it does as the basic ingredient of organic compounds.

Structure of carbon materials

Carbon is an element. It occurs principally in two crystalline forms, diamond and graphite, and in molecular form as fullerenes.

CRYSTAL STRUCTURE

Graphite is the thermodynamically stable crystalline form of carbon under normal conditions. Diamond is a metastable crystalline form, and will revert to graphite if heated to high temperatures, although the transformation is infinitely slow at room temperature. For the materials produced on a commercial scale that will be considered here, the graphite hexagonal structure provides the relevant model. However, it is useful to be aware of the other forms. In addition, the molecular forms of carbon known as fullerenes have been discovered only in recent years (3).

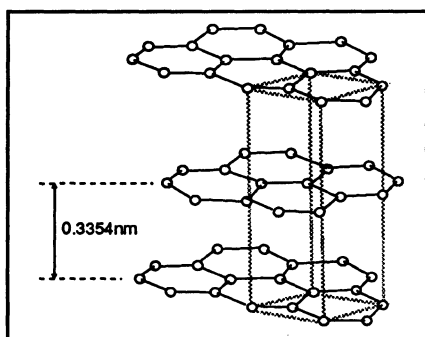


Figure 1. Graphite crystal structure

The arrangement of atoms in the diamond structure is such that the four electrons in the outer shell of each carbon atom are shared with four adjacent atoms to form a three-dimensional lattice entirely connected by covalent bonds. The strength of the attractive forces is such that this carbon structure is the hardest material found in nature and, despite being thermodynamically unstable, diamond has to be heated to above 3300°C before the structure is disrupted to form graphite. In addition to its hardness, which is attractive for many industrial applications, diamond's unusual optical properties (high refractive index and dispersion) make them the most valuable and desired gemstones. Diamonds and diamond films are also produced synthetically.

The crystal structure of graphite is highly anisotropic, Figure 1. It consists of parallel layers or basal planes containing carbon atoms arranged in hexagonal symmetry. The C-C bond distance is 1.415 Angstroms, compared to that in benzene of 1.395 Angstroms: the carbon atom arrangement in the layers is essentially the same as that in polycondensed aromatics. The layers are stacked in alternate sequence ABABAB, with an interlayer spacing of 3.354 Angstroms. Within the layers the bonding is covalent. Between layers the bonding is due to weak van der Waals interactions.

The anisotropic crystal structure gives rise to highly directional properties. For example, the ratio of electrical conductivity along the layers is about 200 times greater than across the layers at room temperature: similar behaviour is found for thermal conductivity. In terms of chemical reactivity, the basal planes are resistant to oxidation and other reactions, the edge planes much less so, where the exposed C atoms are susceptible to oxidative attack. The weak interlayer spacing makes cleavage facile in a direction parallel to the planes, which leads to the use of graphite as a lubricant.

Graphite occurs naturally in certain locations: Borrowdale, Cumberland, England, where the deposit supported a pencil industry in mediaeval times; Madagascar, Sri Lanka; and Ticonderoga, NY, USA. Its occurrence is always associated with proximity to igneous rock. It is also hypothesised that it is formed as the final stage of the maturation process of fossilized biological material.

Graphite crystals can be synthesised by solution crystallization from molten metals such as Fe, Ni or Co. It can also be formed in thin films at lower temperatures (500-1000°C) by vapour phase deposition onto these metals from carbon-containing precursor, when highly crystalline films are produced by solid solution and precipitation (4,5). However, artificial crystals are never very large (up to a few mm) because of their slow growth rate and associated high production cost: natural ones can be of mm to cm

size. Commercial graphites are actually assemblages of many single crystals and are the product of high temperature heat treatment.

DISORDERED CARBONS

All carbon-forming reactions generate C atoms and/or C-containing fragments which try to arrange themselves into the ideal graphitic structure, following the thermodynamic driving force. However, rarely is carbon formed under conditions which allow the time and provide the energy for the individual atoms to arrange themselves into a highly ordered structure. The process is limited due to a combination of factors such as a high rate of carbon production, low rate of carbon atom diffusion, and crosslinking by heteroatoms, which inhibits the processes of crystal growth. Consequently, what is often produced are small disordered crystals or crystallites that are flawed by imperfections. Over the whole range of possible structures, the extent of disorder can vary from the ideal graphite structure to the situation where, in theory, there is a collection of carbon atoms which are arranged in random order without any semblance of spatial arrangement. This never quite happens. There is always some degree of alignment between atoms, but it is convenient to consider these two situations as extremes, between which there can be a spectrum of intermediate structures.

The first level of structural disorder that departs from the ideal graphite crystal structure is due to stacking disorders of the layers: the layers are still parallel but not properly aligned so that they are rotated with respect to each other about an axis perpendicular to the layer planes. The carbon atoms do not sit comfortably in their minimum energy positions, there may be vacancies and interstitial atoms, and there is increased repulsion between the layers; the interlayer spacing increases from 3.354 to about 3.44 Angstroms. This is known as the turbostratic structure.

With further decrease in order, any residual semblance of the stacking sequence disappears and the interlayer spacing increases further to 3.5 to 3.7 Angstroms. That is, the parallel layers are in completely random rotation. This is the type of structure exhibited by carbon black.

Accompanying the increasing disorder, is the inability to sustain any long range coherence in the structure. The crystallites become smaller in the directions parallel and perpendicular to the layer planes - there are less layers in parallel and there are fewer atoms per layer.

The extent of structural order or disorder can be quantified by measurement of the interlayer spacing and the crystallite dimensions parallel and perpendicular to the layer planes, using diffraction techniques. Empirically, it is found that the dimensions parallel to the basal plane, L_a , and perpendicular to it, L_c , inversely correlate with the interlayer or d spacing.

If highly disordered crystallites are heat treated at elevated temperatures (graphitizing temperatures: up to 3000°C), the atoms in individual planes will diffuse into positions so that they start to assemble into the ideal stacking register and the interlayer spacing will decrease. At the same time, carbon atoms from the surrounding less ordered spaces will diffuse and add to the existing edges of planes and new planes can start to form, extending the crystallite dimensions. If possible, the crystallites will try to arrange in parallel orientation. The extent to which this can occur may be limited because strong bonds can restrict the movement of individual atoms and crystallites. Hence, carbons produced at low temperatures can be distinguished as graphitizing and non-graphitizing. Graphitizing carbons develop a highly ordered graphitic structure at temperatures above about 2200°C, while non-graphitizing carbons do not show any significant improvement in crystalline order or growth even after heat treatment to 3000°C. The

differences between these types of carbon become apparent from the earliest stages of carbonization.

CARBON MATERIALS

The properties of carbon and graphite materials depend primarily upon two factors: the structural order of the individual crystallites, their mutual orientation, and the manner in which they are bonded together. Consider the situation where a carbon artefact is composed of single crystals joined by a binder. If the crystals are all oriented in parallel, then the carbon body will have anisotropic properties as do the individual crystals. However, if the crystals are in random orientation, then the properties of the body will be isotropic despite the fact that the individual units are anisotropic. Partial alignment of the crystals will result in an intermediate situation where the properties are anisotropic but not as markedly so as in single crystal graphite.

Carbon bodies formed from different precursor materials consist of crystallites which possess lower degrees of structural order than that of the graphite single crystals and they are aligned randomly or in varying degrees of parallelism to each other. Hence, a broad spectrum of properties can be attained. The extent of alignment and packing of the crystallites also relates to the porosity of the carbon. If there is extensive parallel orientation, there will be few microvoids between the crystallites and low microporosity. If crystallite orientation is random, the carbon can be highly porous and contain a large surface area in the form of micropores which are accessible to small molecules - carbons in which this porosity has been deliberately developed are known as activated carbons and are highly effective adsorbents for removing a variety of contaminants from the liquid and gas phase.

Formation of low-temperature carbons (< 2000°C)

Carbon precursors can be solids, liquids or gases, and be produced by solid, liquid or gas phase reactions. Gases can form carbons by homogeneous reaction (e.g. carbon black) or heterogeneous reaction (deposition of carbon films). Liquids can also form carbons by homogeneous or heterogeneous reaction and solids only by homogeneous reaction. Solid precursors can be divided into two groups, thermosetting and thermoplastic. Thermoplastic solids can be considered to behave similarly to liquid precursors. Examples of thermosetting solids are certain polymers, biomass, peat, lignite, low-rank coals, some bituminous coals and high-rank coals. Examples of thermoplastic solids are common polymers and bituminous coals. Attention will be given here to liquid and solid phase carbonization, as these relate to potential processes for the conversion of shale oil residual liquids, whole shales, and retorted residues, to carbon products.

In a thermal (as apposed to catalytic) process, the onset of significant chemical change starts to take place in the region 400-600°C. At these temperatures, bonds begin to thermally cleave. The free radicals thus generated undergo a variety of reactions. They can stabilise by hydrogen abstraction, adduction to other molecules, and rearrangement. This results in the liberation of smaller molecules, and aromatization and the formation of stronger covalent bonds within the non-volatilized matter. There is a loss of labile hydrogen, and depending on the composition of the precursor, the loss of oxygen and sulphur, mainly as water and hydrogen sulphide, and the loss of volatile hydrocarbons - aromatics, paraffins, olefins. It is at this stage that the basic structure of the solid carbon product is determined.

During the carbonization of thermosetting precursors, there is little opportunity for the diffusion and arrangement of carbon atoms and sheets of polycondensed aromatics into ordered positions before the

structure is made rigid by the formation of a three dimensional network of crosslinks. The carbon produced from a thermosetting material tends to reflect the structure of the precursor because the structural units are maintained in essentially their original orientation. The resulting carbons are hard and possess an open porosity. The use of thermosetting precursors, or precursors that have been rendered thermosetting (for example by oxidative pretreatment), is essential to the formation of high surface area activated carbons.

For thermoplastic precursors and liquid feedstocks (residual oils, pitch, tar distillation residues), mobility in the liquid phase permits the movement of carbon atoms and the formation of large flat molecules of polycondensed aromatics. [Note: The presence of other types of molecule or heteroatoms can interfere with the planarity of the large molecules.] If there is sufficient mobility in the system, these sheets will diffuse into positions of parallel alignment. The liquid phase must not be too viscous and must persist for a reasonable length of time if this orientation is to occur to any great extent.

The formation and ordering of the planar molecules is similar to the process of crystallisation within the liquid phase and produces a liquid crystal structure. This exists as a separate anisotropic phase within the isotropic parent liquid, and is known as carbonaceous mesophase: meso meaning intermediate, and its formation determines the course of conversion of the precursor to a solid carbon product.

By using polarized light, the mesophase nuclei can be seen in an optical microscope, as they contrast against the featureless isotropic background. If a quarter wave plate is inserted, the nuclei show interference colours which alter according to the orientation of the layer planes to the objective of the microscope. Depending upon the carbonization conditions, mesophase development may be minimal, in which case the final solid carbon product is macroscopically isotropic (same as the thermosetting case); it may be arrested at an early stage when the optical appearance of the solid carbon shows a mosaic of small nuclei - hence known as a mosaic optical texture; or it may be extensive when the nuclei have grown and coalesced before solidification to form large domains or "flow domains" known as such because their appearance reflects the swirls and eddies of convection currents in the liquid before solidification. Optical micrographs of mosaic and flow domain structures are shown in Figure 2. The process may be terminated before solidification to produce a mesophase-containing substance (pitch), which may be used to produce specific types of carbon fibers, or as a source of mesophase microbeads (see below).

Mesophase development is curtailed by conditions which increase the rate of carbonization and inhibit free movement of the polycondensed molecules through the formation of covalent crosslinks (associ-

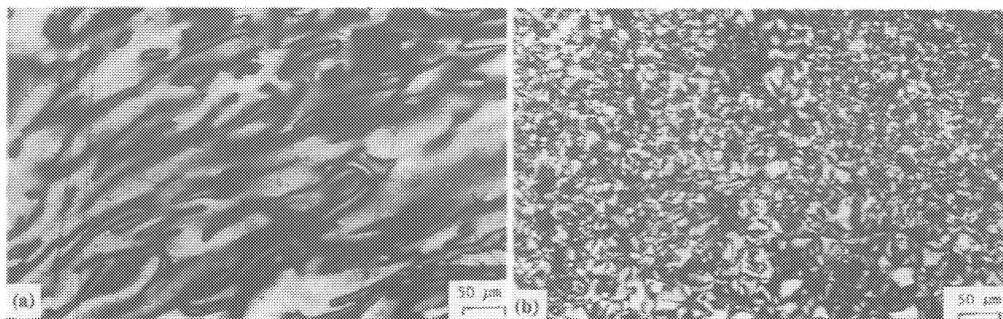


Figure 2. Optical micrographs of cokes showing a) flow domains and b) mosaic structure

ated with the reactions of heteroatoms) and which disrupt planarity (certain species which may be present are non-planar and their incorporation will also prevent the formation of large flat sheets), and the time for which the liquid phase persists before the whole mass becomes solid.

The low density of crosslinks in carbons with extensive mesophase development, and the greater degree of alignment of planar sheets, means that they are of low porosity and relatively weak. Such carbons are graphitizing, whereas carbons with high crosslink density are hard, porous, and non-graphitizing.

The products of residual oil carbonization find different uses depending upon the extent of mesophase development. Specialised (highly aromatic) feeds produce cokes with very extensive flow domains, and are known as needle cokes because the shape of the particles reflects the anisotropy on the molecular scale. They are used to produce graphite electrodes for steel making. For most residues, mesophase development is arrested at an earlier stage. These cokes are used for making carbon anodes for aluminium smelting or fuel. These cokes are known as sponge coke due to their more porous structure.

A second example is in the production of carbon fibers from pitch (coal or petroleum) precursors. High performance carbon fibers can be produced from pitch that has been first heat treated to develop a high mesophase content. General purpose fibers are produced from unmodified (isotropic) pitch.

Activated Carbons

Activated carbons are high surface area adsorbents that are used in diverse applications for purification and chemical recovery. Examples are: potable and waste water treatment; respirators; solvent recovery from process streams; air and gas purification; and the suppression of gasoline vapor emissions from automobiles. More specialized uses, sometimes involving the addition of impregnants, are in catalysis, medicine, military and industrial gas masks, and gold recovery (6-8). Activated carbon can be used to remove SO₂ and NO_x from combustion gases (9), are of interest to natural gas storage for vehicle fuelling (10), and for heat pumping or refrigeration (11). Activated carbons are also used as catalyst supports.

The consumption of activated carbons will continue to increase, spurred on directly and indirectly by environmental issues, and by the continual emergence of new uses. The expansion of the present market could also lead to the more diversified use of biomass and fossil fuel resources, these being the most available and commonly used precursor materials. In addition, the ability to produce activated carbons as by-products could beneficially affect the economics of fossil fuel utilization and conversion processes.

Activated carbons can be produced from a variety of solid precursors, both naturally occurring and synthetic. Common commercial feedstocks include biomass materials such as wood, coconut shell and fruit pits, and fossilized plant matter, peats, lignites and all ranks of coal. The commercial manufacture of carbons generally involves carbonization followed by activation (partial gasification) in steam or CO₂ to generate the required pore structure and surface area. High surface area carbons can also be produced by the reaction of a precursor with a chemical reagent at elevated temperatures. This process is known as chemical activation. Examples include the phosphoric acid activation of cellulosic precursors, such as wood, and the KOH activation of more aromatic structures such as coals, and petroleum cokes (12-14). Porosity is developed in a single heat treatment step, although a subsequent leaching stage is required to recover the reagent for recycle.

Derivation of Adsorbent Carbons from Pyrolyzed Oil Shale Residues

After pyrolysis of oil shale to produce liquid and gaseous products, as much as half of the carbon can remain in the retorted (spent) shale. This carbon-rich product is generally considered a waste material, whose disposal represents an economic and environmental problem. It is, therefore, important that the pyrolyzed shale be utilized, either in the retorting process as a source of energy, or as a source of new products. The former strategy is the basis for the development of the KENTORT II technology for Eastern US oil shales (15, 16). This technology completely utilizes the carbon in the pyrolyzed shale by incorporating integrated gasification and combustion steps. The latter strategy, the utilization of the spent shale carbon for generating new products, specifically activated carbons, is the focus of the study described below.

Previous work has shown that a range of materials can be manufactured from oil shale residues, including cement and asphalt additives (1, 2). However, the utilization of the carbon-rich residues from oil shale pyrolysis, as precursors for the production of adsorbent carbons has not been examined. The objective of this research is to examine the formation of adsorbent carbons from low-ash oil shale residues. The production of such high-value materials, in addition to oil, would make the economics of oil shale development more attractive.

PREPARATION OF ACTIVATED CARBONS BY STEAM ACTIVATION

Two oil shales from the Turkish Goynuk (17) and the Australian Alpha (18) deposits were selected for this study based on the following criteria: low ash contents; and high oil yields upon retorting. The oil shales were pyrolyzed at 550°C under a continuous flow of nitrogen. The N₂-swept fixed bed pyrolysis experiments were performed in a 1.5 inch stainless steel reactor. The reactor configuration has been discussed in detail elsewhere (19). During pyrolysis, the alginite-rich, low-ash oil shales were observed to form a macroporous network of charred carbonaceous material. Heating stage microscopic (HSM) examination, using polarized light, allowed the observation of the spatial relationships between the development of macropores generated by the volatilization of alginite macerals, and the char and minerals that stabilize the macrostructure.

After pyrolysis, the spent shale was activated in steam at 880 °C in a fixed bed reactor, Figure 3. Water is pumped through a 1/16 inch capillary and entered the reactor below a distributor plate, where it is released into the hot zone as superheated steam. The steam passes through the shale bed and exits the reactor, where it is condensed.

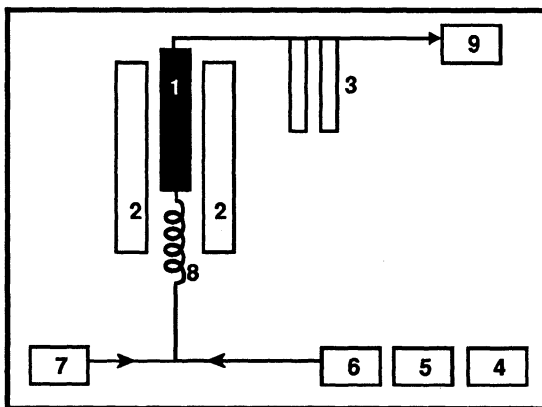


Figure 3. Schematic diagram of the steam retorting apparatus: 1=Reactor; 2=Furnace; 3=Ice-Trap; 4=Water reservoir; 5=Balance; 6=Water pump; 7=N₂-Gas; 8=Steam generator/heating Coil; 9=Gas Chromatograph

Results and Discussion

PYROLYSIS RESIDUES

The pyrolysis-induced porosity (PIP) in the retorted shale corresponds to a BET surface area of only 8-10 m²/g for both shales, Table 1, reflecting the development of, principally, macropores. The HSM experiments showed that the bulk of the macropores are formed during volatilization of the alginite macerals, at 460-470°C. The large elongated macropores are related to the

structure of alginite and vitrinite (desmocollonite) macerals, Figure 4a,b. The macropore framework constitutes an infrastructure that may readily allow steam to infiltrate during activation, and the addition of catalyst metals, facilitating the development of higher surface areas. The validity of this hypothesis was examined by examining catalyzed and uncatalyzed steam activation.

STEAM ACTIVATION

The pyrolysis residues were activated in steam at 880°C for one to ten hours. Examination of the steam treated chars by scanning electron microscopy (SEM) revealed a much rougher surface than the

Table 1. BET - Surface Area Development for Goynuk and Alpha Shales

Sample	BET	BET 1 h*	BET 4h**
Goynuk: Pyrolysed	8.8		
Goynuk: Steam Activated		180	350
Goynuk: Steam Activated/ZnCl ₂ -Catalyst		190	400
Goynuk: Steam Activated/Acid Washed		210	370
Alpha: Pyrolysed	10		
Alpha: Steam Activated		170	280
Alpha: Steam Activated/ZnCl ₂ -Catalyst		170	310
Alpha: Steam Activated/Acid Washed		200	350

* 1 hour steam treatment using steam flow rates of 2 grams/minute
 ** 4 hour steam treatment using steam flow rates of 2 grams/minute
 BET-surface area (calculated using standard BET equation [9])
 Steam Activation at 880°C
 Acid Washing with 0.5 molar HCl for 1 hour

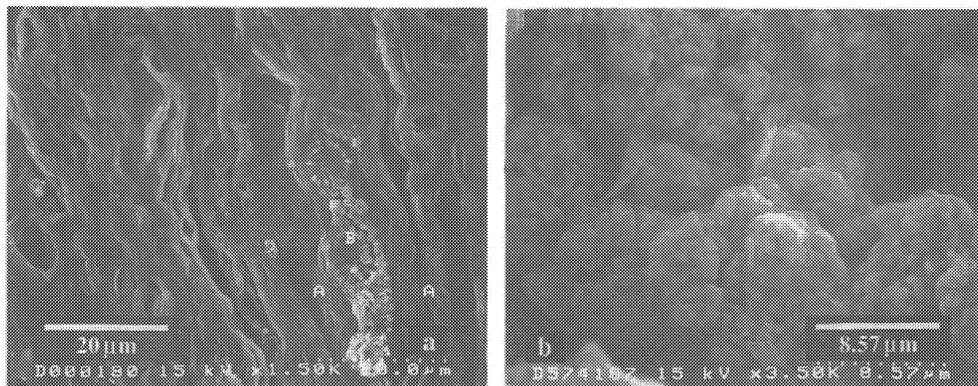


Figure 4. General view of the pyrolysis-induced-porosity (PIP) in the retorted Alpha oil shale. (a) at low magnification the sites of the algal bodies were clearly visible as large elongated cavities. (b) at higher magnification, spheroid structures with abundant fractures and pores are observed within the larger cavities. These structures represent accumulations of precipitated carbon formed as oil vapors are degraded.

pyrolyzed char, Figure 5a,b, with corresponding increases in BET surface area, Table 1. The surface area was further increased after mineral matter removal by acid treatment of the activated product, which may be due to the removal of minerals blocking pore entrances. Similar observations have been made in other studies (20).

It was found that the surface area could be substantially increased by activating under extremely slow steam flow conditions for prolonged periods (up to 10 hours). However this resulted in an extensive loss of carbon. Steam activation at 880°C for four hours, using steam flow rates of 2 grams/minute, developed BET surface areas of around 400 m².g⁻¹, with a 43% loss of carbon, Table 1. An inverse relationship was observed between surface area and carbon yield. Preliminary studies of the effects of added catalysts (ZnCl₂; CaCl₂), indicated some improvement in surface area over non-catalyzed steam activation, Table 1.

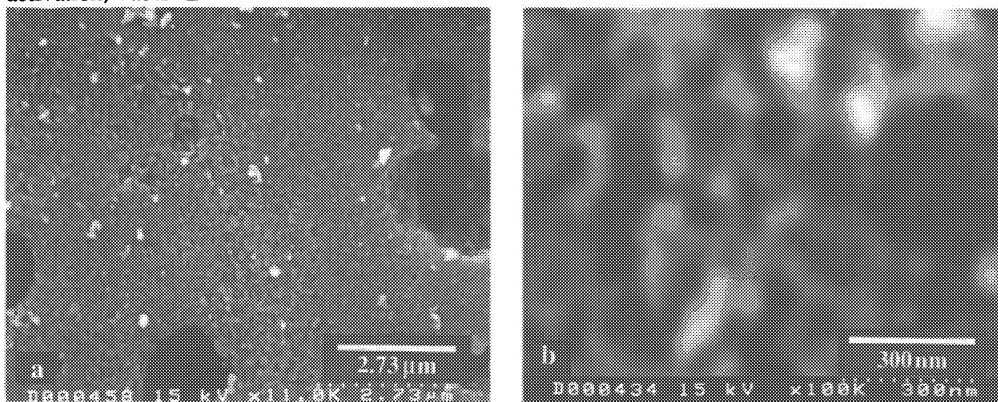


Figure 5. General view of the steam-induced porosity (SIP) in the 880°C steam activated oil shale sample. (a) carbonaceous matrix between large devolatilization pores has abundant micron to sub-micron sized pores after 4 hour steam treatment. (b) enlargement of the area shown in 4a emphasizing the degree of steam processing.

ADSORPTION CHARACTERISTICS

The activated carbon samples were examined for their ability to adsorb selected gases (H₂S, NH₃ and NO) by thermogravimetry/mass spectroscopy (TG-MS), using temperature programmed adsorption/desorption (TPA/D). Both the Goynuk and Alpha derived carbons showed higher adsorptive capacities for H₂S and SO₂ than a commercially available carbon. The H₂S adsorption capacity of the steam activated Goynuk carbon (350 m².g⁻¹) at 70°C was 0.06 g/g of carbon. The adsorption capacity was determined on the weight gain during adsorption, weight loss during desorption, and the identification of H₂S as the only desorbed gas, Figure 6. Samples of shale-derived carbons also

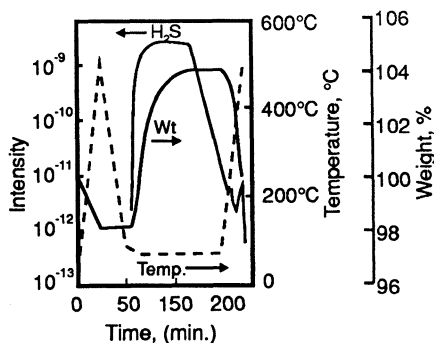


Figure 6. Temperature programmed adsorption/desorption analysis of the Goynuk adsorbent carbon. The carbon was activated at 880°C using ZnCl₂ catalyst. Mineral Matter was reduced after steam activation using 0.5 molar HCl.

demonstrated significant adsorptive capacities for NO and NH₃, Figure 7, indicating their potential use for the treatment of industrial gases.

These investigations have shown that adsorbent carbons, with reasonably high surface areas, can be produced from the pyrolysis residues of the Turkish Goynuk and Australian Alpha oil shales. During pyrolysis, a macroporous network of charred carbonaceous material is formed and provides sufficient access for steam to infiltrate the char during activation at 880°C. Steam activation produced a BET surface area of 300–400 m²/g at 43 % burn off. The activated carbons show promising adsorptive capacities for NO, NH₃ and H₂S.

Carbon Fibers

Carbon fibers are of four main types based upon: rayon; PAN (polyacrylonitrile); pitch; and vapor-grown (21). The focus here is on pitch-based carbon fibers and activated carbon fibers.

In the 1960s, Otani and co-workers (22, 23) described the formation of carbon fibers from isotropic pitch. Such fibers can be produced by melt-spinning, and can be generated either as short, blown fibers or can be drawn as continuous filaments. The as-formed fibers require treatment to render them thermosetting (stabilization), before further thermal treatment. Normally this is achieved by an oxidation step. Processes to produce isotropic fibers from prepared petroleum and coal tar pitches, have been developed by the Ashland Carbon Fibers Division, and by Osaka Gas, respectively (24, 25). The fibers have relatively low tensile strengths and find different markets to high strength or high modulus fibers.

The strength of isotropic fibers can be improved by hot-stretching continuous filaments above 2500°C, which helps to orient the layer planes axially. However, this process is slow and expensive. Orientation can also be achieved by inducing mesophase formation through heat treatment of the pitch prior to fiber formation. The aim is to attain a situation where the liquid crystal phase is the continuous phase, while retaining the fluid state. The liquid crystals can then be oriented by any small force such as a gas bubble, or by the processes of extrusion or elongation (28). Research in this area has focused on the preparation and selection of precursor pitches (including synthetic pitches) that can approach the goal of developing a single anisotropic phase with low softening point to circumvent the onset of solidification during spinning. The process steps for the production of isotropic and mesophase pitch fibers are shown in Figure 8. The structure of the fibers is very dependent upon the precursor structure and the spinning conditions, and a wide range of fiber properties are possible. Schematics of the possible orientation of the layer planes in the fiber cross section are shown in Figure 9.

Generally, mesophase pitch fibers are more graphitizable than PAN fibers, although the extent of structural development will clearly depend upon the orientation of layer planes in the as-formed fibers.

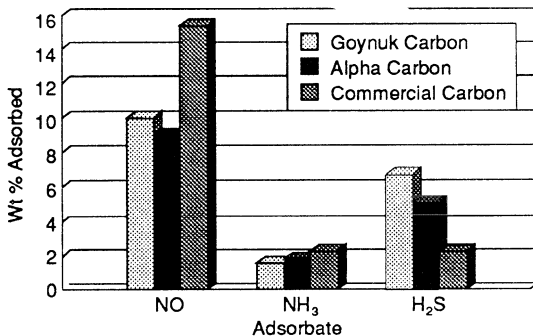


Figure 7. Comparison of the adsorption capabilities of Goynuk and Alpha derived adsorbent carbons with a commercial carbon. Goynuk and Alpha carbons have a BET surface area of about 350 m²/g. BET surface area of the commercial carbon corresponds to 450 m²/g.

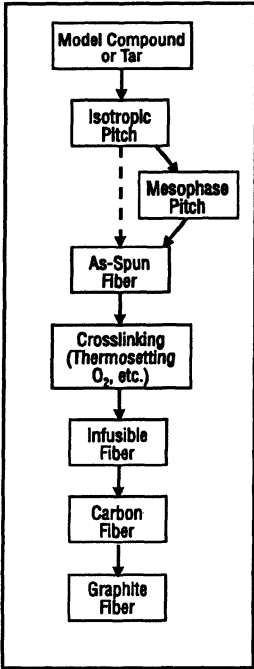


Figure 8. Preparation of isotropic and mesophase pitch carbon fibers.

A comparison of the properties of pitch-based and PAN-based fibers is shown in Figure 10. The graphitized mesophase pitch fibers tend to have higher modulus and lower tensile strength than the PAN-based equivalents, and the former have advantages in applications requiring high stiffness, high electrical and thermal conductivity, low thermal expansion, and high temperature oxidation resistance.

Activated Carbon Fibers

While the industrial use of activated carbons in powder, granular or moulded form, has been established for many decades, interest in the use of activated carbon fibers is relatively recent (24, 27). Carbon fibers have only been commercially available since the 1960s, and the development of activated carbon fibers has been a direct consequence of this technology.

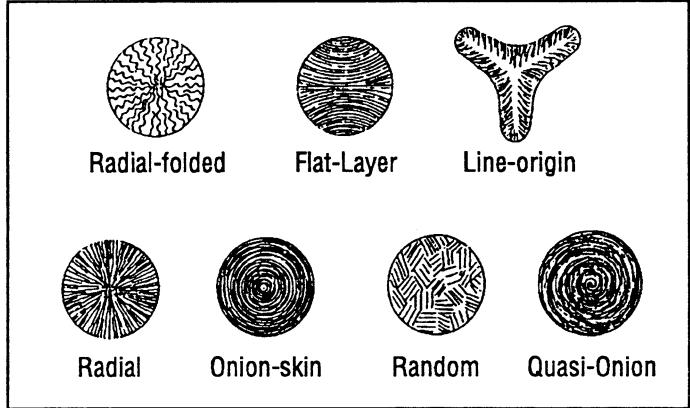


Figure 9. Possible cross-sectional structures of pitch-based carbon fibers. (Adapted from D.D. Edie, *Carbon Fibers, Filaments, and Composites*, 1990)

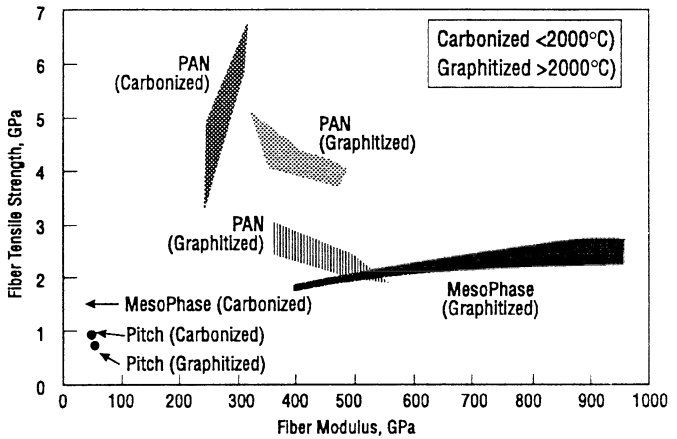


Figure 10. A comparison of tensile strength and modulus ranges for PAN and pitch-based carbon fibers. (Adapted from R. Bacon, *Phil. Trans. Roy. Soc. London*, **A294**, 437, 1979)

Activated carbon fibers have novel properties that make them more attractive than other, more conventional forms for certain applications. They are predominantly microporous, with only a limited proportion of the pores present as fine mesopores. While their bulk density is low, which limits their adsorptive capacity per unit volume, their small diameters essentially eliminate mass transfer effects, allowing very rapid rates of adsorption and desorption. Moreover, their fibrous form facilitates their incorporation into woven and non-woven fabrics, felt, paper, and specific formed shapes (for example filters). Practically all fiber types can be utilized to produce high surface area adsorbents, provided that their thermal history does not include heat treatment to elevated temperatures, when the rate of activation is greatly reduced.

Among the possible applications, activated carbon fibers are of interest for the adsorption and recovery of organic vapors (27, 28), and have been proposed for water treatment (29). Surface treated fibers have been found to have high activity for NO reduction by ammonia (30), and to be effective for SO₂ adsorption (31). A recent article discusses the use of surface treatments for tailoring the adsorptive properties of activated carbon fibers (32).

Carbon Fibers and Activated Carbon Fibers from Residual Shale Oil

Recent research at the University of Kentucky Center for Applied Energy Research (CAER) has focused on investigating the potential of residual shale oil liquids as starting materials for the formation of carbon fibers and activated carbon fibers.

Activated carbon fibers produced from PAN have some unique properties, including the ability to adsorb vitamin B₁₂, NO_x, and SO_x, and are of interest as catalyst supports (30, 33-35). These properties may be related to their nitrogen content, which can lead to the presence of basic functional groups on the adsorptive surface. For similar reasons, it is considered that carbon fibers and activated carbon fibers produced from shale oil residues might exhibit unusual properties that are not possessed by fibers from petroleum or coal tar pitch. Moreover, the ability to generate valuable by-products could enhance the economics of oil shale retorting.

In the study described here, an asphaltene fraction was isolated from a shale oil residuum produced by the Kentort II process (15). The fraction was processed by melt spinning, oxidative stabilization, carbonization and activation to produce isotropic carbon fibers and activated carbon fibers. The products were characterized by SEM, elemental and surface area analyses.

Fiber Formation

A shale oil residue (SOR), produced from eastern oil shale (15), was used as the starting material. The asphaltene fraction, SOA, (hexane insoluble, benzene soluble) was separated as follows: the hexane soluble fraction of the shale oil residue was removed by extraction with boiling hexane (36); the hexane insoluble fraction was then Soxhlet extracted with benzene, following which the benzene was removed from the extract by rotary evaporation. A petroleum-derived pitch precursor (PP) was selected for comparison.

Continuous single filament carbon fibers were produced from both precursors by melt spinning, using a spinneret (capacity ~8g, nozzle diameter 0.3 mm) operated under nitrogen pressure. The shale oil and

petroleum precursors were spun under 150~300 kPa pressure at about 240 and 300°C, respectively. The resulting fibers were then chopped into 15-20 mm lengths and stabilized by oxidation in air for 90 minutes at 180 and 230°C for the oil shale and petroleum pitch fibers, respectively. The spinning temperatures were selected with reference to the precursor softening points, although some additional experimental adjustment was necessary. The stabilized fibers were carbonized in nitrogen at 850°C for 30 minutes. Carbon fibers were activated by reaction at 850°C for 60 minutes in 50 vol% steam or carbon dioxide in nitrogen.

RESULTS AND DISCUSSION

Analyses of the shale oil residue, its asphaltene fraction, and the petroleum pitch are shown in Table 2. The asphaltenes represent about 20 wt% of the original residue. It can be seen that the nitrogen in the SOR is considerably concentrated in the asphaltene fraction. The sulfur contents of the three materials are similar, but the petroleum pitch has a somewhat lower ash content. The shale oil asphaltene fraction has a softening point of 183°C, which is lower than that of the petroleum pitch, consistent with its higher hydrogen content.

Scanning electron micrographs (SEM) of the carbonized fibers are shown in Figure 11. Small particles (100~500 nm) were observed on the fiber surfaces: their origin is tentatively ascribed to the ash components in the precursor. The form of the fibers was clearly retained after carbonization, indicating

Sample	Elemental Analysis (wt %)				Atomic Ratio (%)		Content of Ash (wt %)	Softening Point (°C)
	C	H	N	S	H/C	N/C		
PP	92.88	4.63	0.31	1.99	0.60	0.29	0.21	258
SOR	83.22	9.60	0.51	1.82	1.38	0.53	0.82	<25
SOA	80.98	6.64	2.54	1.96	0.98	2.69	0.97	183

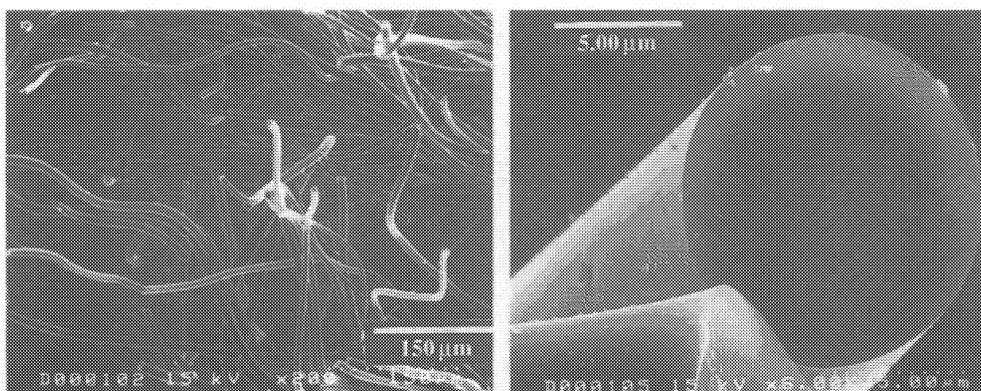


Figure 11. SEM micrographs of carbon fibers produced from shale oil.

that the conditions chosen for stabilization were sufficient. Normally, stabilization reactions are performed at temperatures above 220°C, and for extended periods (37). The low reaction temperature of 180°C used here indicates that the fibers have a high oxidation reactivity.

While the freshly spun fibers had similar diameters, that of the shale oil carbonized fibers was in the range 5~12 μm , and smaller than those produced from petroleum pitch (6-15 μm). The greater degree of thermal contraction of the shale oil fibers reflects their lower carbonization yield (50 versus 71%), which in turn is consistent with the lower softening point of the precursor, and the implied higher volatile matter content.

The morphology of activated carbon fibers derived from petroleum pitch and shale oil asphaltenes is shown in Figures 12 and 13. Ridges are apparent on the surfaces of the petroleum pitch fibers, and they tend to follow the fiber circumference. Despite this, the surface appears relatively smooth and there are no evident cracks or pores. With the shale oil fibers, an irregular distribution of small pits or pores have developed over the fiber surfaces. In addition, particles can be observed on the surfaces of some of the pore walls. It may be that some of the ash components can have a catalytic influence on the activation

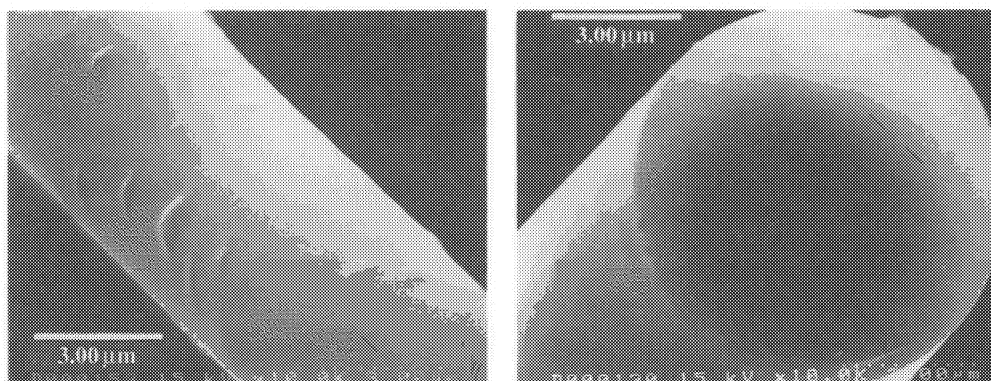


Figure 12. SEM micrographs of activated carbon fibers from petroleum pitch by steam activation.

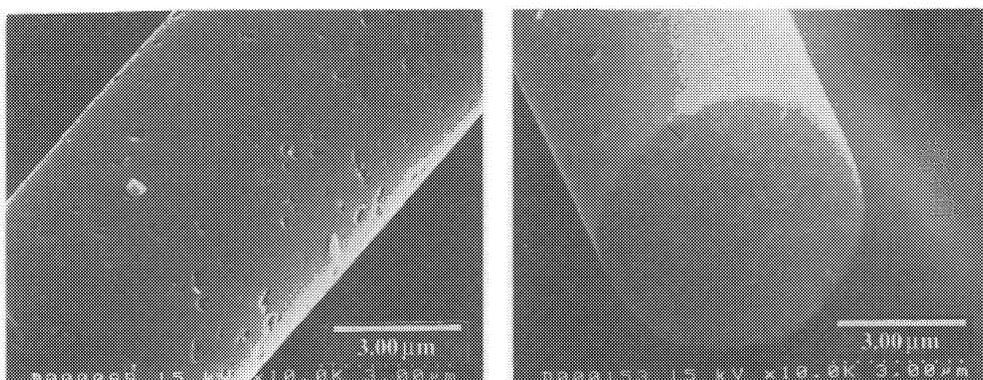


Figure 13. SEM micrographs of activated carbon fibers from shale oil by steam activation.

or gasification of the fibers, and are instrumental in the generation of these features. The SEM micrographs also suggest that there are some differences in the internal morphology of the two types of fiber.

As shown in Table 3, under similar conditions, the shale oil carbon fibers experienced much greater burn-off during steam activation than the petroleum pitch fibers. This finding also indicates that the former are more reactive to oxidation, either due to certain inherent aspects of their composition and structure, or to the catalytic effect of ash constituents. Predictably, activation in carbon dioxide, which is known to be a slower reaction, caused lower burn-off than steam under the same conditions. Despite the different degrees of burn-off, the steam activated fibers from pitch and shale oil had very similar BET surface areas, although there may be differences in their pore size distributions.

These preliminary studies have shown that single filament carbon fibers and activated carbon fibers can be produced successfully from the asphaltene fraction of residual shale oil. The shale oil fibers were more reactive to oxidation than petroleum pitch fibers, as evidenced by the low temperature required for stabilization, and the high burn-off during activation. The greater reactivity of the shale oil fibers may be due to their inherent structure and/or to the catalytic effect of some ash constituents: some evidence for catalysis is provided by microscopic observations. The high reactivity and nitrogen content (3.3 wt%) of the activated shale oil fibers may provide unusual adsorptive or catalytic properties.

These considerations, and the development of mesophase in the shale oil residue, and the formation of mesophase fibers will be examined in future work.

Table 3. Activation of carbon fibers from petroleum and shale oils

Sample Code	Activation (°C-Min)*	Burn-off (wt %)**	Diameter of ACF (µm)	BET Surface Area (m ² /g)
AF-P1	850-60	38	4~12	978
AF-P2	850-90	58	4~12	2080
AF-S1	850-60	68	3~10	960
AF-S2*	850-60	49	3~10	566
AF-S3	820-60	60	3~10	1250

*activating agent, 50 vol% H₂O in N₂;
 *activating agent, 50 vol% CO₂ in N₂;
 **as % of carbonized fibers

References

1. Speight J.G. The Chemistry of Petroleum. Second Edition. Marcel Dekker Inc., New York (1991).
2. Riedhammer M. Zement-Kalk-Gips, 38, No. 7. p. 359, (1985)
3. Kroto, H. W., Angewandte Chemie, 31 (2), 111-129, 1992

4. Derbyshire, F.J., Presland, A.E.B., and Trimm, D.L., *Carbon*, **10**, 114-115, 1972
5. Derbyshire, F.J., Presland, A.E.B., and Trimm, D.L., *Carbon*, **13**, 111-113, 1975
6. Houghton, F.R. and Wildman, J., *Chemical and Process Engineering*, **52** (5), 61-64 , 1971
7. Wilson, J., *Fuel*, **60**, 823-831, 1981
8. Juentgen, H., *Carbon*, **15**, 273-283 , 1977
9. Richter, E., Knoblauch, K. and Juentgen, H., *Gas Separation and Purification*, **1**, 35-43 , 1987
10. Barton, S.S., Dacey, J.R., Evans, M.J.B., Holland, J.A., and Quinn, D.F., 1987, The Development and Performance Testing of Adsorbent Carbon for the Storage of Compressed Natural Gas, Report AF-87-02, Ministry of Transportation and Communications, Ontario, Canada, 57 pp.
11. Critoph, R.E., *Carbon*, **27** (1), 63-70, 1989
12. Jagtoyen, M. and Derbyshire, F.J. "Some Considerations of The Origins of Porosity in Carbons from Chemically Activated Wood". accepted for publication in *Carbon*
13. Heng, S., Verheyen, T. V., Perry, G. J., McAllan, C. G. and Harris, J. A., 1985. Proc. 1985 International Conference on Coal Science, Sydney, Aus., 875-878 , 1985
14. U.S. pat. 4,082,694, Wennerberg, A. N. and O'Grady, T. M, 1978
15. Carter S.D., Robl T.L., Rubel A.M., and Taulbee D.N. *Fuel*, **69**, p.1124, (1990)
16. Carter S.D., Robl T.L., Taulbee D.N., and Rubel A.M. *Fuel*, **70**, p.1347, (1991)
17. Putun E., Akar A., Ekinçi E. and Bartle K.D. *Fuel*, **67**, p. 1106 (1988)
18. Duffy G.J., Udaja P., and Shao-Xin L. *Fuel*, **69**, p. 1134, (1990)
19. Rubel A.M. and Coburn T.T. In Proceedings of the 1981 Eastern Oil Shale Symposium, Kentucky Energy Cabinet, Lexington, KY, p. 21, (1981).
20. Jagtoyen, M., Groppo, J., and Derbyshire, F. J., *Fuel Proc. Tech.*, **34**, 85-96, 1993
21. Singer, L. S., Proc. Eighth Annual Conference on Materials Technology: Structural Carbons, Sept. 1-2, 1992, Southern Illinois University at Carbondal, Carbondale, IL 2901, USA, p3-32
22. Otani, S., *Carbon*, **3**, 31, 1965
23. Otani, S., *Carbon*, **3**, 213, 1965
24. Thwaites, M.W., Stewart, M. L., McNeese, B. E., and Sumner, M. B., *Fuel Proc. Tech.*, **34**, 137-145, 1993
25. Maeda, T., Zeng, S. M., Tokumitsi, K., Mondori, J., and Mochida, I., *Carbon*, **31** (3), 407-412, 1993
26. White, J. L., Dubois, J., and Souillart, C., *J. Chim. Phys. et de Phys.-Chime Biol.*, p33, Special Issue, April, 1969
27. Suzuki, M., Proc. Biennial Carbon Conference, Buffalo, 1993
28. Foster, K. L., Fuerman, R. G., Economy, J., Larson, S. M., and Rood, M. J., *Chem. Mater.*, **4**, 1068-1073, 1992

29. Suzuki, M., *Water Science Technology*, **23**, 1649, 1991
30. Mochida, I., Sun, Y-N., Fijitsu, H., Kisamori, S., and Kawano, S., *Nippon Kagaku Kaishi (J.Chemical Society of Japan)*, **6**, 885-890, 1991
31. Mochida, I., Hirayama, T., Kisamori, S., Kawano, S., and Fijitsu, H., *Langmuir*, **8** (9), 2290-94, 1992
32. Economy, J., Foster, K., Andreopoulos, A., and Jung, H., *Chemtech*, 597-603, October, 1992
33. Ermolenko, I. N., Lyubliner, I. P., and Gulko, N. V. *in* *Chemically Modified Carbon Fibers*, (Translated by E.P.Titovets), VCH Publishers, New York, 1990, p.198
34. Fujitsu, H., and Mochida, I. *in* *Kaseitan (Activated Carbon)*, Edited by Y. Sanada, M. Suzuki and K. Fujimoto, Kotansha Scientific, Tokyo, 1992, p.195
35. Sato, K., Hirai, M., and Shimazaki, K. *TEXTILE TEKHNOLGY'84*, Industrial Fabrics Association International 72nd Annual Convention, 1984
36. Fei, Y.Q., Sakanishi, K., Sun, Y.N., Yamashita, R., and Mochida, I., *Fuel*, **69** (2), 261 (1990)
37. Donnet, J.B., and Bansal, R.C. *in* *Carbon Fiber*, Marcel Dekker, New York, 1990, p.55

COMBUSTION REACTIVITY OF CHARS

Bekir Zühtü Uysal
Department of Chemical Engineering
Gazi University
06570 Ankara, Turkey

ABSTRACT. Combustion of chars with special reference to oil shale in fluidized-beds is discussed. The kinetics of char combustion is reviewed. The total time required for carbon burn off is considered for both kinetic controlled combustion and mass transfer controlled combustion. The importance of intraparticle diffusion on the rate of combustion of oil-shale particles is explained. The effects of the devolatilization, the decomposition reactions, the carbonate and silicate minerals and the presence of sulphur on char combustion are also described.

1. Introduction

Solid fossil fuels, such as coal and oil shale undergo two overlapping stages of reaction during combustion, namely devolatilization and char combustion. When a coal or oil shale particle is introduced to the combustion chamber, it decomposes to produce hydrogen-rich gas derived from the volatile matter and carbon-rich residue, the char.

The time for devolatilization cannot be predicted accurately. The rate of combustion of volatiles is also difficult to determine and is normally considered to be limited by the rate of mixing of fuel and oxygen, which depends on the type of combustor as well as the type of the fuel. The devolatilization rate is usually estimated from the release history of proximate volatiles content ^(1,2) and can be characterized by a total devolatilization time, which is determined either visually by extinction of volatiles flame ⁽³⁻⁵⁾ or by degree of completion of the evolution of volatiles ^(6,7). The flame extinction time is typically correlated with the particle diameter by a power-law relation ⁽⁸⁾ with generally $1 \leq n \leq 2$ ⁽⁹⁾, i.e.

$$t_f = a d_p^n \quad (1)$$

There are though some arguments that this time is shorter than the total evolution time of volatiles. Commonly it is accepted for large particles that the total devolatilization time is proportional to the square of the particle diameter ⁽¹⁰⁾

The time required for the combustion of volatiles is relatively much shorter than that for that of carbon residue. Atimtay ⁽¹¹⁾ showed that for coal particles ranging from 1.5 to 3 mm, the burnout time of volatiles was about 3-12 s in fluidized-beds. This can be compared with the estimate of 1000 s for the burnout time of a 1.5 mm char particle at 1023 K ⁽¹²⁾. It can be thus stated that the devolatilization time or the flame-out time of volatiles is about two orders of magnitude lower than the burnout time of the char. This by no means should lead to the misunderstanding that devolatilization and combustion of volatiles should not be further investigated. Although this topic actually deserves a detailed analysis, the main interest of the present article is the combustion of char derived from oil-shale and combustion of volatiles will not be discussed further here. Nevertheless, it should be added that if oil-shale or coal particles are burned directly, their hydrogen contents decrease monotonously and so the C/H ratios increase significantly during devolatilization, leading to the importance of subsequent char combustion. Similar arguments are also true in case of the combustion of spent oil-shale received from retorting unit. Above a temperature of about 500°C, oil-shale retorting leads to the decomposition of kerogen to gases, shale oil and carbon residue. When subsequent combustion of the spent shale is desired, essentially the combustion of char trapped in the inorganic matrix becomes the point of interest.

2. Combustion of Solid Carbon

Combustion of carbon is a complex process. Combustion of low grade fossil fuels, such as oil-shale and lignite, is further complicated by the presence of high contents of ash. It is very difficult to burn such fuels by conventional methods. Thus, fluidized combustors seem to be more appropriate for such applications. Although essentially the major part of what follows here is applicable to the general aspects and kinetics of carbon combustion, as far as the interparticle mass transfer is concerned, a fluid bed will be visualized as the combustor. Combustion of carbon will be presented first and then the extra difficulties due to the presence of incombustibles will be discussed.

Possible combustion reactions at the carbon surface can be summarized as follows.





Studies reported on the temperature of the burning particles ⁽¹³⁻¹⁶⁾ indicate that the first reaction is dominant at the carbon surface and the other two reactions can be neglected near the first one for practical purposes ⁽¹⁷⁾. CO obtained by the first reaction is subsequently oxidized in the gas phase around the particle to give CO₂.



In other words, it can be stated explicitly that oxygen diffuses to the carbon surface where it reacts to form carbon monoxide according to reaction 1. While CO, thus formed, is diffusing away from the surface, reaction 4 takes place in the gas phase. Summation of reaction 1 and 4 gives the overall reaction.



Rate expressions and kinetic data for the combustion reactions (R1 and R4) as well as those of the gasification reaction (R3) (due to its importance, this is discussed later) are summarized in Table 1 ^(18,19).

Since reaction 4 contributes approximately two thirds of the heat produced by the overall reaction 5, it is important to know where exactly reaction 4 is taking place in the gas phase. There are two models with respect to location ⁽²⁰⁾. According to the first, it is assumed that carbon monoxide is further consumed to CO₂ close to the particle surface, in the diffusion film of the particle to be more exact. According to the second model, the oxidation of carbon monoxide is assumed to take place outside the diffusion film surrounding the particle. Therefore, with respect to the first model, it can be visualized as if one atom of every O₂ molecule diffusing towards the carbon surface is used up for the first reaction and the other one for reaction 4. Since the rate of combustion of a single carbon particle is affected by the rate of diffusion in the film and consumption of oxygen at the surface, the combustion rate of carbon becomes equal to the mass transfer rate of O₂, i.e. $n(C)=n(O_2)$. According to the second model, however, since reaction 4 takes place outside the diffusion film, both atoms from one O₂ molecule reaching the carbon surface across the diffusion film are used by the first reaction and the molar rate of carbon consumption becomes equal to twice the molar rate of diffusion of oxygen to the surface, i.e. $n(C)=2n(O_2)$.

Table 1. Rate Expressions and Kinetic Data for
Combustion and Gasification Reactions of Char.

Reaction	Rate	k	E	(-ΔH)
$C(s) + \frac{1}{2}O_2 \rightarrow CO$	$r = (1 - X_C) k \exp\left(-\frac{E}{RT}\right) P X_{O_2}$ [kg C / s.kg initial C]	$k = 1.41 \times 10^5$ [kg C / s.atm.kg initial C]	9.706×10^4 [J/mol]	2.28×10^5 [J/mol O ₂]
$C(s) + CO_2 \rightarrow 2CO$	$r = (1 - X_C) \frac{k_0 \exp\left(-\frac{E}{RT}\right) P X_{CO_2}}{1 + k_1 P X_{CO_2}}$ [kg C / s.kg initial C]	$k_0 = 7.8 \times 10^6$ [kg C / s.atm.kg initial C] $k_1 = 4.95$ [atm ⁻¹]	1.853×10^5 [J/mol]	1.67×10^5 [J/mol CO ₂]
$CO + \frac{1}{2}O_2 \rightarrow CO_2$	$r = k \exp\left(-\frac{E}{RT}\right) X_{O_2}^{1/2} X_{CO} X_{H_2O}^{1/2} \frac{P^2}{T^2}$ [kmol O ₂ / s.m ³]	$k = 9.67 \times 10^{12}$ [kmol O ₂ - K ² / s.m ³ .atm ²]	1.255×10^5 [J/mol]	5.63×10^5 [J/mol CO ₂]

The order of reaction 1 can be taken as one for temperatures higher than 1000 K ⁽¹⁷⁾. The rate of carbon consumption may be expressed as:

$$n(C) = \pi d_p^2 k_r c_{O_2, s} \quad (2)$$

The rate of mass transfer of oxygen to the surface of carbon can be written as:

$$n(O_2) = \pi d_p^2 k (c_{O_2, \infty} - c_{O_2, s}) \quad (3)$$

Considering both these models, Guades De Calvaro ⁽²⁰⁾ proposed the following expression for the overall rate constant, K.

$$\frac{1}{K} = \frac{1}{k_r} + \frac{1}{\phi k} \quad (4)$$

Expressing the mass transfer coefficient in terms of Sherwood number, equation (4) can be written also as

$$\frac{1}{K} = \frac{1}{k_r} + \frac{d_p}{\phi D Sh} \quad (5)$$

The value of ϕ in equation (4) or (5) is 1 for model 1 and 2 for model 2. Using this definition of the overall rate constant, combination of equations (2) and (3) leads to the following expression for the consumption rate of carbon,

$$n(C) = \pi d_p^2 K c_{O_2, \infty} \quad (6)$$

or, in mass units:

$$\frac{d m(C)}{d t} = M_C \pi d_p^2 K c_{O_2, \infty} \quad (7)$$

2.1. KINETIC CONTROLLED COMBUSTION

If it is assumed that the rate of combustion of carbon is controlled by the kinetic resistance, equation (7) reduces to

$$\frac{d m(C)}{d t} = -4 \pi r_p^2 \rho_C \frac{d r_p}{d t} = M_C 4 \pi r_p^2 k_r c_{O_2, \infty} \quad (8)$$

Integration of equation (8) yields equation (9) for the total time required for combustion of a carbon particle.

$$t_T = \frac{d_p \rho_C}{24 k_r c_{O_2, \infty}} \quad (9)$$

The kinetic rate constant, k_r is expected to be strongly dependent on particle temperature. Estimation of the particle temperature is, however, very difficult due to the uncertainty about where reaction 4 is taking place and whether the heat released from CO generation reaction alone or CO₂ producing reactions contribute to the increase in particle temperature. The following expression has been proposed for the temperature (T_p) of a carbon particle in a fluidized bed combustor at a temperature T ^(21, 22).

$$T_p (K) = T + 66000 c_{O_2} \quad (10)$$

Assuming combustion takes place essentially at the exterior surface of the particle [21,22], k_r can be expressed as:

$$k_r = 594.3 T_p \exp(-149,200/R T_p) \quad (11)$$

2.2. MASS TRANSFER CONTROLLED COMBUSTION

In case of mass transfer controlled combustion equation (7) reduces to:

$$\frac{d m(C)}{d t} = -4 \pi r_p^2 \rho_c \frac{d r_p}{d t} = \phi M_c 4 \pi r_p^2 k c_{O_2, \infty} \quad (12)$$

Total burn-out time obtained from integration of equation (12) becomes:

$$t_T = \frac{\rho_c d_p}{24 \phi k c_{O_2, \infty}} \quad (13)$$

Ross and Davidson ⁽²²⁾ suggest that, for particles smaller than 0.5 mm, CO formed by reaction 1 can diffuse to a greater relative distance before being consumed. For particles larger than about 1 mm, however, CO burns relatively close to the surface. Thus, one may say that for fluidized-bed combustion with particles typically in the size range from 0.5 mm to 15 mm, what actually happens is likely to fall in between the two extremes, i.e. $\phi=1$ and $\phi=2$. However, as the particle size reduces during combustion, an alteration from model 1 to model 2 is very likely. Indeed, recent findings in studies on combustion in fixed-beds and fluidized beds indicate that the value of ϕ can be taken as 2 ^(20,23). This means that the second model, which assumes reaction 4 takes place outside the diffusion film, is more realistic. With $\phi=2$, equation (13) becomes

$$t_T = \frac{\rho_c d_p}{48 k c_{O_2, \infty}} \quad (14)$$

or, in terms of the Sherwood number,

$$t_T = \frac{\rho_c d_p^2}{48 Sh D c_{O_2, \infty}} \quad (15)$$

Usually the Sherwood number is expressed in the form suggested by Frossling ⁽²⁴⁾,

$$Sh = a + b Re^{0.5} Sc^{0.3} \quad (16)$$

There are various arguments for the values of a and b in the literature ^(17, 25-28). For combustion in bubbling fluidized-beds equation (16) can be used in the following form ⁽¹⁷⁾.

$$Sh = 2 \epsilon_{mf} + 0.95 Re_{mf}^{0.5} Sc^{0.3} \quad (17)$$

$$\text{where, } Re_{mf} = \frac{d_p U_{mf} \rho_G}{\mu \epsilon_{mf}}$$

There are other suggestions in the literature for the calculation of the Sherwood number in fluidized combustors. LaNauze et al. ⁽²⁹⁾ proposed:

$$Sh = \frac{k d_p}{D} = 2 \epsilon_{mf} + \sqrt{\frac{4 \epsilon_{mf} d_p (u_{mf} / \epsilon_{mf} + u_b)}{\pi D}} \quad (18)$$

This equation was later modified by Guedes de Carvalho and Coelho ⁽³⁰⁾ as:

$$\frac{Sh'}{\epsilon_{mf}} = \frac{k d_p}{D_e \epsilon_{mf}} = 2 + \sqrt{\frac{4 d_p u_{mf}}{\pi D_e \epsilon_{mf}}} \quad (19)$$

Guedes de Carvalho et al. ⁽²⁰⁾ offered

$$\frac{Sh'}{\epsilon_{mf}} = \frac{k d_p}{D_e \epsilon_{mf}} = [4 + 0.576 \left(\frac{u_{mf} d_p}{D_e \epsilon_{mf}}\right)^{0.78} + 1.28 \left(\frac{u_{mf} d_p}{D_e \epsilon_{mf}}\right) + 0.141 \left(\frac{d_s}{d_p}\right) \left(\frac{u_{mf} d_p}{D_e \epsilon_{mf}}\right)^2]^{1/2} \quad (20)$$

The modified Frossling equation can also be used for

circulating fluidized beds;

$$Sh = 2 + 0.552 Re^{0.53} Sc^{1/3} \quad (21)$$

It should be emphasised that all the above discussion is restricted to combustion of single carbon particles. Other factors characterizing the nature of the combustor should be considered in the overall model as well. For example, the concentration of oxygen in the dense phase in bubbling fluidized bed combustors is affected by the rate of mass transfer between the bubble phase and the dense phase and this should also be considered in any overall model. If, for instance, simple two-phase theory of Davidson and Harrison⁽³¹⁾ is used, following an approach similar to that of Ross and Davidson⁽²²⁾, one can develop the following equation for the burn-out time for a batch of carbon particles;

$$t_b = \frac{m}{12 c_o A (u_o - (u_o - u_{mf}) e^{-X_{bo}})} + \frac{\rho_c d_p^2}{48 Sh D c_{o,\infty}} + \frac{\rho_c d_p}{24 k_r c_{o,x}} \quad (22)$$

3. Combustion of oil-shale particles

Oil-shale or spent shale may behave different in combustion from pure carbon particles, described above due to the presence of large amounts (approximately 80-85 wt-%) of inorganics. The principle constituents of the inorganic material are carbonates (largely calcite and dolomite) and aluminosilicates. The organic fraction, which is largely kerogen, is dispersed in this matrix. A porous structure is developed during combustion of the carbonaceous material of oil-shale. Similar changes are also valid for the combustion of retorted shale particles. Thermal pyrolysis of oil-shale results in decomposition of approximately 60-70% of kerogens to oil and the remaining kerogens to gas and char. Thus, porosity is also developed during the retorting process. Char combustion reactivities are hence affected by the mass transfer inside the porous structure as well as in the surrounding gaseous phase. This means that addition of another term to equations (4) or (5) would be required to account for the resistance for effective intraparticle diffusion of oxygen. Moreover, gasification reaction of carbon with CO₂ (R3) may take place in the pores of the oil-shale particles. Also, in contrast from combustion of pure carbon particles, while CO formed in the pores diffuses to the outer surface, reaction 4 may as well take place within the pores. Considering all these facts an approach similar to the one given above for the combustion of a

pure carbon particle may still be employed, but it would be perhaps reasonable to be more cautious about the value of ϕ in this case.

Assuming negligible attrition with no appreciable change of porosity during combustion, isothermal conditions during reactions and the presence of large excess of oxygen (thus no change in its concentration in bulk gas phase), the following expression for the time for fractional conversion (X) of carbon can be developed using Charlton's approach ^(32,33).

$$t = \frac{d_p \rho_p \omega_c}{24 k_r c_{O_2}} [1 - (1-X)^{1/3}] + P(X) \frac{d_p^2 \rho_p \omega_c}{288 \phi D_{e,p} c_{O_2}} + \frac{d_p^2 \rho_p \omega_c X}{72 \phi Sh D c_c} \quad (23)$$

ρ_p in equation (23) is the particle density and ω_c is the weight fraction of carbon in the particle. The first term at the right hand side of this expression represents the chemical kinetic contribution, the second term the internal diffusion contribution and the third term the external mass transfer contribution. The shrinking core model with constant particle size ⁽³⁴⁾ was assumed for the correction of the kinetic term as given by equation (9). $P(X)$ in the term accounting for the internal diffusion is given for spherical particles as ⁽³²⁾:

$$P(X) = 1 - 3(1-X)^{2/3} + 2(1-X) \quad (24)$$

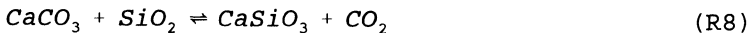
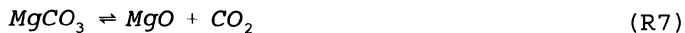
Charlton ^(35,36) proposed that the last term in equation (23) is negligible for spent shales of low carbon concentration and that the overall kinetics are controlled by internal gas diffusion for spent shales of low carbon concentration and by chemical reaction for spent shales of high carbon concentration (38-50%). The intermediate concentration spent shale with approximately 23 % carbon showed a transition from internal diffusion to reaction rate control. The data for large particles at temperatures lower than 900°C were also found to be better described by the internal diffusion function.

There are also many theoretical studies in the literature analysing the combustion process of oil-shale by numerical techniques ⁽³⁷⁻⁴¹⁾. Common features of these studies are the consideration of heterogeneous and homogeneous reactions (R1, R3 and R4, respectively) and the solution of the unsteady state equations of conservation of mass and energy by various numerical methods. Such approaches are especially useful for parametric studies, i.e. to show the effect of various parameters such as ambient temperature and particle size, on the conversion and the carbon burn-off time.

As pointed out earlier, devolatilization and combustion

of volatiles overlap to some extent the char burning stage. This may influence char depletion reactions and the production of active sites. Abd El-Samed et al.⁽⁴²⁾ found that there is enhanced char reactivity in the early stages of combustion and reported that the combustion rates of the chars produced in a flame environment were generally around 1.5 orders of magnitude higher than those observed for prepared chars. As the particles burnout, the decrease in the extent of volatiles production and carbon/ash ratio causes a fall in reactivity. The authors speculated that hydrogen release rate from the carbon surface and from the trapped volatiles can be linked to the reactivity of char. They postulated that the trapped volatiles are the main origin of hydrogen. As the volatiles emerge and crack, they produce free radicals which create active sites and enhance the reaction rate. As the trapped volatiles become depleted, char reactivity falls.

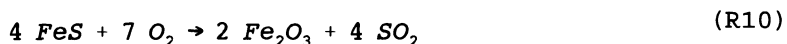
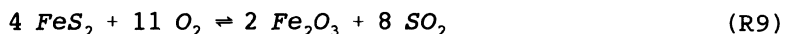
It should be also mentioned that the temperatures at which char combusts are sufficient to affect various other chemical reactions within the supporting mineral matrix. Combustion of oil-shale particles or spent shale particles is, thus, further complicated by the presence of large quantities of calcite (CaCO_3), dolomite ($\text{MgCO}_3 \cdot \text{CaCO}_3$) and silica (SiO_2)⁽⁴⁰⁾. Thermal decomposition of carbonate minerals and at sufficiently high temperatures exceeding 600°C the silication reactions such as:



may also take place in the shale particles. Both types of reactions are endothermic and produce large quantities of CO_2 . When the concentration of CO_2 in the pores increases, gasification reaction (R3), which is negligible for pure carbon combustion, may now become important for shale combustion. Moreover, these mineral reactions produce products (CaO and MgO) that participate as catalysts in the char reactions⁽⁴³⁾. A variation in reactivity by a factor of 100 was observed by Jenkins et al.⁽⁴⁴⁾, with those chars containing large amounts of magnesium and calcium being the most reactive. Similar effects of metal carbonates on the combustion rate of shale char were observed by Cavalieri and Thomson⁽⁴⁵⁾.

The presence of sulphur in oil-shale interferes with char reactivity. Besides the oxidation of organic sulphur to SO_2 , the following reactions of pyrite and iron sulphide

may also affect the consumption rate and concentration of oxygen in the pores.



Another point that is worth mentioning is that the physical properties of char, such as surface area and pore size distribution, change continuously during combustion. The extent of the effect of these changes on char reactivity depends essentially on the initial structure of the particle. Naturally it is reasonable to expect that micropore structure can be dramatically altered while that of the macropores can be only moderately affected. Thus, the change of the surface area of most chars can be modelled successfully by using a single pore micropore model as the surface area contributed by macropores is negligible ⁽⁴⁶⁾. Various types of 2-D and 3-D pore models have been proposed for analysing gas-solid reactions. Although there are some studies on the measurement of physical properties of lignite, anthracite and bituminous chars ⁽⁴⁷⁻⁴⁹⁾, similar comprehensive studies are required for oil-shale chars.

4. Conclusion

Basic combustion reactions for char are reaction 1 and 4. The total combustion rate of oil shale char is, however, affected by the contributions of chemical kinetics, internal diffusion of oxygen and external mass transfer. Although the combustion rate is, generally, controlled initially by the combined effects of chemical reaction and pore diffusion, in the later stages of reaction a transition to greater chemical control is observed. Char reactivity is also affected by the presence of volatiles and sulphur compounds, thermal decomposition reactions of carbonates and silicates and the change in the porosity and internal surface area of the particles. Since oil shale particles may have a large variety in quality and composition, a thorough analysis of every oil shale deposit is necessary before its ultimate use in combustors.

5. Notation

A	cross-sectional area of combustor, m^2
c	concentration, mol/m^3
c_o	oxygen concentration of the inlet gas, mol/m^3
d_p	particle diameter, m
D	molecular diffusivity of oxygen, m^2/s
D_e	effective diffusivity, D/τ , m^2/s
$D_{e,p}$	effective diffusivity in the particle, m^2/s
H	bed height, m
k	mass transfer coefficient, m/s
k^r	reaction rate constant, m/s
K	overall rate constant, m/s
K_{be}	bubble/emulsion phase mass transfer coefficient, s^{-1}
m	mass of carbon, kg
M	molecular weight
n	rate of consumption, mass transfer rate, mol/s
P	pressure, Pa or atm
r	reaction rate constant, mol/s
r_p	particle radius, m
R	universal gas constant, 8.314 J/mol-K
Re	Reynolds number
Sc	Schmidt number
Sh	Sherwood number
t	time, s
t_f	flame extinction time, s
t_r	carbon burnout time, s
T	temperature, K
u_b	bubble velocity, m/s
u_{mf}	minimum fluidization velocity, m/s
u_o	superficial velocity, m/s
w_c	weight fraction of carbon in particle
x	mole fraction
X	fractional conversion
X_{be}	bubble/emulsion phase cross flow factor, $K_{be}H/u_b$

Greek letters

ϵ_{mf}	bed voidage at minimum fluidization conditions
μ	viscosity, Pa-s
ρ	density, kg/m^3
τ	tortuosity of the diffusion path in the emulsion phase of fluidized beds
ϕ	model parameter

Subscripts

C	carbon
O ₂	oxygen
p	particle
s	surface
∞	bulk

6. References

1. Jung, K. and B.R. Stanmore, Fuel, 1980, **59**, 74.
2. Agarwal, P.K., W.E. Genetti and Y.Y. Lee, Fuel, 1984, **63**, 1748.
3. Pillai, K.K., J.Inst.Energy, 1981, **54**, 142.
4. Pillai, K.K., J.Inst.Energy, 1985, **58**, 3.
5. Prins, W., R. Simons and W.P.M. Van Swaaij, Combustion and Flame, 1989, **75**, 57.
6. Morris, J.P., and D.L. Keairns, Fuel, 1979, **58**, 465.
7. Stubington, J.F., and Sumaryano, Fuel, 1984, **63**, 1013.
8. La Nauze, R.D., in Fluidization, Eds. J.F. Davidson, R. Clift and D. Harrison, 631, Academic Press, London (1985).
9. Zhang, J.Q., H.A. Becker and R.K. Code, Can.J.of Chem.Eng., 1990, **68**, 1010.
10. Essenhigh, R.N., J.Eng.Power, 1963, **85**, 183.
11. Atımtay, A., in Fluidization, Eds. J.R. Grace and J.M. Matsen, 159, Plenum Press, New York (1980).
12. Yates, J.G., Fundamentals of Fluidized Bed Chemical Processes, Butterworths, London, (1983).
13. Basu, P., Fuel, 1977, **56**, 390.
14. Chakraborty, R.K., and J.R. Howard, J.Inst.Fuel, 1978, **51**, 220.
15. Roscoe, J.C., A.R. Witkowski and D. Harrison, Trans.I.Chem.E., 1980, **58**, 69.
16. Ross, I.B., M.S. Patel and J.F. Davidson, Trans.I.Chem.E., 1981, **59**, 83.
17. Turnbull, E., and J.F. Davidson, AIChE Jr., 1984, **30**, 881.
18. Thomson, W.J., U.S. DOE Report No. DE-AS07-77-ET12099 (1979).
19. Howard, J.B., J.C. Williams and D.H. Fine, Proc.1973 14th Int.Symp.on Combustion, 975, Combustion Institute.
20. Guedes de Carvalho, J.R.F., A.M.F.R. Pinto and C.M.C.T. Pinho, Trans.I.Chem.E., 1991, **69**, 63.
21. Field, M.A., D.W. Gill, B.B. Morgan and P.G.W. Hawksley, Fuel, BCURA, Leatherhead, England (1967).
22. Ross, I.B., and J.F. Davidson, Trans.I.Chem.E., 1982, **60**, 108.

23. Pinto, A.M.F.R., and J.R.F. Guedes de Carvalho, Chem.Eng.Res.Des., 1990, **68**, 503.
24. Frossling, N., Gerlands Beitr.Geophys., 1938, **52**, 170.
25. Avedesian, M.M., Combustion of Char in Fluidised Beds, Ph.D. Dissertation, University of Cambridge (1972).
26. Xavier, A.M., and J.F. Davidson, in Fluidisation: Proc. of Eng. Found. Conf. on Fluidisation, Eds. J.F. Davidson and D.L. Keairns, Cambridge Univ. Press, 333, (1978).
27. Chakraborty, R.K., and J.R. Howard, J. Inst. Energy, 1981, **54**, 48.
28. LaNauze, R.D., and K. Jung, Proc. 1982 Int. Conf. on Fluidized Bed Combustion, (Philadelphia).
29. LaNauze, R.D., K. Jung and J. Kastl, Chem. Eng. Sci., 1984, **39**, 1623.
30. Guedes de Carvalho, J.R.F., and N.A.N. Coelho, Chem. Eng. Sci., 1986, **41**, 209.
31. Davidson, J.F., and D. Harrison, Fluidised Particles, Cambridge Univ. Press, Cambridge (1963).
32. Charlton, B.G., Fuel, 1987, **66**, 384.
33. Charlton, B.G., Fuel, 1987, **66**, 388-391.
34. Levenspiel, O., The Chemical Reactor Omnibook, OSU Book Stores Inc., Corvallis, Oregon (1984).
35. Charlton, B.G., Fuel, 1988, **67**, 1361.
36. Charlton, B.G., Fuel, 1988, **67**, 1365.
37. Ballal, G., and N.R. Amundson, Chem. Eng. Sci., 1989, **44**, 1763.
38. Daniel Hsuen, H.K., and S.V. Sotirchos, Chem. Eng. Sci., 1989, **44**, 2639.
39. Daniel Hsuen, H.K., and S.V. Sotirchos, Chem. Eng. Sci., 1989, **44**, 2653.
40. Morell, J.I., and N.R. Amundson, Chem. Eng. Sci., 1990, **45**, 3247.
41. Özüm, B., A. Chambers, G. Kovacik and M. Öztörel, Can. J. of Chem. Eng., 1991, **69**, 1142.
42. Abd El-Samed, A.K., E. Hampartsoumian, T.M. Farag and A. Williams, Fuel, 1990, **69**, 1029.
43. Soni, Y., and W.J.I. Thomson, I&EC Proc. Des. & Dev., 1978, **17**, 364.
44. Jenkins, R.G., S.P. Nandi and P.L. Walker, Fuel, 1973, **52**, 291.
45. Cavalieri, R.P., and W.J. Thomson, Fuel, 1990, **69**, 334.
46. Tseng, H.P., and T.F. Edgar, Fuel, 1989, **68**, 114.
47. Tseng, H.P., and T.F. Edgar, Fuel, 1984, **63**, 385.
48. Tseng, H.P., and T.F. Edgar, Fuel, 1985, **64**, 373.
49. Guerin, H., T. Siemieniowska, Y. Grillet and M. Francois, Carbon, 1970, **8**, 727.

A PROBE FOR THE RAPID ANALYSIS OF VANADIUM: AN ELECTRON PARAMAGNETIC RESONANCE AND THEORETICAL PERSPECTIVE

S. M. MATTAR, R. SAMMYNAIKEN AND I. UNGER

Department of Chemistry, University of New Brunswick, Bag Service No. 45222, Fredericton, New Brunswick, Canada E3B 6E2

ABSTRACT The structure and bonding of several substituted benzenes (C_6H_5F , 1,4- $C_6H_4F_2$ and 1,3,5- $(C_6H_3(CH_3)_3)$) with vanadium has been investigated by electron paramagnetic resonance (EPR) spectroscopy and semi-empirical quantum chemical ZINDO/1 calculations. As the arene electron withdrawing ability increases, the vanadium hyperfine splitting of the corresponding organometallic complex decreases. The calculated vanadium-ligand bond dissociation energies for these complexes increases with the increase of the π -electron density in their $2p_z(C)$ orbitals. These observations indicate that EPR may be a rapid probe for the analysis of vanadium organometallic compounds.

1. Introduction

Vanadium is a toxic metal that is harmful to the environment.^(1,2) Since some crude oils are rich in vanadium⁽³⁾ and vanadium itself can act as a poison to cracking catalysts⁽⁴⁾ it would be worthwhile to develop a method that can, in the field, analyze the vanadium content of oil deposits. Since EPR is a rugged and extremely sensitive spectroscopic tool that can quantitatively detect complexed vanadium⁽⁵⁾, it could be the method of choice. Previous studies have shown that EPR is a valuable tool in determining the vanadium content in refinery streams and petroleum deposits.^(6,7) However, these analyses were carried out at high temperatures, and the nature of the vanadium complexes were unknown.

The present work also stems from our interest in the magnetic properties of sandwich compounds and how they relate to molecular structure and bonding. As a prerequisite to the understanding of the structure and bonding in larger systems, smaller transient sandwich complexes were synthesized by matrix isolation in argon at cryogenic temperatures (12 K). These stabilized fractions or transients were then studied by EPR spectroscopy. In cases where the sizes of the trapping sites in the matrix need to be varied, relatively inert organic compounds may be used, instead of rare gases.⁽⁸⁾ In an analogous fashion, a petroleum matrix may be used to isolate a vanadium complex in

crude oils.

In addition, computation of the electronic structure, heats of formation, metal-ligand bond dissociation energies and theoretical simulation of the EPR spectra may be combined with the experimental results to enable one to understand the bonding of these vanadium-sandwich compounds.

In our studies we have isolated several mono- and bis- sandwich complexes of vanadium. In this paper we report the results of some matrix isolated vanadium benzenes that represent the range from strongly electron donating ligands to electron withdrawing ones. The molecules studied together with the methods used in the study are shown in Table 1.

Table 1: Hyperfine Splittings^a and Bond Dissociation Energies^b

Molecule	Vanadium Hyperfine Splitting (Gauss)	Bond Dissociation Energy (kcal/mol.)
(1,3,5-C ₆ H ₃ Me ₃)V	132.27	54.6
(1,3,5-C ₆ H ₃ Me ₃) ₂ V	109.1	---
(1,4-C ₆ H ₄ F ₂)V	---	41.1
(1,4-C ₆ H ₄ F ₂) ₂ V	77.27	83.9
(C ₆ H ₅ F)V	127.27	45.0
(C ₆ H ₅ F) ₂ V	81.81	---

a- Observed experimentally by EPR spectroscopy.

b- Computed by the ZINDO/1 method.

2. Computational Method

The heats of formation, optimized V-C distances and the ionization energies of the vanadium complexes were calculated using the HyperChem version of the ZINDO/1 program.⁽⁹⁾ The ZINDO/1 program is an INDO semi-empirical program that has been specifically parameterized for the first and second row transition metal elements. It is designed to handle and compute the electronic structure and properties of organometallic complexes.⁽¹⁰⁾

First, the ligand geometries were optimized with a convergence criterion of 10⁻⁴ and their heats of formation calculated. The half-sandwich complexes were then geometry optimized and their heats of formation were also computed. The vanadium-arene bond dissociation energies were then determined by subtracting the heat of formation of the ligand from the heat of formation of the complex. This energy is referred to as the ligand-vanadium bond dissociation energy in Table 1. The energy of the separated vanadium atom is not taken into consideration since it remains fixed in all the cases.

3. Experimental

The matrix isolation apparatus used is shown in Figure 1. The operating base pressure of the vacuum system is approximately 2.0×10^{-7} Torr. The sample holder is cooled to 12K by means of an Air Products Displex (APD) system based on a two-stage closed refrigeration cycle of Gifford-McMahon. It consists of an APD HC-2 Helium Compressor and a DE-202 expander head. The cold surface used to deposit the sample is a flat rod made of oxygen free high conductivity copper.

The vanadium atoms were evaporated directly, by resistive heating, from a vanadium filament that was supported on two water cooled electrodes.⁽¹¹⁾ A radiation shield was placed between the electrodes and the cold surface. The atomic vanadium flux was monitored using a calibrated quartz crystal microbalance.⁽¹²⁾ The gas samples were prepared by mixing appropriate ratios of arene and argon in a gas bulb. The best ratio for the half sandwich complexes was 1:250 and 1:50 for the full sandwich. In a typical experiment approximately $.8 \mu\text{mol/hr}$ of vanadium atom were deposited for a total of 8-24hrs. The ligand/ matrix was deposited at a rate of 1 mmol/hr. The EPR spectra were recorded on a Varian E3 spectrometer. The spectrometer frequency was measured by a pre-calibrated Hewlett-Packard X532A wavemeter attached to the spectrometer via a 20db directional coupler. The magnetic field was calibrated by a Bell incremental Gaussmeter. Care was taken not to distort the spectral line shapes either by overmodulation of the magnetic field or by microwave power saturation.

4. Discussion

The EPR spectra of all the complexes that were isolated show eight lines. This is consistent with hyperfine lines arising from the vanadium nuclear spin of $7/2$. The spectra for each complex reported in this study are shown in Figure 2. The eight hyperfine splittings for each complex varied slightly depending on the nature and the number of the arene substituent. These hyperfine splittings are proportional to the net unpaired electronic spin density at the vanadium nucleus.

NMR results have shown that the CH_3 group (Me) as a substituent on the benzene acts as an electron π electron donor and the fluorine acts as a π electron acceptor.⁽¹³⁾ The extent of the π electron withdrawing capability does not depend on the number of fluorines but on the symmetry of the molecule.

Figure 2a shows the epr spectra of *mono*- and *bis*- vanadium complexes $(1,3,5-\text{C}_6\text{H}_3\text{Me}_3)\text{V}$ and $(1,3,5-\text{C}_6\text{H}_3\text{Me}_3)_2\text{V}$. There are 8 vanadium hyperfine lines for the mono complex with a splitting of 132.27 Gauss. The 960 superhyperfine splittings from the hydrogen nuclei are unresolved mainly due to the small spin density of the unpaired electron at these nuclei. The *bis*- complex has a hyperfine of 109.1 Gauss which is smaller than that for the *mono*- complex. Even though the methyl groups are electron donating to the π electrons of the benzene, the ligand still acquires d electron character from the vanadium via d- π bonding. In the case of $(1,3,5-\text{C}_6\text{H}_3\text{Me}_3)_2\text{V}$, the two ligands will deplete the vanadium of a larger quantity of electrons which results in a smaller spin density and hyperfine splitting at the vanadium nucleus. Figures 2b, 2c and 2d show the spectra of $1,4-(\text{C}_6\text{H}_4\text{F}_2)_2\text{V}$, $(\text{C}_6\text{H}_5\text{F})_2\text{V}$ and $(\text{C}_6\text{H}_5\text{F})\text{V}$ with the hyperfine splittings of 77.27, 81.81 and 127.27 Gauss respectively. In these cases, as

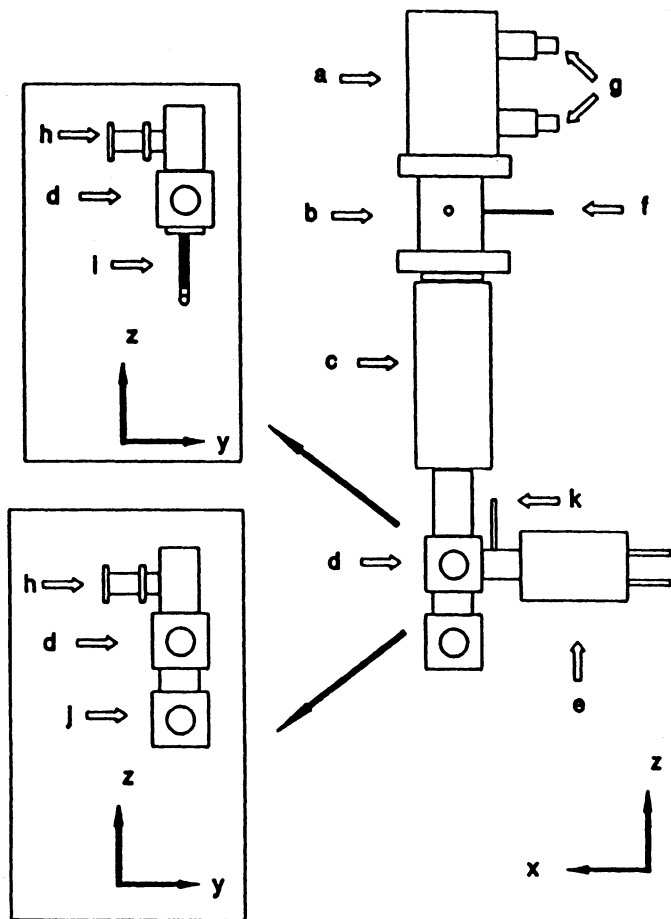


Fig.1 Schematic diagram of the matrix isolation apparatus (not drawn to scale). The two insets show the possible configurations of the system. a) APD DE202 expander head. b) Inner vacuum shroud supporting expander head. c) Outer vacuum shroud. The inner shroud moves vertically inside the outer shroud so that the matrix isolated sample is lowered in to the EPR cavity or the lower compartment j. d) Compartment used for depositions and UV-visible spectroscopy. e) Furnace for creating atomic beams. g) Expander head He inlet and outlet valves. h) Vacuum port. i) Quartz tube used as a shroud for the oxygen-free-high-conductivity copper rod in EPR experiments. j) Lower spectroscopy compartment used for FT-IR, UV-VIS and fluorescence studies. k) Gas inlet port.

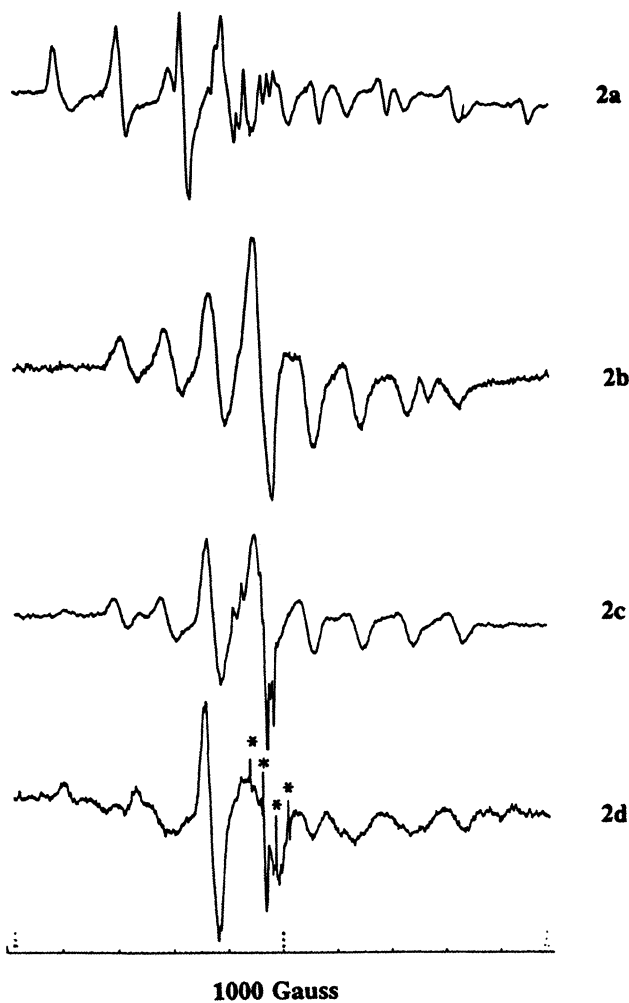


Fig. 2 The EPR spectra of the vanadium benzene sandwich complexes isolated in an Ar matrix at 12 K. The Ar:ligand ratio is 250:1 for the mono complexes and 50:1 for the bis complexes. The deposition time was up to 24 hours. Microwave power incident on the sample: 20 μ W, Modulation amplitude: 1.0 Gauss, microwave frequency: 9.2873 GHz. The four lines of the methyl radical are denoted by asterisks. Figure 2a is due to $(1,3,5\text{-C}_6\text{H}_3\text{Me}_3)\text{V}$ and $(1,3,5\text{-C}_6\text{H}_3\text{Me}_3)_2\text{V}$ with the mono complex having a hyperfine splitting of 132.27 Gauss and the bis 109.10 Gauss, Fig 2b is $(1,4\text{-C}_6\text{H}_4\text{F}_2)_2\text{V}$ with hyperfine splitting of 77.27 Gauss, 2c is $(\text{C}_6\text{H}_5\text{F})_2\text{V}$ where the hyperfine splitting is 81.81 Gauss. Fig. 2d represents $(\text{C}_6\text{H}_5\text{F})\text{V}$ with hyperfine coupling constant of 127.27 Gauss.

expected, the 1,4 di-substituted benzene has less π electron density than the mono-substituted benzene. Thus the resulting complex has a smaller hyperfine splitting. The fluoro-substituted ligands do not show any superhyperfine splitting due to the low symmetry of the molecule and the magnetic inequivalency exhibited by the fluorine centres. This phenomenon is observed only in magnetic resonance spectra of glasses, powder and crystals in the presence of an external magnetic field. It is a direct consequence of the non-alignment of the principal axes of the spin Hamiltonian tensor.⁽¹⁴⁾

The results of the ZINDO calculations (Table 1) indicate that the bond dissociation energy of (1,3,5-C₆H₃Me₃)V is greater than (C₆H₅F)V and (1,4-C₆H₄F₂)₂V by 9.0 and 13.5 kcal/mol respectively. The trends in the hyperfine splittings, and intensities of the EPR spectra for the bis(arene)-vanadium complexes are similar to those observed for the corresponding mono compounds. It is therefore assumed that the bond dissociation energy trends for the *bis*- complexes will be similar to those already found for the mono complexes. Basically one expects that the more π -electron rich benzene rings form stronger bis complexes with the vanadium.

A detailed analysis of the EPR spectra, using computer simulation, and the correlation between the magnetic properties and the molecular structure of these complexes will be published shortly.

5. Conclusions

Electron rich benzenes react readily with atomic vanadium to form EPR active species. This is shown experimentally and confirmed by ZINDO/1 computations. When isolated in an inert matrix the vanadium complex shows eight resolvable vanadium hyperfine lines that are characteristic of vanadium-benzene sandwich complexes. Even for sandwich complexes that have a very low formation probability they are still detected due to the exceedingly high sensitivity of EPR spectroscopy (< 1 ppm). Thus in an analytical sense, EPR could be an extremely valuable tool to detect trace amounts of vanadium.

6. Acknowledgments

SMM would like to thank the Natural Sciences and Engineering Council of Canada for an Operating and Equipment grants. We would also like to acknowledge the University of New Brunswick for financial support in the form of research and operating grants. The authors are grateful to CALGAH Computer Systems, Ville St. Laurent, Quebec, for providing them with a copy of HyperChem.

7. References

1. R. Makhija, R. G. Draper and E. Furimsky, CANMET Report 77-61, Ottawa, Canada (1976).
2. E. M. van Zinderen Bakker and J. F. Jaworski, NRCC No.18132, Ottawa, Canada (1980).
3. R. J. H. Clark, The Chemistry of Titanium and Vanadium: An Introduction to the Chemistry of the Early Transition Elements, Elsevier, Amsterdam (1968).
4. M. J. Ledoux, and S. Hantzer, Catal. Today, 1990, 4, 479-496.
5. K. J. Klabunde and H. F. Efner, Inorg. Chem., 1975, 18, 789.
6. K. Shibata, H. Kikiyama, Y. Sanada and J. Sohma, Fuel, 1978, 57, 561.

- 7 F. E. Dickson, C. J. Kunesh, E. L. McGinnis and L. Petrakis, Anal. Chem., 1972, **44**, 978.
8. G. A. Ozin and M. Moscovits, *Cryochemistry*, Wiley, New York (1976).
9. Product of Autodesk Inc. Sausalito, California USA.
- 10 W. P. Anderson, W. D. Edwards and M. C. Zerner, Inorg. Chem., 1986, **25**, 2728.
11. E. P. Kundig, M. Moscovits and G. A. Ozin, J. Mol. Struct., 1972, **14**, 137.
12. M. Moscovits and G. A. Ozin, Appl. Spectrosc., 1972, **26**, 481.
13. J. L. Fletcher and M. J. McGlinchey, Can. J. Chem., 1975, **53**, 1525.
14. S.M. Mattar and G.A. Ozin, J. Phys. Chem., 1988, **92**, 3511.

CHARACTERIZATION OF JURASSIC BLACK SHALES FROM ASTURIAS (NORTHERN SPAIN): EVOLUTION AND PETROLEUM POTENTIAL

I. Suárez-Ruiz and J.G. Prado

Instituto Nacional del Carbón (C.S.I.C.). Ap.Co. 73, 33080-Oviedo. Spain.

ABSTRACT. The black shale levels for the Jurassic from the province of Asturias (Northern Spain) are mainly Pliensbachian age. They are composed of calcite, quartz, pyrite and illite as inorganic compounds while organic matter corresponds to a type II kerogen in which the autochthonous aquatic material (marine) predominates over that from the continental origin. The rank studies show a differential evolution for these sediments which corresponds to the diagenesis (represented by oil shales) and organic catagenesis (source-rocks of oil and gas) stages. This evolution seems to be linked to the tectonic of the region and to the presence of thermal flows which have occurred from the Paleozoic until after Jurassic sedimentation promoting the generation and migration of hydrocarbons.

KEY WORDS: Northern Spain, Jurassic, Pliensbachian, Organic matter, Black shales, Oil shales, Source-rocks, Rank, Kerogen II, Petroleum potential, Organic petrology, Pyrolysis.

1. Introduction

Even though the greater part of the sedimentary rocks contain particles of dispersed organic matter from the different origins, only a few of them can be considered black shales⁽¹⁾ because of its high organic content (% Carbon > 5) and special characteristics of formation of these black shales. Those having a type of kerogen appropriated to generate hydrocarbons in the conversion process and presenting a high degree of immaturity will be considered as true oil shales.

In the hydrocarbons exploration field, the detailed characterization and study of organic fraction from the sedimentary levels with high organic content as well as the determination of its degree of evolution are important tools for the knowledge of the geothermal history and the petroleum potential of a specific region. From the point of view of the oil shale conversion and application of the resultant products it is essential to know the nature, the properties and characteristics of the organic matter present.

Therefore, considering that in the province of Asturias (Northern Spain) there are important black shales levels mainly from the Pliensbachian (Jurassic) period⁽²⁾, the overall objective of this work has been their characterization. Specifically, inorganic composition and the type of organic content have been analyzed. Moreover, the degree of evolution reached by these black shales, their regional distribution and petroleum potential have been evaluated.

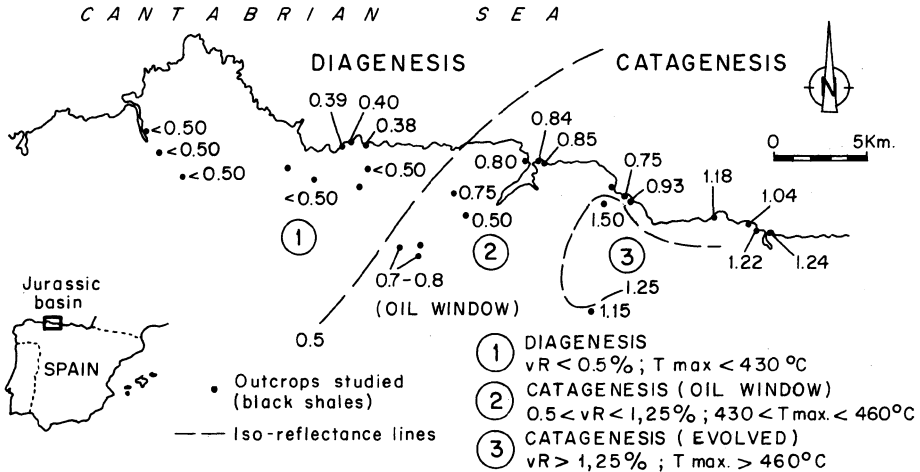


Figure 1. Organic evolution pattern for the Pliensbachian black shales according to different parameters of maturity.

2. Sampling and Analytical Procedures

Samples studied in this work come from 20-25 outcrops over 40 km considering that the black shales levels mainly appear along the shoreline (Fig. 1). Samples were prepared for petrographic and geochemical analysis.

Petrographic analysis. The optical study of organic fraction was achieved by microscopy in white, blue and UV light. The reflectance measurements were performed according to ISO standard⁽³⁾ in oil immersion with objectives of 60X magnification, overall vitrinite particles found in a petrographic section. Spectral analysis on fluorescence were taken from alginite (Tasmanite algae and Lamalginite), organo-mineral groundmass and hydrocarbons found in some samples, using UV light and water lens (50X magnification). The spectral parameters considered in this work have been the classical ones⁽⁴⁾: λ_{max} (98%) and the green/red quotient (Q650/500).

Geochemical analysis. The determination of the petroleum potential and the degree of evolution of the organic matter in the black shales were achieved using pyrolysis techniques: Rock-Eval analysis performed according to Espitalié⁽⁵⁻⁶⁾ and the Gray-King Assay according to ISO standard⁽⁷⁾ exclusively for the oil yield.

The mineral matter was characterized by X Ray Diffraction.

3. Results and Discussion

3.1 COMPOSITION OF THE BLACK SHALES

Globally, the organic fraction of the black shales is composed of the mixed type of organic matter which corresponds to a type II Kerogen (Fig. 2). It is composed of

autochthonous material of aquatic origin (marine) which dominates and comes from the phytoplankton and zooplankton as well as their degradation products. It mainly corresponds to alginite: (Lamalginité⁽⁹⁾) and Tasmanites indicative of brackish waters), bituminite and different fragments of zooclasts as well as elements of the hystrichosperid group. The allochthonous material is represented by pieces of continental vegetable origin which are scarce and reduced in size. They would be classified according to the established maceral groups by the ICCP⁽¹⁰⁻¹¹⁾ as inertinite (fusinites and in lesser amounts semifusinites), huminite/vitrinite (humo/colinite and scarce humo/telinite), liptinite (microspores and few resinites) and products of mechanical and/or biochemical degradation. The main mass of these rocks is the organo-mineral groundmass, an undifferentiated mixture of organic and inorganic substances, over which the other figured components, mentioned above, are found. Moreover, in the case of black shales with reflectance greater than 0.5%, different phases of hydrocarbons are highly fluorescent and solid bitumens have been identified.

The inorganic fraction of these black shales identified by XRD is composed of calcite, quartz, pyrite, illite and in smaller amounts dolomite, ankerite, kaolinite and traces of feldspars.

All of these characteristics represent a sedimentary environment for the black shales which is of marine character, reducing, euxinic and of low energy.

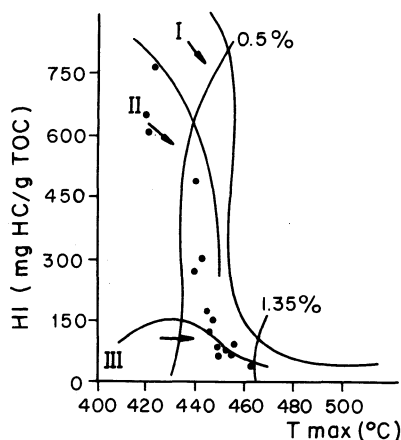


Figure 2. Organic composition of the black shales. (The basic Tmax/HI diagram is from Espitalié⁽⁸⁾)

3.2. ORGANIC EVOLUTION

The degree of evolution presented by the organic matter from the black shales of all the studied outcrops, was achieved using the reflectance, spectral fluorescence data and the Tmax, HI, TOC parameters from Rock-Eval pyrolysis. The results obtained have permitted to define an evolution pattern which varies from the West to the East side (Fig. 1) of the region making it possible to distinguish two different stages of organic evolution⁽¹²⁾ corresponding to the diagenesis and the catagenesis.

Table 1. Evolution of spectral parameters in relation to the different stages of organic maturity (vR = % vitrinite reflectance)

	Tasmanite λ_{max} $Q_{650/500}$	Lamalginite λ_{max} $Q_{650/500}$	Organo-Mineral Groundmass λ_{max} $Q_{650/500}$	Different phases of hydrocarbons			
				λ_{max}	$Q_{650/500}$	λ_{max}	$Q_{650/500}$
1 DIAGENESIS Gijón Area vR < 0.5% $T_{\text{max}} < 430^{\circ}\text{C}$	500 0.37	539 0.66	540 0.70				
2 CATAGENESIS (Oil window) Rodiles-P. Vega Area $0.5 < \text{vR} < 1.25\%$ $430 < T_{\text{max}} < 460^{\circ}\text{C}$	539 0.60	592 1.35	573 1.12	494	0.25		
3 (evolved) Colunga-Ribadesella Area $\text{vR} > 1.25\%$ $T_{\text{max}} > 460^{\circ}\text{C}$			627 1.73	514	0.35	575	1.09 657 2.02
				No Fluorescence			

Diagenetic stage (Figs. 1, 2 and Table 1): This stage is represented by immature organic matter ($vR < 0.5\%$; $T_{max} < 430^{\circ}\text{C}$) having higher hydrogen content ($HI > 600 \text{ mg HC/g TOC}$) which preserves all the textural and structural characteristics and, in general, it shows a strong fluorescence at the shortest wavelength (Table 1). In this stage, the black shales constitute the true oil shales that, when found in the phase before oil generation they keep intact their petroleum potential making it possible to identify all the organic components mentioned above. Semiquantitative data about the composition of these oil shales⁽¹³⁾ show that the principal component was the organo-mineral groundmass (76.6 vol.%) followed by the all specimens of alginite (21.2 vol.%), vitrinite + inertinite (1.1 vol. %), terrestrial liptinite (0.9 vol.%) being scarce the zooclast fragments (0.2 vol.%).

Catagenetic stage (Figs. 1, 2 and Table 1). The organic fraction is evolved as indicated by the modification of rank parameters. For this stage it is possible to distinguish two different and correlative phases of maturity.

The first one corresponds to the oil window or the oil generation phase ($0.5 < vR < 1.25$; $430 < T_{max} < 460^{\circ}\text{C}$; $65 < HI < 600 \text{ mg HC/g TOC}$). A gradual degradation of the organic matter occurs and its properties change. Therefore, it is not possible to identify all the organic components because they are degraded or they have been transformed into hydrocarbons. At the same time, the fluorescence properties of the organic components are modified showing reddish colours with lesser intensities (Table 1). The organo-mineral groundmass has partially lost its fluorescence. The presence of different phases of hydrocarbons and oil traces having strong fluorescence are typically found in this stage. These black shales are source-rocks that have partially generated their hydrocarbons by natural evolution.

In the second phase of the catagenetic stage (Figs. 1, 2 and Table 1) the organic matter of the black shales is clearly evolved ($vR > 1.25\%$; $T_{max} > 460^{\circ}\text{C}$; $HI < 65 \text{ mg HC/g TOC}$). With the exception of a few oil traces, the organic matter is not fluorescent (Table 1) and it is only possible to identify the organic matter of continental origin and some other very degraded fragments. This stage represents the wet gas generation phase.

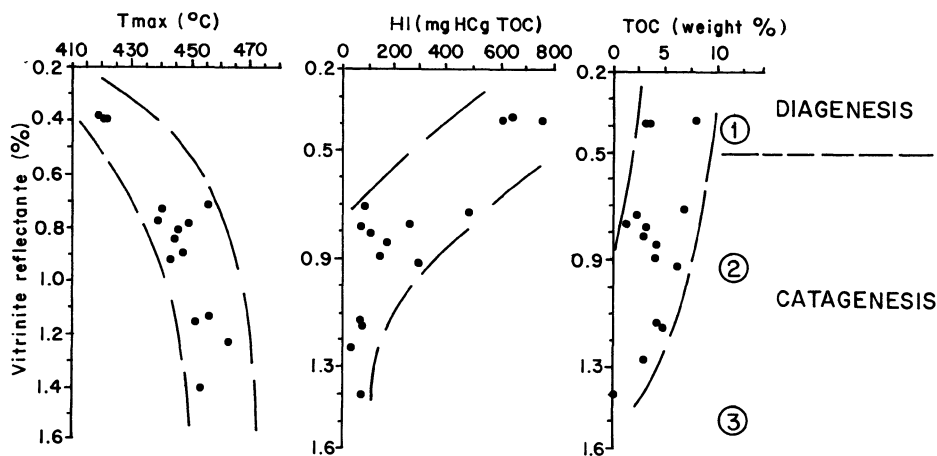


Figure 3. Relation between different parameters of maturity for the defined stages of organic evolution.

There is a good correlation between all the maturity parameters for these black shales in the different stages of evolution as is shown in Fig. 3.

3.3 EVALUATION OF THE PETROLEUM POTENTIAL.

The petroleum potential of the black shales studied depends on the stage of evolution concerned. Parameters considered to evaluate this potential were the S2 and TPI (from Rock-Eval pyrolysis) and the oil yield from the Gray-King Assay. Results are shown in the Fig. 4.

Diagenesis stage (immature): Even though the oil shales have their petroleum potential intact, the real potential depends on the abundance of the organic matter of the rock. In general, oil yields after pyrolysis conversion have been: 40-25 Kg oil/T rock and S2: 55-25 mg HC/g rock (Fig. 4).

Catagenesis stage: For the oil window phase the petroleum potential is variable due to the fact that the black shales have partially generated their hydrocarbons. Therefore, the oil yields obtained were: 28-5 Kg oil/T rock and S2: 20-3 mg HC/g rock (Fig. 4). A diminution in the oil yields was observed with increasing degree of catagenesis. In general, for the black shales evolved (vitrinite reflectance >1.25%) no oil was obtained. Only in some cases the S2 has proportionated values between 0.0 and 1.0 mg HC/g rock. This evolved organic matter could only possibly generate gas.

The variation of the TPI (total production index) is according to the other results (Fig. 4).

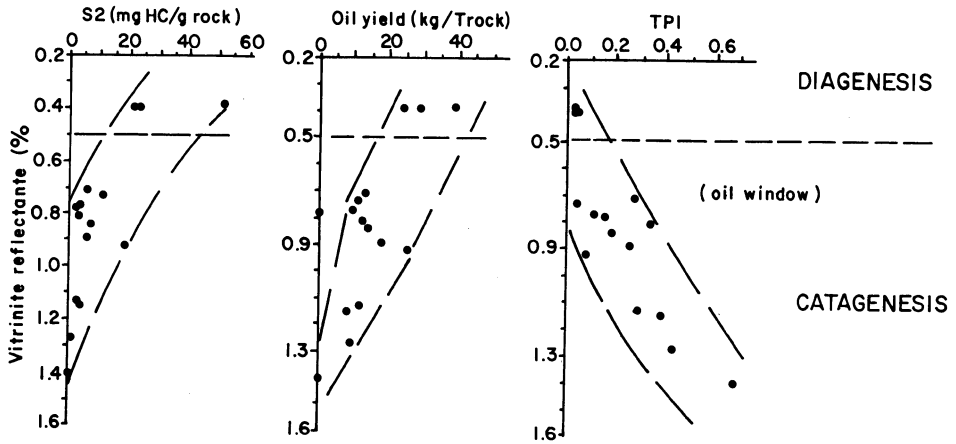


Figure 4. Petroleum potential of the studied black shales in relation to their degree of evolution.

4. Conclusions

1. The black shales of the Pliensbachian from Asturias (Northern Spain) are composed of a type II kerogen (mixed organic matter) having a medium petroleum potential when they are in an immature stage (oil shales).
2. The degree of evolution reached by these black shales varies from the West side (immature stage - diagenesis) to the East side (mature and evolved stages - catagenesis) of the region studied as demonstrated by all the parameters of maturity considered.
3. This evolution seems to be linked to the regional tectonic (opening stages of the rift) and to the presence of thermal flows which have occurred from the Paleozoic until after Jurassic sedimentation. It has promoted the generation and migration of hydrocarbons and it could have partially contributed to their accumulation in younger sediments of the continental platform of the Cantabrian Sea.

5. References

- 1 R.L. Bates and J.A. Jackson (Ed.). Glossary of Geology (3th ed.). Amer. Geolog. Instit., (1987), 788 pp.
- 2 I. Suárez-Ruiz. Caracterización, Clasificación y Estudio de la Evolución de la Materia Orgánica Dispersa (MOD) en el Jurásico de Asturias y Cantabria. Ph.D. Thesis. University of Oviedo. Oviedo, Spain (1988), t. I,II
- 3 ISO 7404/5 - 1984(F) Standard. Méthodes d'analyse pétrographique des charbons bitumineux et de la anthracite, part 5: Détermination au microscope du pouvoir réflecteur de la vitrinite.
- 4 K. Ottenjann, M. Teichmuller and M. Wolf. Fortschr. Geol. Rheinland Westfalen, Dtsch. (1974), 24, 1-36.
J. Espitalié, M. Madec, B. Tissot, J.J. Mening and P. Leplat. Source rock characterization method for petroleum exploration. Proc. 9th Ann. Offshore Techn. Conf., (1977a), 439-444, Houston, Tx.
- 6 J. Espitalié, J.L. Laporte, M. Madec, F. Marquis, P. Leplat, J. Paulet and A. Boutefeu. Rev. de l'Institut Français du Pétrole, (1977b), 32, 23-42
- 7 ISO 502 - 1974 Standard. Gray-King Assay.
- 8 J. Espitalié. Organic Geochem. applied to oil exploration, (1983), 24 pp. Rueil-Malmaison, France.
- 9 A.C. Hutton. Internat. Jour. of Coal Geol., (1987), 8, 203-231
- 10 ICCP. International Handbook for Coal Petrography, (1971), (2th ed.), C.N.R.S., Paris.
- 11 ICCP. International Handbook for Coal Petrography, (1975), (2th ed.), C.N.R.S., Paris.
- 12 B. Tissot and D.H. Welte. Petroleum Formation and Occurrence; a new approach to oil and gas exploration., (1978), Springer Verlag, 538 pp. Berlin.
- 13 I. Suárez-Ruiz and J.G. Prado. Estud. Geológicos, (1990), C.S.I.C., 46, 81-92, Madrid.

***n*-ALKANOIC COMPOUNDS IN SULPHUR-RICH MACROMOLECULAR SUBSTANCES: A DETAILED INVESTIGATION OF SULPHUR INCORPORATION AND CROSS-LINKING**

J. HEFTER, H. H. RICHNOW, R. SEIFERT AND W. MICHAELIS

Institut für Biogeochemie und Meereschemie

Universität Hamburg

Bundesstraße 55

20146 Hamburg

Germany

ABSTRACT. A selective stepwise chemical degradation technique is applied to investigate alkanolic structural subunits in sulphur-rich macromolecular fractions (resins, asphaltenes, kerogens). Emphasis is given to the sulphur speciation in terms of intermolecular (thioether, thiodiether) and intramolecular (thiolane, thiophene) linking of structural subunits. The degradation sequence comprises two steps: (I) a desulphurization and (II) an oxidation of aromatic moieties liberating alkyl substituents as mono- and dicarboxylic acids. In this study, nickel boride is used for the desulphurization. The efficiency of the reagent is compared to other desulphurization reagents (Raney nickel, nickelocene/LiAlH₄). The use of deuteriated nickel boride allows to label the site of former sulphur functionalities with deuterium. The reagent is tested on a set of reference compounds to elucidate the deuteration pattern of various sites and types of sulphur bonds (e. g. thioether, thiolane, thiophene). Ruthenium tetroxide is used to release alkanolic substituents of aromatic subunits.

This chemical degradation sequence is applied to several macromolecular fractions, derived from various sulphur-rich sediments and oils, respectively. Each step of the sequence affords considerable amounts of low molecular weight material (hydrocarbons, carboxylic acids), which is separated by column chromatography and studied by GC and GC-MS, whereas the remaining high molecular weight material is subjected to the following degradation step.

The alkanolic degradation products of several sulphur-rich macromolecular fractions of oils and sediments are discussed with respect to the incorporation of sulphur into the macromolecular structure and the abundance of sulphur bridges.

The labelling with deuterium provided evidence for a simultaneous linkage by sulphur and aromatic units of the released alkanolic products, pointing to their function as constituents and cross-linking subunits of the parent macromolecular network.

1. Introduction

Sulphur is next to carbon and hydrogen the most abundant element in heavy petroleum and kerogen⁽¹⁾. The environmental impact arising from the increasing combustion of sulphur-rich oils and the awkward effects of sulphur on the refining processes and products give rise to a growing interest in the chemical nature of sulphur in oils. Even though various attempts have been made to elucidate the chemical structure of sulphur species in oils and kerogens, at least the forms of sulphur in macromolecular organic matter are partly known on the molecular level.

The chemical structure of a large number of sulphur containing compounds was in-

vestigated using gas-chromatography and mass-spectrometry (2-6). In general, these methods are limited to relative low molecular weight compounds.

Structural investigations of sulphur in macromolecular organic matter were also performed using non-destructive spectroscopic methods such as IR and NMR. These methods reveal bulk information on the abundance of functional groups and of aromatic and aliphatic carbon atoms. However, they allow only limited conclusions on the detailed macromolecular structure (7).

Recently, studies have been carried out applying temperature programmed reduction (TPR)(8) and X-ray spectroscopic techniques such as X-ray adsorption near-edge spectroscopy (XANES)(9, 10). Though these methods allow an estimate of the relative quantities of thiophenic and non-thiophenic sulphur species, they give scarce information on the related carbon atom framework. The scope and limitations of X-ray spectroscopy and other spectrometric methods in the quantitative analysis of sulphur speciation in heavy petroleum have been discussed recently (11).

Progress in the structural analysis of macromolecular material was achieved by the application of chemical degradation techniques (7) developed to study building blocks of macromolecular substances of geological origin. These techniques are based on selective cleavage reactions of distinct bonds within the macromolecular framework. The resulting extractable degradation products of low molecular weight are amenable to GC and GC/MS analysis. Methods applied for the selective degradation of sulphur bonds are the chemolysis of polysulphide bonds (12, 13) and desulphurization with Raney nickel (14-16), nickelocene (17, 18) or lithium/ethylamine (19). Some of these desulphurization methods allow to label the position of the former sulphur linkages by using deuteriated reagents.

A number of oxidation techniques has been applied to investigate the aromatic and aliphatic structural entities of geological macromolecules (20, 21). High yields of products were achieved applying ruthenium tetroxide (RuO₄) as oxidation reagent. By this method, aromatic structural units are oxidized, affording aliphatic substituents as carboxylic acids (22-24).

In this study we applied a sequence of selective chemical degradation techniques, which combined desulphurization and oxidation, to sulphur-rich macromolecular fractions of geological origin. We attempted to demonstrate the different forms of organic sulphur species (e. g. thioether, thiodiether, thiolane, thiophene) by the deuterium signature of the low molecular weight degradation products. The speciation of sulphur is exemplified by *n*-alkanoic subunits released during chemical degradation of the parent macromolecules.

Major goals of this study have been:

1. Elucidation of the cross-linking of low molecular weight compounds by sulphur bridges, aromatic subunits, sulphur bridges and aromatic subunits;
2. Determination of the macromolecularly bound thiolane and thiophene subunits.

Oil samples	Origin	Age	Source rock type	*LMW (wt. %)	Resin (wt. %)	Asphaltene (wt. %)
Monterey oil #4	California	Miocene	silicates carbonates	52.3	24.9	18.6
Monterey oil #8	California	Miocene	silicates carbonates	46.8	26.2	18.0
Boscan	Venezuela	Cretaceous	carbonates	49.3	25.9	18.3
Bati Raman	Turkey	Cretaceous	carbonates	45.1	15.9	25.4

Table 1: Origin, age, source rock type and chromatographic fractions of oil samples (*LMW = low molecular weight compounds).

2. Experimental

2.1. SAMPLES AND GEOLOGY

The investigated macromolecular fractions derived from oils (Boscan, Bati Raman and Monterey) and sediments (Monterey). Data on the origin, age, source rock, lithology, depositional environment and the composition of the respective oil and rock samples are shown in Table 1 and 2. The Monterey sediment and oil samples are part of the Cooperative Monterey Organic Geochemistry Study.

Sediment samples	Origin	Age	Lithology	Environment	*LMW (wt. %)	Resin (wt. %)	Asphaltene (wt. %)
Monterey KG4	California	middle Miocene	calcareous shales and mudstones	anoxic basin, upwelling	5.3	28.9	62.2
Monterey KG8	California	late Miocene	siliceous mudstones (carbonate poor)	anoxic basin, upwelling	6.2	24.1	64.9

Table 2: Origin, age, lithology, depositional environment and chromatographic fractions of sediment samples (*LMW = low molecular weight compounds).

2.2. EXTRACTION AND SEPARATION OF MACROMOLECULAR FRACTIONS

Sediment samples were extracted extensively with a mixture of dichloromethane/methanol (3:1; v:v). Kerogens were prepared by conventional techniques⁽²⁵⁾. Asphaltene fractions from the sediment extracts and the crude oils were precipitated by a fifty-fold excess of *n*-heptane⁽²⁶⁾. The *n*-heptane soluble compounds were separated by column chromatography resulting in a hydrocarbon fraction (*n*-hexane), a fraction of aromatic and sulphur compounds (5-10% diethyl ether in *n*-hexane) and a polar fraction (dichloromethane). The resin fraction was obtained by deactivation of the silica column with a mixture of dichloromethane/methanol/water (70:25:5; v:v:v).

2.3. DESULPHURIZATION

Desulphurization was achieved with nickel boride using a modification of the method previously described^(27, 28). Nickel boride was generated *in situ* from nickel chloride (NiCl₂) and sodium borohydride (NaBH₄). Hefter⁽²⁹⁾ and Schouten⁽³⁰⁾ have used this desulphurization technique with a number of model compounds and macromolecular matter of geological origin. For labelling of the desulphurization products, deuteriated nickel boride was prepared *in situ* by the reaction of NiCl₂ with NaBD₄. The reagent was soluble in the solvent system employed. The macromolecular substrate was dissolved in a mixture of CH₃OD:THF (1:1; v:v). Prior to adding the reagents, the sample was cooled in an ice bath. Typically, the degradation experiment was performed using 20 mol NiCl₂ and 60 mol NaBD₄ per mol organically bound sulphur. The mixture was stirred for 30 min and then kept under reflux for 30 min. The reaction was quenched with water and the reaction products were extracted with an excess of CH₂Cl₂ and filtered. The precipitating nickel salts were dissolved by addition of nitric acid (5%) to liberate trapped material or to recover the solid residue in the case of kerogen degradation. After washing the filter with CH₂Cl₂/CH₃OH (3:1; v:v), the water-solvent mixture was extracted again with CH₂Cl₂ (three times) and diethyl ether, subsequently. The combined organic phases were dried

over anhydrous Na_2SO_4 . The reaction products were further separated on a silica column as described above.

To compare the efficiency of the nickel boride reagent with methods previously used, i.e. Raney nickel, nickelocene/ LiAlD_4 (17, 18), selected samples were desulphurized applying all the three methods.

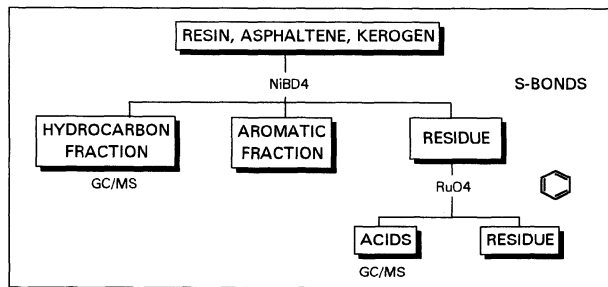


Fig. 1: Flow diagram of the degradation sequence.

2.4. RUTHENIUM TETROXIDE DEGRADATION

The use of RuO_4 for the oxidation of aromatic subunits is well established (17, 18, 22-24). Typically, a 15- to 20-fold molar excess of periodic acid (H_5IO_6), calculated on the organic carbon content of the sample, was used as co-oxidant. The sample and the co-oxidant were dissolved in a mixture of dichloromethane/acetonitrile/water (2:2:3; v:v:v), and a catalytic amount of RuO_2 (20 mg) was added. The mixture was stirred continuously for 15 h at 35 °C. The organic acids yielded by the reaction procedure were extracted subsequently with dichloromethane and diethyl ether, dried with anhydrous Na_2SO_4 and filtered through acid-washed Celite. The carboxylic acids were esterified with diazomethane and purified by column chromatography.

2.5. SEQUENTIAL CHEMICAL DEGRADATION

The degradation sequence applied to the macromolecular fractions is outlined in Fig. 1.

Compounds exclusively linked by sulphur bonds to the macromolecule are released within the initial desulphurization step. Furthermore, intramolecular sulphur functionalities (thiolane, thiophene) are degraded during this step, and the former positions of sulphur are labelled with deuterium atoms. Thereby, the amount of deuterium uptake is related to the former sulphur speciation and thus provides information about the structure of the original organic sulphur compound. After the desulphurization step, the low molecular weight degradation products are separated by column chromatography and the remaining macromolecular fraction is subjected to the next degradation step.

Alkanolic compounds substituted to aromatic ring systems are released by the oxidation of aromatic subunits. Two different types of compounds are obtained:

- non deuteriated compounds which have been exclusively linked to aromatic units within the macromolecule.
- deuteriated products, resulting either from substituents of aromatic structural elements with additionally incorporated thiolane or thiophene moieties, or from alkanolic subunits additionally cross-linked by sulphur bridges to the macromolecular network.

2.6. ANALYTICAL TECHNIQUES

Sulphur and carbon determinations were performed on a *Carlo Erba* 1500 elemental analyzer. Hydrocarbons and methyl esters were analyzed on a *Carlo Erba* 4160 gaschromatograph equipped with a fused silica capillary column (DB-5, 30 m x 0.25 mm; J&W Scientific). The temperature program was: 80 °C, 3 min isothermal; 80-300 °C, 3 °C/min; 300 °C, 30 min

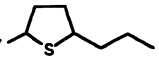
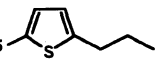
SUBSTRATE	$\xrightarrow[\text{[NiCl}_2\text{/NaBD}_4\text{]}]{\text{Ni}_2\text{B}}$	PRODUCT	YIELD
$\text{CH}_3(\text{CH}_2)_{11}\text{-S-(CH}_2)_{11}\text{CH}_3$	\longrightarrow	$(\text{CH}_2)_{11}\text{CH}_2\text{D}$	93%
$\text{C}_{13}\text{H}_{27}$ 	\longrightarrow	$\text{C}_{20}\text{H}_{40}\text{D}_2$	91%
$\text{C}_{17}\text{H}_{35}$ 	\longrightarrow	$\text{C}_{24}\text{H}_{44}\text{D}_6$	92%

Fig. 2: Desulphurization of standard compounds with nickel boride.

isothermal. Injection mode: on column; carrier gas: H_2 . GC/MS analyses were performed on a *Carlo Erba* 4160 gaschromatograph coupled to a *Varian* CH7A mass spectrometer. MS conditions: 70 eV ionization energy; source temperature 250 °C; mass range m/z 50-800; resolution 1000. The temperature program was: 80 °C, 5 min isothermal; 80-300 °C, 3 °C/min; 300 °C, 30 min isothermal. Injection mode: on column; carrier gas: He.

The number of deuterium atoms incorporated into the low molecular weight degradation products was determined by GC/MS. For assigning the number of deuterium atoms present in the degradation products, intensities of the molecular ions (M^+ , M^++1 , M^++2 ,...) are summed up. Contributions of individual molecular ions are calculated as percentages of this sum. The data are not corrected for carbon and oxygen isotopes.

3. Results and discussion

3.1. DESULPHURIZATION WITH NICKEL BORIDE

The selectivity, reactivity and the labelling efficiency of the nickel boride reagent was tested using synthetic reference compounds (Fig. 2). Aliphatic thioethers are almost completely converted to *n*-alkanes. Thiolanes and thiophenes were desulphurized with good to excellent yields (>90%). Additional experiments showed that ether and ester bonds or aromatic bonds remained unaltered.

The number of deuterium atoms of the degradation products revealed information on the former sulphur functionalities. Desulphurized thioethers were mainly labelled with one deuterium atom, whereas desulphurized thiolanes incorporated two and thiophenes six deuterium atoms (Fig. 3a), respectively. Thioether bound thiolane and thiophene structures should show an uptake of one additional deuterium atom during the desulphurization. Based on this suggestions, we calculated the number of deuterium atoms for those structural elements by combining the known deuteration patterns of the unbound reference compounds. Hence, a thioether-bound thiolane structure three deuterium atoms and a thioether-bound thiophene structure seven deuterium atoms (Fig. 3b).

Aliquots of the Monterey oil #4 resin and asphaltene fractions were treated simultaneously with Raney nickel, nickelocene and nickel boride to compare the efficiencies of the different desulphurization reagents for natural sample material. The carbon to sulphur ratios of the original and the desulphurized fractions are shown in Fig. 4. In general, the C/S values increased after desulphurization which proves a removal of sulphur by all three reagents. Regarding the efficiency, different trends are observed for the respective macromolecular fraction (resin or asphaltene) these methods were applied to. In case of the resin fraction, the highest C/S value after desulphurization was obtained with Raney nickel (26.2), followed by nickelocene (19.8) and nickel boride (17.1). In contrast the C/S ratios of the desulphurized asphaltene fractions

indicated lowest desulphurization with Raney nickel (C/S: 13.5), whereas a ratio of 16.0 and 18.0 resulted from the nickelocene and for nickel boride treatment, respectively. These values suggest desulphurization of the resin fraction to be most efficient with Raney nickel, while highest efficacy for the asphaltene fraction was achieved with the nickel boride reagent. This is probably caused by the enhanced solubility of asphaltene in the solvent system (THF:CH₃OD) used for the nickel boride degradation.

3.2. STRUCTURAL ASPECTS OF SULPHUR IN MACROMOLECULAR FRACTIONS

The major compounds obtained by the desulphurization of the resin, asphaltene and kerogen fractions from the studied samples are aliphatic hydrocarbons with a linear carbon skeleton. These products represent intermolecular building blocks of the macromolecular network which have been bound *via* sulphur bonds. Polydeuteriated products may result from sulphur bound compounds possessing intramolecular sulphur containing structural elements like thiolanes and thiophenes.

The natural mixture of organic sulphur species present in the building blocks of the macromolecular network leads to a deuterium distribution in the obtained desulphurized natural products more complex than in the desulphurized reference compounds. However, the deuteration pattern of compounds deriving from desulphurized geological samples provide information on the different sulphur functionalities in the macromolecular network as the sulphur species leave their imprint on the alkyl moieties degraded from the macromolecule. Thus deuteriated alkanes can be used to differentiate (I) the type of sulphur functionalities in different resins, asphaltenes and kerogens, and (II) the cross-linking of sulphur between structural subunits of variable chain length.

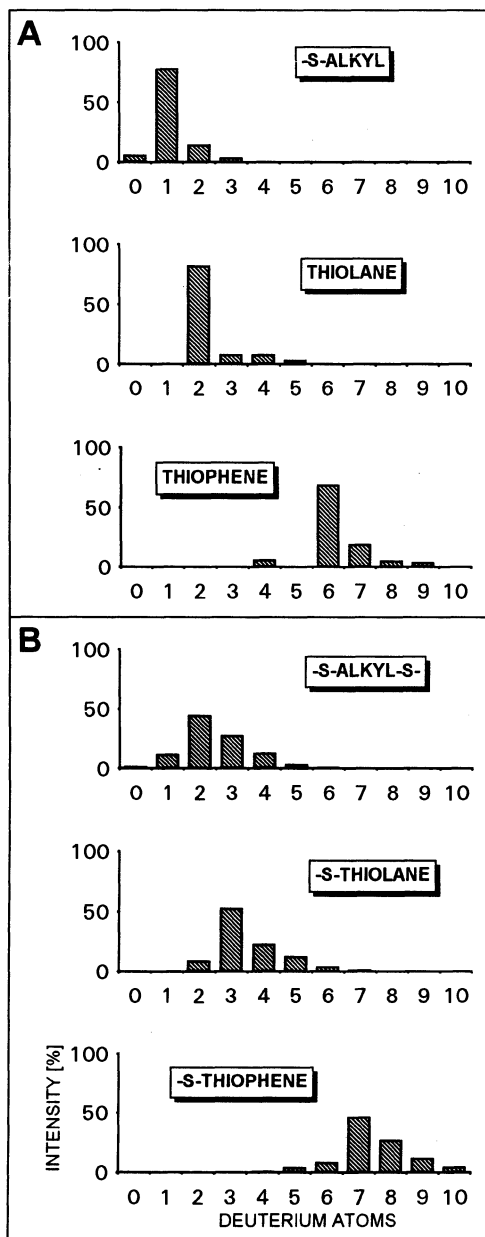


Fig. 3: Deuterium incorporation of desulphurized reference compounds (A) and calculated deuteration patterns for thioether bound reference compounds (B).

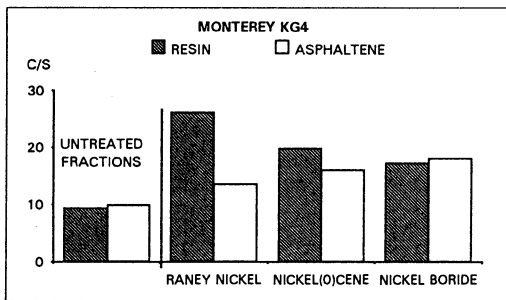


Fig. 4: Carbon to sulphur ratios of Monterey Oil #4 resin and asphaltene fractions before and after desulphurization with different reagents.

uptake of two deuterium atoms. Higher degree of deuterium labelling, up to seven deuterium atoms, may indicate cross-linking of this compound *via* several thioethers. However, small relative amounts of thioether-thiolane structures (three deuterium atoms) and thioether-thiophene moieties (seven deuterium atoms) may be present in this resin fraction.

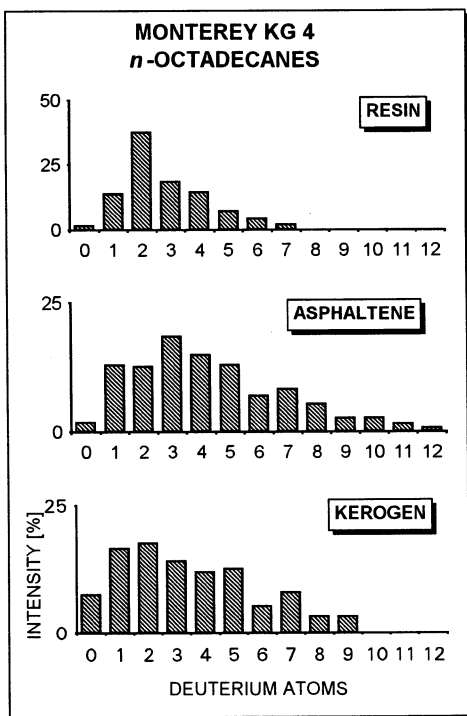


Fig. 5: The deuterium labelling of *n*-octadecanes released by desulphurization of the Monterey KG 4 macromolecular fractions.

(I) A resin, an asphaltene and a kerogen fraction isolated from the Monterey KG4 sediment sample were desulphurized with nickel boride. The incorporation of deuterium is calculated from the analysis of the molecular ion region in mass spectra of selected compounds. Fig. 5 shows of the intensities for the M^+ peak and its deuteriated homologues ($M^+ + 1$, $M^+ + 2, \dots$) for *n*-octadecanes obtained in different desulphurizations. The deuterium incorporation in the desulphurization product of the resin fraction revealed that sulphur is mainly present in thioether and thiodiether linkages, as indicated by the prevalent

A more complex deuterium incorporation pattern is recognized in the desulphurization products of the asphaltene and kerogen. Compared to the resin fraction, the *n*-octadecanes from the degradation of the asphaltene and the kerogen revealed a significantly higher relative amount of multideuteriated compounds. A distinct maximum, accompanied by a regular decrease with increasing numbers of deuterium atoms was not observed. In contrast, an enhanced portion of compounds, which have incorporated three and seven deuterium atoms, was recognized in the asphaltene fraction. This suggests the relevance of sulphur bound thiolane - three deuterium atoms - and sulphur bound thiophene structures (seven deuterium atoms) in this fraction. Sulphur bound thiophene moieties are also prominent building blocks of the kerogen fraction, as indicated by the value of seven deuterium atoms in the desulphurized product.

These findings imply that the resin, asphaltene and kerogen fractions differ not only in their molecular weight but also in the chemical structure of their macromolecular network (16, 18).

(II) The desulphurization of a resin fraction of the Bati Raman oil released high amounts of *n*-alkanes ranging from 12 to 35 carbon atoms. The individual deuteration

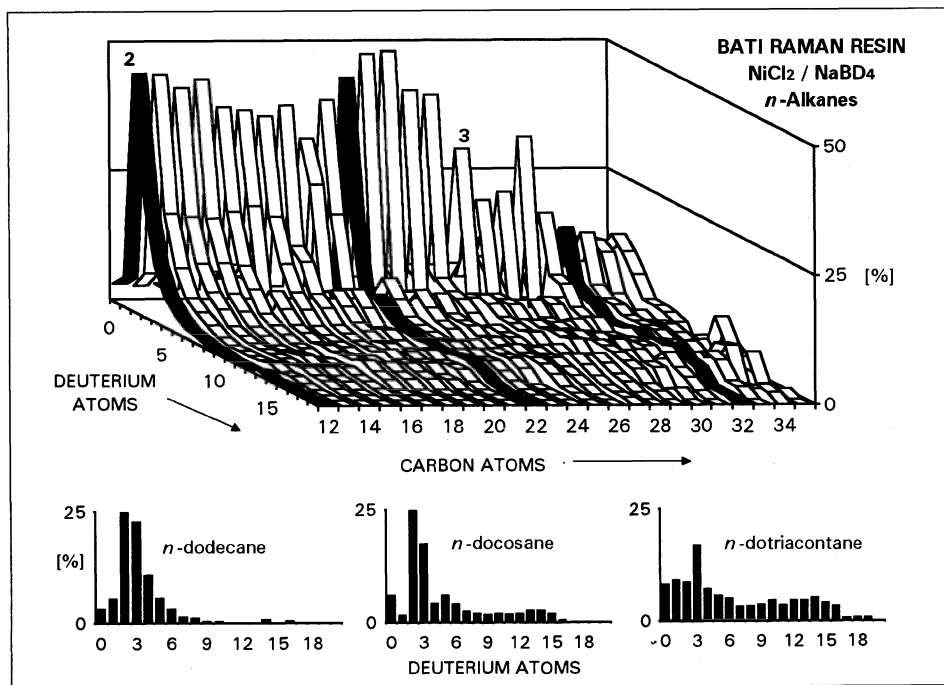


Fig. 6: The deuterium labelling of *n*-alkanes released by desulphurization of the Bati Raman resin.

pattern of these *n*-alkanes revealed an incorporation of up to 20 deuterium atoms. The complete deuterium incorporation of all *n*-alkanes is summarized in a three-dimensional diagram in Fig. 6. The distribution of deuterium atoms in the molecular ions for three *n*-alkanes (*n*-dodecane, C₁₂; *n*-docosane, C₂₂ and *n*-dotriacontane, C₃₂) is accentuated. The deuteriation pattern of *n*-dodecane makes evident a relative high contribution of compounds which have been linked to the macromolecular network by two sulphur bridges (two deuterium atoms) and of sulphur bound thiolanes (three deuterium atoms). These structural elements may also well explain the deuteriation pattern of the *n*-docosane. Additionally, this compound shows a deuterium incorporation of up to 16 deuterium atoms. The molecular ion region in the mass spectrum of the *n*-dotriacontane indicates the presence of up to 19 deuterium atoms with a high relative concentration of multiple deuteriation. Obviously, the degree of polydeuteriation shows a positive correlation with increasing chain lengths of the released *n*-alkanes. Multiple deuteriation may arise for example from the former presence of two thiolane or two thiophene moieties which are linked by several sulphur functions to the macromolecular matrix. Furthermore it seems that long chain aliphatic compounds provide preferred sites for a multiple attack of active sulphur species.

3.3. DEGRADATION OF AROMATIC STRUCTURAL SUBUNITS

Catalytic oxidations using ruthenium tetroxide have been applied to asphaltenes⁽³³⁾, kerogens⁽²³⁾ and macromolecular fractions of coals^(31, 32, 34). This reagent liberates aliphatic substituents of aromatic structural units as carboxylic acids in high yields⁽³¹⁾ bearing one extra

carbon atom from the oxidative degradation of the aromatic system. Dicarboxylic acids extended by two carbon atoms are obtained from aliphatic structures linking two aromatic units.

The RuO_4 oxidation was applied to the residue of the desulphurization reaction in our sequential degradation. The carboxylic acids released by the oxidation of the resin fraction of the Monterey oil #4 are shown in Fig. 7.

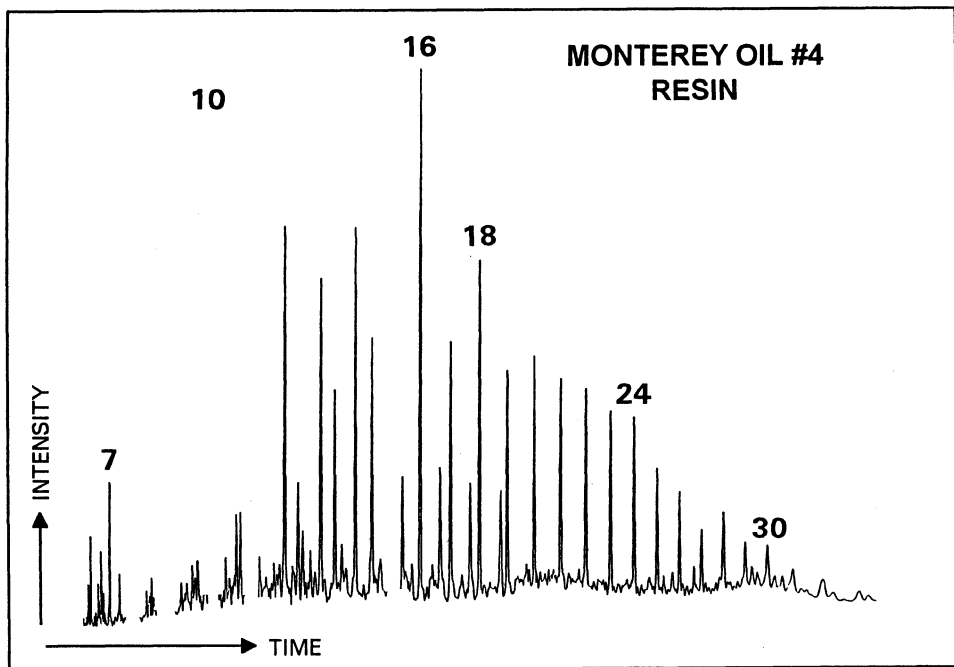


Fig. 7: Gas chromatogram of the carboxylic acid fraction (measured as methyl esters) obtained by the oxidation of aromatic structural units of the Monterey oil #4 resin. Numbers refer to the carbon atom numbers of the *n*-alkanoic acids.

Carbon numbers of the degraded straight chain monocarboxylic acids range from C_7 to C_{30} . A considerable fraction of branched monocarboxylic acids is also present. GC-MS investigations revealed the oxidation products of macromolecular fractions to be a mixture of non deuteriated and deuteriated compounds. For example, the molecular ion region in the mass spectra of heptadecanoic acid (methyl ester), obtained by the oxidation of the Monterey oil #4 asphaltene, indicated a mixture of undeuteriated (m/z 284) and mono- to polydeuteriated (m/z 285-290) compounds (Fig. 8). The undeuteriated components represent alkyl units which had contained no sulphur functionalities but have been attached to an aromatic ring system. The deuteriated acids could arise either from thiolane and thiophene structures in the alkyl substituent of an aromatic system or from alkanolic subunits which had been linked to the macromolecular structure *via* both, sulphur bridges and an aromatic ring as indicated in Fig. 8.

The relative amount of deuterium incorporation of the heptadecanoic acid is shown in Fig. 9. Whereas about 50% of mass intensity for the molecular ion region of the heptadecanoic acid is related to deuterium free species, the remaining percentage reveals an incorporation of 1 to 6 deuterium atoms.

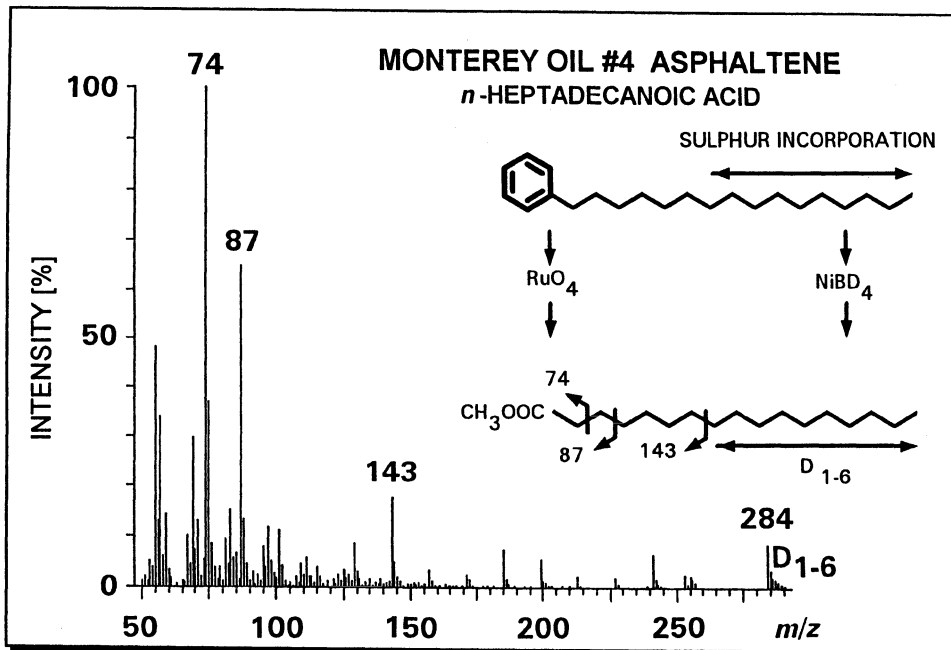


Fig. 8: Mass spectrum and fragmentation pattern of *n*-heptadecanoic acid methyl ester. The molecular ions (*m/z* 284-290) indicate a mixture of non-deuteriated (*m/z* 284) and polydeuteriated (*m/z* 285-290) compounds. The deuterium incorporation of this compound results from the previous desulphurization step.

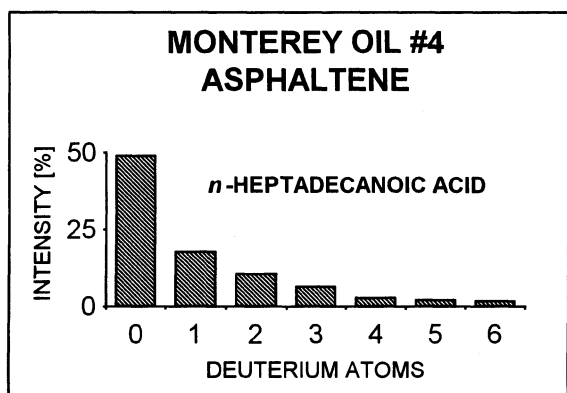


Fig. 9: The deuterium labelling of *n*-heptadecanoic acid (methyl ester) yielded by the oxidation of aromatic structural units of the Monterey oil #4 asphaltene fraction.

4. Conclusions

A selective chemical degradation sequence was applied to macromolecular fractions (resins, asphaltenes, kerogens). This method allows to distinguish between sulphur bound moieties and substituents of aromatic structural units building up the macromolecular network. Deuterium labelling of the former sulphur functionalities provided evidence that thioethers, thiodiethers and sulphur bound thiolanic and thiophenic moieties are important structural subunits of the sulphur-rich macromolecular fractions.

The efficiency of different desulphurization reagents (Raney

nickel, nickelocene and nickel boride) was tested. In general, all three methods are suitable to desulphurize geological samples. Raney nickel was found to be most effective for the desulphurization of a resin fraction, whereas highest efficacy for the desulphurization of an asphaltene fraction was achieved by the use of the nickel boride reagent.

The comparison of the deuterium labelling of *n*-octadecanes derived from the desulphurization of a resin, an asphaltene and a kerogen fraction isolated from the Monterey KG4 sediment sample revealed the thioether and thiodiether bound *n*-alkanoic structures to be more abundant in the resin fraction, while thioether bound thiolanic and thiophenic moieties are more relevant in the asphaltene and kerogen fractions.

A detailed investigation of the deuterium labelling of all *n*-alkanes released by the desulphurization of a resin fraction from a Monterey sediment sample showed a positive correlation between the number of former sulphur functionalities and the carbon number of the *n*-alkanes.

A certain amount of the carboxylic acids released by the oxidation of aromatic subunits had deuterium atoms, which only could result from the desulphurization of former sulphur species. This proves that considerable amounts of *n*-alkanoic substituents of aromatic structures either contain sulphur functionalities (thiolanes, thiophenes) or are additionally linked by sulphur bridges to the high molecular weight fractions.

Thus, *n*-alkanoic subunits with thiolanic and thiophenic moieties can be simultaneously cross-linked *via* sulphur and aromatic structural units to the macromolecular network.

Acknowledgements - We thank J. Laqua for technical assistance. This project was supported by the Deutsche Forschungsgemeinschaft (Mi 157/7-3).

5. References

1. B.P. Tissot and D.H. Welte, *Petroleum Formation and Occurrence*, Springer (1984).
2. J. Valisolalao, N. Perakis, B. Chappe and P. Albrecht, *Tetrahedron Lett.*, 1984, **25**, 1183.
3. J.C. Schmid, J. Connan and P. Albrecht, *Nature*, 1987, **329**, 54.
4. J.D. Payzant, D.D. McIntyre, T.W. Mojeisky, M. Morres, D.S. Montgomery and P.P. Strausz, *Org. Geochem.*, 1989, **14**, 461.
5. J.D. Payzant, Montgomery and P.P. Strausz, *Tetrahedron Lett.*, 1983, **24**, 651.
6. J.S. Sinninghe Damsté and J.W. De Leeuw, *Advances in Organic Geochemistry 1989*, Pergamon Press, 1077 and references therein.
7. J. Rullkötter and W. Michaelis, *Advances in Organic Geochemistry 1989*, Pergamon Press, 829.
8. B. Majchrowicz, J. Yperman, J. Mullens and L. Van Poucke, *Anal. Chem.*, 1991, **63**, 760.
9. G.N. George and M.L. Gorbaty, *J. Amer. Chem. Soc.*, 1989, **111**, 3182.
10. S.R. Kelemen, G.N. George and M.L. Gorbaty, *Fuel*, 1990, **69**, 939.
11. G.S. Waldo, R.M.K. Carlson, J.M. Moldowan, K.E. Peters and J.E. Penner-Hahn, *Geochem. Cosmochim. Acta*, 1991, **55**, 801.
12. P. Adam, J.C. Schmid, J. Connan and P. Albrecht, *Tetrahedron Lett.*, 1991, **32**, 2955.
13. M.E.L. Kohnen, J.S. Sinninghe Damsté, A.C. Kock-van Dalen and J.W. De Leeuw, *Geochim. Cosmochim. Acta*, 1991, **55**, 1375.
14. J.C. Schmid, Ph.D thesis, Université Louis Pasteur, Strasbourg (1986).
15. J.S. Sinninghe Damsté, I.W.C. Rijpstra, J.W. De Leeuw and P.A. Schenck, *Advances in Organic Geochemistry 1987*, Pergamon Press, 593.
16. P. Adam, J.C. Schmid, B. Mycke, C. Strazielle, J. Connan, A. Huc, A. Riva and P. Albrecht, *Geochim. Cosmochim. Acta*, 1993, **57**, 3395.
17. H.H. Richnow, A. Jenisch and W. Michaelis, *Org. Geochem.*, 1992, **19**, 351.
18. H.H. Richnow, A. Jenisch and W. Michaelis, *Geochim. Cosmochim. Acta*, 1993, **57**, 2767

19. I.C. Hoffmann, J. Hutchinson, J.N. Robson, M.I. Chicarelli and J.R. Maxwell, *Org. Geochem.*, 1991, **19**, 371.
20. D. Vitrovic, *Kerogen. Insoluble Organic Matter from Sedimentary Rocks*, Editions Technip (1980).
21. A.O. Barakat and T.F. Yen, *Geochim. Cosmochim. Acta*, 1988, **52**, 359.
22. S. Trifilieff, O. Sieskind and P. Albrecht, *Biological Markers in Sediments and Petroleum - A Tribute to Wolfgang K. Seifert*, Prentice Hall (1992), 350.
23. G. Standen, R.J. Boucher, J. Rafalska-Bloch and G. Eglinton, *Chem. Geol.*, 1991, **91**, 297.
24. G. Standen, R.L. Patience, R.J. Boucher and G. Eglinton, *Organic Geochemistry - Advances and Applications in the Natural Environment*, University Press (1991), 454.
25. W.L. Orr, *Org. Geochem.*, 1986, **10**, 499.
26. R. Pelet, F. Behar and J. Monin, *Advances in Organic Geochemistry 1985*, Pergamon Press, 481.
27. T.G. Back, K. Yang and H.R. Krouse, *J. Org. Chem.*, 1992, **57**, 1986.
28. T.G. Back, D.L. Baron and K. Yang, *J. Org. Chem.*, 1993, **58**, 2407.
29. J. Hefter, Ph.D. thesis, Institut für Biogeochemie und Meereschemie, Universität Hamburg, 1992.
30. S. Schouten, D. Pavlovic, J.S. Sinninghe-Damsté and J.W. De Leeuw, *Org. Geochem.*, 1993, (in press).
31. L.M. Stock and K. Tse, *Fuel*, 1983, **62**, 974.
32. P. Blanc and P. Albrecht, *Advanced Methodologies in Coal Characterization*, Elsevier (1990), 53.
33. S. Trifilieff, Ph.D. thesis, Université Louis Pasteur, Strasbourg (1987).
34. A. Jenisch, H.H. Richnow and W. Michaelis, *Organic Geochemistry - Advances and Applications in Energy and Natural Environment*, University Press (1991), 423.

BIODEGRADATION OF HYDROCARBONS BY SULPHATE REDUCING BACTERIA IN THE CRETACEOUS BAHLOUL FORMATION (TUNISIA)

M. PERVAZ and W. PÜTTMANN
Lehrstuhl für Geologie, Geochemie und
Lagerstätten des Erdöls und der Kohle,
RWTH Aachen, Lochnerstr. 4-20,
52056 Aachen F. R. Germany

ABSTRACT. In the Atlas of Northern Tunisia stratiform lead and zinc sulphide mineralization occur in laminated black shales of the Cenomanian-Turonian Bahloul formation and as Bou Grine orebody along a fault system through Cretaceous series. The age and the mechanism of mineralization processes is still controversially discussed. The precipitation of base metals as sulphides in sediments requires organic matter as hydrogen source both in thermochemical and bacterial sulphate reduction.

In the present study the extractable organic matter of samples from the black shales (Bahloul) and the orebody (Bou Grine) has been investigated by organic geochemical methods in order to clarify the mechanism of involvement of the organic matter in the mineralization processes. Results have shown, that in high grade orebody (Pb+Zn=2-20%) the bitumen is severely biodegraded as indicated by the complete removal of n-alkanes and of aromatic hydrocarbons from the naphthalene and phenanthrene series.

In low grade mineralized black shales of the Bahloul Formation (up to 1% Pb+Zn) the aromatic hydrocarbon fractions indicate severe biodegradation although the alkanes are only slightly biodegraded. Biomarker analyses (hopanes and steranes) and vitrinite reflectance data have shown that the maturity of the indigenous organic matter in the Bahloul formation reached the oil window. Consequently, in present case the degree of hydrocarbons biodegradation is linked with base metal mineralization.

1. Introduction

The precipitation of base metal sulphides in black shales requires the generation of H₂S which can be provided either by biological or thermochemical processes. For both reactions organic matter is essential as reducing agent for sulphate⁽¹⁾.

For many stratiform base metal deposits it is still unclear whether metal precipitation was mediated by biological or abiological (thermochemical) reactions. From the inorganic geochemical and mineralogical aspect it is difficult to differentiate between both processes. An alternative approach is the investigation of the organic matter which was recently applied to the study of Kupferschiefer⁽²⁾. In this case, a thermochemical effect on the organic matter of the Kupferschiefer from the mining districts was evidenced based on the detection of abundant polycyclic aromatic hydrocarbons.

Previous studies of the Cretaceous stratiform zinc/lead deposits in the Tunisian Atlas indicate a completely different mechanism. Here, severe biodegradation of the organic matter was shown to be associated with zinc/lead precipitation as sulphides⁽³⁾.

According to former study⁽³⁾ the Bahloul formation could have served as a conduit for migrating bitumen and metal-bearing brines feeding the Bou Grine orebody in the sense of "lateral secretion". The H₂S was suggested to be generated in the Triassic diapirs and migrated to the Bahloul Formation. The association of mineralization in Bou Grine with diapirism was also discussed in further papers⁽⁴⁻⁵⁾.

2. Sample Description and Geological Setting

The lead and zinc deposits of Bou Grine are found in the dome area of the Northern Tunisian Atlas. The structural sketch of Tunisia, location of salt domes (diapirs) and Bou Grine are shown in Fig. 1. In this area the Bahloul formation occurs as organic rich (black shale facies) sedimentary layer of Cenomanian/Turonian age, vicinal to semi massive Bou Grine orebody (hanging wall). Five types of mineralization have been reported to occur in Bou Grine area (Fig. 2a-b)⁽³⁾.

The average thickness of Bahloul formation in the Upper Cenomanian/Lower Turonian is about 20m. The microfauna used for the dating, occur in fine laminated slightly brown limestone and dark brown clay that is enriched with kaolinite. Both organic petrographic and organic geochemical studies conclude marine planktonic (algal amorphous) origin of organic matter disseminated in carbonate matrix (oil prone). Mineralization in the laminites is dominated by small crystals of sphalerite occurring as fine disseminations or in regular beds of flattened nodular bodies. Pyrite, galena and other ore particles are embedded in the cavities of foraminifera. The alginite is the main maceral of liptinite group.

In the present study the samples from the Bahloul formation well LM1 (Fig. 2b) and from the Bou Grine orebody have been investigated by organic and inorganic geochemical methods.

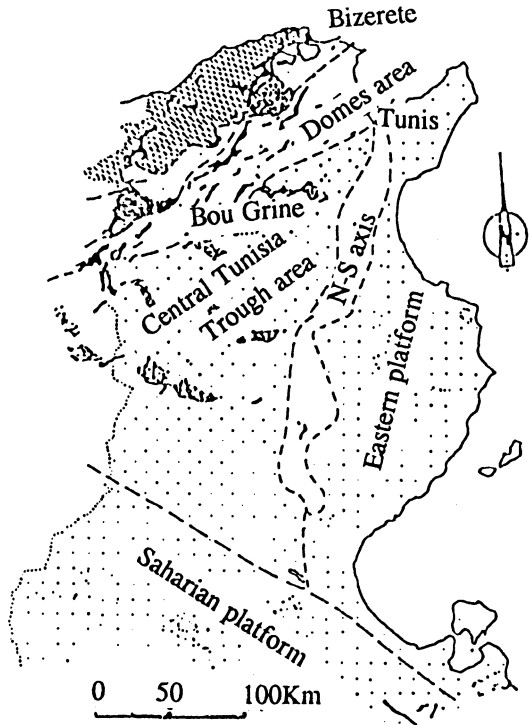


Fig. 1 Structural sketch of Tunisia showing location of the Domes (diapirs) area¹².

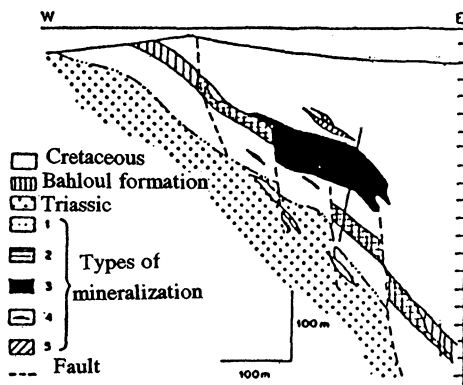


Fig. 2a Schematic west-east geological cross section of the Bou Grine area³. Expl: (1) Lenticular ore body (2) Stratiform mineralization in Bahloul (3) Semi-massive Bou Grine ore body (4) Cenomanian ore formations (5) Turonian ore formations

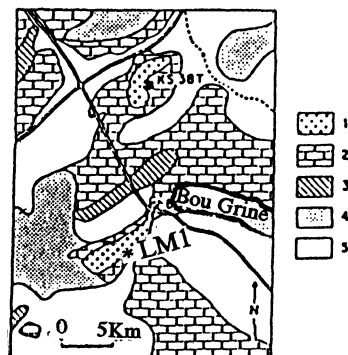


Fig. 2b Geological map of Bou Grine area³. Expl: (1) Triassic (2) Cretaceous (3) Eocene (4) Neogene (5) Quarternary

3. Experimental

Finely ground samples were extracted with dichloromethane in Soxhlet apparatus using pre-extracted thimbles (24h). The extracted bitumens were fractionated into hydrocarbon groups by column chromatography over activated (1h, 110 °C) silica gel (230-400 mesh,). The elution of saturated and aromatic hydrocarbon fractions was achieved with n-hexane, and dichloromethane respectively.

GC analyses of the fractions were performed on a Carlo Erba 5160 high resolution gaschromatograph equipped with 25m x 0.25mm I.D. fused silica column coated with SE 54 silicone (0.25 μm film thickness) as stationary phase using hydrogen as carrier gas. The GC oven was programmed 80-300 °C with heating rate 4°C/min and maintained for 20 min. Quantification of individual compounds was carried out using an internal standard (squalane) and Minichrome software. The saturated and aromatic fractions were investigated by GC-FID.

GC/MS analyses of selected samples have been performed on Varian 3700 GC coupled to a Finnigan MAT 8200 mass spectrometer using the same fused silica capillary column as for GC. Helium was applied as carrier gas and mass spectra were recorded in the cyclic scan mode (1.1 sec). An INCOS data system was used for data processing and interpretations.

The total organic carbon (TOC), total carbon (TC) and total sulphur (TS) were determined with Leco CR 12 and CS 32 respectively. TOC was determined after removal of inorganic carbonate carbon with hydrochloric acid. Inorganic trace and major elements were determined with X-ray fluorescence and atomic absorption spectroscopy. Core samples were also studied with reflectance and fluorescence microscopy (Zeiss) using polished blocks of the samples.

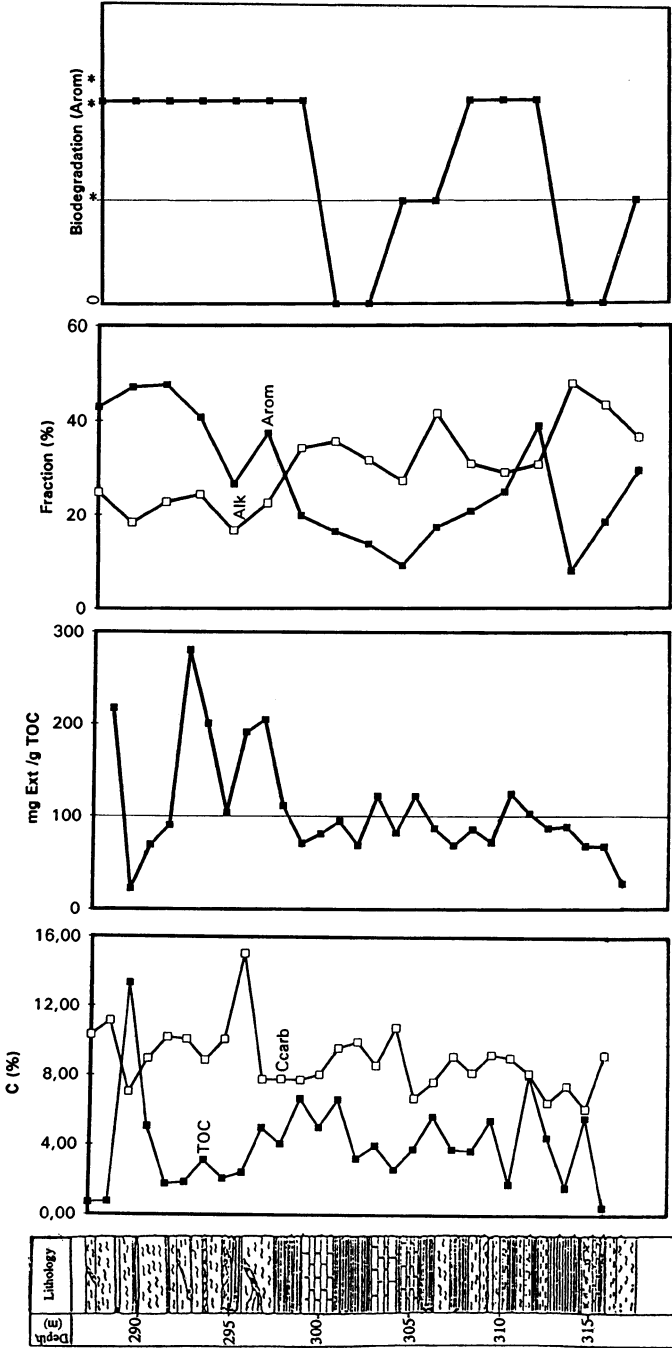


Fig. 3 Geological profile of Bahoul formation and variation of various organic geochemical parameters.

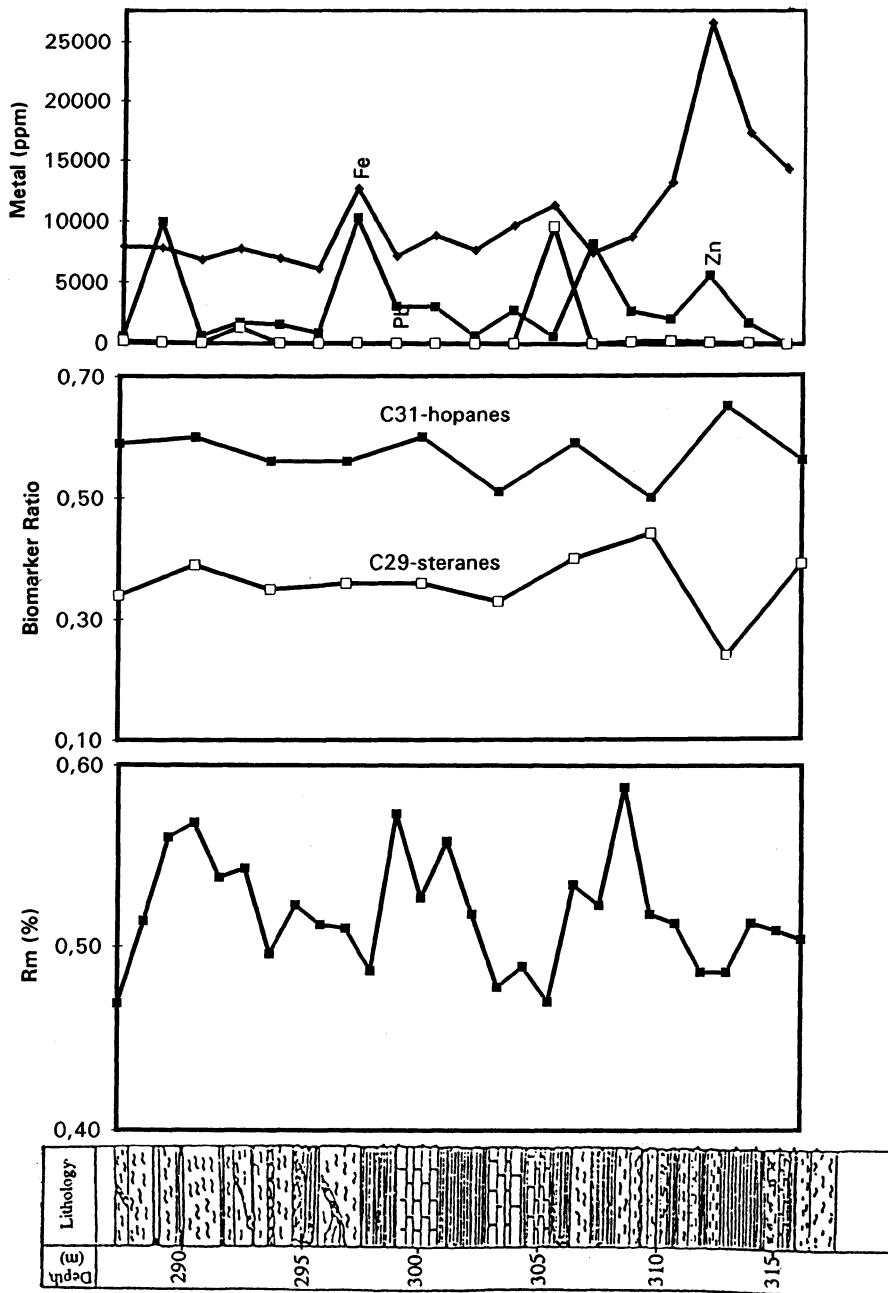


Fig. 4 Geological profile of Bahloul formation and variation of vitrinite reflectance (in oil), biomarker ratios and the metal content (Pb, Zn and Fe), along the profile.

Table 1. Analytical results of core samples

Sample No.	Depth (m)	TOC (%)	Ccarb (%)	mg Ext/gTOC	Alk (%)	Arom (%)	Zn (ppm)
92671	286,80	0,69	10,31	216,55	42,97	24,79	533
92644	288,20	0,74	11,13	22,57			
92645	288,70	13,35	7,04	69,11			
92646	290,00	5,06	8,98	89,98	47,05	18,3	9928
92647	290,80	1,74	10,21	280,43	47,55	22,74	635
92648	291,80	1,83	10,09	200,41	40,78	24,3	1693
92649	292,50	3,09	8,87	103,68	26,54	16,58	1535
92650	293,50	2,06	10,09	191,28	37,36	22,47	884
92651	294,80	2,39	15,07	204,58			
92652	295,10	4,98	7,79	111,19			
92653	296,80	4,08	7,80	70,59	19,75	34,14	10294
92654	298,50	6,68	7,76	80,91			
92655	298,70	5,03	8,08	94,22	16,34	35,55	3097
92656	300,00	6,65	9,58	68,46			
92657	300,20	3,22	9,94	121,31			
92658	302,00	3,97	8,60	81,96	13,66	31,48	3065
92659	303,40	2,59	10,79	121,57	9,06	27,19	659
92660	305,00	3,77	6,74	86,59			
92661	306,10	5,67	7,66	68,86			
92662	306,60	3,77	9,14	85,31	17,28	41,47	2771
92663	308,90	3,68	8,20	71,94	20,67	30,77	598
92664	310,80	5,45	9,24	124,23	24,79	28,92	8227
92665	311,70	1,75	9,06	102,53	38,85	30,57	2703
92666	313,30	8,04	8,19	86,66	7,83	47,82	2095
92667	314,00	4,47	6,49	88,37	18,34	43,21	5643
92668	315,10	1,56	7,45	67,92	29,27	36,34	1762
92669	315,60	5,58	6,13	67,52			
92670	316,70	0,44	9,21	27,89			28

Table 2. Analytical results of orebody

92225	7,50	6,90	86,66	47,80	23,10	139211
92226	7,58	6,22	112,58	1,50	66,30	184025
92227	1,00	10,90	186,45	51,80	16,60	27300
92672	7,56	6,44	76,54			
92673	3,13	6,70	155,76	30,18	44,66	229938
92674	1,05	10,85	169,35	38,88	36,11	21244

Table 1 contd.

Pb (ppm)	Fe (ppm)	Rm (%)	22S/ (22S+22R) C31-Hopanes	20S/ (20S+20R) C29-Steranes	Biodeg. Arom.
147	7910	0,47 0,51 0,56	0,59	0,34	**
56	7840	0,57			**
36	6860	0,54			**
1304	7770	0,54			**
49	7000	0,50			**
12	6160	0,52 0,51 0,51	0,60	0,39	**
60	12740	0,49 0,57	0,56	0,35	**
40	7210	0,53 0,56 0,52	0,56	0,36	0
48	8890	0,48	0,60	0,36	0
24	7700	0,49 0,47 0,53	0,51	0,33	*
41	9730	0,52	0,59	0,40	*
9630	11340	0,59			**
11	7490	0,52	0,50	0,44	**
182	8820	0,51			**
279	13300	0,49	0,65	0,24	0
168	26740	0,49	0,56	0,39	0
113	17430	0,51 0,51			*
9	14420	0,50			

Table 2 contd.

9608	14490				***
7472	14210				***
350	5740				***
		0,44			
5425	10710	0,55			***
403	6510	0,48			***

4. Results and Discussion

4.1. CORE SAMPLES (BAHLOUL FORMATION)

4.1.1. Bulk parameters. Twenty eight (28) samples from the Bahloul formation well (LM-1) ranging from 286-317m have been analyzed using various geochemical methods (Table 1). The analytical results show that TOC is higher than 2% in most of the samples; in few samples the values increase up to 14% (Table 1). In Figure (3) the TOC variation is plotted along the profile of the Bahloul formation. A major cyclicality of variation is not observed, only one sample (92651) falls out of the regular range. Carbonate contents are relatively uniform in the centre of the formation and show irregularities predominantly in the bottom and top section. Increases in carbonate contents are not reflected by concomitant decreases in the organic matter content. Also the variation in the amount of TOC normalized extract yields is low in the bottom and inner part of the section (Fig. 3). Here, the values are around 80 mg extract per gram of total organic carbon (mg ext/g TOC). A few samples provide values higher than 100 mg ext/g TOC.

In the present study, during the Soxhlet extraction no copper foil was added to the flask for the removal of elemental sulphur. After removal of the solvent crystallization of S_8 was observed in most samples from the upper part of the profile (Fig. 3). The increased extract yields in this part of the formation is caused by S_8 , because this molecule is almost completely extractable with organic solvents. The extract yields higher than 100 mg Ext/g TOC, therefore, cannot be used as an argument for the presence of migrated organic material according to the classification of Hunt⁽⁶⁾.

4.1.2. Maturity Assessment. For the determination of the maturity of the organic matter within the Bahloul formation vitrinite reflectance measurements on the kerogen and biomarker analyses in the extracts have been carried out. Along the profile the vitrinite reflectance varies around 0.5 % (Fig. 4). Again, major variations are not observed. The data indicate that with respect to maturation the beginning of the "oil window" has been reached. This is also confirmed by the results obtained from the measurements of molecular maturation parameters by the use of GC/MS. Mass chromatography of m/z 191 was used for the measurement of the hopane distribution. The ratio of $22S/(22R+22S)$ $\alpha\beta$ C_{31} hopanes has reached the equilibrium value of 0.6 in almost all samples. Therefore, the hopane distribution is not an appropriate tool for the recognition of maturity variations in the present case.

The sterane distribution has been determined from the m/z 217 mass chromatograms. Results from the determination of the ratio of $20S/(20S+20R)$ $\alpha\alpha\alpha$ C_{29} -steranes are shown in Figure (4). Here, the equilibrium value has not yet been reached and the values of this ratio are around 0.36 all over the profile. Only one sample near the bottom of the section (92666) provides a significantly lower ratio with 0.24. The ratio of $20S/(20S+20R)$ $\alpha\alpha\alpha$ C_{29} -steranes recently was shown to be affected by biodegradation. Many aerobic bacteria degrade the 20R isomer preferentially which results in an increase of the $20S/(20S+20R)$ ratio⁽⁷⁾.

As mentioned above, in most of the samples from the investigated profile the biodegradation of the organic matter is detectable. However, samples 92666 and 92659 did not show an effect of biodegradation. So the samples with a lower $20S/(20S+20R)$ ratio might be better reflecting the degree of maturity. According to Mackenzie et al⁽⁸⁾ the ratio $20S/(20S+20R)$ $\alpha\alpha\alpha$ C_{29} -steranes with value 0.24 corresponds approximately

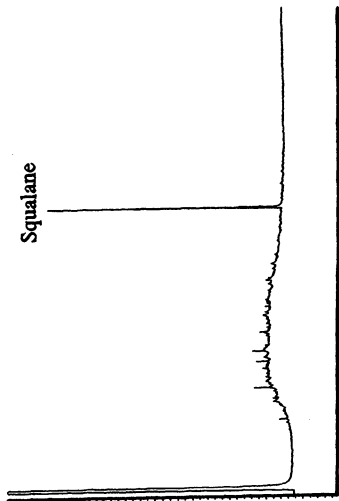


Fig. 6a Typical chromatogram of severely biodegraded alkane fraction (orebody).

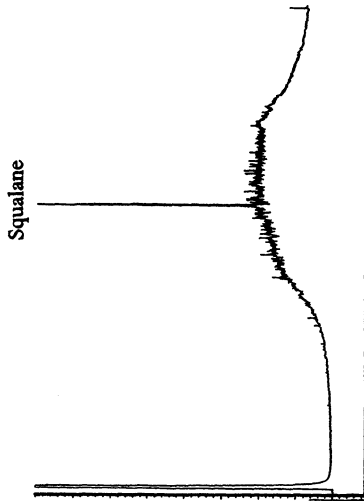


Fig. 6b Chromatogram of biodegraded aromatic fraction (orebody).

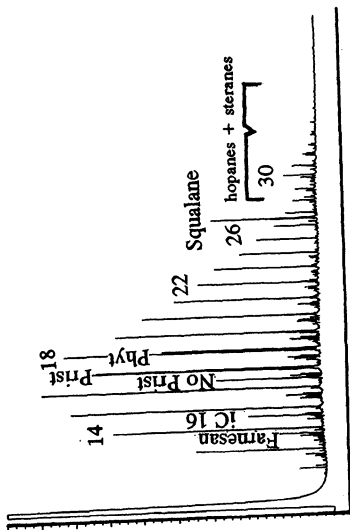


Fig. 5a Chromatogram of non biodegraded alkane fraction (core sample).

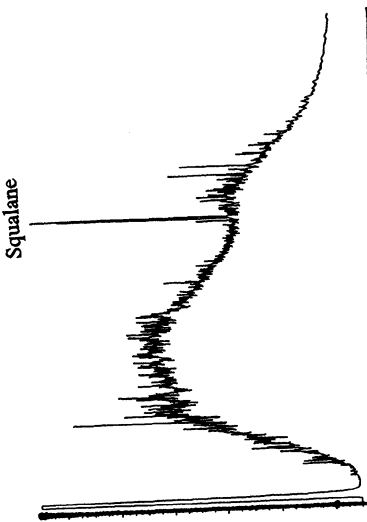


Fig. 5b Chromatogram of biodegraded aromatic fraction (core sample).

to the measured vitrinite reflectance of 0.49%. The measured maturity parameters, therefore, consistently argue for an organic matter maturation near the beginning of the oil window based on the diagram developed by Mackenzie et al⁽⁸⁾ on data from the Toarcian shales in the Paris basin.

At the top of Bahloul formation the extractable organic matter contains higher amounts of alkanes (50%) than other fractions and apparently no biodegradation occurred (Fig. 5a). The gas chromatograms of aromatic hydrocarbons (Fig. 5b) for most of the samples are very complex which is often called Unresolved Complex Mixture⁽⁹⁾ (UCM) due to biodegradation. Apart from hydrocarbons the bitumen also contains considerable amount of elemental sulphur that is correlating with the intensity of (UCM) in the chromatograms of aromatic fractions. Precipitation of iron, zinc and lead as sulphides by sulphate reducing bacteria obviously caused the hydrocarbon degradation.

Normally during biodegradation aliphatic hydrocarbons are attacked first⁽⁹⁾. According to Jobson et al⁽¹⁰⁾ sulphate reducing bacteria are not able to metabolize n-alkanes which results in a preferential degradation of aromatic hydrocarbons in crude oils. This situation was also reported by Connan⁽¹¹⁾ and is confirmed by the results presented here.

4.2. BOU GRINE OREBODY

Six samples from the Bou Grine orebody were also investigated (Table 2). The samples show the following characteristics.

Total organic carbon (TOC) is increased in relation to the Bahloul formation and exceeds in some cases 7%. The TOC normalized extract yields in four samples are higher than 100, preferentially caused by the presence of elemental sulphur. The distribution of aliphatic and aromatic hydrocarbons is composed of only UCM (Fig. 6a-b) indicating a higher degree of biodegradation as compared to Bahloul formation.

4.3. METAL CONTENT

The contents of iron, lead and zinc have been determined in both sample sets (core and orebody). The results are shown in Tables 1 and 2. The variation of the metal content along the profile of the Bahloul formation is shown in Figure 4. The iron content is about 1% and the zinc content is in general around 0.3%. In a few samples an increase to approximately 1% is observed. Apart from one exception, the lead contents are lower than iron and zinc contents.

In the Bou Grine orebody the iron contents are in the same range as in the Bahloul profile. However, lead and zinc content increase significantly to values up to 22% (Table 2). This increase correlates with a severe biodegradation, not only of aromatic, but also of saturated hydrocarbons (Fig. 3, 6a & 6b).

5. Conclusions

The present investigation of samples from the Bahloul formation and from the Bou Grine orebody provided a close correlation between biodegradation of organic material and sulphide precipitation (Pb/Zn). Samples from the ore body with higher metal contents show higher degree of biodegradation of the organic matter. The presence of elemental sulphur is consequence of microbial activities which governed the composition of ores (Pb, Fe and Zn) at the same time.

The underlying Triassic diapirs were apparently the source of base metals and sulphate whereas the Bahloul formation contributed the hydrocarbons for the activity of bacteria. In the present case aromatic hydrocarbons were degraded before saturated hydrocarbons in the Bahloul formation while in orebody the sequence of degradation could not be determined clearly because both saturated and aromatic hydrocarbons are completely biodegraded (Fig. 6a-b). Biomarker analyses (steranes and hopanes) have shown that the maturity of bitumen in Bahloul formation has reached the oil window.

6. Acknowledgements

We are grateful to Metalgesellschaft, Frankfurt for providing samples for the present investigation and to Dr. A. Bechtel University of Bonn, Germany for the analyses of metals. Financial support to one of us (M. Pervaz) from Deutscher Akademischer Austauschdienst (DAAD) is also thankfully acknowledged.

7. References

1. P.A. Trudiger, L.A. Chambers and J.W. Smith Low temperature sulphate reduction: biological versus abiological. Can. J. Earth Sci. **22**, 1910-1918 (1985).
2. W. Püttmann, H. Heppenheimer and R. Diedel, Accumulation of copper in the Permian Kupferschiefer: A result of post-depositional redox reactions. Org. Geochem. **16**, 1145-1156 (1990).
3. M. Montacer, J.R. Disnar, J.J. Orgeval and J. Trichet, Relationship between Zn-Pb ore and oil accumulation process example of the Bougrine deposits (Tunisia). Org. Geochem. **13**, 423-431 (1988).
4. A. Charef and M.S.F. Simon, Pb-Zn mineralization associated with diapirism. Chemical Geology **61**, 113-33 (1987).
5. J.J. Orgeval, D. Giot, J. Karoui, J. Monthel and R. Sahli, The discovery and investigation of the Bou Grine Pb-Zn deposit (Tunisian Atlas) Chron. Rech. Min. special issue. 53-68 (1989).
6. J. Hunt, "Petroleum Geochemistry and Geology". W.H. Freeman and Company, San Francisco (1979).
7. P. Chossen, C. Lanau, J. Connan, and D. Dessort, Biodegradation of refractory hydrocarbon biomarkers from petroleum under laboratory conditions. Nature **351**, 640-642 (1991).
8. A.S. Mackenzie, S.C. Brassell, G. Eglinton and J.R. Maxwell, Chemical fossils: The geological fate of steroids. Science **271**, 491-504 (1982).
9. N.J.L. Bailey, A.M. Jobson and M.A. Rogers, Bacterial degradation of crude oil, comparison of field and experimental data. Chem Geol **11**, 203-221 (1973).

10. A. Jobson, F.D. Cook and D.W.S. Westlake, Interaction of aerobic and anaerobic bacteria in petroleum biodegradation. Chem. Geol. 24, 355-365 (1979).
11. J. Connan, Biodegradation of crude oils in reservoirs. In: Advances in Organic Geochemistry Vol. 1. pp. 299-335, Academic Press, London (1984).
12. V. Perthuisont, Dynamique et petrogenese des extrdsions transique et Tunisie septentrionale. Travaux du Labo. Geol. Ecole Normale Sup. 12, Ph.D thesis, Paris (1978).

ORIGIN, EVOLUTION AND PETROLEUM POTENTIAL OF A CAMBRIAN SOURCE ROCK: IMPLICATIONS OF PYROLYSATE AND BITUMEN COMPOSITION

SUNIL BHARATI
Geolab Nor
P.B. 5740 Fossegrenda
7002 Trondheim, Norway

ABSTRACT. The Upper Cambrian Alum Shale of Scandinavia, which was historically used to produce oil using conventional retorting methods, is not at present regarded as a significant potential source rock for oil generation. The shale, deposited in a shallow-marine environment have neither experienced any major tectonic events nor have they been deeply buried. This is perhaps why the Alum Shales have not been characterised in detail geochemically earlier and available data in the literature is scarce. We present here the chemistry of the flash pyrolysates and solvent extracts of the Alum Shales using 37 outcrop samples from numerous locations in southern Scandinavia. The Alum Shales have very high organic matter content, primarily algal, and are anomalously enriched in uranium. However, they generate gaseous petroleum on simulated maturation and the free hydrocarbons present are aromatic in nature. Hypothesis suggested earlier, such as radiation damage of kerogen, are examined in light of the present findings. A combination of several chemical and optical techniques has allowed us to estimate the true petroleum potential of this formation and model the composition of the petroleum that can be generated from the Alum Shales.

1. Introduction

The Middle Cambrian to Lower Ordovician age Alum Shale Formation, which is extensively developed in the Balto-scandian Platform of Scandinavia, has a long exploitation history dating back over 300 years. The Alum Shales were mined for the hydrated salt, potassium aluminium sulphate in the early years (from ca 1637 to 1900's). Towards the end of the 19th century, its high kerogen content was realized and oil produced through conventional retorting methods up to nearly 500 tonnes of shale oil/year. Fischer assays indicate oil yields of about 1000 MMT from the richest areas of Narke and Gotland. The Alum Shales were also mined to recover uranium, especially from the kolm lenses within the Alum Shale Formation, which were anomalously rich in uranium (2000 to 7000 ppm). However, the Alum Shales were never regarded as a significant petroleum source rocks, despite their very high TOC content, as they were never deeply buried to reach the required thermal maturity for oil generation. This has perhaps been the primary reason for the Alum Shales not being geochemically characterised in detail earlier and the scarcity of geochemical data in the literature.

In the present study, we have attempted to elucidate and understand the chemistry of the flash pyrolysates and solvent extracts of the Alum Shales using 37 outcrop samples from numerous locations in southern Scandinavia (Figure 1). A combination of several chemical techniques has allowed us to estimate the true petroleum potential of this formation and model the composition of the petroleum that can be generated from the Alum Shales.

2. Geology and Depositional Environment of the Alum Shales

The Alum Shales, which extended in a paleo-basin measuring more than 2000 sq. km., were deposited in low energy, shallow marine conditions and at a very slow rate estimated to be around 3-10 mm/1000 years ⁽¹⁾. It is also likely that their deposition took place in an epicontinental sea environment, with limited access to the open ocean in the south. The Alum Shales are represented today as a thin (10-60 m) black, laminated mudstone facies ⁽²⁾. The highest concentrations of organic matter (up to 21% TOC) are found in the Late Cambrian sub-unit, namely the Olenid Series and the samples in the present study are restricted to this stratigraphic interval. The formation is also enriched in trace elements, particularly uranium and vanadium. The highly anoxic depositional conditions proposed for the Alum Shales ⁽¹⁾ perhaps explains the high organic carbon and pyrite content. Due to low sedimentation rates (also implying low clastic dilution), the degree of primary organic matter preservation is also believed to be very high.

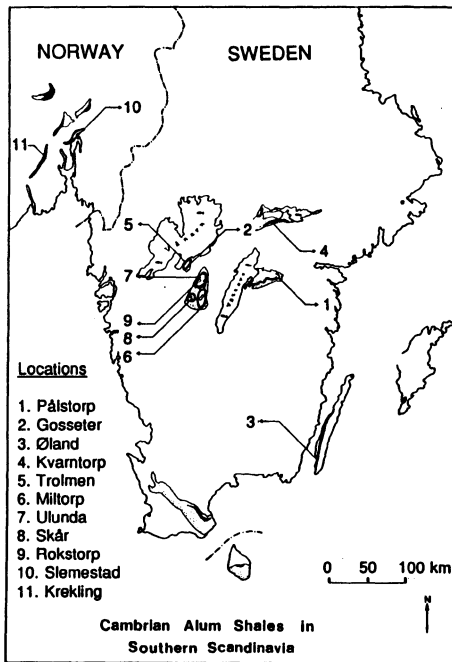


Figure 1. Locations of samples of the present study ordered according to increasing maturity (location 1. Pålstop is least mature and location 11. Krekling is most mature).

Most Alum Shale occurrences today are isolated erosional outliers, underlain by a thin bituminous lime-stone band - the Stinkstone band and generally capped by Permian dolerite sills. The paleo-thickness of these sill emplacements is not known, but they are believed to have caused some heating of the underlying Alum Shales⁽³⁾ although no clear evidence is available on their thermal influence. The sample suite considered in the present study however, represents a natural maturation series from immature to post-mature (Figure 1), this being based on bituminite reflectance^(3,4). The Alum Shales are most developed in Billingen and Kinekulle regions of Gotland, and generally are the least mature too in these areas. The most mature Alum Shales are found in Oslo region in southern Norway. This is perhaps due to some burial and regional subsidence associated with the Alum Shales of Oslo contra the other occurrences in Sweden where little or no subsidence has taken place.

3. Composition of the Alum Shales

X-ray diffraction analysis (XRD) show that the Alum Shales have uniform mineralogical composition over a large basinal area. The relative X-ray percentages of quartz, clay minerals, pyrite+carbonate and feldspars in each of the 9 locations of south-central Sweden are quite comparable. Typical quartz+feldspars / clay minerals ratio is 2, while quartz / feldspar ratio is around 1.5. Uranium content in the present sample suite is however slightly variable, ranging 27-172 ppm (Table 1), although no definite relationships are observed between uranium content and TOC or maturity. There is also no direct evidence of any geographical location being particularly enriched in uranium. Scanning electron microscopy shows that uranium occurs as uniformly distributed and disseminated fine particles all over the inorganic mineral matrix and is conspicuously absent in the organic carbon rich areas such as bituminite lenses⁽³⁾.

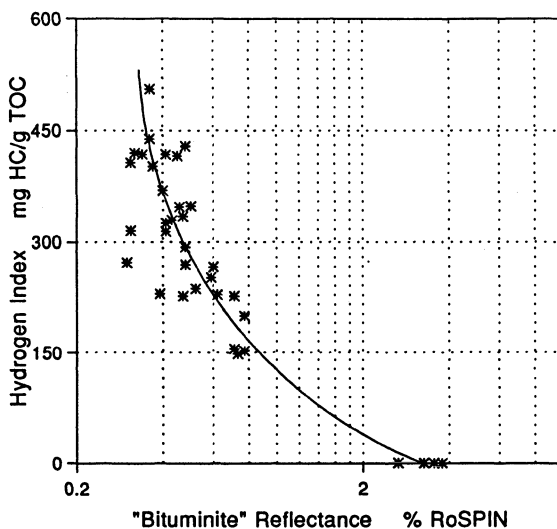


Figure 2. Relationship of "bituminite" reflectance (R_o) and Rock-Eval's hydrogen index.

TABLE 1 : Selected analytical data for the Alum Shale arranged in the order of increasing thermal maturity (decreasing hydrogen content) (sample 1 is least mature).

S.No.	TOC %	U ppm	HI mg/g TOC	OI	Ro %	AL vol % rock	EOM mg/g	HC %	NHC %
1	3	58	505	26	0.32	5	3.45	15	85
2	22	87	439	10	0.36	-	1.88	16	84
3	18	128	429	7	0.48	24	3.99	19	81
4	15	125	420	17	0.32	28	3.13	11	89
5	10	140	418	20	0.41	10	1.49	11	89
6	14	96	418	15	0.34	9	3.27	10	90
7	10	66	416	11	0.45	18	1.51	20	80
8	13	106	407	6	0.31	-	4.16	23	77
9	12	130	402	16	0.37	19	0.90	17	83
10	10	95	369	21	0.40	16	0.90	22	78
11	10	75	348	12	0.50	18	2.49	17	83
12	22	93	347	13	0.45	28	1.51	12	88
13	14	54	334	11	0.47	20	2.55	23	77
14	16	75	325	15	0.41	-	1.02	17	83
15	15	110	329	19	0.43	9	2.47	11	89
16	2	107	315	67	0.31	-	4.47	4	96
17	17	121	314	10	0.41	35	0.98	18	82
18	12	66	293	14	0.48	8	4.96	5	95
19	11	36	272	31	0.30	10	2.06	17	83
20	12	68	269	35	0.48	12	3.51	9	91
21	13	106	266	11	0.60	6	1.27	27	73
22	13	145	252	10	0.59	8	7.66	9	91
23	18	145	231	11	0.52	26	1.74	10	90
24	15	172	230	19	0.39	40	5.59	5	95
25	10	111	229	8	0.62	3	1.73	20	80
26	19	113	227	23	0.47	24	6.14	4	96
27	10	138	227	12	0.71	4	2.05	29	71
28	10	98	200	7	0.77	3	0.95	28	72
29	8	118	197	15	-	2	9.26	5	95
30	15	98	155	9	0.71	3	2.22	29	71
31	13	58	152	7	-	1	1.69	19	81
32	16	72	148	10	0.73	2	12.3	4	96
33	11	52	0	3	3.25	0	12.3	4	96
34	3	29	0	36	3.53	0	0.24	81	29
35	15	57	0	10	2.65	0	0.22	16	84
36	12	27	0	7	3.26	0	0.18	25	75
37	11	27	0	5	3.77	0	0.23	18	82

Abbreviations: TOC= total organic carbon; U= uranium; HI= hydrogen index; OI= oxygen index; Ro= bituminite reflectance; AL vol= alginite volume (% of total rock volume); EOM= extractable organic matter (mg/g rock); HC= % hydrocarbons; NHC= % non-hydrocarbons.

Total organic carbon (TOC) analysis of crushed whole rock samples using LECO CR12 carbon analyzer shows that the Alum Shales are very rich in TOC, typically over 10% and occasionally up to 22%. This is in strong contrast to the average TOC content of source rocks worldwide (2.16% in shales to 0.67% in carbonates) ⁽⁶⁾. Optical analyses (reflected white and UV light microscopy) show that in the rich Alum Shale samples, up to 35% of rock volume is occupied by organic macerals (see below). Preliminary evaluation of the bulk pyrolysis data using Rock-Eval indicates that the Alum Shale kerogens are of type II. There is a vast variation in the hydrogen indices of the sample suite - 505 to 0 mg hydrocarbons/g TOC (Table 1). This is perhaps partially related to the varying thermal maturity of these samples (immature to post-mature) in a way that with increasing maturity there is a proportional decrease in the samples hydrogen content. A similar large variation is observed in the net residual genetic potential (about 75 to almost 0 kg hydrocarbons/ ton rock). However, samples with very low genetic potential do not exhibit corresponding decrease in the TOC content, suggesting that a substantial portion of the organic carbon (kerogen) is not capable of contributing to the pyrolysate yield (Rock-Eval's S2). This implies that this substantial portion of organic carbon can be considered as inert carbon, as regards to thermal lability.

Petrographic examination of polished whole rock mounted in epoxy, both parallel and perpendicular to bedding, reveal that the principle maceral type in the Alum Shales is bright yellow fluorescing alginite (typically over 90% of the total content) (Plate 1) and these are most developed in hydrogen rich samples, as observed in reflected UV light. In the immature samples, alginites typically measure up to 400 microns long in a section perpendicular to bedding. In a section parallel to bedding, algal colonies occur as clusters measuring up to about 250 microns in diameter. The other major maceral is grey coloured (as observed in reflected white light) spindle or lens shaped (in a section perpendicular to bedding) bituminite (?) lenses, as described by Bharati and Larter ⁽⁴⁾. These non-fluorescing lenses generally measure 100-250 microns along their long axis in a section perpendicular to bedding and appear circular in shape in a section parallel to bedding (Plate 1). Reflectance measurements on these bituminite lenses using reflected white light shows that there is a systematic variation in reflectance values (%Ro) with decreasing hydrogen content (Figure 2) ; the hydrogen rich samples giving minimum values (around 0.2-0.3% Ro) indicating thermal immaturity, while the hydrogen poor samples giving higher values (around 0.7-0.8% Ro) indicating higher thermal maturity (Table 1). The nature of alginites also changes with increasing bituminite reflectance in a way that their fluorescence intensity decreases, from about 4 to 1, with increasing maturity. Polished thin sections, when viewed by multi-mode illumination technique (simultaneous use of reflected white and UV light and transmitted white light) show that bituminite lenses are dense, untextured and partially translucent. They also do not show any signs of deformation due to sedimentary compaction.

4. Bitumen Composition

The maximum recorded average solvent extract (EOM) of an immature Alum Shale location (Øland) is about 4 mg EOM/g rock (27 mg EOM/g TOC) and that of a mature Alum Shale location (Ulunda) is about 9 mg EOM/g rock (84 mg EOM/gm TOC) (Table 1). These values are far below those reported earlier ⁽⁶⁾ for Lower Toarcian Shales from the Paris Basin, where the kerogen is also of type II. When immature, the total extract yield of the Toarcian Shales is 40 mg EOM/g TOC and it increases to about 100 mg/g TOC at 1500 m (early mature) and to 180 mg/g TOC at 2500 m (mature) in the principal zone of oil formation. Apparently, the Alum

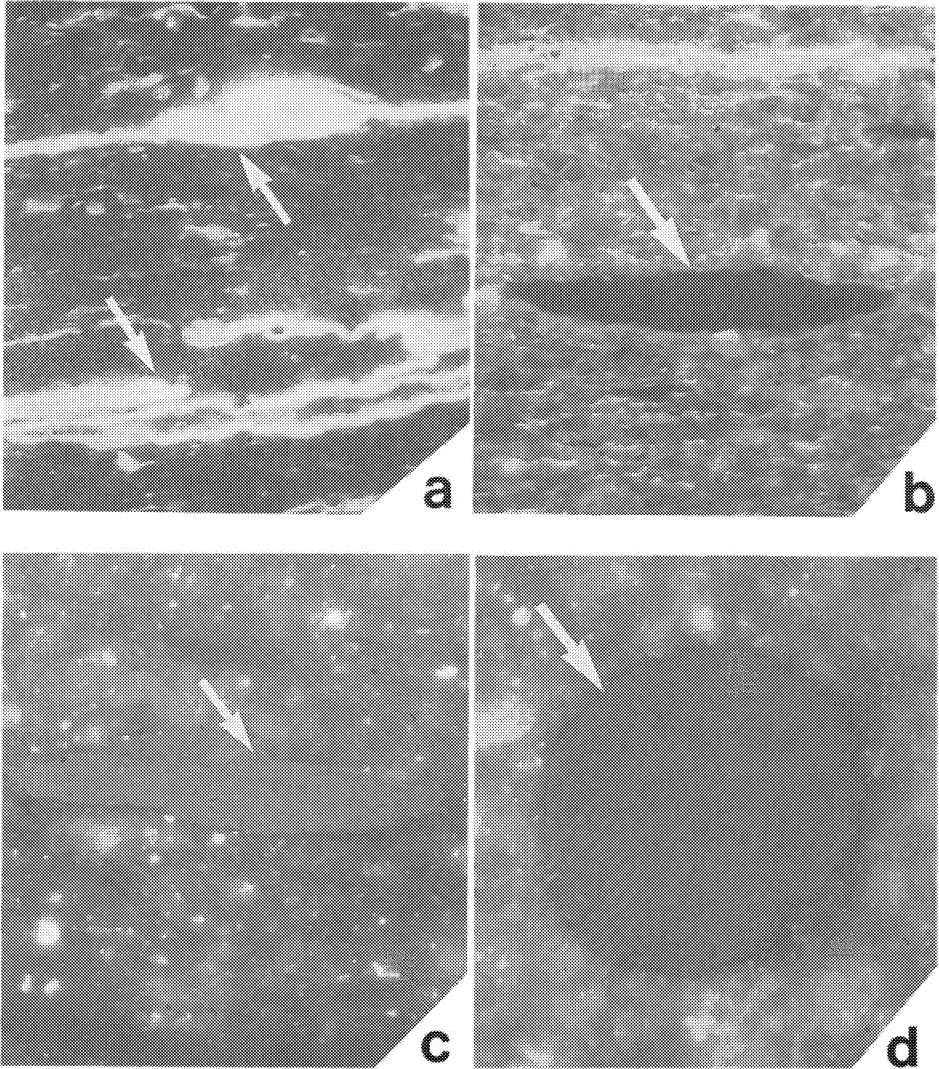


Plate 1. Photomicrographs of an immature Alum Shale sample using polished whole rock epoxy blocks. a) a section perpendicular to bedding in UV light mode where large (up to 400 μ long) bright yellow fluorescing alginite which is a dominant maceral, are seen. In a section parallel to bedding, algal colonies are seen as circular clusters. b) view of another major maceral in a section perpendicular to bedding - the non-fluorescing (black) spindle shaped "bituminite" lenses in UV light mode and c) in reflected white light mode where it appears as grey bodies. d) view of the "bituminite" lens in a section parallel to bedding, where it appears as a grey circular disc. SCALE: Width of micrographs in a) and b) is 120 μ and in c) and d) is 60 μ .

Shales despite their high TOC content, are deficient in soluble organic matter (bitumen) present in the rock, confirming the findings from Rock-Eval analysis.

Latroscan analysis show that major portion of the extractable organic matter (generally greater than 75 %) comprise non-hydrocarbons (Table 1) which includes resins and asphaltenes (collectively termed as polars), with asphaltenes being more dominant. While the total EOM yield is very low for the Alum Shales, it is also highly depleted in hydrocarbons, the hydrocarbons being relatively rich in aromatic hydrocarbons ⁽⁹⁾.

4.1 SATURATED AND AROMATIC HYDROCARBONS

Saturated hydrocarbon fractions, which were obtained by separating maltenes using medium pressure liquid chromatography (MPLC), were analysed using capillary- gas chromatography after adding squalane as an internal standard. A typical saturated hydrocarbon gas chromatogram, is characterised by a dominant hump comprising unresolved complex hydrocarbon mixture, with the mode of the hump occurring generally at around nC22. This feature is common for all the samples irrespective of their thermal maturity (Figures 3a-d, which show GC traces of 4 different samples of varying maturity- immature, early mature, late mature and post mature).

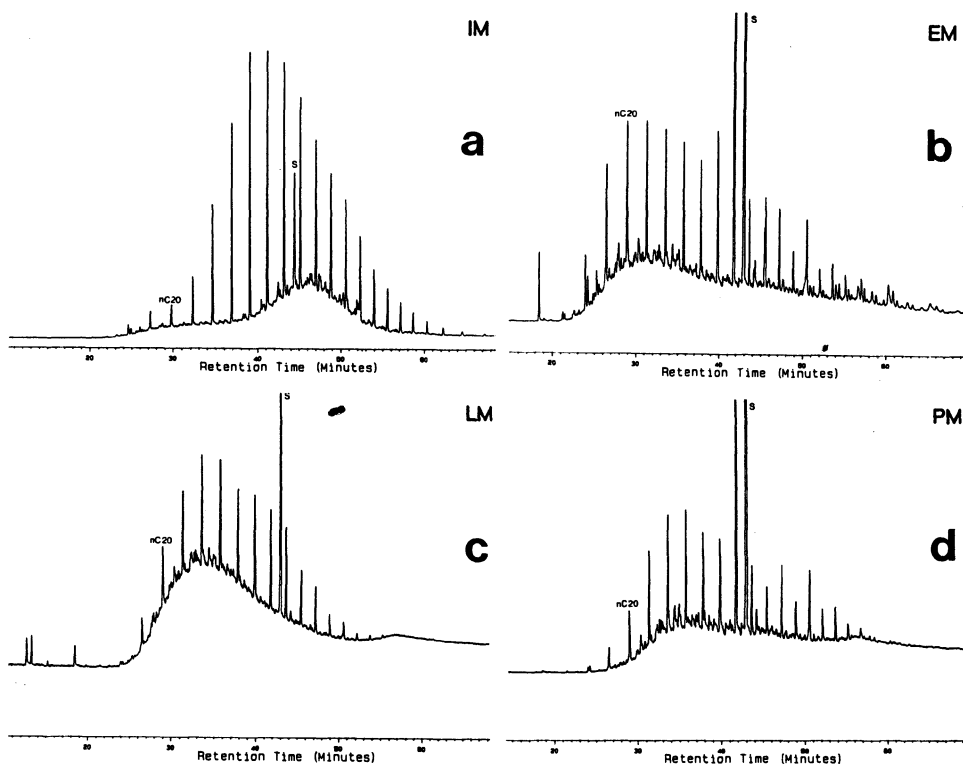


Figure 3. Typical saturated hydrocarbon gas chromatograms for thermally immature (a), early mature (b), late mature (c) and post mature (d) Alum Shale samples.

In most of the cases, the first distinct n-alkane recorded is either nC18 or nC19, the medium molecular weight n-alkanes and acyclic isoprenoids (norpristane, pristane and phytane) occurring only in low concentrations in the early mature and late mature samples. High molecular weight n-alkanes (nC20 to nC35) dominate the signature, with nC25 or nC26 having maximum yields. N-alkanes with more than 37 carbon atoms are rare. The carbon number distribution for the 4 samples typical of the 4 maturation stages (immature, early mature, late mature and post-mature) is shown in Figure 4. Apparently, there is a decrease in the net yield of the individual saturated hydrocarbon species with increasing maturity.

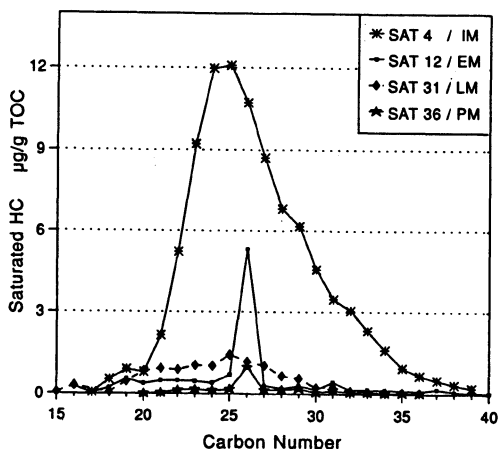


Figure 4. Net yield of individual n-alkanes in the C15-C40 range for 4 Alum Shale samples representing the 4 stages of maturity - immature, early mature, late mature and post mature.

Although aromatic hydrocarbon yields from the Alum Shales are relatively greater than the saturated hydrocarbons, their absolute amounts remain very low (4.38 mg/g TOC) when compared to Lower Toarcian of the Paris Basin (up to 40 mg/g TOC in the principle zone of oil formation)⁽⁶⁾. Moreover, their composition is quite different when compared to other type II kerogen source rocks in that the Alum Shale bitumens lack the dominance of commonly encountered compounds, such as methylnaphthalenes, methylphenanthrenes etc. As seen in their gas chromatograms (Figure 5), the aromatic hydrocarbons are also characterised by a dominant hump comprising mainly of a complex unresolved mixture.

5. Kerogen Composition

The isolated Alum Shale kerogens were characterised by flash (800°C for 20 sec) quantitative pyrolysis-gas chromatography (Q-Py-GC) using a Varian 3700 GC equipped with a CDS 100 pyroprobe and using a temperature program of -50°C for 5 minutes, then 4°C/minute to 300°C for 15 minutes and helium as the carrier gas. The pyrolysates released by all the Alum Shale kerogens were very similar in composition, resulting in nearly identical pyrogram signatures; a

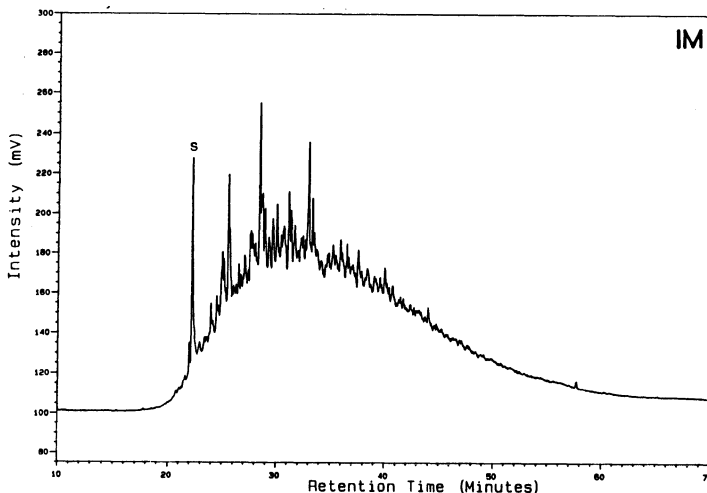


Figure 5. A typical aromatic hydrocarbon gas chromatogram for the Alum Shales.

typical pyrogram is shown in Figure 6a. The only significant difference between samples of varying maturity was the general decrease in the net pyrolysate yield with increasing maturity, as also noted during bulk pyrolysis. However, the consistency in the pyrolysate composition points towards uniform organic facies in the Alum Shale sea. Apparently, gaseous compounds (C1-C5) form the major portion of the pyrolysate, with methane, ethane and ethene (MEE) being the most abundant species; followed by propene/propane (Table 2). Several branched hydrocarbons are also present in the gas fraction (C1-C5) and in the oil fraction (C5+). Phenolic species were not found to be present in the Alum Shale kerogen pyrolysates. It is evident from the pyrograms that the principle products of pyrolysis are low molecular weight compounds with a dominance of aromatic hydrocarbon species, particularly benzene and alkylbenzenes (toluene, xylenes and C3-benzenes) and to a lesser extent alkylnaphthalenes (Table 2). Straight chain hydrocarbons (n-alkenes and n-alkanes) are surprisingly in very low concentrations, with n-alkanes heavier than n-nonane being extremely difficult to detect. Gas to oil ratio for the Alum Shale pyrolysates typically lie in the range of 0.5 kg/kg (2500 scf/bbl) (Table 3) which is quite high when compared to other type II kerogens such as the Toarcian from Paris Basin or Upper Kimmeridge clay from the North Sea (around 0.25 kg/kg).

These observations and results for the Alum Shales are in strong contrast with the results reported for algal kerogens ^(7,8). It was noted that alginites, which is what the Alum Shale kerogens are principally comprised of, generate generally n-paraffinic or in some cases paraffinic / naphthenic type pyrolysates on flash pyrolysis. In addition, low molecular weight normal alkyl moieties are more abundant in sporinite pyrolysates and liquid petroleum components generated from sporinites and vitrinites are aromatic-naphthenic and aromatic respectively ⁽⁹⁾. Kerogens of Permian age Australian Torbanites derived from Botryococcus braunii algae have been shown to yield waxy and high paraffinic pyrolysates, while Permian Tasmanites kerogens from Australia give both paraffinic and naphthenic pyrolysates. Upper Jurassic Kimmeridge clay kerogens of

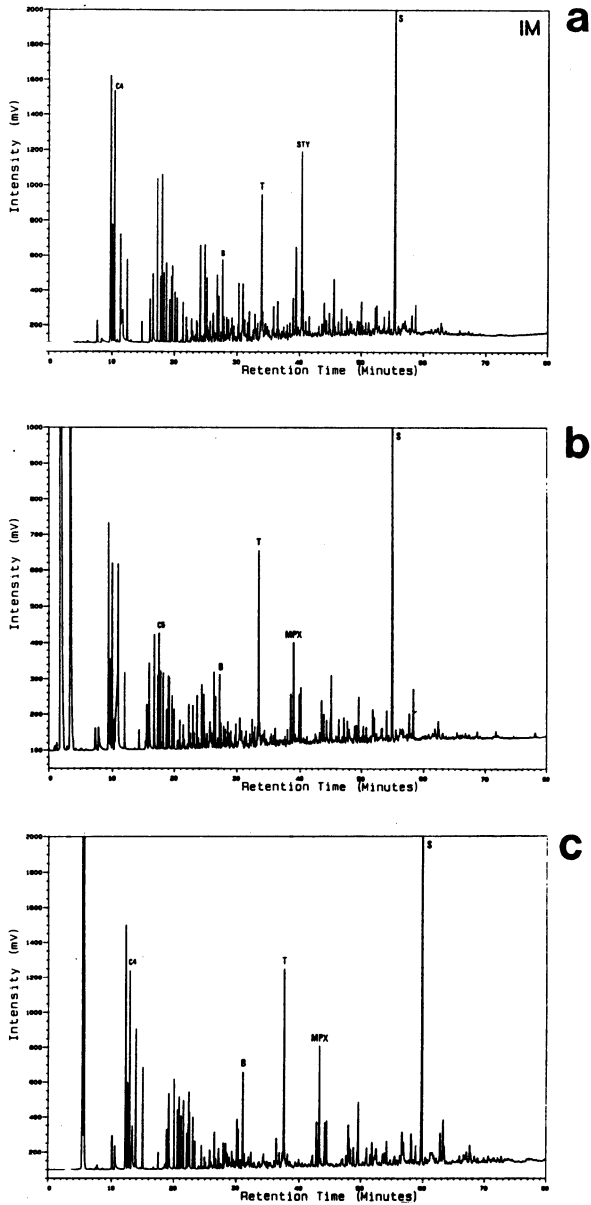


Figure 6. Flash pyrogram of a) atypical Alum Shale kerogen, b) organic concretions isolated from the underlying carbonate bed (The Great Stinkstone band) and c) uranium rich Kolm lens. Peak identifications: C4 = n-propane, C5 = n-pentane, B = benzene, T = toluene, MPX = m,p-xylene, S = standard (polybutylstyrene). The first broad peak is methane+ethane+ethene.

the North Sea, a typical Type II marine alginite, which was analysed for comparison also produced mostly paraffinic and naphthenic species. Therefore the most striking feature of the Alum Shale pyrolysates was the absence of a strong n-hydrocarbon homology.

In addition to the Alum Shale kerogens, a kolm sample (*a kolm is a organic rich (TOC 40-70%), coaly, lens shaped body, measuring up to 30 cm. in length parallel to bedding, anomalously enriched in uranium, typically 2000-7000 ppm*), which is normally found randomly distributed within the Alum Shale Formation, particularly in the Kinnekulle area ⁽²⁾ and a nodular bitumen, chemically separated from the underlying Great Stinkstone band, were analysed by Q-Py-GC. Nodular bitumen, which is bead-like in appearance under a stereo microscope, is believed to represent early migrated petroleum. The composition of the pyrolysates released by uranium rich kolm, and nodular bitumen are very similar to that of the Alum Shale (Figures 6b and 6c respectively), despite that the two pyrograms represent two entirely different source sections. The two samples also differ by several magnitudes in their uranium content. The general distribution of compounds and their relative abundances are nearly

TABLE 2 : Selected molecular peak integration data based on Q-Py-GC analysis for selected samples. All molecular concentrations expressed in mg/g TOC. Samples in the 1st column ordered according to locations of increasing maturity. For example, 1/5 in the first column indicates location 1 (Pålstop) (cf. Figure 1) and sample 5 (cf. Table 1).

Loc/ S.No.	1	2	3	4	5	6	7	8	9	10
1/5	47.33	21.53	15.56	2.50	10.56	3.75	4.31	116.35	20.26	136.60
1/9	54.07	21.20	17.50	3.00	10.16	3.11	5.39	117.34	20.62	137.96
2/2	51.98	26.09	21.68	2.95	13.58	4.16	3.41	129.78	23.01	152.79
2/15	60.73	26.72	21.97	3.14	12.65	4.41	5.37	141.28	24.37	165.65
3/7	35.56	28.17	21.56	2.53	11.56	3.67	5.44	115.86	22.69	138.55
3/13	53.43	30.42	22.88	2.55	11.11	3.90	6.07	137.54	23.14	160.69
4/12	67.46	33.39	32.72	4.29	14.37	4.51	6.12	173.20	27.71	200.91
4/26	66.36	32.87	27.78	4.59	15.26	4.23	3.66	166.42	25.88	192.30
5/20	54.33	27.41	23.18	3.79	14.17	4.02	4.33	142.82	24.74	167.55
6/21	42.58	20.58	15.52	2.51	11.21	2.85	3.66	101.61	19.31	120.92
7/22	34.93	25.09	18.06	2.34	10.36	2.98	3.67	105.57	18.78	124.36
8/31	35.27	16.59	11.49	1.83	7.63	2.04	3.07	80.90	14.00	94.90
9/30	32.95	15.29	12.12	1.52	8.70	1.91	2.98	77.77	14.72	92.49
10/34	0.86	2.26	0.65	0.18	2.71	0.61	2.31	5.55	5.95	11.51
11/36	1.23	0.79	0.18	0.06	1.25	0.27	1.05	2.69	2.76	5.45

Column Explanations: 1 = methane+ethane+ethene ; 2 = Σ n-alkenes (C3-C10); 3 = Σ n-alkanes (C3-C10); 4 = Σ xylenes ; 5 = Σ alkylbenzenes ; 6 = Σ indenenes ; 7 = Σ alkyl-naphthalenes ; 8 = Σ aliphatic hydrocarbons ; 9 = Σ aromatic hydrocarbons ; 10 = total hydrocarbons.

TABLE 3: Summary Q-Py-GC data in mg/g TOC, calculated by using a horizontal baseline.

Loc./ S.No.	Gas (C1-C5)	Light Oil (C6-C14)	Heavy Oil (C15+)	Total Oil (C5+)	Total Pyrolysate (C1-C5/C5+)	GOR
1/5	97.23	57.60	160.01	217.62	314.85	0.45
1/9	100.69	41.11	160.29	201.40	302.09	0.50
2/2	107.46	25.04	163.58	188.61	296.07	0.57
2/15	118.66	32.77	177.93	210.70	329.36	0.56
3/7	91.78	54.35	169.37	223.70	315.70	0.41
3/13	111.56	57.05	176.52	233.57	245.13	0.48
4/12	161.94	203.67	59.57	263.24	425.18	0.62
4/26	154.97	217.27	59.06	276.32	431.29	0.56
5/20	129.59	201.69	57.27	258.96	388.55	0.50
6/21	86.52	105.29	37.21	142.51	229.03	0.61
7/22	85.93	151.57	63.31	214.88	300.81	0.40
8/31	76.40	93.09	31.24	124.34	200.74	0.61
9/30	67.82	84.92	33.93	118.86	186.68	0.57
10/34	16.12	28.32	45.13	73.45	89.57	0.22
11/36	8.37	13.65	8.09	21.73	30.10	0.39

the same in all the samples- the Alum Shales, the nodular bitumen (probably derived from the Alum Shale) and kolm (with several 1000 ppm uranium).

In a larger context therefore, the Alum Shale pyrolysates are similar in gross composition to the free hydrocarbons present in them, in that both are relatively rich in aromatic hydrocarbons and depleted in normal hydrocarbons. One significant difference is however noticed in case of pyrolysates that there is a systematic decrease in the net yield of pyrolysate- both in the gas and oil fractions. GOR on the other hand seem to be rather constant with increasing maturity, perhaps suggesting little change in the basic chemistry of the kerogen molecule. No major trends are observed even when the data are plotted at molecular level using conventional bivariate or trivariate methods, which provide only limited discrimination between the samples and the variables. A more sophisticated and powerful statistical approach was therefore necessary to exemplify the effects of a single given variable, such as maturity, on the samples when other variables such as molecular yield, uranium content etc. also seem to influence the net results.

6. Principal Component Analysis of Kerogen Pyrolysate's Molecular Data

As multivariate analytical methods reduce large number of variables into a manageable number of factors, with the first factor accounting for maximum total variance of the total data matrix, this exercise was particularly useful in elucidating the main controlling variable(s) affecting the whole set of current objects (37 samples) and recognize the overall pattern. Principal Component Analysis (PCA) essentially makes use of the correlation or covariance matrix or the original set of variables (representing multidimensional space) and decomposes the total variance of the total data matrix to produce uncorrelated (orthogonal and independent) principal components

(representing a lower dimensional space) which are linear combinations of the original variables that explain or account for maximum variability.

In the present PCA, a total of 55 variables were used as input for all the 15 samples which were analysed by quantitative-pyrolysis- gas chromatography (Q-Py-GC). The variables included 48 quantitative measurements of all the major peaks in the pyrograms, which account for more than 90 % of total peak area of the pyrogram. In addition, the input data included several bulk measurements such as hydrogen indices from Q-Py-GC (TotPyr) and Rock-Eval (HI ker), uranium content ($\mu\text{g/gm TOC}$), $R_o\text{SPIN}$ (reflectance of bituminite lenses) and sample transmission (SANT) and dimensionality (SAND) from small angle neutron scattering (SANS). Figure 7a and 7b show respectively the loadings and scores plots along the first two principal components which account for 76.1 and 8.2% of total variance (cumulative 84.4% variance) and hence the 2-dimensional representation of the PC1 and PC2 gives a good picture of the most significant aspects of the data.

The key features of the loadings plot include distinct separation of the bulk parameters from whole rock analysis (which also happen to be non chemical parameters such as reflectance of bituminite lenses, small-angle neutron scattering (SANS) transmission and dimensionality) from all the other variables. Amongst the bulk physical variables, bituminite reflectance - $R_o\text{SPIN}$ (which is a maturity parameter) clearly is an outlier and somehow seem to control with equal intensity all the chemical variables (yields of pyrolysis products) (Figure 7a), suggesting that maturity (as determined by reflectance) was the prime controlling factor responsible for each chemical moiety. This is based on the observation that the variable $R_o\text{SPIN}$ seem to occupy the centre of a hypothetical circle formed by the chemical variables, each of the latter being almost equidistant from the former. There is a large horizontal separation between this maturity parameter (cluster I) and all the chemical variables (clusters II,III and IV) (Figure 7a). Hence PC1 can perhaps be regarded as a maturity based component, which accounts for 76.1 % of total variance. Hydrogen index data from Q-Py-GC is exactly at 180° from $R_o\text{SPIN}$, indicating a very good negative correlation, as expected. Small angle neutron scattering (SANS) dimensionality and uranium content, which seem to cluster together, also have some horizontal separation from the chemical variables, but this separation is apparently far less influential compared to the maturity variable ($R_o\text{SPIN}$).

Along the second PC, which accounts for 8.23 % of total variance, most similar molecular species tend to cluster together. Cluster III mainly has aromatic hydrocarbons, branched hydrocarbons and non-hydrocarbons of gas the fraction; cluster IV mainly has branched hydrocarbons and non-hydrocarbons of the oil fraction and C1-C5 n-hydrocarbons and cluster V has dominantly n-hydrocarbons of oil fraction (C5+). The most interesting feature however is, that the chain length of pyrolysate n-hydrocarbons systematically increases along the second PC in the positive direction (indicated by the solid line and arrow) while relative aromaticity seem to increase along the second PC in the negative direction (indicated by the broken line and open arrow). This effect can also be seen in cluster V, in which C4-alkylbenzenes and 2-methylnaphthalene also plot. A C4-alkylbenzene has a total of 10 carbon atoms but it plots relatively more negative along PC2 than n-decane (C10a) and n-decene (C10e) due to presence of an aromatic ring. The effect on relative aromaticity is even more pronounced in the case of 2-methylnaphthalene, which despite having 12 carbon atoms plots even more negative along PC2 due to the presence of 2 aromatic rings.

Styrene (STY) and 1-methyl naphthalene (1MeN) apparently are outliers and can be rejected, as in a separate PCA performed without styrene and 1-methylnaphthalene, no significant change was observed in the overall pattern of the loading and score plots. No significant change was

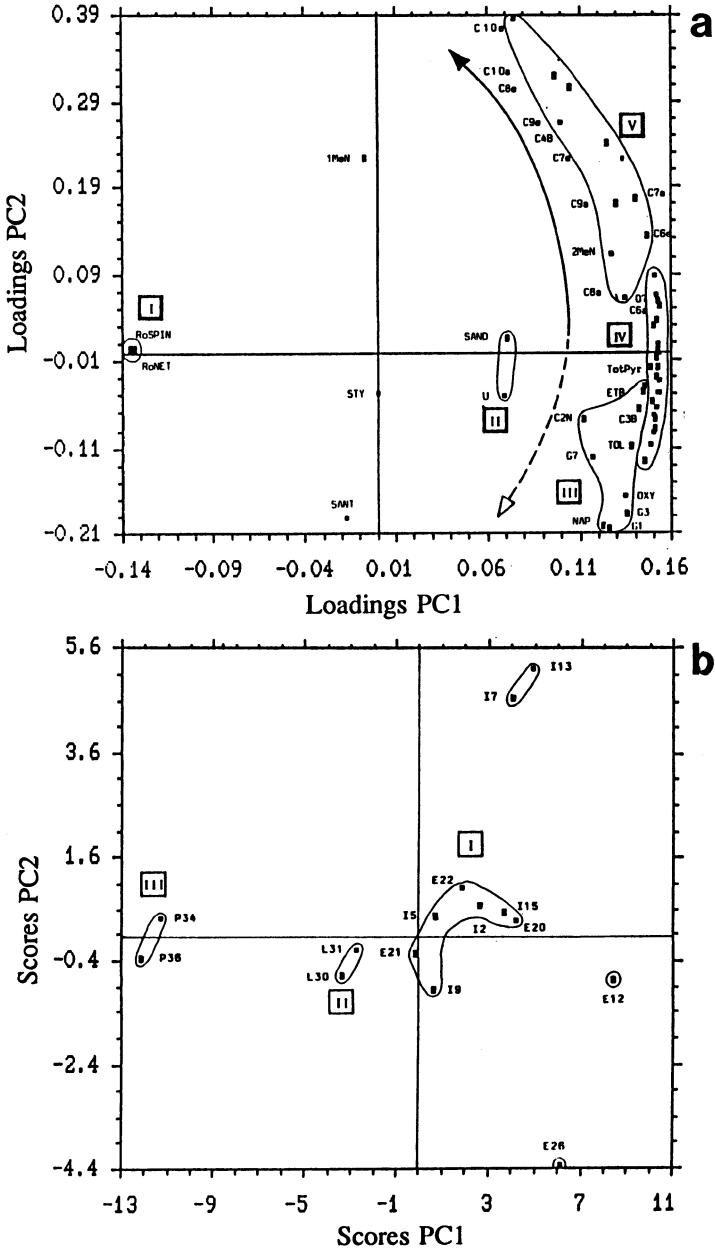


Figure 7. Principal Component Analysis (PCA) of the Alum Shale analytical data. a) loadings Plot showing the discrimination of the variables. b) Scores Plot showing the discrimination of the samples.

observed in the patterns even when uranium was excluded, perhaps suggesting that uranium does not seem to play an overriding role in defining the pattern of variability. In summary, therefore, the discrimination of the variables is found to be most significantly related to maturity along the first PC, independent of whether the variables are bulk (non-chemical) or molecular (chemical) along the first PC. In addition, the carbon chain length of a compound is decisive along the second PC in the positive direction and relative aromaticity of compounds along the second PC in the negative direction. Hence PC1 can be regarded as the maturity based principal component while PC2 is a compound type based principal component, both being related to the Alum Shale kerogens' pyrolysate data.

In the scores plot (Figure 7b) where the samples are plotted, there is maximum and most pronounced separation of the clusters horizontally, or along the maturity based principal component (PC1) with the immature samples (including a few early mature) (cluster I) being furthest apart on the positive side of the scale and post mature samples (cluster III) being most closely associated with the reflectance data. The late mature samples (cluster II) occupy an intermediate position, as expected. Evidently, an increase in maturity or reflectance is more significant and critical in defining a sample position on the scores plot. The positions of samples KER/26 and KER/12 (both early mature) on the scores plot suggest that these two samples should be enriched in aromatic hydrocarbons; the chemical data shows that this is true (Table 3).

7. Composition of artificially produced petroleum from the Alum Shales

As a follow-up of the previously described Q-Py-GC analysis, which was flash pyrolysis of the entire kerogen portion, a similar analysis was performed in 2 stages. The first stage consisted of mere thermovapourisation- gas chromatography (T-GC) at 300°C of crushed whole rock samples, which gave the composition of only the free hydrocarbons present in the Alum Shales. The second stage consisted of pyrolysis- gas chromatography (Py-GC) of pre-extracted kerogen of the same samples following a temperature programme (300 - 550°C at 50°C/minute, then 10 minutes at 550°C). It was necessary to perform these analyses to obtain compositional information on these samples under conditions similar to those that would be employed during artificial maturation. Finally, micro-scale sealed vessel (MSSV) simulated maturation was performed on the least mature pre-extracted kerogen employing 3 temperature conditions - 300, 330 and 350°C for 72 hours each, the results of which are described in detail elsewhere⁽¹⁰⁾. The products were analysed by T-GC and the residues by Py-GC.

The results of T-GC of whole rock samples suggest that the bitumen present in the Alum Shales consist mainly of low molecular weight hydrocarbons, these being primarily C1-C9 n-alkenes and alkanes, C1-C3 alkyl benzenes and C1-C2 alkyl naphthalenes (Figure 8a). This is true for all the samples, irrespective of their thermal maturity, except for the post-mature sample from Oslo, which is depleted in free hydrocarbons. This finding is consistent with the earlier results obtained from Iatroscan analysis where aromatic hydrocarbons were relatively more abundant with respect to the total hydrocarbon content. Also, the signatures of kerogen pyrolysates obtained by Py-GC (Figure 7b) are very similar to those produced by 800°C Q-Py-GC described earlier (Figure 6a) and the relative abundance of the molecular species is also comparable. The Py-GC technique also releases low molecular weight compounds with alkylbenzenes and alkyl naphthalenes being the dominant components. These results are in contrast with most alginites (botryococcus, tasmanite, gloeocapsomorpha) which generate only

low proportions of aromatic hydrocarbons and relatively high proportions of straight chain hydrocarbons⁽⁹⁾. The Alum Shale kerogens seem to be more gas prone than most other alginites in that the typical GOR for any Alum Shale sample is in 0.4-0.5 range, irrespective of maturity (Table 3).

MSSV simulated maturation induced different levels of kerogen conversion and mass balance calculations reveal that the Py-GC hydrogen index parameter fell from 387 in the original unheated sample to 277, 121 and 77 in the sequential heating experiments (300, 330 and 350°C respectively)⁽¹⁰⁾. The molecular composition of the products and residues of simulated maturation are however very similar to those of the natural series as is apparent from the respective GC traces (Figures 8c and 8d). The principle products formed are low molecular weight, primarily aromatic hydrocarbons. The gassy nature of products and residues is further exemplified in the ternary plot of C1-5, C6-15 and C15+ n-paraffin distribution (Figure 9) where the Alum Shale alginites clearly are different from most alginites. The Alum Shale pyrolysates as well as simulated maturation products, are highly depleted in medium and high molecular weight n-paraffins which is unusual^(9,11).

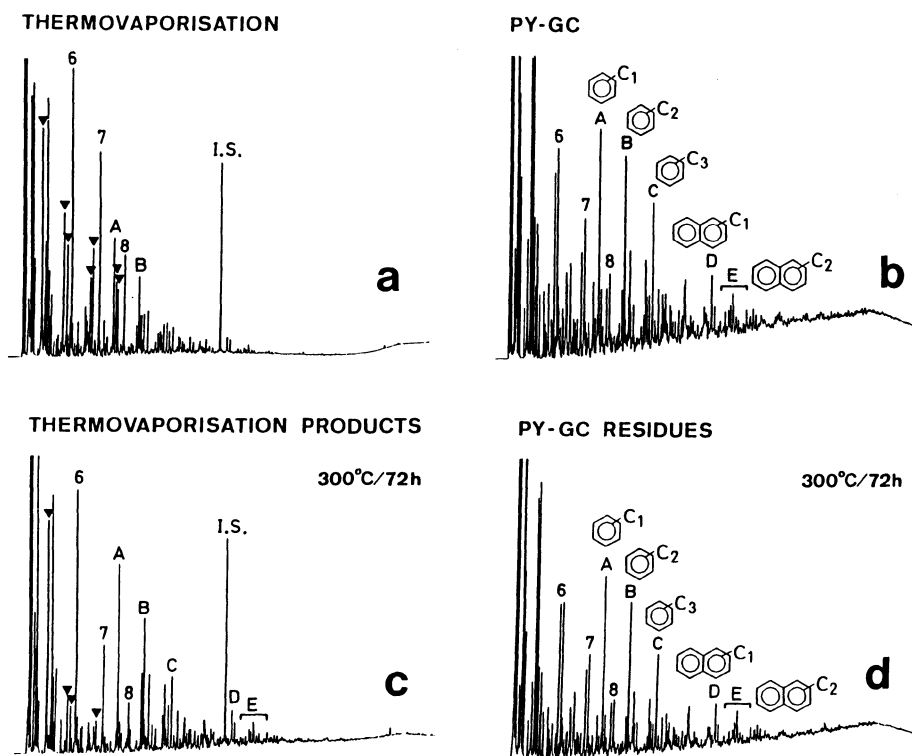


Figure 8. a) Thermovapourization of crushed whole rock. b) Py-GC of extracted kerogen. c) Thermovapourization of hydrocarbons produced by artificial maturation. d) Py-GC of the residual kerogen after artificial maturation.

Another unusual, but significant fact that is revealed by mass balance calculation is that 15%, 25% and 32% respectively of originally volatile moieties in the unheated kerogen are not detected in the 300, 330 and 350°C heating experiments. This appears to represent 'dead carbon' formation and suggests that the process might be quantitatively very significant not only in the simulation experiments, but also in the natural series. The fact that a substantial portion of original organic carbon (labile kerogen) present in the Alum Shales is converted into 'dead carbon' may partially explain the high TOC content (up to 21%) in the late mature and post mature samples. Therefore, any calculations made regarding the petroleum generating potential of the Alum Shales, say from instance from Rock-Eval and TOC data will be highly overestimated and erroneous.

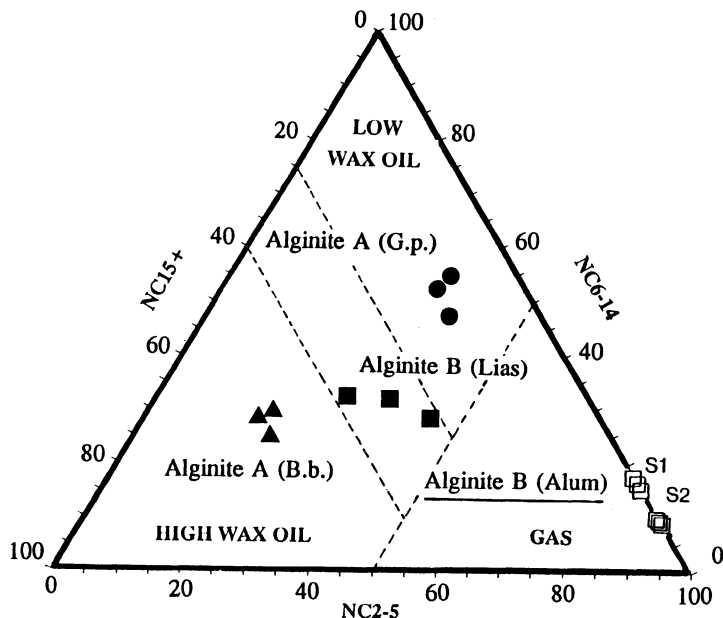


Figure 9. Distribution of normal paraffins in the products released and residues of artificially matured Alum Shale kerogen, as compared to other alginites.

8. Radiation effects on the Alum Shale Kerogen

It was recently postulated ⁽¹²⁾ that the extractable organic matter (bitumen) of the Alum Shales have been affected by radiation due to uranium decay and that the yields of total extract, saturated and aromatic hydrocarbons decrease with increasing amounts of uranium and that the aromatic hydrocarbon species tend to be more abundant in samples with higher content of uranium. In addition, an idea was conferred ⁽¹³⁾ that it is the primary sedimentary matter (kerogen) has been structurally altered due to radiation and have proposed a mechanism involving polymerisation of alkyl chains through free radical cross linking. Dahl et al. ⁽¹²⁾ have

in their sample suite uranium ranging from 7-250 ppm while Lewan and Buchardt ⁽¹³⁾ have a sample suite with uranium ranging from 18-440 ppm. Both the studies cited above have assumed their respective sample suites to be of uniform maturity and have regarded the samples studied as thermally immature. Factors such as source, thermal maturity, petroleum migration (mixing), weathering and biodegradation were not adequately considered to be responsible in establishing the present composition of the EOM.

The present study considers a larger number of locations and samples, and has established the presence of a natural maturation series within the Alum Shale Formation. The results of the present study also indicate that the locations considered by other workers ^(12,13) are not uniform as regards their thermal maturity, but are of variable maturity, mostly from thermally immature to early mature. There is therefore a clear discrepancy between the findings of the present study and the assumptions of other studies ^(12,13) as regards thermal maturity of the Alum Shales from various locations.

Average uranium content of shales worldwide is around 4 ppm while that in black shales is as high as 8 ppm ⁽¹⁴⁾. A wide variation is also reported ⁽¹²⁾ in total extract yield (55-154.8 mg EOM/gm TOC), total saturated hydrocarbons (5.7-37.7 mg/g TOC) and total aromatic hydrocarbons (10.5-66.4 mg/g TOC) for samples containing uranium in the range of 7-15 ppm. In samples with more than 15 ppm uranium, all the yields are comparable, irrespective of uranium content. Assuming that the unusual and atypical results obtained with regard to the Alum Shale bitumens, pyrolysates, simulated maturation products and petroleum generating potential are primarily due to irradiation, the above observation implies that the threshold amount of uranium required to cause such an alteration lies between 8-10 and about 15 ppm i.e. a margin of 5 - 7 ppm. Considering the extent of atypicality observed in case of the Alum Shales with regard to composition of bitumens and pyrolysates, it seems unlikely that alteration of such a large magnitude could be caused by such a small increment in uranium content, bearing in mind the average uranium content of 8 ppm in black shales worldwide.

Some convincing arguments have been presented in the radiation dosage approach ⁽¹³⁾, but it is likely that radiation caused alteration might not be the only reason for Alum Shale's anomalous geochemistry and other factors such as a "different" original biota may also be responsible. Principal components analysis of Alum Shales pyrolysate molecular data has also shown that relative to maturity (interpreted from bituminite reflectance), uranium content plays a less important role when considering total pyrolysate yield or even molecular distribution and abundance. Moreover, exclusion of uranium as a contributing variable, did not seem to bring about any change in the geometric pattern of PCA. In addition, kolm sample which has relatively been subjected to extremely high radiation dosage as compared to the Alum Shales, does not exhibit any differences in its chemical composition, implying no effect what so ever by its uranium content, which is as high as 2000-7000 ppm.

9. Expulsion of petroleum and effects of migration in the Alum Shales

The results presented in the previous sections indicate the Alum Shale to be unusual and atypical with regards to petroleum generation as a function of thermal maturation. Sedimentary organic matter in the Alum Shales from various locations is also qualitatively very similar and uniform, both petrographically and chemically. In qualitative terms, the Alum Shales are extremely rich in organic carbon, but simulated maturation studies show that in addition to the original hydrogen index being sequentially reduced from 387 in the unheated sample to 277, 121 and 77 mg

HC/gm TOC on 300, 330 and 350°C heating respectively, there is also a simultaneous formation of inert carbon to the extent of 15, 25 and 32% respectively. Petroleum expulsion, as a result of thermal maturation, therefore is thought to be very limited in the case of Alum Shales.

The Alum Shales in the Oslo region, despite their overmature state, contain 105 mg C_{org} /gm rock (10.5 % TOC), but they neither contain any free petroleum ($S_1 = 0$) nor yield any pyrolysate ($S_2 = 0$). This suggests that all the organic carbon present (105 mg/gm rock) is inert or 'dead' carbon. In addition, it must be noted that the present TOC value in the Oslo region is in the same range as in the immature sections. This might suggest that the original TOC in Oslo region must have been nearly double of the present TOC, if at all there was some petroleum generation and expulsion. Due to this unique inherent characteristic of the Alum Shale, petroleum generation / expulsion calculations made according to some previously proposed models^(15,16) will be highly erroneous and meaningless.

Theoretically therefore, the Alum Shales seem to realise major portion of their petroleum potential and large quantities of generated petroleum seem to have been expelled. In reality however, a process of simply rearrangement of carbon atoms within the Alum Shales is more prevalent rather than conversion of labile kerogen into expellable petroleum. Perhaps in this process of labile kerogen (initially hydrogen rich) converting into inert carbon (kerogen) (relatively hydrogen poor) and this finally transforming into graphite (pure carbon), hydrogen was the principle product. It has been suggested⁽¹⁷⁾ that rich source rocks are compacted as a result of expelling petroleum and the density changes observed in source rocks during maturation reflect not only conventional compaction, but expulsion of primary petroleum with little associated water too. However, in the case of the Alum Shales, this does not seem to have occurred, as no generation or expulsion is believed to have taken place.

10. Summary and Conclusions

While the preliminary analyses indicate the Alum Shales to contain type II kerogen with a substantial petroleum potential, subsequent detailed chemical and optical examination reveals that this primarily algal organic matter does not produce liquid petroleum on maturation. The primary maturation products include low molecular weight compounds, mainly aromatic with anomalously high gas:oil ratios. In addition, the organic carbon which is found to be labile at an immature stage, partially converts into inert or 'dead' carbon, resulting in considerable reduction in the actual petroleum masses which are expellable. The Alum Shale organic matter is therefore different and unusual than most other algal kerogens, in more than one ways. Perhaps the only similarity between these is the physical appearance of bright yellow fluorescing alginite, which is found in the Alum Shales in great abundance. Chemically however, none of the findings of the Alum Shales are comparable to other type II algal source rocks such as the Upper Kimmeridge Clay from the North Sea or the Lower Toarcian from the Paris Basin. Radiation damage of kerogen, as suggested by other workers, is a possibility, but our data indicates that this may not be the sole or an overriding factor; the original composition of the precursor biota may have been unusual. Clearly, far greater multi-disciplinary approach is required to fully understand the structural peculiarities of the Scandinavian Alum Shales.

Acknowledgements

Thanks to Prof. Henning Dypvik, Dept. of Geology, Univ. of Oslo for providing samples. Thanks to Prof. Steve Larter, NRG, Univ. of Newcastle upon Tyne, U.K. for fruitful discussions and support during the study and suggestions to improve the manuscript.

11. References

1. Thickpenny, A. (1987) In: Marine Clastic sedimentology (Eds: Leggett, J.K. and Zuffa, G.G.) Graham and Trotman, 156-171.
2. Andersson, A., Dahlman, B., Gee, D.G. and Snäll, S. (1985) Swedish Geo. Survey No. 56
3. Bharati, S. (1989), Cand.scient. thesis. University of Oslo, Norway.
4. Bharati, S. and Larter, S.R. (1991). In: Advances & Applications in Energy & The Natural Environment (Ed. Manning, D.A.C.), Manchester Univ. Press, U.K.
5. Bharati, S., Larter, S. and Horsfield, B. (1992) In: Generation, Accumulation and Production of Europe's Hydrocarbons II (Ed. Spencer, A.M.) Springer-Verlag, Berlin.
6. Tissot, B.P and Welte, D.H (1984) Petroleum Formation and Occurrence, Springer-Verlag, New York, 699 p.
7. Larter, S.R. and Douglas, A.G. (1980) In: Adv. in Org. Geochem. 1979 (Eds. Douglas, A.G. and Maxwell, J.R.) Pergamon Press, London, 579-584.
8. Larter, S.R. and Senftle, J.T. (1985) Nature, vol. 318, 277-280.
9. Horsfield, B. (1990) In: Proc. of 7th Int. Palynological Cong., Aug 1988, Brisbane, Australia
10. Horsfield, B., Bharati, S., Larter, S.R., Leistner, F., Lütke, R., Schenk, H.J., Dypvik, H. (1992). In: Early Organic Evolution : Implications for Mineral and energy Resources. (Ed. Schidlowski, M.) Springer-Verlag, Berlin, 257-266.
11. Larter, S.R. (1985) In: Petroleum Geochemistry in Exploration of the Norwegian Shelf (Ed. Thomas, B.L.) Graham & Trotman, London, 269-286.
12. Dahl, J., Hallberg, R. and Kaplan, I.R. (1988) Org. Geochem. Vol. 12/6, 559-571.
13. Lewan, M.D. and Buchardt, B. (1989) Geochim. Cosmochim. Acta vol 53, 1307-1322.
14. Swanson, V.E. (1961) U.S. Geol. Surv. Prof. Paper 356-C, 67-110.
15. Cooles, G.P., Mackenzie, A.S. and Quigley, T.M. (1986) In: Adv. Org. Geochem. 1985 (eds: Leythaeuser, D. and Rullkotter, J.), 235-245.
16. Mackenzie, A.S. and Quigley, T.M. (1988) Am. Asso. Petr. Geol. Bulletin, Vol.. 72/4, 399-415.
17. Larter, S.R. (1988) Marine and Pet. Geol. Vol. 5, No.13, 194-205.

CARBON-ISOTOPIC COMPOSITIONS OF INDIVIDUAL ALKANES/ALKENES IN LEAF FOSSILS AND SEDIMENTS FROM THE P-33 SITE OF THE MIOCENE CLARKIA DEPOSIT

Yongsong Huang, Matthew J. Lockheart, James W. Collister,
and Geoffrey Eglinton
Organic Geochemistry Unit, School of Chemistry, University of Bristol, Bristol,
BS8 1TS, UK.

ABSTRACT. The alkanes/alkenes from the Clarkia sediments and fossils were analysed by GC, GC/MS and irm-GC/MS. The results indicate that the sediment has an extremely low thermal maturity and the *Sycamore* fossil analysed still preserves a distinctive *n*-alkane distribution comparing with the surrounding sediments. The presence of isotopically depleted hopenes suggests input from methanotrophic bacteria and hence the presence of an active methane cycle.

1. Introduction

The Miocene lacustrine Clarkia deposit (Northern Idaho, U.S.A.) has attracted a great deal of research interest in the last two decades because of its exceptionally well preserved leaf fossils ⁽¹⁾. Among its five fossil sites, the fossiliferous site P-33 has received the most intense investigation since its discovery by Francis Kienbaum in 1972. The amazing degree of preservation of leaf fossils can be seen in the pigmentation retained in the leaves. When initially removed from the finely laminated lacustrine clays, the fossil leaves are green, red or brown, but rapidly turn black upon exposure to air. Fossil leaf tissues have also shown exceptional ultrastructure preservation ⁽²⁾, and more recently, have yielded DNA through amplification by the polymerase chain reaction (PCR) ⁽³⁻⁴⁾. This high degree preservation of leaf fossils taken in conjunction with the finely laminated nature of the sediments and the lack of bioturbation is in accordance with the lake having been stratified, with an anoxic hypolimnion which excluded metazoan grazers ⁽¹⁾.

Identification and quantitation of biological markers in sediments is a powerful technique for assessing sources of organic matter in ancient environments and can aid in the paleoreconstruction of ancient sedimentary environments. However, because many biological markers are non-specific, being produced by a variety of organisms, interpretations based only on their distributions and abundances in sediments can be problematic. Additional information can be gained from isotopic analysis of individual biomarkers. Carbon-isotopic compositions of lipids reflect both the isotopic

composition of the carbon source utilised by the organism and isotopic fractionations accompanying assimilation and biosynthesis. Thus, while two classes of organisms may produce the same lipids, the isotopic compositions of these lipids can be significantly different. This technique has greatly extended the ability to trace carbon flows in ancient environments (5-6).

Previous studies by Logan (7) of the solvent extractable lipids have shown that the Clarkia sediment and leaf fossils contain abundant functionalised compounds of biological origin, indicating a high degree of molecular preservation after 17-20 Ma of burial. Indeed Logan (7) demonstrated that the leaf wax components were located at the fossils and had not moved. The present study attempts to reconstruct more fully the depositional environment of the Clarkia deposit by combining structural identification of biomarkers with their carbon-isotopic compositions.

2. Materials and Methods

Two sediment samples were collected from 2.5m and 3m below the top of the 2b region in the stratigraphic column from the P-33 site of the Clarkia deposit. Fossil leaves, identified by Dr Jack Smiley as *Magnolia* sp. and *Sycamore* sp., were taken from the same stratigraphic horizons and were scraped into sample vials and extracted by immersion in DCM/methanol (9:1) on the site. Sediment samples were lyophilised and then ground into fine powder. About 50g of sediment were soxhlet-extracted with DCM/methanol (2:1) containing pure copper granules to remove elemental sulphur, for 24 hrs. Each fossil sample was extracted ultrasonically five times with DCM/methanol (2:1) and the supernatants combined after centrifugation. Two modern leaf samples collected from the Bristol University Botanical Gardens (identified as *Magnolia delabayi* and *Quercus turneri*), were cleaned of foreign particles and dust with pre-extracted cotton wool/double distilled water and oven-dried overnight at 80°C under nitrogen. Waxes were removed from each species by washing/shaking both sides of the leaves in a watch glass with DCM for 30 seconds, repeating three times using fresh solvents and combining washings.

Total extracts were separated into aliphatic hydrocarbon, aromatic, ketone, alcohol and acid fractions, using solid phase extraction (Aminopropyl Bond Elut®, Varian) to isolate acids, followed by silica gel flash column chromatography eluting with solvents of increasing polarity. Aliphatic hydrocarbons were obtained by eluting with hexane. About 1-2mg of the sedimentary aliphatic hydrocarbon fractions were further separated into branched/cyclic and *n*-alkane fractions using a urea adduction procedure as follows. The sample was transferred to a teflon-capped tube, blown down with nitrogen and redissolved in toluene (300µl). The tube was pre-heated to 65°C and to it added hexane (a few drops) and urea-saturated methanol (4ml at 65°C). The sample tube was agitated for 1 min at 65°C and cooled in air whilst crystals formed, followed by re-refrigeration (1 hr) and centrifugation (3000 rpm for 5 mins). The supernatant (the 'non-adduct')

was removed using a cotton-stoppered pipette. The crystals were gently washed by shaking twice with cold urea-saturated isoctane and combining with 'non-adduct'. The 'adduct' was recovered by dissolution of the crystals in 0.1N HCl (3ml) and extracting three times with hexane. The recovery of C₂₁ to C₃₅ n-alkanes from the aliphatic hydrocarbon fraction was greater than 96% using this procedure. A further 10mg of sediment aliphatic hydrocarbons were fractionated into saturated, monounsaturated and diunsaturated fractions on TLC (SiO₂ plates impregnated with 20% AgNO₃) and developed with hexane. The appropriate fractions were subjected to GC, GC-MS and irm-GC-MS analyses as described before (8).

3. Results and Discussion

3.1 DISTRIBUTION AND CONCENTRATION

Histograms showing the distribution and abundance of the C₂₂ to C₃₄ n-alkanes (in µg/g dry weight of sample) from the six 'hydrocarbon' fractions are displayed in Figure 1. A unimodal distribution of n-alkanes maximising at C₂₉ with strong odd/even predominance is observed for 2.5m and 3m sediments and the *Magnolia* fossil. The two modern leaves show similar distribution patterns to these samples (maximised at C₂₉) but with a higher odd/even carbon number predominance. The *Sycamore* fossil has a distinct bimodal distribution of n-alkanes, differing from that of the sediments and the *Magnolia* fossil. A much higher concentration of C₃₁ to C₃₅ n-alkanes is observed in this fossil; the alkanes from the original *Sycamore* leaf waxes are evidently still preserved in the fossil leaf after millions of years in the sediment. Previous work by Logan (7), analysing the total extracts of different fossil species, found that the gross characteristics of the original epicuticular wax were preserved in the fossils. The parallel comparison of the alkane/alkene fractions from the fossils and sediments in this work has provided further evidence of molecular preservation.

The concentration of n-alkanes in the 2.5m sediment is approximately two times higher than that in the 3m sediment, suggesting a greater amount of terrigenous input in the upper (2.5m) horizon. However, the similarity in the n-alkane distributions suggest a relatively uniform higher plant flora around the ancient lake Clarkia during the time of deposition, as indicated by geological and paleontological evidence (1).

The identification of the major terpenoid hydrocarbons is shown on the GC trace of the branched/cyclic fraction of 2.5m sediment in Figure 2. The terpenoids are mainly composed of des-A-triterpenes of higher-plant origin and hopene derivatives of bacterial origin. Hop-17(21)-ene (E) and hop-21-ene (H) are present in rather high abundance but no hop-22(29)-ene is found, suggesting that the isomerisation of hop-22(29)-ene has been completed. However, the saturated hopanoids are dominated by the isomers with 17β(H), 21β(H) configurations, indicating extremely low thermal maturity (10), as reported by Logan (7) (22R-30α-homohopane was identified in sediment in the work).

3.2 UREA ADDUCTION

Figure 2 shows the GC traces for the total, urea adducted and urea non-adducted aliphatic hydrocarbon fractions of the 2.5m sediment. The *n*-alkanes must be separated from co-eluting terpenoids before irm-GC/MS analyses, as co-elution affects measured values considerably ⁽¹¹⁾. Urea adduction was found not to cause isotopic fractionation; a high recovery of the *n*-alkanes is particularly important and a recovery of 96% to 100% has been achieved for C₂₁ to C₃₅ *n*-alkanes in the samples analysed in this study using the procedure described above. Table 1 compares the isotopic data measured on the total aliphatic hydrocarbon fraction (TAHF) and urea adducted *n*-alkanes from the same fraction of the 2.5m sediment. The values for the C₂₇, C₂₈ and C₂₉ *n*-alkanes (with no obvious co-elution in TAHF) show differences (Δ) of smaller than 0.2‰, which is within the range of irm-GC/MS instrumental error (± 0.3 ‰). Hence, there is no isotopic fractionation associated with the separation of *n*-alkanes by urea adduction. The *n*-alkanes with apparent co-elution on GC and irm-GC/MS, for instance C₂₃, C₂₄, C₃₀, C₃₁, show the greatest differences before and after adduction of up to 2.7‰ (Table 1). Co-elution was also a problem for C₂₅ and C₂₆ *n*-alkanes on irm-GC/MS runs (but not apparent on the GC runs), which is attributed to the lower peak resolution power and use of helium as carrier gas (peak positions may shift) on irm-GC/MS. Thus urea adduction is necessary to obtain accurate measurement of isotopic composition.

3.3 ISOTOPIC COMPOSITIONS

$\delta^{13}\text{C}$ Values for *n*-alkanes and hopenes are summarised in Table 2. Values for 2.5m and 3m sediment *n*-alkanes show a similar range of $\delta^{13}\text{C}$ values (-27.4 to -32.8‰). The *Magnolia* fossil show values ranging from -26.0 to -28.4‰ (bulk isotopic analysis of *Magnolia* gave -26.6‰). The *Sycamore* fossil gave values in a similar range to those of the sediments of -26.5 to -30.8‰ (bulk *Sycamore* was -23.9‰).

A general trend of increasing ¹³C depletion with chain length was observed for both the fossils and sediments. The *Magnolia* fossil exhibited slightly more positive values (about 1‰ for the same carbon number) than those of the other *Clarkia* samples, which suggests the variation of $\delta^{13}\text{C}$ values between individual fossil plant species, as is observed in modern plants ⁽⁸⁾. This difference may also suggest that the *n*-alkanes of the original *Magnolia* leaf waxes are still localised inside the fossil leaf. The $\delta^{13}\text{C}$ values for individual *n*-alkanes in the sediment samples suggest a major source from C₃ higher plants ⁽⁸⁾, consistent with paleontological evidence.

Hopenes in *Clarkia* sediments and fossils are highly depleted in ¹³C relative to the *n*-alkanes (Table 2), with $\delta^{13}\text{C}$ values ranging between -49.5 and -61‰. Such depleted values suggest they derive from methanotrophic bacteria ⁽¹²⁾, and is compelling evidence for the presence of a methane cycle. In contrast, 22R-homohopane has a $\delta^{13}\text{C}$

Figure 1: *n*-alkane distributions in *Clarkia* P-33 samples and modern leaf waxes.

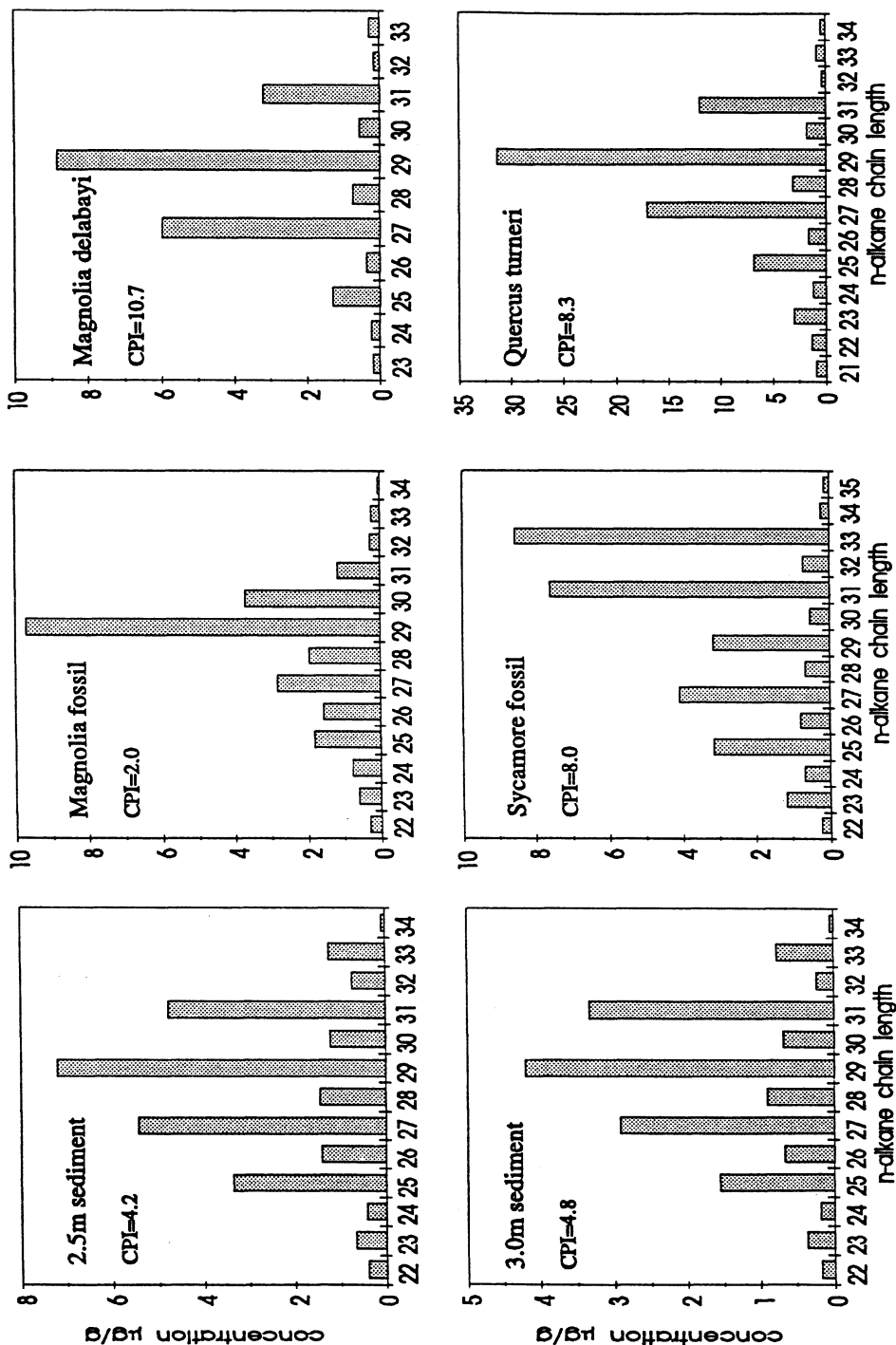
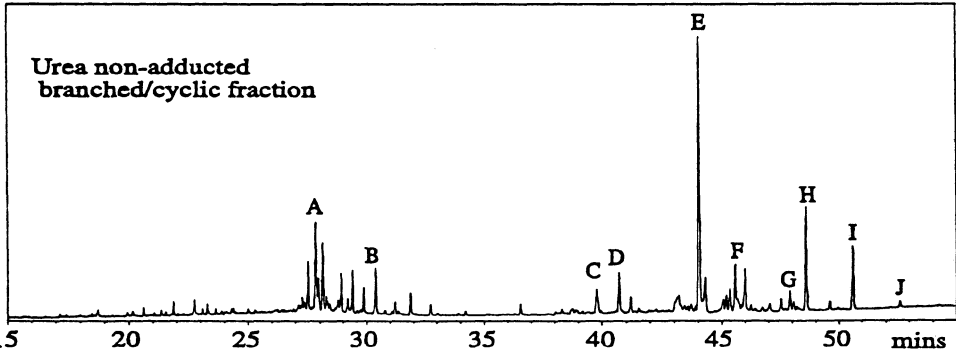
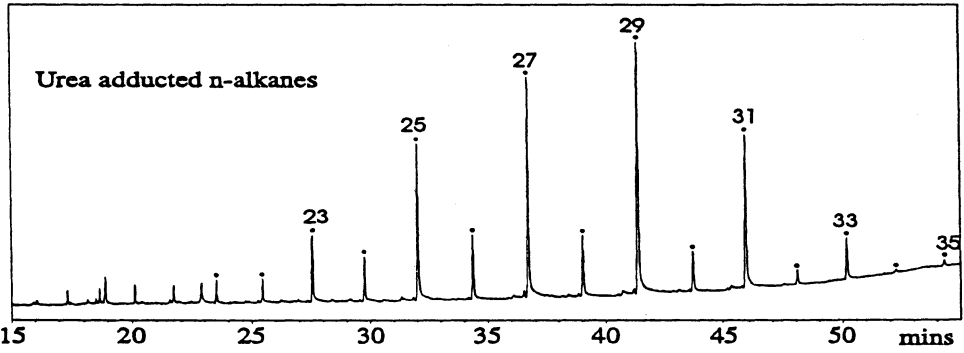
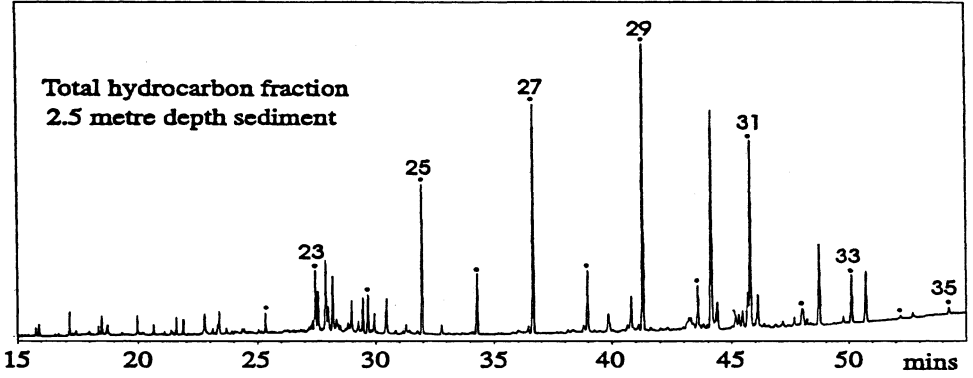


Figure 2: GC traces displaying urea adduction of the 2.5m sediment hydrocarbon fraction



- | | |
|--|---|
| A. des-A-olean-13(18)-ene | F. 17 β (H), 21 β (H)-30-nor-hopane |
| B. des-A-lupane | G. homo-neohop-13(18)-ene |
| C. 22,29,30-trisnor-hop-17(21)-ene | H. hop-21-ene |
| D. 17 β (H)-22,29,30-trisnorhopane | I. 22R-17 β (H), 21 β (H)-homohopane |
| E. hop-17(21)-ene | J. 22R-17 β (H), 21 β (H)-bishomohopane |

Table 1: Comparison of *n*-alkane isotopic data obtained from urea adducted and total aliphatic hydrocarbon fractions of 2.5m sediment.

<i>n</i> -alkane chain length	22	23	24	25	26	27	28	29	30	31	32	33
values from total alkane/alkene fraction	-25.7 (0.2) *	-25.5 *	-26.2 (0.1) *	-27.3 (0.1) *	-29.1 (0.1) *	-30.7 (0.1) *	-29.2 (0.1) *	-31.8 (0.3) *	-29.7 (0.1) *	-30.8 (0.1) *		
values from urea adducted fraction	-28.9 (0.4)	-27.4 (0.1)	-28.2 (0.1)	-27.7 (0.2)	-28.2 (0.1)	-29.0 (0.2)	-30.5 (0.1)	-29.1 (0.2)	-30.5 (0.2)	-30.5 (0.1)	-32.8 (0.1)	-29.9
Δ	1.7	2.7	1.5	0.9	0.1	0.2	0.1	1.3	0.8	0.9		

Values are deviations per mil relative to Pee Dee Belemite standard, calculated according to the equation:

$$\delta^{13}\text{C} = \{(R_{\text{sample}} - R_{\text{standard}})/R_{\text{standard}}\} \times 1000, \text{ where } R = {}^{13}\text{C}/{}^{12}\text{C} \text{ of the standard and sample.}$$

Figures indicated in parentheses are standard deviations of two runs.

Where no standard deviation is listed, only one isotopic value was obtained.

* indicates that these peaks were co-eluting with other compounds on irm-GC-MS runs.

Table 2: Comparison of isotopic data from *n*-alkanes and hopanoids obtained from Clarkia P-33 samples.

<i>n</i> -alkane chain length	22	23	24	25	26	27	28	29	30	31	32	33	X	Y	Z
2.5m sediment	-28.9 (0.4)	-27.4 (0.1)	-28.2 (0.1)	-27.7 (0.2)	-28.2 (0.1)	-29.0 (0.2)	-30.5 (0.1)	-29.1 (0.2)	-30.5 (0.2)	-30.5 (0.1)	-32.8	-29.9	-49.5	-61.0	-35.9
3.0m sediment	-29.5 (0.1)	-29.0 (0.3)	-29.3 (0.2)	-28.2 (0.5)	-28.7 (0.1)	-29.0 (0.3)	-29.5 (0.1)	-29.2 (0.2)	-30.5 (0.4)	-30.2 (0.4)	-31.2 (0.3)	-30.0 (0.3)	nd	nd	nd
<i>Magnolia</i> fossil				-26.8 (0.2)	-26.0 (0.1)	-27.8 (0.1)	-27.7 (0.1)	-27.9 (0.1)	-28.4 (0.2)				-52.9		
<i>Sycamore</i> fossil		-26.9 (0.1)		-28.4 (0.1)		-29.2 (0.1)		-28.8 (0.1)		-30.6 (0.1)		-30.9 (0.1)	-55.1		
<i>Magnolia delabayi</i>						-33.2 (0.1)		-34.0 (0.1)		-34.3 (0.1)					
<i>Quercus turneri</i>		-30.5	-31.4	-31.6 (0.1)		-32.8 (0.2)		-33.2 (0.3)		-35.7 (0.2)					

X. hop-17(21)-ene Y. hop-21-ene Z. 22R-17β(H), 21β(H) homohopane nd. not determined

Values are deviations per mil relative to Pee Dee Belemnite standard, calculated according to the equation:

$$\delta^{13}\text{C} = \left\{ \left(\frac{R_{\text{sample}}}{R_{\text{standard}}} \right) / \left(\frac{R_{\text{sample}}}{R_{\text{standard}}} \right) \times 1000, \text{ where } R = \frac{^{13}\text{C}}{^{12}\text{C}} \text{ of the standard and sample.} \right.$$

Figures indicated in parentheses are standard deviations of two runs. Where no standard deviation is listed, only one isotopic value was obtained.

value of -35.9‰, suggesting it was derived from a different group of bacteria, such as cyanobacteria or heterotrophic bacteria.

$\delta^{13}\text{C}$ values for modern leaf *n*-alkanes are about 3‰ more negative (-33.2 to -34.3‰ for *Magnolia delabayi* and -30.5 to -35.7‰ for *Quercus turneri*). This might be attributed to differing atmospheric concentration and isotopic composition of CO_2 at the time of deposition compared with modern levels.

4. Conclusions

The Miocene *Clarkia* sediment has an extremely low thermal maturity. The *Sycamore* fossil analysed shows a distinctive *n*-alkane distribution when compared with the surrounding sediments, providing the evidence of excellent molecular preservation. The higher plant flora around the ancient lake *Clarkia* was mainly C_3 species and remained relatively stable during the deposition of P-33 sediment. The presence of isotopically depleted hopenes in the sediments suggests input from methanotrophic bacteria and hence the presence of an active methane cycle. This further supports the idea that the water column was stratified with an anoxic hypolimnion.

Acknowledgements: We are grateful to Dr. Torren Peakman for useful discussions. We acknowledge the financial support provided by the NERC through its TIGER (Terrestrial Initiative in Global Environment Research) Programme, award number GST/02/613. We also thank the NERC for the GC-MS facility (Grants GR3/2951 and GR3/3758) and irm-GC/MS facility (Grant GR3/7731).

5. References

1. C.J. Smiley and W.C. Rember, Late Cenozoic paleogeography of the Western United States. (ed. C.J. Smiley), pp.11-30. AAAS, San Francisco (1985).
2. K.J. Niklas, R.M. Brown, and R. Santos, Late Cenozoic History of the Pacific Northwest. (ed. C.J. Smiley), pp. 143-159. AAAS, San Francisco (1985).
3. E.M.Golenberg, Phil. Tran. Roy. Soc. Lond , 1991, **B333**, 419.
4. P.S. Soltis, D.E. Soltis and C.J. Smiley, Proc. Nat. Acad. Sci, 1992, **89**, 449.
5. K.H. Freeman, J.M. Hayes, J.-M. Trendel and P. Albrecht, Nature, 1990, **343**, 254.
6. J.M. Hayes, K.H. Freeman, B.N. Popp and C.H. Hoham, Org. Geochem., 1990, **16**, 1115.
7. G.A. Logan, Ph.D thesis. University of Bristol (1992).
8. G.Rieley, J.W. Collister, B.Stern and G. Eglinton Rapid Communications in Mass Spectrometry, 1993, **7**, 488-491.

9. G.A. Logan and G. Eglinton, Org. Geochem., in Press.
10. A.S. Mackenzie, R.L. Patience, J.R. Maxwell, M. Vandenbroucke and B. Durand, Geochim. Cosmochim. Acta 1980, **45**, 1345-1355.
11. E. Lichtfouse, K.H. Freeman, J.W. Collister and D.A. Merritt, J. Chromatography, 1991, **585**, 177.
12. J.W. Collister, R.E. Summons, E. Lichtfouse and J.M. Hayes, Org. Geochem., 1992, **19**, 265.

Atmospheric Pressure Temperature Programmed Reduction (AP-TPR) as a tool to investigate the changes in sulphur functionalities in solid fuels

J. YPERMAN¹, D. FRANCO¹, J. MULLENS¹, G. REGGERS¹,
M. D'OLIESLAEGER² and L.C. VAN POUCKE¹

1) *Laboratory of Inorganic and Physical Chemistry*

2) *Materials Physics Division*

IMO, Limburgs Universitair Centrum, B-3590 Diepenbeek, Belgium

S. P. MARINOV

*Institute of Organic Chemistry, Bulgarian Academy of Sciences,
Sofia 1040, Bulgaria*

ABSTRACT. This research contribution reports the preliminary interpretation of the results of selective desulphurization procedures of a Bulgarian lignite, Maritza-Iztok. The AP-TPR profiles can be explained in view of the selective treatments used. In addition, the importance of heat recovery for the products obtained is discussed.

1. Introduction

A major problem in the utilization of oil shales and coal is the presence of sulphur, which is present in both inorganic and organic forms. Inorganic sulphur (pyrite, sulphides and sulphates) is not a major problem as it can be removed by conventional physical cleaning methods. ⁽¹⁾ With the rigorous emission regulation however the knowledge of organic sulphur will be necessary in view of an adapted treatment (precleaning and/or end-of-pipe methods).

Several efforts are made to characterize the organic sulphur in solid materials. The use of X-ray photoelectron spectroscopy (XPS) ⁽²⁻⁴⁾ utilizing the sulphur 2p signal, together with a curve fitting procedure and sulphur K-edge X-ray absorption spectroscopy (XANES) ⁽⁵⁻⁶⁾ using the third derivative analysis have been employed for identification and quantification of sulphur in coal. In addition in more recent studies it has been demonstrated that sulphur L-edge X-ray absorption near edge structure is used to distinguish organosulphur species in coal ⁽⁷⁻⁸⁾.

Besides these X-ray techniques, oxidation (CAPTO) ⁽⁹⁾ as well as temperature programmed reduction (TPR) - atmospheric ⁽¹⁰⁻¹²⁾ and high pressure ⁽¹³⁾ - have made substantial progress. Further details on these techniques can be found in the chapter by C. E. Snape and K. D. Bartle.

Analysis of model compounds ⁽¹⁴⁾ as well as selective desulphurization of real coal samples can be useful, in order to interpret the TPR profiles. In view of these aspects, this study presents the first results of several desulphurization treatments of a Bulgarian lignite, Maritza-Iztok. The degree of global desulphurization and the changes of the calorific values are reported. Also a first attempt is performed to interpret the changes in the sulphur functionalities as determined by AP-TPR. For some desulphurized products,

the possible contribution of pyrite reduction to the H₂S profiles is not always clear, confirming the need for the control for effective pyrite removal, before a final assignment and quantification are possible.

2. Experimental

2.1. COAL SPECIES

The lignite sample used, was obtained from M. Iztok deposit in Bulgaria [(wt % daf) C 59.8 %, S_t 4.17 % (S_p 1.56, S_s 1.00, and S_{org.} 1.61), H 6.4 %, N 0.7 %, O (diff) 28.93 %]. The proximate analyses and other characteristics are given in Table 1.

2.2. TREATMENTS

The desulphurization treatments are described in literature and only a brief outline is given below.

2.2.1. Hydrothermal Treatment. ⁽¹⁵⁾ These experiments were carried out in an autoclave of 500 ml capacity, fitted with a temperature regulator, a pressure gauge and a thermocouple. Sodium hydroxide (4 g) and CaO (1 g) were dissolved in 150 ml of water and placed in the autoclave. To this solution 20 g dry, raw coal was added and the slurry was thoroughly mixed. The autoclave was closed and heated to 200 °C with a reaction pressure of 1.66 Mpa. The autoclave was kept at this temperature and pressure for 1 h to complete the reaction and then cooled to 50 °C.

After opening the autoclave, the mixture was acidified with 1 M HCl to pH 4-5 and distilled with water vapour. Next the mixture was washed with hot distilled water (4-8 l) and centrifuged. The treated coal was then dried under vacuum at 90 °C for 48 h (method A).

2.2.2. Treatment with sodium alkoxide. ⁽¹⁶⁾ The organometallic compound was made by adding 1 g sodium metal, in a round bottom flask under inert atmosphere, to 200 ml n-BuOH, which was magnetically stirred at ambient temperature for 1 h to ensure complete dissolution. The dry raw coal sample (20 g) was added to this solution and the mixture was refluxed under nitrogen atmosphere, for 20 min. In the next step, the mixture was acidified with 1 M HCl to pH 4-5 and the mixture was distilled with water vapour. The mixture was then washed with hot distilled water (4-8 l) and centrifuged. The treated product was then dried under vacuum at 90 °C for 48 h (method B).

2.2.3. Metallation followed by protonation. ⁽¹⁷⁾ Metallation was performed by adding 5 g dry raw coal to 100 ml dry THF and 50 ml tetramethylethylenediamine in a round bottom flask under nitrogen atmosphere. After cooling with liquid nitrogen, this solution was slowly added to 100 ml BuLi/hexane 15 % and stirred for 2 h. In the next stage, 25 ml nBuOH was added and the mixture was stirred for 3 h at ambient temperature under nitrogen atmosphere. Thereafter the mixture was acidified with 1 M HCl to pH 4-5 and distilled with water vapour. Then the mixture was washed with hot distilled water (4-8 l) and centrifuged. The resultant product was then dried under vacuum at 90 °C for 48 h (method C). The sequence of acidification and the steam distillation has also been reversed and this treatment is designated as method D.

2.2.4. Molten caustic. ⁽¹⁰⁾ A modified treatment to that in ref. 10 was used. The lignite was treated with molten (non-aqueous) caustic at 360 °C for 20 min. These experiments were carried out in a stirred autoclave. First 200 g of a 50/50 wt % mixture of NaOH / KOH was heated up to 360 °C, while nitrogen gas was swept constantly through the reactor. Thereafter 40 g of the raw, dry coal sample was introduced quantitatively also under nitrogen atmosphere. The coal reacts then for 20 min and after dilution with water, the reaction products were transferred to a glass filter and the filter cake was washed three times with hot water to remove the caustic. During each wash process the coal product was stirred for 30 min in hot water at 80 °C and then filtered. The desulphurized coal was dried at 50 °C under nitrogen gas before being analysed (method E).

In addition to obtain a raw coal free of ash and pyrite, HF extractions were performed of the lignite. The raw coal was demineralized with 40 % HF at 60 °C, according to the procedure of Bishop and Ward ⁽¹⁸⁾. Before and after HF treatment the coals were treated with 12 M HCl (method F).

2.3. CHARACTERIZATION

2.3.1. Elemental, proximate and ultimate analyses. Moisture, ash, total sulphur and the calorific value were analysed with the classical ASTM methods D3173, D3174, D3175 and D2015 respectively ⁽¹⁹⁾ and TG standard methods ⁽²⁰⁾.

2.3.2. Atmospheric pressure temperature programmed reduction (AP-TPR). The reactor used in this study, being made completely out of glass (fig. 1), is different to that used previously ⁽¹⁰⁻¹²⁾. The upper part comprises borosilicate glass in order to secure the sealing. The lower part is of quartz glass, so that the reduction of a sulphur compound can be executed up to 1000 °C. As no differences are found with and without a preheated carrier gas stream, the carrier gas - pure hydrogen - is no longer preheated and is let directly into the reaction mixture. (It was found that pure hydrogen leads to better reduction characteristics than a 5 % H₂ / 95 % Ar mixture.) The flow is held constant on 75 ml/min during the whole experiment, and is controlled regularly by a callibrated flow meter. All experiments were recorded at a heating up rate of 5 °C/min during the whole temperature range. A further improvement in comparison with the previous reactor is the presence of a collector, nearby the top of the reactor. The function of the collector is to prevent the reducing solvent mix returning into the reactor part. If it returns, tar will be formed, leading to retrogressive reactions including the conversion of sulphides into more complex structures. This results in very poor sulphur balance and additional signals due to secondary reactions.

The inner glass tube is made in such a way that the internal free volume is as small as possible. The small internal volume is needed to optimize the continuous contact between sample, reducing solvent mix and reducing gas stream. Also a better control and faster transport of the carrier gas from the reactor to the detector is possible.

In the same context, it is found that the use of make-up gas is no longer necessary. The fix place connection of the thermocouple on the reactor is undoubtedly very important. This reactor is considered to be vastly superior to the previous set-up ^(10,11).

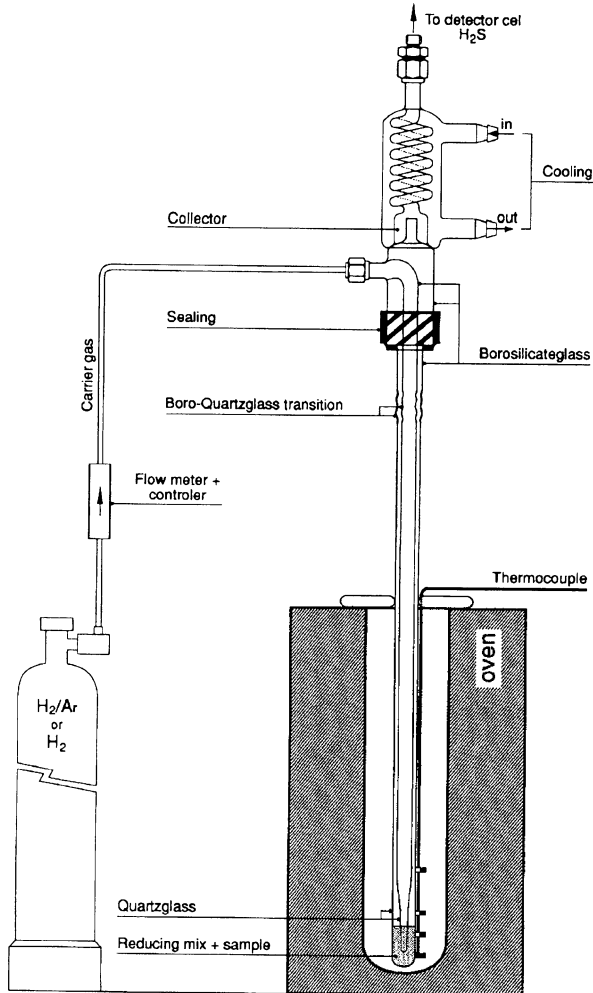


Fig. 1. Total reactor set-up

3. Results and discussion

After HF extraction, the lignite is nearly ash free (see TGA fig. 2a -b). In addition the presence of pyrite in the treated sample is studied by means of SEM-EDX. The coals are mounted on an aluminium stub and coated with carbon. No pyrite particles are found in the treated coal sample (method F), and in addition the iron/sulphur ratio, which strongly varies for the raw coal, is close to zero for the HF extracted coal sample.

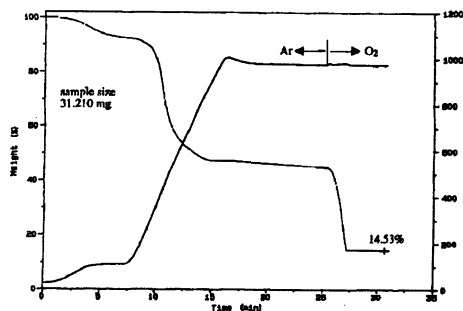


Fig. 2a. TGA plot of raw lignite flow 100 ml/min. Ar or O₂

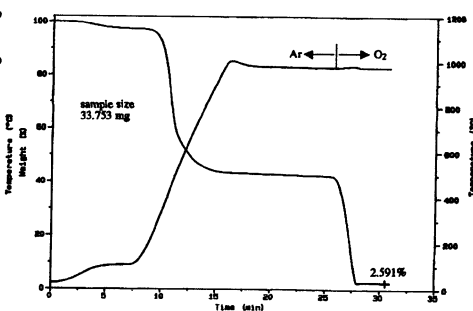


Fig. 2b. TGA plot of desulphurized lignite (method F) flow 100 ml/min. Ar or O₂

The results for the desulphurization are reported in Table 1.

Table 1 : Analysis and calorific values of samples desulphurized with different methods.

	Raw coal	method A	method B	method C	method D	method E
Moisture wt %	7.5	4.5	6.5	4.6	4.2	4.2
Ash wt %	14.5	15.7	5.3	8.1	2.4	2.6
Volatile matter wt %	47.5	41.1	50.3	54.6	59.9	43.7
Fixed carbon (wt % daf)	39.1	48.9	42.9	37.3	35.8	53.1
Calorific value (daf) (cal/g)	6092	6780	5826	6773	6566	7452
Recovery (%) (* = daf)	100.0 (78.0*)	63.5 (50.6*)	80.0 (70.6*)	90.0 (84.0*)	64.0 (55.8*)	42.0 (39.1*)
S _t (wt % daf)	4.17	3.14	2.99	2.34	1.90	0.64
ΔS (%)	0.0	- 24.7	- 28.3	- 43.9	- 54.4	- 84.6

With method A and B only a slight desulphurization is obtained (24.7 - 28.3 %). Looking at the high ash content (15.7 %) for the treated sample from method A, there is probably some incorporation of CaO during this treatment. From previous studies (15-16) it is shown that pyritic and sulphate sulphur are removed to an extent of 90 % or more

under these conditions. For method C and D a higher level of desulphurization is obtained (43.9 → 54.4 %). The reversed wash procedure seems to increase the desulphurization. This effect requires further study together with the reaction mechanisms of the desulphurization. For method E, the level of a desulphurization is 84.6 %. It is clear that the treatment with molten caustic can remove both inorganic and organic sulphur.

Table 1 lists also the calorific values (on daf basis) of the treated samples. It is however clear that besides the sulphur removal also, the calorific heat recovery is an important parameter. Treatment E causes, beside a large desulphurization (84.6 %) also a strong decrease of organic matter (78.0 → 39.1 %). On the other hand the calorific heat value on daf basis is also strongly increased (+22 %) so that in view of possible applications both the sulphur removal as well as the calorific recovery should be investigated for each treatment.

AP-TPR profiles of the several treated samples are shown in fig.3 a, b, c, d, e and f. The full line is always the raw, untreated coal and the dotted line represents the corresponding treated samples. Although the AP-TPR are recorded until 1000 °C, the profile above 600 °C is dubious in nature, as has been demonstrated in previous studies, because the presence of the reducing mix can cause anomalies in this temperature region. Therefore only the temperature region up to 600 °C is discussed here. The recoveries are expressed in mg S/g sample on the profiles. Values of peak temperatures are given in °C on the figures.

It is clear that for the HF extracted coal (fig. 3a) the peak at 570 °C has disappeared in comparison with the raw coal. This suggests that the signal at 570 °C should be assigned to pyrite.

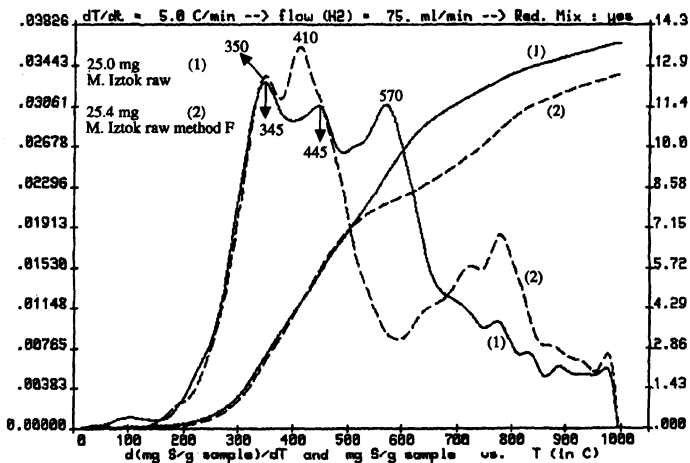


Fig. 3a. AP-TPR analysis of the desulphurized lignite (method F) in comparison with the AP-TPR analysis of the raw lignite

The TPR profile of the hydrothermal treated sample is reported in fig. 3b. Again the peak at 570 °C disappears together with a decrease of the signals around 345 °C. From previous studies (10,11,15) it is known that pyrite is removed under these experimental conditions. In addition the decrease of the signal at 345 °C can probably be attributed to the thermal labile sulphur containing groups like aliphatic and aromatic thiols (low temperature shoulder) and aliphatic mono and disulphides (peak).

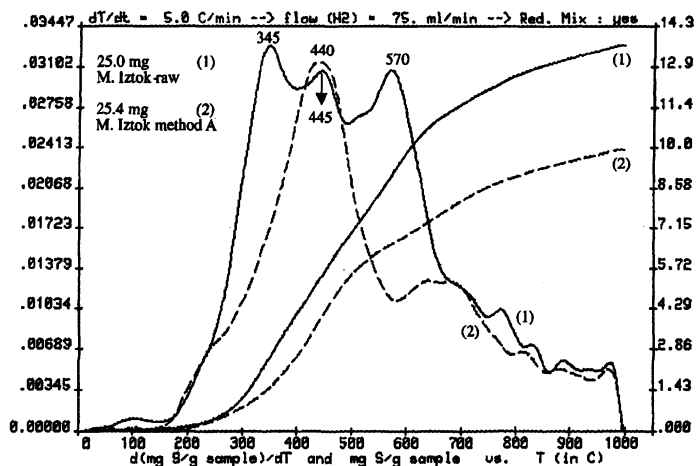


Fig. 3b. AP-TPR analysis of the desulphurized lignite (method A) in comparison with the AP-TPR analysis of the raw lignite

This is also in good agreement with previous analysis⁽¹⁰⁾. The low temperature region of the signal at 445 °C (raw coal) can be attributed to mixed aromatic aliphatic sulphides and the peak to aromatic sulphides⁽¹⁴⁾. The low temperature shoulder of the pyrite signal at 570 °C can be assigned to aromatic disulphides⁽¹⁴⁾.

For method B (fig. 3c), a higher yield in detectable sulphur is obtained for the desulphurized sample (28.3 %) than for the raw coal together with this increase, the signal in the region at 345 °C is increased. A possible explanation for these results might be that due to treatment B, these sulphur groups are now more accessible for the AP-TPR but are not desulphurized at this stage. As Maritza Iztok is a low rank coal it is logical that the contribution of the reduction to the H₂S profile of the original present groups, occurs at low temperature (345 °C) indicating the presence of aliphatic and aromatic thiols, aliphatic sulphides and disulphides. This hypothesis of the increased porosity of the treated sample will be further investigated with the use of SEM-EDX and burning profiles.

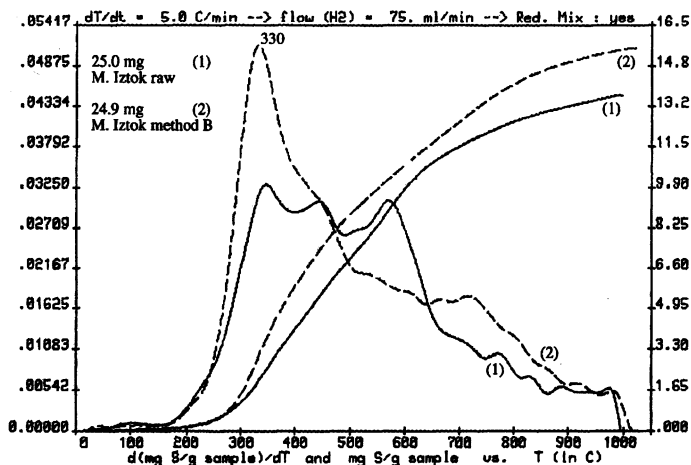


Fig. 3c. AP-TPR analysis of the desulphurized lignite (method B) in comparison with the AP-TPR analysis of the raw lignite

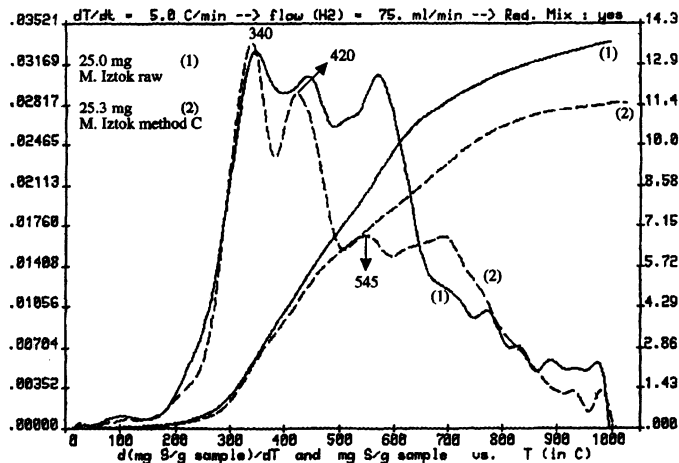


Fig. 3d. AP-TPR analysis of the desulphurized lignite (method C) in comparison with the AP-TPR analysis of the raw lignite

The TPR profiles of the treated samples from methods C and D are represented in fig. 3d and 3e, respectively. These treatments cause a cleavages of sulphur bridges and sulphur ether groups, resulting in new thiols aliphatic as well as aromatic, which can be, eventually, further desulphurized. It is thus logical that the TPR profiles for both have a significant signal in the lower temperature region (345 °C) and a less pronounced signal

starting from 450 °C. That the intensity is lower for the sample treated with method D versus method C is logical because of an increased desulphurization.

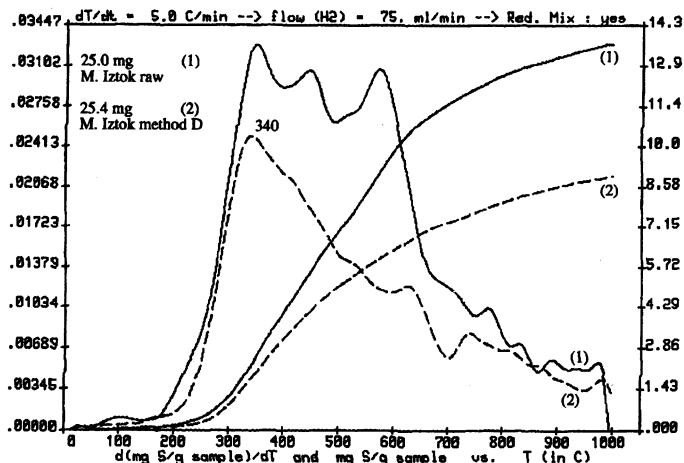


Fig. 3e. AP-TPR analysis of the desulphurized lignite (method D) in comparison with the AP-TPR analysis of the raw lignite

When the lignite is treated with molten caustic a virtually desulphurization is obtained (84.6 %) and consequently much less pronounced TPR signals are obtained in comparison with the raw coal (fig. 3f).

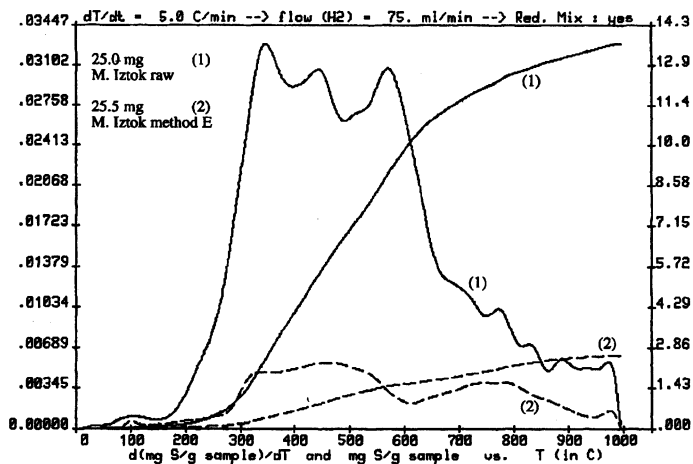


Fig. 3f. AP-TPR analysis of the desulphurized lignite (method E) in comparison with the AP-TPR analysis of the raw lignite

4. Conclusions

It is demonstrated that selective desulphurization can be followed by AP-TPR. In addition, it is possible to assign some of the signals to sulphur containing functionalities. Although for some experiments the degree of pyrite removal must be confirmed, the observed trends in the TPR profiles of the desulphurized products can be explained in view of these selective desulphurization treatments.

The product obtained after the treatment with the molten caustic is nearly completely desulphurized (organic and inorganic), and the calorific value is considerable higher on daf basis. This higher calorific value compensates for the low organic recovery (39 % on daf basis).

5. Acknowledgement

The authors like to thank Miss Martine Vanhaemel for the technical help with several experiments. This work was supported by the European Community through the Go-East Go-West program.

6. References

1. T.D. Wheelock, in *Physical Cleaning of Coal* (Ed. Y.A. Lin) Marcel Dekker, New -York USA, (1982).
2. S.R. Kelemen, G.N. George and M.L. Gorbaty, *Fuel*, 1990, **69**, 939.
3. D.C. Frost, B. Wallbank and W.R. Leeder, in *Analytical Methods for Coal and Coal Products* (Ed. C. Karr Jr), Academic Press, New York, Vol. I. pp. 349-376, (1978).
4. J.P. Boudou, J. Boulegue, L. Malechaux, M. Nip, J.W. de Leeuw and J.J. Boom, *Fuel*, 1987, **66**, 1558.
5. G.P.Huffman, F.E. Huggins, S. Mitra, N. Shah, R.J. Pugmire, B. Davis, F.W. Lytle and R.B. Greegro, *Energy & Fuels*, 1989, **3**, 200.
6. M.L. Gorbaty, G.N. George and S.R. Kelemen, *Fuel*, 1990, **69**, 945.
7. M. Kasrai, J.R. Brown, G.M. Bancroft, K.H. Tan and J.M. Chen, *Fuel*, 1990, **69**, 411.
8. J.R. Brown, M. Kasrai, G.M. Bancroft, K.H. Tan and J.M. Chen, *Fuel*, 1992, **71**, 649.
9. R.B. LaCount, D.G. Kern, W.P. King, R.B. LaCount Jr., D.J. Miltz Jr., A.L. Stewart, T.K. Trulli, D.K. Walker and R.K. Wicker, *Prep. Pap. Am. Chem. Soc. Div. Fuel Chem.*, 1991, **33** (3), 1217.
10. B.B. Majchrowicz, D. Franco, J. Yperman, G. Reggers, J. Gelan, H.J. Martens, J. Mullens and L.C. Van Poucke, *Fuel*, 1991, **70**, 434.
11. B.B. Majchrowicz, J. Yperman, J. Mullens and L.C. Van Poucke, *Anal. Chem.*, 1991, **63**, 760.
12. J. Mullens, J. Yperman, R. Carleer, D. Fanco, L.C. Van Poucke and J. Van der Biest, *Applied Clay Science*, 1993, **8**, 91.
13. C.E. Snape and C.J. Lafferty, *Prep. Am. Chem. Soc. Div. Fuel Chem.*, 1990, **35** (1), 1.
14. K. Ismail, R. Garcia, S.C. Mitchell, C.E. Snape, A. C. Buchanan^{III}, P.F. Britt, D. Franco and J. Yperman, *Proc. Inter. Conf. Coal Sci.*, Banff Canada, (1993).

15. B. Sain, P.C. Saika, B.P. Buruah, C.S. Bordoloi and B. Mazumder, Fuel, 1991, **70**, 753.
16. B. Mazumder, P.C. Saikia, B. Sain, B.P. Baruah and C.S. Bordoloi, Fuel, 1989, **68**, 610.
17. L. Lazarov, S.P. Marinov, M. Stefanova and G. Angelova, Proc. Inter. Conf. Coal Sci., Moulijn J. A., et al. Eds.; Elsevier : Amsterdam, pg. 745, (1987).
18. M. Bishop and D.L. Ward, Fuel, 1958, **37**, 191.
19. ASTM, Annual Book of ASTM Standards, Part 26, Coal and Coke, (1979).
20. S. St. J. Warne, Trends in Analytical Chemistry, 1991, **10**, no 6.

**ORGANIC GEOCHEMICAL CHARACTERIZATION OF SOME
CARBONIFEROUS COAL SEAMS OF THE ZONGULDAK BASIN
(NW TURKEY)**

M. N. YALÇIN

*University of Istanbul, Faculty of Engineering,
TR-34850 Avcılar, Istanbul, Turkey*

and

*TÜBİTAK Marmara Research Center
Research Institute for Basic Sciences
Department of Earth Sciences,
P.O.Box 21, TR-41470 Gebze, Turkey*

ABSTRACT. The Carboniferous clastic sequence of the Zonguldak Basin contains several coal seams that have been mined since 1848 as the only major bituminous coal deposit of Turkey. Recently, a study was initiated aimed at determining the coalbed methane potential of the basin. Within the framework of this study, in addition to coal geology and numerical basin modelling, organic geochemical methods have been used to define the relevant properties of the coals. The coal seams are located in a Namurian to Westphalian D progradational delta and fluid plane sequence. This sequence was originally up to 3500 m thick prior to being eroded during two major uplift periods caused by the Hercynian and Alpine orogenic movements. There exists up to 8 coal seams in Namurian, 20 to 26 in Westphalian A and up to 8 coal seams in Westphalian B,C and D.

Geochemical analysis were carried out on 42 coal samples from wells and mines. The procedures applied includes total organic carbon (TOC) determination, Rock-Eval pyrolysis, proximate and elemental analysis and organic petrography. Additionally, kinetic parameters of bulk hydrocarbon generation from coal were determined by open-system non-isothermal pyrolysis. The majority of the coals in the Zonguldak basin are typical humic coals of high volatile C to A bituminous rank. Vitrinite reflectance values in general vary between 0.55 and 1.20 % (R_o mean). However, data from a recent deep test well showed that the maturity of the coals at the base of the Westphalian A can increase up to 1.45 % (R_o mean). Further details of the type, maturity, maceral composition, hydrocarbon generation potential of the coals and relations between various geochemical parameters are presented.

1. Introduction

Coal seams of the Carboniferous Zonguldak Basin have been the subject of great interest because they have been mined for more than 100 years as the only major bituminous coal deposits of Turkey. Consequently, several studies on the geology, tectonics, palynology and mining engineering aspects exist⁽¹⁻³⁾. However, studies on the organic geochemical properties of the coal seams are limited to only some organic petrographical investigations⁽⁴⁻⁸⁾.

Within the frame of a research project aimed at determining the coalbed methane potential of the Zonguldak Basin⁽⁹⁻¹³⁾ coals were also investigated for some of their geochemical properties. The aim of this paper is to present the results of the organic geochemical analysis of the Zonguldak coal seams.

2. Geological Setting

The Zonguldak Basin is located in NW Turkey on the Black Sea coast (Fig.1). The coal seams are located in a thick Carboniferous (Namurian to Westphalian D) clastic sequence, which lies on a platform type limestone unit of Visean age (Yılanlı Fm).

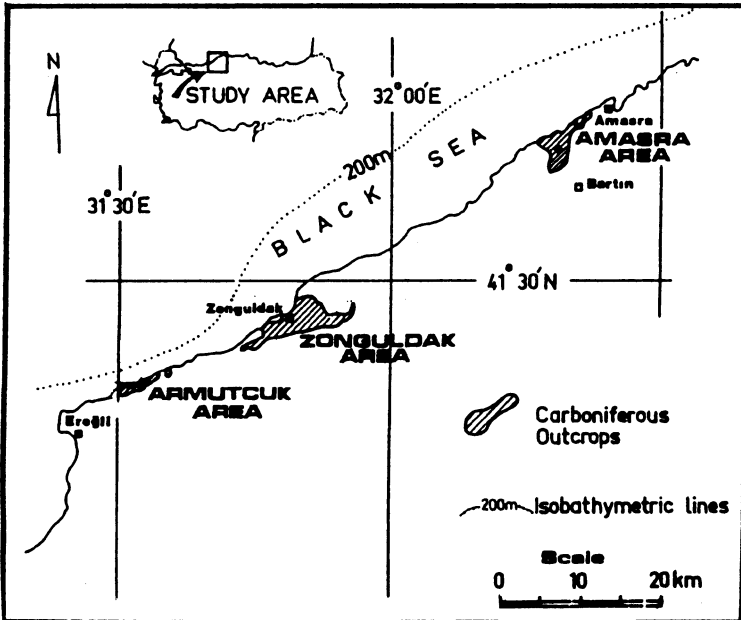


Figure 1. Location map of the Zonguldak Basin (modified from Yalçın et al.⁽¹³⁾)

As a result of uplift and erosion on the northern margin of the area the carbonate platform was converted to a molasse type basin where first a progradational delta and then a fluid plane sequence was deposited. Within this very thick clastic sequence 3 rock-stratigraphic units are differentiated. The Namurian Alacağzı formation consists of prodelta fine clastics and towards the upper parts some coal seams. The Westphalian A deltaic unit (Kozlu Fm) is composed mainly of sandy lithologies and bears most of the coal seams. The Upper Westphalian (Westphalian B to D) unit (Karadon Fm) is composed of by fluid plane deposits mainly by coarse clastics with few coal seams. There exits up to 8 coal seams in the Namurian, 20 to 26 in the Westphalian A and up to 8 coal seams in the Westphalian B,C and D. But, due to the lateral changes in seam thickness and extension and due to erosion, the number and combined thickness of coal seams change considerably.

The Carboniferous sequence is overlain by different units with an angular unconformity. While the Upper Permian-Lower Jurassic continental Çakraz Formation and the Upper Jurassic carbonates of the İnalı Formation have only a limited extension mainly in the eastern part of the basin, units of the Lower Cretaceous - Eocene sedimentary cycle are found almost in the entire study area (Fig.2). Shallow marine clastics (İncüvez Fm) and carbonates (Zonguldak Fm) are the basal units of this sedimentary cycle. Çağlayan Fm represents the transition to a deeper marine depositional environment. Flysch type deposits and pyroclastics of the Yemişliçay formation indicate the culmination of deepening. Sedimentation continued with detrital shelf type deposits of Maastrichtian, Paleocene and Eocene age. In some parts of the basin all these units have been totally eroded during the uplift-erosion period which began at Late Eocene and is still continuing at present.

3. Samples and Methods

Geochemical analysis were carried out on 42 coal samples which were obtained either as cores from wells or as outcrop samples from mines. The majority of the coal samples belong to Westphalian A Kozlu Formation. Few samples are from Namurian Alacağzı Fm. and from Upper Westphalian Karadon Fm.

Total Organic Carbon (TOC) concentrations and Rock-Eval pyrolysis parameters were determined using LECO TOC-analyser and a Rock-Eval II instrument, respectively. Polished sections of coals are used to measure vitrinite reflectance values (R_o %) and on 7 selected samples maceral analysis (500 points) has been carried out. The proximate analysis of the coal samples were carried out according to well established procedures given by ASTM standards. Elemental analyses of 15 selected samples were performed by Carlo Erba Mod 1106 Elemental Analyzer where hydrogen, carbon and nitrogen contents were measured and the oxygen values were determined by the difference.

4. Results and Discussions

Moisture, volatile matter, ash and fixed carbon contents were determined on air dried samples. Respective values are listed in Table-1 where values of volatile matter, ash and fixed carbon are given on dry coal basis. Moisture content of the coals range between 0.52 and 4.90 % which is relatively low. This can be explained by the fact that most of the coal samples are stored in atmospheric conditions for a long time prior to the analysis. Ranges of volatile matter, ash and fixed carbon are 20.27 % to 44.07 %, 3.68 % to 29.78 % and 42.54 % to 72.19 %, respectively. High ash content and low fixed carbon values of some samples are in general due to the impurities. The majority of the measured properties are within the range of high volatile bituminous coals ⁽¹⁴⁾.

Elemental analysis were carried out on 15 selected coal samples. A diagram of H/C atomic ratio vs the O/C atomic ratio (van Krevelen diagram) is shown in Fig.3. The evolution pathway of the elemental composition of humic coals with increasing coalification taken from Bertrand ⁽¹⁵⁾ and of Type III kerogen are also superimposed on the diagram. Although some of the relatively mature samples are located in the area of low coalification a fit is in general ensured.

Total organic carbon (TOC) values for 42 coal samples range from 50.0 % to 82.7 %. TOC and fixed carbon values are plotted in Fig. 4 to test a possible correlation between them. From Fig. 4 only a rough correlation can be observed.

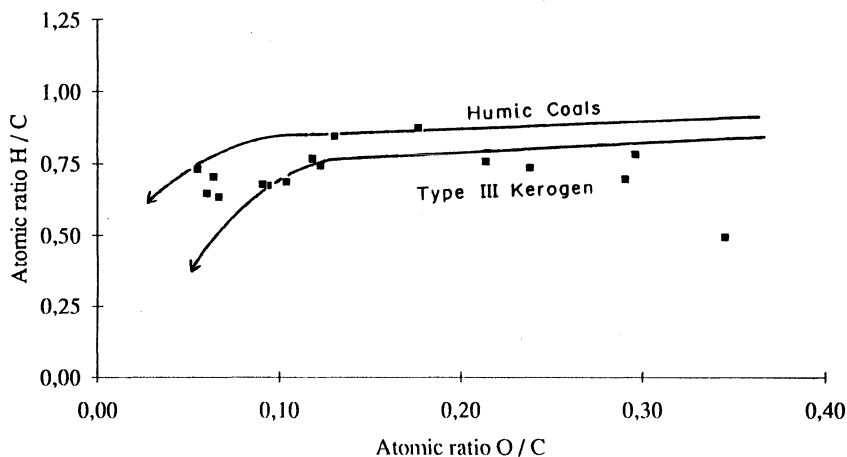


Figure 3. Van Krevelen diagram showing the position of some Zonguldak coals. Evolution pathway of the humic coals after Bertrand ⁽¹⁵⁾ and of Type III kerogene are indicated by the solid line curves.

Table 1. Proximate analysis results of Zonguldak coal seams. Nam = Namurian, W_A = Westphalian A; W_C = Westphalian C. (O) on original air dried coal, (d) on dry coal.

Sample No	Unit	Moisture(o) (%)	Volatile M.(d) (%)	Ash(d) (%)	Fixed C(d) (%)	Cal. Val. (Kcal/kg)
YBL-1	W _A	1,66	31,95	11,36	56,69	7371,1
YBL-2	W _A	1,65	28,89	5,17	65,94	7510,4
YBL-3	W _A	1,45	31,92	8,19	59,19	7267,5
YBL-4	Nam	1,14	33,09	5,69	61,22	7927,2
YBL-5	W _A	1,52	35,64	4,99	59,37	7824,3
YBL-6	W _A	1,70	33,55	7,13	59,32	7560,0
YBL-7	W _A	1,47	36,42	18,8	44,78	6069,5
YBL-8	W _A	1,06	33,3	4,98	61,72	7816,2
YBL-9	W _A	1,10	35,29	3,68	61,02	8144,8
YBL-10	W _A	1,14	32,82	7,47	59,71	7835,3
YBL-11	W _A	0,97	36,31	4,43	59,26	7916,9
YBL-12	W _A	0,78	31,51	20,49	48,00	6307,6
YBL-13	W _A	1,08	28,71	26,32	44,97	5656,6
YBL-14	W _A	0,74	20,27	29,78	49,95	5759,8
YBL-15	W _A	0,80	26,64	4,22	69,14	8292,4
YBL-16	W _A	0,69	25,43	6,11	68,46	7969,4
YBL-17	W _A	0,85	28,46	5,48	65,86	8057,1
YBL-18	W _A	1,45	29,49	5,32	65,19	8020,0
YBL-19	W _A	0,71	28,57	9,88	61,55	7341,2
YBL-20	W _A	0,52	22,53	5,28	72,19	8092,9
YBL-21	W _A	1,38	29,33	20,2	68,65	8354,0
YBL-22	W _A	0,83	24,47	5,88	69,65	8071,0
YBL-23	W _A	0,90	26,86	13,48	59,66	6950,8
YBL-24	W _A	1,22	22,22	37,3	40,48	4860,2
YBL-25	W _A	1,52	25,79	8,68	65,53	7582,6
YBL-26	W _A	0,52	21,85	12,15	66,00	7531,9
YBL-27	W _A	1,21	20,29	26,73	52,35	6231,3
YBL-28	W _A	0,70	26,78	14,74	58,48	6096,3
YBL-29	W _A	1,02	30,18	6,62	63,20	7884,0
YBL-30	W _A	0,92	24,85	5,42	69,73	8291,7
YBL-31	W _A	0,94	21,53	21,92	56,92	6723,3
YBL-32	Nam	0,74	23,42	8,27	68,31	7910,0
YBL-33	W _A	1,45	30,88	4,16	64,96	7980,3
YBL-34	W _C	2,31	32,20	12,96	54,84	6886,9
YBL-35	W _A	2,75	35,95	4,75	59,30	7495,4
YBL-36	W _C	4,40	38,37	4,65	56,98	7027,0
YBL-37	W _C	4,06	37,03	15,40	47,57	6456,2
YBL-38	W _C	4,70	32,48	13,26	54,26	63,83,1
YBL-39	W _C	4,90	35,76	7,38	56,86	6920,6
YBL-40	W _C	4,78	36,65	10,59	52,76	6743,6
YBL-41	W _C	3,64	44,07	13,39	42,54	6350,0
YBL-42	W _C	3,58	34,22	20,88	44,90	5582,2

Rock-Eval measurements performed after Espitalie et al. ⁽¹⁶⁾ allowed the evaluation of various geochemical aspects. Typing of Zonguldak coals with the help of an HI - OI diagram (a van Krevelen diagram based on Rock-Eval analysis) is represented in Fig. 5. Whereas the Hydrogen Index values are within the range of normal humic coals, the Oxygen Index values are remarkably low. Thompson et al. ⁽¹⁷⁾ pointed out that the coals of coastal plain environments of Indonesia have hydrogen indices often above 300 and oxygen indices usually below 15 and therefore different from coals of North-West Europe. That the low oxygen indices of Zonguldak coals can be explained by this organic facies aspect requires further investigations.

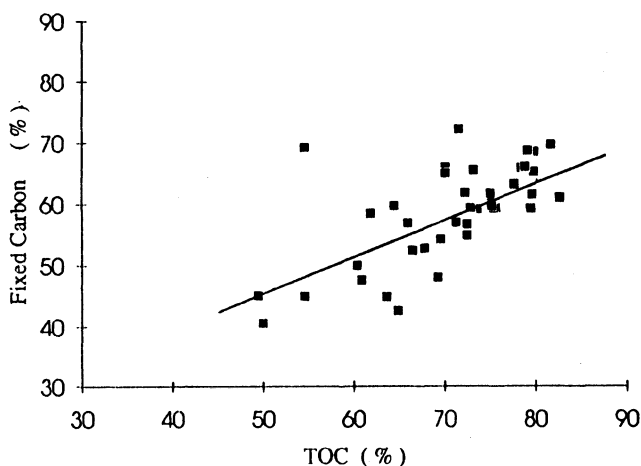


Figure 4. Correlation between Fixed Carbon and TOC values

From the Rock-Eval pyrolysis data, both the Rock-Eval pyrolysis temperature (T_{max}) and the Hydrogen Index may be considered as maturity indicators ⁽¹⁸⁾. When T_{max} increases the Hydrogen Index has to decrease. This is true for organic matter of types I and II, but not completely true for type III as shown by Durand and Paratte ⁽¹⁹⁾ on coals. They showed that the hydrogen indices increase with the maturity up to a level around 435-440 °C T_{max} , so that less mature coals have lower hydrogen indices. This phenomenon is explained by the fact that during pyrolysis the quantities of hydrogen transformed into water and carbon transformed into carbondioxyde are higher than during the natural coalification process. Although not very obvious a similar trend can also be observed in Zonguldak coals (Fig. 6).

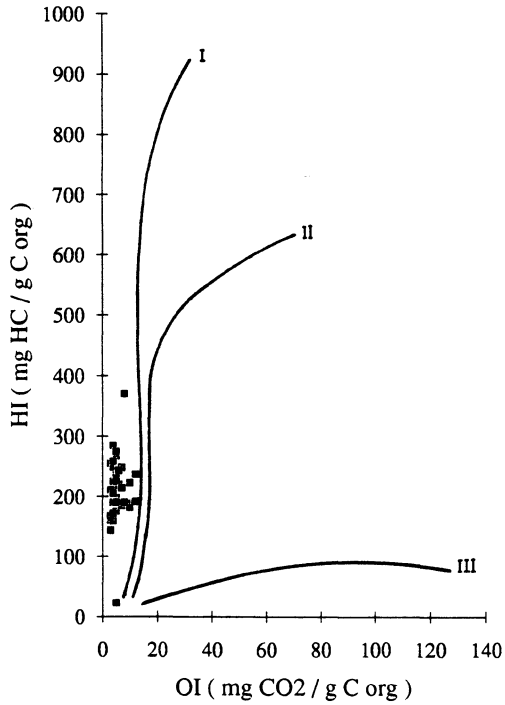


Figure 5. Rock-Eval Hydrogen Index (HI) vs Oxygen Index (OI) diagram of Zonguldak coals. Pathways of different kerogen types are included for comparison reasons.

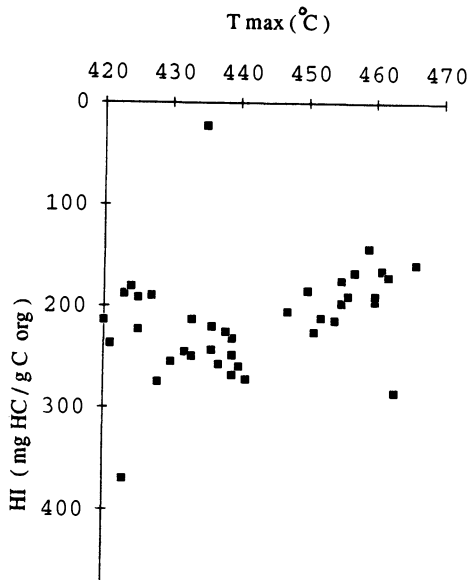


Figure 6. Correlation between Tmax and Hydrogen Index (HI)

Within the frame of a study aiming to model the gas generation in Zonguldak coals⁽¹³⁾ an open system pyrolysis at heating rates of 0.1, 0.7 and 5.0 K/min was performed with the furnace setup described by Schaefer et al.⁽²⁰⁾. A low maturity coal (YBL-36) was used for pyrolysis. In order to determine the kinetic parameters of bulk hydrocarbon generation in Zonguldak coals, the mathematical model described by Schaefer et al.⁽²⁰⁾ was utilized. This model is based on the kinetic analysis of bulk hydrocarbon formation rate (dM / dT) versus temperature (T) curves assuming $n=25$ first order parallel reactions with activation energies E_i regularly distributed between 46 and 70 kcal/mol and a single pre-exponential factor. A total number of 26 parameters, namely 25 initial potentials in combination with 25 activation energies and a pre-exponential factor A are optimized using a special method which compares measured and calculated formation rates until the corresponding error function presents a well-defined absolute minimum⁽²⁰⁾. The pyrolysis curves computed with the determined kinetic parameters and the input data are shown in Fig. 7 with solid and dotted lines, respectively. The fit between these two curve sets is almost perfect. Hence, the optimization may be considered successful and the kinetic parameters shown in Fig. 8, as the hydrocarbon generation potential vs activation energy distribution, are representative.

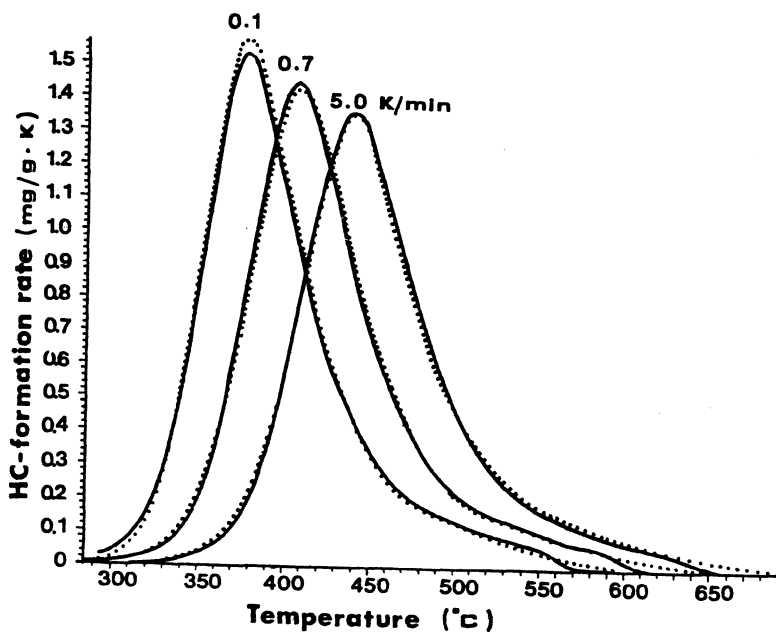


Figure 7. Rates of bulk hydrocarbon generation obtained by the pyrolysis at three different heating rates (dotted lines) and the calculated values (solid lines). The calculation is carried out with the activation energy distribution presented in Fig. 8 (from Yalçın et al.⁽¹³⁾)

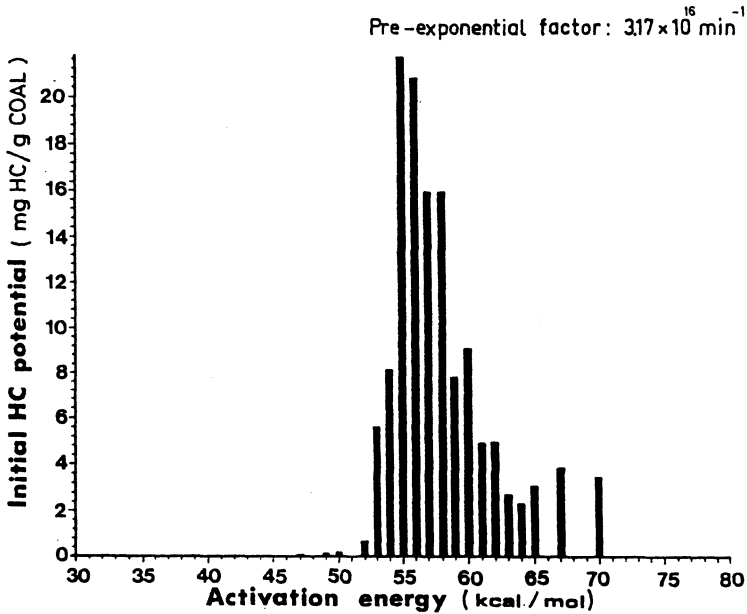


Figure 8. Hydrocarbon generation potential vs activation energy for Zonguldak coal (from Yalçın et al.⁽¹³⁾)

Organic petrographic analysis were carried out to determine the coal rank by measuring the vitrinite reflectance ($\% R_o$) and to define the petrographical composition by maceral analysis. The latter is carried out by 7 selected samples. For another additional 10 samples the ratio of maceral groups are determined semiquantitatively by visual observation. Respective values are listed in Table-2. As shown in (Fig.9) Zonguldak coals can be classified as typical humic coals. Vitrinite reflectance data indicate a very scattered distribution ranging from 0.45 $\% R_o$ to 1.14 $\% R_o$. It is difficult to derive a depth - maturity trend when all measurements are considered. This is an expected phenomenon since the investigated coal seams are effected by erosional periods in very different ways.

If only one particular well or a small area is considered an obvious depth - maturity trend can be observed. This is also confirmed by the maturity values obtained from a recent deep well (Fig. 10). Here, the coals at the base of Westphalian A unit have a rank of 1.45 $\% R_o$ at a depth of 1720 m.

Table 2. Petrographic data of Zonguldak coals. V=vitrinite, I=inertinite, L=liptinite.
 (*) indicates samples where percentages of V,I and L are determined semiquantitatively.

Sample Nr.	Overall Composition(%)			Vitrinite Reflectance (% R_o)
	V	I	L	
YBL-1*	75	7	18	0.75
YBL-3	64	22	14	0.83
YBL-4*	60	14	26	0.86
YBL-5	46	30	24	0.72
YBL-7*	68	22	10	0.81
YBL-8*	73	12	15	0.87
YBL-9*	75	20	5	0.82
YBL-10*	70	12	18	0.75
YBL-11	55	33	12	0.76
YBL-14	53	37	10	0.99
YBL-21*	70	15	15	0.92
YBL-22*	68	25	7	1.12
YBL-23*	57	32	11	0.92
YBL-24*	65	20	15	0.94
YBL-25	57	21	22	0.80
YBL-27	76	14	10	1.04
YBL-36	70	8	22	0.50

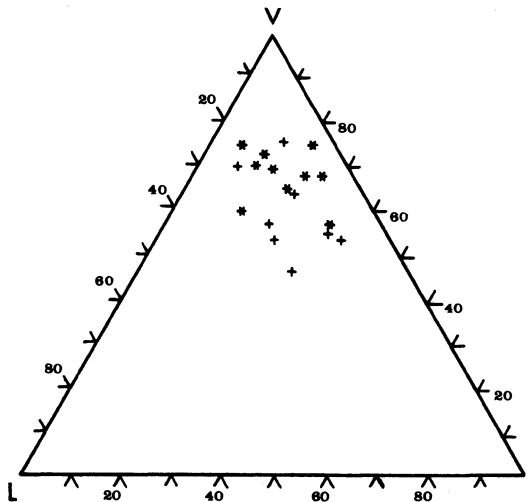


Figure 9. Triangular diagram showing petrographic composition of Zonguldak coals.
 (*) indicates samples analyzed semiquantitatively.

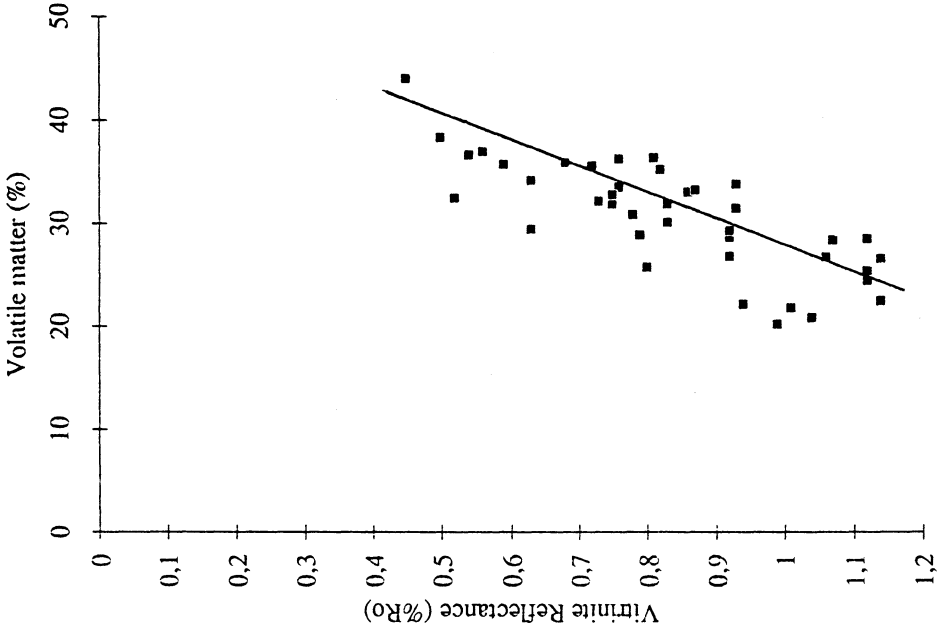


Figure 11. Correlation between vitrinite reflectance and volatile matter

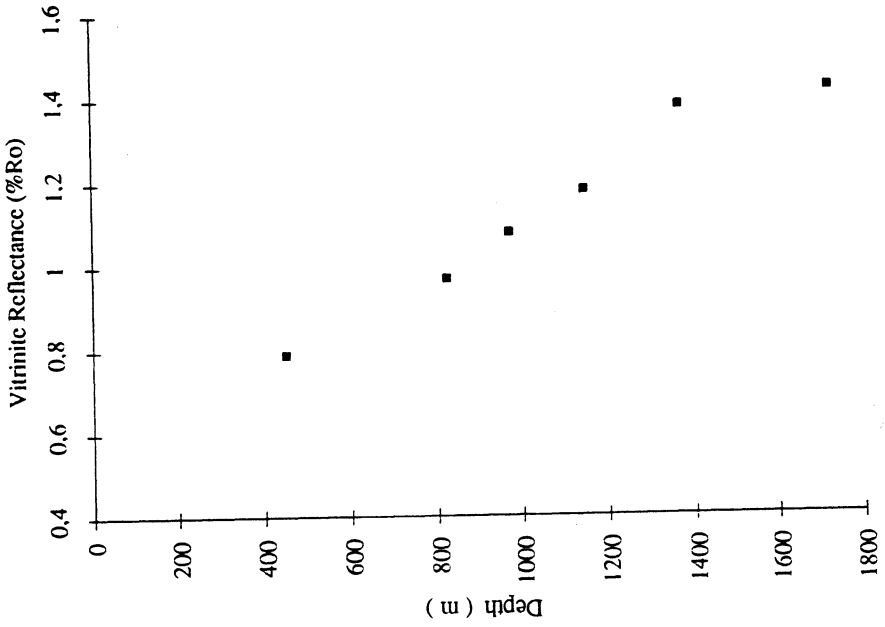


Figure 10. Vitrinite reflectance vs depth in the well K20/G

The measurement of vitrinite reflectance, which is probably the most reliable indicator of coal rank enable a comparison with other maturity parameters such as volatile matter, Rock - Eval Tmax and despite of the already mentioned limitations the Hydrogen Index. For this purpose diagrams of these parameters vs vitrinite reflectance are prepared (Figs. 11, 12 and 13). On the diagrams either the already published correlation trends and/or a line drawn after best fit (regression) is also implemented. Although the number of measurements is relatively low, a certain correlation could be derived eventhough some scattering does exit.

5. Summary and Conclusions

A thick Namurian - Westphalian clastic sequence in the Zonguldak Basin contains several coal seams. Within the framework of a study aimed at evaluating the coalbed methane potential of the basin coals from some of the seams have been analyzed by different geochemical methods. The obtained results can summarized as follows:

- Most of the coals can be classified as high volatile bituminous after analyzing their rank, volatile matter, ash and moisture contents.
- Both the atomic O/C and H/C ratios and the Hydrogen and Oxygen Index values are within the ranges of typical humic coals. But almost all the analyzed coal samples have very low Oxygen Indices which has been reported as a typical characteristics of coastal plain environment.
- Kinetic parameters of bulk hydrocarbon generation determined by a non-isothermal open system pyrolysis are similar to those obtained for coals from other regions.
- Organic petrographical composition coincides with the results of other analysis indicating humic coals some of which are liptinite rich.
- Between the maturity parameters vitrinite reflectance, volatile matter content, Hydrogen Index and Tmax a reasonable correlation does exit.

Acknowledgements

The TOC, Rock - Eval and organic petrographic analysis were carried out at the laboratories of Institute of Petroleum and Organic Geochemistry of KFA - Jülich. I wish to express my thanks to Prof. Dr. D.H. Welte for providing this opportunity and to Dr. R. Littke for his valuable support by microscopic analysis. I am grateful to G. Gürdal for her assistance during the study. The financial support of the Alexander von Humboldt - Stiftung, Germany is also acknowledged.

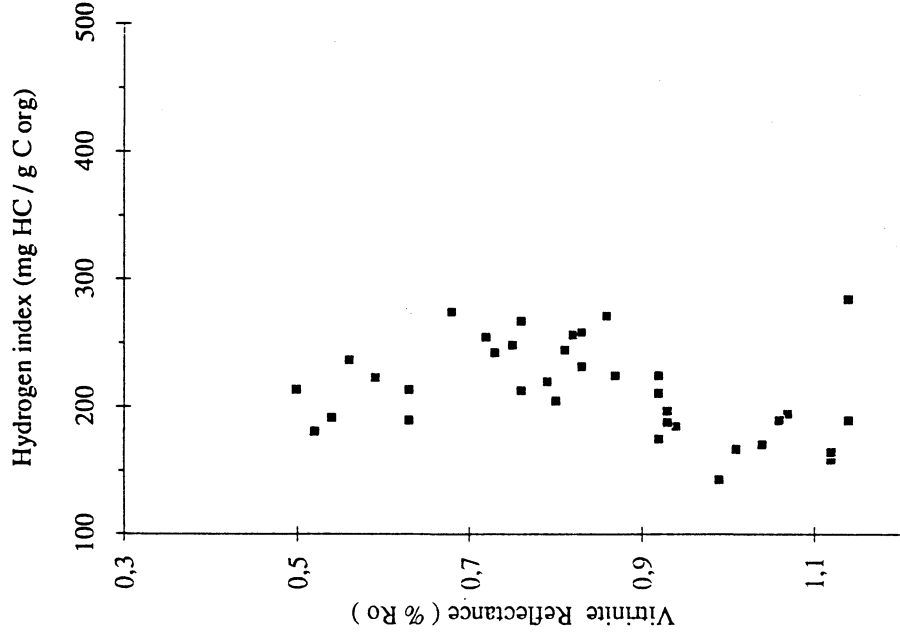


Figure 13. Correlation between vitrinite reflectance and Hydrogen Index

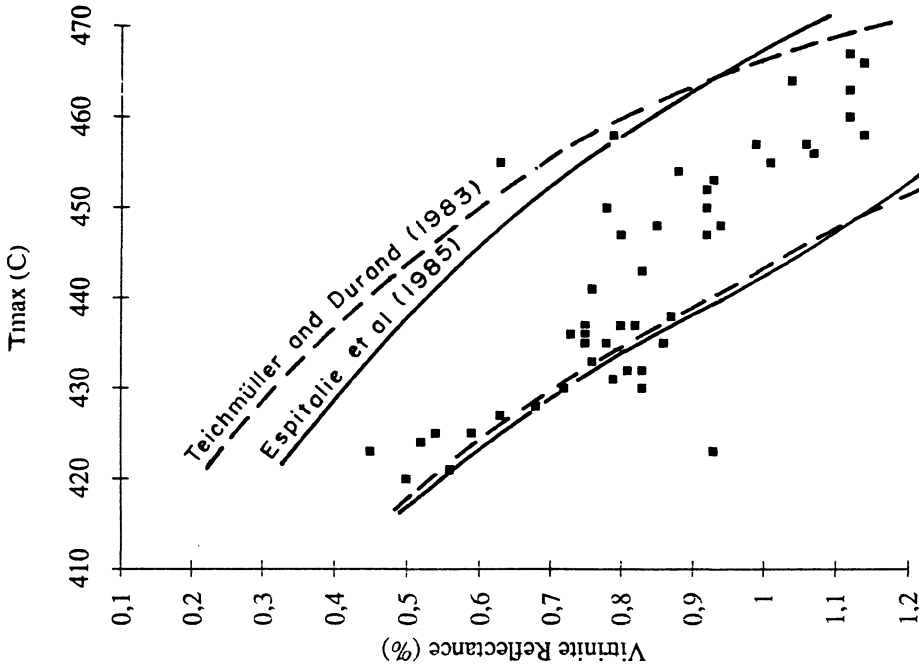


Figure 12. Correlation between vitrinite reflectance and Tmax. Trends given by Espitalie et al.⁽²¹⁾ and Teichmüller and Durand⁽²²⁾ are also indicated.

REFERENCES

1. A.S. Derman, Petrol İşleri Genel Müdürlüğü Dergisi, 1984, 208-220.
2. İ.E. Kerey, The Geological Evolution of the Eastern Mediterranean, Spec. Pub. of the Geol. Soc.17, 123-128, Blackwell, Oxford, (1985).
3. F. Akgün and E. Akyol, Doğa, Türk Yer Bilimleri Dergisi, 1992, 1, 1, 49-56.
4. A.İ. Okay, Revue de la Faculté des Sciences de l'Univ. d'Istanbul, 1939, IV, 3,4,1-17.
5. A.İ. Okay, MTA Mecmuası, 1944, 1,31, 137-138.
6. S. Artüz, İstanbul Üniversitesi Fen Fakültesi Monografileri, 21, (1971) .
7. S. Artüz, İstanbul Üniversitesi Fen Fakültesi Monografileri, 24, (1974).
8. A.İ. Karayığit, Türkiye 7. Kömür Kongresi Bildiriler Kitabı, 261-278, (1990).
9. M. N. Yalçın, Türkiye 7. Kömür Kongresi Bildiriler Kitabı, 245-260, (1990).
10. M.N. Yalçın, AAPG Bull., 1991, 75, 3, 697.
11. G. Gürdal and M.N. Yalçın, Türkiye 8. Kömür Kongresi Bildiriler Kitabı, 307-318, (1992).
12. E. Can and M.N. Yalçın, Türkiye 8. Kömür Kongresi Bildiriler Kitabı, 367-380, (1992).
13. M.N. Yalçın, H.J. Schenk, R.G. Schaefer, Int. J. of Coal Geology, 1994, 25, 2, 195-212.
14. E. Stach, M-Th. Mackowsky, M. Teichmüller, G.H. Taylor, D. Chandra, R. Teichmüller, Stach's Textbook of Coal Petrology. Gerbrüder Borntraeger, Berlin, Stuttgart, (1982).
15. P. Bertrand, Org. Geochem. 1984, 6, 482-488.
16. J. Espitalié, J.L. Laporte, M. Madec, F. Marquis, P. Leplat, J. Paulet, and A. Boutefeu, Rev. Inst. Fr. Pét. 1977, XXXII, 23-42.

17. S. Thompson, B.S. Cooper, R.J. Morley, and P.C. Barnard, *Petroleum Geochemistry in Exploration of the Norwegian Shelf*. Norwegian Petroleum Society, pp.59-73, (1985).
18. B.P. Tissot and D.H. Welte, *Petroleum Formation and Occurrences*. Springer Verlag, Berlin, Heidelberg, New York, Tokyo, (1984).
19. N. Durand and M. Paratte, *Petroleum Geochemistry and Exploration of Europe*, Geol. Soc. Spec. Publ. 12, 255-265, Blackwell, Oxford, (1983).
20. R.G. Schaefer, H.J. Schenk, H. Hardelauf and R. Harms, Org. Geochem., 1990, **16**, 115-120.
21. J. Espitalie, G. Deroo and S.F. Marquis, Rev. Inst. Fr. Pet., 1985, **40**, 755-784.
22. M. Teichmueller and B. Durand, Int. J. Coal Geol., 1983, **2**, 197-230.

X-RAY STUDIES OF THE STRUCTURE OF COALS AND COKES

P. WILK and S. JASIEŃKO
Institute of Chemistry and Technology
of Petroleum and Coal,
Technical University of Wrocław,
Wrocław, ul. Gdańska 7/9, POLAND

ABSTRACT

The results from studies on both the organic matter in coals and cokes and mineral compositions by X-ray diffraction (XRD) technique are presented. The results obtained by applying an Atomic Radial Distribution Function (RDF) method are analysed with models. The most important minerals occurring in vitrains are determined. Vitrains from gas coal, orthocoking coal and semicoking coal and the corresponding cokes have been analysed.

1. Introduction

Physical methods, especially XRD and microscopic methods, play an important role in the investigation of coal and carbon structure. The main aim of this paper was to determine the structural parameters of organic matter of vitrains from medium rank coals (gas coal, orthocoking coal and semicoking coal) and their cokes using the classical X-ray Diffraction and Atomic Radial Distribution Function methods. The other aim was to determine the mineral substance content by using the computer program XRAYAN recently described by H. Marciniak and R. Diduszko. Hard coals of medium rank are the basic raw material for metallurgical coke production and they are also used in production of formed coke and graphite materials.

A literature review of X-ray studies on coals can be found elsewhere^[1].

2. RDF method

The Radial Distribution Function (RDF) method is based on the following equation

$$4\pi r[\rho(r) - \rho_o] = \frac{2}{\pi} \int F(k) \sin kr dk$$

where: $G(r) = 4\pi r[\rho(r) - \rho_o]$ - reduced RDF, $\rho(r)$ - density function, ρ_o - average density, r - interatomic distance, $F(k) = k[cI - f^2]/f^2$ - reduced intensity, $k = 4\pi \sin\theta/\lambda$ - scattering vector, λ - wavelength, c - normalization constant, f - scattering factor, I - experimental intensity corrected for polarization and absorption, θ - scattering angle.

This equation is important because it relates the directly obtainable experimental function, $F(k)$ with the function, $G(r)$ which describes the real space structure of an amorphous solid (for instance coal). From the RDF method, information about interatomic distances, and the range of structure ordering can be obtained.

Fig.1 presents a fragment from single graphite-like layer with the marked first several interatomic distances. These numbers will be used while presenting the plots of $G(r)$ function for models and experimental results.

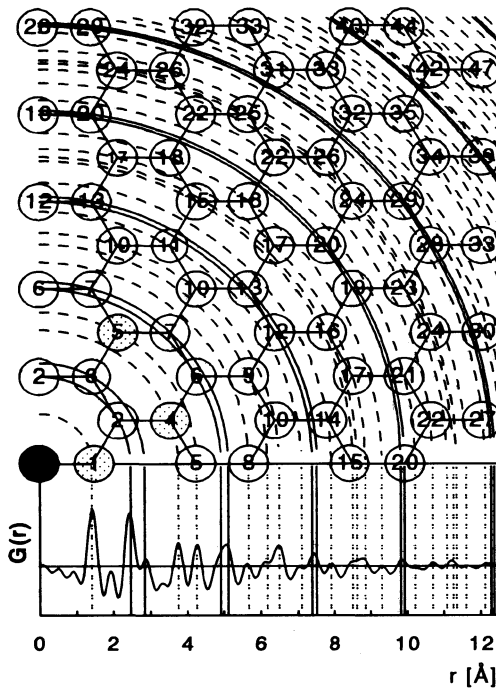


Fig.1. The correspondence between fragment of single graphite-like layer and the due reduced RDF plot.

3. Experimental

The characteristics of the vitrains used are presented in Table 1.

Table 1. Characteristics of vitrains studied

Sample	Coal type	Proximate and ultimate analysis			R	SI	RI
		V ^{daf} %	C ^{daf} %	H ^{daf} %			
A	gas coal	36.8	82.9	5.2	0.97	5.1	66
B	orthocoking coal	27.7	87.2	5.1	1.16	8.5	87
C	semicoking coal	22.1	88.6	4.8	1.41	5.0	26

R - reflectance, SI - Free Swelling Index, RI - caking power according to Roga method

In order to determine structural parameters for the organic matter by employing the classical XRD method as well as mineral substance analysis, diffraction experiments were carried out by using $\text{CuK}\alpha$ radiation in reflecting geometry. For the case of Atomic Radial Distribution Function method, Moka radiation was used.

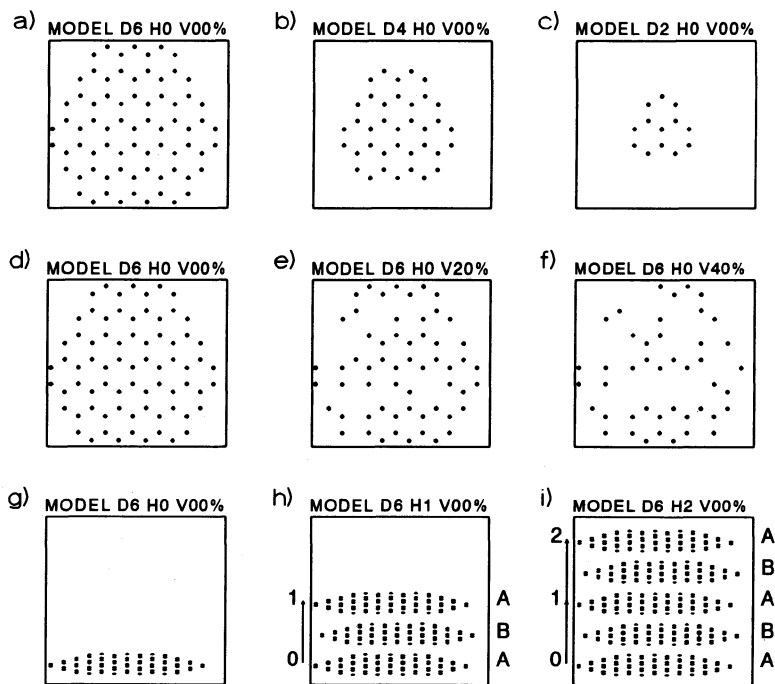


Fig.2. Examples of models (D-diameter in units of hexagonal graphite lattice constant $a = 2.456\text{\AA}$, H - height of stack of layers in units of hexagonal graphite lattice constant $c = 6.696\text{\AA}$ and V percentage of vacancies).

4. Models

For the purpose of interpretation of the experimental reduced RDF plots, the following base of simplified structural models (which correspond to the hexagonal structure of graphite) is proposed. Each component of the base can be described by three coefficients i.e. diameter D, height H and percentage of vacancies V. For example the model denoted by D6 H0 V00% means the single layer of diameter of six aromatic rings, without any vacancies (see Fig.2.a) while notation D6 H0 V20% means a single layer of the same diameter but with a 20% content of vacancies (see Fig.2.e). Finally, the model denoted by D6 H2 V00% represents a stack of 5 layers each of diameter of 6 rings arranged in hexagonal sequence ABABA; the stack height being equal to 2 lattice constants $c=6.696\text{\AA}$ (see Fig.2.i).

In Fig.3, the calculated plots of reduced RDFs corresponding to the models illustrated in Fig.2 are presented. All the reduced RDFs were calculated by Fourier transforming the reduced intensities $F(k)$; the latter being assumed to be equal to zero for $k < 1\text{\AA}^{-2}$ and $k > 16\text{\AA}^{-2}$ and attenuated by the dumping factor $\exp(-\gamma k^2)$ with $\gamma = 0.003$.

It is seen that the decrease of the layer diameter (Fig.2.a, b, c) as well as increase of the vacancies content (Fig.3.d, e, f) do not influence the peak positions but decrease the peaks heights. Obviously, it is valid within the range where the correlation holds.

Stacking of layers causes changes of both the peaks positions and peak heights mainly for r ranging within the $3.5 - 8\text{\AA}$ interval (Fig.3.g, h, i).

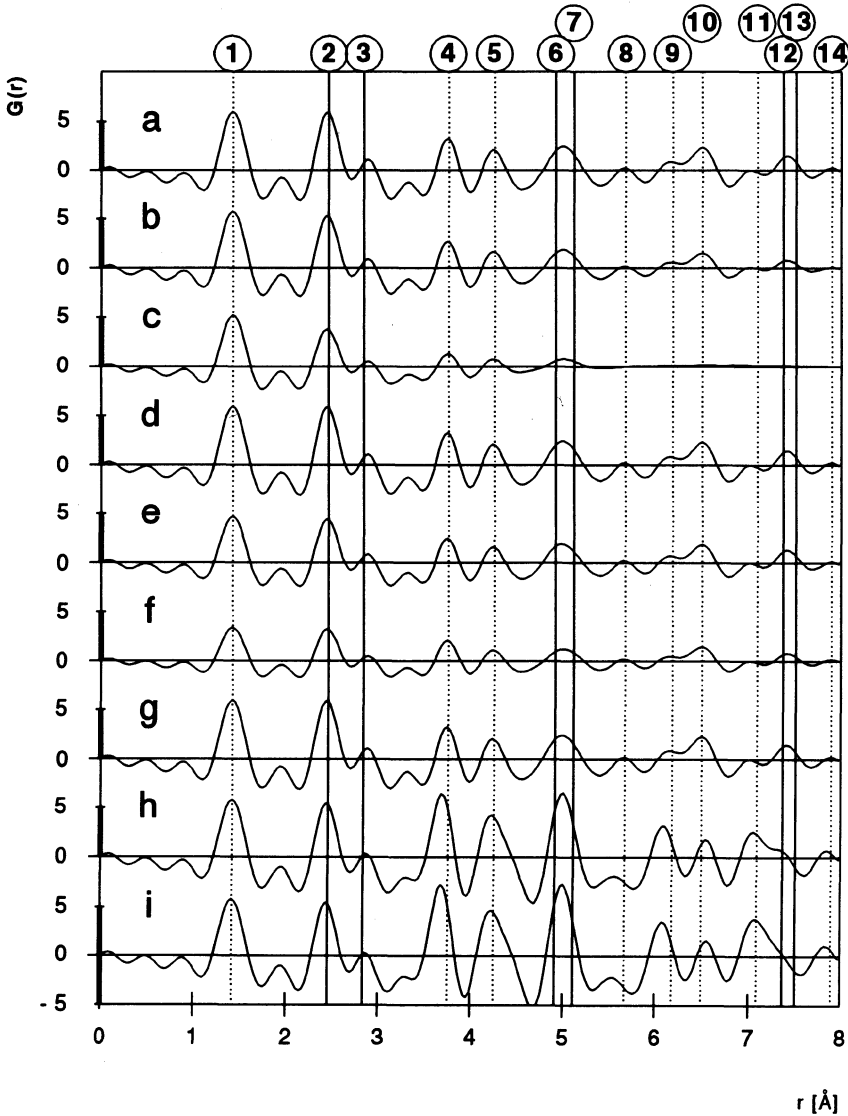


Fig.3. The plots of the $G(r)$ functions corresponding to the models presented in Fig.2.

- the influence of the diameter value on the shape of $G(r)$ function
 a) model D6 H0 V00%, b) model D4 H0 V00%, c) model D2 H0 V00%
- the influence of the vacancies content on the shape of $G(r)$ function
 d) model D6 H0 V00%, e) model D6 H0 V20%, f) model D6 H0 V40%
- the influence of stacking of layers in hexagonal graphite order on the shape of $G(r)$ function
 g) model D6 H0 V00%, h) model D6 H1 V00%, i) model D6 H2 V00%

5. Results and discussion

5.1 ORGANIC MATTER STRUCTURE OF COALS AND COKES

The structural parameters of studied samples are presented in Table 2. Structural ordering expressed in pseudocrystalline dimensions L_c , L_a , and interlayer spacing d_{002} increase with the coal rank. In a case of the cokes from the vitrains, the best ordered structure is for the coke from the orthocoking coal. It is connected with the liquid structure which is characteristic for this type of coal.

Table 2. X-ray parameters of coals and cokes studied

Sample	d_{002} [Å]	L_c [Å]	L_a [Å]			
				d_{002} [Å]	L_c [Å]	L_a [Å]
vitrains			cokes from vitrain			
gas coal	3.594	9.4	14.3	3.564	12.2	33.0
orthocoking coal	3.562	12.8	15.5	3.500	15.8	31.8
semicoking coal	3.559	13.4	15.5	3.509	14.9	30.2

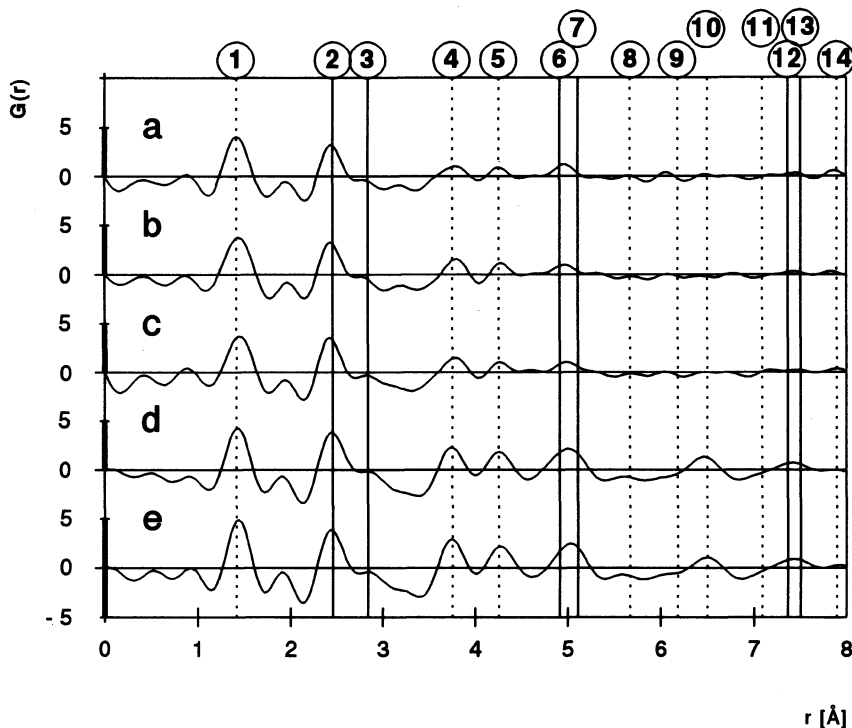


Fig.4. The plots of experimental reduced RDFs for:

a) vitrain from gas coal, b) vitrain from orthocoking coal, c) vitrain from semicoking coal, d) coke from vitrain of gas coal, e) coke from vitrain of semicoking coal

When looking at the $G(r)$ plots (Fig.4.a, b, c) of the vitrains, it is evident that the correlation range is very low (up to two aromatic rings only). The degree of structure ordering is weakest for the gas coal vitrain whereas the highest ordering is for the semicoking coal. Experimental reduced RDFs are shifted to the right hand side in the regions of the peaks number 1, 4 and 5, respectively, which can be explained by a contribution from aliphatic compounds with a predominant interatomic distance of 1.54Å. These aliphatic compound, if separated should influence the peak number 1. If, however there any radicals on aromatic rings then the distances corresponding to 4 and 5 peak increase.

Table 3. Interatomic distances found in samples studied

Interatomic distances in perfect hexagonal graphite [Å]	Distance between layers [x 3.348Å]	Distances found in experimental reduced RDFs [Å]					
		vitrains			cokes from vitrains		
		sample A	sample B	sample C	sample A	sample C	
1 ⁾	1.418	0	1.42	1.44	1.46	1.43	1.41
2	2.456	0	2.42	2.41	2.41	2.42	2.44
3	2.836	0	2.83	2.81	2.84	2.90	2.87
	3.348	1					
	3.636	1					
4	3.752	0	3.78	3.80	3.78	3.74	3.75
	4.152	1					
5	4.253	0	4.25	4.26	4.25	4.26	4.26
	4.388	1	4.61	4.62	4.61		
6	4.912	0					
	5.028	1	4.97	4.97	4.98	5.02	5.01
7	5.113	0					
	5.413	1	5.34	5.34	5.33		
8	5.671	0	5.67	5.70	5.68	5.59	5.67
	5.944	1					
	6.111		6.06	6.07	6.05	6.00	6.07
9	6.180	0					
10	6.498	0	6.45	6.42	6.44	6.48	6.49
	6.586	1					
	6.696	2	6.78	6.78	6.75		
	6.844	2					
	7.029	1					
11	7.090	0					
	7.132	2	7.14		7.15		
	7.272	2					
	7.310	1					
12	7.368	0				7.41	7.46
13	7.503	0	7.46	7.44	7.49		
	7.675	2					
	7.841	1		7.84			
14	7.895	0	7.87		7.88	7.88	7.89
	7.933	2					

⁾ Numbers corresponding to the numbers in Fig. 1.

No interatomic distances connected with the staking layers in perfect hexagonal graphite order were found, indicating the absence of the ordered graphite crystallites. On the other hand the presence of 002 and 004 bands in diffraction patterns should indicate the existence regions of turbostratic structure.

For the case of cokes from vitrains, the ordering range is much higher. The peak positions in the 0-8Å range are highly consistent with those of perfect single graphite-like layer (see Fig. 4.d, e). Also, the peak heights are close to those of models of diameters larger than 5 rings. Similarly to the previous case, no distances were observed which could be attributed to the three dimensional ordered graphite structure.

5.2 MINERAL SUBSTANCE CONTENT

XRD patterns were measured with the step $2\theta = 0.05$ degree in the 5 - 65 degree interval range which gives resolution good enough to obtain at least ten points for each structural peak. Very low peaks (of intensities comparable to the noise level) were also taken into account by repeating the measurements twice for each sample and only those small peaks which occurred in patterns obtained from both the measurements were taken into account.

The data, constituting the base of standard patterns of mineral substances considered in this work, were restricted to the chemical compositions reported to occur in coals. The computer program XRAYAN described by H.Marciniak and R.Diduszko^[2] was used to find the set of standard patterns which fit the experimental pattern in the best way. The program searches the base of standard patterns to find the phase for which FP parameter takes the minimal value. The FP parameter is defined as follows:

$$FP = FP_d FP_I \left(\frac{L_s}{L_f} \right)^2 \sqrt{\frac{L_E}{L_f}} \sqrt{SCALE}$$

where

FP_d - fitting parameter of positions of lines (standard deviation)

FP_I - fitting parameter of intensities

L_s - number of standard lines in the measurement range

L_E - number of experimental lines

L_f - number of fitted lines

SCALE - the ratio of intensities of lines of standard to intensities of fitted lines of a sample.

Table 4. A list of mineral substances found in studied samples of vitrains

Vitrain of:	FP	FP_d	L_E/L_s	SCALE	Phase(JCPDS)	Mineral name
gas coal	24.17	1.71	3/6	0.26	29-1499	Montmorillonite
	62.96	1.55	7/33	0.50	14-691	Strontium-apatite
	64.66	1.88	4/9	0.28	26-801	Pyrite
orthocoking coal	1.75	0.71	6/6	0.98	6-710	Pyrite
	11.77	1.71	3/3	0.25	29-696	Siderite
	37.02	1.30	6/12	0.12	6-221	Kaolinite
	12.33	1.30	2/2	0.20	5-490	Quartz
	18.90	1.71	2/2	0.15	35-752	Chalcopyrite
	11.34	1.59	3/3	0.24	14-691	Strontium-apatite
semicoking coal	5.30	0.90	11/14	0.43	6-221	Kaolinite
	57.44	1.48	5/12	0.64	29-696	Siderite
	99.00	1.30	1/9	0.03	6-710	Pyrite

The quality of the fitting procedure described above is illustrated in Fig.5. The results obtained by applying the procedure described above are presented in Table 4. In cokes only troilite and oldhamite were found. However only minerals present in higher concentration are identified.

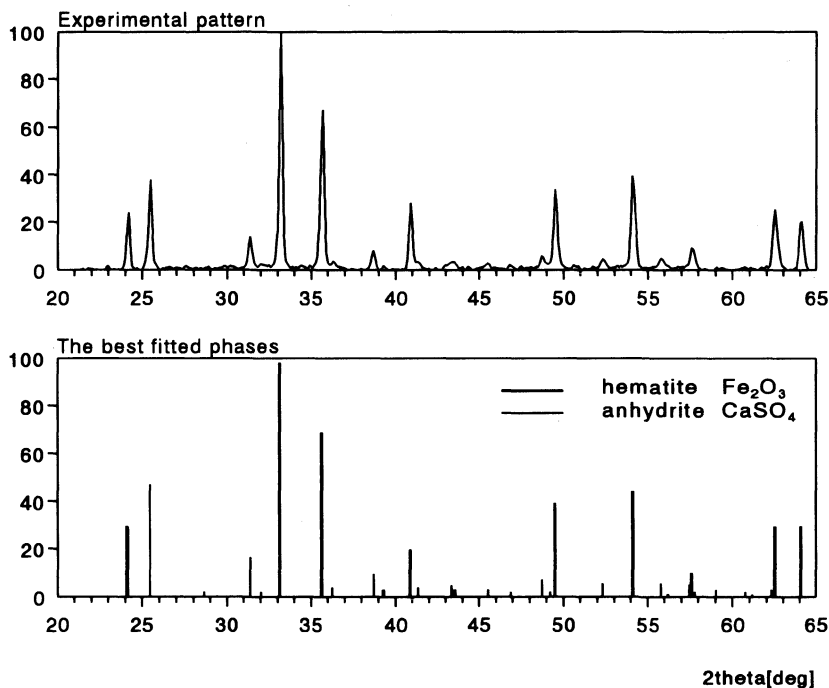


Fig.5. Illustration of the quality of fitting for the case of ash from the orthocoking coal.

6. Conclusions

The models presented in this paper are simplified to a high degree since the influence of aliphatic and alicyclic compounds is ignored. In spite of this, they appear to be very useful to explain the type of ordering in both coalification and coking processes. The simulations of models accounting the effect of aliphatic compounds will be subject of further investigations.

It's worth noting that the methodology of this kind should be applicable to the examination of mineral substances occurring in oil shales deposits and of oil shale structure and pyrolysis and extraction products.

7. References

1. S.Jasieńko and J.Pielaszek, "X-ray Methods in the Investigations of Coals Structure", 1992, Polish Academy of Science, Department of Coal Chemistry, Gliwice (in Polish).
2. H.Marciniak and R.Diduszko, XRAYAN, X-ray phase analysis, version 2.85, 1991-1993, computer program

THE ASPECTS OF MICROSCOPIC STUDIES AS EXEMPLIFIED BY THE MACROPOROUS STRUCTURE OF COKES FROM BITUMINOUS COAL RANGE

P. WILK and K. BRATEK
Institute of Chemistry and Technology
of Petroleum and Coal,
Technical University of Wrocław,
Wrocław, ul. Gdańska 7/9

ABSTRACT

A methodology for the microscopic study of coke macroporous structure (expressed in terms of open, closed and intergrain macropores) has been used to differentiate pore configurations both qualitatively and quantitatively. The method can be applied to any porous matter. The relation between the macroporous structure of coke and the properties of the parent coal is discussed. Cokes obtained from vitrains of coals ranging from flame coal to anthracitic coal have been investigated.

1. Introduction

Coke consists of a configuration of micro-, meso- and macropores. These pores influence coke properties, such as reactivity and strength.^[1-2] They can also characterize the raw material from which the coke has been obtained. The aim of this work was to determine the macroporous structure of cokes for vitrains from low rank, medium rank and high rank coals in terms of open, closed and intergrain pores introduced in our previous papers.^[3-5]

2. Experimental

2.1. SAMPLES and APPARATUS

Vitrains separated from the coals listed in Table 1 were used. Cokes were obtained in a Gray-King apparatus (heating rate 5°C/min, up to 1000°C). The characteristics of vitrains used to obtain the coke are presented in Table 2.

For microscopic observations, polished blocks of the cokes were prepared. In the case of sintered cokes (samples C, D, E, F, G), slices of cokes of 1 cm thickness cut transversely at the middle of cokes were mounted in epoxy resin and then polished. The routine averaging procedure was applied before mounting coke powders in epoxy resin for the case of non-sintered cokes (samples A, B, H, I, J). The macroporous structure of the cokes was determined by using the Mini-Mop semiautomatic image analyser.

2.2. MEASURING AND EVALUATING PROCEDURES

The concept of pores categorization as suggested in references^[3-5] into geometrically *closed*, *open* and *intergrain* ones is illustrated in Fig. 1. The criterion of differentiation between the irregular part of a pore and an open pore is based on the "20%" rule which states: the irregular part of a pore is treated as a separated open pore if the length of the common border (see dashed line in Fig. 1.c) is less than 20% of

Table 1. List of coals the vitrains of which were used to produce the cokes examined.

Sample	Coal type	ICC	Mine
A ⁾	flame coal	700	Chwałowice mine
B	gas-flame coal	711	Ignacy mine
C	gas coal	622	Rydułtowy mine
D	gas coal	633	Kleofas mine
E	gas-coking coal	634	Dębieńsko mine
F	orthocoking coal	434	1 Maja mine
G	semicoking coal	432	Nowa Ruda mine
H	semicoking coal	311	Warszowice bore-hole
I	lean coal	311	Warszowice bore-hole
J	anthracitic coal	200	Warszowice bore-hole

⁾ The above notation (sample names A, B, C,...) will be used in tables, photos and pictures presented in this paper.

Table 2. Characteristics of vitrains used for obtaining the cokes.

Sample	Proximate and Ultimate Analysis					R %	SI	RI
	W ^a %	A ^a %	V ^{dar} %	C ^{dar} %	H ^{dar} %			
A	6.3	1.9	39.5	78.2	5.0	0.65	0.0	6
B	5.2	2.6	38.8	81.0	5.2	0.81	1.0	30
C	2.3	2.6	37.8	83.8	5.3	0.87	4.0	60
D	3.0	1.0	36.8	82.9	5.2	0.97	5.5	66
E	2.3	2.4	35.9	86.5	4.9	0.96	6.0	75
F	1.0	0.9	28.0	88.4	5.0	1.25	9.0	77
G	1.1	2.1	22.1	88.6	4.8	1.41	5.0	26
H	0.9	1.6	15.7	91.4	4.5	1.70	3.5	20
I	0.9	0.9	12.9	91.5	4.4	1.79	1.5	9
J	0.9	0.8	8.2	91.8	4.0	2.36	0.0	0

Sample	Dilatometric Properties (Audibert-Arnau method)					Plastic Properties (Gieseler method)			
	t _I °C	t _{II} °C	t _{III} °C	a %	b %	t _S °C	t _{F(max)} °C	t _R °C	F(max) %/min
A	375	420		9					
B	362	438		36		352	418	466	8
C	363	410	429	35	25	360	419	452	42
D	373	407	427	33	17	370	426	451	85
E	358	414	453	29	85	361	428	457	1500
F	394	427	483	28	228	368	452	486	9920
G	402	437	450	28	-21	396	437	468	17
H	235	484		27		429	460	493	7
I	470	500		5					
J									

t_I - melting temp., t_{II} - max. contraction temp., t_{III} - max. dilatation temp., a - contraction, b - dilatation; t_S - temp. of softening, t_{F(max)} - temp. of max. fluidity, t_R - temp. of resolidation, F(max) - max. fluidity.

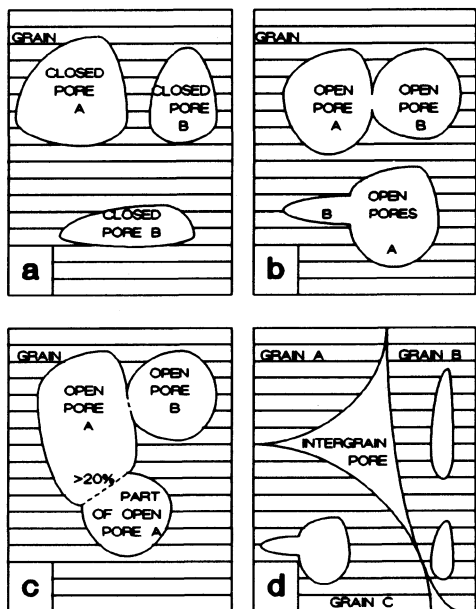


Fig.1. A graphic illustration to the definition of geometrically closed, open and intergrain pores:

- a) Examples of closed pores
- b) Examples of open pores
- c) Exemplified illustration of the 20% rule to distinguish the open pores between the irregular part of a complex pore
- d) Example of intergrain pore

the whole perimeter of that part of pore.

The distributions of the pore sizes were obtained basing on the sequence of magnitudes 1,2,4,...,512 μm (2^n rule). Numbers of pores belonging to the respective pore diameter intervals ($2^n - 2^{n-1}$) were counted and the corresponding contributions to porosities evaluated. All the pore size distributions were normalized to the same reference area of one square millimeter. For the case of non-sintered cokes (samples A, B, H, I, J) the reference area was taken as a sum of areas of all examined grains. For sintered and swollen cokes (samples E, F) the reference area was that of coke walls defined as regions not including pores of sizes greater than 1mm. For sintered but not swollen cokes (samples C, D, G) the reference area was taken as a sum of areas of separated grains and the areas of conglomerates of partially glued grains which formed intergrain pores as the result of glueing. The magnification of 250x was used.

3. Results and discussion

Results obtained are illustrated in series of plots and photos presented in Figures 2-5. The principal findings are presented below.

1. From the vitrains of low coalified coals (flame and gas-flame coal) powder cokes of low porosity (1.9 and 4.0, respectively) are obtained in the coking process. In these cokes the closed pores of dimensions 1-32 μm and 2-64 μm appear in larger grains, exclusively. Gas flame coal passes to a small degree through the plastic stage which facilitates the creation of a number of larger pores. Therefore, the porosity of the resultant coke becomes a little higher.

2. Vitrains of gas coals showing certain plasticity in the coking process give baked cokes which are only slightly fused. A great number of pores appear in cokes from both these coals. The total number of pores

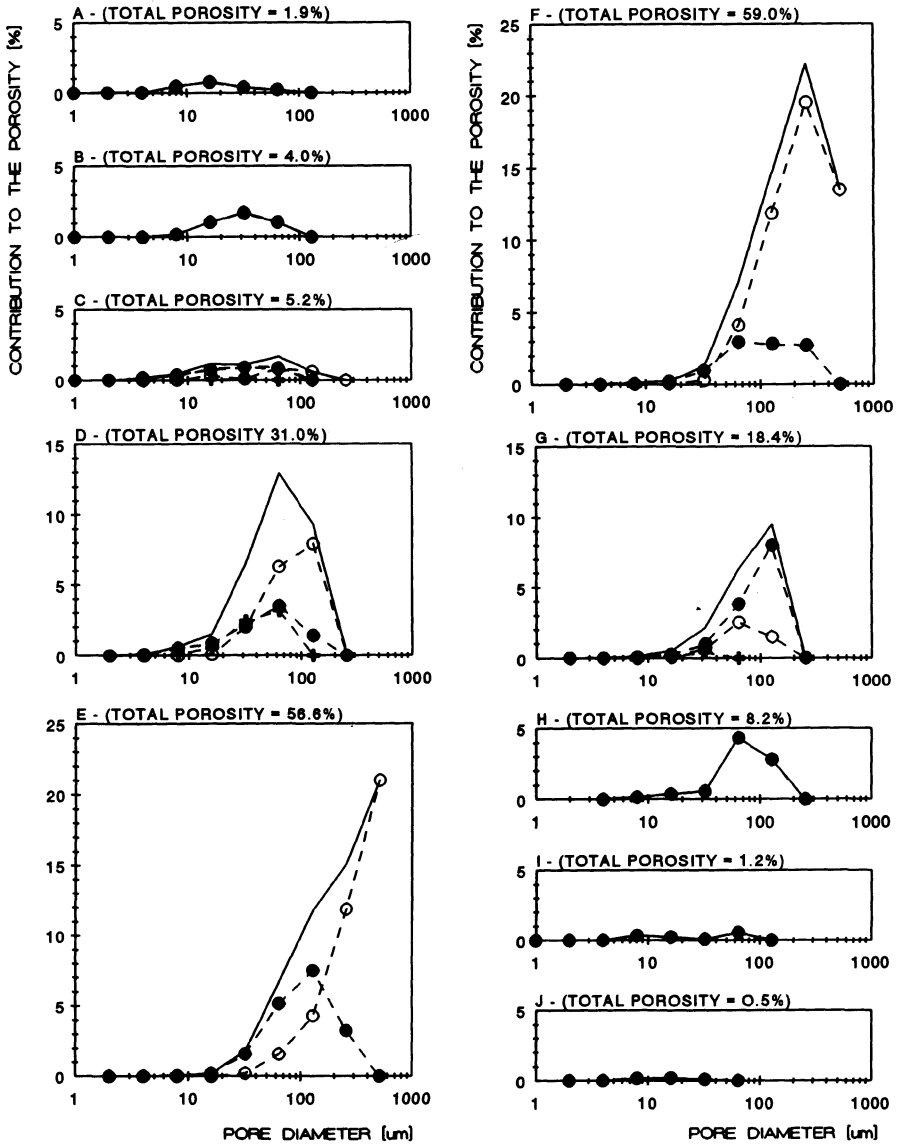
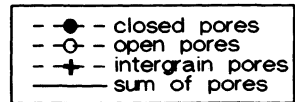


Fig.2. Contribution to the porosity as a function of the pore diameter for different coke samples A, B, C,..., J. For the sample notation see Table 1.



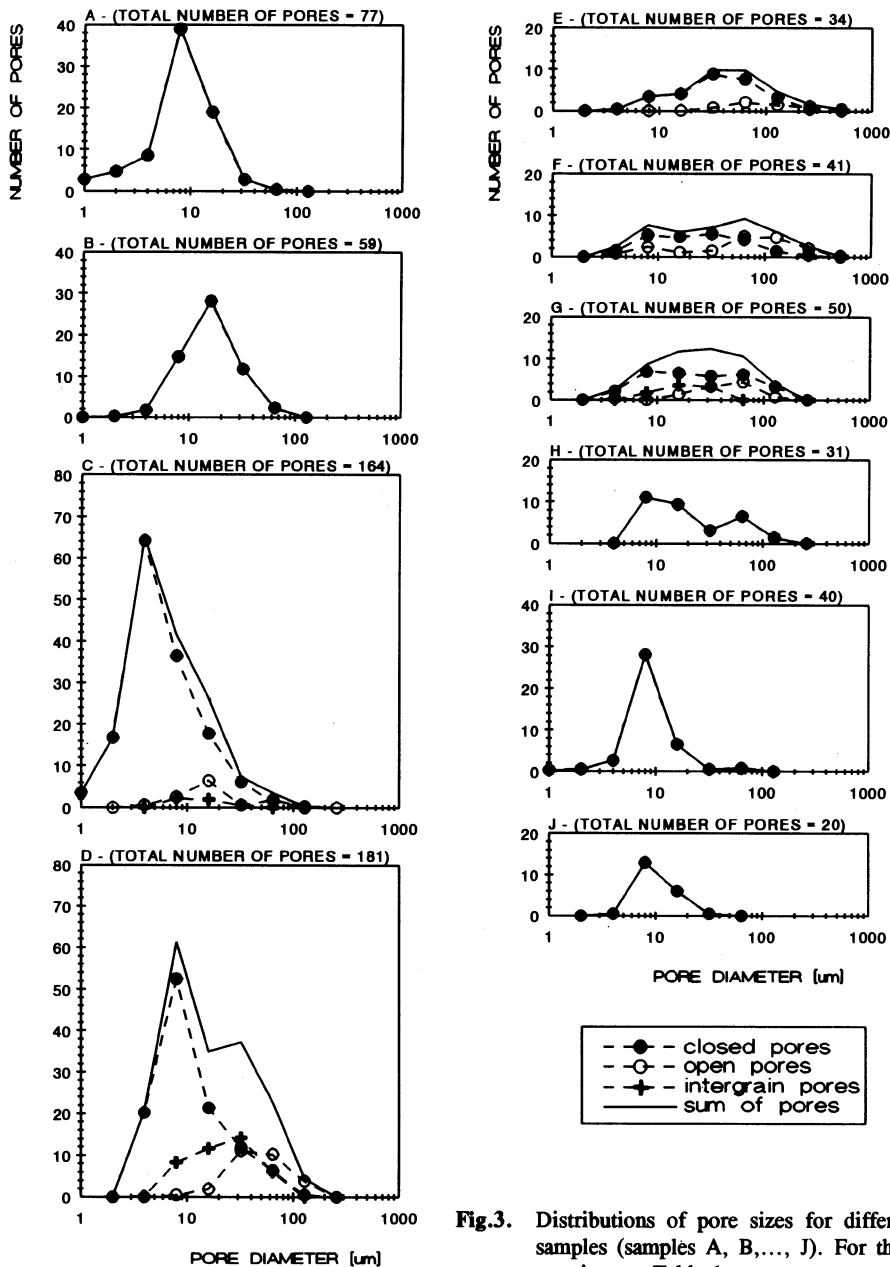


Fig.3. Distributions of pore sizes for different coke samples (samples A, B,..., J). For the sample notation see Table 1.

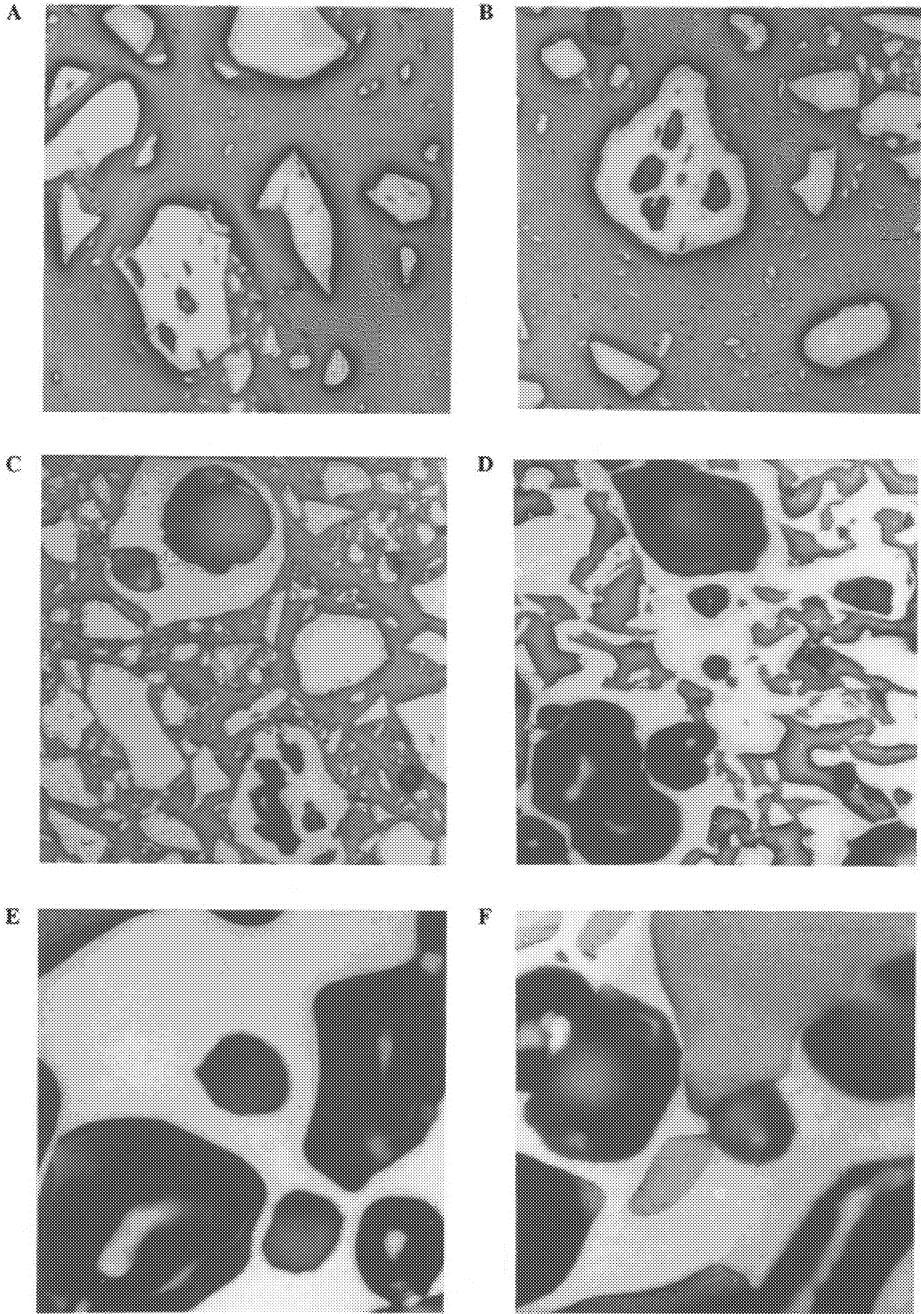


Fig.4. Representative photos of a different coke samples (samples A, B, C, D, E, F).

in these cokes are comparable. However, coke from the higher coalified gas coal (sample D) shows much higher porosity and a greater number of large open and intergrain pores. Thus, it may be concluded that a lower viscosity of plastic vitrain grains facilitates pores to grow and coalesce and grains to stick to one another to create intergrain pores.

3. Vitrains of coking coals (gas coking and orthocoking coal) give sintered and highly swollen cokes. These coals pass through the plastic stage completely. In the stage of higher plasticity, a strong emission of gases occurs which facilitates the production of large pores of spherical shapes, which then increase in sizes and consequently coalesce. A greater number of open pores was observed in coke from the orthocoking coal so it may be concluded that pores in this coke show higher tendency to coalesce. This can be explained by the higher plasticity of this coal.

4. In the coking process, vitrain of semicoking coal may create:

- baked (though only slightly fused) coke for the case of lower coalified semicoking coal (ICC 432 - sample G).

- weakly agglutinated coke for the case of higher coalified semicoking coal (ICC 311 - sample H).

A relatively small number of pores appears in the cokes from vitrains of semicoking coals. In a case of lower coalified semicoking coal (sample G) open, closed and intergrain pores appear while only closed pores appear in the case of higher coalified semicoking coal (sample H). Pores in coke from vitrain of coal ICC 432 are of much larger sizes than those of coke from vitrain of coal ICC 311. Therefore, it may be stated that similarly to the case of vitrains of gas coals, higher plasticity facilitates the increase of pore sizes and the coalescence of pores as well as the fusion of the grains.

5. It is interesting to compare the macroporous structure of cokes from vitrains of gas coal from the Kleofas mine (sample D) and that from vitrain of semicoking coal from the Nowa Ruda mine (sample G). Both cokes are characterized by high porosity and significant contribution of large pores. However, the macroporous structure of coke from gas coal vitrain comprises mainly large open pores while large closed pores contribute mainly to the porosity of the semicoking coal. This is due to the fact that gas coal is richer in "centers" from which the pores may be created and developed than semicoking coal. Therefore the probability of meeting a neighboring pore in the process of pore sizes increasing in the plastic phase is significantly higher in the gas coal than that in the semicoking coal. Thus not only plasticity but also the "nature" of coal substance determines the macroporous structure of coke obtained in the coking process.

6. Vitrains from lean and anthracitic coals neither transit through the plastic stage nor soften in the coking process, consequently giving powder cokes of very low porosity (1.2%, 0.4%, respectively). Pores appear only in larger coke grains being of closed type exclusively and sizes 2-32 μm . Note that in coke from lean coal vitrain the number of pores of sizes 2-16 μm is relatively higher than in coke from anthracitic coal vitrain.

7. In cokes from higher coalified non baking coals (samples I, J), there appear to be many fewer pores than in cokes from lower coalified non baking coal vitrains (samples A, B). Pores created in cokes from vitrains of lean and anthracitic coals are also smaller than those in coke from gas and gas-flame coal vitrains.

4. Conclusions

The method describing the macroporous structure of cokes presented in this paper seems to be universal enough to describe any porous structure. The representation of porous structure of cokes in the form of the plots presented in Figures 2, 3 allows to specify the particular kind of coke with much higher precision than it would be possible by observing the photographs only. This is because the plots are sensitive to three kinds of information, independently i.e.

- distribution of sizes
- shapes of pores
- mutual location of pores.

In this sense the method allows a representative picture of the configuration of pores for particular coke case to be designed.

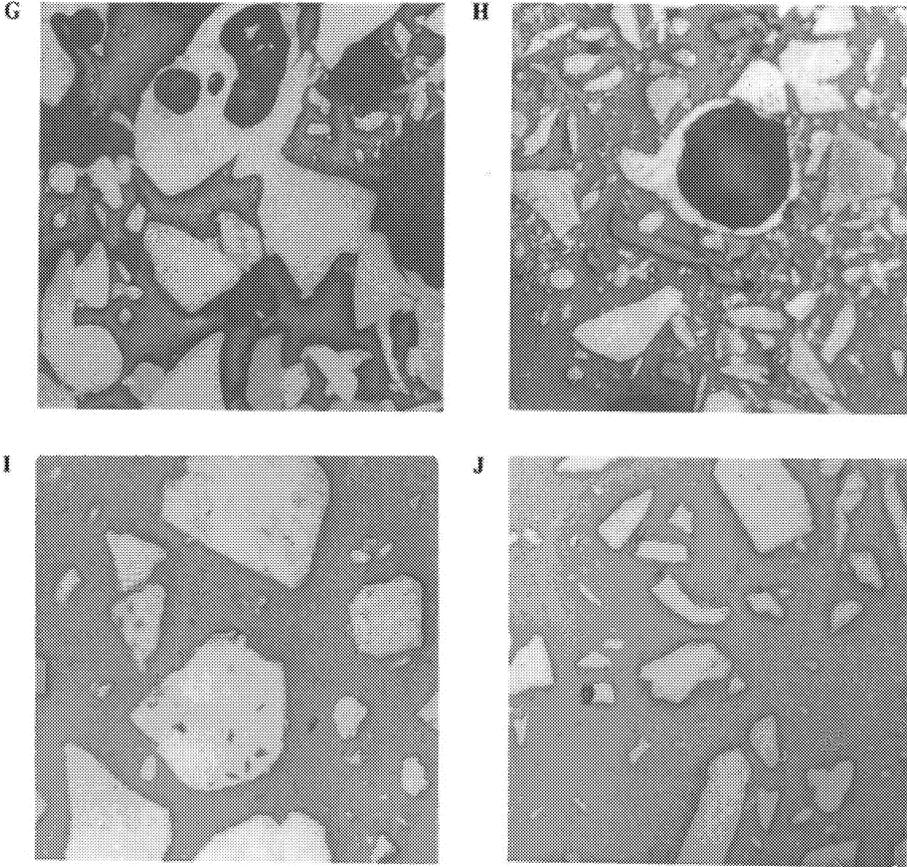


Fig.5. Representative photos of a different coke samples (samples G, H, I, J). For the sample notation see Table 1.

5. References

1. J.W.Patrick and A.Walker, Fuel, 1985, **64**, 136.
2. D.Hays and J.W.Patrick and A.Walker, Fuel, 1976, **55**, 297.
3. K.Bratak and P.Wilk, Koks Smola Gaz, 1989, **34**, 239.
4. K.Bratak and P.Wilk, Fuel Proc. Techn., 1990, **26**, 197.
5. S.Jasieńko, K.Bratak and P.Wilk, Polish Journal of Applied Chemistry, 1993, **XXXVII**, 1-2, 25

DETERMINATION OF ORGANIC SULPHUR FORMS IN TYPE I/II KEROGENS BY HIGH PRESSURE TEMPERATURE PROGRAMMED REDUCTION (TPR)

S.C. MITCHELL and K. ISMAIL
*University of Strathclyde
Department of Pure and Applied Chemistry
Glasgow G1 1XL
Scotland, U.K.*

R. GARCIA and S. R. MOINELO
*Instituto Nacional del Carbon
Apartado 73
33080 Oviedo
Spain*

Summary

The temperature programmed reduction (TPR) technique has been extended to two kerogens: Goynuk oil shale, a type I kerogen, and Kimmeridge (Dorset-Cuddle), a type II kerogen. In each case thiophenic sulphur was confirmed as the dominant organic sulphur form with sulphides accounting for ≈ 40 -50% of Goynuk and $\approx 35\%$ in Kimmeridge. From the hydrogen sulphide (H_2S) profiles obtained from TPR, the position of the T_{max} gives a good indication of the average ring size of the thiophenic structures, suggesting that the type I kerogen contains mainly single ring thiophenes, whilst the higher T_{max} , displayed by the type II kerogen implies a prevalence of 2-3 ring thiophenes, consistent with the recognised structural differences between the two kerogen types. Additionally, for Goynuk oil shale, the proportion of H_2S evolving from non-thiophenic forms below $250^\circ C$ indicates the probable presence of polysulphides.

1. Introduction

As yet, there is no one established procedure for determining organic sulphur forms, despite recent advancements in the use of X-ray techniques (XPS and XANES)¹⁻⁴, and continued research into temperature programmed reduction (TPR)⁵⁻¹⁰, oxidation (CAPTO)^{11,12} and fluidised-bed pyrolysis^{13,14}.

The TPR method, pioneered by Attar⁵⁻⁷ and used by others^{8,9}, has met with only limited success, primarily because only the labile non-thiophenic sulphur forms were actually observed. Poor sulphur balances resulted from the use of low pressures with virtually all the thiophenic sulphur remaining in the residue. Further, little account was taken of the reduction of pyrite to pyrrhotite and of any retrogressive chemistry including the conversion of sulphides into thiophenes⁶.

As described in the contribution by Snape and Bartle in this volume, a novel high pressure TPR approach for determining the distribution of organic sulphur forms in coals, kerogens and related materials has recently been developed^{10,15-17}. The extent of any secondary reactions has been reduced considerably by using a well-swept reactor operating at relatively high hydrogen pressures (15 MPa). The extent of desulphurisation has previously been reported as being over 95% for both lignites and high volatile bituminous coals at temperatures above $500^\circ C$ ¹⁵. Typically over 75-80% of the organic

sulphur being reduced to H₂S with the remainder being released as mainly thiophenic compounds in the tars which can be accounted for by GC analysis¹⁷.

The technique has already been applied to a number of coals and this contribution describes the extension to two kerogens, namely Goynuk oil shale, a type I kerogen, and Kimmeridge (Dorset-Cuddle), a type II kerogen.

2. Experimental

Samples

The analyses of the two oil shales are given in Table 1. The sample of Kimmeridge (Dorset-Cuddle) was prepared by standard procedures using hydrochloric and hydrofluoric acids¹⁸. Goynuk oil shale was used directly. Pyrite was removed using lithium aluminium hydride^{19,20}.

Table 1. Analytical data (dry basis).

Sample	C	H	N	S	S ¹	H/C
Goynuk ²	56.1	7.6	0.9	3.3	2.4	1.63
Kimmeridge ³	55.5	6.2	2.1	8.3	5.8	1.34

¹After pyrite removal

²Oil shale

³Kerogen

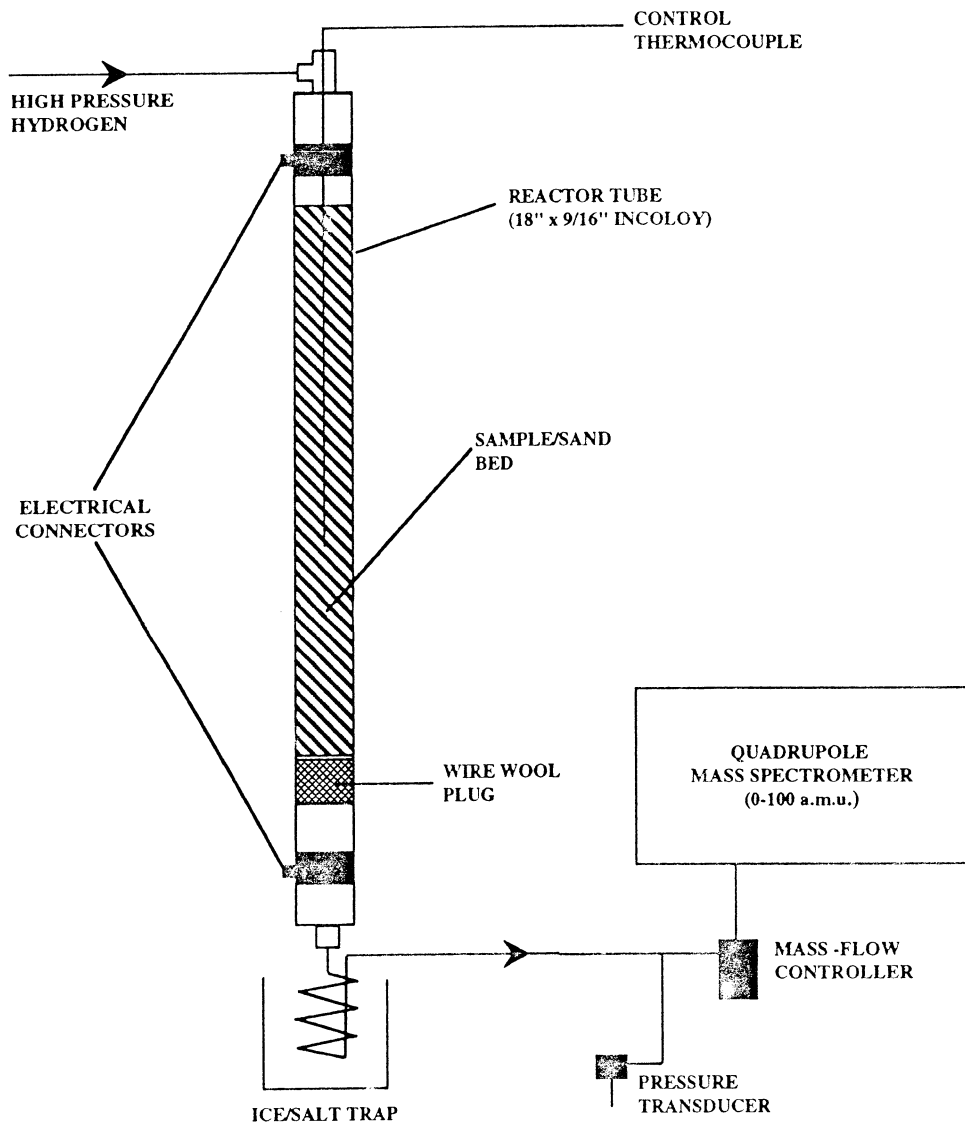
Apparatus

A schematic of the TPR apparatus is shown in Figure 1. The fixed-bed tubular down-flow reactor is heated resistively from 100 to 600°C at 5°C min⁻¹. A hydrogen pressure of 15 MPa was used with a superficial gas velocity of *ca* 0.5 m s⁻¹. Temperature was monitored by a thermocouple situated in the coal bed. For all the tests between 0.2 to 0.5 g sample, depending on the organic sulphur content, was diluted with sand (*ca* 10:1 mass ratio) and packed into the reactor, supported by a wire wool plug. Any tar formed was condensed in a high pressure trap cooled with ice/water. Following pressure let-down through a mass flow controller, the gas stream was sampled through a 1.8 m length of heated capillary tubing at a rate of 25 cm³ min⁻¹ into a quadrupole mass spectrometer (VG Monitorr 100D) for on-line monitoring of H₂S and other volatiles. The signal from the control thermocouple situated in the sample bed was also fed directly to the mass spectrometer facilitating plots of evolved gas concentrations against temperature. At the end of each run, the sand/char mixture left in the reactor was emptied and the tar recovered by thoroughly washing with dichloromethane.

3. Results and discussion

The temperatures (T_{\max}) at which H₂S evolves from different sulphur compounds has been assessed using sulphur-containing silica immobilised substrates and phenol-formaldehyde resins as solid calibrants²¹(see contribution by Ismail and Mitchell). Figure 2 shows two hydrogen sulphide (H₂S) evolution profiles for Goynuk oil shale (Type I kerogen), as received and pyrite removed. The latter profile displays a dominant high-temperature feature centred at 400°C, which strongly suggests that the thiophenic sulphur is largely present as single rings, and a leading low temperature shoulder between 200 and 380°C from non-thiophenic forms²¹. Although thiophene and benzothiophene calibrants have not yet been synthesised, their T_{\max} can be anticipated to occur in the range 380-450°C on the above evidence. Indeed from studies on two well-characterised high-sulphur lignites (Mequinenza and Rasa), the reduction temperature at which H₂S evolution reaches a maximum (430 and 460°C, respectively)^{10,16} is close to that of 470°C determined for immobilised dibenzothiophene²¹. The large difference in T_{\max} obtained for immobilised dibenzothiophene and diphenylsulphide samples also indicates the potential of high pressure TPR to give a good indication of the average ring size of the thiophenic structures present, the implication being that Goynuk contains mainly single

Figure 1. TPR APPARATUS



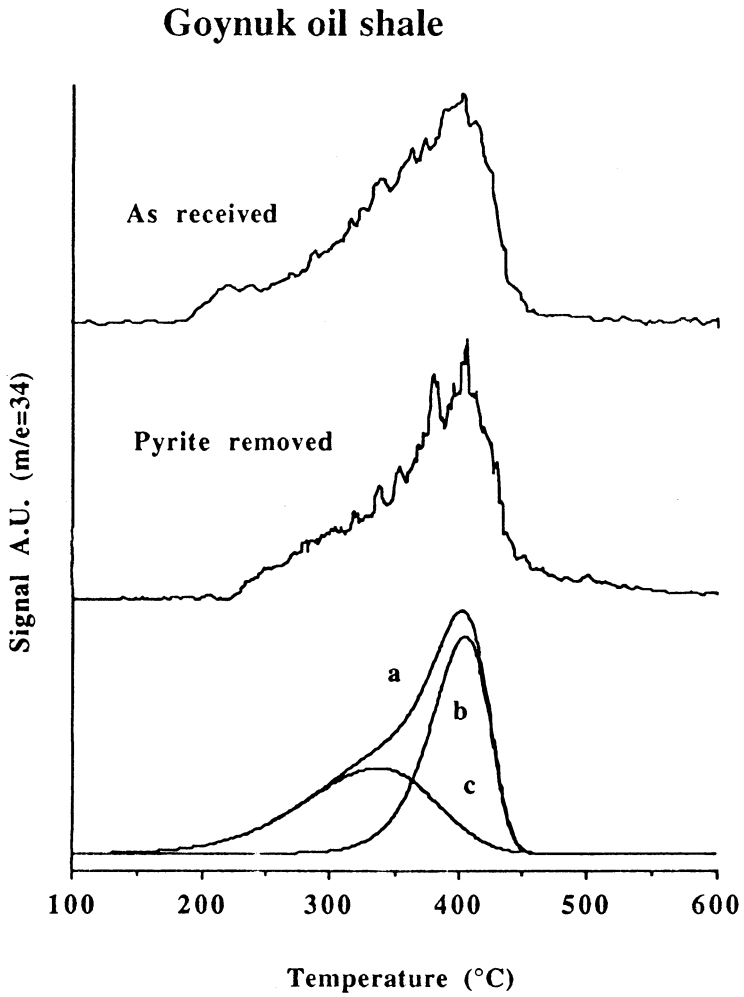


Figure 2. H₂S evolution for Goynuk oil shale: a. overall evolution; b. thiophenic sulphur; c. non-thiophenic sulphur.

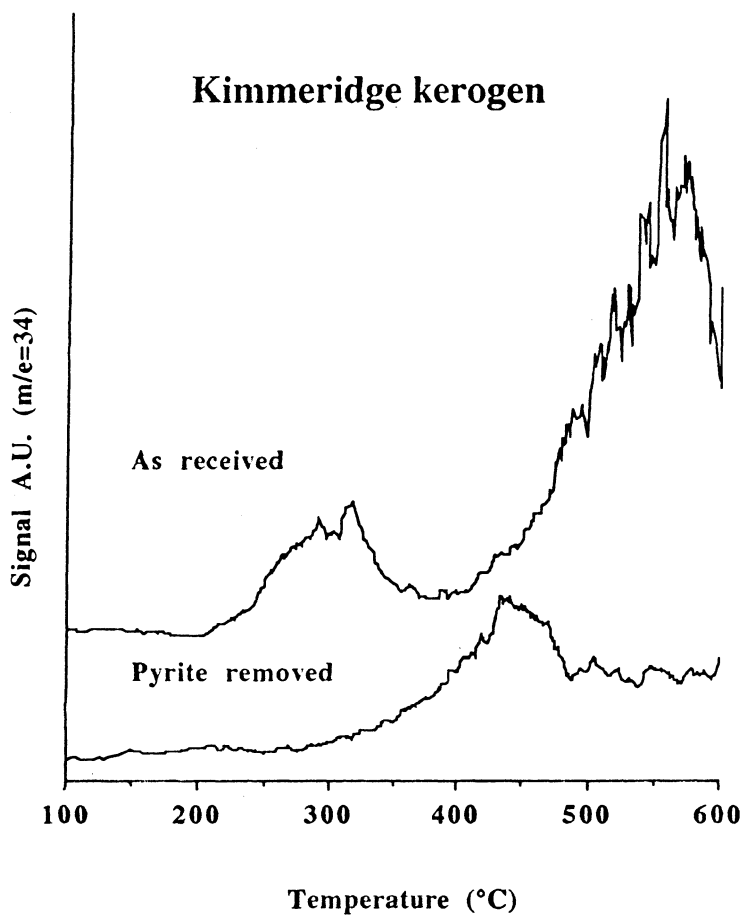


Figure 3. H₂S evolution profiles for Kimmeridge kerogen.

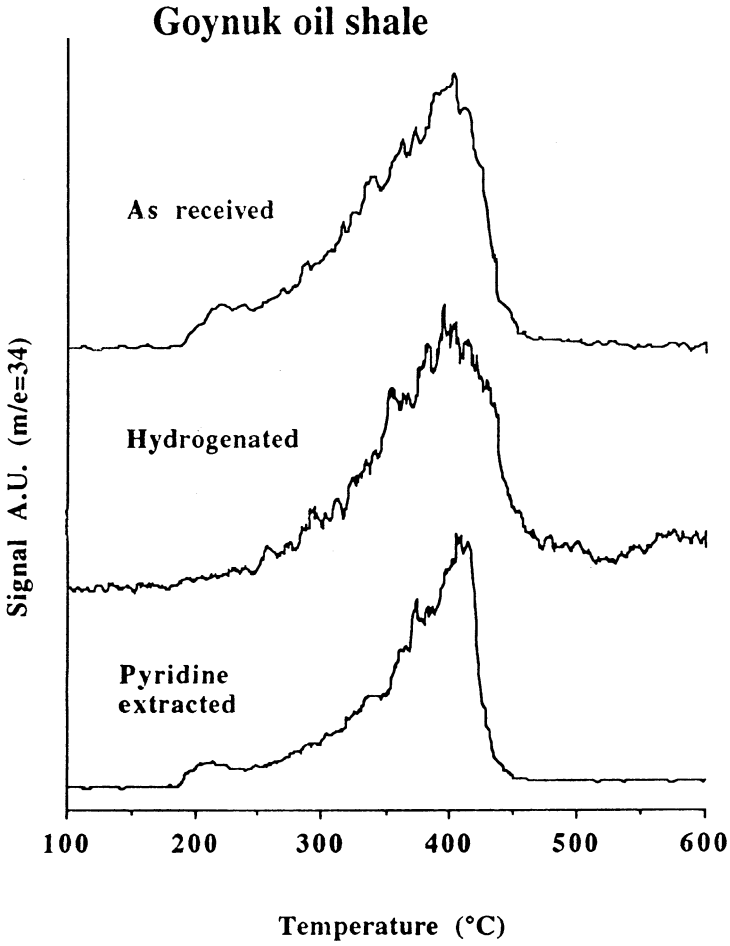


Figure 4. H₂S evolution profiles for Goynuk oil shale.

ring thiophenes, as compared to the lignites which contain 2-3 or more ring thiophenes. In addition, the proportion of H₂S evolving below 350°C indicates a relatively high concentration of sulphides, possibly di-/polysulphides.

The H₂S evolution profiles can be fitted to the Redhead equation as shown in Figure 2 by a simple two-component fit for Goynuk oil shale, after pyrite removal. At 15 MPa hydrogen pressure, the breakdown results in sulphidic sulphur accounting for *ca* 50% of that evolved as H₂S. Correcting this value for the 20% found in the tar (Table 2), it is deduced that sulphidic sulphur accounts for 40-45% of the total organic sulphur content. Simply dividing the traces at *ca* 380°C for both kerogens gives roughly the same proportions of thiophenic and non-thiophenic sulphur forms as fitting the profile to two components using the Redhead equation.

Table 2. Distribution of organic sulphur in TPR products.

Sample ^a	%Schar	%Star	%Sgas ^b
Goynuk	<2	20	80
Kimmeridge	10	10	80

^aFollowing treatment with lithium aluminium hydride

^bDetermined by difference

There is the possibility that retrogressive chemistry might still be occurring at 15 MPa hydrogen pressure resulting in the interconversion of sulphides to thiophenes but the fact that the profile returns to baseline at a relatively low temperature (Figure 2) suggests that secondary reactions have been minimised.

Kimmeridge kerogen (as received) is dominated by a low temperature peak close to 300°C followed by a more intense high temperature peak at *ca* 550°C (Figure 3). It is clearly essential to remove the pyrite to obtain any meaningful information at all on the organic sulphur forms. The lithium aluminium hydride treatment used to remove the pyrite has been shown to have little or no effect on the organic sulphur present.

The profile obtained for the type II kerogen following pyrite removal comprises a broad band between 280 and 400°C followed by the dominant thiophenic peak with a Tmax of 440°C (Figure 3). The failure of the H₂S concentration to return to its initial baseline value is probably due to the incomplete removal of pyrite. The lower proportion of non-thiophenic sulphur compared to Goynuk is however entirely consistent with the structural differences between the two kerogens, the carbon aromaticity of Kimmeridge of *ca* 0.50 being 15 mole % carbon higher than that for Goynuk.

Figure 4 compares the H₂S profile for the as-received Goynuk with a sample which has been catalytically hydrogenated at 360°C (1% Mo loading, using a tubing bomb/sandbath arrangement) and the profile of the kerogen after pyridine extraction at 160°C. After catalytic hydrogenation at 360°C, two major changes on the profile are evident. Firstly, the profile has lost a considerable proportion of the low temperature feature between 200-300°C as a result of the breaking of the more labile sulphur bonds (di-/polysulphides and perhaps aliphatic sulphides). Secondly, although changes above 300°C are less important, the main peak at *ca* 400°C is broader with the intensity being considerable less than the as-received sample. Additionally, there are high temperature features at 460 and 560°C resulting from retrogressive chemistry taking place. This may be due to mass transfer limitations inherent to the tubing bomb set up.

4. References

1. S.R. Kelemen, G.N. George, and M.L. Gorbaty, *Fuel*, 1990, **69**, 939.
2. M.L. Gorbaty, G.N. George, and S.R. Kelemen, *Fuel*, 1990, **69**, 945 and 1065.
3. G.P. Huffman, S. Mitra, F.E. Huggins, N. Shah, S. Vaidya and F. Lu, *Energy & Fuels*, 1991, **5**, 574.
4. G.P. Huffman, N. Shah, M.M. Taghiei, F. Lu and F.E. Huggins, *Prepr. Am. Chem. Soc., Div. Fuel Chem.*, 1991, **36(3)**, 1204.
5. A. Attar, *Fuel*, 1978, **57**, 201.

6. A. Attar, in "Analytical Methods for Coal and Coal Products" (C. Karr, Jr., Ed.), Academic Press, New York (1979), Vol. III, Ch. 56, p. 585.
7. A. Attar, DOE/PC/30145TI Technical Report, US DOE (1980).
8. B.T. Dunstan and L.V. Walker, Final Report to Australian National Energy Research Development and Demonstration Council, Canberra (1988).
9. B.B. Majchrowicz, D.V. Franco, J. Yperman, G. Reggers, J. Gelen, J. Martens, J. Mullens, and L.C. van Poucke, Fuel, 1991, **70**, 434.
10. C.J. Lafferty, S.C. Mitchell, R. García and C.E. Snape, Fuel, 1993, **72**, 367.
11. R.B. LaCount, R.R. Anderson, S. Friedman and S. Blaustein, Fuel, 1987, **66**, 909.
12. R.B. LaCount, D.G. Kern, W.P. King, T.K. Trulli and D.K. Walker, Prepr. Am. Chem. Soc., Div. Fuel Chem., 1992, **37(3)**, 1083.
13. W.H. Calkins, Energy & Fuels, 1987, **1**, 59.
14. W.H. Calkins, R.J. Torres-Ordonez, B. Jung, M.L. Gorbaty, G.N. George and S.R. Kelemen, Proc. 1991 Int. Conf. on Coal Science (Newcastle upon Tyne), p. 985.
15. R. García, S.R. Moinelo, C.J. Lafferty and C.E. Snape, Energy & Fuels, 1991, **5**, 582.
16. S.C. Mitchell, C.J. Lafferty, R. García, C.E. Snape, A.C. Buchanan, III, P.F. Britt and E. Klavetter, Energy & Fuels, 1993, **7**, 331.
17. R. García, S.C. Mitchell, C.E. Snape, S.R. Moinelo and K.D. Bartle, Proc. 1993 Int. Conf. on Coal Science (Banff), Vol I, p.445.
18. J.D. Saxby, "Oil Shale" (T.F. Yen, Ed.) (1975), 103.
19. D.L. Lawlor, J.I. Fester and W.E. Robinson, Fuel, 1963, **42**, 239.
20. J.W. Smith, N.B. Young and D.L. Lawlor, Anal. Chem., 1964, **36**, 618.
21. K. Ismail, R. Garcia, S.C. Mitchell, C.E. Snape, A.C. Buchanan, III, P.F. Britt, D. Franco and J. Yperman, Proc. 1993 Int. Conf. on Coal Science (Banff), p.3.
22. P.A. Redhead, Vacuum, 1962, **12**, 203.

Index

A

Activated carbon	352
Steam activation	353
Acyclic isoprenoids	54
Algae	23
Alginite	23, 41, 421
Alkanes	27, 426, 439
Branched	53
Bicyclic	54
Hexacyclic	58
Monocyclic	54
Normal	52, 407, 440, 447
Pentacyclic	56
Tetracyclic	55
Tricyclic	55
Alkanoic compounds	395
Alkenes	27, 439
Alkyl naphthalenes	433
Aliphatic carbon	200, 202
Aqueous organic chemistry	313
Aromatic carbon/aromaticity	202, 204, 307
Aromatic hydrocarbons	425
Asphalt	347
Asphaltenes	358, 401, 404
Asphaltites	
Fluidized-bed combustion	338
Hydrogen-donor solvent extraction	337
Pyrolysis	332
Rare metals	339
Solvent extraction	334
Supercritical gas extraction	337
Turkish	330, 331
Autocatalysis	321

B

Bacteria	
Sulphate-reducing	408
Behenic acid	322
Beneficiation	29, 164, 175

Benzyl aryl ethers	321
Biodegradation	407
Biomarkers	51, 439
Parameters	57
Bitumen	18, 213, 295
Formation	430
Heating, isothermal, non-isothermal	298
Formation	304
Bituminite	298
Bituminite	426, 21
Botryococcus	19, 21, 27, 427

C

Carbon distribution	242
Carbon fibres	356, 358
Activated	357
Carbon isotope composition	439
Carbonates	36
Decomposition	270, 374
Carbons	347
Adsorbent	353
Disordered	349
Low temperature	350
Turbostratic structure	350
Carboxylic acids	148, 409
Catagenesis	317, 392
Catalysts, dispersed	281
Hydrous titanium oxides	283
iron	282
Lewis acids sulphided	281
molybdenum	281
Char reactivity	270
Combustion	365
Gasification	368
Rate expressions	368
Clay	
Upper Kimmeridge	427
Clay minerals	324
Coals	450
Definition	7
Petrography	2, 6
Carboniferous	461
Types	478
Coalification	15, 315
Cokes	481
Macroporous structure	485, 491
Porosity	487

Combustion	160
Fluidized-bed	338
Kinetically controlled	369
Mass transfer controlled	370
Oil shale particles	374
Combustion emissions	
sulphur	272
NO _x	273
Comminution	176
Conversion processes	162
D	
Demineralization	35, 145
Density	197
Density gradient centrifugation (DGC)	39, 41, 43
Desulphurization	397, 493
Lignite	457
Molten caustic	451
Sodium alkoxide	450
Deuterium incorporation	398
Deuterium labelling	402
Devolatilization	365
Diagenesis	315, 392
DNA	439
E	
Economic considerations	159
Electron spin resonance (ESR)/ electron paramagnetic resonance (EPR)	198, 379
Matrix isolation	379
Superhyperfine splittings	379
Vanadium complexes	381
Esters	149
F	
Fischer assay	28, 192, 200, 230, 297
Colorado	297, 307
New Albany	297, 307
Flotation	
Equipment	180
Cells	186
Fossil leaf	440
Fourier transform infra-red (FTIR)	41, 44

G	
Gas chromatography	
Flame ionization detection (FID)	110
On-column injection	109
Open-tubular	107
Nitrogen-phosphorus detector (NPD)	110
Retention indices	112
Split injection	108
Splitless injection	109
Stationary phase coatings	115
Gas chromatography - mass spectrometry (GC-MS)	52, 395, 409, 414
Isotope ratio, δ ¹³ C	442
Geraniol	319
Graphite	348, 479
Gravity concentration	178
H	
Hopanes	56, 414, 441
Hydrodesulphurization	137
Hydrofluoric acid	37, 452
Hydrolysis	320
Hydropyrolysis	277
Oil composition	281
Reactor types	278
Fixed-beds	279
Two-stage reactors	284
Hydroretorting	167, 284
Assays	290
Carbon conversion	288
Pressurized fluidized bed	285
Process development unit (PDU)	285
I	
Inertinite	2, 10, 11, 389
Iron sulphides	374, 416
K	
Kerogen	24, 25, 35, 150, 388, 401, 404, 493

	426	Autochthonous	2
Green River	324		
Kimmeridge	324	N	
Ketones	149	Nitrogen,	
Kinetics	211, 263	bases	147
hydrocarbon		hydrolyzable	147
generation	265, 469	NMR, Solid state ¹³ C	70, 146,
oil generation	267		199
parameters	469	Cross polarisation	75, 79
Kukersite	21	Dipolar dephasing	77
		High power	
L		decoupling	71
Lamalginite	18, 27,	Magic-angle spinning	70, 72
	389	Sideband removal	74
Lamosite	21, 25, 31	Single pulse excitation	81
Tertiary	25		
Lead sulphides	407, 416	Q	
Lignite	457, 494	Oil/Shale oil	26
Limonene	319	Cracking	269
Lipids	440	Generation	391
Liptinite	2, 10, 12,	Molecular weights	307
	21, 389	Window	391
Lithium aluminium hydride	149, 395	Yields	28, 268
Lithotypes	13	Oil shales	
Lochmann's base	139	Algal	214
		Alum shales	419
M		Analysis	197
Macerals	2	Bahloul formation	408
Marine	47	Black shales	387, 407
Properties	36	Boscan	397
Separation	35, 39, 40	Carbonaceous	22
Terminology	7, 10	Co-processing	254
Terrestrial	47	Classification	18
Marinite	21, 26	Cleveland	43
Mass spectrometry (MS)	93	Decomposition	
Chemical ionization	98	models	295
Electron ionization	96	Devonian	232
Field ionization	98	Geochemistry	59
High resolution	99	Eastern US	232
Low voltage	101	Green River	37, 143,
Magnetic sector	96		155, 157
Mass analyzers	95		214, 230
Mesophase	351	Goynuk	159, 248
Metal sulphides	407, 416		353
Microlithotypes	13, 14, 22	Lacustrine	20
Microscopy		Messel	323
Fluorescence	2, 409	Marine	21
Reflectance	409	Monterey	221, 396
Microwave radiation	197	New Albany	43
Minerals		Petrographic	
Allochthonous	2	classification	19

Process design	263	Steam	253
Resource allocation	83		
Rotem	37	Q	
Rundle Ramsey		Quaternization	139, 147
Crossing	143, 154,		
	156	R	
Seyitomer	249	Raney nickel	137, 395
Structural analysis	150		399
Terrestrial	20	Reactions	
Toarcian	427	Condensation	318
Types	20	Bond cleavage	319
Upper Devonian	35	Reduction	137
Western US	292	Refining costs	169
Olefins	150	Reflectance	9
Organic petrography	1, 17, 43	Reflected light microscope	5
Techniques	3	Resins	401
Organic sulphur forms	125	Retorting	165
Oxidation	137	Fluidized-bed	229
Perchloric acid	144	Kentort II	231, 239
		Steam	247
P		Retorts	
Parallel reaction model	224	Combustion	264
Pediastrum	27	Heinze	248
Petroleum pitch	360	Hot recycled solids	265
Petrographic analysis	388, 470	Gray-King	248, 392
Fluorescence	421	Rock-Eval	195, 425,
Phenols	148		435, 461,
Polyacrylonitrile	356		463, 467
Polymerase chain reaction	439	Hydrocarbon index	219, 389
Principal component analysis	430	Ruthenium tetroxide	396, 398
Pyridyl derivatives	318		
Pyrite	30, 126,	S	
	374, 449	Scanning electron	
	452	microscopy (SEM)	452
Pyrroles	148	Silicates	38
Pyrolysates	27, 217,	Small angle neutron	
	427, 437	scattering (SANS)	431
Pyrolysis	160	Sodium borohydride	149, 397
Flash	135	Sporinite	41
Fluidized-beds	232, 238,	Steranes	55, 414
	251	Styrene	321
Fluidizing medium	235	Sulphides	39
Gas chromatography	431, 433	Sulphur	268
High pressure	211	Distribution	243
Hydrous	211, 216,	Incorporation	395
	323	Cross-linking	395
Kerogen	212	Functionalities	449
Laser	195	Supercritical fluid	
Non-hydrous	213, 323	chromatography	52
Open	211	Sycamore fossil	439
Residence time	236		

T		Atomic radial distribution function	477, 479
Tasmanite	21, 389, 427	Minerals	483
Telalginite	18	X-ray photoelectron spectroscopy (XPS)	127
Temperature programmed adsorption	355	Z	
Temperature programmed desorption	355	Zinc sulphides	407, 416
Temperature programmed oxidation (TPO)	135, 449, 493		
Temperature programmed reduction (TPR)	125		
Atmospheric pressure	449, 451, 454		
High pressure	130, 493		
Low pressure	130		
Terpenoids	441		
Thermal chromatography	195		
Thermogravimetric analysis (TGA)	453		
Thermogravimetry - mass spectrometry (MS)	355		
Thiolanes	396		
Thiophenes	395		
Torbanite	21, 159, 353, 427		
Total organic carbon (TOC)	409, 414, 420, 423, 437		
U			
Uranium	419, 420		
Urea adduction	442, 461, 463, 467		
V			
van Krevelen diagram	424, 65		
Vanadium	420		
Complexes	381		
Vitrains	478		
Vitrinite	8, 10, 12, 388, 390, 414, 461, 463, 465		
Reflectance			
X			
X-ray absorption near-edge structure (XANES)	127, 396		
X-ray diffraction (XRD)	145, 388, 421, 477		